Contaminated Sediments

Evaluation and Remediation Techniques

STP 1482

Editors:
M. Fukue
K. Kita
M. Ohtsubo
R. Chaney

ASTM INTERNATIONAL
Standards Worldwide

STP 1482

Contaminated Sediments: Evaluation and Remediation Techniques

M. Fukue, K. Kita, M. Ohtsubo,
and R. Chaney, editors

ASTM Stock Number: STP1482

ASTM
100 Barr Harbor Drive
PO Box C700
West Conshohocken, PA 19428-2959

Printed in the U.S.A.

ISBN: 0-8031-3408-8

Peer Review Policy

Each paper published in this volume was evaluated by two peer reviewers and at least one editor. The authors addressed all of the reviewers' comments to the satisfaction of both the technical editor(s) and the ASTM International Committee on Publications.

The quality of the papers in this publication reflects not only the obvious efforts of the authors and the technical editor(s), but also the work of the peer reviewers. In keeping with long-standing publication practices, ASTM International maintains the anonymity of the peer reviewers. The ASTM International Committee on Publications acknowledges with appreciation their dedication and contribution of time and effort on behalf of ASTM International.

Printed in Lancaster, PA
May 2006

Foreword

This publication, *Contaminated Sediments: Evaluation and Remediation Techniques* is the proceedings of the Third International Symposium on Contaminated Sediments, held in Shizuoka, Japan from May 23 to 25, 2006. This symposium was sponsored by the D18 Committee on Soil and Rock, ASTM International.

The symposium chairman was Dr. Masaharu Fukue, Tokai University, the symposium co-chairmen were Dr. Ronald. C. Chaney, Humbolt State University and Dr. Masami Ohtsubo, Kyushu University, and the symposium secretary was Dr. Katsutoshi Kita, Tokai University.

Contents

Overview

This Special Technical Publication is a compilation of technical papers which were reviewed for the On-line *Journal of ASTM International* and used as the proceedings of the 3rd International Symposium on Contaminated Sediments held in Shizuoka, Japan from May 23 to 25, 2006. Papers and presentations were targeted to deliver information on current knowledge in scientific and engineering topics. Emphasis on remediation technology is a key feature of the symposium. This volume is also part of the overall technical program of ASTM Committee D18 on Soil and Rock.

Since the Industrial Revolution, surface water including sediments and benthos has been exposed to a wide variety of contaminants, such as organic compounds and metals. Recent research has shown that sediments play an important role in the preservation of surface water quality and thus the sediments must be protected to ensure a safe environment for life through the food-chain and to avoid the biological concentration of contaminants. Eutrophication in enclosed and semi-enclosed lakes, estuaries and bays due to the leaching of nutrients from the beds is another subject relating to sediments. Thus, the objective of the symposium is to acquaint the attendees with the latest advances in the fields of environmental science and underwater engineering related to sediments, and to determine the various courses of future research.

The symposium covers the areas of characterization, evaluation, mitigation, restoration and management of contaminated sediments in the fields of oceanography, limnology, sedimentology, geochemistry, marine geotechnology, environmental science and civil engineering, etc. The subjects also include physical, chemical and biological aspects of sediments. There are many advances presented in the papers which are separated into four sections; (1) monitoring and field investigation in relation to the quality of sediments and water, (2) physical properties of sediments, which also affect the fate and transport of contamination, (3) specific topics and issues concerning heavy metals and (4) different, potentially more sustainable, approaches for remediation technology including capping of contaminated sediments and cement stabilization of dredged contaminated materials.

The subjects vary from physico-chemical interactions between substances and sediments or suspended particles to global environmental problems, which are often difficult to solve. However, it is emphasized that future courses are indicated through the presentations by authors and the discussion by panelists in the special discussion session.

Finally, the editors would like to thank all authors for their contribution. We also would like to thank the members of the Organizing Committee, International Advising Committee, ASTM International (Committee D-18), Tokai University and Marine Geoenvironmental Research Association, for their strong cooperation and support. The editors are very grateful to Mrs. Crystal Kemp for her dedication towards ensuring the completion of this Special Technical Publication.

Masaharu Fukue
Tokai University

Katsutoshi Kita
Tokai University

SECTION I: MONITORING AND FIELD INVESTIGATION

Journal of ASTM International, Vol. 3, No. 7
Paper ID JAI13374
Available online at www.astm.org

H. E. Keenan,[1] *M. Dyer,*[1] *A. Songsasen,*[2] *S. Bangkedphol,*[2] *and U. Homchan*[2]

Environmental Monitoring of the Sediment Pollution along the Thai:Laos Mekong

ABSTRACT: The Mekong is an essential source of water and protein for the denizens of Thai Laos countries. However historic pollution is adversely affecting the water and sediment quality that threatens the short- and long-term supply/use of this major river system. This can have a major impact on the health and population of the marine life and ultimately adversely affect human health and the economy for both countries. As a first stage in the assessment of the scale and extent of the pollution problem, an in-depth program of sampling and analysis has been carried out for both water and sediments for three seasons since 2000. A range of water quality parameters were measured from ten sampling stations. These included the PolyAromatic Hydrocarbons (PAHs) initially measured as chrysene equivalents, then as individual compounds of fluorene, phenanthrene, anthracene, fluoranthene, pyrene, benzo(a)anthracene, chrysene, benzo(b)fluoranthene, benzo(k)fluoranthene, benzo(a)pyrene, dibenzo(a,h)anthracene, benzo(g,h,i)perylene, and indeno(1,2,3,cd)pyrene. A range of heavy metals were measured including chromium, cadmium, mercury, copper, zinc, lead, and titanium. This paper presents the results of the field study to date and provides a preliminary evaluation of the extent of the pollution and potential for bioaccumulation within the local food chain.

Introduction

The Mekong River rises in Tibet and travels 4425 km south through China, Myanmar, Thailand, Laos, and Cambodia before discharging to the South China Sea via the delta in Vietnam. It is the eleventh longest in the world and more than sixty million people inhabit the environs of the river. The river is essential to provide water, protein, electricity, and other valuable resources. Pollution of the quality of both the water and sediments may adversely impact on wildlife and human health. The objective of this study is to measure various parameters in both water and sediments in the Thai:Laos Mekong and relate the values found to environmental quality and impact assessment. This paper is particularly concerned with 13 polyAromatic hydrocarbons (PAHs) and a range of metals in the Thai:Laos Mekong for several seasons since 2000. PAHs are known persistent organic pollutants (POPs) characterized by their hydrophobicity with a capacity to persist in the environment with concomitant bioaccumulation and biomagnification effects.

Using a persistence, bioaccumulation, and toxicity profiler (Environmental Science Center 2004) several parameters for each of the PAHs were obtained. These included the percentage of the compound expected in each environmental compartment (calculated from the chemical and physical properties of the compound) the bioconcentration factor (BCF) and the fish chronic value (ChV). Using (ECOSAR) (USEPA 2000) the predicted 14 day lethal concentration 50 (LC_{50}) for fish was also obtained.

Water and sediment samples were analyzed using optimized methodology already developed by the authors (Songsasen et al. 2004) reference standards were used to calculate the efficiency of the methodology. The results were collated to give average annual concentrations at each sampling station.

Samples for metal analysis were analyzed using an acid digest inductively coupled plasma (ICP) method. The values obtained were assessed in terms of sediment quality guidelines and probable effect level as pollution indicators, as there are currently no sediment quality guidelines in either UK or Thailand, the Canadian values were used (Canadian Environmental Quality Guidelines 2003).

Manuscript received May 10, 2005; accepted for publication September 28, 2005. Presented at ASTM Symposium on Contaminated Sediments: Evaluation and Remediation Techniques on 23–25 May 2006 in Shizuoka, Japan; M. Fukue, K. Kita, M. Ohtsubo, and R. Chaney, Guest Editors.

[1] Civil Engineering, University of Strathclyde, Glasgow, Scotland.
[2] Faculty of Science, Kasetsart University, Bangkok, Thailand.

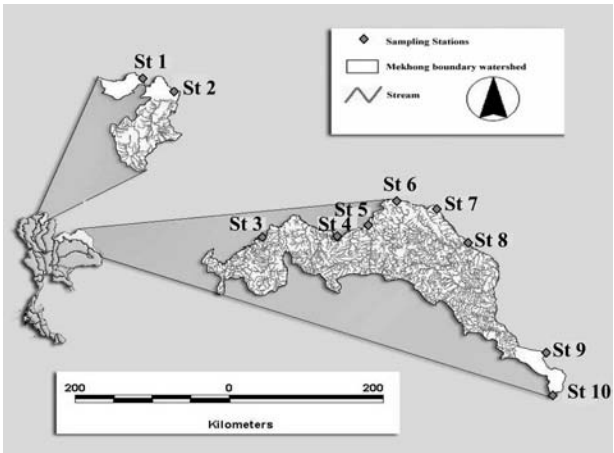

FIG. 1—*Sampling stations on the Thai: Laos Mekong.*

The location of the sampling stations (1–10) are shown in Fig. 1. At each station, samples (water and sediment) for analysis were taken from the river edge.

However due to the seasonal changes these points are not identical but as closely related as physically possible. The reasons for the choice of sampling stations are listed in Table 1 below.

Methods of Analysis

PAHs

Trace enrichment of water samples was carried out using C18 solid phase extraction tubes, the eluted compounds were analyzed for each PAHs by (HPLC) (EPA 8310) using standard additions methodology.

For the analysis of the sediments, the samples were sonicated for 50 min using an optimized solvent mix of cyclohexane:acetone 3:2 as the extracting solvent. The concentration of each PAH was determined by HPLC (EPA 8310). A certified reference sediment (Laboratory of Government Chemist, London, LGC6188) was analyzed to determine the extraction efficiency (%) of each PAH present.

The values of the analysis were collated, averaged and tabulated ($N=10$). The values obtained by analysis were recalculated to adjust for the extraction efficiency of each compound. The actual water concentration was multiplied by the BCF for each compound to define a potential bioaccumulation value. This was compared to the ChrV and LC50 (14 day) values for fish.

TABLE 1—*Sampling points along the Thai:Laos Mekong.*

Station No.	Rational for sampling at specific locations
1	Golden Triangle—Mekong River enters Thailand
2	Wat Jam Pong—Mekong leaves Thailand into Laos (mountain range then forms the border until station 3)
3	Chiang Karn—Mekong reenters Thailand
4	Nong Khai—Thai-Laos friendship bridge (currently only bridge that joins the two countries)
5	Phonpisai—near a large town
6	Wat ArHong—the deepest point of Mekong
7	Sri Song Kram—Sri Song Kram River meets Mekong
8	Dhat Panom—busy port between Thai-Laos
9	Wat Khongchiampurawat—river from Laos meets Mekong
10	Khong Chaim—the last point before Mekong leaves Thailand into Laos and Cambodia

TABLE 2—*Environmental quality guidelines (metals) for freshwater sediment.*

Metals	ISQG ($mgkg^{-1}$) dry wt	PEL ($mgkg^{-1}$) dry wt $
Cr	37.3	90
Cu	35.7	197
Zn	123	315
Pb	35	91.3
Cd	0.6	3.5
Hg	0.17	0.486

$ Shading in tables represents those values above the stated EQG.

For metals the samples were analyzed by Standard Method (Eaton et al. 1995) 3120B which involved acid digest followed by ICP. All samples were analyzed wet and using the moisture content (sample oven dried at 105 °C) was recalculated to a dry basis.

Results

Initially the extraction efficiency for each PAH was calculated from the triplicate analysis of the certified reference standards ($N=3$).

The results obtained from the metal analysis (dry weight $mg\text{-}kg^{-1}$) were compared to the Environmental Quality Guidelines for freshwater sediment in Table 2 to assess pollution levels. The data presented in subsequent Tables 3–7 for sampling between 2000 and 2002 are shaded in two different tones to indicate where concentration levels exceed either the interim sediment quality guideline (ISQC) or probable effect level (PEL). The darker shading refers to the PEL values.

Discussion

The results show that the PAHs were successfully analyzed qualitatively and quantitatively for both water and sediment samples. Using reference standards the extraction efficiency was found to be different for

TABLE 3—*Trace element composition of sediments ($mg\text{-}kg^{-1}$-dry-wt) November 2000.*

Metals	Station Number									
	1	2	3	4	5	6	7	8	9	10
Cr	...	...	49	<dl	53	54	59	<dl	37	...
Cu	...	...	78	79	81	75	85	80	6	...
Zn	...	...	152	199	189	188	196	153	86	...
Pb	...	...	49	55	60	61	59	37	27	...
Cd	...	...	25	26	27	26	28	25	10	...
Mn	...	...	364	353	68	418	479	204	379	...
Ti	...	...	212	175	161	238	203	89	159	...

TABLE 4—*Trace element composition of sediments ($mg\text{-}kg^{-1}$-dry-wt) April 2001.*

Metals	Station Number									
	1	2	3	4	5	6	7	8	9	10
Cr	...	...	27	16	27	32	27	36	...	...
Cu	...	...	21	17	15	16	8	8	...	...
Zn	...	...	82	51	72	76	73	79	...	...
Pb	...	...	23	15	23	27	24	32	...	...
Cd	...	...	9	7	9	10	9	10	...	...
Mn	...	...	355	189	314	378	349	427	...	...
Ti	...	...	184	141	165	143	140	163	...	...

TABLE 5—*Trace element composition of sediments (mg-kg^{-1}-dry-wt) December 2001.*

Metals	Station Number									
	1	2	3	4	5	6	7	8	9	10
Cr	71	63	96	26	72	78	90	122	123	134
Cu	9	2	10	<dl	<dl	2	7	16	9	27
Zn	164	55	62	32	49	70	65	83	76	99
Pb	46	48	41	24	13	16	21	28	35	44
Cd	<dl	<dl	12	20	25	<dl	6	24	14	31
Hg	13	26	43	21	42	38	48	52	15	106

each PAH analyzed as shown in Table 8. The quicker sonication method produces variable results although the method is reproducible. As each PAH is a component of a single sample the experimental methodology is consistent and the range of efficiencies may be due to the different chemical and physical properties of the PAHs. The more volatile hydrophilic PAHs may be lost during the procedure (Napthalene was discounted from the study as reproducible efficiencies were not obtained) the more hydrophobic PAHs are

TABLE 6—*Trace element composition of sediments (mg-kg^{-1}-dry-wt) April 2002.*

Metals	Station Number									
	1	2	3	4	5	6	7	8	9	10
Cr	51	54	89	6	69	69	83	100	190	142
Cu	0.2	0.9	7	<dl	0.1	<dl	7	12	9	30
Zn	69	69	85	96	63	67	78	80	83	116
Pb	32	32	38	26	40	37	45	47	47	65
Cd	35	36	39	0.5	18	15	20	18	22	29
Hg	6	34	17	14	27	11	12	20	24	36

TABLE 7—*Trace element composition of sediments (mg-kg^{-1}) August 2002.*

Metals	Station Number									
	1	2	3	4	5	6	7	8	9	10
Cr	94	. . .	. . .	99	122	116	93	102	112	99
Cu	15	. . .	. . .	29	25	29	24	20	23	16
Zn	97	. . .	. . .	35	117	102	95	103	110	98
Pb	55	. . .	. . .	55	62	67	62	61	68	58
Cd	41	. . .	. . .	45	18	46	36	27	43	44
Hg	69	. . .	. . .	1	24	87	0.5	13	4	11

TABLE 8—*Recovery (%) of PAHs calculated from reference materials* (N = *3).*

PAHs	Water percent	Solids percent
Fluorene	73.42	38.76±3.85
Phenanthrene	75.32	69.22±14.94
Anthracene	70.23	78.09±5.34
Fluoranthene	63.98	58.46±2.26
Pyrene	51.36	54.49±0.81
Benzo(a)anthracene	53.88	33.27±5.86
Chrysene	49.78	89.42±3.62
Benzo(b)fluoranthene	58.41	112.48±0.30
Benzo(k)fluoranthene	64.58	163.99±0.98
Benzo(a)pyrene	63.18	44.79±8.36
Dibenzo(a,h)anthracene	67.38	53.02±1.01
Benzo(g,h,i)perylene	65.98	82.27±3.10
Indeno(1,2,3,cd)pyrene	68.61	61.42±3.56

Note: The efficiency of the extraction (percent recovery) was taken into account for subsequent calculations.

TABLE 9—*Relationship between Caq and Cbio Compared with the ChrV and LC50 values for average results from each sampling station (N = 10) of PAHs (April 2003, dry season).*

PAHs	C_{aq} (mean ppb)	C_{bio} (mean ppm)	ChrV/LC_{50} (ppm fish)
Fluorene	1.67	0.55	↑/↓
Phenanthrene	0.23	0.12	↓/↓
Anthracene	0.26	0.14	↓/↓
Fluoranthene	1.15	2.19	↑/↑
Pyrene	1.35	1.49	↑/↑
Benzo(a)anthracene	5.60	30.24	↑/↑
Chrysene	2.69	15.87	↑/↑
Benzo(b)fluoranthene	1.22	6.83	↑/↑
Benzo(k)fluoranthene	1.23	12.30	↑/↑
Benzo(a)pyrene	2.10	21.00	↑/↑
Dibenzo(a,h)anthracene	1.54	33.88	↑/↑
Benzo(g,h,i)perylene	1.06	26.50	↑/↑
Indeno(1,2,3-cd)pyrene	1.18	34.22	↑/↑

Note: $C_{aq} \times BCF = C_{bio}$ (potential bioaccumulation).

ChrV: chronic value, LC_{50} lethal concentration 50 (14 days).

↑: C_{bio} values above threshold for water.

↓: C_{bio} values below threshold for water.

difficult to remove from glassware and to reconstitute. Where efficiencies are >100 % as occurred with the benzo fluorane isomers, this may be due to poor automated integration of peaks on the chromatograms. However the study is valid as each PAH was reproducible as seen by the standard deviation (σn-1). The authors have further optimized the methodology since the production of this work (Songsasen et al. 2005).

With regard to the results measurable quantities of PAHs were detected in both water (Tables 9 and 10) and sediments (Tables 11 and 12) at most stations. Generally water concentrations were lower in the wet season than the dry, this is due to dilution by the greater volume of water in the wet season.

As expected the more hydrophobic the PAH the greater the BCF (Table 13) and the greater the percent partitioning to solids, this is associated with lower aquatic concentrations for the ChrV and LC50 values.

Higher BCF values will increase the biomagnification, thus very low levels of PAHs in water may exert adverse physiological effects through the food chain.

Although the ChrV and LC50 values relate to toxic concentrations in water these were used comparatively with the potentially accumulated concentrations. Toxicity tests for accumulated PAHs are difficult to assess due to variation in BCFs for each PAH and each species of fish. Further work on this project has demonstrated a correlation between PAHs and adverse physiological effects in fish dosed with various

TABLE 10—*Relationship between Caq and Cbio Compared with the ChrV and LC50 values for average results (N = 10) of PAHs (August 2003, wet season).*

PAHs	C_{aq} (mean ppb)	C_{bio} (mean ppm)	$ChrVLC_{50}$ (ppm fish)
Fluorene	0.22	0.07	↓/↓
Phenanthrene	0.14	0.08	↓/↓
Anthracene	0.27	0.14	↓/↓
Fluoranthene	0.50	0.95	↑/↑
Pyrene	0.58	0.64	↑/↓
Benzo(a)anthracene	<dl	…	…
Chrysene	<dl	…	…
Benzo(b)fluoranthene	0.18	1.01	↑/↑
Benzo(k)fluoranthene	0.14	1.4	↑/↑
Benzo(a)pyrene	<dl	…	…
Dibenzo(a,h)anthracene	<dl	…	…
Benzo(g,h,i)perylene	0.27	6.75	↑/↑
Indeno(1,2,3-cd)pyrene	0.15	4.35	↑/↑

Note: $C_{aq} \times BCF = C_{bio}$ (potential bioaccumulation).

ChrV: chronic value, LC_{50}: lethal concentration 50 (14 days).

↑: C_{bio} values above threshold for water.

↓: C_{bio} values below threshold for water.

TABLE 11—*Comparison of Csed and quality standards of PAHs average values (N = 10) (April 2003 dry season).*

	Csed actual	Standards ($\mu g \cdot kg^{-1} \cdot dry \cdot wt$)	
PAHs	($\mu g \cdot kg^{-1} \cdot dry \cdot wt$)	ISQG	PEL
Fluorene	52.85	21.2 ↑	144
Phenanthrene	153.35	41.9 ↑	515
Anthracene	82.78	46.9 ↑	245
Fluoranthene	180.67	111 ↑	2355
Pyrene	79.30	53 ↑	875
Benzo(a)anthracene	32.77	31.7 ↑	385
Chrysene	13.98	57.1	862
Benzo(b)fluoranthene	34.60	nv	nv
Benzo(k)fluoranthene	79.26	nv	nv
Benzo(a)pyrene	30.34	31.9	782
Dibenzo(a,h)anthracene	55.08	6.22 ↑	135
Benzo(g,h,i)perylene	101.30	nv	nv
Indeno(1,2,3-cd)pyrene	7.66	nv	nv

Note: ISQG: Interim sediment quality guideline.
PEL: Probable effect level } Canadian environmental quality guidelines (freshwater sediment).
↑ Csed actual value above guideline. Csed actual = Csed measured × 100/recovery %.
nv: No value.

PAHs (Phanwichien 2004). In this investigation the potential accumulative values for PAHs almost always exceed the ChrV and LC50 values for water (Tables 9 and 10). This is particularly true for the dry season when water volume levels are low. High sediment concentrations may have a greater impact and associated adverse physiological effects in bottom dwelling fish such as the giant catfish.

The fugacity model (Table 13) shows that most of the PAHs partition into sediment with the exception of phenanthrene and anthracene. However this is based on a default model where the values are obtained from chemical and physical properties and not experimental data. Work on this project has shown that the Mekong sediments are low in total organic carbon (TOC) with all stations having values of <5 %, this may lead to elevated concentrations in water concomitant with greater bioaccumulation. Also hydrophobic compounds that strongly adhere to solids are less bioavailable therefore persisting in the sediments and being transported downstream. Experimental data, particularly the partitioning between water and the organic carbon of the sediment (Koc) would define the model more accurately.

The concentration of PAHs in sediment always exceeds the ISQG (Tables 11 and 12) regardless of the

TABLE 12—*Comparison of Csed and quality standards of PAHs average values (N = 10) (August 2003 wet season).*

	Csed actual	Standards ($\mu g \cdot kg^{-1} \cdot dry \cdot wt$)	
PAHs	($\mu g \cdot kg^{-1} \cdot dry \cdot wt$)	ISQG	PEL
Fluorene	70.72	21.2 ↑	144
Phenanthrene	377.11	41.9 ↑	515
Anthracene	209.53	46.9 ↑	245
Fluoranthene	290.57	111 ↑	2355
Pyrene	85.84	53 ↑	875
Benzo(a)anthracene	35.16	31.7 ↑	385
Chrysene	18.38	57.1	862
Benzo(b)fluoranthene	16.11	nv	nv
Benzo(k)fluoranthene	85.05	nv	nv
Benzo(a)pyrene	28.03	31.9	782
Dibenzo(a,h)anthracene	61.62	6.22 ↑	135
Benzo(g,h,i)perylene	88.55	nv	nv
Indeno(1,2,3-cd)pyrene	12.25	nv	nv

Note: ISQG: Interim sediment quality guideline.
PEL: Probable effect level } Canadian Environmental Quality Guidelines (freshwater sediment).
↑ Csed actual value above guideline.
Csed actual = Csed measured × 100/recovery %.
nv: No value.

TABLE 13—*Bio concentration factors, percent PAH predicted in each environmental compartment and ChrV and LC50 values (from PBT profiler and ECOSAR).*

PAHs	BCF	Partitioning (scenario 6)[a]			ChrV(mg/L)/ LC_{50}(mg/L) (Fish)
		Percent solid	Percent air	Percent liquid	
Fluorene	330	82	2	16	0.28/3.88
Phenanthrene	540	47	0	53	0.16/2.15
Anthracene	530	47	0	53	0.16/2.15
Fluoranthene	1 900	81	0	19	0.055/0.76
Pyrene	1 100	70	0	30	0.055/0.76
Benzo(a)anthracene	5 400	93	0	7	0.019/0.263
Chrysene	5 900	94	0	6	0.019/0.263
Benzo(b)fluoranthene	5 600	94	0	7	0.006/0.089
Benzo(k)fluoranthene	10 000	96	0	4	0.006/0.089
Benzo(a)pyrene	10 000	96	0	4	0.006/0.089
Dibenzo(a,h)anthracene	22 000	97	0	3	0.002/0.03
Benzo(g,h,i)perylene	25 000	97	0	3	0.002/0.03
Indeno(1,2,3-cd)pyrene	29 000	97	0	3	0.002/0.03

[a]Scenario 6 derived from 100 % discharged to water.

season, the exceptions being chrysene and benzo(a)pyrene. The PEL was never breached, however as partitioning is mainly to sediments the accumulative values may increase. This may impact directly on mud dwelling and bottom feeder fish.

PAHs are only one group of a range of POPs present in the river system. Adverse physiological effects from exposure to these chemicals may include: mutagenic, teratogenic, carcinogenic, and endocrine disrupting processes. The additive and synergistic effects of groups of chemicals may also have to be considered.

For metals in sediment the values obtained by analysis were compared to the Canadian Quality Guidelines (Table 2). The silt and clay fraction (<63 m fraction) of the sediment, is a primary carrier of adsorbed chemicals, especially phosphorus, chlorinated pesticides and most metals.

Tables 3–7 show the mean values obtained at different times. Table 3 for samples taken in November 2000, show levels of Cr, Cu, Zn, and Pb above the ISQG for most stations sampled, the levels of Cd exceeded the PEL values for all stations. April 2001 (Table 4) showed concentrations in the sediments had dropped but all stations still exceeded the PEL for Cd. For December 2001 (Table 5) mercury had been added to the suite of metals measured and was found to exceed the PEL at every station. Again high concentrations of Cd were found at most stations. Tables 5–7 all show both Cd and Hg at levels above the PEL From December 2001 to August 2002 consistently high values (above the PEL) for chromium were also noted but only in the south most stations suggesting that this pollutant (and others) may be transported downstream. It is difficult to find clear association between the seasons and the data obtained, this is not surprising considering the variables involved. The river undergoes vast changes in volume and flow rate due to the monsoonal type climate, this affects the amount and transportation of sediment. Transformation mechanisms (volatalization, biodegradation, etc.) ensure that pollutant levels are never static. Additionally the sources and quantities of pollutants entering the river are extremely variable. However, generally the most problematic (elevated) concentrations measured were for Cd and Hg, which exceed the PEL by several orders of magnitude. Mercury salts and compounds are commonly used in agriculture and may be a major source of this pollutant. Cadmium is used mainly in industry and since there are no major industries on the Thai:Laos Mekong, this suggests that the high levels of cadmium are inherited pollution, however it is difficult for downstream countries to exert any control over inherited pollution.

The presence of aquatic metals particularly cadmium and mercury adversely affects fish health, particularly those mechanisms that protect against diseases (Rand 1995). This results in a depletion of fish stocks and would be devastating for the 60 million inhabitants of the Mekong as fish is the major source of protein. Biomagnification that occurs through the food chain may attain levels dangerous for the consumer, although the animal exposed may not exhibit adverse physiological effects. The most documented evidence of this comes from two episodes of mercury poisoning in Japan (FDA consumer 1995) that resulted in many human fatalities. Such levels as found in the Mekong may result in similar scenarios.

Conclusions

From the study undertaken and by comparison to the guidelines used it is clear that the Thai:Laos Mekong may be considered polluted for some of the parameters measured. PAHs, Cd, and Hg levels are of particular concern due to their adverse physiological effects on both animals and humans. Canadian sediment standards should be used with caution and the findings treated as indicative because the guidelines are developed specifically for the country in which they were developed and the species used in deriving the guidelines may have different sensitivities to those in the Mekong. Also variations in climate throughout the year may have to be considered, particularly river water temperature as this affects the chemical and physical properties of pollutants and their rate of removal. Thailand or the Mekong River Commission should develop their own guidelines for sediment quality.

Acknowledgment

Thanks to the British Council for financial support through the Higher Education Link between Strathclyde and Kasetsart Universities.

References

Canadian Environmental Quality Standards, 2003, http://www.ec.gc.ca/CEQG-RCQE/English/default.cfm

Eaton, A. D., Clesceri, L. S., and Greenberg, A. E., 1995, *Standard Methods for the Examination of Water and Wastewater*, United Book Press, Inc., Baltimore, Maryland.

Environmental Science Center, 2004, http://www.pbtprofiler.net

FDA, *Consumer*, 1995, http://www.fda.gov/fdac/reprints/mercury.html

Phanwichien, K., "Pathogenesis of Mekong Fish," *International Workshop, Environmental Monitoring and Modelling of the River: The Mekong River Case Study*, Bangkok, Thailand. October 6th–8th 2004.

Rand, G. M., *Fundamentals of Aquatic Toxicology, Effects, Environmental Fate and Risk Assessment*, Taylor & Francis, Philadelphia, 1995.

Songsasen, A., Bangkedphol, S., and Keenan, H. E., "Comparative Evaluation of the Microwave-Assisted Extraction in a Closed System and Sonication for the Extraction of PAHs from Sediments," *2nd Asian International Conference on Ecotoxicology and Environmental Safety*, Songkla, Thailand, September 26th–29th 2004.

Songsasen, A., Bangkedphol, S., and Keenan, H. E., Comparison of the Closed System, Microwave-Assisted Extraction of Polycyclic Aromatic Hydrocarbons from Sediment 2006, *J. Environ. Sci. Health*, A 41, p. 6.

USEPA, http://www.epa.gov/oppt/newchems/21ecosar.htm, 2000.

Journal of ASTM International, Vol. 3, No. 6
Paper ID JAI13330
Available online at www.astm.org

YongSung Kim,[1] *MyoungHak Oh, Ph.D.,*[2] *SunYoung Bang,*[3] *and Junboum Park, Ph.D.*[4]

Monitoring Heavy Metal Transport in Aquifer Based on Electrical Property Measurements

ABSTRACT: Monitoring the movement of subsurface contamination using the electrical properties of soils has the economical merits of providing continuous and automated soil profiles. However, identification on the sensitivity of this property in reflecting both the presence and concentration of different contaminant types has been validated for soils under static conditions. For application, electrical properties of soils must be verified under an active state where contaminant migration by means of groundwater migration is considered. The objective of this study is to provide the groundwork required in applying the electrical properties of soil as a means of monitoring contaminant migration by performing column tests. Two parameters representing the electrical property of materials are examined in this study; the electrical resistivity and the dielectric constant. Measurements for these parameters are performed at a low frequency range where the spatial polarization takes place and increases the sensitivity of the electrical property against the presence of the contaminant. In order to detect the contaminant movement in the subsurface level, electrical measurements were performed during column tests for saturated sand and weathered granite soil. In addition, three different contaminants (aluminum, lead, and cadmium) were selected to groundwater contaminated by heavy metals. As a result, the relationships between the contaminant migration against the electrical resistivity, real, and imaginary parts of the dielectric constant were derived for different time intervals during the column tests.

KEYWORDS: electrical resistivity, dielectric constant, subsurface contamination

Introduction

Subsurface contamination has the potential to pollute the groundwater through various migration mechanisms. Conventional method of monitoring the migration of subsurface contaminant involves taking representative samples in the field for laboratory analysis. However, sampling is a laborious and destructive method which is inappropriate for continuous monitoring of subsurface contamination. In order to overcome such limitations, electrical properties of soils have become a topic of extensive research because it has the potential to provide a means of continuous and nondestructive monitoring of subsurface contaminants.

Electrical methods for contaminant monitoring is based on the concept that contaminant intrusion alters the electrical properties of soil and pore water. Such changes can be perceived through fluctuations in two representative parameters: dielectric constant and electrical resistivity. Dielectric constant represents the ability of a material to store electrical energy through the application of an alternating current (ac) field. Electrical resistivity is a basic property of a material to transmit electrical charge under the application of an electrical potential. The reported studies based on laboratory tests have been focused on finding the factors that affect the dielectric constant and electrical resistivity of soils (Arulanandan and Smith 1973, Fukue et al. 1999). The governing factors of the dielectric constant of soils have been reported in the past to include water content, type, and amount of electrolyte in pore water (Francisca and Rinaldi 2003, Kaya and Fang 1997). Keller and Frischknecht (1996) reported that porosity, electrical resistivity of the pore fluid, and degree of saturation governs the electrical resistivity of soils.

Although the sensitivity of the dielectric constant and electrical resistivity against contaminant intru-

Manuscript received March 31, 2005; accepted for publication June 28, 2005. Presented at ASTM Symposium on Contaminated Sediments: Evaluation and Remediation Techniques on 23–25 May 2006 in Shizuoka, Japan; M. Fukue, K. Kita, M. Ohtsubo, and R. Chaney, Guest Editors.

[1] Graduate Student, Seoul National University, San 56-1, Sillim-dong, Gwanak-gu, Seoul, 151-742, Korea.
[2] Post Doctoral Researcher, Seoul National University, San 56-1, Sillim-dong, Gwanak-gu, Seoul, 151-742, Korea.
[3] Researcher, Korea Electric Power Research Institute, Munji-dong, Yoosung-gu, Daejon, 305–380, Korea.
[4] Professor, Seoul National University, San 56-1, Sillim-dong, Gwanak-gu, Seoul, 151-742, Korea.

TABLE 1—*Index properties of weathered granite soil and silica sand.*

Weathered granite soil	Maximum dry density $\gamma_{d\,max}=1.95(t/m^3)$	Coefficient of gradation 1.3	Uniformity gradation 8.1	Specific gravity 2.56	USCS[a] Well graded sand
Silica sand	Maximum dry density $\gamma_{d\,max}=1.66(t/m^3)$	Coefficient of gradation 1.01	Uniformity gradation 1.51	Specific gravity 2.64	USCS Poorly graded sand

[a]Unified Soil Classification System.

sion has been validated by many reported works, this is founded on laboratory experiments performed under static conditions. Therefore, the applicability of monitoring based on the electrical properties needs to be verified under an active state where migration of contaminant is simulated similar to the field conditions such as in contaminated groundwater. The objective of this study is to monitor the electrical properties of soils against time-dependent migration of contaminants by performing column tests. In order to model contaminant migration, silica sand and weathered granite soil were used as representative soils while heavy metals with various concentrations were selected as representative contaminants.

Experimental Section

Materials

Two kinds of soils were used in this study, the weathered granite soil and silica sand. Weathered granite soil is a commonly distributed soil around the Korean peninsula, and it was collected from the vicinity of the Seoul National University for this study. The soil was sieved through the No.10 sieve and oven-dried for 24 h at 105°C. Index properties of the soils used in the study are shown in Table 1.

Cadmium, lead, and aluminum were selected as representative heavy metal contaminants in this study. Standard solutions (Cica-reagent, Kanto Chemical Co. Inc., Japan) were diluted with deionized water (Milli-Q, Millipore Corp., Billerica, MA) to have concentrations varying between 0 and 100 mg/L.

Preliminary Test

Prior to the column test, preliminary tests were performed to verify the effect of heavy metal contamination on the electrical properties of silica sand and weathered granite soil. Measurements were performed on an acrylic mold designed for this study. The acrylic mold employs the parallel plate capacitor method, and is connected to either the 4263B *LCR* Meter (Agilent Co., Kobe, Japan) or the 4285A *LCR* Meter (Agilent Co., Kobe, Japan) for capacitance measurements. The 4263B and 4285A *LCR* meters are capable of capacitance measurement under the frequency ranges of 100 Hz–100 kHz and 100 kHz–10 MHz, respectively. The electrical resistance was calculated by measuring the electrical potential difference between the electrodes under the direct current (dc) of 0.1 mA by the 2400 SourceMeter (Keithley Co., Cleveland, OH). Calibrations were made with solutions of known resistance and capacitance in order to eliminate the fringing effect and residual impedance effect. The measured capacitance and electrical potential difference are substituted to the following equations to calculate the real and imaginary parts of the dielectric constant and the electrical resistivity. For real and imaginary parts of the dielectric constant

$$\varepsilon' = \frac{C}{\varepsilon_0 \times \frac{A}{d}} \tag{1}$$

$$\varepsilon'' = \varepsilon' \tan \delta = \frac{\varepsilon'}{\omega RC} \tag{2}$$

where A is the area of the plate electrode, d is the distance between the electrodes, ω is the measurement frequency ($=2\pi f$), C is the capacitance, R is the direct current resistance, and ε', ε'',ε_0 are real part, imaginary part of the dielectric constant, and permittivity of vacuum ($=8.854\times10^{-12}$ F/m), respectively. For the electrical resistivity

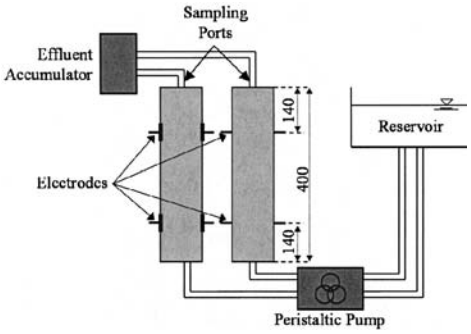

FIG. 1—*Schematic diagram of the column test fixture.*

$$\rho = \frac{A}{d}\frac{V}{I} \tag{3}$$

where ρ is the electrical resistivity, V is the electrical potential difference, and I is the magnitude of the electrical current.

Column Test

Column tests were prepared to model permeation of heavy metal contaminant in the subsurface level. As shown in Fig. 1, electrodes were installed at two different levels of the column in order to evaluate the electrical properties of the soil during contaminant movement. Two separate acryl columns with 4 cm diameter and 40 cm length were designed to calculate the dielectric constant and the electrical resistivity. As shown in the cross-sections of Fig. 2, this was because two-electrode and four-electrode configurations were adopted for capacitance and potential difference measurements, respectively. These electrodes were connected to either the *LCR* meter or the 2400 SourceMeter reported earlier in this study.

Parasnis (1975) introduced a simple experimental setup for determining the electric resistivity of a borehole core, as shown in Fig. 2. The electrical resistivity of cylindrical core measured from point electrodes that are φ degrees apart from the source electrodes is given by

$$\rho = \frac{b}{k}\frac{V}{I} \tag{4}$$

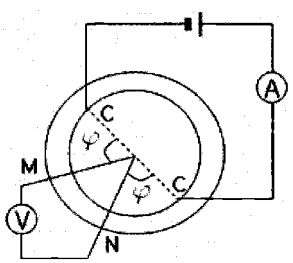

FIG. 2—*Electrical resistivity measurement of borehole core proposed by Parasnis (1975). M and N are the measurement electrodes reading the difference in voltage (V) of the specimen, and C marks the source electrodes that provide direct current.*

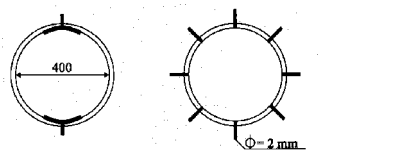

FIG. 3—*Cross-sections of columns with two-electrode and four-electrode configurations.*

$$k = \frac{1}{\pi} \ln \frac{1 + \cos \varphi}{1 - \cos \varphi} \tag{5}$$

where b is the length of current electrode. Similar to Eq 3, V is the electrical potential difference, and I is the magnitude of the electrical current. The specimens in the columns prepared for this study have an identical geometry to the drill core samples. Therefore, Eq 4 proposed by Parasnis was used to calculate the electrical resistivity in order to take the geometry of the four-electrode configuration into consideration. The real and imaginary parts of the dielectric constant were calculated using the equation described in the preliminary test section.

Figure 1 is a schematic diagram of the test fixture. Prior to the actual test, effluent solutions were collected for ion chromatography (IC) analysis during a tracer test using Cl^- solution. From the breakthrough curves obtained, the time required for the outflow of one pore volume at a constant inflow rate of 2 ml/min was estimated to be 95 and 120 min for silica sand and weathered granite soil, respectively. Therefore, electrical measurements were performed in 5 min intervals for a time period of 120 min. Lead, cadmium, and aluminum solutions with 50 ppm concentration were used as the influent solutions, and an upflow was induced by peristaltic pumps (MasterFlex, Coleparmer Co., Vernon Hills, IL) at a rate of 2 ml/min. (See Fig. 3.)

Test Results

Preliminary Test

Results of the preliminary tests are shown in Fig. 4. Results for weathered granite soil and those for lead and aluminum are omitted since their results show identical tendencies to that of cadmium. Both the real and imaginary part of the dielectric constant decreased with increasing frequency and increasing heavy metal concentration. Dielectric constant of soils show dispersed behavior against frequency because different polarization mechanisms are operative at different frequency ranges. Space charge polarization mechanism which is operative only at low frequencies ($<$100 kHz) account for the increase in the real part of the dielectric constant with decreasing measurement frequency. In addition, increase in the heavy metal concentration leads to a greater amount of polarized ions, which in turn increases the real part of the dielectric constant.

The imaginary part of the dielectric constant increased and the electrical resistivity decreased with increasing heavy metal concentration. This can be understood in terms of increased energy loss by the conductive heavy metal ions. Increase in the amount of conduction loss for increasing heavy metal concentration leads to a increase in the imaginary part of the dielectric constant. In addition, heavy metal ions which act as charge carriers increase the electrical conductivity of the medium, which in turn decreases the electrical resistivity.

Column Test

Variations in the measured dielectric constant and electrical resistivity during column tests for the two soils used in this study are plotted against time in Figs. 5 and 6. Results for lead and aluminum are omitted since their results showed identical tendencies to that of cadmium. The real and imaginary parts of the dielectric

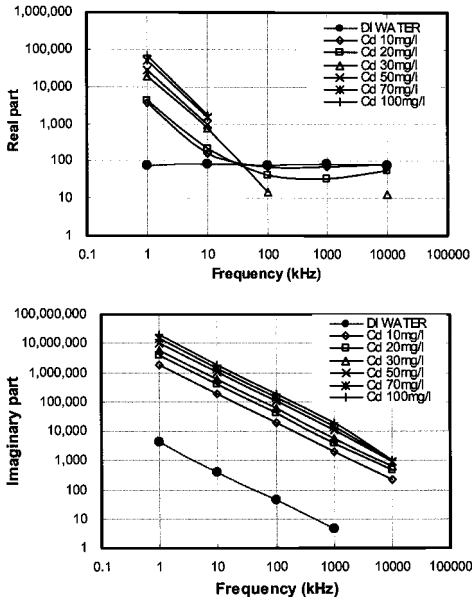

FIG. 4—*Variations in the real and imaginary parts of the dielectric against cadmium concentration for silica sand.*

constant were calculated for measurement frequencies of 10 and 100 kHz. All of the values are plotted according their measurement location: either the top or the bottom pair of electrodes In addition, results for aluminum and lead showed similar behavior to that of cadmium.

The real part of the dielectric constant for a column test performed on silica sand shows no significant tendency of increase or decrease according to the movement of influent cadmium solution. Although the time at which variations start to take place for both the bottom and the top electrodes are similar to that found in the results of the electrical resistivity, random fluctuations continue to have no significant importance beyond this point. This could be attributed to the continuous movement of pore water in soils during the column test which may have an adverse effect in capacitance measurement. Capacitance measurements found in literature were generally performed in a closed volume and are considered to be sensitive to the subject of investigation and measurement environment. Although the real part of the dielectric constant

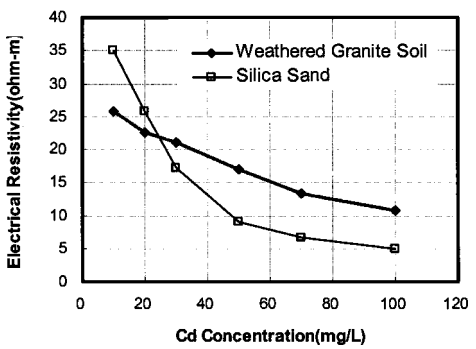

FIG. 5—*Variations in electrical resistivity against cadmium concentration for weathered granite soil and silica sand.*

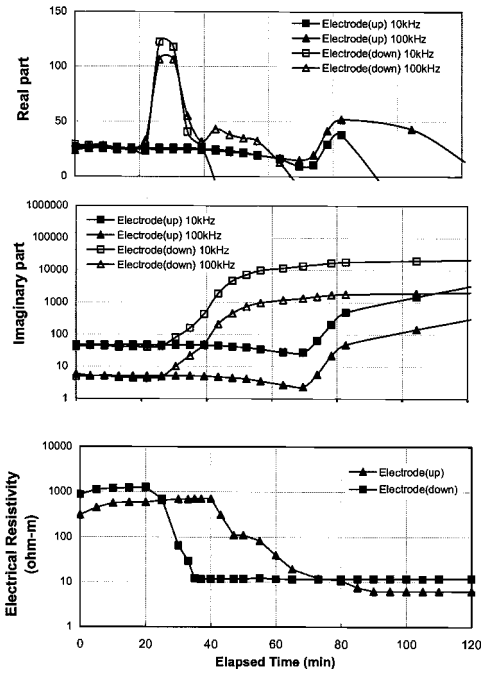

FIG. 6—*Variations in real and imaginary parts of the dielectric constant and electrical resistivity during column test for silica sand with cadmium migration.*

showed random fluctuations, this value remained almost consistent for the first 20 and 60 min of the column test for bottom and top pairs of electrodes, respectively. Therefore, random fluctuations may indicate that change in the compositional property of the subject under measurement is taking place. Variations occur almost concurrently with the electrical resistivity, which demonstrates that the real part of the dielectric constant is sensitive to the movement of cadmium ions. Therefore, the real part of the dielectric constant is sensitive to the influent cadmium ions in pore water but shows no qualitative correlation against time.

From the results of preliminary tests, presence of heavy metal ions in pore water was found to give a rise in the imaginary part of the dielectric constant in all measurement frequencies. Therefore, an increase in the imaginary part of the dielectric constant for silica sand shown in Fig. 4 can be understood as a result of movement in cadmium ions. Movement of influent cadmium ions increases the amount of ions that act as charge carriers, consequently increasing the conduction loss and thus the imaginary part of the dielectric constant. Although the bottom and the top pair of electrodes did not give recurring identical curves, a clear increase was notable in both measurements, indicating possibilities of monitoring the movement of heavy metal ions based on the imaginary part of dielectric constant. Further research is required to validate whether such increases took place at accurate time intervals considering the different mechanisms of transport in pore water.

The electrical resistivity of soil is sensitive to heavy metal contamination, owing to the highly conductive characteristic of heavy metal ions present in pore solution. As a result, a decrease in the measured electrical resistivity was evident in the column tests performed on silica sand. Figure 6 shows a decrease in electrical resistivity with a magnitude of over two-orders for measurements made at both the bottom and top pairs of electrodes. Although the points of fluctuation vary for the electrical resistivity and the imaginary part of the dielectric constant, this may be due to the fact that these measurements were made on separate columns with discrete levels of compaction and different pore structure. In addition, the steady decrease observed for the measurements made with the top pair of electrodes can be attributed to diffusion

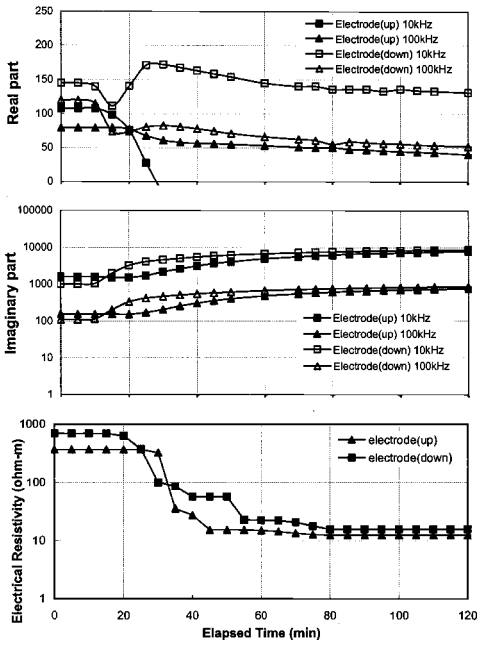

FIG. 7—*Variations in real and imaginary parts of the dielectric constant and electrical resistivity during column test for weathered granite soil with cadmium migration.*

and dispersion mechanisms which bring about a gradual increase in cadmium concentration. Varying values of electrical resistivity for the two pairs of electrodes at the beginning and the end of the test may be a result of geometrical differences that arise in electrode configuration, even with error compensation through electrode calibration. Nonetheless, sensitivity against heavy metal movement was found to be apparent, verifying the applicability of electrical resistivity measurement for monitoring heavy metal contamination in a qualitative basis.

Results for column tests performed on weathered granite soil shown in Fig. 7 are similar to that of silica sand. The real part of the dielectric constant did not give a clear correlation against varying cadmium concentration in the pore water. An increase in the imaginary part of the dielectric constant was evident for weathered granite soil, but its magnitude was clearly smaller than that of silica sand. This may be attributed to the presence of fine particles in weathered granite soil which brings about conduction loss prior to the loss due to the increase in cadmium concentration. Results for electrical resistivity in weathered granite soil were analogous to that for silica sand. However, the exceeding rate of decrease in the electrical resistivity measurements made on the top pair of electrodes must be validated.

Conclusion

The following conclusions are drawn based on the preliminary tests and column tests performed in this study.

The value of the real part of the dielectric constant varied from the introduction of heavy metal ions in pore water, which indicates that it may be sensitive to migration of contaminants. However, it did not show a clear tendency of increase or decrease against cadmium migration in the column tests performed. Although the real part of the dielectric constant showed a clear tendency of increase against cadmium concentration in preliminary tests, its applicability for monitoring heavy metal contaminant may be limited for in situ conditions.

Imaginary part of the dielectric constant and the electrical resistivity showed a clear correlation against

transport of heavy metal contaminant. Increase in imaginary part of the dielectric constant and a decrease in electrical resistivity was clear in both silica sand and weathered granite soil. This can be interpreted as a result of increased conductivity loss and a greater number of ions that act as charge carriers. Therefore these two parameters may have a potential applicability for monitoring the migration of ionic contaminants.

Acknowledgment

This work was supported by Grant No. R-2002–B-257 from the Korean Electrical Engineering & Science Research Institute.

References

Arulanandan, K. and Smith, S. S., 1973, "Electrical Dispersion in Relation to Soil Structure," *Journal of the Mechanics and Foundations Division*, ASCE, 99(SM12), 1113–1133 (1973).

Francisca, F. M. and Rinaldi, V. Á., "Complex Dielectric Permittivity of Soil-Organic Mixtures (20 MHz–1.3 GHz)," *J. Environ. Eng.*, 129(4), 347–357 (2003).

Fukue M., Minato T., Horibe M., and Taya N., "The Micro-Structures of Clay Given by Resistivity Measurements," *Eng. Geol. (Amsterdam)* 54, pp. 43–53 (1999).

Kaya, A. and Fang, H. Y., "Identification of Contaminated Soils by Dielectric Constant and Electrical Conductivity," *J. Environ. Eng.* 123(2), 169–177 (1997).

Keller, V. George, and Frischknecht, C. Frank, *Electrical Methods in Geophysical Prospecting*, Pergamon Press Ltd., Headington Hill Hall, Oxford, 1996.

Parasnis, D. S., *Mining Geophysics*, Elsevier Scientific Publishing Company, Amsterdam, Netherlands, 1975.

Journal of ASTM International, Vol. 3, No. 7
Paper ID JAI13346
Available online at www.astm.org

Yoshio Sato,[1] *Masaharu Fukue,*[2] *Kuniaki Yasuda,*[1] *Katutoshi Kita,*[3] *Shozo Sawamoto,*[4] *and Yasuhito Miyata*[5]

Seawater Quality, Suspended Solids, and Settling Particles in the Wood Pool Area of Shimizu Port, Japan

ABSTRACT: The transport and contamination of suspended solids in a wood pool were quantitatively studied as a case study for the environmental assessment of an enclosed sea area. To assess the present contamination of Shimizu Port (Japan), seawater, suspended solids, and settling particles were collected from three rivers, the wood pool, and Shimizu Port. Physical and chemical properties of the samples were analyzed. In addition, tidal currents were observed to investigate the transport process of chemical substances by suspended solids. The results showed that the amount of lithogenic particles discharged into Shimizu Port was approximately 12 000 kg/day. Suspended solids discharged from rivers and the biological particles produced in the port caused a reduction in seawater transparency and an increase in chemical oxygen demand. Trace metals, such as Mn, Co, and Pb, were highly concentrated in suspended solids. Tributyltin adsorbed onto settling particles was approximately 300 μg/kg. Concentration factors for Mn, Fe, Cd, and Pb from water and settling particles are comparable to those of plankton. Hydroxides were found in suspended solids from the wood pool, which locates in the inner part of Shimizu Port. The results showed that these suspended particles could accumulate metals from seawater as effectively as biogenic particles. After particle deposition, trace metals are regenerated into seawater under anaerobic conditions. This process plays an important role in the accumulation of chemicals in seawater and sediments, especially in enclosed sea areas.

KEYWORDS: seawater quality, suspended solids, sediment quality, trace metals, TBT

Introduction

There are various types of suspended solids of different origins. Chemicals, which are dissolved solutes or particulate substances, are leached from land into the sea. Dissolved chemicals become particulate substances if ingested by plankton in the euphotic layer. In turn, phytoplankton is ingested by zooplankton and the fecal pellets excreted. These biogenic particles are mixed with particles discharged from land and deposited on the sea bottom. These sediments can adsorb hazardous substances, such as exogenic hormone-disrupting chemicals, trace metals, etc. (Rozan and Benoit 1999; Takada and Yanagi 2000; Santschi et al. 2001; García-Ruelas et al. 2004). These particles are ingested by benthic invertebrates, i.e., suspension feeders. These suspension feeders include bivalves, polychaetes, ascidians, etc. Therefore, toxic substances are accumulated in these invertebrates and, subsequently, animals feeding on them. As a result of this accumulation, an increase in imposex and cancer is to be feared (Hashimoto 2000; Okuda et al. 2000).

Suspended organic solids, including algal blooms, damage the ecosystem in two ways. First, they cloud the water and block sunlight, causing seagrasses to die. Because these seagrasses provide food and shelter for aquatic animals, spawning and nursery habitats are destroyed, and waterfowl have less to eat when grasses die off. Second, when organic matter decomposes, oxygen is exhausted. Dissolved oxygen is essential to most organisms living in an aquatic environment.

To investigate chemical contamination of sediments, it is necessary to understand the cycle and role of

Manuscript received March 24, 2005; accepted for publication June 3, 2005. Presented at ASTM Symposium on Contaminated Sediments: Evaluation and Remediation Techniques on 23–25 May 2006 in Shizuoka, Japan; M. Fukue, K. Kita, M. Ohtsubo, and R. Chaney, Guest Editors.

[1] Professor, Department of Marine Science, Tokai University, Shizuoka, 424-8610, Japan.
[2] Professor, Department of Marine Civil Engineering, Tokai University, Shizuoka, 424-8610, Japan.
[3] Associate Professor, Department of Marine Civil Engineering, Tokai University, Shizuoka, 424-8610, Japan.
[4] Professor, Ocean Research and Development, Tokai University, Shizuoka, 424-8610, Japan.
[5] Senior Researcher, Steel Research Laboratory, JFE Steel, Co., Fukuyama, 721-8510, Japan.

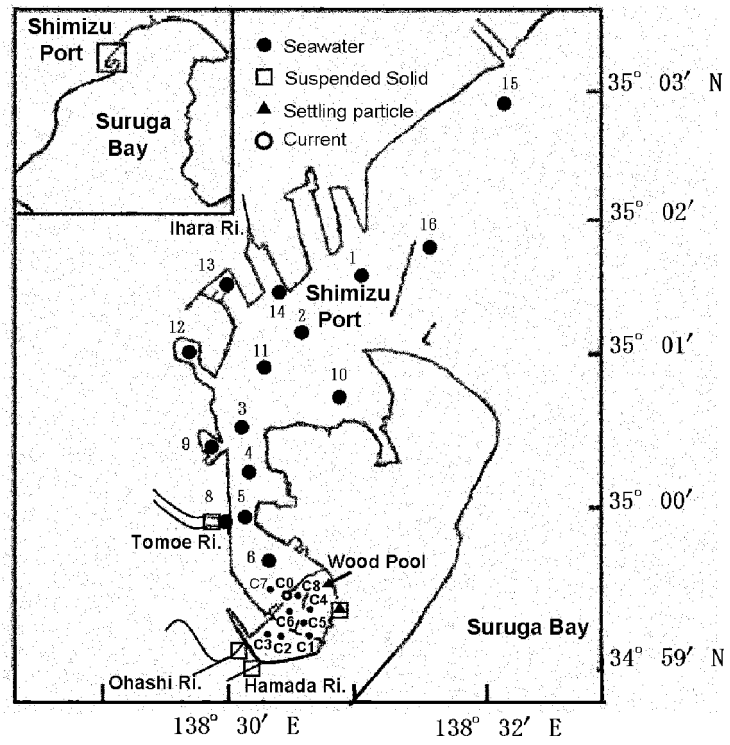

FIG. 1—*Sampling sites for seawater, suspended solid and settling particles, and observation sites for water currents.*

suspended particles in transporting these materials (Hoshika et al. 1994; Yanagi 1997; Tanimoto et al. 2001). In this study of Shimizu Port, the physical and chemical properties of suspended solids were analyzed to understand the role of suspended solids in the contamination process. Similarly, the properties of settling particles in the wood pool were also analyzed.

Investigation and Methods

Sampling of Seawater

Seawater samples were collected from Shimizu Port and the wood pool in May, July, September, and December 2004. The sampling sites are indicated in Fig. 1. Water samples were obtained using a Van Dorn sampler at depths of 0, 2, and 5 m. Water temperature, salinity, dissolved oxygen (DO), chemical oxygen demand (COD) and suspended solids of the samples were measured. Trace metals in the surface seawater were analyzed by (ICP–AES), after preparation using chelating resin disks.

Observation of Water Current

To investigate the exchange of seawater in Shimizu Port and the wood pool, water currents were observed using electromagnetic current recorders (Alec Electronics Co.Compact-EM) at depths of 0.5 and 4 m, near the opening of the wood pool (St. C0 in Fig. 1). Simultaneously, salinity and temperature were also measured with conductivity recorders (Alec Electronics Co., Compact-CT). Recordings were carried out at 1-s intervals for 48 h. The velocity components of the flow direction, into and out from the wood pool, were determined using the water current data. To neglect the effects of waves and swells, data of the axial

velocity components and salinity were smoothed through a humming filter with a bandwidth of 1 min. Furthermore, the change in tidal period was separated from the seiche, which usually occurs in Shimizu Port, by passing through a 60-min band filter. The typical seiche has a period of about 40 min. Salt flux was calculated using the changes in water velocity and salinity. To confirm the vertical profile of salinity, in and around the wood pool, the salinity obtained at the eight sites (i.e., Sts, C1–C8 in Fig. 1) in September 2004 was used. Data were obtained with temperature and conductivity recorders (Alec Electronics) at 0.5-m intervals of depths between 0.5 and 3 m and at 1-m intervals at depths below 3 m.

Sampling of Plankton

Plankton was collected from five sites, at the surface and bottom (1 cm above the bottom), in the wood pool. To collect zooplankton, seawater was pumped and filtered through a cone net with mesh size of 0.1 mm. The volume of water filtered varied between 26 and 40 L. The Zooplankton collected were identified and classified in detail. To collect phytoplankton, seawater was obtained using the Van Dorn sampler; 1 L was then filtered through a 25-μm mesh and concentrated into 10 mL. A 0.1-mL aliquot was used for identification of phytoplankton, which were classified to species level, if possible.

Suspended Solids and Settling Particles

To analyze the element concentration of suspended solids (SS) in the Tomoe, Ohashi, and Hamada rivers, and the wood pool, 4 L of water was filtered through a 0.4-μm nuclepore filter. After removal of sea salt, suspended solids were weighed and digested in a sealed Teflon vessel (Noriki et al. 1980). Settling particles in the wood pool were collected using containers with a height of 30 cm and volume of 1000 cm^2. The containers were installed on the flat bottom of the wood pool at a depth of 4 m and collected by a diver 3, 6, and 9 months later. Sediments in the containers were subjected to physical and chemical analyses, after removal of sea salt. The salt was washed out by 3 % $(NH_4)_2CO_3$.

Trace metals (Mn, Fe, Ni, Cu, Zn, Cd, Pb) were analyzed using ICP-AES, and tributyltin (TBT) was measured with (GC-MS). Samples were dried at 110°C and about 0.1 g of dried samples ere digested in a sealed Teflon vessel with a mixture of 2 mL perchloric acid, 2 mL 65 % nitric acid and 0.6 mL hydrofluoric acid at 150°C for 5 h. Texture and components of suspended solids and settling particles were analyzed using an electron probe microanalyzer (EPMA–JEOL, JXA8900R). Measurements of TBT and tributyltin (TPT) were performed following the GC-MS method of Takahashi et al. (1999).

Chemical oxygen demand (COD) was measured following Japanese Industrial Standard (JIS K 0102), using potassium permanganate.

Total nitrogen (T-N) and total phosphorus (T-P) were measured following the methods described in the literature (Grasshoff et al. 1983), and widely used for monitoring seawater quality.

Results and Discussion

Seawater in Shimizu Port

The Shimizu Port area is approximately 1560 ha and is fed by five rivers, i.e., the Hatauchi, Ihara, Tomoe, Hamada, and Ohashi Rivers. The volume of water flow from the Tomoe, the largest of the five rivers, is approximately 10 m^3/s. This is more than ten times the total volume of the other four rivers. Since the Tomoe river runs through urban and industrial districts, the discharged water is contaminated with organic matter from municipal and industrial waste. The amounts of COD and SS from the Tomoe river are 5400 and 8600 kg/day, respectively. Treated water from the three sewage plants, i.e., at Hokubu (20 000 m^3/day), Seisei (15 000 m^3/day), and Nanbu (30 000 m^3/day), is also discharged into Shimizu Port. Biochemical oxygen demand (BOD) and SS are 20 and 30 mg/L, respectively. Therefore, the amount of SS, which is discharged daily into Shimizu Port, is approximately 12 000 kg. Assuming that, in Shimizu Port, the average water depth is 10 m, the amount of SS discharged can be estimated at 0.08 mg/L/day.

The wood pool, which is located in the inner part of Shimizu Port, has an area of 35 ha and an average water depth of 4.7 m. This wood pool has been used for the pest control of wood since 1927. The average

TABLE 1—*Salt flux at the entrance to the wood pool (St.C0).*

		Average value		Salt flux ($kg/m^2/s$)		
		Current (cm/s)	Salinity (psu)	Average	By average current	By tidal current or current with short period
Tidal variation + Average value	Upper layer	−2.50	28.50	−0.718	−0.712	−0.006
	Lower layer	1.61	34.41	0.554	0.555	−0.000
Short period variation	Upper layer	0.002	0.000	0.000	0.000	0.000
	Lower layer	0.006	−0.001	0.000	−0.000	0.000

flow rates of the Ohashi and Hamada rivers are 0.6 and 0.1 m^3/s, respectively, and discharges of COD and SS from the two rivers are 600 and 400 kg/day, respectively. The amount of SS from the rivers is calculated to be approximately 0.3 mg/L/day.

Observations on water current were carried out at the opening of the wood pool in December 2004. Approximately 20 cm/s flow velocity was observed at water depths of 0.5 and 4 m. However, the average flow velocity from the bay was −2.5 cm/s at a water depth of 0.5 m, and about 1.6 cm/s in the inner bay at a depth of 4 m. The tidal current was less than 5 cm/s. The strongest current flow was due to the short seiche with a period of 40 min.

Average flow velocity, salinity and salt flux for the two tidal periods (58 h and 38 min) are presented in Table 1. Average salt fluxes in upper and lower layers are −0.718 and 0.554 $kg/m^2/s$, respectively. Almost all fluxes are due to the average flow and salinity; however, the contribution due to tidal currents, which are almost zero in the upper and lower layers, is extremely low.

Salinity was recorded at eight sites in and around the wood pool, in September 2004. The vertical profile is shown in Fig. 2, where there are double layers, separated by a halocline, corresponding to a pycnocline at a depth between 1 and 2 m. It is possible that there is a large difference between the double layers in September and December. However, the halocline may be different in September and December. Therefore, the depths of the interface between the upper and lower layers were estimated from the average flow velocities (−2.50–1.61 cm/s) in the upper and lower layers.

The interface depth, when the sum of the flow volumes in the upper and lower layers becomes zero,

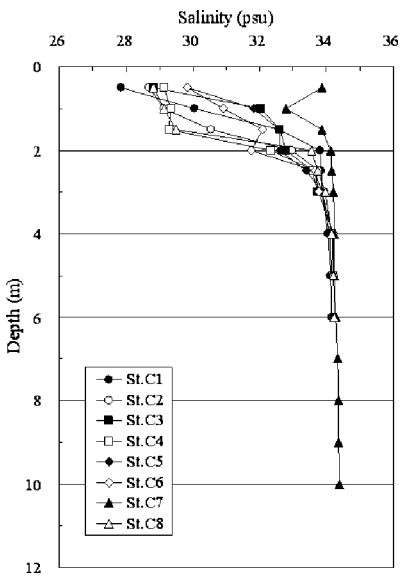

FIG. 2—*Vertical profiles of salinity in wood pool of Shimizu Port.*

TABLE 2—*Average salt flux in a vertical section at the breakwater (St.C0).*

	Average salt flux in vertical section ($kg/m^2/s$)		
	Average	By average current	By tidal current or current with short period
Tidal variation+Average value	0.055	0.058	−0.003
Short period variation	0.000	−0.000	0.000

is estimated to be 2.55 m. It is possible that the halocline (interface) deepens from autumn through winter. Assuming double layers separated by a depth of 2.55 m, the sectional average salt flux in the entire upper and lower layers is presented in Table 2. Salt flux at the average flow (0.058 $kg/m^2/s$) accounts for nearly all of them, and the effects of tidal current and short period flow (−0.003−0.000 $kg/m^2/s$) are relatively small.

As mentioned above, the seawater in the wood pool is exchanged mainly due to density current, but the contribution of tidal current and short period flow is very small. The total amount of average salt flux in the vertical section is estimated to be 0.055 $kg/m^2/s$ toward the inner bay, which is about one tenth of the average salt flux in the upper and lower layers.

In general, tidal currents play an important role in the exchange of seawater within ports and harbors, except in unique circumstances, such as floods and the rise of river water from heavy rainfall. However, the effect of tidal currents in this study is small, as estimated by analysis, implying that the exchange of seawater of the wood pool is insignificant.

Table 3 shows seawater quality in Shimizu Port. Average salinity varied from approximately 27 to 30 psu through May to December, respectively. The results indicate that a great deal of fresh water is discharged into Shimizu Port. In particular, the impact of the Tomoe River is significant inside sampling site St. 3 (Fig. 1). As shown in Fig. 3(*a*), transparency increases exponentially with decreasing SS. It seems that transparency in Shimizu Port is low in May and high in December. The reason why transparency decreased can be described as follows:

Since DO is approximately 8.4 mg/L in May, this oversaturated condition may cause the production of phytoplankton. Therefore, a relationship between pH and DO can be described as a linear function, as shown in Fig. 3. COD value of the surface water was more than 3 mg/L, where the impact of the Tomoe River cannot be neglected and this trend was observed throughout the year. The data points deviate from the conservative dilution line, as shown in Fig. 3(*c*), which means the load of COD, attributing to the existence of phytoplankton in Shimizu Port. As phytoplankton increase in May, SS becomes relatively high. However, the SS value becomes relatively low in December because activity is low. The COD has a

TABLE 3—*Transparency, temperature, salinity, pH, dissolved oxygen, chemical oxygen demand, suspended solids, total phosphorus, and total nitrogen in seawater collected from Shimizu Port.*

Date	May	July	Sep.	Dec.
Tr. (m)	1.5–3.0	2.0–4.0	2.0–5.5	3.0–5.5
ave.	2.0	2.7	2.5	3.9
W. Temp. (°C)	20.1–22.2	26.3–26.9	25.8–27.0	15.4–18.8
ave.	21.0	26.6	26.7	17.4
S (psu)	3.87–30.73	17.42–31.13	8.78–32.79	20.50–33.13
ave.	27.21	29.68	29.09	30.17
pH	7.68–8.41	7.82–8.41	7.48–8.37	8.11–8.40
ave.	8.28	8.35	8.17	8.34
DO(mg/L)	5.83–10.54	6.97–9.47	3.86–9.81	7.33–8.74
ave.	8.45	7.80	7.13	8.00
COD(mg/L)	1.27–4.32	1.18–4.06	1.53–3.88	0.79–4.03
ave.	2.53	2.13	2.53	2.03
SS(mg/L)	0.7–8.8	1.6–9.2	0.2–5.3	0.7–4.4
ave.	4.7	3.3	2.5	1.9
T-P(mg/L)	0.014–0.152	0.016–0.137	0.011–0.231	0.014–0.118
ave.	0.043	0.035	0.047	0.036
T-N(mg/L)	0.254–4.022	0.379–4.768	0.203–2.473	0.130–1.522
ave.	0.944	0.892	0.753	0.553

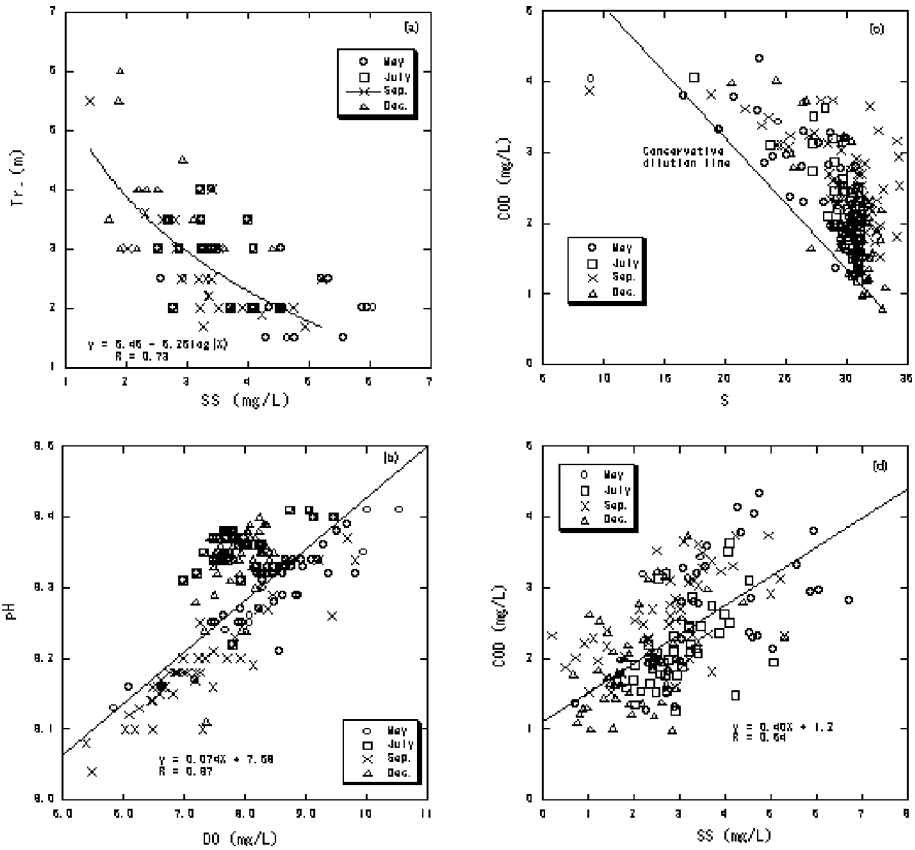

FIG. 3—*Relationships between transparency and suspended solids (a), pH and dissolved oxygen (b), chemical oxygen demand and salinity (c) and chemical oxygen demand and suspended solids (d).*

linear relationship with SS, as shown in Fig. 3(*d*). The particulate organic carbon (POC) concentration of Shimizu Port is 120 μg/L and organic content is about 12 % (Sato 1985). Therefore, the dispersal of SS in Shimizu Port may be dependent on phytoplankton, with the exception of materials from the rivers.

The concentration of total phosphorus (T-P) in Shimizu Port varied from 0.011 to 0.231 mg/L, while total nitrogen (T-N) concentration varied from 0.130 to 4.768 mg/L. These values may be sufficient to cause red tides if other requirements are satisfied. From the correlations between TP and salinity (Fig. 4(a)), and T-N and salinity (Fig. 4(b)), it can be deduced that the T-P and T-N are supplied from the rivers. Thus, seawater in Shimizu Port has been contaminated with organic matter.

Metal concentrations of seawaters in Shimizu Port, the wood pool, Hiroshima Bay (Hirata et al. 2002) and the open sea (Nozaki 1992) are presented in Table 4. The average concentrations of Mn, Fe, Ni, Cu, Zn, Cd, and Pb in surface seawater of Shimizu Port are also presented in Table 4, which are 1–300 times greater than those in the open sea. The comparison between Shimizu Port and Hiroshima Bay shows that the concentrations of Fe, Ni, Cu, and Zn are higher in Shimizu Port, while the concentrations of Mn, Cd, and Pb are higher in Hiroshima Bay.

The concentrations of trace metals in the wood pool, except Ni and Cd, are a few times greater than in Shimizu Port. The main reason for this is that the wood pool is an enclosed sea area, where various kinds of discharged materials remain for long periods inside the pool and are easily deposited. In this case, accumulation of chemical elements in suspension feeders becomes a serious problem.

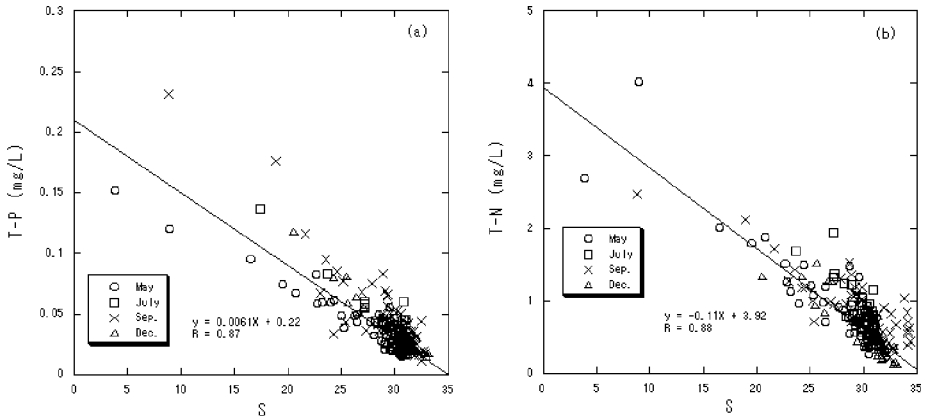

FIG. 4—*Relationships between total phosphorus and total nitrogen versus salinity.*

Suspended Solids and Settling Particles

As mentioned above, tidal currents contribute little to the exchange of seawater in the wood pool. Therefore, materials discharged from the two rivers remain as suspended solids for a long time and are deposited in the wood pool. Texture and primary components of the suspended solids and settling particles were observed using Electron Probe Micro Analyzer (EPMA), as shown in Fig. 5. Suspended materials from the rivers consist of small particles (a few micrometres) and their aggregates, in which no plankton was found, as shown in Figs. 5(*a*) and 5(*b*). On the other hand, the suspended solids in the surface water and the settling particles in the wood pool contain fragments of plankton, with a size of approximately 10 μm.

A great deal organic matter, which consists mainly of plankton, is contained in the suspended solids of Shimizu Port. Investigations on phytoplankton and zooplankton were carried out in the wood pool in September 2004. The results are presented in Table 5. Phytoplankton, such as diatoms and dinoflagellates (Dinophyceae), was sometimes found, but species numbers were very small. Though diatoms (Bacillariophyceae) were dominant, only two species, i.e., *Leptocylindrus danicus* and *Thalassionema nitzschioides*, were found. It is noted that *Skeletonema costatum* and *Chaetoceros* spp., which are usually found in Shimizu Port, were not found in the wood pool.

On the other hand, zooplankton was composed of many phyla, such as Arthropoda (Copepoda, Cirripedia, and Decapoda), Annelida, Mollusca, Chaetognartha, Echinodermata, and Chordata. These were meroplankton and holoplankton, with cirriped larvae and bivalve larvae being dominant in the meroplankton, and Copepoda being dominant in the holoplankton. Paracalanidae and *Oithona davisae* were the dominant Copepoda.

TABLE 4—*Concentration of dissolved trace metals in Shimizu Port, wood pool, Hiroshima Bay, and North Pacific. (1) Hiroshima Bay (Hirata et al. 2002), (2); North Pacific (Nozaki 1992).*

	Mn	Fe	Ni	Cu	Zn	Cd	Pb
	($\times 10^{-6}$ mg/L)						
Shimizu Port July	626–7580	1020–3090	323–1440	241–979	6600–23000	7.87–109	14.5–70.4
Shimizu Port Sep.	813–5530	1800–2920	294–587	203–985	8370–34700	11.2–25.9	22.8–74.6
Average: Ca	2580	2090	499	515	18400	37.1	35.2
Wood Pool Sep.	4770–4830	2790–3140	505–804	1740–1970	22 600–24 700	28.1–36.0	97.4–162
Average: Cb	4800	2970	652	1860	23700	32.6	131
Hiroshima Bay[(1)]	999–16 800	72.6–771	205–393	241–616	307–4120	50.6–253	128–3830
Average: Cc	4870	285	305	343	2000	146	1120
Seawater[(2)]: Cd	16.5	33.5	470	127	392	84.3	2.69
Cb/Ca	1.9	1.4	1.3	3.6	1.3	0.9	3.7
Ca/Cc	0.5	7.3	1.6	1.5	9.2	0.3	0.03
Cb/Cd	291	89	1.4	14.6	60	0.4	49

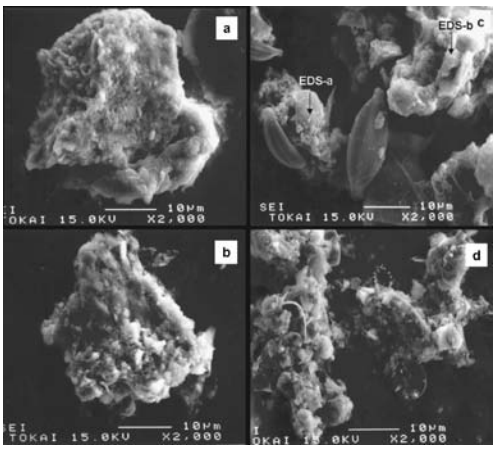

FIG. 5—*SEM images of suspended solids and settling particles. (a) Suspended solids in the Ohashi River, (b) suspended solids in the Hamada River, (c) suspended solids in the wood pool, and (d) settling particles in the wood pool.*

Meroplankton occupies from 16 to 40 % of the total number of zooplankton in surface water, while it decreased to approximately 15 % near the bottom. However, meroplankton was only 10 % of the total biomass, even in surface water at the opening of the wood pool. Therefore, the wood pool can be characterized by a relatively large number of planktonic larvae (meroplankton) in the surface water.

The grain size characteristics of both the settling particles and sediments are presented in Table 6. The settling particles collected in January 2005 have a clay content greater than that obtained in November 2004. The reason for this can be explained by the amount of water flow from the rivers into the wood pool. In general, heavy rainfall decreases fine content, because greater particles can be washed out. In fact, rainfall was 1300 mm from July through December 2004, while it was only 100 mm from November to January 2005.

Chemical Concentrations of Suspended Solids and Settling Particles

Table 7 shows a comparison between the physical and chemical properties of particles in the major rivers of the world and data obtained in this study. The ignition loss of suspended solids in the rivers ranged from 2 to 7 %, while that of plankton at stations northwest and southwest of Puerto Rico was 30 % (Martin 1970). The ignition loss of settling particles in the wood pool was 15 % and, in this area, the sedimentation rate is approximately 2.0 g/cm^2/year. This value is four times greater than that of the inner part of Tokyo Bay (Matsumoto 1983). This difference is thought to result from the variation in the amount of SS, primary productivity, inflow area, and the different exchange rates of seawater with the outside seawater.

With the exception of copper, metal concentrations of suspended solids in the Ohashi and the Hamada rivers are comparable to the average values in the major world rivers (Martin and Meybeck 1979).

A comparison between metal concentrations in the suspended solids from the rivers and wood pool showed that the concentrations of Mn, Fe, Co, and Pb were higher for the materials in the rivers. On the other hand, from a comparison between suspended solids in the surface water and settling particles near the bottom in the wood pool, metal concentrations were lower for suspended solids in the surface water. This may be because suspended solids in surface water include more plankton, which contain less amounts of metals (Martin 1970).

Jenne (1968) pointed out that suspended solids, such as aluminosilicate, in river water were coated with oxides and organic matter. According to Gibbs (1977), the amounts of Mn, Fe, Co Ni, and Cu, which accumulate in the oxide phase, are 50.0, 47.2, 27.3, 44.1, and 8.1 %, respectively. If the organic matter which coats suspended solids is humus, their functional groups are carboxyl (–COOH), phenolic (–OH), and hydroxyl (–OH).

TABLE 5—*Phytoplankton and zooplankton collected from the wood pool, Orido, Shimizu*

	St. 1		St. 2		St. 4		St. 6		St. 7	
Phytoplankton (cells/L)	Surface	Bottom	Surface	Bottom	Surface	Bottom	Surface	Bottom	Surface	Bottom
Bacillariophyceae										
Leptocylindrus danicus	39 400		14 200	6000	10 200	1500	23 400	900	2700	
Thalassionema nitzschioides	3700	no	3100	2000	3600	500	3000	1900	500	3300
Dinophyceae		sample								
Protocentrruns sp.							200			
Protoperidinium sp.				600	200					
Total	43100	···	17300	8600	14000	2000	26600	2800	3200	3300
Zooplankton (individuals/10 L)										
Annelida										
Polychaeta larvae	0.6		1.4	3.1	1.7	2.3	1.4	1.1	2.1	2.2
Mollusca										
Bivalvia larvae	2.2	6.1	4.1	8.5	1.3	4.5		6.8		4.7
Arthropoda										
Decapoda larvae	0.6		0.7	1.5	0.3		0.3	0.3		0.5
Cirripedia larvae	15.9	4.7	13.9	5.0	15.9	11.7	21.4	7.4	10.3	3.7
Echinodermata										
Ophiuroidea larvae										0.5
Meroplankton total	19.4	10.8	19.9	18.1	19.3	18.5	23.1	15.7	12.3	11.7
Arthropoda										
Euphausiidae larvae						1.1				
Acetes spp. (larvae)		1.0		4.2		0.4		1.4	0.7	2.5
Luciferidae larvae				1.9				0.6		1.2
Copepoda										
Paracalanidae	13.7	26.7	21.3	38.8	20.6	49.1	10.3	39.3	68.8	59.5
Acrocalanus spp.	6.4	6.4	5.1	8.8	6.3	6.4	2.8	5.7	5.1	11.2
Centropages sp.					0.3					
Temora turdinata	0.6	2.4	1.7	3.8	2.7	1.9	1.4	4.8	3.1	8.5
Lucictia sp.		0.3								
Acartia omori		0.7	1.4	1.9	4.3	2.3	1.0	2.3	6.2	3.5
Oithona davisae	2.2	14.5	2.4	22.3	4.0	26.0		22.2	7.5	75.1
Corycaeus sp.	0.3	0.7					0.7	0.9	1.0	1.0
Euterpina acutifrons	1.3	1.0	1.0		1.3	0.8	2.1	2.0	1.4	
Copopoda larvae	16.2	6.8	9.5	8.5	10.6	4.9	14.8	6.8	8.2	4.5
Chaetognatha										
Saggita spp.		2.0	0.7	3.8	1.7	2.3		2.6	3.1	
Chordata										
Appendicularia	1.9	3.0	1.0	2.3	1.0	0.8	1.0	1.1	2.4	2.5
Doliolida								0.3		
Holoplankton total	42.7	65.5	43.9	96.5	52.8	95.8	34.1	90.0	107.5	169.4
Ground total	62.1	76.4	63.9	114.6	72.1	114.3	57.2	105.7	119.9	181.1

Figure 6 shows the primary components of suspended solids (arrow in Fig. 5(*c*)) from the wood pool. It should be noted that the intensity of Pd in the figure resulted from Pd-coating during sample preparation. The results show that suspended solids contain oxides of Mn and Fe.

TABLE 6—*Percentage finers of riverine sediments and settling particles.*

	Gravel $D \geqq 2$ mm (%)	Sand 2 mm $> D \geqq 0.075$ mm (%)	Silt $0.075 > D \geqq 0.005$ mm (%)	Clay 0.005 mm $> D$ (%)
Sediments				
Hamada River	22.3	53.9	14.4	9.4
Ohashi River	0.0	89.8	10.2	0.0
Tomoe River	0.0	37.2	35.4	27.4
Settling particles				
Nov. 2004	0.0	3.9	49.7	46.4
Jan. 2005	0.0	5.4	33.6	61.0

TABLE 7—*Ignition loss, heavy metal concentration, TBT concentration, and sedimentation rate for suspended solids and settling particles.*

	Ig. loss (%)	Mn	Fe	Co	Cu (mg/kg)	Zn	Cd	Pb	TBT (μg/kg)	Sedimentation rate (g/cm^2/y)
Suspended Solid										
Hamada River	2.5	2990	35 500	17.8	211	626	<0.1	175	⋯	
Ohashi River	6.9	1690	41 400	24.0	155	931	<0.1	131	⋯	
Tomoe River	2.0	1830	55 200	26.2	150	471	0.4	181	⋯	
Wood Pool	-	737	22 700	1.7	142	419	⋯	77	⋯	
Organisms[a]	33[b]	8	882	<1	27	540	2.3	12	⋯	
River[c]	⋯	1050	48 000	20	6	350	⋯	150	⋯	
Settling Particle										
Sep., 2004	15.0	847	47 100	22.0	269	825	0.5	87	310	2.3
Nov., 2004	15.0	840	43 500	15.6	286	678	0.4	101	270	2.0
Jan., 2005	16.6	525	⋯	13.2	178	427	0.4	60	⋯	1.7

[a]Average contents of marine organisms and world major river suspended solid (Martin and Knauer 1973).
[b]Average contents of marine organisms and world major river suspended solid (Martin and Meybeck 1979).
[c]Ignition loss of organisms (Martin 1970).

It was reported that the concentration of Co is dependent on the amount of Mn and Fe oxides in the sea environment (Halbach et al. 1982; Takematsu et al. 1984). It was also pointed out that Co is absorbed into Mn oxides more easily than Fe oxides (Takematsu 1979a; Moorby and Coronan 1981; Sato 1989). In addition, it is known that Pb, as well as Co, show a scavenge-type distribution (Whitfield and Turner 1987; Cowen and Li 1991). Therefore, the data on ignition loss clearly show that the reason why suspended solids in the rivers contain greater concentrations of Mn, Co, and Pb is due to the coating of oxides on the particles, because of a higher redox potential. In fact, Mn, Co, and Pb concentrations of settling particles are lower in the month in which ignition loss is higher.

TBT concentration of settling particles is approximately 300 μg/kg dry weight in the wood pool. Previous data showed that the TBT concentrations of sediments from Osaka Bay, Tokyo Bay, and Uwa Sea were in the range 10–2100, 4.0–180, and 9.2–930 μg/kg dry weight, respectively (Sakai et al. 2003).

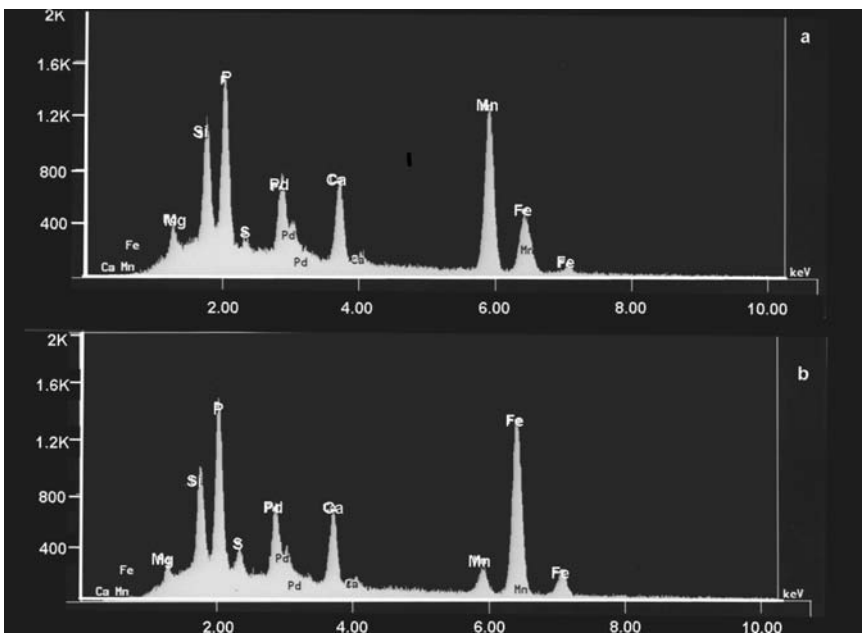

FIG. 6—*Energy dispersive spectroscopy of suspended solids in the wood pool.*

TABLE 8—*Concentration factors of heavy metals for settling particles, zoo- and micro-plankton.*

Concentration factor	Mn	Fe	Co	Cu	Zn	Cd	Pb
Wood Pool							
Settling Particles	2.8×10^{6}	2.2×10^{7}	3.3×10^{4}	1.3×10^{4}	3.5×10^{4}	1.2×10^{4}	2.3×10^{6}
(Martin 1970) (Martin and Knauer 1973)							
Zooplankton	2.6×10^{5}	3.0×10^{6}	$<8.0\times10^{5}$	9.0×10^{4}	4.6×10^{5}	2.7×10^{4}	7.8×10^{5}
Microplankton	9.1×10^{5}	5.9×10^{7}	$<8.0\times10^{5}$	4.5×10^{5}	2.0×10^{6}	1.9×10^{4}	1.2×10^{7}
(Masuzawa 1989)							
Settling Particles (890 m)	3.7×10^{7}	1.6×10^{8}	5.2×10^{6}		2.9×10^{5}		
Settling Particles (1870 m)	7.1×10^{7}	6.6×10^{8}	1.2×10^{7}		4.0×10^{5}		
Settling Particles (3240 m)	2.4×10^{8}	6.7×10^{8}	1.8×10^{7}		4.9×10^{5}		

From these data, the concentration of TBT in the wood pool is considered to be relatively high. Because water velocity is relatively low and most suspended material is deposited in this area, the TBT adsorbed on suspended solids tends to remain near the origin of the pollution. Thus, the transport of substances is confined to this area and they accumulate in sediments.

Table 8 presents the concentration factors (CF) of trace metals for settling particles and plankton in the Japan Sea (Masuzawa 1989), compared with the data from this study. The average trace metal concentrations in Shimizu Port were used for the calculation of suspended solids and data from the North Pacific Ocean, presented in Table 4 (Nozaki 1992), were used for settling particles and plankton.

The CF values of Mn, Fe, Cd, and Pb for settling particles in the wood pool are comparable to those of plankton. However, the CFs for Cu and Zn are considerably lower. The CFs in the Japan Sea increase with increasing depth and it is believed that this increase with depth is due to the formation of Mn and Fe oxides. The CFs of Co, Cu, Zn, and Cd, to Mn and Fe are 10^{4}–10^{6}, 10^{6}–10^{7}, 10^{4}–10^{5}, and 10^{3}–10^{4}, respectively, which are comparative to those of plankton and settling particles (Takematsu 1979b; Sato 1989). Accordingly, suspended solids in the wood pool will take a longer time to be deposited on the bottom. When seawater is stratified, photosynthesis is active and aerobic, from the surface to a water of about 2 m, although there is an oxygen-deficient water layer just near the bottom. As a result, Mn and Fe oxides are formed on the suspended solids (Fig. 5(*c*)). This means that suspended solids remove trace metals in seawater, as with plankton. After these materials are deposited on the bottom, the trace metals in the sediments are regenerated because of a low redox potential. The repeated cycle plays an important role for the accumulation of chemicals in sediments.

Thus, suspended solids retain a considerable amount of hazardous substances and their removal is one of the easiest ways to clean seawater (Fukue et al. 2004).

Concluding Remarks

The transport and contamination of suspended solids in the wood pool were quantitatively investigated, as an assessment case study of an enclosed sea area. The amount of suspended materials discharged from rivers and sewage plants into Shimizu Port is approximately 12 000 kg/day. The amount from two small rivers discharged into the wood pool is about 12 % of the total amount. Suspended particles, as well as plankton generated in the port, cause a reduction in the transparency of seawater, an increase in COD, etc.

From analyses of salt flux, the seawater in the wood pool is exchanged mainly by density currents. The impact of tidal currents on seawater exchange is extremely weak; therefore, suspended particles discharged into the wood pool remain there for a long period of time.

Concentrations of Mn, Fe, No, Cu, Zn, Cd, and Pb were 10–1000 times greater than the average values of the open sea. Mn, Cd, and Pb concentrations of surface water in Shimizu Port was lower than that in Hiroshima Bay, while Fe, Ni, Cu, and Zn concentrations were higher. In the wood pool, trace metal concentrations, except Ni and Cd, were a few times greater than in Shimizu Port.

The ignition loss of suspended solids from the rivers was 2–7 %, while it is 16 % for settling particles in the wood pool. Mn, Co, and Pb concentrations of suspended solids from the rivers were higher than that of the settling particles in the wood pool. Cu and Cd concentrations were a little lower for the suspended solids from the rivers. Concentration factors of Mn, Fe, Cd, and Pb for settling particles are comparable to those of plankton. TBT concentrations in settling particles were approximately 300 μg/kg. It is found that suspended particles in the wood pool contain Mn and Fe oxides. Trace metals in the sediments are

regenerated because of a low redox potential. The repeated cycle plays an important role in the accumulation of chemicals in sediments.

Acknowledgments

This study was financially supported by the Project of the Institute of Oceanic Research and Development, Tokai University and also by Grant-In-Aid for Scientific Research, No. 16510067. The authors thank Professor Y. Kato, Professor M. Nishimura, T. Mizushima, N. Hagiwara, and S. Saito for their useful suggestions.

References

Cowen, J. P. and Li, Y. H., "The Influence of a Changing Bacteria Community on Trace Metal Scavenging in a Deep-Sea Particle Plume," *J. Mar. Res.* 49, 517–542 (1991).

Fukue, M., Sato, Y., Inoue, T., Minato, T., Yamasaki, S., and Tani, S., "Seawater Purification with Vessel Installed Filter Units," *Geoenvironmental Engineering-Integrated Management of Groundwater and Contaminated Land*, edited by Yong, R. N. and Thomas, H. R.,Thomas Telford, London, 2004, pp. 510–515.

García-Ruelas, C., Botello, A. V., Ponce-Vélez, G. and Díaz-González. G., "Polycyclic Aromatic Hydrocarbons in Coastal Sediments from the Subtropical Mexican Pacific," *Mar. Pollution Bull.* 49, 514–524 (2004).

Gibbs, R. J., "Transport Phases of Transition Metals in the Amazon and Yukon Rivers," *Bull. Geol. Soc. Am.* 88, 829–843 (1977).

Grasshoff, K., Ehrhardt, M., and Kremling, K., Eds., *Methods of Seawater Analysis*, Second, Revised and Extended Edition, Verlag Chemie, Weinheim (1983).

Halbach, P., Giovanoli, R., and Borstel, D., "Geochemical Processes Controlling the Relationship Between Co, Mn and Fe in Early Diagenetic Deep-Sea Nodules," *Earth Planet. Sci. Lett.* 60, 226–236 (1982).

Hashimoto, S., "Elevated Vitellogenin and Gonadal Abnormalities in Wild Male Flounder (*Pleuronectes yokohamae*) from Tokyo Bay, Japan," *Bull. Coast. Oceanogr. Jpn.* 37, 85–88 (2000). (in Japanese).

Hirata, S., Ishihara, Y., Kajiya, T., and Takeda, K., "Heavy Metal Concentrations of Coastal Seawater in Hiroshima Bay," *Proceedings of Sea Environment and Living Things, and Rehabilitation of Coastal Environment*, 2002, pp. 19–24.

Hoshika, A., Tanimoto, T., and Mishima, Y., "Sedimentation Processes of Particulate Matter in the Osaka Bay," *Umi no Kenkyu* 13, 419–425 (1994) (in Japanese).

Jenne, E. A., "Controls on Mn, Fe, Co, Ni, Cu and Zn Concentrations in Soils and Waters: The Significant Role of Hydrous Mn and Fe Oxides," *Adv. Chem. Ser.* 73, 337–387 (1968).

Martin, J. H., "The Possible Transport of Trace Metals Via Molted Copepod Exoskeletons," *Limnol. Oceanogr.* 15, 756–761 (1970).

Martin, J. M. and Knauer, G. A., "The Elemental Composition of Plankton," *Geochim. Cosmochim. Acta* 37, 1639–1653 (1973).

Martin, J. M. and Meybek, M., "Elemental Mass-Balance of Materials Carried by Major World Rivers," *Mar. Chem.* 7, 173–206 (1979).

Masuzawa, T., "Compositional Change of Settling Particles with Water Depth in the Japan Sea," *Mar. Chem.* 27, 61–78 (1989).

Matsumoto, E., "The sedimentary environment in the Tokyo Bay," *Geochemistry (USSR)* 17, 27–32 (1983). (in Japanese).

Moorby, S. A. and Coronan, D. S., "The Distribution Elements Between Coexisting Phases in Some Marine Ferromanganese Oxides Deposits," *Geochim. Cosmochim. Acta* 45, 1855–1877 (1981).

Noriki, S., Nakanishi, K., Fukawa, T., Uematsu, M., Uchida, T., and Tsunogai, S. "Use of A Sealed Teflon Vessel for the Decomposition Followed by the Determination of Chemical Constituents of Various Marine Samples," *Bull. Fac. Fish. Hokkaido Univ.* 31, 354–361 (1980) (in Japanese).

Nozaki, Y., "Trace Elements in Seawater: Their Mean Concentration and North Pacific Profiles," *Geochemistry (USSR)* 26, 25–39 (1992).

Okuda, K., Nakada, N., Isobe, T., Nishiyama, H., Sanada, Y., Sato, F., and Takada, H., "Endocrine

Disruptors in a Sediment Core Collected from Tokyo Bay: The Historical Trends During the Past 50 Years," *Bull. Coast. Oceanogr. Jpn.* 37, 97–106 (2000) (in Japanese).

Rozan, T. F. and Benoit, G., "Heavy Metal Removal Efficiencies in a River-Marsh System Estimated from Patterns of Metal Accumulation in Sediments," 48, 335–351 (1999).

Sakai, H., Kasai, R. Takahasi, S., and Tanabe, S., "Contamination by Butyltin Compound in Sediment, Cultured Fishes (*Seriola quinqueradiata* and *Pagrus major*) and Pearl Oysters (*Pinctada martensii*) Collected from Uwa Sea, Japan," *Nippon Suisan Gakkaishi* 69, 10–22 (2003) (in Japanese).

Santschi, P. H., Presley, B. J., Wade, T. L., Garcia-Romero, B., and Baskaran, M., "Historical Contamination of PAHs, PCBs, DDTs, and Heavy Metals in Mississippi River Delta, Galveston Bay and Tampa Bay sediment cores," 52, 51–79 (2001).

Sato, Y., "Studies on Marine Environments and Productivities in Suruga Bay, Japan:Chemical Constituents of Seawater and Particulate Matter of Suruga Bay," *Bull. Inst. Ocean. Res. Dev. Tokai Univ.* 7, 1–6 (1985) (in Japanese).

Sato, Y., "The Rate of Oxidation of Ferrous Iron in Seawater and the Partition of Elements Between Iron Oxides and Seawater," *J. Oceanogr. Soc. Jpn.*, 45, 270–278 (1989).

Takada, H. and Yanagi, T., "A Summary of Behaviour of Endocrine Disrupting Chemicals in Coastal Environments Symposium," *Bull. Coast. Oceanogr. Jpn.* 37, 83–84 (2000). (in Japanese).

Takahashi, S., Tanabe, S., Takeuchi, I., and Miyazaki, N., "Distribution and Specific Bioaccumulation of Butyltin Compounds in a Marine Ecosystem," *Arch. Environ. Contam. Toxicol.* 37, 50–61 (1999).

Takematsu, N., "Sorption of Transition Metals on Manganese and Iron Oxides, and Silicate Minerals," *J. Oceanogr. Soc. Jpn.* 35, 36–42 (1979a).

Takematsu, N., "The Incorporation of Minor Transition Metals into Marine Manganese Nodules," *J. Oceanogr. Soc. Jpn.* 35, 191–198 (1979b).

Takematsu, N., Sato, Y., and Okabe, S., "The Formation of Todorokite and Birnessite in Seawater Pumped from Under ground," *Geochim. Cosmochim. Acta* 48, 1099–1106 (1984).

Tanimoto, T., Hoshika, A., Nishimura, Y., and Yanagi, T., "Budget of Suspended Materials and Nutrients in Osaka Bay," *Umi no Kenkyu* 10, 397–412 (2001) (in Japanese).

Whitfield, M. and Turner, D. R., "The Role of Particles in Regulating the Composition of Seawater," *Aquatic Surface Chemistry*, edited by Stumm, W., Wiley, New York, 1987, pp. 457–493.

Yanagi, T., "Budget Model in the Coastal Area," *Umi no Kenkyu* 16, 163–171 (1997). (in Japanese).

Journal of ASTM International, Vol. 3, No. 7
Paper ID JAI13318
Available online at www.astm.org

Masaharu Fukue,[1] *Yoshio Sato,*[2] *Kouji Uehara,*[3] *Yoshihisa Kato,*[4] *and Yukio Furukawa*[5]

Contamination of Sediments and Proposed Containment Technique in a Wood Pool in Shimizu, Japan

ABSTRACT: The objective of this study is to evaluate the contamination of sediments, in order to determine a remediation method for a local bay bottom. To achieve this, 12 surface-sediment samples were obtained from a wood pool located in the inner part of Shimizu Port, Japan, and were subjected to physical and chemical analyses. The results show that the concentrations of the heavy metals measured were relatively high. The concentrations of copper and zinc in the sediment samples were higher than the probable effect levels of marine sediments provided by the Canadian Sediment Quality Guidelines. The high concentrations obtained are probably due to the high organic content resulting from humus. The separation of organic matter might be useful as a remediation technique for dredged materials. A containment technique for dredged sediments using permeable bags is therefore proposed.

KEYWORDS: background, dredged materials, enclosed sea, heavy metals, ignition loss, sediments

Introduction

Since Shizuoka city was designated by ordinance in April 2005, the surrounding areas of Orido Bay and Shimizu Port have been targeted for redevelopment. Orido Bay is located in the inner part of Shimizu Port. The bay has been used as a pool in which wood is floated for pest control since 1927. However, since the bay has become surrounded by many industries, it might have been contaminated. An integrated investigation is therefore needed to assess its potential for the following uses: the farming of fish and shellfish; tourism; anchorage, moorage, and roadstead areas for ships and seaplanes; or a waterfront public park.

All of these projects require a clean waterside and uncontaminated seawater, which can be obtained by measures based on integrated investigations and studies. The current paper focuses on sediment quality, because the bioaccumulation of contaminants by benthic organisms in sediments is a major problem for individual projects. Furthermore, the resuspension of the contaminated sediments can greatly increase their exposure to the water column.

If the sediments are contaminated, the following items should be taken into account: first, isolation of the contaminated sediment from the benthic environment; and second, cleanup of the bottom (i.e. preventing resuspension and transport to other sites).

The items presented here are important not only at this site, but also at many other enclosed sea areas.

Site Locations

The investigation sites were within a wood pool that occupies most of Orido Bay, as shown in Fig. 1. The inner part of the wood pool has been enclosed by breakwaters and used as a pool in which wood is floated for pest control since 1927. The wood pool has an area of 717 000 m^2 and a maximum water depth of 8 m. Therefore, wood chips have accumulated on the bottom and have been subjected to degradation. The pool is fed by two streams, the Ohashi River and the Hamada River, both of which run through residential

Manuscript received April 6, 2005; accepted for publication December 12, 2005. Presented at ASTM Symposium on Contaminated Sediments: Evaluation and Remediation Techniques on 23-25 May 2006 in Shizuoka, Japan; M. Fukue, K. Kita, M. Ohtsubo, and R. Chaney, Guest Editors.

[1] Professor, Department of Marine Civil Engineering, Tokai University, Shizuoka, 424-8610, Japan.
[2] Professor, Department of Marine Science, Tokai University, Shizuoka, 424-8610, Japan.
[3] Manager, Japan Industrial Land Development, Co., Tokyo, 108-8432, Japan.
[4] Professor, Department of Marine Science, Tokai University, Shizuoka, 424-8610, Japan.
[5] Professor, Department of Civil Engineering, Nihon University, Kooriyama, 963-8642, Japan.

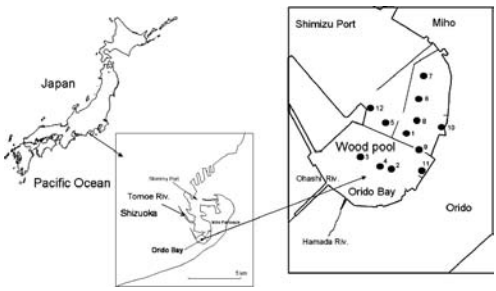

FIG. 1—*Sampling sites of sediments in the wood pool.*

districts and small factory sites, as shown in Fig. 1. The flow rates of the streams are relatively low (i.e., 0.17–0.76 m^3/s and 0.02–0.24 m^3/s, respectively). The wood pool contains several breakwaters and many driven mooring piles, to which wood rafts are moored. The Tomoe River, which is larger than the two streams mentioned above, flows into Shimizu Port, as shown in Fig. 1. The flow rate of the Tomoe River is approximately 6.0 m^3/s, but its impact on the wood pool is not significant.

Twelve surface-sediment samples were obtained using a grab sampler from the bottom of the wood pool. Because of the presence of wood and ropes discarded on the bottom, it was difficult to obtain sediment samples at some sites. The sampling depth was less than 8 cm from the top surface. The sampling site locations were designated St. 1 to St. 12, as indicated in Fig. 1.

Tests and Measurements

Physical tests on the sediment samples were carried out to obtain the specific gravity of particles, grain-size distribution, water content, and so on. These tests were carried out using the methods provided by the Japanese Industrial Standards (JIS) and the Japanese Geotechnical Standards (JGS), except for grain-size analysis, which was performed using the laser method (Furukawa et al. 2001). Ignition loss, concentrations of sulfide, heavy metals and tributyltin (TBT), redox potential, and pH were measured by chemical tests and analyses. A temperature of 750°C was used to determine the ignition loss. The chemical analyses of some metals—i.e., iron (Fe), lead (Pb), copper (Cu), zinc (Zn), manganese (Mn), and cobalt (Co)—were carried out using inductively coupled plasma atomic-emission spectrometry (ICP-AES), after digestion (HNO_3, HF, and $HClO_4$). As some metals appeared to be present at relatively high concentrations, a cross check was made using atomic-absorption analysis. This technique was also used to measure the concentrations of elements such as cadmium (Cd), arsenic (As), aluminum (Al), and chromium (Cr). The concentrations of TBT were measured using gas chromatography/mass spectrometry (GC/MAS). The detection limit for TBT was approximately 0.1 μg/kg dry weight.

Results and Discussions

Physical and Chemical Properties

The results obtained from the different measurements are presented in Table 1, along with the water depths of the sampling points, which varied from 3.0 m to 7.8 m. The water contents of the sediment samples varied from 89 % to 300 %, where the water content is defined as the percentage of water to solid, by weight. The specific gravities of the samples were smaller than those of ordinary inorganic sediments; the smallest specific gravity value was 2.17 and the largest was 2.63.

Correlations between Properties and Ignition Loss

The physical and chemical properties of the sediments could be correlated to the magnitude of ignition loss, as demonstrated later. At all sites, except for Sts. 3 and 11, the ignition loss exceeded 15 %, as shown in Fig. 2. The highest value of the ignition loss was 29.2 % for St.12, and the values exceeded 20 % for

TABLE 1—*Physical and chemical properties of sediment samples from the wood pool.*

	Site											
	St.1	St.2	St.3	St.4	St.5	St.6	St.7	St.8	St.9	St.10	St.11	St.12
Water depth (m)	5.7	4.1	3.5	4.0	5.9	5.9	5.8	5.8	7.8	3.0	3.0	3.0
Water content (%)	210	286	171	300	192	136	214	175	156	280	89	300
Specific gravity	2.55	2.17	2.53	2.36	2.58	2.53	2.63	2.47	2.59	2.26	2.56	2.29
Ignition loss (%)	16.4	25.2	13.7	24.2	16.3	15.0	15.2	19.0	15.8	25.3	9.1	29.2
Organic carbon content (%)	....	....	....	....	....	....	....	....	....	3.8	2.2	4.5
Fe (g/kg)	36.2	40.1	39.1	35.1	47.6	41.7	47.5	35.7	48.0	39.8	25.7	22.9
Al (g/kg)	27.0	29.0	31.0	28.0	24.0	20.0	24.0	18.0	20.0	34.0	37.0	31.0
Zn (mg/kg)	429	365	405	382	417	327	454	466	379	729	402	719
Pb (mg/kg)	83	75	45	72	62	46	81	60	83	96	57	103
Cu (mg/kg)	250	240	190	240	190	130	250	210	200	310	139	320
Cd (mg/kg)	0.67	0.38	0.59	0.41	0.71	0.88	0.55	0.81	0.39	0.71	0.38	0.69
Co (mg/kg)	22	16	22	20	19	12	23	15	23	22	11	24
Mn (mg/kg)	670	580	610	530	690	500	760	730	700	700	400	700
Cr (mg/kg)	7	16	6	10	11	17	10	7	15	11	17	....
As (mg/kg)	10	9.4	7.9	7.5	11	22	18	11	7.2	6	6.2	....
TBT (μg/kg)	340	....	360	....	....	....	....	....	....	....	....	....
Sulfide (mg/g)	1.1	2.5	3.2	3.2	1.25	1.2	1.7	1.25	0.6	1.13	0.42	1.24
pH	7.34	7.4	7.3	7.1	6.9	6.8	6.7	6.8	6.9	7.3	7.4	7.3
Eh (mV)	−150	−178	−158	−175	−76	−109	−112	−132	−130	−8	25.5	−61
Clay content (%)	46.2	55.6	43.3	48.7	45.2	44.6	57.7	55.8	45.2	38.2	8.6	40.7
Fine content (%)	91.1	96.4	93.6	95.6	94.1	94.2	96.6	95.3	91.8	91.0	18.0	95.2

Sts. 2, 4, 10, and 12. As stated above, the high ignition loss was possibly due to the deposits of the bark. Pieces of bark had been deposited on the bed and cellulose-decomposing bacteria were active in the wood pool.

The ignition loss of soils can represent the organic matter content. Organic matter contains organic carbon. Therefore, the ignition loss can be correlated to the organic carbon for soils. Figure 3 shows the relationship between the ignition loss and organic carbon for various types of soil (Japanese Geotechnical Society 2000). The data obtained for the Orido Bay sediments (Sts. 10 to 12) and the Lake Sanaru sediments are also presented in Fig. 3. The figure shows a strong correlation between ignition loss and organic carbonate content for various soils and sediments (R^2=0.809). When the ignition loss is high, the ratio of organic carbon content is also high.

Because organic matter can contain more water, higher ignition loss usually leads to higher water content. Furthermore, a lower specific gravity of organic matter can also make the water content higher. A similar pattern is seen in peat, which consists mostly of organic matter. The relationship between ignition loss and water content is shown in Fig. 4. For example, clean sand without organic matter has a water content of around 30 %. However, there might be water content, depending on the particle characteristics of the sediments. The variation in the data in Fig. 4 results mainly from variation in particle characteristics, such as grain-size distribution and mineralogical aspects.

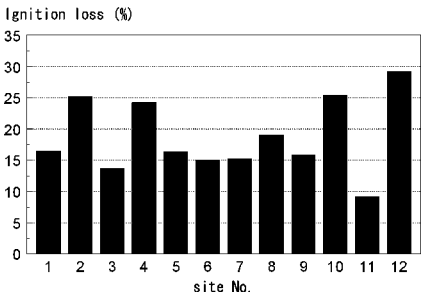

FIG. 2—*Ignition loss of the sediments from the wood pool.*

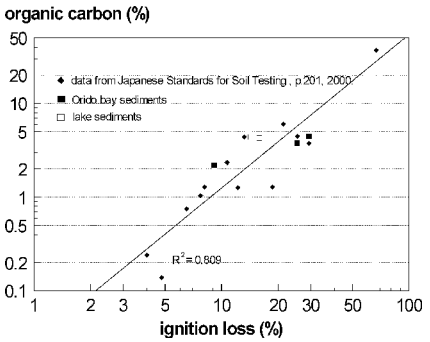

FIG. 3—*Relationship between organic carbon and ignition loss for various types of soil and sediments.*

The specific gravity of sediments depends mainly on the organic matter content. As the organic matter content is reflected by the ignition loss value, there is a correlation between specific gravity and ignition loss. The correlation cannot be expressed by a single and straight line, because of the limited maximum and minimum specific gravities depending on the respective specific gravities of inorganic and organic constituents, as shown in Fig. 5.

Heavy Metals and Ignition Loss

The organic component of sediments has a high affinity for heavy metal cations because of the presence of ligands or groups that can form chelates with the metals (Yong et al. 1992). If this is the case, the heavy metal contents must increase with increasing ignition loss. Figure 6 shows the Cu concentration versus the

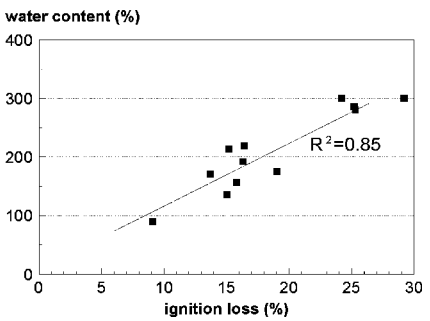

FIG. 4—*Relationship between water content and ignition loss for sediments from the wood pool.*

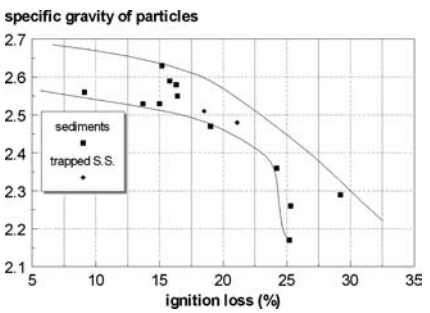

FIG. 5—*Specific gravity versus ignition loss for the wood pool sediments.*

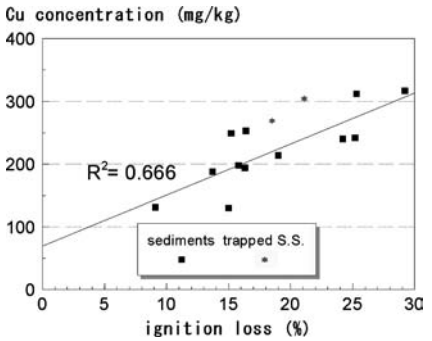

FIG. 6—*Concentrations of Cu versus ignition loss for the wood pool sediments.*

ignition loss for sediment samples and trapped suspended solids from the wood pool. As might be expected, the Cu concentration increases with increasing ignition loss; the rate of increase of the Cu concentration with ignition loss is greater than 10 mg/kg/%. The trend indicated by the straight line in Fig. 6 is important for evaluating the background concentration of Cu. It should be noted that the intercept with the vertical axis provides the Cu concentration of the sediments without ignition loss.

A similar relationship between Pb concentration and ignition loss is shown in Fig. 7. From the gradient in Fig. 7, the rate of increase of the Pb concentration with ignition loss is at least 2.7 mg/kg/%. Figure 8 shows the relationship between Zn concentration and ignition loss. The relationship presented in Fig. 8 is

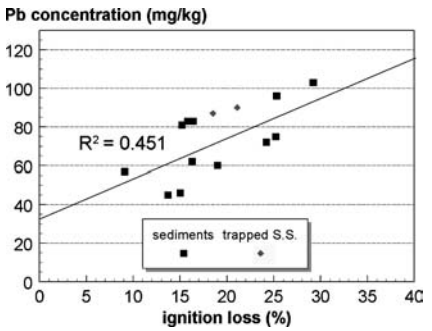

FIG. 7—*Concentration of Pb versus ignition loss for the wood pool sediments.*

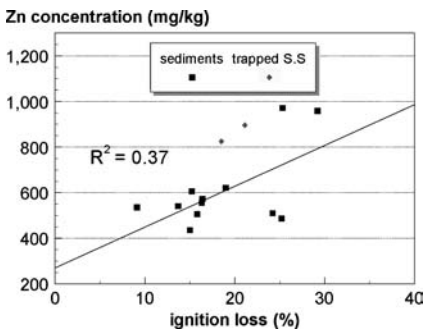

FIG. 8—*Relationship between Zn concentration and ignition loss.*

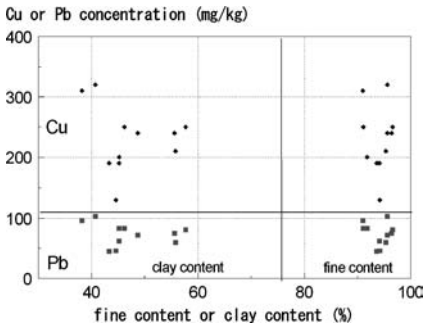

FIG. 9—*Concentrations of Cu and Pb versus fine content* (<0.075 mm) *and clay content* (<0.005 mm)*, showing that grain size is not a dominant factor determining heavy metal concentrations.*

similar to those shown in Figs. 6 and 7, although some scatter is seen. The rate of increase of the Zn concentration with ignition loss is relatively high (i.e., approximately 20.3 mg/kg). Thus, the heavy metals measured showed a strong affinity for the organic matter.

The results shown in Figs. 6–8 might be affected by grain size, because, generally, the finer the sediments, the higher the ignition loss. However, this is contradicted by the fact that, in Fig. 9, there is no correlation between the heavy metal concentrations and grain-size characteristics. Figure 9 shows the concentrations of Cu and Pb versus fine content (<0.075 mm) and clay content (<0.005 mm) for the wood pool sediments. The data for St. 11 was omitted from this analysis, because Fig. 9 shows only an independence of the grain size with the metal concentration of contaminated sediments. The other analyses include the data for St. 11. The figure shows that the concentrations of Cu and Pb were not significantly correlated with grain-size characteristics. Therefore, the concentrations of heavy metals in the wood pool sediments might have been strongly influenced by the organic content. Consequently, in this region, the effect of grain size vanished, as seen in Figs. 6 and 7. Thus, for contaminated sediments, the concentration of metals tends to be dependent on the degree of contamination, not on grain size. The degree of contamination can be evaluated from the comparison between the concentration and the background concentration which can be dependent on the grain size characteristics.

By contrast, there was no significant correlation between Fe concentration and ignition loss, as seen in Fig. 10. The correlation coefficient R^2 is only 0.064. As Fe exists as oxides, pyrites, or hydroxides in sediments, its concentration is largely independent of the amount of organic matter. Some studies reported that Fe and Al concentrations could be used for normalization when the sediment contamination was evaluated (Cobelo-Garcia and Prego 2003; Din 1992). However, normalizing techniques with elements such as Fe and Al could not be used in the present study, because no data were obtained on uncontaminated sediments.

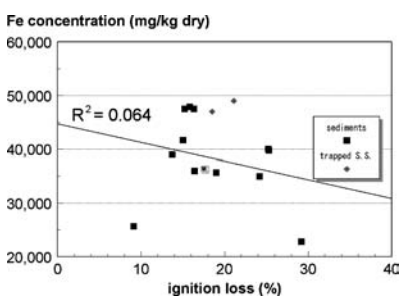

FIG. 10—*Concentration of Fe versus ignition loss for the wood pool sediments, showing no significant correlation between these factors.*

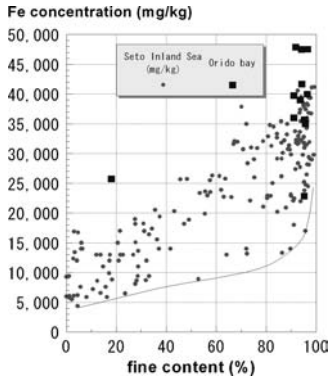

FIG. 11—*Concentration of Fe and fine content for sediments from the Seto Inland Sea and the wood pool.*

The background concentrations of metals were found to be in agreement with the average values reported for gneisses rocks (Carral et al. 1995). However, the background values for Cu, Zn, and Pb did not always agree with those obtained previously.

Fukue et al. (1999) used carbonate as a normalizing substance and measured its content. Cobelo-Garcia and Prego (2003) determined the baseline relationships between the concentrations of Fe and pollutants. Din (1992), Corteäo and Vale (1995), Morrison et al. (2001), and Santschi et al. (2001) used Al to normalize the concentrations of heavy metals in sediments. The basic idea when using Al as a normalizing substance is that this is one of the main constituents of clay crystals, and the larger the amount of clay minerals, the smaller the grain size. Therefore, Al concentration can be used as an index of grain size.

Background Baseline Values and Evaluation of Contamination

The contamination of the sediments is discussed with reference to data obtained from other sites. Figs. 11–14 show the concentrations of Fe, Pb, Cu and Zn, respectively, in terms of fine content ($>$0.075 mm).

The data presented in Fig. 11 are from the Seto Inland Sea and the wood pool in Orido Bay. The data from the Seto Inland Sea include measurements taken on uncontaminated sediments, which were obtained using a core sampler. A lower limit line for Fe concentration against fine content is drawn in Fig. 11. This is considered to be a baseline relating to grain-size characteristics. Figure 11 shows that the baseline

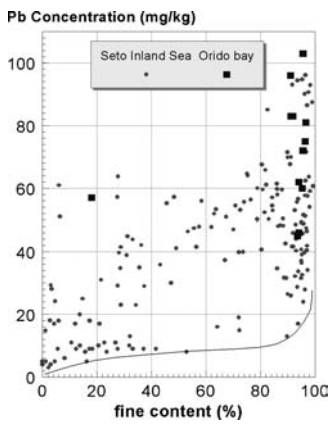

FIG. 12—*Concentration of Pb versus fine content for sediments from the Seto Inland Sea and the wood pool.*

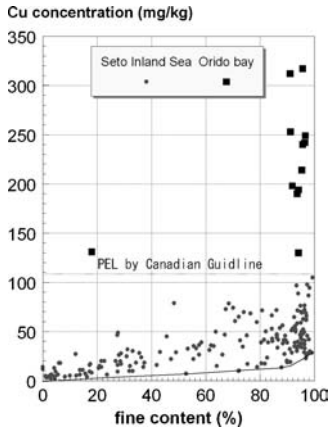

FIG. 13—*Concentrations of Cu and fine content for sediments from the Seto Inland Sea and the wood pool.*

increases with increasing fine content, which is defined as a finer percentage of fractions smaller than 0.075 mm. The concentrations of Fe in the wood pool sediments were relatively high in comparison with those from the Seto Inland Sea, and were comparable to those from Tokyo Bay (Matsumoto 1983). The Tokyo Bay sediments showed values of approximately 45 000 mg/kg. It is noted that most of the data for the Seto Inland Sea and Orido Bay show the effects of anthropological activity, because the concentrations are considerably greater than the baseline which is probably non-contaminated.

Figure 12 shows the concentrations of Pb for sediments from both the Seto Inland Sea and the wood pool. The baseline of Pb is also indicated in the figure. The wood pool sediment values were considerably higher than the baseline. If the effect of ignition loss is taken into account, the excess Pb retention in the sediments might be due to organic matter. The probable effect level (PEL) of Pb is 112 mg/kg (Canadian Sediment Quality Guidelines 2003); thus, all the data presented in Fig. 11 are within the allowable range. In Tokyo Bay, the Pb concentration obtained by Matsumoto (1983) was approximately 20 mg/kg to 110 mg/kg. This value was similar to those of the wood pool sediments.

The Cu concentration of the wood pool sediments was relatively high, as shown in Fig. 13. The highest Cu concentration from the Seto Inland Sea was approximately 100 mg/kg, whilst some data from the wood pool was higher than 300 mg/kg. The highest Cu concentration of the Tokyo Bay sediments was

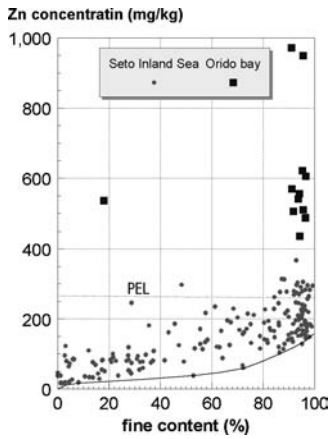

FIG. 14—*Concentration of Zn and fine content for sediments from the Seto Inland Sea and the wood pool.*

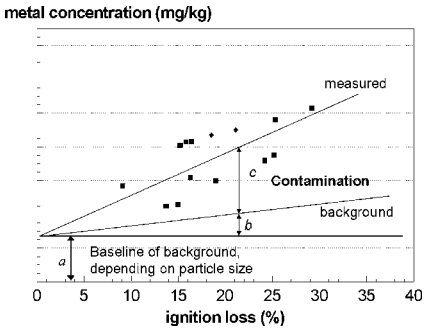

FIG. 15—*Background concentrations in terms of ignition loss for fine sediments.*

around 100 mg/kg (Matsumoto 1983). The values from all three sites were relatively high in comparison with the baseline presented in Fig. 13. The PEL for Cu according to the Canadian Sediment Quality Guidelines is 108 mg/kg, as indicated in Fig. 13.

One reason why the Cu concentration of the wood pool sediments is high might be the large amount of organic matter. The effect of organic matter is clear from the relationship between Cu concentration and ignition loss shown in Fig. 6. The estimated concentration at zero ignition loss (approximately 70 mg/kg) shown in Fig. 6 is a little higher than the baseline for fine sediments indicated in Fig. 13. Thus, the high concentration of heavy metals in the wood pool sediments might be due to the retained capacity of organic matter. The large amount of organic matter might be attributable to chips from wood floating in the bay. This could become a serious problem as the organic matter provides food for benthic organisms, which can lead to bioaccumulation.

The Zn concentrations of the wood pool sediments and Seto Inland Sea sediments are shown in Fig. 14. The maximum Zn concentration from the wood pool was approximately 700 mg/kg, whereas Matsumoto (1983) obtained a value of 900 mg/kg for Tokyo Bay sediments. All of the samples from the wood pool exceed the PEL given in the Canadian Sediment Quality Guidelines (i.e., 271 mg/kg).

Although considerable scattering is present in Fig. 8, the Zn concentration decreases with decreasing ignition loss. The intercept of the straight line in Fig. 8 is comparable to the baseline of the fine sediments (i.e., approximately 130 mg/kg). Thus, the results obtained can be interpreted according to the effect of ignition loss or organic matter.

Comparing the metal concentrations and PEL values revealed that the surface sediments of the wood pool were heavily contaminated. If we assume that these data include anthropological effects, the background concentration must be lower than the results obtained. Therefore, the background can be interpreted as shown in Fig. 15. First, a background baseline *a* is dependent on particle-size characteristics or by other normalizations. The line *c* shows an apparent contamination of sediments with a given particle size distribution or for a similar type of sediments. The *b* is an increasing concentration attributed to the increase in ignition loss, but not resulting from contamination due to anthropological activity. The *b* can be almost zero, because the metal concentration is almost constant due to increasing ignition loss (Nagaoka et al. 2004). Nagaoka et al. (2004) compared relationships between the concentrations of heavy metals and ignition loss for contaminated and noncontaminated sea areas. Their results were very similar to Fig. 15. In the current study, the baseline was tentatively represented as a function of the fine content. The baseline was determined as the lower limit of the data, as seen in Figs. 11 to 14. Finally, the background might be regarded as a function of organic content or ignition loss, as shown in Fig. 15. This suggests that if organic matter is removed from the sediments, the metal concentration will be decreased to the background value.

A comparison of the results shown in Table 1 and the Canadian Sediment Quality Guidelines revealed that the Cd concentration from the wood pool did not exceed the PEL value. The average Cd concentration of the twelve sediment samples from the wood pool was 0.6 mg/kg, whereas the PEL was 4.2 mg/kg. The average concentrations of Cr and As were relatively low and were lower than the respective PELs.

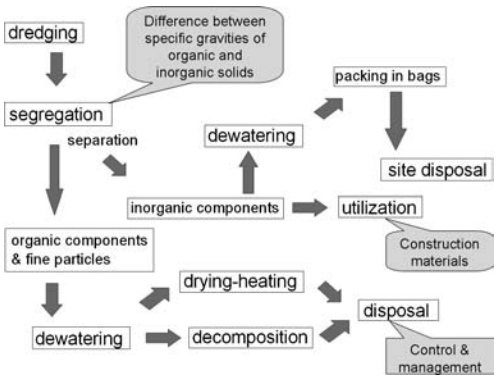

FIG. 16—*Procedures for treatment and disposal of dredged sediments.*

Proposal for Remediation

Dredging is an effective way to clean up the bottom sediments. As the sedimentation rate was slow in the wood pool, the contaminated thickness might be relatively small. Therefore, the dredging volume for cleanup might not be too large. For example, if we assume that a surface sediment thickness of 30 cm is contaminated, then the total volume to be dredged is estimated as 215 000 m^3. The dredged materials have an average water content of 200 % and a low strength. Therefore, the dredged sediments need to be solidified for treatment (Yamasaki et al. 1995).

In Japan, dredged materials are difficult to dispose of, because there is no further disposal space for dredged materials. The dumping of contaminated dredged sediments into the ocean is prohibited. At present, two technical options remain: The first is washing out the contaminants and using the dredged sediments as construction materials, although it is necessary to improve the materials before use; the second is to dispose of the dredged materials at the dredging site.

As shown previously, hazardous substances are retained by organic matter. Therefore, it might be better to separate the organic matter from the sediments as the next step. The differences between the specific gravities of organic matter and inorganic minerals can be utilized for this separation. The segregation of particles with different specific gravities is a useful technique for separating organic matter from sediments and can be achieved during the washing of the dredged sediments. If the coarse inorganic particles are not contaminated, they can be used as construction materials, although a dewatering process is required before use.

The volume of contaminated organic matter can be reduced by dewatering, drying, and heating. The materials can also be decomposed by burning at a high temperature, although the concentration of heavy metals will increase. Appropriate treatment and disposal are essential when the materials are seriously contaminated. The procedures for the treatment and disposal of dredged sediments are shown in Fig. 16.

Suspended solids are washed by seawater during sedimentation. This is the reason why the results of leaching tests on contaminated dredged sediments show little desorption. For example, even when contaminated sediments from Osaka Bay were washed with acid, the desorption amounts of Cu and Zn were less than 1 % of the amount retained (Fukue et al. 2001). It is natural that, in many cases, contaminated sediments adsorb greater amounts of metals when they are submerged in a metal solution.

Methods for the treatment and disposal of contaminated dredged sediments are demonstrated in Figs. 16 and 17. The main steps in this process are as follows: first, the contaminated surface sediments are dredged; second, the dredged materials are solidified to some extent; third, the materials are poured into permeable bags; fourth, the bags are laid on the seabed; and fifth, the bags are covered with sand.

Permeable bags can promote the consolidation of dredged materials. Although the contaminants could potentially leach out from the bags, hazardous substances are strongly adsorbed onto the solid particles and the sediment particles are washed by seawater, so any leachate from the bags will be diluted. These bags are used to isolate contaminated sediments from benthic organisms and fish.

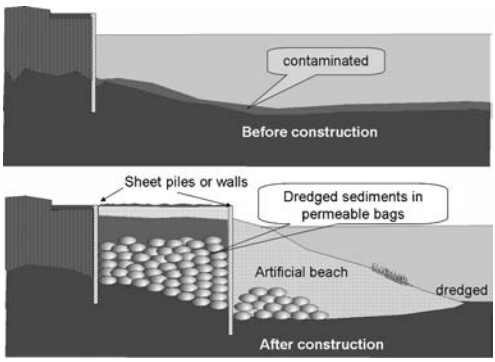

FIG. 17—*Disposal of dredged sediments onsite.*

Concluding Remarks

The quality of sediment samples obtained from a wood pool was evaluated in terms of heavy metals, and other physical and chemical properties. The ignition loss of the sediment samples was so high that their physical and chemical properties could be correlated. Comparisons between the metal concentrations and PEL values provided by the Canadian Sediment Quality Guidelines showed that the sediments were heavily polluted with Cu and Zn. However, the concentrations of As, Cd, and Pb were lower than the respective PELs.

The concentrations could be correlated to ignition loss when the effect of grain size vanished. This implies that these elements are strongly adsorbed onto organic matter. Therefore, a more accurate evaluation of the background could be made using ignition loss. By contrast, Fe and Al showed no significant correlations with ignition loss, because these elements were constituents of the sediment particles themselves.

Dredging might be effective in preserving the environment of the wood pool. According to the results of our investigation, it is better to separate heavily contaminated organic matter from the dredged sediments. This separation can be achieved by segregation during washing and sedimentation in water.

The disposal of dredged contaminated sediments is problematic in small countries like Japan, because no more land is available for waste disposal. Moreover, it might become illegal to dump dredged sediments into the ocean in the near future. An appropriate disposal technique or the remediation of contaminated sediments is, therefore, essential. In the current study, an onsite disposal technique using permeable bags was proposed.

Acknowledgments

This research study was part of the Orido Bay Project of Tokai University, Japan. The authors wish to thank Professor Shin-ichi Ono for useful suggestions. Toshihide Fujikawa, who is a graduate student at Tokai University, carried out the tests and analyses.

References

Canadian Sediment Quality Guidelines (CSeQGs), 2003, "Summary of Existing Canadian Environmental Quality Guidelines," Summary table.

Carral, E., Villares, R., Puente, X., and Carballeira, A., 1995, "Influence of watershed lithology on heavy metal levels in estuarine sediments and organism in Galicia (north-west Spain)," *Mar. Pollution Bull.*, Vol. 30, pp. 604–608.

Cobelo-Garcia, A. and Prego, R., 2003, "Heavy metal sedimentary record in a Galician Ria (NW Spain) background values and recent contamination," *Mar. Pollution Bull.*, Vol. 46, pp. 1253–1262.

Corteäo, C. and Vale, C., 1995, "Metals in sediments of the Sado Estuary, Portugal," *Mar. Pollution Bull.*,

Vol. 30, No. 1, pp. 34–37.

Din, Z., 1992, "Use of aluminum to normalize heavy metals data from the estuarine and coastal sediments of the strait of Melaka," *Mar. Pollution Bull.*, Vol. 24, pp. 484–491.

Fukue, M., Nakamura, T., Kato, Y., and Yamasaki, S., 1999, "Degree of pollution for marine sediments," *Eng. Geol. (Amsterdam)*, (Amsterdam) Vol. 53, pp. 131–137.

Fukue, M., Yanai, M., Takami, Y., Kuboshima, S., and Yamasaki, S., 2001, "Containment, sorption and desorption of heavy metals for dredged sediments," *Clay Science for Engineering*, Adachi, K. and Fukue, M., Ed., Balkema, The Netherlands, pp. 389–392.

Furukawa, Y., Fujita, T., Kunihiro, T., and Fukazawa, M., 2001, "Investigation of particle size distribution of soil using a particle size analysis equipment automated by laser and its applicability to soil samples (text in Japanese)" Journal of Geotechnical Engineering," *Japan Society of Civil Engineers*, Vol. 56, No. 687, pp. 219–231.

The Japanese Geotechnical Society, 2000, "Japanese Standards for Soil Testing," The Japanese Geotechnical Society, p. 201.

Matsumoto, E., 1983, "The sedimentary environment in the Tokyo Bay (text in Japanese with English Abstract)," *Geochemistry*, Vol. 17, pp. 27–32.

Morrison, R. J., Narayan, S. P., and Gangaiya, P., 2001, "Trace element studies in Laucala Bay, Suva, Fiji," *Mar. Pollution Bull.*, Vol. 42, No. 5, pp. 397–404.

Nagaoka, C., Yamamoto, Y., Eguchi, S., and Miyazaki, N., 2004, "Relationship between distribution of heavy metals and sediment condition in the sediment of Osaka Bay (text in Japanese with English summary)," *Nippon Suisan Gakkaishi*, Vol. 70, No. 2, pp. 159–167.

Santschi, P. H., Presley, B. J., Wade, T. L., Garcia-Romero, B., and Baskaran, M., 2001, "Historical contamination of PAHs, PCBs, DDTs, and heavy metals in Mississippi River Delta, Galveston Bay and Tampa Bay sediment," *Mar. Environ. Res.*, Vol. 52, pp. 51–79.

Yamasaki, S., Yasui, S., and Fukue, M., 1995, "Development of solidification technique for dredged sediments," *Dredging, remediation, Containment for Dredged Contaminated Sediments*, ASTM STP1293, ASTM International, West Conshohocken, PA, pp. 136–144.

Yong, R. N., Mohamed, A. M. O., and Warkentin, B. P., 1992, *Principles of Contaminant Transport in Soils*, Elsevier, Amsterdam, p. 154.

Journal of ASTM International, Vol. 3, No. 6
Paper ID JAI13357
Available online at www.astm.org

Tomohiro Umeki,[1] *Akira Mano,*[2] *and Yoshinobu Ishibashi*[3]

Groundwater Flow and Arsenic Contamination Analyses in Southern Bangladesh

ABSTRACT: Arsenic contamination had been found all over Bangladesh in 1993, however, the groundwater flow and the mechanism of arsenic contamination have not been made clear yet. Because the arsenic contamination spreads through the groundwater, it is important to understand the groundwater flow. We performed the field measurement from December 23rd to 25th, 2003 and from May 19th to 21st, 2004. Then we performed the numerical analyses of groundwater flow and arsenic transportation using MODFLOW to grasp the field groundwater condition. As a result of the field measurement, the underground condition of our study area is reductive. Besides, using MODFLOW, we could reproduce the groundwater flow properly and estimate a flux of groundwater drawn from wells, and then, predict the future contamination.

KEYWORDS: arsenic, groundwater, MODFLOW

Introduction

Following the wide use of the tube well since 1971, 95–97 % of an approximately 140 million population in Bangladesh now depends on groundwater for drinking. However, arsenic contamination of the groundwater beyond the Bangladesh arsenic safety standard, 0.05 mg/l, had been found all over the country since 1993, especially for shallow wells. Continuous consumption of the water in human bodies causes melanosis, kertosis, skin cancer, etc. It is an urgent issue to find safe and sufficient water resources.

One basic approach for the issue is to clarify the macroscopic behavior of the groundwater. Operation of a huge number of the wells implies the pumping affects transport of the groundwater as well as arsenic. To know the pumping amount we analyzed groundwater flow by using the numerical simulation code MODFLOW, developed by the U.S. Geological Survey. We also conducted field measurement to know the arsenic feature. Finally by combining the two knowledges and others, we performed the numerical analysis on arsenic transport to show the future change of the contamination.

Study Area

Our study area is surrounded by the Gorai River on the western side, the Padma River on the eastern side, the Bay of Bengal on the southern side, and is approximately 17 000 km^2 (Fig. 1).

The arsenic contamination is remarkable in shallow tube wells, which have less than 40 m in depth, but in contrast, the contamination is not found at almost all deep wells, which are greater than 150 m in depth. Therefore, the deep well is becoming a main water source. Besides, there is a distinct regional pattern of arsenic contamination with the greatest contamination in the south and southeast of the country and the least contamination in the northwest and in the uplifted areas of north-central Bangladesh. However, there are occasional strongly contaminated spots in the generally low-arsenic regions of northern Bangladesh. Moreover, the Holocene alluvial and deltaic deposits are most affected, whereas the older alluvial sediments in the northwest and the Pleistocene sediments of the uplifted areas normally provide the low-arsenic water.

The arsenic is of natural origin and believed to accumulate underground and then be released to

Manuscript received March 28, 2005; accepted for publication September 4, 2005. Presented at ASTM Symposium on Contaminated Sediments: Evaluation and Remediation Techniques on 23–25 May 2006 in Shizuoka, Japan; M. Fukue, K. Kita, M. Ohtsubo, and R. Chaney, Guest Editors.

[1] Student, Faculty of Engineering Tohoku University, Sendai, Miyagi, Japan.
[2] Professor, Faculty of Engineering Tohoku University, Sendai, Miyagi, Japan.
[3] Professor, Faculty of Engineering Tohoku Gakuin University, Sendai, Miyagi, Japan.

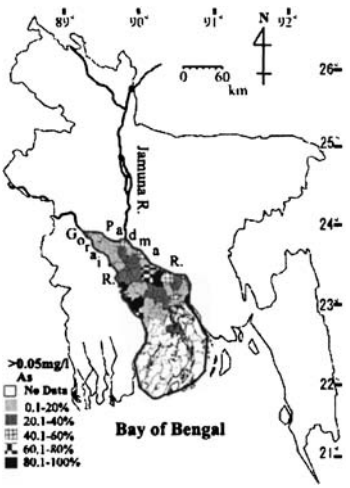

FIG. 1—*Study area.*

groundwater as a result of some mechanisms that are poorly understood. There are mainly two hypotheses about arsenic release. One is called iron oxide reduction hypothesis, in which the arsenic is thought to be desorbed and be dissolved from iron oxides that had earlier absorbed the arsenic from river water during their transport as part of the normal river sediment load under the reductive condition. The other is called pyrite oxidation hypothesis, in which the underground condition changed from reduction to oxidation as a result of the wide use of the tube well and drawing of water, and then the arsenic desorption resulted from the oxidation of pyrite that had already accumulated underground (Kinniburgh and Smedley 2001). However, the arsenic desorption depends on the regional geology, and there is not a unified view. It is the reason why we focus on these regions for a study area.

The high arsenic contamination is spreading in the upper and the middle part of corresponding area, 80 % of all tube wells exceeded the Bangladesh standard for arsenic in drinking water in some regions.

Methods

Field Measurement

The field measurement was carried out at 33 tube wells for drinking and irrigation in Kushtia, which is the region near the distributary of the Gorai River and the Padma River, during a dry season, from December 23rd to 25th, 2003 and from May 19th to 21st, 2004 (Fig. 2). The measurement items were groundwater level, arsenic concentration, water temperature, DO, pH, electric conductivity, and redox potential. The authority had analyzed simply the water from almost all tube wells at the site before our measurement. When the high concentration arsenic had been found at the well, the well had been painted a red color, which means that the well is not suitable for drinking. In contrast, when the water from the well had not exceeded the Bangladesh standard for arsenic in drinking water, the well had been painted a green color, which means that the well is thought to be arsenic-free. We sampled and measured the water at three different wells in depth in each region.

As for the arsenic concentration, sampled water was analyzed at the (KTH) laboratory in Sweden and Bangladesh University of Engineering and Technology (BUET). About the method of the analysis, first the total arsenic concentration was measured, and then As(III) was measured from two samples of each location separating the arsenic into As(III) and As(V) by the use of a resin that absorbs As(V) preferentially and does not absorb As(III). The determination of concentration of As(V) results from a subtraction of the As(III) from the total arsenic.

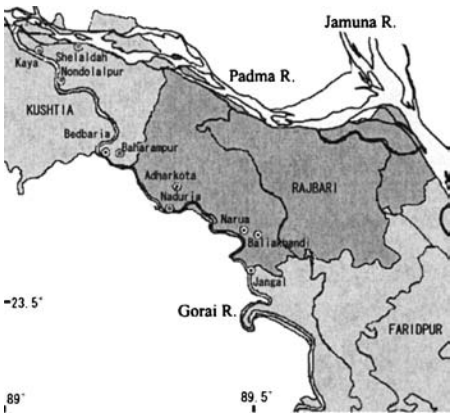

FIG. 2—*Observation points in study area.*

Numerical Analysis

As for the flow movement of groundwater, we use MODFLOW, which is the three-dimensional finite difference code made by U.S. Geological Survey. This program applies Darcy's law and the principle of the conservation of mass, and then it outputs the simulated water level and the water balance through the input of initial water level, hydraulic conductivity, specific storage coefficient, precipitation, recharge, withdrawal, evapotranspiration, and so on.

The fundamental equation of groundwater flow applying Darcy's law and the conservation principle is given as Eq 1. Where S_s is specific storage coefficient, $K_{x,y,z}$ is hydraulic conductivity, r is recharge, and q is discharge.

The water levels of the Padma River, the Gorai River, and the Bay of Bengal are used as a boundary condition. Also, we use the groundwater level based on the observed groundwater level as an initial condition.

The elevation data is available at the U.S. Geological Survey GTOPO30. As for the other input data, the measured values of precipitation, evaporation and river data were obtained from the Institute of Water Modelling, and hydraulic conductivity and specific storage coefficient are based on the field experiment, which was performed by Miyazaki University (Hamambe, Yokota, Jinno, and Nakagawa 2001). The groundwater level is based on the field investigation and is also obtained from the Institute of Water Modelling.

Because the flux of groundwater drawn from a well is not measured specifically, we estimated it by reproducing the measured groundwater level properly using MODFLOW. Considering a large scale of a flood in rainy season, from May to November, and a relatively small population in the south part of the corresponding area, we changed it according to the situation.

In this simulation, we consider the model layer as only one layer and the groundwater flow as an unconfined flow.

As for the fundamental equation of the arsenic transportation, we apply the conservation principle and the reaction rate equation, considering the absorption and desorption of the arsenic. They are given as Eqs 2 and 3. Where ε is porosity, C and $\bar{C}$ are volumetric concentration and the mass concentration of solute sorbed on or contained within the solid aquifer material respectively, ρ_b is the bulk density of the aquifer material, V is a vector of interstitial fluid velocity components, D is a second-rank tensor of dispersion coefficient, W is a volumetric fluid sink or fluid source rate per unit volume of aquifer, C' is the volumetric concentration in the sink/source fluid, λ is the decay rate, k_r is the parameter for the reaction, and k_d is the sorption coefficient. The fluid sink here corresponds to water intake by pumping. W and C' were determined by pumping discharge which is later shown and the arsenic concentration at the pumping. We used 0.05 mg/l for C and 12 mg/kg for $\bar{C}$ based on the safety standard and representative measured value in

TABLE 1—*Results of the field measurement in May, 2004.*

Village name	Well depth, m	As(III), mg/l	As(V), mg/l	AsT, mg/l	DO(mg/l)	pH	Eh(mV)
Kaya	36.6	<0.01	<0.01	bdl[a]	0.00	7.0	−60
Kaya	21.3	<0.01	<0.01	bdl	0.00	6.8	−45
Kaya	27.4	<0.01	<0.01	bdl	0.00	7.0	−50
Shelaldah	18.0	<0.01	<0.01	bdl	0.00	7.0	−60
Shelaldah	27.4	<0.01	<0.01	bdl	0.00	6.9	−50
Nondolalpur	33.5	0.01	0.01	0.02	0.00	6.7	<−100
Nondolalpur	13.7	0.03	0.02	0.05	0.00	6.9	<−100
Nondolalpur	36.6	0.14	0.01	0.15	0.00	7.0	<−100
Bedbaria	39.6	0.02	0.01	0.03	0.00	6.9	<−100
Baharampur	39.6	0.01	0.00	0.01	0.00	7.0	<−100
Nadria	39.6	0.36	0.08	0.45	0.00	6.9	<−100
Adrarkota	137.2	0.01	<0.01	0.01	0.00	7.0	<−100
Narua	42.7	0.15	0.01	0.16	0.06	6.8	<−100
Narua	48.8	0.13	0.00	0.13	0.00	6.8	<−100
Narua	36.6	0.02	0.00	0.02	0.00	6.7	<−100
Jangal	50.3	<0.01	<0.01	bdl[a]	0.00	7.0	80

[a]bdl represents below the detectable level.

Holocene sediments of upper Bengal delta (Anwar 2000), respectively. The bulk density and porosity are obtained from Reynolds Global Soil Data. Velocity is based on the estimated flux of groundwater drawn from wells. As for the parameter for the reaction and the sorption coefficient are set 2.2×10^{-10} s^{-1} and 2.4×10^{-7} m^3/mg, respectively, based on reported values (Bruce and Donald 2000), and this reaction parameter represents that the solute reaches equilibrium in approximately one month. Arsenic decay was not considered in Eq 2.

In this simulation, we picked one inland point up representatively and performed the one-dimensional vertical analysis and explain about it later.

$$S_s\frac{\partial h}{\partial t}=\frac{\partial}{\partial x}\left(K_x\frac{\partial h}{\partial x}\right)+\frac{\partial}{\partial y}\left(K_y\frac{\partial h}{\partial y}\right)+\frac{\partial}{\partial z}\left(K_z\frac{\partial h}{\partial z}\right)+r-q \tag{1}$$

$$\frac{\partial(\varepsilon C)}{\partial t}+\frac{\partial}{\partial z}(\varepsilon C V_z)-\frac{\partial}{\partial z}\left(\varepsilon D_{zz}\frac{\partial C}{\partial z}\right)-\sum C'W+\lambda(\varepsilon C+\rho_b\bar{C})-k_r(\bar{C}-k_dC)\rho_b=0 \tag{2}$$

$$\frac{\partial\bar{C}}{\partial t}=k_r(\bar{C}-k_dC) \tag{3}$$

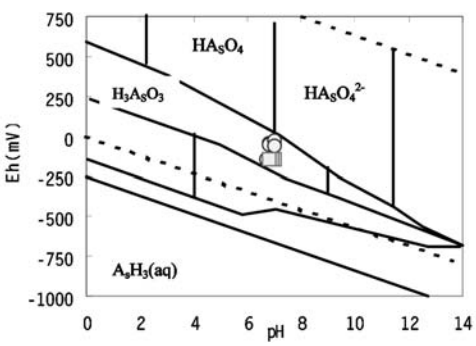

FIG. 3—*Eh-pH diagram for arsenic (Montgomery 1985). Circles and squares show our measurements for As concentration* <0.05 *and* >0.05 mg/l*, respectively*

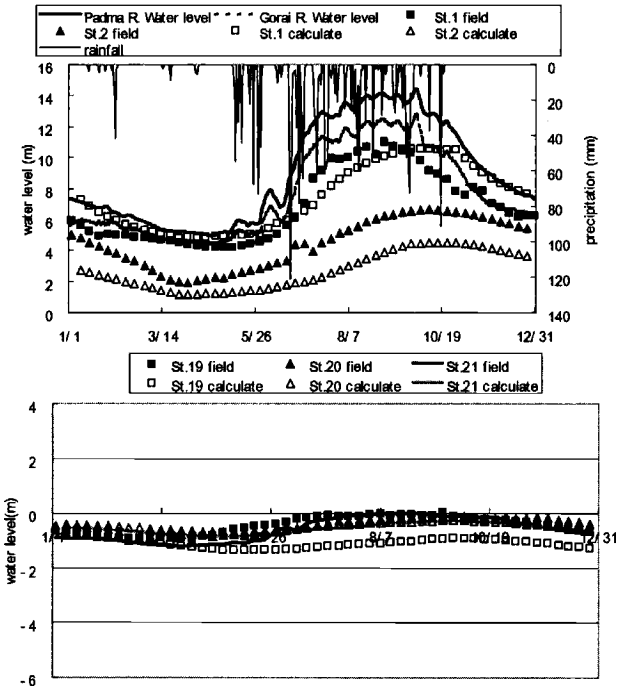

FIG. 4—*Comparison between observed water level and calculated water level.*

Results and Discussion

Field Measurement

The major results of the measurement in May 2004 are shown in Table 1. The shallow tube well is mainly used in corresponding area. As a result of the values of DO and Eh, which represents the redox potential, generally the groundwater in the corresponding area is under reductive condition, moreover, such reductive condition is developing especially in the area where the arsenic contamination is becoming aggravated. Besides, the iron was precipitated when the sampled water had been left for a few days and this reaction may represent the fact that the arsenic had coprecipitated with the iron in this area.

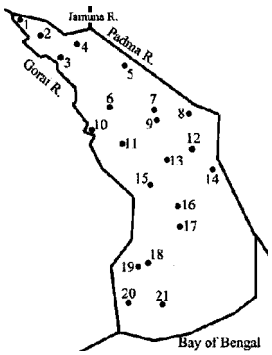

FIG. 5—*Observation points of groundwater level.*

TABLE 2—*Water balance calculated with MODFLOW.*

	Discharge, mm/month		Recharge, mm/month		Storage, mm/month
	Pumping	Evapotranspiration	River	Rain	
Dry (Nov–Apr)	315.9	119.7	115.3	32.2	−288.1
Rainy (May–Oct)	111.7	130.2	189.2	282.6	229.8

On the other hand, there were some places where the smell of sulfur was noted, and it is possible that the accumulated sulfur compounds affect the arsenic release resulting from the oxidation of the groundwater.

The predominant As form in Eh and pH diagram (Montgomery 1985) is shown in Fig. 3 with our data in Table 1. The samples with lower and higher As concentration are plotted by the circles and squares, respectively. Our data locate in H_3AsO_3 domain of As(III) and higher As concentration is found in more reductive conditions.

As for the toxicity of arsenic, toxicity of As(III) is stronger than As(V), and consequently, the arsenic contamination is much more serious in the area where the underground condition and the form of arsenic are reductive, in contrast, the contamination is not remarkable where the ground condition and the form of arsenic are oxidative.

Numerical Analysis

Three-Dimensional Groundwater Flow Analysis—The comparison between the observed groundwater level and the calculated groundwater level using MODFLOW is represented in Fig. 4. Also, the observed points of groundwater level are shown in Fig. 5. The water levels of both the Gorai River and the Padma River strongly affect the groundwater level at Kushtia because Kushtia is located near both rivers. This indicates that the groundwater at Kushtia is recharged much from both rivers and the residence time of groundwater is shorter than the other regions. It also may represent the fact that the groundwater at Kushtia is less contaminated than the other regions if the river water does not include the arsenic. On the other hand, the groundwater level at Rajbari, St. 2 is not strongly affected from rivers and the groundwater cycle is thought to be slow. The result of the numerical analysis matches the observed water level properly.

The water balance calculated with MODFLOW is shown in Table 2. In this case, the discharge is composed of the pumping and the evapotranspiration, on the other hand, the recharge consists of the recharge from rivers and the precipitation. A subtraction of the discharge from the recharge is reflected on the storage of groundwater. As shown in the table, the discharge from the pumping occupies as much as the discharge from the evapotranspiration and it indicates the pumping strongly affects the groundwater level, especially in the dry season.

Vertical Arsenic Contamination Analysis—According to the result of the groundwater flow analysis, a horizontal flow is dominant near the distributary point because of the recharge from rivers. On the other

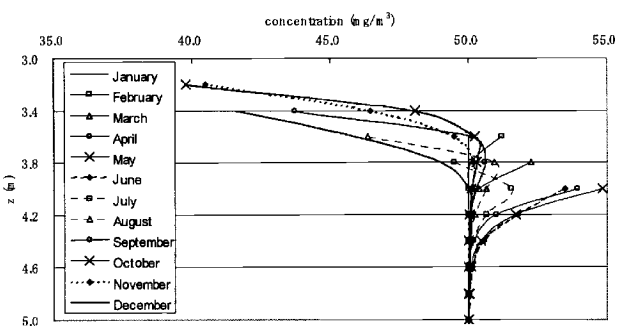

FIG. 6—*Vertical concentration change of solute.*

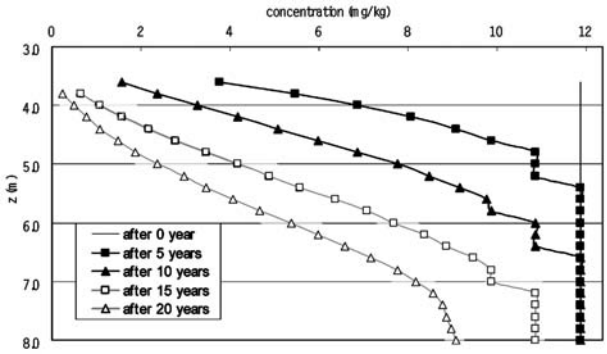

FIG. 7—*Concentration change of the arsenic sorbed on the soil.*

hand, vertical flow is dominant at the inland area because of extremely mild slope less than 1:10,000 and low hydraulic conductivity. Therefore, we picked one inland point up representatively and performed the one-dimensional vertical analysis. The increase or decrease of groundwater is due to only pumping, evapotranspiration, and rainfall. In this analysis, we use the flux of pumping estimated from the groundwater flow analysis, and the groundwater is drawn from the deepest point of the aquifer.

The vertical concentration change of solute and the concentration change of the arsenic sorbed on the soil are shown in Figs. 6 and 7. Near the groundwater surface, as the volume of groundwater decreases in the dry season, arsenic concentration increases by concentrate. On the other hand, in rainy season, the concentration decreases because of the dilution by inflow of rain, which does not include the arsenic. Moreover, such a concentrated solute will be sorbed on the soil in dry season, on the contrary, the arsenic sorbed on the soil will elute into groundwater in the rainy season because of the concentration gradient. As a result of the analysis, after 20 years, the initial arsenic sorbed on the soil reduces to half at the 3 m deep from the groundwater surface.

Recently, the pumping from deep wells is increasing. Moreover, the pumping strongly affects groundwater because the ratio of pumping occupies more than 50 % of the water balance. It will cause the contamination of the deeper arsenic-free aquifer in the future because contaminated groundwater infiltrates into the deeper aquifer. Then, it is predictable that deep wells will also be contaminated. In this case, it is possible to estimate the flux of contaminated water infiltrating toward the deeper aquifer and how deep we can draw the arsenic-free water by performing the analyses of the groundwater flow and the arsenic transportation. Then, it is also possible to estimate how long all of arsenic sorbed on the soil elute into groundwater.

Conclusion

Generally the groundwater in the corresponding area corresponding to arsenic contamination is under reductive condition and such a reductive condition is developing especially in the area where the arsenic contamination is becoming aggravated. Besides, we reproduced the groundwater flow properly and estimated the flux of groundwater drawn from wells. According to the water balance, the pumping from the well strongly affects the groundwater level in the study area. As a result of the arsenic contamination analysis, we predicted the long-term distribution of the arsenic elution from the soil, applying the reaction rate equation.

References

Anwar, J., *Arsenic Poisoning in Bangladesh*, Palash Media, Dhaka, 2000, 336 p.

Bruce, A. M. and Donald, L. S., "Modeling Arsenic(III) Adsorption and Heterogeneous Oxidation Kinetic in Soils," *Soil Sci. Soc. Am. J.*, Vol. 64, 2000, pp. 128–137.

Hamambe, K., Yokota, H., Jinno, K., and Nakagawa, K., "Pumping Tests of Deep and Shallow Tube wells and Numerical Analysis of Groundwater Flow in Samta Village, Bangladesh," 6th forum on *Arsenic Contamination of Groundwater*, organized by Asia Arsenic Network, Joetsu City, 2001, pp. 23–32

Kinniburgh, D. G. and Smedley, P. L., *Arsenic Contamination of Groundwater in Bangladesh*, Vol. 1 Summary, BGS Technical Report, Dhaka, 2001, pp. 1–14

Montgomery, J. M., *Water Treatment Principles and Design*, A Wiley-Interscience Publication, New York, 1985, 696 p.

Journal of ASTM International, Vol. 3, No. 7
Paper ID JAI13315
Available online at www.astm.org

S. Hayashi[1] *and Y. J. Du*[2]

Effect of Acid Treatment Agent of Sea Laver on Geoenvironmental Properties of Tidal Flat Muds in the Ariake Sea

ABSTRACT: Recently the amount of catch of some specific benthos (e.g., shells) in the Ariake Sea of Japan has reduced dramatically. Researchers are questioning if it is the acid treatment practice undertaken in the Ariake Sea tidal flats that changed the geoenvironmental properties of the tidal flat muds, and consequently caused impacts on the benthos living in the muds. However, so far, relatively few detailed studies have been done in this regard. The purpose of this study is to investigate the effect of acid treatment practice on the geoenvironmental properties of muds in the Ariake Sea tidal flats. The field investigation data as well as laboratory test data are presented. It is found that as a consequence of the acid treatment practice, considerable reduction of salt concentration and pH of the muds has taken place. Furthermore, the measured increased sulfide content of the muds indicate that the acid treatment practice in the tidal flats of the Ariake Sea may have produced serious consequences for some benthos inhabiting the shallow depth of the muds.

KEYWORDS: acid treatment, benthos, mud, pH, salt concentration, sulfide content

Introduction

The Ariake Sea, which is located in the Kyushu region of Japan, is a typical shallow sea. It has the largest tidal flat area in Japan with an average area of about 207 km^2, which is almost 40 % of the total tidal flat areas in Japan. These tidal flat areas provide large inhabiting spaces for fishery such as sea laver, *Agemaki* shell, *Tairagi* shell and oysters, and the Ariake Sea is famous for its large amount of fishery products. However, the annual catch of some benthos registered a decline (see Fig. 1). For example, the catch of oysters, usually living near the surface of the mud, dropped from 799 tons in 1976 to 126 tons only in 1999; that of *Tairagi*, living in the upper 10–15 cm, declined from 13 395 tons in 1976 to 79 tons in 1999,

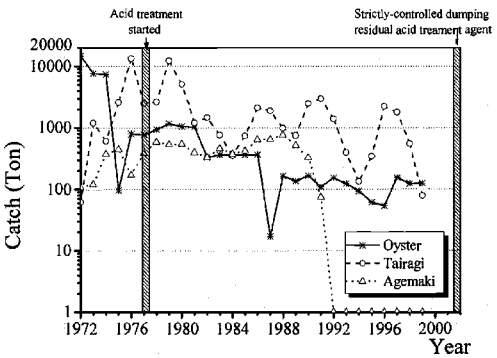

FIG. 1—*Annual catch of some benthos and remarkable epochs related to acid treatment practice.*

Manuscript received February 24, 2005; accepted for publication June 2, 2005. Presented at ASTM Symposium on Contaminated Sediments: Evaluation and Remediation Techniques on 23–25 May 2006 in Shizuoka, Japan; M. Fukue, K. Kita, M. Ohtsubo, and R. Chaney, Guest Editors.

[1] Professor, Institute of Lowland Technology, Saga University, Saga 840-8502, Japan.
[2] Corresponding author, Professor, Institute of Geotechnical Engineering, Southeast University, Nanjing 210096, P.R. China.

and the situation in the case of *Agemaki*, living in the depth of 0–70 cm of the mud, was even worse: 170 tons catch in 1976 dropped to practically nil by 1992. The reason for this observed decline in the fishery catch is still arguing. So far, the possible reasons that are argued can be concluded as: (1) the sea water quality in the Ariake Sea is polluted due to the exchange with the land rivers; (2) the man-made changes such as the Isahaya reclamation project started from 1988; and (3) the deteriorated environment in the mud of the Ariake Sea. The aspect (1) is mostly addressed by the change in the chemical oxygen demand (COD) and concentrations of nutrients in the Ariake Sea water (Araki et al. 2002; Yamanish et al. 2002). The aspect (2) is addressed by the change in the water quality in the reservoir of the Isahaya reclamation projection (Koga et al. 2003). The aspect (3) is from the questionnaires of the Kyushu local fishermen. The questionnaires reveal that most fishermen thought that the mud in the tidal flat areas of the Ariake Sea has been deteriorated, accompanying with the observation that unpleasant odor from the mud was found in the Ariake Sea tidal flats. These fishermen thought that the observed unpleasant odor was toxic and harmful to the *Agemaki* shells and *Tairagi* shells. The preliminary investigations have shown that the sea laver acid treatment practice would be one of the mostly possible causes for the mud deterioration (Ushihara 2002). However, so far, detailed studies on how the acid treatment agent of the sea laver affects the geoenvironmental properties of the mud, have not received sufficient attention. This raises the question of whether the acid treatment practice has caused the significant change in the geoenvironmental properties of the Ariake Sea mud, and consequently disturbed the ecosystem balance for those benthos inhabiting the shallow depth of the mud.

The purpose of this study is to investigate the possible effects of acid treatment practice on the geoenvironmental properties of the tidal flat muds in the Ariake Sea. The field investigation and the laboratory test results are presented. Based on the observed test results, the possible reason for the decrease in the catch of the benthos living in the shallow depth of the muds is discussed.

Background of Acid Treatment Practice

Each year, during the period of January to March, the acid treatment agent is used by the local sea laver farmers as the disinfectant acid to treat the sea lavers cultivated in the sea. This acid treatment practice has been widely undertaken all over Japan from 1977 to present. In the Kyushu region before 2002, the residual acid treatment agents were directly dumped into the Ariake Sea without any pretreatment. According to the unpublished data from the Ministry of Agriculture, Forest and Fisheries of Japan, during the period of 1977 to 2001, annually about 2900 tons of acid has been dumped into the Ariake Sea water within the sea laver farming areas. Since 2002, in some Kyushu regions such as Saga Prefecture, the direct dumping of the acid treatment agent into the Ariake Sea has been strictly controlled. The residues of the acid treatment agent are required to be treated to lower its acidity and sufficiently dilute its concentrations before finally being dumped into the Ariake Sea. The chemical compositions of the acid treatment agent are varied depending on the areas. The one used in the Saga Prefecture has the main chemical compositions of 18 % of DL-Malic Acid ($HOOCCHOHCH_2COOH$), 15 % of ammonia sulfate $[(NH_4)_2SO_4]$, 14 % of sodium dihydrogenphosphate (NaH_2PO_4), 1 % of amino acid, 0.6 % of coloring matter. The pH of the acid treatment agent used in the Saga Prefecture is about 2.0.

Description of Study Area

Two tide flat areas in the Ariake Sea, the Iida and Higashiyoka sites, were selected as study areas. Figure 2 shows the locations of the two sites. Before setting the study areas, the field investigations have been undertaken. The results show that the Iida site mud seems to be the most affected caused by the acid treatment practice, whereas the Higashiyoka site appears to be the least affected in terms of two aspects: (1) the mud samples at the Iida site gave out a strong unpleasant odor [which is thought to be the gas-phased hydrogen sulfide (H_2S)], whereas the mud samples at the Higashiyoka site did not give out an unpleasant odor; and (2) the sulfide content of the mud at a depth of 0–20 cm at the Iida site is much higher. According to the Fishery Water Quality Standard (Japan Fisheries Resource Conservation Association 2000), higher sulfide contents are harmful to the benthos such as *Agemaki* and *Tairagi* shells living in the mud. 0.2 mg/g is the safe limit of the mud sulfide content for the benthos living in the shallow depth of the mud, as suggested by the Fishery Water Quality Standard. The field investigation shows that for the

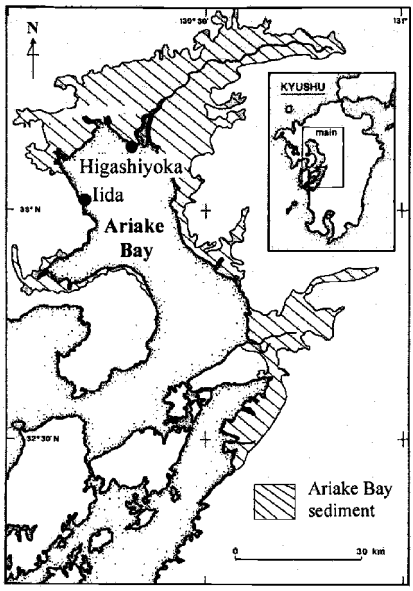

FIG. 2—*Location map of the study areas (after Ohtsubo et al. 1995).*

Iida site mud, the sulfide content at the depth of 0–20 cm is higher than this limit. Based on these field investigation results, the Iida and Higashiyoka sites were selected as the study areas.

Test Methods

Field Investigation

Undisturbed samples were obtained by pushing a 20 cm diameter PVC pipe down in the muds at a depth of about 20 cm at both the Iida and Higashiyoka sites. The samples were extruded and sliced to measure the salt concentration, pH, and sulfide content. The measured results are depicted in Figs 3, 4, and 5,

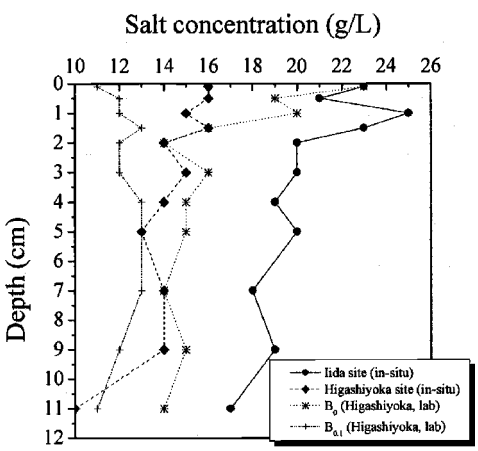

FIG. 3—*Variation of the salt concentration with depth for the Ariake Sea muds.*

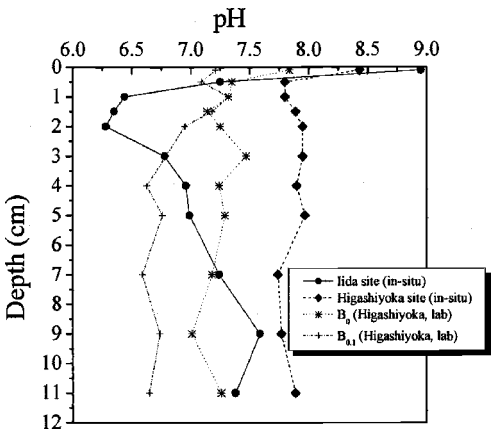

FIG. 4—*Variation of pH with depth for the Ariake Sea muds.*

respectively. The reason for measuring pH and sulfide content is mainly because these two geochemical indexes can well represent the inhabiting conditions of the benthos (Japan Fisheries Resource Conservation Association 2000). The reason for measuring the salt concentration is mainly because that previous study indicated that the change in the Ariake Sea mud salt concentration could represent the change in the Ariake Sea mud pH (Ohtsubo et al. 1996). The pH was measured using a portable pH meter HORIBA D-52. The measuring process consists of inserting the probe of the pH meter in the mud with a shallow depth, 0.5 cm, and read the value from the display. The salt concentration was measured using the compact salt meter HORIBA C-121. This salt meter is capable of making accurate measurements of sodium chloride (NaCl) concentration from a single-drop mud sample. The measuring of the mud sulfide content was based on the standard method prescribed by the Japan Fisheries Resource Conservation Association (1980). Briefly, measuring sulfide content consists of placing 0.1 g of mud at field moisture content on a fine porous disk placed in a 10 mL glass tube. Two millilitres of diluted sulfuric acid (H_2SO_4) (1 mL of distilled water is mixed with 1 mL of H_2SO_4 with concentration of 18 N) was put on the mud sample, and the generated H_2S (gas phase) was collected. The weight of the resulted H_2S was measured and expressed as milligrams per grams of the mud. These studies were performed in mud samples from the top 12 cm only.

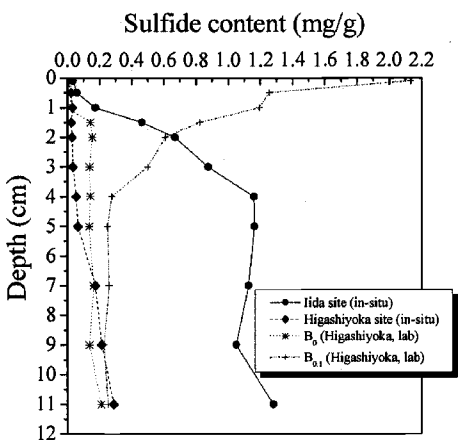

FIG. 5—*Variation of the sulfide content with depth for the Ariake Sea muds.*

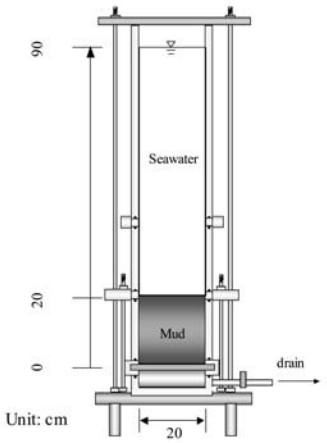

FIG. 6—*A schematic of apparatus setup for laboratory test.*

Laboratory Investigation

In order to better understand the effect of acid treatment practice on the muds at the Iida site, the laboratory one-dimensional infiltration tests were performed. The infiltration test was thought to simulate the field scenario in which the dumped acid treatment agent in the Ariake Sea infiltrates through the Iida muds during the high tide period. About 6 kg of mud at the field moisture content taken from the Higashiyoka site was thoroughly mixed with the seawater. The slurry was poured into a 20 cm diameter acrylic cylinder (see Fig. 6) and the remaining portion of the cylinder was filled up to 90 cm with the seawater.

Two parallel tests were conducted over a period of 30 days. In one test, called herein B_0, the seawater was continuously drained from the base of the setup (see Fig. 6) and every day the sea water level was brought up to the 90 cm mark. This process was repeated for 30 days after which the water above the mud was drained away and the sample extruded and sliced for determining salt concentration, pH, and sulfide content. The results are depicted in Figs 3, 4, and 5, respectively. For this test, B_0 means the concentration of the acid treatment agent was 0 %. Another test, called herein as $B_{0.1}$, was carried out with the seawater mixed with the acid treatment agent with the concentration of 0.1 % (by volume of water). The acid treatment agent used in the laboratory test has the same composition with that used in the field of the Saga Prefecture. Its pH value is about 2.0. The sample was subjected to the same process as described in the case of B_0 test. After 30 days of acid treatment, the seawater was again fully drained, and the mud sample was extruded and sliced for determination of salt concentration, pH, and sulfide content. These results are also shown in Figs 3, 4, and 5, respectively.

In addition to 0.1 % acid treatment agent of Higashiyoka mud, a similar test was conducted at 0.01 and 0.03 %. The variation of sulfide content with acid concentration is depicted in Fig. 7.

Results and Discussions

Figure 3 indicates that the salt concentrations of the mud at the Iida site are larger than those of the muds at the Higashiyoka site. The pH of the mud at the Iida site is lower than that of the mud at the Higashiyoka site (Fig. 4). The sulfide content of the mud at the Iida site is higher than that of the mud at the Higashiyoka site (Fig. 5). The results in Figs 3–5 for the Iida site and the Higashiyoka site are for the month of November 2002.

Figures 3, 4, and 5 also compare the in situ conditions at the Iida and Higashiyoka sites with the results of laboratory simulation tests B_0 and $B_{0.1}$. It is noted that during the B_0 test, the salt concentration increased and pH decreased as compared to the original Higashiyoka mud (Figs. 3 and 4, respectively). The treatment of the Higashiyoka mud with the acid treatment agent, $B_{0.1}$ test, has resulted in a significant

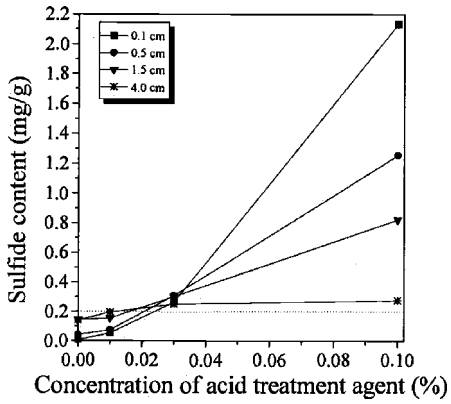

FIG. 7—*Relationship between the sulfide content and the concentration of acid treatment agent from laboratory tests.*

decrease in the salt concentration. This reduction in the mud salt concentration and pH values as a result of acid treatment seems to have also occurred at the Iida site, as discussed later.

The sulfide content in the case of the Higashiyoka mud after treatment of the acid treatment agent ($B_{0.1}$ test) are significantly higher than the original low values, especially at the depth of 0–4 cm (Fig. 5). At the depth of 4–12 cm, the sulfide content is practically constant. The $B_{0.1}$ test results would suggest that the Iida site muds, affected by the continued acid treatment practice over a long period (between 1977 and 2001 as shown in Fig. 1), would have undergone changes similar to those experienced by the Higashiyoka mud in the laboratory study. On the basis of such observations, it is thought that the sulfide content in the case of the Iida muds also would have shown an increasing trend, similar to one noted for $B_{0.1}$ test (Fig. 5) at the depth of 0–4 cm in the mud during the continued acid treatment practice period. Such a result seems to be plausible for explaining the phenomenon that the catch of the *Agemaki* and *Tairagi* shells living in the shallow depths of the mud decreased during the period of acid treatment practice, as depicted in Fig. 1.

Based on the observations, it may be suggested that as a result of acid treatment practice in the sea laver farming areas, the Iida site muds experienced significant changes: decrease in salt concentration, decrease in pH values, and increase in the sulfide content. The increase in the sulfide content with the acid treatment agent concentration, based on the laboratory infiltration tests, is depicted in Fig. 7. For the sake of comparison, the sulfide content=0.2 mg/g threshold level (thought to be the safe limit for the benthos living in the shallow depth of the mud) is also shown in Fig. 7. The decrease in the sulfide content at the depth of 0–4 cm of the Iida site mud (Fig. 5), in contrast to the increase observed in the $B_{0.1}$ test, may be partly due to the result of the strictly controlled acid treatment practice since 2002. It would appear that this change in the acid treatment practice since 2002 has resulted in the decrease in the mud sulfide content and consequently the improvement of the inhabiting condition for the benthos living in the shallow depth of the mud. A recent field investigation shows that there are some indications of recovery of the benthos at the Iida site.

The observed changes in salt concentration and pH values as a result of acid treatment are better visualized by examining the relationship between pH and salt concentration for these muds, both in field and laboratory situations. Figure 8 depicts the decrease in pH with increasing salt concentration, based on field data for the Megurie site which is very close to the Iida site (Ohtsubo et al. 1996), and the laboratory test for another Ariake Sea mud sample (Kanayama et al. 2000). The original Higashiyoka mud (thought to be much less affected by the acid treatment practice in the field) fits the observed field and laboratory trends, while most of the data from the Iida site and $B_{0.1}$ test are located below the trends.

Superposed on these trends are the results of changes in the salt concentration and pH as a result of acid treatment ($B_{0.1}$ test) for Higashiyoka mud. Two significant results were observed: first, the treatment with acid treatment agent reduces the salt concentration and pH values (almost down to 6.5); and second, these changes do not follow the trends shown in Fig. 8. Also shown are the results for the affected Iida site

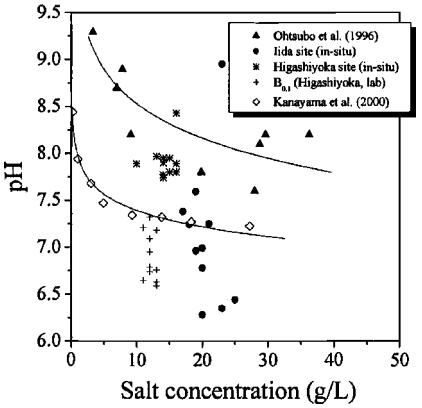

FIG. 8—*pH-salt concentration relationship for the Ariake Sea muds.*

mud. Once again it was observed that changes at the Iida site are well simulated by the $B_{0.1}$ test, and the earlier discussions of the similarity in the mud sulfide profiles between the Iida site and the laboratory test $B_{0.1}$, seems justified.

The relationship between the sulfide content and pH for these muds is depicted in Fig. 9. The laboratory data from $B_{0.1}$ test suggests an increase in the sulfide content with a decrease in pH as a result of acid treatment of the original Higashiyoka site mud. Also superposed are the results of the affected Iida site mud. The values of pH higher than 7.0 in the case of the Iida mud (at shallow depth), and the reduced sulfide content are indications of some possible recovery following the strictly controlled acid treatment practice since 2002. A value of $R^2=0.726$ indicates that the pH appear to be one of the important factors controlling the sulfide content when these muds are treated with the acid treatment agent.

Conclusions

This paper presents an investigation of the effect of the acid treatment practice on the geoenvironmental properties of the Ariake Sea mud. The field/laboratory test is undertaken to investigate the effect of the acid treatment agent on the salt concentration, pH, and sulfide content of the muds. Results of this study show that in the sea laver farming areas of the Ariake Sea tidal flats, the acid treatment practice during the long period of 1977 to 2001 had impacts on the geo-chemical balance of these muds. Consequences of the

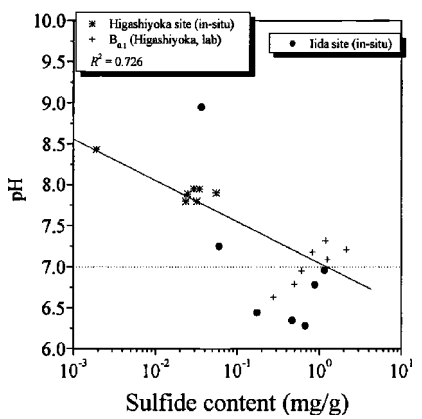

FIG. 9—*Relationship between pH and sulfide content for the Ariake Sea muds.*

acid treatment practice resulted in a significant reduction of the salt concentration and pH values and an increase of the sulfide content. The sulfide content increased to the levels even higher than the safe limit for the benthos inhabiting the shallow depth of the mud. This change in the geoenvironmental properties of the Ariake Sea mud, seems to be plausible in explaining the recorded decrease in the catch of some benthos living in the shallow depth of the mud.

Acknowledgments

The authors thank Dr. Yudhbir, the former guest professor of the Institute of Lowland Technology, Saga University, for his comments. Thanks are also due to Mr. Ushihara, U., a former graduate student of Saga University, for his help with performing the tests. This work is financially supported by a large grant research project entitled "Technological Development for Bottom Sediment Improvement and Benthos Restoration in Ariake Sea" founded by Bio-oriented Technology Research Advancement Institution (BRAIN), Japan.

References

Araki, H., Vongthanasunthorn, N., Koga, K., Yamanishi, H., and Ohgushi, K., "Water Quality and Simulation by the Box Model in the Ariake Sea (in Japanese)," *Environmental Engineering Research*, 39, 229–234 (2002).

Japan Fisheries Resource Conservation Association, *The Method for the Testing of Water Pollution* (in Japanese), Kouseisha-kouseikaku Corporation, 1980.

Japan Fisheries Resource Conservation Association, *Fishery Water Quality Standard* (in Japanese), Kouseisha-kouseikaku Corporation, 2000.

Kanayama, M., Ohtsubo, M., Higashi, T., Hiyama, H., and Takayama, M., "Effects of Pore Water Salinity on the Consolidation Characteristics of Clay," *Proceeding of International Symposium on Lowland Technology*, Saga, 2000. pp. 113–120.

Koga, K., Vongthanasunthorn, N., Araki, H., Yamanishi, H., Kawabe, M., and Ohwa, N., "Study on Water Quality Analysis in the Reservoir of Isahaya Bay Land Reclamation Project (in Japanese)," *Environmental Engineering Research*, 40, 541–550 (2003).

Ohtsubo, M., Egashira, K., and Kashima, K., "Depositional and Post-Depositional Geochemistry, and its Correlation with Geotechnical Properties of the Marine Clays in Ariake Bay, Japan," *Geotechnique*, 45, 263–282 (1995).

Ohtsubo, M., Egashira, K., and Takayama, M., "Mineralogy and Chemistry, and Their Correlationship with the Geotechnical Properties of Marine Clays in Ariake Bay, Japan: Comparison of Quick and Nonquick Clay Sediments," *Marine Georesources and Geotechnology*, 14, 263–282 (1996).

Yamanishi, H., Araki, H., Koga, K., and Kimitoshi, S., "Study on Water Quality and Mud Property in Inner Part of the Ariake Sea (in Japanese)," *Environmental Engineering Research*, 39, 219–227 (2002).

Ushihara, U., Hayashi, S., Hino, K., Du, Y. J., and Setoyama, J., "Fundamental Study on the Change in the Geoenvironmental Properties of the Ariake Sea Mud (in Japanese)," *Proceeding of 57th Annul Conference of Japanese Society of Civil Engineers*, 2002, pp. 699-670.

Journal of ASTM International, Vol. 3, No. 6
Paper ID JAI13336
Available online at www.astm.org

Masaru Mizoguchi,[1] *Yuji Abe,*[2] *Noriko Yamaguchi,*[3] *and Tsuyoshi Miyazaki*[4]

Cadmium Transport in Volcanic Ash Soil during Citric Acid Solution Flow

ABSTRACT: Cadmium contamination of soil is one of the most serious environmental problems in Japan. As basic research toward the development of a decontamination method to remove cadmium from soil, cadmium transport has been measured in a volcanic ash soil during citric acid solution flow. After a soil column that was polluted artificially by cadmium nitrate was saturated with distilled water, citrate solution was passed through the soil column. Leachate from the soil column was collected for the measurement of cadmium concentration. At the end of the flow experiment, the soil column was sliced into 2-cm-thick pieces and the residual cadmium in soil was analyzed. As a result, it was found that the higher the concentration of citrate, the faster the cadmium discharged from the soil. This result can be explained in terms of the downward movement of the soluble complex of citrate with cadmium in the soil.

KEYWORDS: cadmium transport, citric acid, decontamination, soluble complex, volcanic ash soil

Introduction

Soil polluted by heavy metals is hard to clean up because the heavy metals are strongly associated with soil particles. Some symptomatic decontamination methods, such as soil dressing or solidification, are predominantly used at sites that require clean-up. The number of sites identified as being polluted is increasing and people are beginning to become concerned regarding environmental contamination of the land. Therefore, clean-up technologies to decontaminate polluted soils should be developed.

Organic acids have shown the potential with respect to the desorption of cadmium adsorbed to soil particles (Cieslinski et al. 1998) because organic acids form soluble complexes with metals (Krishnamurti et al. 1997). Therefore, we herein examine a method of leaching cadmium from polluted soil using organic acid. The method examined herein is to collect cadmium by washing polluted soil with organic acid. However, a number of questions remain. For example, how much cadmium can be desorbed from the polluted soil during organic solution flow? Moreover, how does the desorbed cadmium move in the soil? Kedziorek et al. (2000) investigated solubilization of cadmium during the percolation of EDTA though a polluted soil column, but no one has investigated cadmium transport during the percolation of natural organic acid through a polluted soil column.

In the present study, we investigate the effect of citric acid, which is often secreted by plant roots in the rhizosphere, on the desorption and transport of cadmium in the soil as basic research in order to develop a decontamination method for removing cadmium from the soil.

Manuscript received April 1, 2005; accepted for publication August 29, 2005. Presented at ASTM Symposium on Contaminated Sediments: Evaluation and Remediation Techniques on 23–25 May 2006 in Shizuoka, Japan; M. Fukue, K. Kita, M. Ohtsubo, and R. Chaney, Guest Editors.

[1] Associate Professor of Soil Physics and Soil Hydrology, Dept. of Biological and Environmental Engineering, The University of Tokyo, 1-1-1 Yayoi, Bunkyo-ku, Tokyo 113-8657, Japan.

[2] Graduate Student of Soil Physics and Soil Hydrology, Dept. of Biological and Environmental Engineering,The University of Tokyo, 1-1-1 Yayoi, Bunkyo-ku, Tokyo 113-8657, Japan.

[3] Senior Researcher of Soil Environmental Chemistry, National Institute for Agro-environmental Sciences, 3-1-3 Kan-nondai, Tsukuba, Ibaraki 305-8604, Japan.

[4] Professor of Soil Physics and Soil Hydrology,Dept. of Biological and Environmental Engineering, The University of Tokyo, 1-1-1 Yayoi, Bunkyo-ku, Tokyo 113-8657, Japan.

TABLE 1—*Soil properties.*

Bulk Density, Mg/m^3	Soil Particle Density, Mg/m^3	pH (H_2O)	pH (KCl)	Total C, 10 g/kg	Total N, 10 g/kg	CEC, $cmol_c/kg$	Specific surface area[a], m^2/g
0.78	2.56	6.62	5.65	4.4	0.38	20.2	135

Exchangeable Cations, cmolc/kg				Acid Ammonium Oxalate, 10 g/kg			Dithionite-citrate-Bicarbonate, 10 g/kg			Na-pyrophosphate, 10 g/kg	
Ca	Mg	K	Na	Si_{ox}	Al_{ox}	Fe_{ox}	Si_d	Al_d	Fe_d	Al_p	Fe_p
14	2.8	1.4	0.6	0.60	1.15	2.13	0.68	2.49	2.43	0.50	0.09

[a]Specific surface area was determined by the BET method based on N_2 adsorption.

Materials and Experimental Methods

Materials

Andosol samples (Melanudant) were taken from the plowed layer (0–20 cm) of experimental upland fields of the University of Tokyo, Nishi-Tokyo, Japan. The soils were air-dried and passed through a 2 -mm sieve. Relevant soil properties are given in Table 1 (Editor's Commission of Method of Soil Analysis, 1996).

Batch Experiment

Sorbate solutions were prepared by dissolving $Cd(NO_3)_2$ in 15 mmol L^{-1} $NaNO_3$ and the pH was adjusted to 4, 5, 5.5, and 6 by the addition of 15 mmol L^{-1} of HNO_3 or NaOH dissolved in 15 mmol L^{-1} of $NaNO_3$. The initial concentrations of Cd were 0.2, 0.4, 0.6, 0.8, and 1.0 mmol L^{-1}, respectively. Ten milliliters of the sorbate solution were added to 0.5 g of soil and the suspension was shaken for 24 h. After pH measurement, the suspension was centrifuged (5000 rpm, 10 minutes) and filtered through a 0.22-μm membrane filter (Sartorius SM 16534K). The cadmium concentration in the filtrate was determined using an atomic absorption spectrometer (AAS, SHIMADZU AA-680). The sorption amounts of Cd were calculated by subtracting the moles of Cd initially added to the soil from the moles of Cd remaining in the filtrate solution after reaction for 24 h.

The sedimented soil after the sorption experiment was washed using 10 mL of deionized distilled water and was centrifuged at 5000 rpm for 10 min. Then, 10 mL of citric acid solution (25, 50, 100, 200, and 400 mmol L^{-1}) were added and shaken for 1 h. The suspension was centrifuged at 5000 rpm for 10 min and was filtered through a 0.22-μm membrane filter. The concentration of Cd was determined by AAS in order to estimate the desorption amounts of Cd.

Flow Experiment

The soil was packed with a bulk density of 0.80 Mg/m^3 in an acrylic tube with a height of 10 cm and a diameter of 5 cm. The hydraulic conductivity of the packed soil was 3.3×10^{-4} cm/s. Two soil columns were prepared for a laboratory experiment. One was a column of which the top layer (2 cm) was artificially polluted by cadmium nitrate, and the other was a column of which the bottom layer (2 cm) was polluted. In order to make the polluted soil layer, a 1.5 pore volume of cadmium nitrate solution (0.6 or 0.2 mmol L^{-1}) was passed upward through the soil column to drive out the air in the soil. After distilled water was passed though the polluted soil column for 6 h to remove the residual cadmium in the soil pores, a citrate solution (0, 25, 100, and 400 mmol L^{-1}) was passed through the soil column under a constant hydraulic head of 56 cm, or a hydraulic gradient of 5.6. Leachate from the soil column was then collected at a certain time interval for the measurement of cadmium concentration (Fig. 1). At the end of the flow experiment, the soil column was sliced into 2-cm-thick pieces and the acid soluble fraction of the residual cadmium in the soil was analyzed by 0.1 mol L^{-1} HCl extraction (Editor's Commission of Method of Soil Analysis, 1996).

The experimental conditions of the flow experiment are given in Table 2. In the table, "Time" denotes the time that the citrate solution was flowed in the soil column. The concentration of the citrate solution was 100 mmol L^{-1} for each run, except for Runs 1 and 3, which were conducted in order to determine the

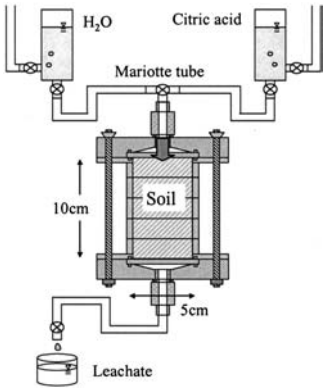

FIG. 1—*Schematic diagram of the flow experiment for a Cd-contaminated soil column.*

influence of the citrate concentration. Runs 1–4 were flow experiments for the soil column with a contaminated bottom layer, and Runs 5–8 were flow experiments for the soil column with a contaminated top layer.

Results and Discussion

Adsorption Isotherms of Cadmium to Soil

Figure 2 shows the adsorption isotherms of cadmium to Andosol for each pH. The adsorption isotherm denotes the relationship between the amount of cadmium adsorbed by soil, W (mmol/kg), and the equilibrium concentration of cadmium nitrate, C_i (mmol L^{-1}):

$$W = \frac{C_0 - C_i}{M}$$

where C_0(mmol L^{-1}) is the initial concentration of the cadmium nitrate solution, and M(kg L^{-1}) is soil concentration in the cadmium nitrate solution. The dots denote experimental data, and the solid lines are the fitting lines based on the following Langmuir model:

$$W = W_s(bC_i)^n/[1 + (bC_i)^n]^{m/n}$$

where W_s is the saturated amount of cadmium adsorbed by the soil (mmol kg^{-1}), b is the equilibrium adsorption constant, and m and n are adsorption constants.

The experimental data are in good agreement with the Langmuir model. The amount of cadmium adsorbed into soil increased with pH because the negative charge of the soil surface increased with pH.

TABLE 2—*Experimental conditions and various results of the flow experiments.*

Run	Site	Cd Conc., mmol/L	Citrate Conc., mmol/L	Time, hour	80%p.v.[a]	Max Cd Conc.,[b] mmol/L	p.v. at the Max Cd Conc.[c]
1	bottom	0.6	400	18	1.8	0.76	0.9
2	bottom	0.6	100	18	2.9	0.56	1.2
3	bottom	0.6	25	18	8.1	0.13	2.4
4	bottom	0.2	100	18	4.0	0.08	1.6
5	top	0.6	100	6	…	…	…
6	top	0.6	100	18	…	…	…
7	top	0.6	100	40	16.3	0.08	6.0
8	top	0.6	0	38	…	…	…

[a]Pore volume (p.v.) required to remove 80% of the cadmium in the soil column.
[b]Maximum cadmium concentration in the leachate.
[c]Pore volume at which the leachate Cd concentration is maximum.

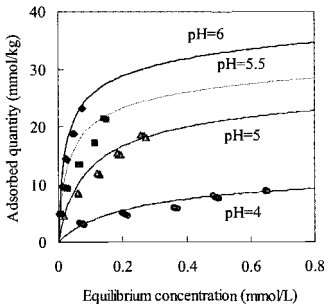

FIG. 2—*Adsorption isotherms.*

Desorption Rate of Cadmium

Figure 3 shows the relationship between the desorption rate of cadmium and citrate concentration. The desorption rate of cadmium increased with citrate concentration, and approached a constant value. The cadmium desorption rate from polluted soil by citrate was more than 80%, independent of the initial concentration of cadmium adsorbed. This result suggests that citrate could extract cadmium adsorbed onto the soil particles by forming a soluble complex with cadmium, but that some cadmium remains on soil particles. In the batch experiment, an amount of citrate 33 to 1600 times greater than the amount of cadmium sorbed on the soil (molar basis) was added in order to remove cadmium from the soil. Assuming that no citrate was sorbed onto the soil or complexed with metals other than cadmium, divalent cadmium that was not complexed with citrate (Cd^{2+}) was not present in solution based on MINEQL calculation. Since sufficient amounts of citrate to complex with cadmium existed, variations in pH between 4 to 7 did not influence the speciation of citrate-cadmium complex in the solution. A fraction of the added citrate was likely to be sorbed on the soil or complexed with metals such as Fe and Al. At lower citric acid concentrations, less citrate would be available to be complexed with the sorbed cadmium on the soil.

Breakthrough Curve and Desorption Rate of Cadmium

Figure 4 shows the breakthrough curves, which represent the cadmium concentration of leachate as a function of pore volume. Figure 5 shows the cadmium desorption rate, which is defined as a ratio of desorption to the initial adsorption amounts of cadmium. From comparison of Runs 2 and 4, it was found that the maximum Cd concentration in the leachate was higher in the column that was polluted by the 0.6 mmol L^{-1} cadmium nitrate solution compared to that polluted by the 0.2 mmol L^{-1} cadmium nitrate solution and that 10-pore volume of citrate solution was sufficient in order to remove most of the cadmium from the polluted soils. In addition, comparison of Runs 1 through 3 revealed that as the citrate concentration increased, the cadmium discharge from the soil became faster. Moreover, as the concentration of the citrate solution increased, the maximum Cd concentration in the leachate increased and the volume of

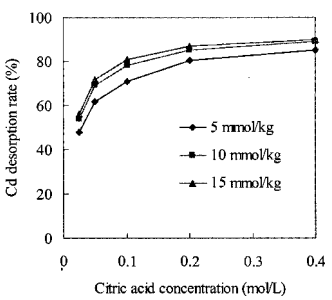

FIG. 3—*Cd desorption rate as a function of citric acid concentration.*

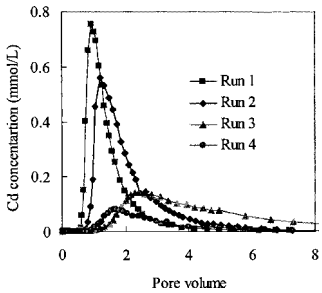

FIG. 4—*Breakthrough curves of Cd.*

the citrate solution required to remove 80% of cadmium from the polluted soil decreased (Fig. 6). These results suggest that as the citrate concentration increased, the soluble complex with cadmium was formed more easily.

Transport of Cadmium in Soil

Figure 7 shows the relationship between cadmium desorption rate and pore volume for the top or bottom layer polluted soil column. The volume of 100 mmol L^{-1} citrate solution required to remove 80% of cadmium from the soil column was 5.6 times larger for the top layer polluted soil column (16.3 p.v.) than the bottom layer polluted (2.9 p.v.). Considering that no desorption occurred due to distilled water (Run 8), this result suggests that cadmium desorbed by citrate from soil particles at the top layer to form a soluble complex of citrate and moved downward. Because of the downward movement of the soluble complex, more citrate solution might be required for the top layer polluted soil column.

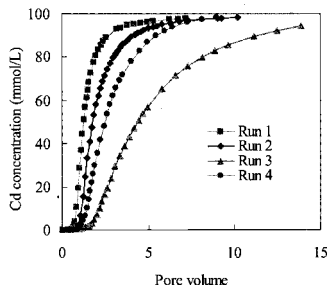

FIG. 5—*Cd desorption rate as a function of pore volume.*

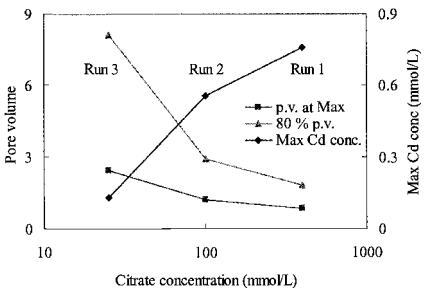

FIG. 6—*Maximum Cd concentration in leachate and pore volume of citrate solution required in order to remove 80% of cadmium from polluted soil.*

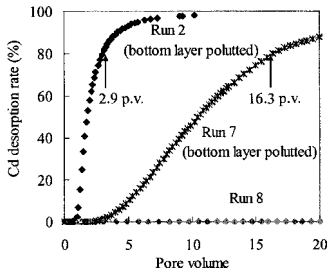

FIG. 7—*Cd desorption rate as a function of pore volume.*

Figure 8 shows the residual cadmium distributions in the soil columns with the top layer polluted after citrate solution flow for 0, 6, 18, and 40 h (Runs 5–7). Figure 9 shows the mass balance of the cadmium performed to compare initial and final analysis. The error of the mass balance was at most 10%. As the citrate solution flowed, the cadmium concentration in the top layer decreased while the cadmium concentrations in the lower layers increased. The cadmium distribution became linear, and eventually 90% of the cadmium was removed after 40 h (21 p.v.). This result indicates that the soluble complex of cadmium formed by citrate in the top layer moves downward and flowed out of the soil column. However, in order to clarify the flow mechanism of such a soluble complex in soil, we need to study the soluble complex transport including the chemical reaction of citrate and cadmium.

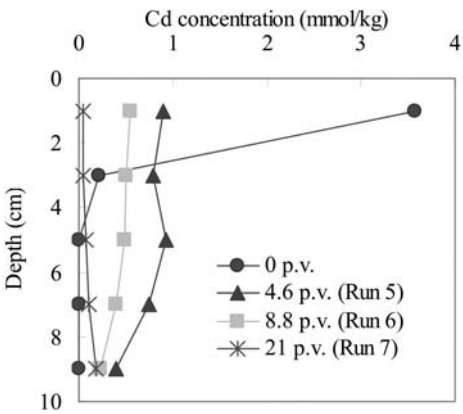

FIG. 8—*Changes in Cd distribution in the soil with a contaminated top layer (0–2 cm).*

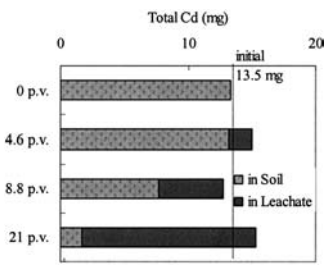

FIG. 9—*Mass balance of the cadmium.*

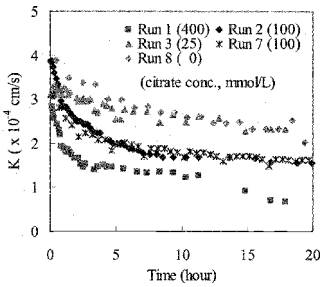

FIG. 10—*Change in hydraulic conductivity of soil.*

Changes in Hydraulic Conductivity of Soil

Figure 10 shows changes in hydraulic conductivity (K) of soil with time. K decreased gradually with time. Although it is difficult to compare the absolute values of K because the initial Ks were different for each experiment, the decrease of K was fast as the citrate concentration became high. Kedziorek et al., (2000) pointed out the importance of peptization, which induces the formation of colloids and clogging of the porous medium in their EDTA solution percolation experiment. In addition, they also observed the retarded elution of Fe and Ca that are originally contained in soil. The decrease of K with time is most likely due to the clogging of the soil, which is caused by the formation colloids and their downward movement. In fact, the color of the leachate changed yellow with time, as shown in Fig. 11. Figure 12 shows absorbance of the leachate at 400 nm. The absorbance increased with time, and approached a constant value which became large with the citrate concentration. The change in the color of the leachate may be related to dissolution of Fe as citrate-Fe complex. However, more study is needed with regard to the formation of colloids.

Conclusions

The effect of citric acid on the desorption and transport of cadmium in soil was investigated as a basic study toward the development of a decontamination method to remove cadmium from soil. From batch and flow experiments, it was found that (1) the cadmium desorption rate from polluted soil ($<$15 mmol/kg) by citrate was more than 80%, independent of the initial concentration of cadmium

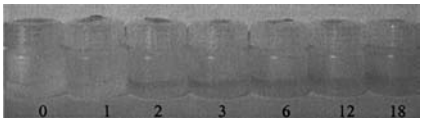

FIG. 11—*Change in color of the leachate at 0, 1, 2, 3, 6, 12, and 18 h (Run 1).*

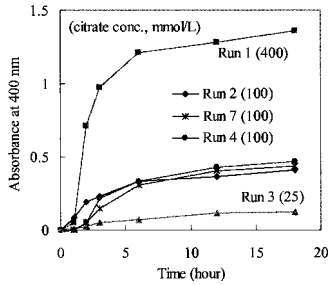

FIG. 12—*Absorbance of the leachate at 400 nm.*

adsorbed; (2) the volume of citrate solution required to remove cadmium from polluted soil decreased as the concentration of citrate solution increased; (3) a longer time was required to remove cadmium from the soil with the top layer polluted than the bottom layer polluted; (4) cadmium desorbed by citrate to form a soluble citrate-cadmium complex and moves downward in soil; and (5) hydraulic conductivity of the soil decreased according to the citrate concentration during the solution flow.

References

Cieslinski, G., Van Rees, K. C. J., Szmigielska, A. M., Krishnamurti, G. S. R., and Huang, P. M., "Low-Molecular-Weight Organic Acids in Rhizosphere Soils of Durum Wheat and Their Effect on Cadmium Bioaccumulation," 1998, *Plant Soil*, Vol. 203, No. 1, pp. 109–117.

Editors Commission of Method of Soil Analysis, 1996, "Methods of Soil Analysis Part 3 Chemical Methods."

Kedziorek, M. A. M., and Bourg, A. C. M., 2000, "Solubilization of Lead and Cadmium during the Percolation of EDTA through a Soil Polluted by Smelting activities," *J. Contam. Hydrol.*, Vol. 40, No. 4, pp. 381–392.

Krishnamurti, G. S. R., Cieslinski, G., Huang, P. M., Van Rees, K. C. J., 1997, "Kinetics of Cadmium Release from Soils as Influenced by Organic Acids: Implication in Cadmium Availability," *J. Environ. Qual.*, Vol. 26, No. 1, pp. 271–277.

Journal of ASTM International, Vol. 3, No. 7
Paper ID JAI13328
Available online at www.astm.org

Seiji Iwasaki,[1] *Makiko Sakka,*[2] *Tetsuya Kimura,*[3] *Kazuo Sakka,*[4] *Tomonari Matsuda,*[5] *and Saburo Matsui*[6]

Current Status of Estrogenlike Compounds in Sediments in Enclosed Sea Areas

ABSTRACT: The concentrations of estrogenlike compounds in sediment were surveyed in Ise Bay and Ago Bay, which are typical of enclosed sea areas. Fourteen sediment samples were collected from the deepest part at the entrances to these bays. The examination of estrogenlike compounds was performed by a yeast screen assay developed by Professor J. P. Sumpter. The highest concentrations of estrogenlike compounds of sediment were found in the deepest part of Ise Bay (6.54 μg kg^{-1}), and quantified as 17β-estradiol (E2) active equivalent. The concentration gradually decreased approaching the entrance of the bay from the deepest part of the bay. It was suggested that this decrease could be the result of biodegradation. The sediment assay samples were fractionated by high performance liquid chromatography and assayed to determine the chemical species of estrogenlike compounds. The detected estrogenlike compounds corresponded with E1 and E2, and were found in all of the samples. They are typical natural female hormones, and their origin is presumably domestic sewage and other wastewater containing feces and urine.

KEYWORDS: estrogenlike compounds, enclosed sea areas, 17β-estradiol (E2), estrone (E1), total organic carbon (TOC)

Introduction

Endocrine disrupting chemicals in the environment have become an issue of public concern (Ahel et al. 1994, 1996; Desbrow et al. 1998). In particular, the biological effects of estrogenlike compounds in water are serious issues. As many estrogenlike compounds are present in water (Ahel et al. 1994, 1996; Desbrow et al. 1998), examination of these compounds by instrumental analysis requires great cost and effort. Bioassay is used for the examination of toxic compounds in the environment, including estrogenlike compounds in water (Routledge et al. 1996). Since the degree of toxicity in samples can be easily measured at low cost using a bioassay, this method is considered suitable to screen for estrogenlike compounds. However, it is difficult to identify chemicals with endocrine-disrupting activity by conventional bioassay.

In this study, we applied a new bioassay system to analyze estrogenlike compounds, consisting of a bioassay using genetically modified yeast expressing human estrogen receptor (hER) (yeast method) combined with high performance liquid chromatography (HPLC), in which the advantages of instrumental analysis and bioassay are combined (Iwasaki et al. 2004). Then we surveyed estrogenlike compounds in sediment samples from Ise Bay and Ago Bay, which are typical of enclosed sea areas.

Manuscript received May 2, 2005; accepted for publication December 15, 2005. Presented at ASTM Symposium on Contaminated Sediments: Evaluation and Remediation Techniques, on 23–25 May 2006 in Shizuoka, Japan; M. Fukue, K. Kita, M. Ohtsubo, and R. Chaney, Guest Editors.

[1] Graduate Student, Faculty of Bioresources, Mie University, Tsu 514-8507, Japan.
[2] Research Engineer, Faculty of Bioresources, Mie University, Tsu 514-8507, Japan.
[3] Professor, Faculty of Bioresources, Mie University, Tsu 514-8507, Japan.
[4] Professor, Faculty of Bioresources, Mie Universiyt, Tsu 514-8507, Japan.
[5] Professsor, Department of Technology and Ecology Graduate School of Global Environment Studies, Kyoto University, Kyoto, 606-8501, Japan.
[6] Professsor, Department of Technology and Ecology Graduate School of Global Environment Studies, Kyoto University, Kyoto, 606-8501, Japan.

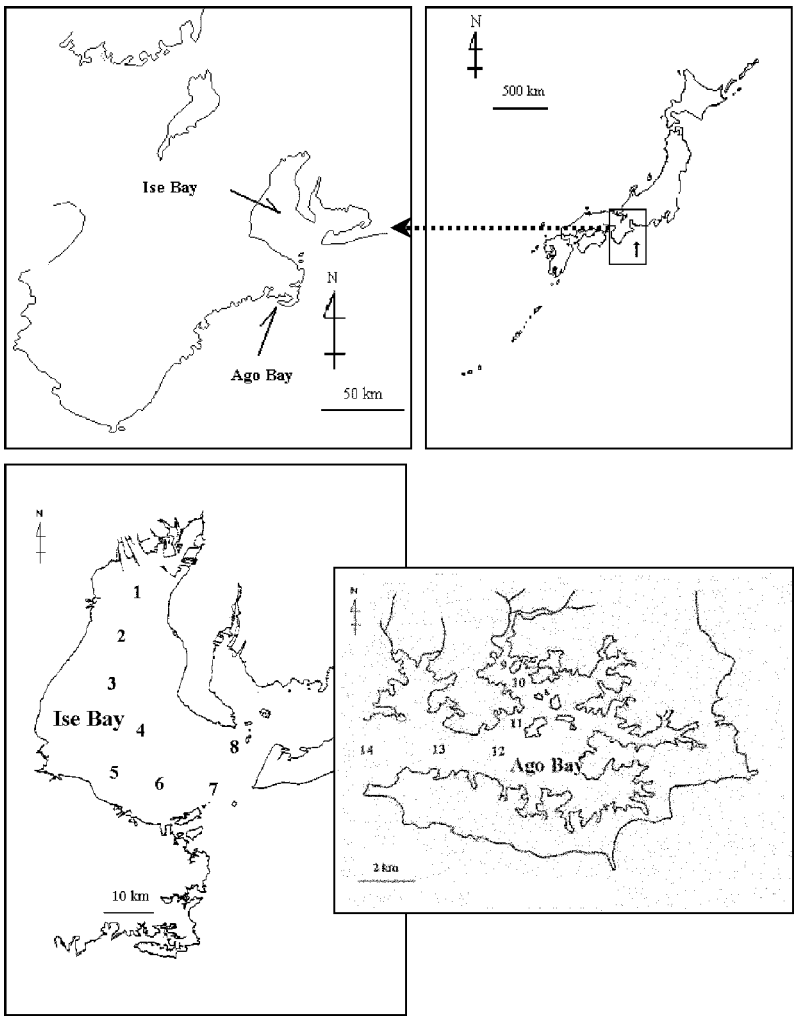

FIG. 1—*Sampling sites.*

Materials and Methods

Field Site and Sample Collection

Sediments were sampled from 11 sites shown in Fig. 1. Sediment samples were taken at each site using a core sampler; aliquots from the top 3 cm of the sample were collected.

Analytical Method

Total organic carbon (TOC) and oxidation-reduction potential (ORP) were examined by the Manuals for Sediment Monitoring Methods.

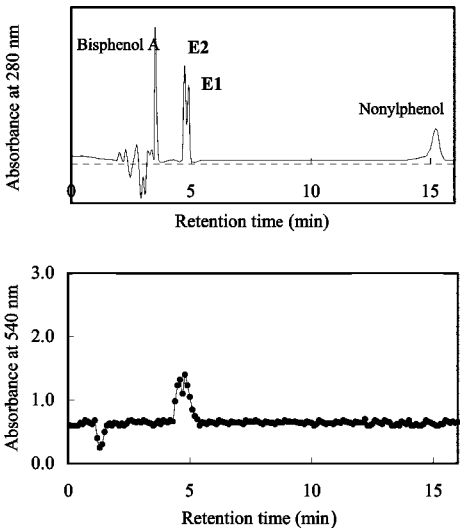

FIG. 2—*Examples of fractionation of sediment sample by HPLC. Upper panel: Standard solution of four kinds of estrogenlike substances, detected by UV absorption. Lower panel: Sediment sample, detected by yeast screen assay.*

Yeast Screen Assay

Preparation of Assay Sample—Estrogenlike compounds were examined by the yeast screen assay developed by Routledge et al. (1996). The human estrogen gene recombinant yeast was obtained from Professor J. P. Sumpter (Brunel University, Uxbridge, UK). Assay of water samples was performed according to the method of Takigami et al. (2000). The analytes were extracted with 10 mL of methanol by ultra-sonic agitation. The extract was reduced in volume to approximately 2 mL using a vacuum evaporator at 40°C. The concentrate was dried by nitrogen gas flow and dissolved in 200 μL of dimethyl sulfoxide.

Yeast screen assay: Calibration standards were prepared in ethanol at a concentration of 100 μgL^{-1} of 17β-estradiol (E2) and serially diluted (×3) in ethanol. Samples were diluted serially by the same method as the standards. Ten-microlitre aliquots of each diluted standard and sample were transferred to a 96-

TABLE 1—*Concentration of estrogenlike substances and another pollution indexes in sediments.*

Sea area	Sampling sites	E2+E1	E2	El	TOC	ORP
		E2 eq. ng g^{-1}	E2 eq. ng g^{-1}	E2 eq. ng g^{-1}	mg g^{-1}	mV
	1	6.54	4.07	2.47	2.01	−384
	2	5.82	5.15	0.67	2.09	−313
	3	2.58	0.83	1.75	3.08	−320
Ise Bay	4	2.38	1.19	1.19	1.31	−285
	5	1.39	0.0	1.39	0.39	−83
	6	1.12	0.0	1.12	0.37	−92
	7	1.98	0.0	1.98	0.40	−106
	8	2.88	1.43	1.45	0.62	−97
	9	4.34	2.58	1.76	3.94	−384
	10	6.61	4.17	2.45	3.24	−282
Ago Bay	11	4.68	2.21	2.47	3.52	−300
	12	3.68	1.31	2.37	2.91	−295
	13	3.45	0.84	2.61	3.01	−264
	14	0.22	0.08	0.13	0.80	−58

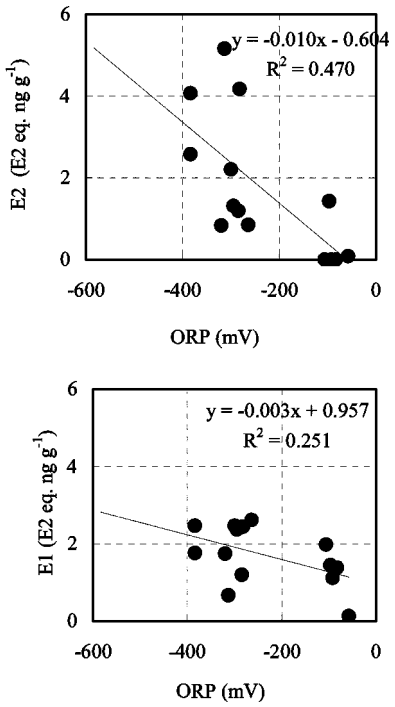

FIG. 3—*Relationship between ORP and estrogenlike substances.*

microwell plate. The solvents were dried by allowing them to stand and assay medium [containing recombinant yeast and substrate for β-galactosidase CPRG(Chlorophenol red-β-D-galactopyranoside)] was added to each well and incubated for 3-4 days at 32°C. After that, the absorbance of the medium developed red was measured. Concentration of an estrogenic substance was determined from the concentration of E2 and assay sample that produced 50 % induction of β-galactosidase activity (EC50) and was calculated by dividing the E2 EC50 by the concentration factor of the assay sample EC50. The estrogen activity detected by the yeast screen assay was defined as estrogenlike compounds and the value was shown as the E2 activity equivalent without Fig. 5.

Fractionation of the Assay Sample by HPLC—The sample was fractionated by injecting 50 μL through a high performance liquid chromatography (HPLC) column Lichrosorb RP-18 10 μm 4.6 ×250 mm (GL Sciences) at a flow rate of 1 mL/min using acetonitrile-acetic acid-water (70:5:25) (Lønning 1989). The separate fractions were collected at 0.1 ml intervals, and dried by nitrogen gas flow. They were dissolved in 20 μl of dimethyl sulphoxide and assayed for estrogenlike compounds. Ten milligrams per liter of estron (E1) and E2 standard solution as applied to the same HPLC column, and these compounds were monitored through an ultraviolet detector at 280 nm to determine their retention times.

Results and Discussion

Distribution of Estrogenlike Compounds

Estrogen activity was examined in sediment samples collected from eleven sites along the coast in Mie Prefecture (Fig. 1). Since detection of estrogen activity by the conventional yeast screen assay is difficult due to yeast growth inhibitor substances abundantly present in sediment samples, the samples were first fractionated by HPLC, and the estrogen activity of each fraction was analyzed by the yeast screen assay.

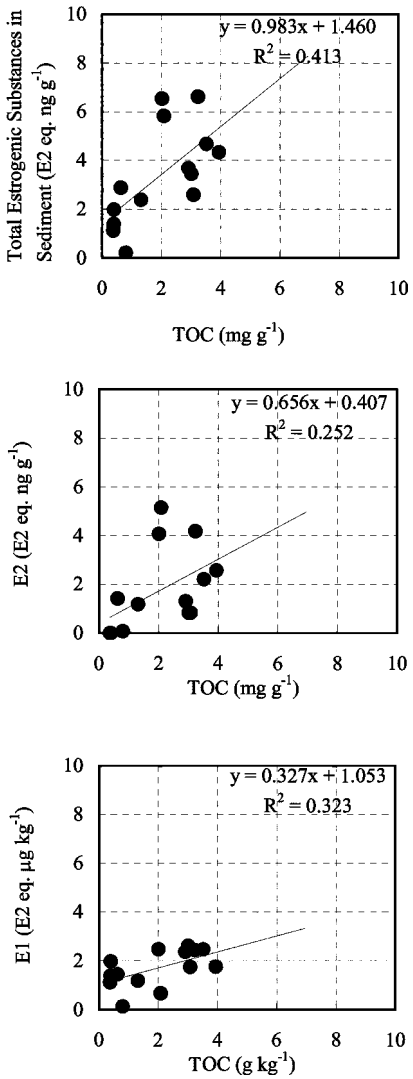

FIG. 4—*Relationship between TOC and estrogenlike substances.*

An example of the fractionation is shown in Fig. 2. Table 1 summarizes the results, with the activities shown as the E2 activity equivalent. Estrogenlike compounds were extracted with methanol, and subjected to analysis by the yeast screen assay. Typical estrogenlike compounds detected in water environments include chemical compounds such as nonylphenol and bisphenol A, and steroid hormones present in raw sewage, such as E1 and E2. We compared the elution patterns of the active fractions in the samples with those of standard substances, and identified activities at the same positions as E1 and E2 in all samples. The detection sensitivity of E1 and E2 is several thousand-fold higher than that of nonylphenol and bisphenol A in the yeast screen assay. These compounds are present at high concentrations in sewage, septic tanks, and waste water from stock farms, and are detected in water samples from rivers flowing into the sea along the coast in Mie Prefecture (Hayakawa et al. 2001). Therefore, the estrogenlike compounds detected in the samples of this study may have been mainly E1 and E2 derived from raw sewage. (See Fig. 3.)

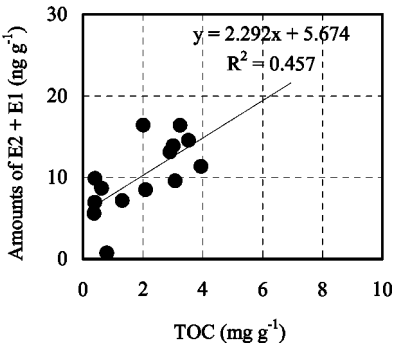

FIG. 5—*Relationship between TOC and amounts of E2 and E1.*

Relationship between Estrogen Activity and TOC in the Sediment Quality

Considerable experimental data show positive correlations between the amount of TOC contained in sediment samples and the concentrations of chemical substances absorbed in the sediment samples, such as E2 (Taniguchi 1998). In this study, a positive correlation was also found between TOC and the estrogen activity (Fig. 4). The estrogen activity is shown as the E2 activity equivalent in this study. Since the estrogen activity of E1 is about 1/5 that of E2, the approximate amount of E1 can be obtained by multiplying the estrogen activity of E1 by 5. Figure 5 shows the relationship between the amounts of E1 and E2 and TOC. The correlation between the amounts of these substances and TOC was closer than that between their estrogen activities and TOC. Little is known about the effects of estrogenlike compounds contained in the sediment on the ecosystem. However, the concentrations of chemical substances absorbed in the sediment are often over 1000-times higher than that in water. The life cycle, such as spawning and growth, of benthic organisms occurs in the sediment. Since estrogenlike compounds are likely to strongly influence the ecosystem even at very low concentrations, it is necessary to monitor their conditions and to make efforts to promote their elimination or reduction. Since not only estrogenlike compounds but also all other water pollutants are difficult to remove once released into public water areas, waste should be treated at the source as much as possible. The results of this study suggested that most of the estrogen activity in sediment samples along the coast in Mie Prefecture is due to steroid hormones, such as E1 and E2. These compounds are detected at the order of $\mu g l^{-1}$ in domestic waste water and animal waste water, but more than 90 % is removed by the activated sludge method. Water after sewage treatment contains steroid hormones at the order of 10 ng L^{-1}, but this can be reduced to a lower order by applying advanced waste treatment methods.

Expedient of Reducing TOC

As shown in the figures, there is a correlation between the concentrations of the sediment TOC and estrogenlike compounds. Therefore, reduction of the sediment TOC concentration will reduce the amount of absorbed estrogenlike compounds. The sediment TOC along the coast partially originates from inland water, but in the regions several kilometers offshore, it is believed that nearly 100 % consists of phytoplankton produced at the site. It is known that the production of phytoplankton in the sea is proportional to the concentration of nutritional salts, nitrogen, and phosphorus. Therefore, reduction of the concentration of nutritional salts in the sea would lead to reduction of sediment TOC, which would decrease the amounts of chemical substances absorbed in the sediment. The amount of sediment TOC and the degree of anaerobic condition are also proportional. If the sediment is aerobic, oxidative degradation of chemical substances, such as E2, proceeds. From the perspective of maintaining the oxidative capacity of the sediment, reduction of sediment TOC is important. Furthermore, the decrease in the amount of plankton would result in the increase in the transparency of seawater, which would increase the intensity of light reaching the seabed, and enhance seaweed growth. Seaweed would contribute to the maintenance of the oxidative condition in the seabed by generating oxygen by photosynthesis, enhancing oxidation of chemi-

cal substances, such as E2. Biodegradation of chemical substances by micro-organisms attached to seaweed would also be enhanced. In addition, solar UV light may also contribute to the degradation of these substances.

Conclusions

Fourteen sediment samples were examined by yeast screen assay, and estrogenlike compounds were found in all of the samples. Estrogenlike compounds in sediments originate from wastewater containing fecal and urine. As estrogenlike compounds are absorbed to TOC in the sediments, it is important to decrease the TOC in sediments to prevent accumulation of the compounds. To reduce estrogenlike compounds in sediments, sources of TOC, such as COD nitrogen and phosphorus, must be reduced as well as estrogenlike compounds. It is also important to maintain aerobic conditions in the sediments to accelerate the oxidation of E2.

According to the fifth regulation on total allowable volumes of pollutants enacted in 2001 by the Ministry of the Environment, the goal is reduction of nitrogen and phosphorus loads in Ise Bay to 96 % and 92 %, respectively, of the present values. The production of phytoplankton is proportional to the smallest amount of the necessary salts, according to Liebich's law. Therefore, if the goal of the regulation is to be achieved, the amount of phytoplankton would theoretically be reduced to 92 % of the present amount. On the assumption that the amount of sediment TOC is proportional to the amount of estrogenlike compounds, the sediment estrogenlike compounds would be reduced to 92 %. Taking the secondary effects described above into consideration, further reduction may be expected. For other chemical substances absorbed in the sediment, similar results would be obtained. The regulation on total allowable volumes of pollutants is intended as a countermeasure against problems caused by eutrophication, such as red tide and water mass with low oxygen concentrations, but it will also be indirectly effective in reducing sediment chemicals, such as estrogenlike compounds.

In daily life, we can contribute to the reduction of TOC and nitrogen/phosphorus loads. Movements for the reduction of these substances in domestic waste water by local residents, which have been conducted for years, will effectively contribute to preventing pollution of the sediment with chemicals, such as estrogenlike compounds, and to protecting the ecosystem of the seabed.

References

Ahel, M., Giger, W., and Schafener, C., 1994, "Behaviour of Alkyiphenol Polyethoxylate Surfactants in the Aquatic Environment – 2: Occurrence and Transformation in Rivers," *Water Res.*, Vol. 28, pp. 1143–1152.

Ahel, M., Schafener, C., and Giger, W., 1996, "Behaviour of Alkyiphenol Polyethoxylate Surfactants in the Aquatic Environment – 3. Occurrence and Elimination of Their Persistent Metabolites During Infiltration of River Water to Groundwater," *Water Res.*, Vol. 30, pp. 37–46.

Desbrow, C., Routledge, E. J., Brighty, G. C., Sumpter, J. P., and Waldock, M., 1998, "Identification of Estrogenic Chemicals in STW Effluxent. 1. Chemical Fractionation and in Vitro Biological Screening," *Environ. Sci. Technol.*, Vol. 32, No. 11, pp. 1549–1558.

Routledge, E. J., and Sumpter, J. P., 1996, "Estrogenic Activity of Surfactants and Some of Their Degradation Products Assessed Using a Recombinant Yeast Screen," *Water Sci. Technol.*, Vol. 15, No. 3, pp. 241–248.

Takigami, H., Taniguchi, N., Matsuda, T., Yamada, T., Shimizu, Y., and Matsui, S., "The Fate and Behavior of Human Estrogens in a Night Soil Treatment Process," *Water Sci. Technol.*, Vol. 42, Nos. 7–8, pp. 45–51.

Lønning, P. E., Skulstad, P., Sunde, A., and Thorsen, T., 1989, "Separation of Urinary Metabolites of Radiolabelled Estrogens in Man by HPLC," *J. Steroid Biochem.*, Vol. 32, No. 1A, pp. 91–97.

Hayakawa, S., Sarai, E., and Yamakawa, M., 2001, "Survey of Endocrine Disrupters in River Water in Mie Prefecture," 2nd Annual Report of Public Health and Environment Research Division of Mie Prefectural Science and Technology Promotion Center, Vol. 3, pp. 94–99.

Taniguchi, N., 1998, "The Behavior of 17β-Estradiol between Solid and Aqueous Phases," Master's thesis, Department of Grobal Environment Engineering Graduate School of Engineering Kyoto University.

Iwasaki, S., Kato, S., Takahashi, M., Kimura, T., Sakka, K., Ohmiya, K., Matsuda, T., and Matsui, S., 2004, "Analysis of Estrogen-like Compounds in the Environment by High Performance Liquid Chromatography Bioassay," *J. Biosci. Bioeng.*, Vol. 97, No. 3, pp. 216–218.

SECTION II: PHYSICAL PROPERTIES

Journal of ASTM International, Vol. 3, No. 6
Paper ID JAI13331
Available online at www.astm.org

M. Kimura[1] *and K. Ishida*[2]

Development of an Acoustical Method for Measuring the Transition Layer of Surficial Marine Sediments

ABSTRACT: A new acoustical method for measuring the physical properties for the transition layer of surficial marine sediments is proposed. In the proposed method, the frequency characteristics of the reflection coefficients for the acoustical normal incidence are utilized. The frequency characteristics of the reflection coefficients are influenced by the depth dependence of the porosity and the density. First, the relationships between the frequency characteristics of the reflection coefficients and the porosity variation with the depth are theoretically shown using Ocean Acoustics and Seismic Exploration Synthesis (OASES) (Biot-Stoll model). Then, the frequency characteristics of the reflection coefficients are measured in water tank and in situ. The measured results are compared with the calculated results using OASES (Biot-Stoll model). Finally, the usefulness of this method is demonstrated.

KEYWORDS: marine sediment, transition layer, acoustical method, reflection, porosity

Introduction

The monitoring of the top transition layer of the surficial contaminated marine sediments such as Hedoro is required. However, the method for the monitoring has not been developed. In this study, a new acoustical method for measuring the transition layer of surficial marine sediments is proposed. It has been recently reported that the physical properties such as the porosity and density in the surfical marine sediment vary largely with the depth [1–3]. The characteristics of acoustic wave reflection from the homogeneous sediment are known in detail [4–6]. However, the characteristics of acoustic wave reflection from such a transition layer of the surficial marine sediment have not been analyzed in detail, and the characteristics seem to be very different from those of the homogeneous sediment. It has been reported that the measured results of the characteristics of the incident angle for the reflection coefficient almost agreed with the calculated results for the transition layer [7] using OASES (Biot-Stoll model) [8]. OASES (Ocean Acoustics and Seismic Exploration Synthesis) is a general purpose computer code for modeling seismo-acoustic propagation in horizontally stratified waveguides using wave-number integration developed by H. Schmidt [8] which can be used for the calculations in underwater acoustics, such as acoustic wave propagation, reflection, etc. In this method, it is necessary to measure the characteristics of the incident angle which are not easy to measure in situ. In the proposed method, the frequency characteristics of the reflection coefficients for the acoustical normal incidence are utilized. The frequency characteristics of the reflection coefficients are influenced by the characteristics for the depth dependence of the porosity and density. First, the relationships between the frequency characteristics of the reflection coefficients and the porosity variation with the depth are calculated using OASES (Biot-Stoll model). Then, the frequency characteristics of the reflection coefficients are measured in water tank and in situ. The measured results are compared with the calculated results using OASES (Biot-Stoll model). Finally, the usefulness of this method is demonstrated.

Manuscript received March 31, 2005; accepted for publication July 12, 2005. Presented at ASTM Symposium on Contaminated Sediments: Evaluation and Remediation Techniques on 23–25 May 2006 in Shizuoka, Japan; M. Fukue, K. Kita, M. Ohtsubo, and R. Chaney, Guest Editors.

[1] Professor, School of Marine Science and Technology, Tokai University, Japan.
[2] Graduate Student, Graduate School of Marine Science and Technology, Tokai University, Japan.

Reflection Coefficients

Sediments are sea water-saturated porous media that are composed of the frame, which is the aggregate of the grain, and the pore water, which fills the pore. The Biot-Stoll model [9–12], which is the acoustic wave propagation model in fluid-saturated porous media, is used for modeling marine sediments.

The wave equations for fluid-saturated porous media are expressed as follows [13]:

$$\mu\nabla^2\mathbf{u} + (H-\mu)[\nabla(\nabla\bullet\mathbf{u})] - C[\nabla(\nabla\bullet\mathbf{w})] = \rho\frac{\partial^2\mathbf{u}}{\partial t^2} - \rho_f\frac{\partial^2\mathbf{w}}{\partial t^2}, \tag{1}$$

$$C[\nabla(\nabla\bullet\mathbf{u})] - M[\nabla(\nabla\bullet\mathbf{w})] = \rho_f\frac{\partial^2\mathbf{u}}{\partial t^2} - \alpha\frac{\rho_f}{\beta}\frac{\partial^2\mathbf{w}}{\partial t^2} - \frac{F\eta}{k}\frac{\partial\mathbf{w}}{\partial t}, \tag{2}$$

$$\mathbf{w} = \beta(\mathbf{u}-\mathbf{U}), \tag{3}$$

where **u** is the displacement of the frame, **U** is the displacement of the fluid, **w** is the relative displacement of the frame to the fluid, μ is the shear modulus, β is the porosity, ρ is the density of the sediment, ρ_f is the density of the fluid, k is the permeability, α is the structure factor, η is the viscosity, F is the viscous correction factor, and H, C, M are the constants determined by the moduli of the grain, fluid, and frame.

As shown in Fig. 1, we consider a normal incidence of plane longitudinal wave to a sediment half-space at $z=0$. There exist incident and reflected waves in the seawater, and two transmitted waves—the first kind of longitudinal wave (fast wave) and the second kind of longitudinal wave (slow wave), in the sediment. The incident and reflected waves in the seawater will have the displacement potentials

$$\phi_i = A_i\exp[j(\omega t - k_w\cdot z)], \tag{4}$$

$$\phi_r = A_r\exp[j(\omega t + k_w\cdot z)], \tag{5}$$

where, $k_w=\omega/c_w$. ω is the angular frequency, and c_w is the sound velocity in the seawater. Two displacements **u** and **w** can be represented by scalar potentials ϕ_s and ϕ_f

$$\mathbf{u} = \nabla\phi_s, \tag{6}$$

$$\mathbf{w} = \nabla\phi_f. \tag{7}$$

In the sediment, the scalar potentials defined in Eqs 6 and 7 are

$$\phi_s = A_1\exp[j(\omega t - k_{1z}\cdot z)] + A_2\exp[j(\omega t - k_{2z}\cdot z)], \tag{8}$$

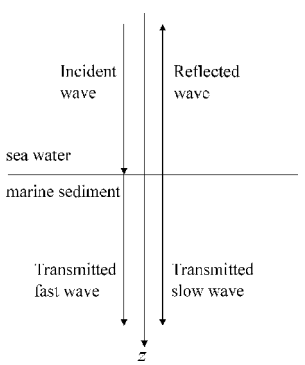

FIG. 1—*Incident and reflected longitudinal waves in seawater and transmitted fast and slow waves in marine sediment.*

$$\phi_f = B_1 \exp[j(\omega t - k_{1z} \cdot z)] + B_2 \exp[j(\omega t - k_{2z} \cdot z)], \tag{9}$$

where, k_{1z} and k_{2z} are the vertical wave numbers for the first and second kinds of longitudinal waves. The relationships between the complex amplitude A_1, A_2, B_1, and B_2 are

$$\frac{B_1}{A_1} = H \frac{\frac{Hk_{l1}^2}{\rho\omega^2} - 1}{\frac{CHk_{l1}^2}{\rho\omega^2} - \frac{\rho_f H}{\rho}}, \tag{10}$$

$$\frac{B_2}{A_2} = H \frac{\frac{Hk_{l2}^2}{\rho\omega^2} - 1}{\frac{CHk_{l2}^2}{\rho\omega^2} - \frac{\rho_f H}{\rho}}, \tag{11}$$

where, k_{l1} and k_{l2} are the complex wave numbers for the first and second kinds of longitudinal waves, and

$$H = \frac{(K_r - K_b)^2}{D - K_b} + K_b + \frac{4}{3}\mu, \tag{12}$$

$$C = \frac{K_r(K_r - K_b)}{D - K_b}, \tag{13}$$

$$D = K_r\left[1 + \beta\left(\frac{K_r}{K_f} - 1\right)\right], \tag{14}$$

where, K_f, K_r, K_b are the bulk moduli of the pore fluid, grain, and frame, respectively. μ is the shear modulus.

The following three boundary conditions are required at a seawater-sediment interface.

1. For continuity of fluid movement

$$\frac{\partial\phi_i}{\partial z} + \frac{\partial\phi_r}{\partial z} = \frac{\partial\phi_s}{\partial z} - \frac{\partial\phi_f}{\partial z}. \tag{15}$$

2. For equilibrium of normal traction

$$H\frac{\partial^2\phi_s}{\partial z^2} - - C\frac{\partial^2\phi_f}{\partial z^2} = \rho_f\left(\frac{\partial^2\phi_i}{\partial t^2} + \frac{\partial^2\phi_r}{\partial t^2}\right). \tag{16}$$

3. For equilibrium of fluid pressure

$$M\frac{\partial^2\phi_f}{\partial z^2} - C\frac{\partial^2\phi_s}{\partial z^2} = -\rho_f\left(\frac{\partial^2\phi_i}{\partial t^2} + \frac{\partial^2\phi_r}{\partial t^2}\right), \tag{17}$$

where

$$M = \frac{K_r^2}{D - K_b}. \tag{18}$$

By combining Eqs 4, 5, and 8–18, the following three linear complex equations can be obtained:

$$\begin{pmatrix} c_{11} & c_{12} & c_{13} \\ c_{21} & c_{22} & c_{23} \\ c_{31} & c_{32} & c_{33} \end{pmatrix} \begin{pmatrix} A_r \\ A_1 \\ A_2 \end{pmatrix} = \begin{pmatrix} Y_1 \\ Y_2 \\ Y_3 \end{pmatrix}. \tag{19}$$

In Eq 19, the components of {c} and {Y} are given by the physical parameters of seawater and sediment. A_r is the complex amplitude of the reflected wave. Therefore, the reflection coefficient can be obtained by solving Eq 19, once A_i is specified.

Calculations for Frequency Characteristics of Reflection Coefficients

Recently, it has been reported that the physical properties such as the porosity and the density in the surficial marine sediment vary largely with the depth [1–3]. The characteristics of the acoustic wave reflection from such a transition layer of the surficial marine sediment seem to be very different from that of the homogeneous sediment. Thus, the frequency characteristics of the reflection characteristics from the surface of the sediments with the top transition layer are calculated. The equation for porosity variation with the depth is assumed by referring Carbo's paper [14] as follows:

$$\beta = \beta_{\min} + (1 - \beta_{\min})\exp(-\alpha z^n), \tag{20}$$

where $\beta_{\min}$ is the minimum value of the porosity, z(cm) is the depth from the surface of the sediment and the values of α and n are constants determining the depth dependence of the porosity. It is difficult to calculate the reflection coefficients for the sediment whose porosity continuously varies with the depth such as the transition layer [15]. Thus, these calculations are performed by separating the layer into thin layers using OASES (Biot-Stoll model), as shown in Fig. 2. The calculated results using OASES are $|A_r/A_i|$ for the transitional sediment. In this calculation, the transition layer whose thickness is 20 cm, is divided into 199 layers. Below the depth of 20 cm, the porosity is constant, that is, the medium below the depth consists of semi-infinite sediments. The characteristics of porosity variation with depth are shown in Fig. 3 with the constant value of $n=0.75$ and the variable values of $\alpha=3.0$, 1.5, 0.75, and Fig. 4 with the constant value of $\alpha=1.5$ and the variable values of $n=1.50$, 0.75, 0.375. In these figures, the porosity at a depth below 20 cm, $\beta_{\min}$ is constant, and the value is 0.62 for silt model.

According to the change of the porosity with the depth, the bulk and the shear moduli of the frame [16], the permeability and pore size parameter are changed using the following equations.

$$\log K_{\text{br}} = -2.20\beta + 8.52, \tag{21}$$

$$\log \mu_r = -0.265\frac{\beta}{1-\beta} + 7.07, \tag{22}$$

$$k = \frac{d^2}{36k_0}\frac{\beta^3}{(1-\beta)^2}(k_0 = 5), \tag{23}$$

$$a = \frac{d}{3}\frac{\beta}{1-\beta}. \tag{24}$$

In this calculation, the values of the parameters used are as follows, the diameter of the grain $d=22.1$ μm, the density of the grain $\rho_r=2650$ kg/m^3, the bulk modulus of the grain $K_r=3.60\times10^{10}$ Pa, the density of the water $\rho_f=1000$ kg/m^3, the bulk modulus of the water $K_f=2.25\times10^9$ Pa, the viscosity of the water $\eta=1.00\times10^{-3}$ Pa·s. The sound velocity in the seawater is assumed to be 1500 m/s.

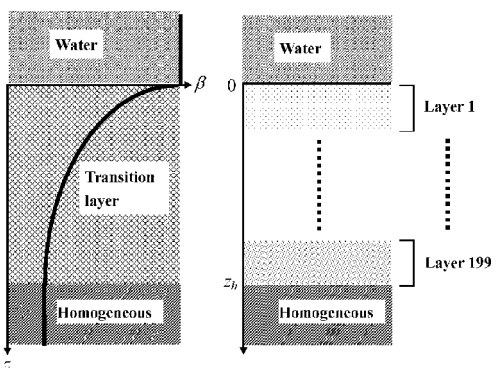

FIG. 2—*Model for the transition layer which is divided into 199 layers.*

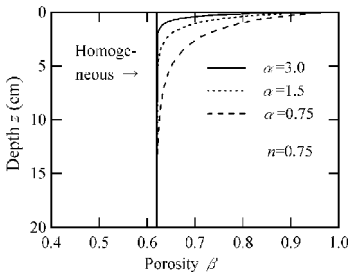

FIG. 3—*Porosity versus depth for transition layer of silt model* (β_{min}=0.62, n=0.75).

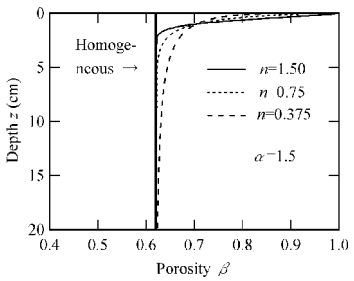

FIG. 4—*Porosity versus depth for transition layer of silt model* (β_{min}=0.62, α=1.5).

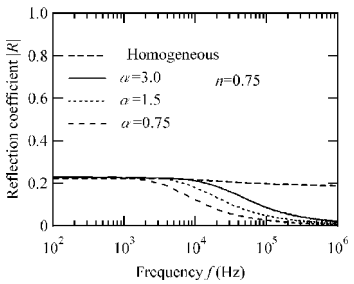

FIG. 5—*Reflection coefficient versus frequency for silt model* (β_{min}=0.62, n=0.75).

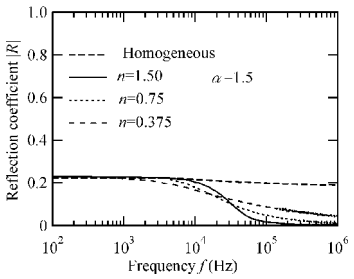

FIG. 6—*Reflection coefficient versus frequency for silt model* (β_{min}=0.62, α=1.5).

The depth dependence of the porosity seems to be different depending on the seabed areas and the type of the sediments. Thus, the changes of the frequency characteristics of the reflection coefficient due to the change of the depth dependence of the porosity are investigated. The calculated results for the frequency characteristics of the reflection coefficients are shown in Figs. 5 and 6. Figure 5 is for silt model ($\beta_{min}=0.62$, $n=0.75$) with the parameter of α. Figure 6 is for silt model ($\beta_{min}=0.62$, $\alpha=1.5$). with the parameter of n. In both figures, the calculated results for the homogeneous sediment are also shown. The reflection coefficient for the transition layer decreases, as the frequency increases such as the frequency characteristics of low pass filter. From Fig. 5, it is seen that the cut-off frequency decreases, as the α decreases. From Fig. 6, it is shown that the slope of the characteristics at the frequency range near the cut-off frequency decreases, as n decreases. These phenomena seem to be due to the fact that the effective depth of the reflection coefficient decreases as the frequency increases, and the porosity increases as the depth decreases. The effective depth of the reflection coefficient is determined by the interrelation between the wavelength of the acoustic wave and the thickness of the transition layer. From these calculated results, an estimation of the types of sediments and the porosity profile with the depth from the measured results of the frequency characteristics of the reflection coefficients is expected to be possible.

Experiments for Acoustic Wave Reflection

Tank Experiments

Silt with the diameter of 30 μm sampled at the Shimizu harbor which depth is about 20 m is used as a sediment model. This model is set in the bottom of the cylindrical tank whose inner diameter is 20 cm and height is 50 cm. The thickness of the medium is 10 cm. Experimental arrangement for the acoustic wave reflection for normal incidence is shown in Fig. 7.

Piezoelectric transducer whose resonant frequency is 500 kHz, and diameter is 25.4 mm is used for transmitting transducer. The propagation distance is 30 cm. A short pulse with wide frequency band is applied to the transmitting transducer. The reflected signal $g(t)$ for the normal incidence obtained by the same transducer is inputted to a digital oscilloscope, averaged 64 times. The reflected signal from the water-air interface $g_s(t)$ is used for the reference signal for obtaining the reflection coefficients. The wave forms of $g_s(t)$ and $g(t)$ are shown in Fig. 8. Both wave forms are processed using the half-Hanning window to reduce the noise. The Fourier transforms of the reflected signals from the water-sediment model interface $G(\omega)$ and that from the water-air interface $G_s(\omega)$ are obtained. Then the absolute value of the reflection coefficient can be obtained as follows:

$$|R| = \left| \frac{G(\omega)}{G_s(\omega)} \right| . \tag{25}$$

The characteristics of the porosity versus the depth are shown in Fig. 9. These characteristics are obtained from the depth dependence of the longitudinal wave velocity, using the relationship between the porosity and the longitudinal wave velocity [17]. In Fig. 9, the measured results and the regressive curve are shown. The regressive equation is as follows:

$$\beta = 0.472 + (1 - 0.472)\exp(-2.29z^{0.695}). \tag{26}$$

The measured and calculated results of the frequency characteristics of the reflection coefficients are shown in Fig. 10. In Fig. 10, the calculated results for the homogeneous sediment model and the coherence function are also shown. In this calculation, the values of the parameters used are as follows: the diameter of the grain $d=30$ μm; the density of the grain $\rho_r=2643$ kg/m^3; the bulk modulus of the grain $K_r=1.20\times10^{10}$ Pa; the density of the water $\rho_f=998$ kg/m^3; the bulk modulus of the water $K_f=2.20\times10^9$ Pa; and the viscosity of the water $\eta=1.00\times10^{-3}$ Pa-s. From Fig. 10, it is seen that the measured result of the frequency characteristics of the reflection coefficients is relatively the same as the calculated result for the transitional sediment model.

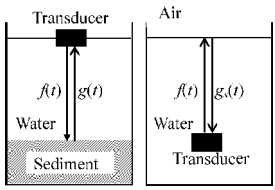

FIG. 7—*Experimental arrangement of the acoustic reflection for normal incidence.*

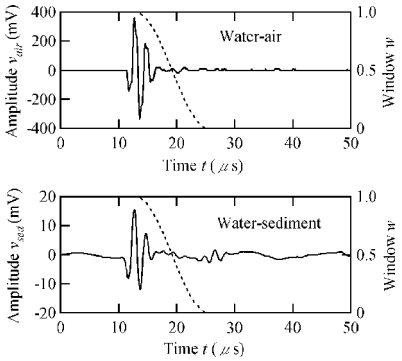

FIG. 8—*Reflection wave forms from the water-air interface (for reference) and water-sediment model interface in tank experiments. Dotted-line curves indicate the half-Hanning window to reduce the noise.*

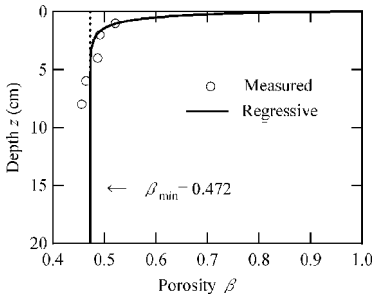

FIG. 9—*Porosity versus depth for transition layer of sediment model.*

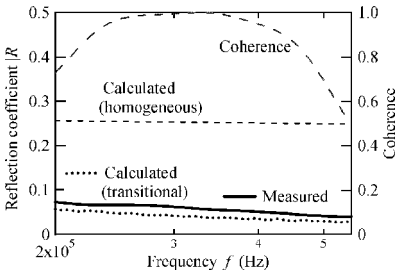

FIG. 10—*Reflection coefficient versus frequency for sediment model in tank.*

In Situ Experiments

In situ experiments were performed in the Shimizu harbor with the water depth about 20 m. The surficial marine sediment is silt with a mean diameter of 30 μm. The measuring system was taken down from a small ship, and set on the surface of the sea bottom. Piezoelectric transducer which resonant frequency is 100 kHz, and the diameter is 38.1 mm, is used for transmitting and receiving transducer. The wave forms

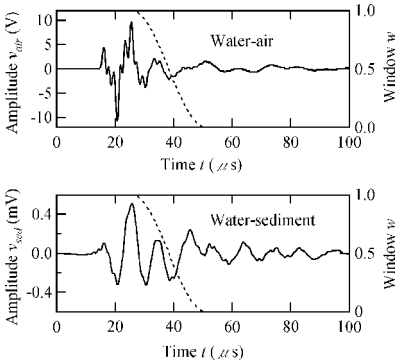

FIG. 11—*Reflection wave forms from the water-air interface (for reference) and water-seabed silt interface in situ experiments. Dotted-line curves indicate the half-Hanning window to reduce the noise.*

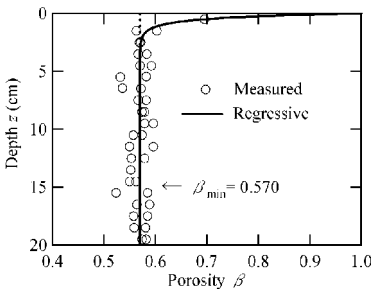

FIG. 12—*Porosity versus depth for transition layer of seabed silt.*

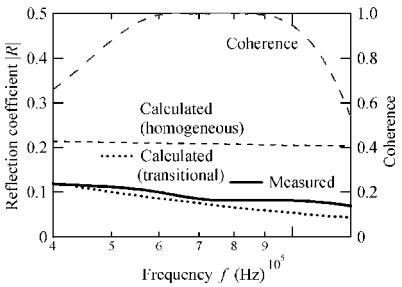

FIG. 13—*Reflection coefficient versus frequency for seabed silt.*

of $g_s(t)$ and $g(t)$ are shown in Fig. 11. The propagation distance is 60 cm. The absolute values of the reflection coefficient are obtained using the same method as the tank experiments.

The characteristics of the porosity versus the depth are shown in Fig. 12. The porosity was measured for 1-cm-long sample from the top of the sediment, after taking sample using a GS-type core sampler manufactured by RIGO Co. (Tokyo, Japan). This core sampler has three core samplers with diameters of 82 mm and lengths of 600 mm. A pair of porosity data at the same depth in Fig. 12 was obtained using two core samples. The regressive equation is as follows:

$$\beta = 0.570 + (1 - 0.570)\exp(-2.33z^{0.929}). \tag{27}$$

The measured and calculated results of the frequency characteristics of the reflection coefficient are shown in Fig. 13. In Fig. 13, the calculated results for the homogeneous sediment model and the coherence function are also shown. The values of the physical parameters are the same as for tank experiments. From Fig. 13, it is recognized that the measured results of the reflection coefficients relatively agree with the calculated result for the transitional sediment.

Conclusions

The frequency characteristics of the reflection coefficient from the transition layer of surficial marine sediment were calculated using OASES (Biot-Stoll model). It is seen that frequency characteristics of the reflection coefficients for the transitional sediment are very different from that for the homogeneous sediment at the higher frequency. These phenomena seem to be due to the effective depth to the reflection coefficient decreases as the frequency increases, and the porosity increases as the depth decreases.

The measured results of the frequency characteristics of the reflection coefficients from the silt model in tank experiments and silt in situ experiments relatively agreed with the calculated results from the transitional sediments. From these results, an estimation of the types of sediments and the porosity profile with the depth using the measured results of the frequency characteristics of the reflection coefficients are possible.

The depth dependence of the porosity in the variety of sediments seems to be different from each other. Therefore, it is required that the frequency characteristics of the reflection coefficients for the different kinds of sediments with the transition layer are analyzed in detail.

References

[1] Stephens, K. P., Fleisher, P., Lavoie, D., and Brunner, C., "Scale-Dependent Physical and Geoacoustic Property Variability of Shallow-water Carbonate from the Dry Tortugas, Florida," *Geo-Mar. Lett.*, 17, 299–305 (1997).

[2] Briggs, K. R. and Richardson, M. D., "Small-Scale Fluctuations in Acoustic and Physical Properties in Surficial Carbonate Sediments and Their Relationship to Bioturbation," *Geo-Mar. Lett.*, 17, 306–315 (1997).

[3] Kimura, M., Shimizu, R., Tsurumi, T., and Ishida, K., "Measurements of Acoustic and Physical Characteristics of Surficial Marine Sediment," *Proc. Autumn Meet. Acoust. Soc. Jpn.*, 2001, pp. 1221–1222.

[4] Stoll, R. D. and Kan, T. K., "Reflection of Acoustic Waves at a Water Sediment Interface," *J. Acoust. Soc. Am.* 70, 149–156 (1981).

[5] Kimura, M., "Reflection of Plane Acoustic Wave at a Seawater-Marine Sediment Interface," *Jpn. J. Appl. Phys., Part 1* 35, 2948–2951 (1996).

[6] Kimura, M., "Acoustic Wave Reflection from Water-Saturated and Air-Saturated Sediments," *Jpn. J. Appl. Phys., Part 1* 41, 3513–3518 (2002).

[7] Kimura, M. and Tsurumi, T. "Acoustic Wave Reflection from the Transition Layer of Surficial Marine Sediment," *Acoust. Sci. & Tech.*, 25, 188–195 (2004).

[8] Schmidt, H., *OASES, Ver. 2.2, User Guide and Reference Manual*, http://acoustics.mit.edu/ faculty/ henrik/oases.html, 1999.

[9] Biot, M. A., "Theory of Elastic Waves in a Fluid-Saturated Porous Solid. 1. Low Frequency Range," *J. Acoust. Soc. Am.* 28, 168–178 (1956).

[10] Biot, M. A., "Theory of Elastic Waves in a Fluid-Saturated Porous Solid. 2. Higher Frequency Range," *J. Acoust. Soc. Am.* 28, 179–191 (1956).
[11] Stoll, R. D., "Wave Attenuation in Saturated Sediments," *J. Acoust. Soc. Am.*, 47, 1440–1447 (1970).
[12] Stoll, R. D., *Sediment Acoustics*, Springer-Verlag, Berlin, 1989, pp. 5–36.
[13] Chotiros, N. P., "Biot Model of Sound Propagation in Water-Saturated Sand," *J. Acoust. Soc. Am.* 97, 199–214 (1995).
[14] Carbo, R., "Wave Reflection from a Transitional Layer between the Seawater and the Bottom," *J. Acoust. Soc. Am.* 101, 227–232 (1997).
[15] Stern, M., Bedford, A., and Millwater, H. R., "Wave Reflection from a Sediment Layer with Depth-Dependent Properties," *J. Acoust. Soc. Am.* 77, 1781–1788 (1985).
[16] Kimura, M., and Kawashima, S., "Study on Physical Parameters of the Biot-Stoll Marine Sediment Model," *J. Marine Acoust. Soc. Jpn.* 22, 54–63 (1995).
[17] Kimura, M, Takarada, S., and Edo, M., "Longitudinal Wave Velocity and Attenuation in High Porosity Marine Sediment," *Technical Report of IEICE*, US2004-36, 2004, pp. 25–28.

Journal of ASTM International, Vol. 3, No. 7
Paper ID JAI13325
Available online at www.astm.org

Goro Imai,[1] *Yuko Komatsu,*[2] *and Masaharu Fukue*[3]

Consolidation Yield Stress of Osaka-Bay Pleistocene Clay with Reference to Calcium Carbonate Contents

ABSTRACT: Sea bottom has been used as landfill sites to dispose various types of waste and dredged materials. Therefore, the geotechnical properties of seabed are of great importance for the design and practice of reclamation projects. Marine clay layers are known to be geologically normally consolidated. Those clays, however, show pseudo-overconsolidation behavior with a consolidation yield stress p_c larger than the in situ overburden pressure p_0. As consolidation behavior of those clays under a load around p_c is not normal but very complex, the prediction of possible settlement under loading is presently quite difficult. In this study, the Osaka-Bay Pleistocene clays were sampled and subjected to physical and mechanical tests. Based on previous studies, it is assumed in this paper that the disagreement between p_0 and p_c results from the cementation of marine soils, and that their cementation is mainly due to calcium carbonate. If the assumption made is valid, p_c value of a clay sample of which calcium carbonates had been chemically dissolved must be equal to p_0 value. In order to verify this assumption, experimental studies has been done. Carbonic-acid water of enough volume to dissolve the calcium carbonates in a clay sample was percolated without breaking fabric structure of the clay skeleton, and p_c value of the sample was determined by the constant strain rate of consolidation test. The results showed a definite decrease of the p_c value. Consequently, the pseudooverconsolidation ratio of the specimens decreased with the removal of calcium carbonates.

KEYWORDS: reclamation, calcium carbonates, Osaka-Bay Pleistocene clay, consolidation yield stress

Introduction

Because of the contamination of sediments, the disposal problems of dredged materials have become increasingly important (Wakeman and Themelis 2001, Stronkhorst et al. 2003). In Japan, the lack of available space for waste disposal in land alternatively necessitates the use of coastal region (Aburatani et al. 1998). Under this situation, site characterizations of the seabeds from the geotechnical point of views may be primarily important to ensure the safety against not only contamination but also mechanical stability. The geotechnical properties of marine sediments can be characterized by the following variables and constants:

1. Physical properties: such as water content; grain size characteristics; and permeability; and
2. Mechanical properties; relating to shear strength and consolidation characteristics.

Marine sediments are composed of terrigenous materials, assemblage of dead marine organisms, fecal pellet, etc. Although diatom is one of the typical marine organisms found in marine sediment (de Jonge 1985), and it influences the physical and mechanical properties of the sediment, it is silicate material without cementation action. Coccolith and foraminifer have their shells mainly made of calcium carbonate, and their dead bodies have been buried in marine sediments with an almost constant rate through the past several million years. Therefore, the amount of calcium carbonate in marine sediments depends on the sedimentation rate of terrigenous materials. If the supplying rate of terrigenous materials is low, as found in the ocean's bottom, the carbonate content becomes relatively high. On the other hand, since the terrigenous materials are highly contained in the sediments near coastlines, bay, and estuary, their carbonate content is relatively low (Broecker and Peng 1982).

Manuscript received March 31, 2005; accepted for publication January 5, 2006. Presented at ASTM Symposium on Contaminated Sediments: Evaluation and Remediation Techniques on 23–25 May 2006 in Shizuoka, Japan; M. Fukue, K. Kita, M. Ohtsubo, and R. Chaney, Guest Editors.

[1] Professor, Yokohama National University, Yokohama, 240-8501, Japan.
[2] Graduate Student, Yokohama National University, Yokohama, 240-8501, Japan.
[3] Professor, Tokai University, Shizuoka, 424-8610, Japan.

TABLE 1—*Physical properties of samples used in this study.*

Formation	Depth from sea level (m)	Bulk density (g/cm^3)	Density of particles (g/cm^3)	Void ratio	Liquid limit (%)	Plasticity limit (%)	Plasticity index	Overburden pressure (kPa)
Dtc	60.49	1.716	2.685	1.35	72	27	45	286
Ma12U	70.10	1.534	2.640	2.08	99	39	60	338
Ma12L	73.47	1.573	2.657	1.91	87	33	54	361
Ma11	108.47	1.678	2.674	1.48	89	34	55	618
Ma10	141.85	1.701	2.691	1.35	84	36	48	870
Ma9	166.07	1.635	2.704	1.55	98	37	61	1052
Doc5	184.45	1.544	2.573	1.97	115	41	74	1188
Ma8	208.07	1.721	2.724	1.37	92	36	56	1372
Ma7	222.40	1.684	2.699	1.39	100	38	63	1489
Ma4	264.10	1.664	2.667	1.41	94	35	58	1866
Ma3	283.92	1.736	2.696	1.24	82	36	47	2012
Ma2	305.50	1.717	2.664	1.33	84	33	51	2201

The cementation of soil particles due to calcium carbonates had been qualitatively known, because of the occurrence of calcareous rocks (limestone and calcareous sandstone) and cemented carbonate soils. Quantitative studies on the cementation of sediments due to calcium carbonate were carried out by Fukue et al. (1992), while Molenaar and Venmans (1993) tried to produce artificially cemented samples to understand the cemented layer in Holocene calcareous sands.

Most marine bed clays are normally consolidated in the sense of geology. However, some of them show pseudo-overconsolidation behavior with a consolidation yield stress p_c, larger than the in situ overburden pressure p_0 (Tsuchida 2001). While this mechanical behavior can be interpreted from the cementation between particles (Kang et al. 2001), the cementation of marine sediments has been interpreted from the effects of salt (Rosenqvist 1953), organic matter (Pusch 1973), and carbonate (Fukue et al. 1992; Molenaar and Venmans 1993). Although such an essential discussion on cementation or bonding between particles has been required to understand the inherent properties of soils, it has been remained as a black box in geotechnical engineering.

The cementation due to calcium carbonates is very likely for marine sediments that have not been subjected to the leaching of salt. Therefore, this study examines the effects of carbonate on the consolidation yield stress of Osaka Pleistocene clay, based on the previous studies on the surface sediments (Fukue et al. 1999).

Methods

The main purpose of the present study is to quantitatively discuss the largeness of consolidation yield stress of Osaka Pleistocene clay showing pseudo-overconsolidation behaviors, with special reference to the amount of calcium carbonate contents in those clays. For this purpose, two kinds of tests were carried out by use of samples obtained from the Osaka Pleistocene clay layers above which Kansai International Airport had been constructed. One of the two is the test to measure the amount of calcium carbonate contents C and another is the strain-rate controlled consolidation test to determine the largeness of consolidation yield stress p_c. If a p_c value larger than the in situ overburden pressure p_0 had been resulted from only cementation action of calcium carbonates, a strong correlation between $(p_c - p_0)$ and C could be found. Furthermore, the p_c value of a clay should decrease down to its p_0 value if calcium carbonate in a sample had been artificially dissolved with no fabric destruction of the specimen.

Carbonate Content Measurement

To measure carbonate content, only about 5 g of testing material is necessary. In the case where only a C value is wanted, a fragment shaved from a block sample was used for the measurement. In the case where a C value should be related to p_c, fragments obtained from trimming of a specimen for the consolidation test were used to determine a C value before consolidation, and a fragment obtained from the specimen was used to determine a C value after consolidation.

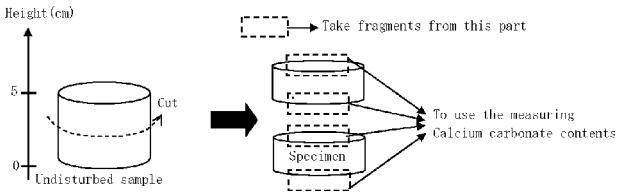

FIG. 1—*Specimen for the consolidation test and samples for measurement of carbonate contents.*

Strain-Rate Controlled Consolidation Test

Two types of specimens were used for the consolidation tests. One is the specimens just trimmed from undisturbed block samples. Another type is the specimens of which carbonates were chemically removed by percolating carbonic-acid water. These two types of specimens are consolidated with the same strain rate. It should be noted here that CO_2 in the carbonic-acid water can dissolve calcium carbonate in the specimen. Based on the results obtained, the effects of calcium carbonate on the consolidation behavior will be discussed.

Sample Preparation

Undisturbed block samples were obtained from off Senshu in Osaka Bay, with cooperation of Kansai International Airport Co. Ltd and Port and Airport Research Institute, Japan. The physical properties of the samples are listed in Table 1. A cylindrical undisturbed block sample with 10 cm or 7.5 cm in height was first cut into sliced samples of 2.5 cm in thickness. As shown in Fig. 1, each of these sliced samples was trimmed to form a specimen ($\phi 60 \times 20$ mm) for the consolidation test. Fragments shaved from the upper and lower surfaces of the intact specimen was used to measure its original C value. In this study, carbonate contents were measured also for the specimens of which carbonate had been removed by the percolation of carbonic-acid water. In this case, a fragment obtained from the center part of the specimen after percolation followed by consolidation was used for the measurement of the C value.

Measurement of Calcium Carbonate Content

The device used for measuring carbonate content of soils is shown in Fig. 2. Its original idea was developed by Kato and Okabe (1998). About 5 g of dry soil sample is used for the measurement. The calcium carbonate in the sediments reacts with hydrogen chloride HCl, and produces calcium chloride, water, and carbon dioxide. The CO_2 gaseous pressure produced in a closed chamber will depend on the amount of calcium carbonate reacting with HCl. The chemical reaction is as follows:

$$CaCO_3 + 2HCl = CaCl_2 + H_2O + CO_2\uparrow$$

When other types of carbonates and sulfates are contained in the soil samples, it may have an influence on the measures. However, in marine soils, calcium carbonate is dominant and other carbonates are possibly neglected (Sverdrup et al. 1972). The features of this device are as follows:

1. The chamber is made of acrylic resin to enable the use of HCl,

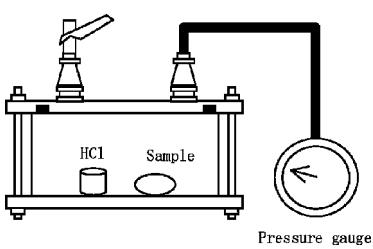

FIG. 2—*Device for measuring carbonate content.*

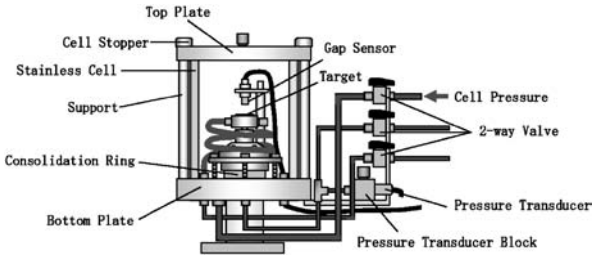

FIG. 3—*Apparatus for the strain-rate controlled consolidation test.*

TABLE 2—*Preparation of specimens for consolidation test.*

Formation	Without percolation of carbonic-acid water	Percolation of carbonic-acid water (degassed water)
Dtc	1	1
Ma12U	1	1
Ma12L	1	2
Ma11	1	1
Doc5	1	1
Ma8	1	1(1)
Ma4	1	1
Ma2	1	1

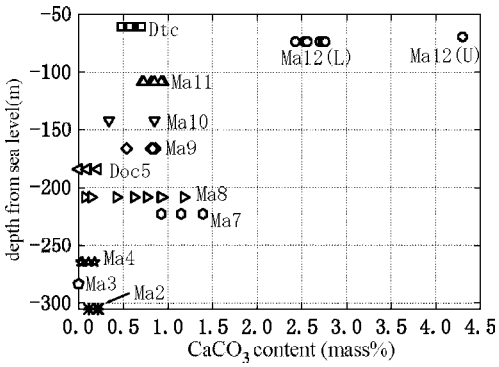

FIG. 4—*Depth profile of calcium carbonate content for the Osaka Pleistocene clay.*

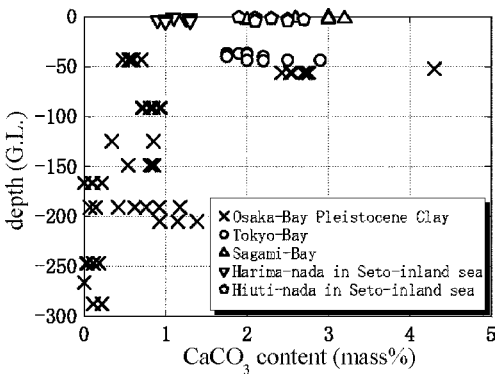

FIG. 5—*Comparison of calcium carbonate contents for various sites.*

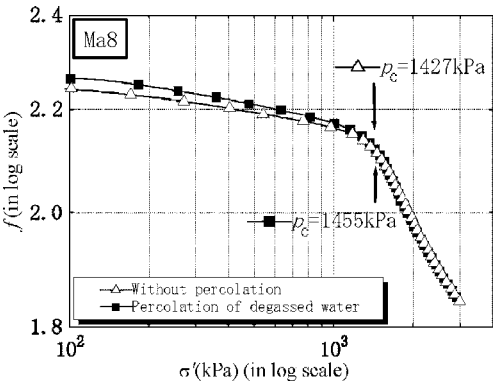

FIG. 6—*Compression curves for specimens with and without the percolation of degassed water.*

2. Only gaseous pressure is measurable when the chamber is closed, and
3. The measurement range of pressure is between zero and several.

Strain-Rate Controlled Consolidation Test

Test Apparatus

Figure 3 shows the consolidation apparatus used in this study. The features of this apparatus are as follows:

1. A cell made of stainless steel is adopted to use high pressure,
2. A gap sensor (noncontact type displacement transducer) attached to the piston rod is used to precisely measure the compression of the specimen,
3. Copper tubes which can hardly be deformed under high pressure are used for the pouring and drainage of water, and
4. Specimen is sealed completely with the bellowphragm. This enables one to measure an accurate pore water pressure induced in the specimen.

Test Conditions

In this study, a consolidation test was carried out by following the Japanese Industrial Standard (JIS A 1227). The test conditions were set up as follows:

1. Strain rate: Considering strain rate effects on p_c, all tests were performed at a strain rate of 0.01 %/min.
2. Final effective stress: Considering the capacity of air pressure which can be controlled, a final effective stress of 3000 kPa was set up. Exceptionally, a final effective stress of 3600 kPa was used for Ma2 formation.
3. Percolation of carbonic-acid water (removal of carbonates): Table 2 shows the specimens used for the consolidation test, including the specimens percolated by carbonic-acid water. The number of specimens tested are also presented in Table 2. The amount of carbonic-acid water used is assumed to be sufficient to dissolve the carbonates in the specimen. In order to examine the possible disturbance of specimen due to infiltration of water, the Ma8 specimen was per-

TABLE 3—*Carbonate contents of Ma8 before and after consolidation.*

Specimen	Before consolidation (%)	After consolidation (%)
Without percolation	0.6	0.6
Percolation of degassed water	1.2	1.2

TABLE 4—*Permeabilities for different pressure difference.*

Specimen	k_{20}(m/s)	k_{50}(m/s)	k_{100}(m/s)
Ma8	2.1×10^{-10}	2.4×10^{-10}	2.3×10^{-10}

colated by degassed water, and its consolidation behavior was compared with another specimen without percolation.

Results and Discussions

Calcium Carbonate Content of Each Clay Layer

The results of carbonate contents measured are shown in Fig. 4. The carbonate contents vary from nearly zero to 4 % showing a considerable scattering with depth. The samples from the same formation show a wide range of carbonate contents, as indicated by plots of Ma12U and Ma12L. Furthermore, the carbonate contents of block sample (e.g., Ma8) also widely vary.

Carbonate contents of various marine sediments have been measured by Fukue et al. (1999). A comparison with those results is shown in Fig. 5. The results show that the Osaka Pleistocene clay layers have relatively low carbonate contents in comparison to those of the surface sediments in Tokyo Bay, Sagami, Bay, and Hiuchi-Nada of Seto Inland Sea. Some formations of the Pleistocene clay layers, such as Doc5, Ma4, Ma3, and Ma2, have very low contents of carbonates, i.e., less than 0.5 %, and they are possibly fresh water or brackish deposits (Fukue et al. 1999), although its possibility will be examined in the near future.

Effects of Percolation of Degassed Water

In this study, carbonic-acid water is percolated through soil specimens in order to dissolve carbonates and to see its possible influence on p_c value. The value of p_c, however, is very sensitive to mechanical disturbance of soil fabric, and the percolation of liquid may cause such a disturbance because of the application of a large difference of liquid pressure within the specimen. For the purpose to previously examine this effect, degassed water was percolated through a specimen and the consolidation behavior was compared with that of an intact specimen without percolation. The obtained compression curves in terms of volume ratio $f(=1+e)$ and effective stress σ' are presented in log-log scale, as shown in Fig. 6. As was noted, Ma8 sample was used for this examination. As shown in Fig. 4, the initial calcium carbonate contents of Ma8 have some variations among specimens. In this test, calcium carbonate content between the two specimens for percolation and without percolation is originally different, but each carbonate contents did not change by consolidation. Therefore, degassed water does not dissolve carbonate (see Table 3).

The $\log f$-$\log \sigma'$ relations without percolation and after the percolation of the degassed water are almost the same, as shown in Fig. 6. This means that the passage of degassed water does not provide any change from the intact sample. In addition to this confirmation, possible disturbance of fabric was further examined from the viewpoints of permeability. Table 4shows the coefficient of permeability k obtained under a load between overburden pressure p_0 and p_c. The suffix numbers 20, 50, and 100 mean the water

TABLE 5—p_c, p_c^*, *and the changes in carbonate contents of each formation.*

Formation	p_c (kPa)	p_c^* (kPa)	C (%)	C^* (%)	$\Delta C=C-C^*$ (%)
Dtc	336	331	0.55	0.18	0.37
Ma12U	398	341	4.3	1.5	2.9
Ma12L	460	440	2.8	1.9	0.9
		394	2.6	0.52	2.1
Ma11	835	783	0.86	0.54	0.33
Doc5	1403	1318	0.22	0.18	0.034
Ma8	1455	1288	0.92	0.74	0.18
Ma4	2291	2284	0.18	0.10	0.081
Ma2	2881	2808	0.21	0.18	0.034

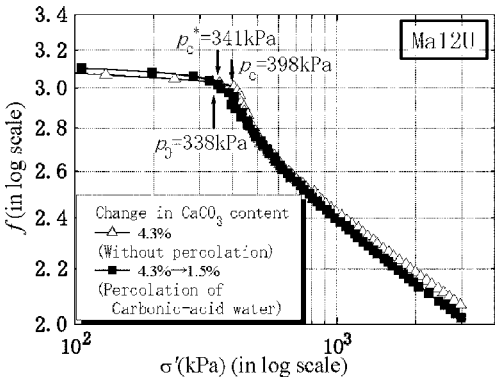

FIG. 7—*Compression curves of Ma12U.*

pressure difference in kPa applied on the specimen to percolate degassed water. Little difference in k value also verified little damage on soil fabric. Thus, it was confirmed that the passage of water through a specimen does not damage the fabric.

Change in Consolidation Behavior Due to the Passage of Carbonic-Acid Water

The results of the strain-rate controlled consolidation tests are summarized in Table 5. A strong effect of the removal of carbonates is seen for Ma12U formation, as shown in Fig. 7, while Ma4 formation shows little influence of carbonate dissolution, as shown in Fig. 8.

In this study, the following definitions are used in order to distinguish between the consolidation yield stresses of specimens with and without the passage of carbonic-acid water.

p_c: consolidation yield stress without the passage of carbonic-acid water (kPa)

p_c^*: consolidation yield stress after the passage of carbonic-acid water (kPa)

The decreasing rate of carbonate content ΔC is defined as follows:

ΔC:(before percolation, C)−(after percolation, C^*)(%)

All the data obtained show that calcium carbonate content decreases if carbonic-acid water is percolated through the soil specimens. If calcium carbonates were dissolved by carbonic-acid water, the reaction may be as follows:

$$CaCO_3 + CO_2 + H_2O \rightarrow Ca^{2+} + 2HCO_3^-$$

Thus, calcium carbonate will dissolve under the occurrence of water and carbon dioxide.

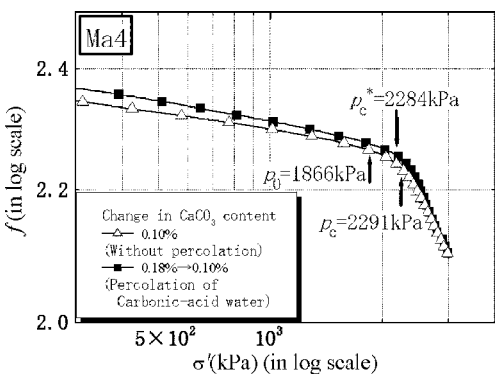

FIG. 8—*Compression curves of Ma4.*

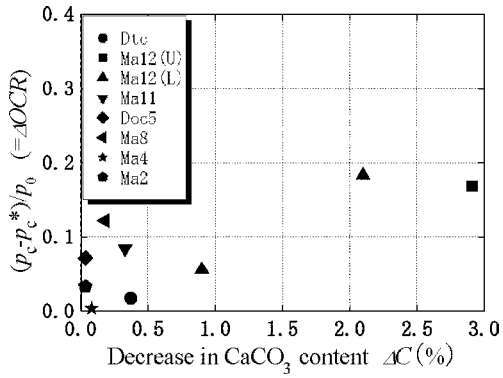

FIG. 9—*Correlation between* ΔOCR *and* ΔC.

The dissolution of carbonate generally causes the decrease in p_c value. However, the initial carbonate contents are less than 1 % for Dtc, Doc5, Ma4, and Ma2 formations, and the decreasing rates of p_c for these formations are relatively small. Thus, it is deduced that the decreasing rate of p_c resulting from the dissolution of carbonate is dependent on the initial carbonate content. If the initial carbonate content is higher than about 1 %, the decreasing rate of p_c is also high.

Change in OCR Caused by Dissolution of Carbonate

Figure 9 shows a relation between ΔC and the decrease in p_c normalized by the in situ overburdened pressure p_0. The changes in (OCR) of each formations are presented in Table 6. About Ma12(L)'s two plots, there are smaller and higher ΔC value(ΔOCR). This is due to the difference in the concentration of carbonic-acid water percolated.

In Fig. 9, the vertical axis is defined as

$$(\text{Decrease in } p_c)/p_0 = p_c/p_0 - p_c^*/p_0$$

$$= \text{OCR} - \text{OCR}^*$$

$$= \text{Decrease in OCR}(=\Delta\text{OCR})$$

where:

p_0=the in situ overburdened pressure (kPa),

OCR=the overconsolidation ratio without the passage of carbonic-acid water, and

OCR^*=the overconsolidation ratio after the passage of carbonic-acid water.

The results show that the greater the ΔC, the greater the ΔOCR. Thus, it is deduced that the $\log f$ -$\log \sigma'$ relationship represented by the pseudo-overconsolidation behavior of the Osaka Pleistocene clays can be partly contributed by the cementation effects due to calcium carbonate.

TABLE 6—*OCR and* OCR^* *of each formations.*

Formation	OCR	OCR^*
Dtc	1.17	1.16
Ma12U	1.18	1.01
Ma12L	1.27	1.22
		1.09
Ma11	1.35	1.27
Doc5	1.18	1.11
Ma8	1.06	0.939
Ma4	1.23	1.22
Ma2	1.31	1.28

Concluding Remarks

This study was performed to know the range in calcium carbonate contents involved in the Osaka Pleistocene clays, and to obtain the change of consolidation behavior due to the removal of the carbonate. The results can be summarized as follows:

1. For the Osaka Pleistocene clays, there is no strong correlation between carbonate content and consolidation yield stress.
2. If carbonate content is greater than 1 %, the removal of carbonate causes the decrease in p_c.
3. When the removal of carbonate becomes greater (as shown in Fig. 9), then the OCR becomes smaller.
4. The pseudo-overconsolidation behavior found in the Osaka Pleistocene clays is possibly dependent on the structure cemented by carbonates.

References

Aburatani, S., Matsui, T., Kamon, M., and Wada, M., 1998, "Geotechnical Characteristics of Incinerated MSW Ash Reclamation Sites of Osaka Bay Phoenix Project," *Environmental Geotechnics*, Seco e Pinto, ed., A. A. Balkema, Rotterdam, pp. 95–100.

Broecker, W. S. and Peng, T. -H., 1982, *Tracers in the Sea*, Eldigio Press, New York.

de Jonge, V. N., 1985, "The Occurrence of 'Epipsammic' Diatom Populations: A Result of Interaction Between Physical Sorting of Sediment and Certain Properties of Diatom Species," *Estuarine Coastal Shelf Sci.*, Vol. 21, No. 5, pp. 606–622.

Fukue, M., Nakamura, T., and Kato, Y., 1999, "Cementation of Soils Due to Calcium Carbonate," *Soils and Foundations*, Vol. 39, No. 6, pp. 55–64.

Fukue, M., Nakamura, T., Nagata, K., and Cheung, S. C. H., 1992, "Cementation of Marine Soils Due to Calcium Carbonate," *Proc. of the 1992 CSCE Annual Conference*, CSCE, pp. 145–152.

Kang, M., et al., 2001, "Consolidation Behavior of Osaka Pleistocene Clay with Well-Developed Structure by Separated-Type Consolidometer of High Capacity(in Japanese)," Report of the Port and Harbour Research Institute, Vol. 40, No. 2, pp. 23–44.

Kato, Y., and Okabe, S., 1988, "High Precise and Rapid Gasmetric Determination of Carbonate in Marine Sediments," *Journal of Faculty of Marine Science and Technology*, Vol. 27, pp. 1–8. (text in Japanese)

Molenaar, N., and Venmans, A. A. M., 1993, "Calcium Carbonate Cementation of Sand* A Method for Producing Artificially Cemented Samples for Geotechnical Testing and a Comparison with Natural Cementation Processes," *Eng. Geol. (Amsterdam)*, Vol. 35, No. 1–2, pp. 103–122.

Pusch, R., 1973, "Influence of Salinity and Organic Matter on the Formation of Clay Microstructure," *Proc. of the International Symposium on Soil Structure*, Gothenburg, Sweden, pp. 161–173.

Rosenqvist, I. Th., 1953, "Consideration on the Sensitivity of Norwegian Quick Clay," *Geotechnique*, Vol. III, No. 5, pp. 195–200.

Stronkhorst, J., Ariese, F., van Hattum, B., Postma, J. F., de Kluijver, M., Den Besten, P. J., Bergman, M. J. N., Daan, R., Murk, A. J., and Vethaak, A. D., 2003, "Environmental Impact and Recovery at Two Dumping Sites From Dredged Material in the North Sea," *Environ. Pollut.*, Vol. 124, pp. 17–31.

Sverdrup, H. U. Johnson, M. A., and Fleming, R. H., 1973, *The Oceans*, Modern Asia Editions, pp. 998.

Tsuchida, T., 2001, "General Interpretation on Natural Void Ratio-Overburden Pressure Relationship of Marine Deposits," domestic edition of *Soils and Foundations*(in Japanese), Vol. 41, No. 1, pp. 127–143.

Wakeman, T. H., and Themelis, N. J., 2001, "A Basin-Wide Approach to Dredged Material Management in New York/New Jersey Harbor," *J. Hard Mater.*, Vol. 85, pp. 1–13.

Journal of ASTM International, Vol. 3, No. 7
Paper ID JAI13349
Available online at www.astm.org

Takaharu Shogaki[1]

Microstructure, Strength, and Consolidation Properties of Ariake Clay Deposits Obtained from Samplers

ABSTRACT: The effect of tube wall friction on the microstructure of Ariake clay samples obtained from a small diameter sampler (45-mm sampler) and their strength and consolidation properties are examined from use of a color laser three-dimensional profile microscope plus unconfined compression, triaxial compression, and standard oedometer tests. The microstructure within 2 mm of the tube wall was disturbed due to wall friction. However, the disturbance in the rest of the sample had other causes and the samples were mechanically homogeneous. The unconfined compressive strength and preconsolidation pressure values obtained from the 45-mm sampler were 20 % to 40 % greater than those of the 75-mm sampler and their sample quality therefore higher.

KEYWORDS: microstructure, clay deposits, strength, consolidation, sample disturbance

Introduction

The quality of soil samples used in laboratory testing has directly influenced test results and design reliability based on them. Undisturbed soft clay deposits have been sampled by using a thin-walled tube sampler with fixed piston (JGS-1221) in Japan. However, studies on the sample disturbance caused by tube wall friction and their effect on the strength and consolidation properties are few. In this paper, the effect of tube wall friction on the microstructure of Ariake clay deposits obtained from a small diameter sampler (Shogaki 1997a) and their strength and consolidation properties are examined by use of a color laser three-dimensional profile microscope (CTM) plus Unconfined Compression (UCT) and Step Loading Oedometer Tests (SLOT).

Soil Samplers and Test Procedures

The undisturbed soil samples used in this study were obtained from the Holocene clay deposit located in the Ariake plain in Japan. Field sampling was performed with 45-mm sampler (Shogaki 1997a) for the depths (z) at z=5, 8, 10 and 12 m. The plasticity index (I_p), effective overburden pressure (σ'_{vo}) and the mean values ($\bar{\rho}_t$, $\bar{w}_n$, and $\bar{q}_u$) of wet density (ρ_t), natural water content (w_n), and unconfined compressive strength (q_u) are summarized in Table 1. The samples, 45 mm in diameter (d), were cut to 40 mm in length from the extruded section. The specimen size used in UCT is d=15 mm and height (h) is 35 mm and that is called a small (S) size specimen in this paper. One to four S specimens were sheared at a strain rate of 1 %/min from a sample using portable unconfined compression apparatus (Shogaki 1997b). It was confirmed that the strength properties between S and ordinary size specimens are similar (Sakamoto and Shogaki 2003). The TCT and SLOT are examined in accordance with JGS 0525-2000 and JIS A1217, respectively.

The microstructure of Ariake clay using CTM is examined for the samples at z=5, 10, and 12 m. The points of examination are Hh and Hv for the sedimentation surface (horizontal section) of soils and Vv and Vh for their vertical direction (vertical section), as shown in Fig. 1(*a*). The examination sites are 0, 0.3, 2, 5, and 22 mm inward (D_w) from the wall to tube center, as shown in Fig. 1(*b*). The D_w=22 mm is the center of the cross section of the sample.

Manuscript received March 31, 2005; accepted for publication December 8, 2005. Presented at ASTM Symposium on Contaminated Sediments: Evaluation and Remediation Techniques on 23–25 May 2006 in Shizuoka, Japan; M. Fukue, K. Kita, M. Ohtsubo, and R. Chaney, Guest Editors.
[1] National Defense Academy, Yokosuka, Kanagawa, Japan.

TABLE 1—$\bar{\rho}_t$, $\bar{w}_n$, I_p, $\bar{q}_u$, *and* σ'_{vo} *values.*

Depth (G.L.-m)	$\bar{\rho}_t$ (g/cm^3)	$\bar{w}_n$ (%)	I_p	$\bar{q}_u$ (kPa)	$\bar{\sigma}_{vo}$ (kPa)
5	1.32	131	68	25	32
8	1.36	120	70	37	42
10	1.35	125	73	31	49
12	1.40	103	52	35	56

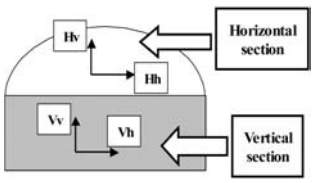

(a) Directions of examination

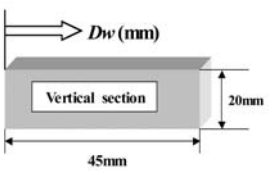

(b) Points of examination

FIG. 1—*Definitions of* Hh, Hv, Vv, Vh *and* D_w.

The mean distance (S_m) of surface irregularity of soil is the mean length of one cycle (X_{si}) of a contour in a certain base length (L_s) and defined as Eq. 1 (JIS B0610) from Fig. 2.

$$S_m = \frac{1}{m}\sum_{i=1}^{m} X_{Si} \tag{1}$$

where, m is the contour's number, including the L_s and 4, as in Fig. 2. The S_m values are calculated using a measurement accuracy of 0.1 μm for the surface irregularity.

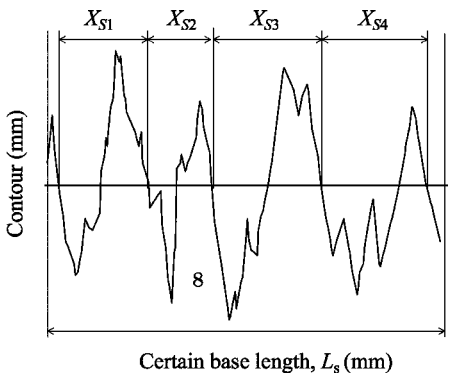

FIG. 2—*Definition of* S_m.

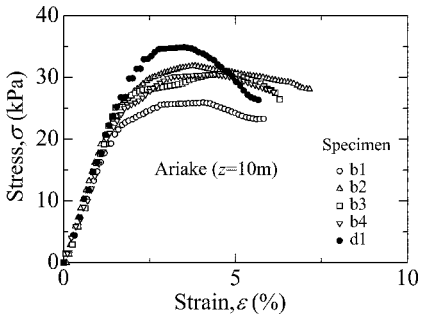

FIG. 3—*Relationships between stress and strain.*

Natural clay surface irregularity is formed by the ped and pore structures. If a soft clay deposit receives sample disturbance caused by shear, the surface irregularity becomes small since the ped structures are divided and soil particles enter the pores. Therefore, the S_m value can be used as an index to indicate sample disturbance.

Effect of D_w on Unconfined Compressive Strength Properties

Figure 3 shows the relationships between stress and strain obtained from specimens at a distance from the cutting edge of the tube (D_s) of 226 mm ($d1$) and 135 mm ($b1$, $b2$, $b3$ and $b4$) for the sampling tube depth of 10 m and test results are summarized in Table 2. The $d1$ specimen is taken from the center of the cross section of a sample and the $b1$, $b2$, $b3$ and $b4$ specimens are taken from a sample with $d45$ mm and $h40$ mm. The periphery of the $b1$, $b2$, $b3$ and $b4$ specimens are located at about 3 mm from the tube wall. It can be seen from Fig. 3 and Table 2 that the $d1$ and 4 ($b1$, $b2$, $b3$ and $b4$) specimens have similar sample quality since the relationships between stress and strain, w_n, q_u, strain at failure (ϵ_f), specimen suction (S_0) and secant modulus (E_{50}) are similar. Figure 3 and Table 2 show that sample disturbance, caused by tube wall friction, does not extend inward more than 3 mm.

Effect of D_w on S_m Value

To examine the effect of D_w on the S_m value, the ratio (RS_m) of the mean value $[\bar{S}_m(D_w)]$ of S_m of each D_w to that $[\bar{S}_m(22)]$ of $D_w=22$ mm are plotted against the D_w in Fig. 4. Figure 4 shows the results for the Vh section under $L_s=100$ μm. The RS_m values in the range of $D_w=0$ mm to 2 mm are greater than 1 and decrease with increasing D_w. However, the RS_m values in the area of $D_w>2$ mm are almost 1, therefore the soil microstructure shows no change.

The results of the Vv and Hh sections, obtained in the same way in Fig. 4, are shown in Figs. 5 and 6, respectively, to give a two-dimensional (2D) analysis. The relationships between RS_m and D_w, as shown in Fig. 4, are unrelated to the Vv, Vh, and Hh sections.

Figures 7 and 8 show the results of the Vv and Vh sections under $L_s=50$ μm and have the same tendency as Figs. 4 and 5, respectively. Clayton et al. (1998) analyzed the strain of soils, when the tube penetrates the ground, using the strain path method and showed the relationship between the maximum axial strain (ϵ_a) of the center of the sample and the ratio of the outer diameter to the tube thickness. The ϵ_a value is calculated by using this relationship as ±1.3 % and ±0.4 % for the 45-mm and 75-mm sampler, respectively. In the analysis by Clayton et al. (1998), the decrease in shear strength of soils caused by sample disturbance increases with increasing ϵ_a value. However, the sample quality obtained from the 45-mm sampler is similar to or greater than that of the 75-mm sampler (Shogaki 1997a; Shogaki et al. 2004; Shogaki and Sakamoto 2004). It is also shown in the next paragraph that the 45-mm sampler can take an equally high quality sample as the Sherbrooke sampler. In the analysis by Clayton et al. (1998), the soils were considered as homogeneous and isotropic materials and the shear strength was not taken into consideration as Baligh et al. did in 1987. The sample quality is controlled by many factors, including

TABLE 2—*Results of unconfined compression test.*

Specimen	D_s (mm)	w_n (%)	q_u (kPa)	ϵ_f (%)	S_0 (kPa)	E_{50} (MPa)
b1	135	135.7	25.9	4.43	7.38	1.4
b2	135	127.8	31.8	3.32	9.84	2.0
b3	135	130.6	30.7	4.63	11.80	2.5
b4	135	129.6	30.5	4.29	10.82	1.4
d1	226	135.3	34.9	3.50	7.38	1.6

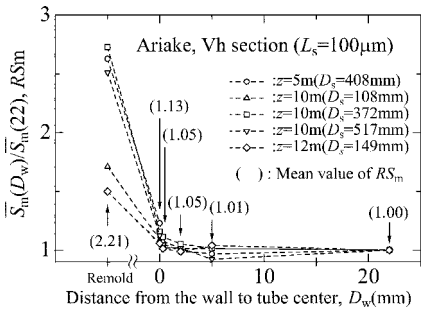

FIG. 4—*Relationships between RS_m and D_w.*

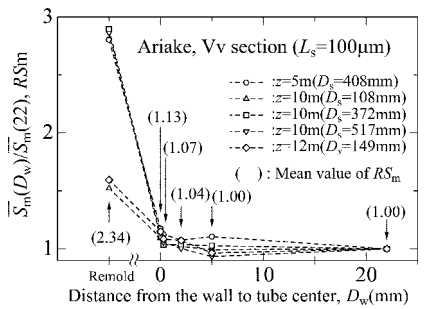

FIG. 5—*Relationships between RS_m and D_w.*

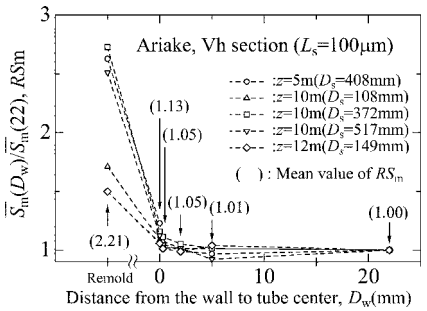

FIG. 6—*Relationships between RS_m and D_w.*

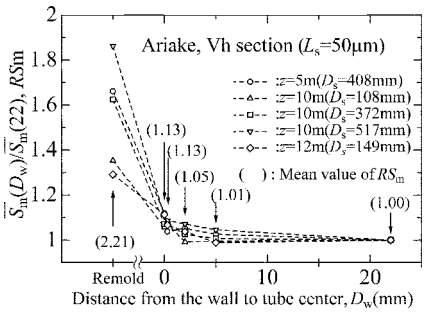

FIG. 7—*Relationships between RS_m and D_w.*

sample tube diameter. The effect of tube wall friction on the microstructure and undrained shear strengths of Ariake clay deposits, as one of many factors, was determined based on the results shown in Figs. 3–8.

Strength and Consolidation Properties of Ariake Clay Deposits Samples Obtained from Various Types of Samplers

Tanaka and Tanaka (1999) compared the sample qualities obtained from Shelby, NGI 54, ELE 100, Laval, Sherbrooke, and 75-mm samplers through UCT for the same site at Ariake. The specifications for the 45-mm, 75R and other samplers are also shown in Table 3. The area ratio (C_a) of the 45-mm sampler is greater than that of the 75-mm sampler (JPN).

The results of UCT and SLOT for all of the specimens tested from the 45-mm and 75-mm samplers are shown in Fig. 9. E and H in the remarks section of Fig. 9 mean the extension rod and hydraulic type samplers, respectively. The w_n values at the same depths are similar to the samples obtained from both

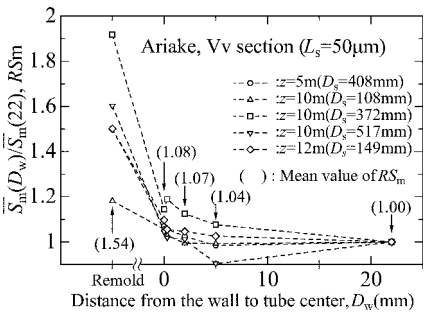

FIG. 8—*Relationships between RS_m and D_w.*

TABLE 3—*Specifications for each sampler.*

Sampling tube	Inside diameter (mm)	Tube length (mm)	Thickness (mm)	Area ratio C_a (%)	Piston
JPN	75	1000	1.5	8.2	yes
LAVAL	208	660	4	7.3	yes
Shelby	72	610	1.65	8.6	no
NGI54	54	768	13	54.4	no
ELE100	101	500	1.7	6.4	yes
Sherbrooke	350[a]	250[a]	…	…	no
45-mm	45	600	1.5	13.8	yes

[a]Dimension of the soil sample. $C_a = D_2^2 - D_1^2 / D_1^2 \times 100(\%)$ where D_1 is the inside diameter of cutting edge and D_2 is the outside diameter of the sampling tube.

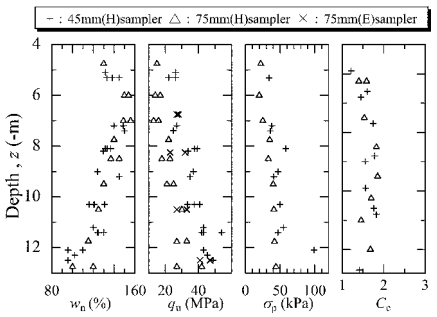

FIG. 9—*Results of UCT and SLOT.*

samplers. It can be seen that the index properties of samples obtained from different types of samplers are therefore almost similar. The ratios of the mean values of q_u, E_{50}, σ'_p and C_c of the 75-mm sampler to those of the 45-mm sampler are plotted against the depth (z) in Fig. 10. The ratios $R(q_u)$ of the mean values of q_u for the hydraulic and extension rod type samplers are 0.67 and 0.85, respectively, and the ratios $R(\bar{\sigma}'_p)$ of the mean value of the preconsolidation pressure (σ'_p) for the hydraulic type sampler are 0.71, as shown in Fig. 10. The q_u and σ'_p values obtained from the 45-mm sampler are 20 % to 40 % greater than those of the 75-mm sampler and their sample quality therefore higher.

The stress-strain curves for the specimens at about 10-m depths, obtained from these samplers, are shown in Fig. 11. The tests, except for the 45-mm sampler, were performed by the Geotechnical Survey Laboratory of the Port and Airport Research Institute (Tanaka and Tanaka 1999). However, only one particular engineer only, using different samplers, did the Ariake clay soil sampling. It can be assumed that this engineer's sampling methods had no effect on sample quality, but he has never used the 45-mm sampler. The specimen sizes used in UCT were d=15 mm and h=35 mm for the sample taken with the 45-mm sampler and d=35 mm, h=80 mm for the 75-mm sampler. However, there were no differences in strength characteristics between the small and the ordinary size specimens for Ariake clay (Sakamoto and Shogaki 2003). In Fig. 11, it can be seen that the q_u values obtained from the 45-mm sampler are larger than the ones by Sherbrooke, Laval, JPN 75 samplers, etc. The specimen depths are also listed in Fig. 11 and the depths are similar for each specimen. However, it is difficult to examine closely the test results of each specimen related to sampler types since the index properties of specimens are not shown in the Tanaka and Tanaka paper.

The $q_u/2$ values are plotted against the z in Fig. 12. The $q_u/2$ values (•) of z=5, 7, 8, 9, 10, 11 and 12 m obtained from the 45-mm sampler are similar or greater than those of Sherbrooke (◇) or other Japanese and foreign samplers. The Sherbrooke sampler can take a block sample. However, its design, compared to that of the tube sampler, limits its capability to be used effectively in soft clay deposits or hard soils due to the cutting action required, which causes sample disturbance and it also requires a longer sampling time, which also contributes to sample stress.

The characteristics of the 45-mm sampler influencing sample quality are as follows;

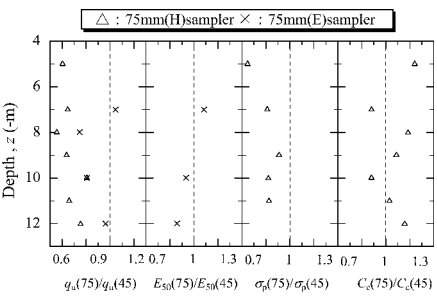

FIG. 10—*Relationships between z and ratios of the mean values of q_u, E_{50}, σ'_p and C_c.*

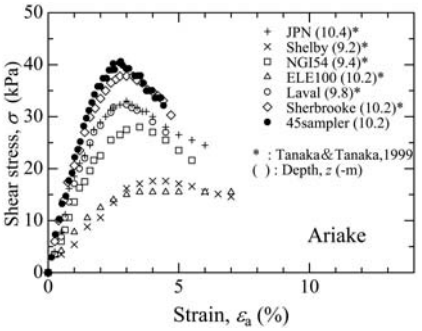

FIG. 11—*The stress-strain curves* ($z \fallingdotseq 10$ m).

1. The sampling tube penetration is smoother due to the longer outer tube.
2. The penetration force is strong and the penetration speed is higher.

It is difficult to control the angle of penetration into the soil. However, the penetration speed for time is almost constant in the 45-mm sampler and the mean penetration speed of the tube was about twice that of the single tube type sampler with an inner diameter of 70 mm for Niigata sand (Shogaki et al. 2002). For the Pleistocene Osaka Ma 12 clays with $q_u \fallingdotseq 500$ kPa, the sampling times for 50 cm penetration were as short as 5 s to 10 s and high quality samples could be taken (Shogaki et al. 2004a). Therefore, it is considered that these characteristics of the 45-mm sampler are the main reasons why high quality samples can be taken with this sampler.

Conclusions

The conclusions obtained in this study are summarized as follows:

1. The microstructure within 2 mm of the tube wall was disturbed due to wall friction. However, the disturbance in the rest of the sample had other causes and the samples were mechanically homogeneous in the case of the 45-mm sampler.
2. From the comparison of the strength and consolidation properties for samples obtained from the 75-mm sampler, the samples obtained from the 45-mm sampler did not received soil strain, when the tube penetrated the ground, as analyzed by Clayton et al. (1998) for other small sized samplers. It can be judged that the soils were considered as homogeneous and isotropic materials and the shear strength was not taken into consideration in his analysis.
3. The undrained shear strength obtained from the 45-mm sampler were similar or greater than those of Sherbrooke or other Japanese and foreign samplers.

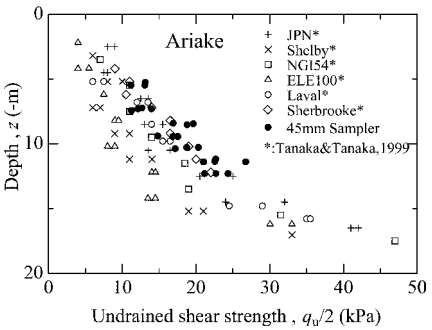

FIG. 12—*Relationships between* $q_u/2$ *and* z.

4. The unconfined compressive strength and preconsolidation pressure values obtained from the 45-mm sampler were 20 % to 40 % greater than those of the 75-mm sampler and their sample quality therefore higher.

References

Baligh, M. M., Azzouz, A. S., and Chin, C. T., 1987, "Disturbance Due to Ideal Tube Sampling Disturbance," *J. Geotech. Eng. Div., Am. Soc. Civ. Eng.*, Vol. 113, No. GT7, pp. 739–757.

Clayton, C. R. I., Siddique, A., and Hopper, R. J., 1998, "Effects of Sampler Design on Tube Sampling Disturbance—Numerical and Analytical Investigations," *Odontol. Din*, Vol. 48, No. 6, pp. 847–867.

Japanese Geotechnical Standards, 1996, "Method for K_0 Consolidate-Undrained Triaxial Compression Test on Soils with Pore Water Pressure Measurement," JGS 0525-1996, pp. 349–358 (in Japanese).

Japanese Geotechnical Society, 2005, "The Method for Obtaining Undisturbed Soil Sampling Thin-Walled Tube Sampler with Fixed Piston (JGS 1221-1995)," Standards of Japanese Geotechnical Society for Soil Sampling–Standards and explanations, pp. 1–7.

Japanese Standards Association, 2000, "Test Method for One-Dimensional Consolidation Properties of Soils," JIS A1217-2000, pp. 1–13.

Japanese Standards Association, 2000, "Geometrical Product Specification (GPS)—Surface Texture: Profile Method—Definitions and Designation of Rolling Circle Waviness," JIS B0610-2000, pp. 1–13.

Sakamoto, R. and Shogaki, T., 2003, "Effect of Specimen Size on Unconfined Compressive Strength Properties for Natural Clay Deposits," *The 13th International Offshore and Polar Engineering Conference and Exhibition*, Honolulu, pp. 426–431.

Shogaki, T., 1997a, "A Small Diameter Sampler with Two-Chambered Hydraulic Piston and the Quality of its Samples," *Proc. of the 14th ICSMFE*, Hamburg, pp. 201–204.

Shogaki, T., 1997b, "Strength Properties of Clay by Portable Unconfined Compression Apparatus," *Proc. of Int. Conf. on Geotechnical Engineering for Coastal Development*, Yokohama, pp. 85–88.

Shogaki, T., Nakano, Y., and Shibata, A., 2002, "Sample Recovery Ratios and Sampler Penetration Resistance in Tube Sampling for Niigata Sand," *Soils Found.*, Vol. 42, No. 5, pp. 111–120.

Shogaki, T., Sakamoto, R., Kondo, E., and Tachibana, H., 2004, "Small Diameter Cone Sampler and its Applicability for Pleistocene Osaka Ma12 Clay," *Soils Found.*, Vol. 44, No. 4, pp. 119–126.

Shogaki, T. and Sakamoto, R., 2004, "The Applicability of a Small Diameter Sampler with a Two-Chambered Hydraulic Piston for Japanese Clay Deposits," *Soils Found.*, Vol. 44, No. 2, pp. 113–124.

Tanaka, M. and Tanaka, H., 1999, "The Current Position of Japanese Sampling Method in the Worldwide Standard," *The 44th Geotechnical Symposium*, pp. 223–232, (in Japanese).

Journal of ASTM International, Vol. 3, No. 7
Paper ID JAI13348
Available online at www.astm.org

Takaharu Shogaki[1]

Effect of Specimen Size on Consolidation Parameters of Marine Clay Deposits

ABSTRACT: The effect of specimen size on consolidation parameters of undisturbed marine clay deposits and their remolded samples are examined through the standard incremental loading oedometer test I.A.W. JIS A 1217. There are two sizes of specimens, a *d*60 specimen (60 mm *d* and 20 mm*h*) and a *d*30 specimen (30 mm*d* and 10 mm*h*). The relationships between void ratio and consolidation load were unrelated to specimen size in the loading and unloading process. The coefficients of consolidation (c_v) obtained from the *d*30 specimen were smaller than those of the *d*60 specimen in the over-consolidated stage. This was caused by larger t_{90} values (the required time for 90% consolidation) of the *d*30 specimen than those of the *d*60 specimen. The t_{90} ratio was about 1.3 in this stage. In the normally consolidated stage, the c_v, coefficient of volume compressibility (m_v), and permeability (k) were unrelated to specimen size. The consolidation parameters obtained from the *d*30 specimen were almost the same as those of the *d*60 specimen in the normally consolidated stage. The *d*30 specimen, retrieved from the 45 mm, small tube sampler or a 75-mm sampler, is more effective for sample testing purposes.

KEYWORDS: size effect, clay deposits, consolidation parameters, oedometer test

Introduction

A new type of 45-mm soil sampler and cone sampler having a two-chambered hydraulic piston were developed by Shogaki (1997) and Shogaki et al. (2004) and it has been confirmed that these samplers can take high quality samples from organic soil, soft and hard clays and Niigata sand (Shogaki and Sakamoto 2004; Shogaki et al. 2002a). The specimen size usually used in Japan for Step Loading Oedometer Tests (SLOT) and Direct Shear Tests (DST) is a specimen 60 mm in diameter (d) and 20 mm in height (h). The thin-walled tube sampler normally used in Japan for obtaining undisturbed soil samples is the 75S, in accordance with the Japanese Geotechnical Standard (1998a) (JGS 1221-1995), having an inner diameter of 75 mm and a length of 1 m. The reason for using *d*60 specimens in Japan is that one specimen can be taken from a sample 75 mm in diameter and 30 mm in height. However, the number of samples required for testing and laboratory work preparation is limited by use of this sampler, due to the size of the sample obtained, latent cracks, or inhomogeneity. In addition to this, undisturbed sampling of hard soils like Pleistocene is difficult. Therefore, the smaller size specimen presents a more effective use of samples.

In this paper, the effects of specimen size on the consolidation parameters of undisturbed marine clay deposits and their remolded samples are examined through the SLOT in accordance with JIS A 1217. There are two sizes of specimens, a *d*60 specimen and a *d*30 specimen (30 mm *d* and 10 mm *h*).

Soil Samples and Test Procedures

The undisturbed soil samples used in this study were obtained from the Holocene and Pleistocene clay deposits located in the Holocene plains of Hachirougata, Urayasu, Yokohama, Isogo, Nagoya, Osaka, Kobe, Iwakuni, Tokuyama, Kumamoto, Ariake, Sakai, Saigou, and Kahokugata in Japan, as shown in Fig. 1, Bothkennar clay in the United Kingdom and Kimhae and Pusan new port clays in Korea.

The 75-mm rotary double-tube sampler identified as 75R, in accordance with the Japanese Geotechnical Standard (JGS 1222-1995) for obtaining undisturbed soil samples using a rotary double-tube sampler,

Manuscript received March 31, 2005; accepted for publication December 8, 2005. Presented at ASTM Symposium on Contaminated Sediments: Evaluation and Remediation Techniques on 23-25 May 2006 in Shizuoka, Japan; M. Fukue, K. Kita, M. Ohtsubo, and R. Chaney, Guest Editors.
[1] National Defense Academy, Yokosuka, Kanagawa, Japan.

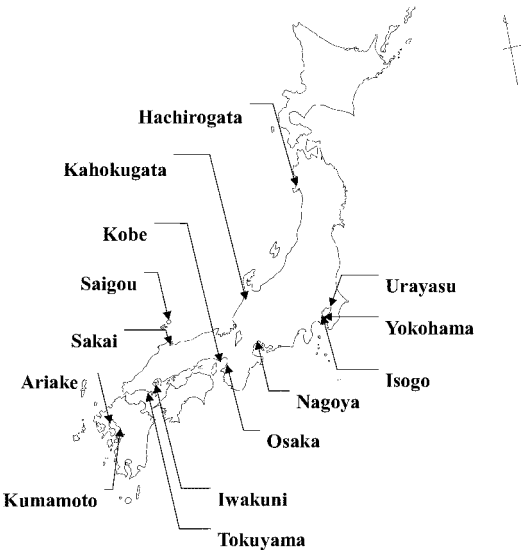

FIG. 1—*Soil sampling sites used in this study.*

was used instead of the 75-mm sampler normally used in Japan in accordance with JGS 1221-1995 for the Pleistocene clay deposits of Nagoya, Iwakuni, and Osaka. The water content (w_n), plasticity index (I_p), effective overburden pressure (σ'_{vo}), unconfined compressive strength (q_u), preconsolidation pressure (σ'_p) and over-consolidated ratio (OCR) (defined as the ratio of σ'_p to σ'_{vo}) are summarized in Table 1. The I_p and q_u values are in the ranges of 22 to 150 and 25 kPa to 670 kPa, respectively.

Figure 2 shows the location of specimens for a sample, 75 mm in *d* and 50 mm in *h*, from the 75-mm sampler. Two *d*30 specimens and one *d*60 specimen can be taken from a sample, as shown in Fig. 2. Shogaki et al. (1995) shows that the strength and deformation properties of ten S (small size) specimens, 15 mm in *d* and 35 mm in *h*, obtained from a sample 75 mm in *d* and 45 mm in *h* are similar in an engineering sense. The specimen site, as shown in Fig. 2, does not affect the sample disturbance caused by tube penetration and friction between soil and tube during sample extrusion. That was also confirmed by using a Scanning Electron Microscope (Shogaki and Matsuo 1985; Shogaki et al. 2002b) The *d*30 specimen can be taken from a sample obtained from the 45-mm and cone samplers.

The SLOT was performed using a load increment ratio of unity and the duration of loading for each load increment was one day. The values of the σ'_p and the compression index (C_c) were determined from the void ratio (e) to consolidation pressure (σ'_v) curves corresponding to 24-h compression. Mikasa (1964) was used to identify preconsolidation pressure on the 24-h $e-\log\sigma'_v$ curve. This method has been employed in Japan as the Japanese industrial standard for determining one-dimensional consolidation properties of soils (JIS A 1217-2000). It was shown by Shogaki et al. (2000) that the mean values of σ'_p, according to Casagrande's method (1936), in the range of $4<b/a<10$ are within ±5 % of that of Mikasa's method and unrelated to the I_p, q_u, and sample disturbance where b is the length of one cycle in logarithm scale of $\sigma'_v$for a length (a) of $e=0.1$.

The coefficient of consolidation (c_v) and coefficient of volume compressibility (m_v) are also calculated in accordance with JIS A1217-2000.

Equality of Index Properties and Sample Quality of and Specimens

The w_n, initial void ratio (e_0) and volumetric strain (ϵ_{vo}) of both specimens are compared in Figs. 3–5, respectively. The ϵ_{vo} value is defined by Eq 1 using e_0 and e_1, where e_1 is the void ratio under σ'_{vo} value, and can be used as an index to indicate the sample disturbance (Shogaki 1996).

TABLE 1—w_n, I_p, σ'_{vo}, q_u, *and* σ'_p *of each sample*

No.	Soil	w_n(%)	I_p	σ'_{vo}(kPa)	q_u(kPa)	σ'_p(kPa)	σ'_p/σ'_{vo}
1	Ariake F6	118.0	46.1	46.0	32.0	52	1.13
2	Hachirogata JPN-1	191.8	150.2	36.0	25.0	46	1.30
3	Isogo 5	52.3	31.0	120.0	106.0	238	1.98
4	Iwakuni 16-1	83.5	58.6	130.0	538.0	170	1.31
5	Iwakuni 16-2	83.5	58.6	130.0	538.0	170	1.31
6	Iwakuni 16-3	80.0	59.0	130.0	538.0	315	2.42
7	Iwakuni 16-4	80.0	59.0	130.0	538.0	315	2.42
8	Kahokugata 19	111.8	88.0	174.0	135.0	154	0.89
9	Kumamoto 9-1	90.7	32.0	87.0	80.0	98	1.13
10	Kumamoto 9-2	90.7	32.0	87.0	80.0	98	1.13
11	Kumamoto 9-3	90.7	32.0	87.0	80.0	98	1.13
12	Kumamoto 15-1	97.5	56.5	143.0	99.0	145	1.01
13	Kumamoto 15-2	97.5	56.5	143.0	99.0	145	1.01
14	Nagoya 2-1	56.4	38.0	355.0	592.0	790	2.23
15	Nagoya 2-2	56.4	38.0	355.0	592.0	790	2.23
16	Nagoya 2-3	56.4	38.0	355.0	592.0	790	2.23
17	Nagoya 6-1	36.9	22.0	432.0	670.0	950	2.20
18	Nagoya 6-2	36.9	22.0	432.0	670.0	950	2.20
19	Osaka 47-1	35.8	33.4	730.0	442.0	845	1.16
20	Osaka 47-2	35.8	33.4	730.0	442.0	845	1.16
21	Kobe 9-1	91.3	81.0	57.0	72.0	98	1.72
22	Kobe 9-2	91.5	81.0	57.0	72.0	95	1.67
23	Kobe 9-3	91.3	81.0	57.0	72.0	95	1.67
24	Kobe 9-4	91.3	81.0	57.0	72.0	95	1.67
25	Saigou 2-2	67.6	42.0	15.0	29.3	34	2.27
26	Saigou 6-1	60.3	23.0	43.0	41.0	22	0.51
27	Saigou 13-1	58.5	24.0	86.0	67.0	126	1.47
28	Sakai 7-1	52.7	34.5	81.0	100.0	196	2.42
29	Tokuyama 2-4	86.5	26.2	51.0	42.0	56	1.10
30	Urayasu 12-1	72.9	27.0	104.0	150.0	280	2.69
31	Urayasu 12-2	72.4	27.0	104.0	150.0	270	2.60
32	Yokohama 2	47.9	29.7	156.0	86.0	150	0.96
33	Yokohama 8	73.9	61.5	230.0	183.0	264	1.15
34	Bothkennar 13-1(UK)	57.6	50.1	102.0	121.0	200	1.96
35	Bothkennar 13-2(UK)	57.6	50.1	102.0	121.0	200	1.96
36	Kimhae 4-7-1(Kr)	38.7	25.5	95.0	91.0	143	1.51
37	Kimhae 4-7-2(Kr)	38.7	25.5	95.0	91.0	143	1.51
38	Kimhae 4-15-1(Kr)	55.0	34.1	151.0	107.0	167	1.11
39	Kimhae 4-15-2(Kr)	55.0	34.1	151.0	107.0	167	1.11
40	Kimhae 7-15-1(Kr)	66.2	40.0	154.0	93.0	128	0.83
41	Kimhae 7-15-2(Kr)	66.2	40.0	154.0	93.0	128	0.83
42	Pusan new port 2.2m②	59.5	29.4	3.7	42.3	30	8.11
43	Pusan new port 2.2m⑤	47.8	29.4	3.7	42.3	50	13.51
44	Pusan new port 5.8m①	61.2	34.5	27.8	32.9	38	1.37
45	Pusan new port 7.8m②	60.2	38.5	40.8	57.5	56	1.37
46	Pusan new port 7.8m⑤	59.3	38.5	40.8	57.5	63	1.54
47	Pusan new port 13.8m②	68.5	45.1	77.8	73.6	60	0.77
48	Pusan new port 13.8m⑤	67.5	45.1	77.8	73.6	89	1.14
49	Pusan new port 17.8m②	66.9	47.9	108.2	96.9	105	0.97
50	Pusan new port19.8m②	65.8	46.5	114.9	94.1	125	1.09
51	Pusan new port 21.8m②	67.3	44.7	127.1	90.6	125	0.98
52	Pusan new port ④21.8m②	67.4	44.7	127.0	90.6	160	1.26
53	Pusan new port ④21.8m⑤	66.0	44.7	127.0	90.6	155	1.22
54	Pusan new port 25.8m②	75.8	48.5	148.4	95.8	150	1.01
55	Pusan new port 25.8m⑤	74.5	48.5	148.4	95.8	152	1.02
56	Pusan new port 26.09m②	53.6	29.9	148.1	64.1	120	0.81
57	Pusan new port 34.09m②	37.7	22.8	205.4	117.4	280	1.36

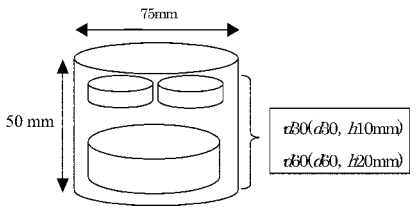

FIG. 2—*The location of specimens in a sample.*

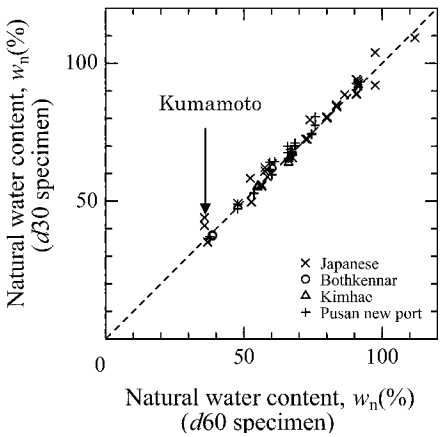

FIG. 3—w_n *values.*

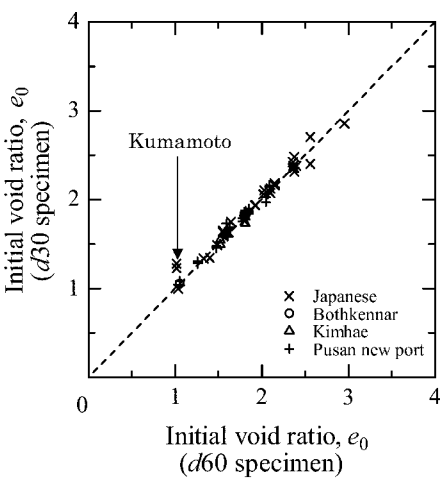

FIG. 4—e_0 *values.*

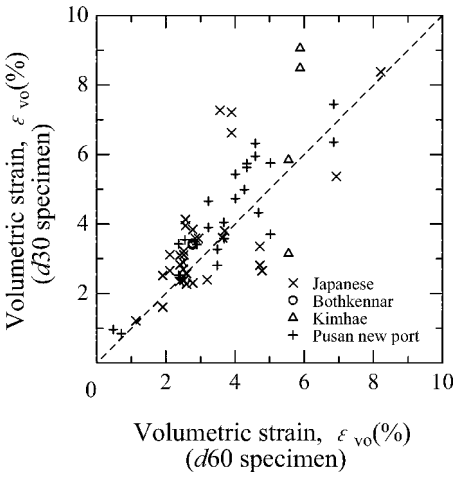

FIG. 5—ϵ_{vo} *values.*

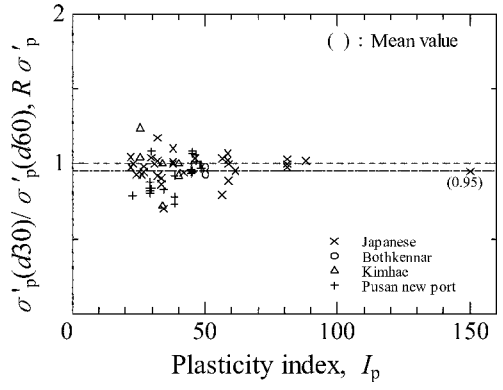

FIG. 6—*The relationship between* $R\sigma'_p$ *and* I_p.

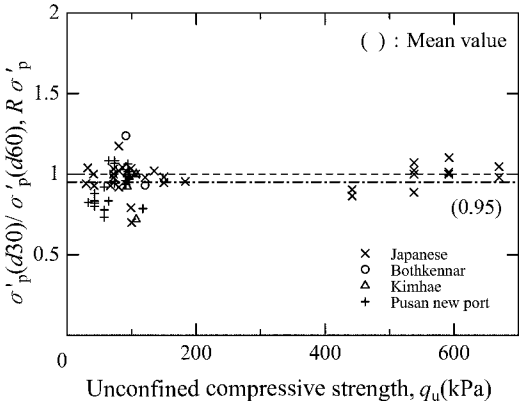

FIG. 7—*The relationship between* $R\sigma'_p$ *and* q_u.

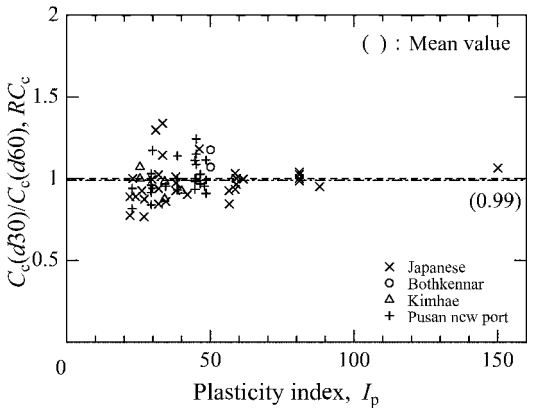

FIG. 8—*The relationship between* Rc_c *and* I_p.

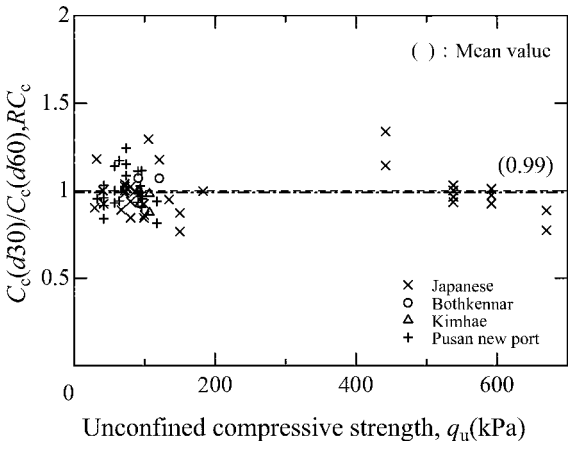

FIG. 9—*The relationship between* Rc_c *and* q_u.

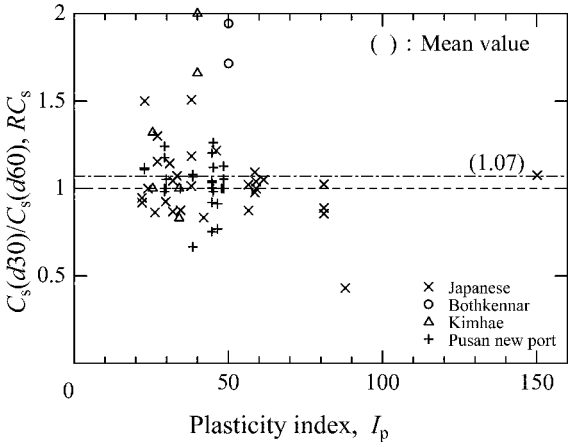

FIG. 10—*The relationship between* Rc_s *and* I_p.

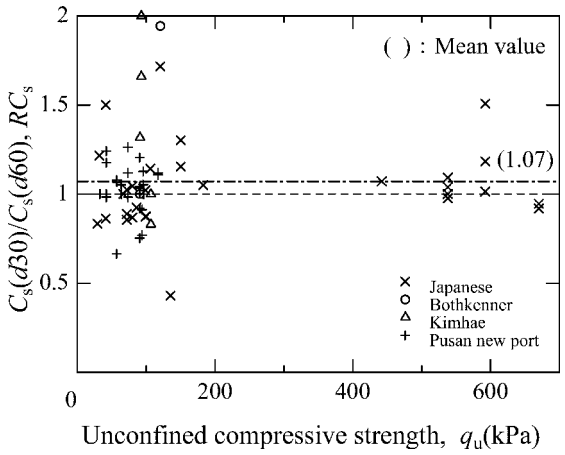

FIG. 11—*The relationship between* Rc_s *and* q_u.

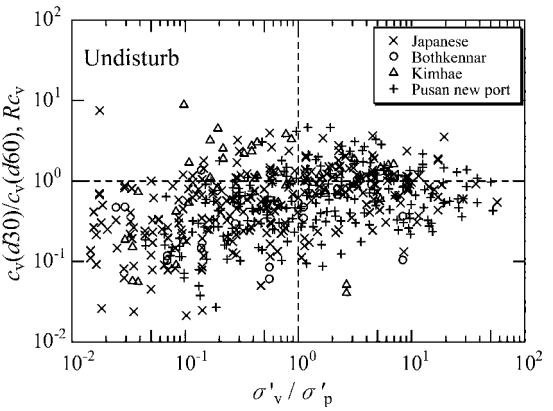

FIG. 12—*The relationship between* Rc_v *and* σ'_v/σ'_p.

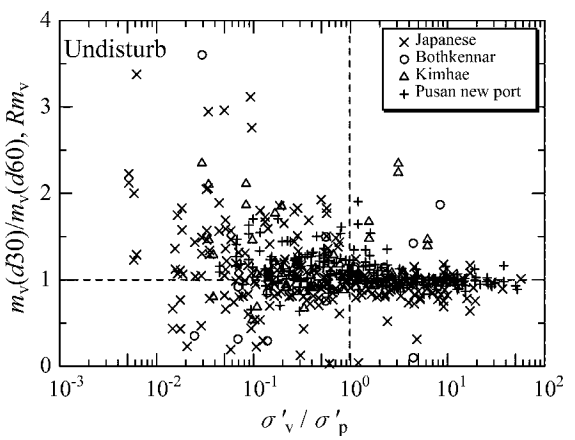

FIG. 13—*The relationship between* Rm_v *and* σ'_v/σ'_p.

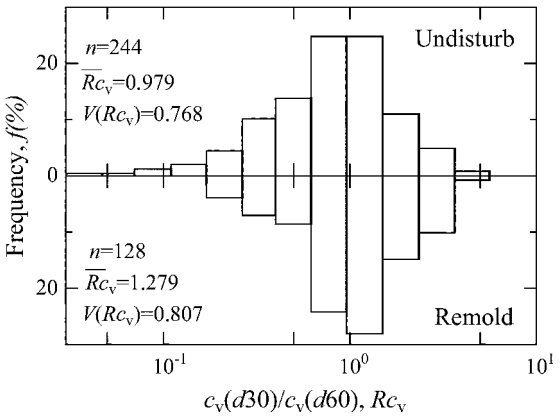

FIG. 14—*The frequency distributions of* Rc_v.

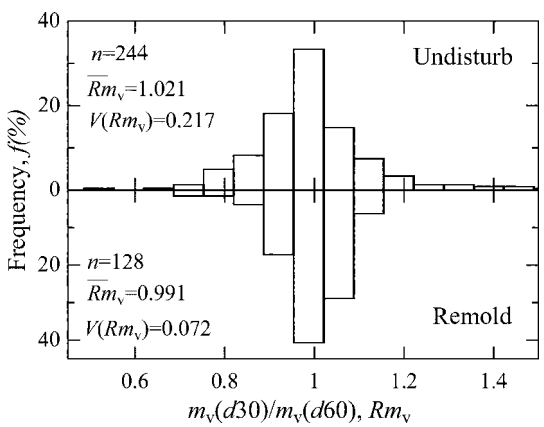

FIG. 15—*The frequency distributions of* Rm_v.

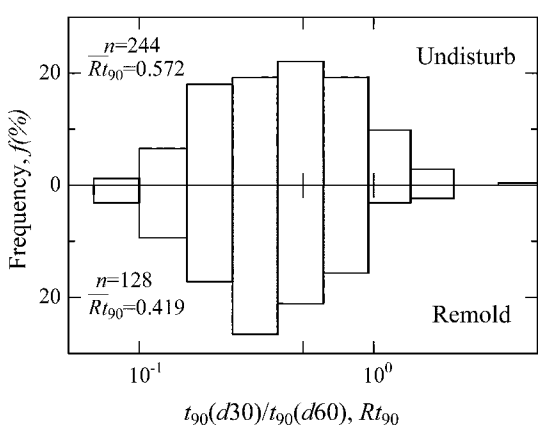

FIG. 16—*The frequency distributions of* Rt_{90}.

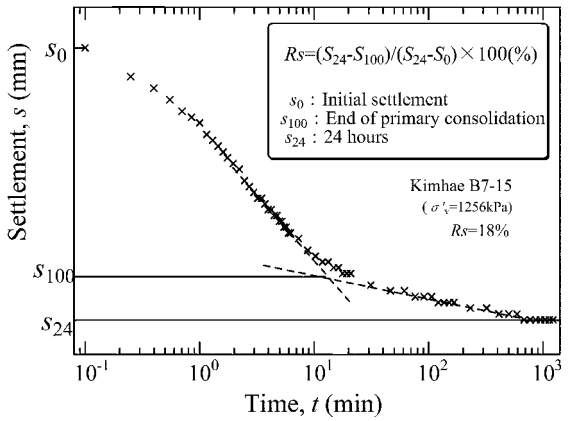

FIG. 17—*The relationship between s and t.*

$$\epsilon_{vo} = \frac{e_0 - e_1}{1 + e_0} \times 100(\%) \tag{1}$$

The symbols used in these figures are classified as Japanese, Bothkenner, Kimhae, and Pusan new port clays to avoid complication. The specimen having the largest difference of w_n in both specimen sizes is Kumamoto clay and the w_n value of the *d*30 specimen is 5 % larger than that of the *d*60 specimen. However, the w_n and e_0 values obtained from both specimens, except Kumamoto clay, are similar and unrelated to specimen size. The consolidation parameters of both specimens were similar, as shown in the next paragraph, including Kumamoto clay. It is considered that the difference of 5 % in w_n of Kumamoto clay is based on the accuracy of the consolidation test or there is no effect for consolidation parameters. Therefore, Kumamoto clay is treated the same as other Japanese clays from Fig. 5 on.

The sample quality of specimens for both sizes is similar since the ϵ_{vo} values are similar. Therefore, it can be seen that the sedimental environment, initial stress conditions, and sample quality for both specimen sizes are also similar since all specimens for both sizes were obtained from a sample 75 mm in *d* and 40 mm in *h*. Therefore, the test results can determine the effect of specimen size on the consolidation parameters of marine clay deposits.

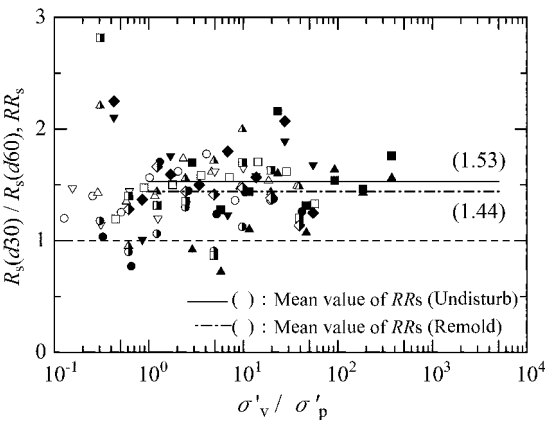

FIG. 18—*The relationship between* RR_s *and* σ'_v/σ'_p.

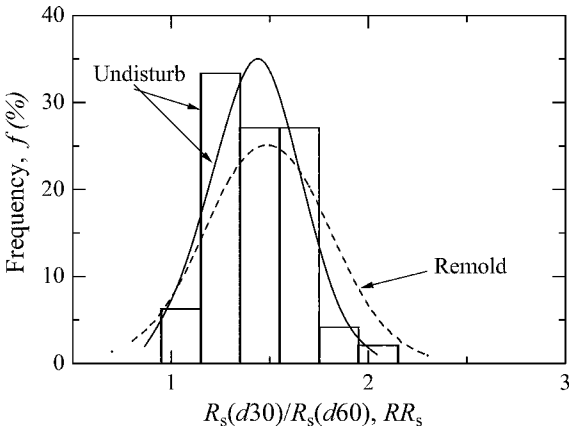

FIG. 19—*The frequency distributions of* RR_s.

Effect of Specimen Size on Consolidation Properties under Primary Consolidation

The ratios ($R\sigma'_p$) of σ'_p values obtained from the $d30$ specimen to those of the $d60$ specimen are plotted against the I_p and q_u values in Figs. 6 and 7, respectively. The ratios (RC_c) of C_c, arranged in the same manner, are also shown in Figs. 8 and 9. The $R\sigma'_p$ and RC_c values are unrelated to the I_p and q_u values and the mean values for all samples are 0.95 and 0.99, respectively.

Figures 10 and 11 also show the ratios (RC_s) of swelling index (C_s). The RC_s values are 0.4 to 2.0 in the range of $q_u \fallingdotseq (80-150)$ kPa. The C_s values of the $d60$ and the $d30$ specimens are 0.024 to 0.276 and 0.021 to 0.297, respectively, and they are similar. The large RC_s values are caused by the effect of the range of the ratio on C_s. Figures 6 to 11 show that the consolidation properties of the load and unload stages in $e-\log \sigma'_v$ relations are unrelated to specimen sizes. It was confirmed that those remolded samples have similar characteristics as those shown in Figs. 6 to 11(Shogaki et al. 2002c).

The ratios (Rc_v and Rm_v) of the $d30$ to $d60$ specimens for undisturbed samples are plotted against the σ'_v/σ'_p values in Figs. 12 and 13, respectively, where the σ'_p values were obtained from $d60$ specimens. The c_v values obtained from the $d30$ specimen were smaller than those of the $d60$ specimen in the over-consolidated stage. This was caused by larger t_{90} values (the required time for 90 % consolidation) of the $d30$ specimen. The t_{90} ratio was about 1.3 in this stage. The histograms for the Rc_v and Rm_v values are

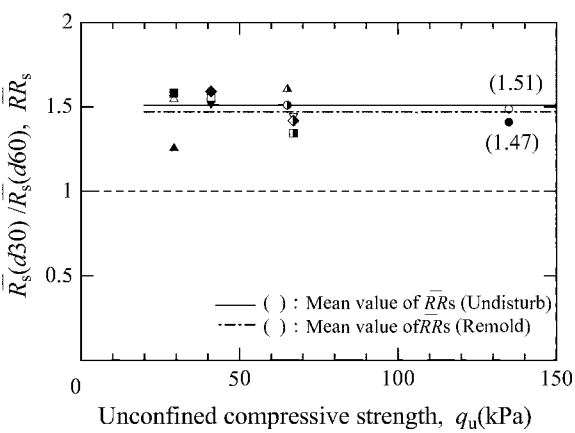

FIG. 20—*The relationship between* $\bar{R}R_s$ *and* q_u.

TABLE 2—*The symbols for plots used in Figs. 20 and 21.*

Condition	Symbol	Soil
Undisturb	○	Kahokugata19
	△	Saigou2-1
	□	Saigou6-1
	▽	Saigou13-1
	⊗	Pusan new port7.8
	⊕	Pusan new port25.8
	•	Kahokugata19
	▲	Saigou2-1
	■	Saigou2-2
	▼	Saigou6-1
	◆	Saigou6-2
Remold	◑	Saigou10-1
	◇	Saigou10-2
	◨	Saigou13-1
	◈	Saigou13-2
	×	Pusan new port7.8
	+	Pusan new port25.8

shown in Figs. 14 and 15, respectively. The c_v and m_v values in Figs. 14 and 15 are obtained from the normally consolidated stage greater than the σ'_p values since they are used for consolidation analysis of soils. The upper and lower graphs in these figures show the frequency distribution for the undisturbed and remolded samples, respectively. The number (n) of specimens, mean values ($\bar{R}c_v$ and $\bar{R}m_v$) of Rc_v and Rm_v, and the coefficient of variation [$V(Rc_v)$ and $V(Rm_v)$] are also shown in Figs. 14 and 15. These statistical values were unrelated to soil types. Therefore, Japanese and Pusan new port clays were used for remolded samples. The I_p values of remolded samples were in the range of 23 to 88 and included with those of other clays. The Rc_v and Rm_v values were about 1 for the undisturbed clays. On the other hand, the $V(Rc_v)$ and $V(Rm_v)$ values are 0.77 and 0.22 for undisturbed samples and 0.81 and 0.07 for remolded samples, respectively, and the $V(Rc_v)$ values are larger than those of $V(Rm_v)$ since the variation of Rc_v is larger than those of Rm_v.

The histograms of the ratios (Rt_{90}) of t_{90} obtained from the same manner as the Rc_v value are shown in Fig. 16. The mean value (Rt_{90}) of Rt_{90} are 0.57 for undisturbed and 0.42 for remolded samples.

Effect of Specimen Size on Consolidation Phenomenon under Secondary Consolidation

It is well known (e.g., Aboshi 1973) that the amount of secondary consolidation is influenced by the specimen size. The ratio (R_s) of the amount of secondary consolidation to settlement (s_{24}) at 24 h after

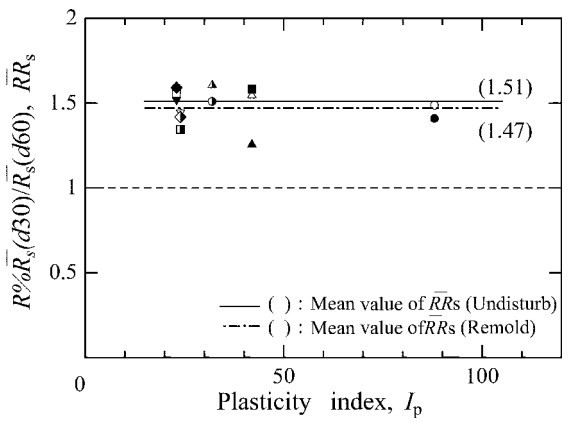

FIG. 21—*The relationship between* $\bar{R}R_s$ *and* I_p.

TABLE 3—*Statistical values of* RR_s.

	Number	Mean value	Coeficient of variation
Undisturb	48	1.43	0.154
Remold	72	1.49	0.208

loading is defined as shown in Fig. 17, where s_{100} is the settlement for the end of primary consolidation obtained from the Casagrande method. The ratios (RR_s) of the R_s of the $d30$ specimen to those of the $d60$ specimen are plotted against σ'_v/σ'_p values in Fig. 18. The symbols for plots used in Figs. 18, 20, and 21 are summarized in Table 2. These are undisturbed and their remolded samples chosen at random from Bothkenner, Japanese, and Pusan new port clays. The RR_s values in the area of $\sigma'_v/\sigma'_p > 1$ are unrelated to σ'_v/σ'_p values and the mean values are 1.53 and 1.44 for undisturbed and remolded soils, respectively. The RR_s values are independent of sample disturbance and have a constant value for the σ'_v/σ'_p in the area of $\sigma'_v/\sigma'_p > 1$. The ratios of secondary consolidation to total consolidation obtained from the $d30$ specimens for each $\sigma'_v$are almost 50 % greater than those of the $d60$ specimens.

Figure 19 and Table 3 show the frequency of distribution and the statistical values of the RR_s for the plots in the area of $\sigma'_v/\sigma'_p > 1$, as shown in Fig. 18. The coefficient of variation for the remolded sample is slightly greater than that of the undisturbed one. However, the mean values ($\bar{R}Rs$) of RR_s are similar. Figures 18 and 19 show that there is no effect of sample disturbance on RR_s value.

To examine the effects of q_u and I_p on the RR_s value, the $\bar{R}Rs$ values of each sample in the area of $\sigma'_v/\sigma'_p > 1$ are plotted against the q_u and I_p in Figs. 20 and 21, respectively. The symbols for plots used in these figures are shown in Table 2. The reason for different mean values in Figs. 18 and 20 is that the mean values in Fig. 18 were calculated from the mean value of each sample. The $\bar{R}Rs$ values for the undisturbed and remolded samples are also unrelated to q_u and I_p values.

It was described in a previous paragraph that the consolidation parameters under primary consolidation are unrelated to the sample disturbance and specimen size used in this study. The amount of secondary consolidation to the s_{24} differs by specimen size. However, this has no effect on the consolidation parameters obtained from the standard incremental loading oedometer test.

Conclusions

The conclusions obtained in this study are summarized as follows:

1. The relationships between void ratio and consolidation load and their characteristics values were unrelated to specimen size in the loading and unloading process for samples having $I_p = 22-150$ and $q_u = 25-670$ kPa ranges.
2. The coefficients of consolidation (C_v) obtained from the $d30$ specimen were smaller than those of the $d60$ specimen in the over-consolidated stage. This was caused by larger t_{90} values (the required time for 90 % consolidation) of the $d30$ specimen. The t_{90} ratio was about 1.3 in this stage. In the normally consolidated stage, the c_v, coefficient of volume compressibility (m_v) and permeability (k) were unrelated to specimen size.
3. The consolidation parameters obtained from the $d30$ specimen were almost the same as those of the $d60$ specimen in the normally consolidated stage. The $d30$ specimen, retrieved from the 45-mm, small tube sampler or a 75-mm sampler, is more effective for sample testing purposes.
4. The ratios of secondary consolidation to total consolidation obtained from the $d30$ specimens for each σ'_v were almost 50 % greater than those of the $d60$ specimens. However, this has no effect on the consolidation parameters obtained from the standard incremental loading oedometer test.

References

Aboshi, H., 1973, "An Experimental Investigation on the Similitude in the Consolidation of a Soft Clay, Including the Secondary Creep Settlement," *8th ICSMFE*, Vol. 4–3, p. 88.

Casagrande, A., 1936, "The Determination of the Preconsolidation Load and its Practice Significance,"

Proc. 1st ICSMFE, Cambridge, Mass. Vol. 1, pp. 60–64.

Japanese Geotechnical Society, 1998a, "The Method for Obtaining Undisturbed Soil Sampling Thin-Walled Tube Sampler with Fixed Piston (JGS 1221-1995)," Standards of Japanese Geotechnical Society for Soil Sampling—Standards and Explanations, pp. 1–7.

Japanese Geotechnical Society, 1998b, "The Method for Obtaining Undisturbed Soil Samples using Rotary Double-Tube Sampler (JGS 1222-1995)," Standards of Japanese Geotechnical Society for Soil Sampling—Standards and Explanations, pp. 8–11.

Japanese Standards Association, 2000, "Test Method for One-Dimensional Consolidation Properties of Soils," JIS A1217-2000, pp. 1–13.

Mikasa, M., 1964, "Calculation of Standard Oedometer Test Results," *Proc. 19th National Conf. on JSCE*, pp. 29–32 (in Japanese).

Shogaki, T., 1996, "A Method for Correcting Consolidation Parameters for Sample Disturbance Using Volumetric Strain, " *Soils and Foundations*, Vol. 36, No.3, pp. 123–131.

Shogaki, T., 1997, "A Small Diameter Sampler with Two-Chambered Hydraulic Piston and the Quality of its Samples," *Proc. of the 14th ICSMFE*, Hamburg, pp. 201–204.

Shogaki, T., and Matsuo, M., 1985, "Factor Analysis Approach to Unconsolidated Undrained Shear Strength of Clay with Some Consideration on Microscopic Structures," *Proc. Symposium on Sampling*, pp. 109–116 (in Japanese).

Shogaki, T., Moro, H., and Kogure, K., 1995, "Statistical Properties of Soil Data within Thin-walled Samplers, *Proc. 5th Int. Offshore and Polar Eng. Conf.*, Hague, pp. 406–414.

Shogaki, T., Sakamoto, R., and Kawata, S., 2000, "Human Errors Concerning Preconsolidation Pressure by Casagrande's Method and their Correction," *Tsuchi-to-kiso*, Vol. 48, No. 2, pp. 9–12 (in Japanese).

Shogaki, T., Nakano, Y., and Shibata, A., 2002a, "Sample Recovery Ratios and Penetration Resistance in the Tube Sampling for Niigata Sand," *Soils and Foundations*, Vol. 42, No. 5, pp. 111–120.

Shogaki, T., Ichino, H., and Sakamoto, R., 2002b, "Microstructure, Strength and Consolidation Properties of Ariake Clay Deposits Obtained from Samplers," *Proc. of 47th Geotechnical Symposium*, pp. 107–112.

Shogaki, T., Nochikawa, Y., and Ichino, H., 2002c, "Effect of Specimen Size on Consolidation Parameters of Undisturbed Natural Clay Deposits and the Remolded Clays," *Proc. of Symposium on Current Studies and Practice for Clay Ground*, pp. 107–112 (in Japanese).

Shogaki, T., Sakamoto, R., Kondo, E., and Tachibana, H., 2004, "Small Diameter Cone Sampler and its Applicability for Pleistocene Osaka Ma12 clay," *Soils and Foundations*, Vol. 44, No. 4, pp. 119–126.

Shogaki, T., and Sakamoto, R., 2004, "The Applicability of a Small Diameter Sampler with a Two-Chambered Hydraulic Piston for Japanese Clay Deposits," *Soils and Foundations*, Vol. 44, No. 2, pp. 113–124.

Journal of ASTM International, Vol. 3, No. 6
Paper ID JAI13327
Available online at www.astm.org

Munehide Ishiguro,[1] *Ryouichi Iwamoto,*[2] *Akiko Hamabe,*[3] *Tomoyuki Ishida,*[4] *and Takeo Akae*[5]

Permeability Characteristics of Lake Kojima Sediment and Their Improvement

ABSTRACT: As lake sediments are one of the causes of eutrophication, their removal and effective use has been considered. When they are used as soil in a land, proper permeability is required. However, soil permeability has not completely been understood due to diversity of clays and organic compounds. We clarified permeability characteristics of Lake Kojima sediment, nonswelling clayey soil, by measuring saturated hydraulic conductivity (*K*). A decrease in *K* during percolation of dilute electrolyte solution was small when Ca was adsorbed by the soil; *K* became 3.4×10^{-5} cm/s at pH 5, 2.9×10^{-5} cm/s at pH 7, 7.5×10^{-6} cm/s at pH 9, and 2.3×10^{-5} cm/s at pH 11 after pure water percolation. Although the permeability tended to decrease as pH increased, *K* at pH 11 became larger than that at pH 9 due to chemical reaction between soil particles and Ca. On the other hand, when Na was adsorbed, *K* drastically decreased with pH increase; *K* became 7.1×10^{-6} cm/s at pH 5, 3.1×10^{-6} cm/s at pH 7, 1.7×10^{-7} cm/s at pH 9, and 1.3×10^{-7} cm/s at pH 11 after pure water percolation. The obtained results could be explained qualitatively by the theory. Next, an improvement method of permeability of Lake Kojima sediment with hydrated lime and gypsum were investigated. Three application methods were compared in the saturated hydraulic conductivity experiment; mixing, surface distribution and solution infiltration. Hydrated lime application with mixing maintained high hydraulic conductivity. The soil structure was supposed to be stabilized by chemical reaction between soil and heterogeneously distributed hydrated lime. On the other hand, gypsum application with solution infiltration maintained the same hydraulic conductivity as that of hydrated lime application with mixing. In that case, electrostatic adsorption of Ca was considered to generate flocculation and kept high permeability.

KEYWORDS: sediment, pH, saturated hydraulic conductivity, Ca, Na

Introduction

Sediments from rivers sometimes become sludge in lakes and bays. They cause eutrophication and oxygen shortage in water. Sediment treatment method has been examined for improvement of water quality. In Lake Kojima, the Ministry of Agriculture, Forestry and Fisheries in Japan has been dredging the sediment in order to improve the eutrophicated lake water. Thus, how to use the dredged sediment is becoming a problem. If the clay content is large in the sediment, the permeability becomes a problem when it is used in a land.

The permeability of clayey soil is very low when the soil swells and disperses because the soil pores become very small. Such a soil has improved its permeability by restricting soil dispersion and keeping flocculated condition. For example, for polder soils affected by sea water and sodic arid soils, sodium (Na) in soils is exchanged with calcium (Ca) and soil dispersion is restricted [1].

Soils have a negative permanent charge and a pH-dependent variable charge. Therefore, pH affects soil dispersion and its permeability. Allophanic soil, a typical volcanic ash soil in Japan, has a large amount of pH-dependent charge. Its saturated hydraulic conductivity decreases under low and high pH conditions [2]. When the predominant anion is sulfate (SO_4), hydraulic conductivity does not decrease even at low pH [3–5]. Suarez et al. [6] indicated that the saturated hydraulic conductivity of soils with montmorillonite and

Manuscript received March 23, 2005; accepted for publication July 6, 2005. Presented at ASTM Symposium on Contaminated Sediments: Evaluation and Remediation Techniques on 23–25 May 2006 in Shizuoka, Japan; M. Fukue, K. Kita, M. Ohtsubo, and R. Chaney, Guest Editors.

[1] Associate Professor, Okayama University, Okayama, 700-8530 Japan.
[2] Engineer, Science Micro, Kobe, 651-1331 Japan.
[3] Engineer, Okayama Prefectural Federation of Land Improvement Association, Okayama, 700-0824 Japan.
[4] Professor of blessed memory, Kagawa University, Miki-cho, Kagawa, 761-0795 Japan.
[5] Professor, Okayama University, Okayama, 700-8530 Japan.

kaolinite at pH 9 is smaller than that at pH 6. However, the effect of pH on permeability of soils and sediments is not fully understood.

In this research, the influence of pH and cation species on the saturated hydraulic conductivity of the sediment of Lake Kojima is examined experimentally for the basic understanding in order to find a good way of improving permeability. Hydrated lime [$Ca(OH)_2$] and gypsum ($CaSO_4$) were also applied as improving materials to investigate a better method.

Materials and Methods

Materials

A sediment dredged from Lake Kojima was used in the experiments. The sediment density was 2.65 Mg/m^3, the ignition loss was 14.9 %, the clay content was 54.3 %, the silt content was 38.0 %, the sand content was 7.7 %, and the soil texture was heavy clay. The predominant clay minerals were vermiculite, kaolinite and illite by x-ray diffraction method. The cation exchange capacities (CEC) were 0.073 mol_c/kg at pH 7, 0.13 mol_c/kg at pH 9, and 0.15 mol_c/kg at pH 11 by using Ca.

The electric conductivity (EC) of the soil water in the sampled sediment which was affected by sea water was about 1 S/m. The value corresponds to that of 0.1 mol_c/L sodium chloride (NaCl) solution. The solution pH was about 7.

The sediment for the saturated hydraulic conductivity experiment was equilibrated with a 0.1 mol_c/L NaCl solution and its pH was adjusted at pH 5, 7, 9, or 11 before the experiment. The sediment for the dispersion flocculation experiment for a Na solution was also prepared the same way. The sediment for the dispersion flocculation experiment for a Ca solution was equilibrated with a 0.1 mol_c/L calcium chloride ($CaCl_2$) solution and its pH was adjusted at pH 5, 7, 9, or 11 before the experiment. The pH was adjusted with hydrochloric acid (HCl), sodium hydroxide (NaOH) for a Na solution, or calcium hydroxide [$Ca(OH)_2$] for a Ca solution.

Dispersion Flocculation Experiment

The dispersion flocculation condition was examined under different pH (pH 5, 7, 9, 11), different concentrations, and different cations (Na, Ca). The procedure was as follows;

1. The pretreated sediment (0.2 g by dry weight) was well mixed with a 40 cm^3 solution at different concentrations (0.001, 0.01, or 0.1 mol_c/L) in a tube. The pH and the cation for the mixed solution was the same as those in the sediment solution.
2. After settling for 4 or 5 h the pH and EC of the supernatant were measured. If the pH changed from the prescribed value, it was adjusted. The concentration was estimated from the EC.
3. The tube was well mixed and it was stood still.
4. After 8.3 h, a 10 cm^3 solution was sampled at 3 cm below the water surface. Its light transmittance at 500 nm was measured with a spectrophotometer. The light transmittance of pure water was set to 100 %.

Saturated Hydraulic Conductivity Experiment under Different pH Condition

The saturated hydraulic conductivities were investigated under different pH conditions (pH 5, 7, 9, and 11). The gravimetric water content of the material was 370 %. The experimental procedure was as follows;

1. The sediment was packed into a experimental column 3 cm in diameter. The length of the packed sediment was 1 cm. A permeable paper filter was set under the packed sediment.
2. The experimental sediment column was filled with the same solution which was used for the saturation of the sediment (0.1 mol_c/L NaCl or $CaCl_2$ solution at the same pH of the material).
3. The same solution was infiltrated and the change of flow rate was measured during the experiment. The total water head difference between the upper side and lower side of the packed sediment was maintained at 10 cm using a mariotte bottle.
4. When cumulative discharge became 3 cm (the height of the discharged water when collected into a cylinder with the same cross-sectional area as the sediment column), the influent was changed to a 0.01 mol_c/L solution at the same pH with the same cation. At 6 cm cumulative discharge, it was

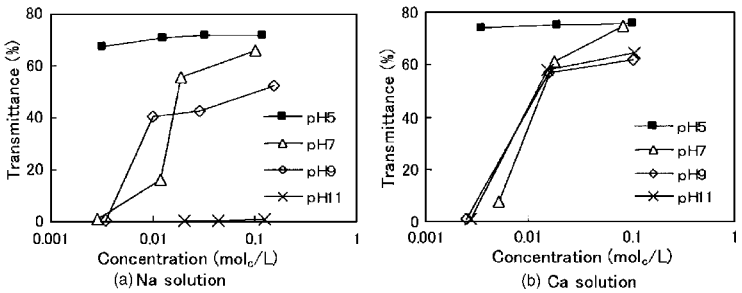

FIG. 1—*Light transmittance of the sediment suspensions. Larger transmittance indicates dispersive condition and smaller transmittance indicates flocculative condition.*

changed to a 0.001 mol$_c$/L solution, and at 9 cm cumulative discharge, to pure water. In case of Ca solution at pH 11, a 0.0035 mol$_c$/L solution was used instead of a 0.001 mol$_c$/L solution because $Ca(OH)_2$ was used for pH adjustment.

5. The change of the sediment length in the experimental column was also measured during the experiment.
6. The saturated hydraulic conductivity was derived by using discharge, sediment length, and the total water head difference.

Saturated Hydraulic Conductivity Experiment for Application of Hydrated Lime and Gypsum

The sediment saturated with 0.1 mol$_c$/L NaCl solution at pH 7 was used for this experiment. Saturated hydraulic conductivities after an application of hydrated lime, gypsum and no application were compared. The experimental column which was mentioned in the above conductivity experiment was also used. Three applications of hydrated lime and gypsum were as follows;

(1) Mixing method: Ca material and the sediment were mixed well in a tube for 1 min by hand. Then, they were mixed using ultrasonic wave for 1 min. The mixed sediment was packed in the experimental column. Then, the measurement started after infiltration of pure water.
(2) Surface distribution method: After packing the sediment, Ca material was distributed on its surface evenly. Then, the measurement started after infiltration of pure water.
(3) Solution infiltration method: After packing the sediment, a 0.01 mol$_c$/L solution of hydrated lime or gypsum was infiltrated. After the prescribed Ca amount was percolated, the influent was changed to pure water.

Ca application amounts were 0.1 mol/kg dry soil, 0.3 mol/kg dry soil, and 1 mol/kg dry soil. 0.1 mol/kg dry soil corresponds to the amount slightly larger than the CEC. In case of hydrated lime, 0.7 mol/kg was applied instead of 1 mol/kg.

The devise setting condition for the saturated hydraulic conductivity experiment was the same as those written above.

Results

Dispersion Flocculation Experiment

The results of the dispersion flocculation experiment are shown in Fig. 1. Smaller light transmittance indicates more dispersive and larger light transmittance denotes more flocculative. The light transmittance was smaller and the sediment was more dispersive with decreasing concentration. When compared between the Na and Ca solutions, light transmittance of the Na solution was smaller and the sediment was more dispersive. In both cases, the light transmittance was smaller and the sediment was more dispersive with pH increase. At pH 5, the light transmittance did not decrease even at the lowest condition and the sediment was flocculative. At pH 11 for the Na solution, the transmittance became zero even at the highest

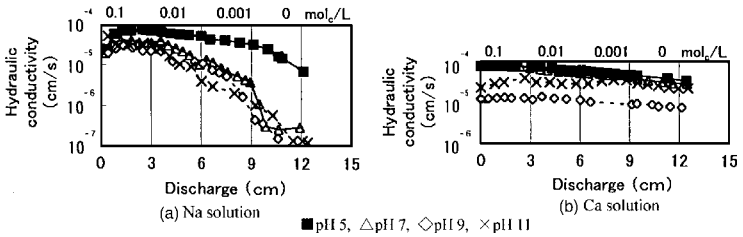

FIG. 2—*Effects of solution pH and concentration on saturated hydraulic conductivity. Values on the upper horizontal lines denote infiltration solution concentrations.*

condition and the sediment dispersed well. For the Ca solution, the transmittance was large and the sediment was flocculative at a concentration larger than 0.01 mol$_c$/L. The transmittance was small and the sediment was dispersive at a concentration lower than 0.001 mol$_c$/L.

Saturated Hydraulic Conductivity Experiment under Different pH Condition

Saturated Hydraulic Conductivity—The results of the saturated hydraulic conductivity experiment are shown in Fig. 2. The saturated hydraulic conductivity decreased as the influent concentration decreased. For the Ca solution, a slightly increasing part was observed at pH 11 as an exception. For the Na solution, the hydraulic conductivity decreased well with decreasing the concentration. For the Ca solution, however, only a slight decrease was observed. For the Na solution, it decreased much as pH increased. On the other hand, for the Ca solution the difference was little among those at pH 5, 7, and 11. At pH 9 for the Ca solution, it was obviously smaller than others.

Sediment Length—Changes of the sediment length of the experimental column during the saturated hydraulic conductivity experiment under different pH conditions are shown in Fig. 3. The length decreased from the initial length, 1 cm, during the experiment. At the beginning, the length for the Ca solution was smaller than that for the Na solution in Fig. 3. However, it was because a 0.1 mol$_c$/L Na solution was percolated before the percolation of a 0.1 mol$_c$/L Ca solution for the Ca solution. After that part, the length for the Na solution decreased much more than that for the Ca solution. However, at pH 5, the decrease was restricted even for the Na solution.

Saturated Hydraulic Conductivity Experiment for Application of Hydrated Lime and Gypsum

In the Case of No Ca Application—The two sets of results of the saturated hydraulic conductivity experiment with pure water infiltration are shown in Fig. 4. The saturated hydraulic conductivity gradually decreased at the initial 2 to 4 cm discharge and it significantly decreased after that. The effluent EC decreased with the pure water percolation. The effluent pH ranged between pH 7 and pH 8. The final sediment length ranged from 0.7 to 0.8 cm.

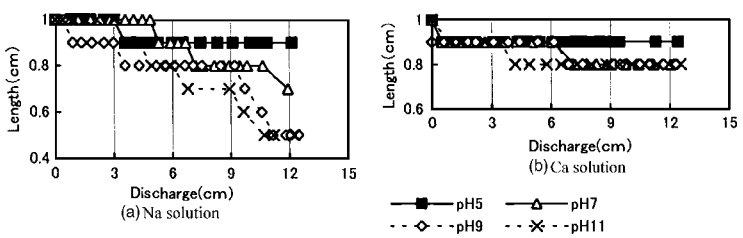

FIG. 3—*Sediment length during the saturated hydraulic conductivity experiment.*

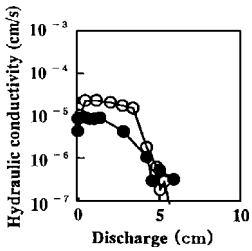

FIG. 4—*Saturated hydraulic conductivity during pure water infiltration. The experiment was duplicated.*

In the Case of Gypsum Application—Each two sets of the results of the saturated hydraulic conductivity experiment for application of gypsum are shown in Fig. 5(*a*). A significant decrease of the saturated hydraulic conductivity smaller than 10^{-6} cm/s, which was observed for pure water infiltration, was not observed. For the solution infiltration method with 0.3 and 1 mol/kg applications, the saturated hydraulic conductivity kept the largest order of 10^{-4} cm/s. Next largest were the cases of the surface distribution method with all application amounts and the mixing method with 0.3 and 1 mol/kg applications; the order of 10^{-5} cm/s. The smallest hydraulic conductivities were observed for the mixing method with 0.1 mol/kg and the solution infiltration method with 0.1 mol/kg; the order of 10^{-6} cm/s. The saturated hydraulic

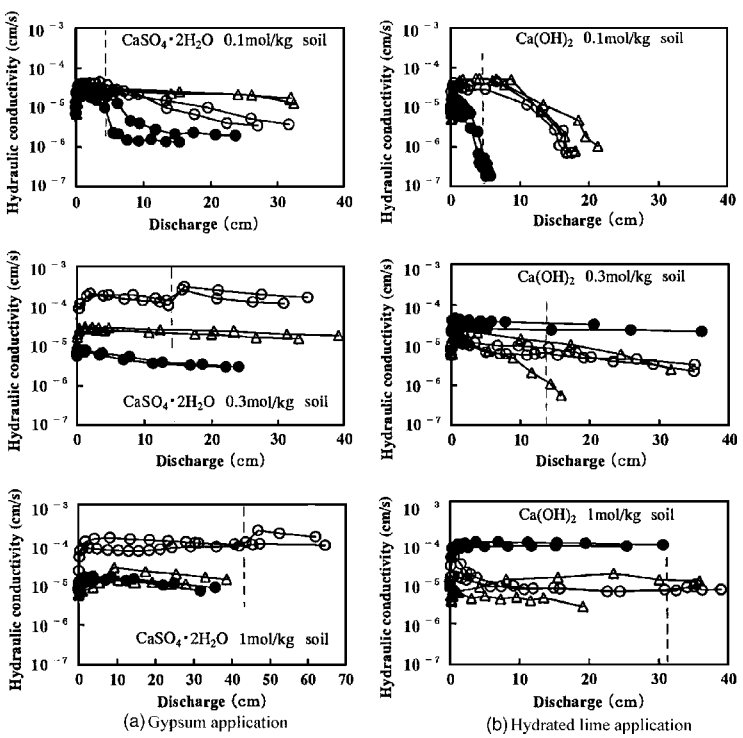

FIG. 5—*Saturated hydraulic conductivity after application of gypsum and hydrated lime.* ● *denotes mixing method,* △ *surface application method, and* ○ *solution infiltration method. Dotted line indicates the point where the influent was changed from solution to pure water in the solution infiltration method.*

conductivity for the mixing method became the smallest compared to other methods. The effluent pH ranged from pH 5.7 to 7.8. The sediment length ranged from 0.8 to 1 cm. The clear differences among the methods were not observed about the sediment length.

In the Case of Hydrated Lime Application—Each two sets of the results of the saturated hydraulic conductivity experiment for application of hydrated lime are shown in Fig. 5(*b*). Obvious decreases of the saturated hydraulic conductivity were observed for the smallest applications, 0.1 mol/kg. For the mixing method with 1 mol/kg application, the saturated hydraulic conductivity kept the largest order of 10^{-4} cm/s. Next largest was the case of the mixing method with 0.3 mol/kg; an order of 10^{-5} cm/s. In general, the saturated hydraulic conductivity kept larger values with larger application amount. Especially, it kept the largest value for the mixing method. The effluent pH became larger with an increase of the application amount. During pure water percolation, the pH decreased. The final effluent pH was an order of pH 8 for 0.1 and 0.3 mol/kg applications, and an order of pH 9–11 for 1 mol/kg applications. The sediment length ranged from 0.8 to 1 cm. The clear differences among the methods were not observed with regard to the sediment length.

Discussion

Saturated Hydraulic Conductivity Experiment under Different pH Condition

Interpretation with the DLVO Theory—The saturated hydraulic conductivity decreased with a decreasing solution concentration and the decrease was more significant for the Na solution than that for the Ca solution (Fig. 2). The result corresponded with the result of the dispersion flocculation experiment; the suspension became more dispersive with decreasing the concentration, and that in Na solution was more dispersive than that in the Ca solution (Fig. 1). These phenomena can be interpreted with the (DLVO) theory. When the electrolyte concentration is higher, the diffuse double layer becomes thinner and the electrical repulsive force is smaller than the attraction due to the London-van der Waals force between the sediment particles [7]. Therefore, the particles keep flocculative condition. When the concentration becomes lower, the diffuse double layer develops and the electrical repulsive force increases between the sediment particles. Then, the particles disperse well and they clog the larger pores in the sediment. Therefore, the saturated hydraulic conductivity decreases with decreasing the concentration. Because Ca is divalent cation while Na is monovalent, the diffuse double layer becomes thinner in the Ca solution than that in the Na solution. The electrical repulsive force in the Ca solution is smaller than that in the Na solution, and the sediment is more flocculative in the former case. Therefore, the decrease of the saturated hydraulic conductivity is restricted in Ca solution.

Saturated Hydraulic Conductivity for Na Solution—The saturated hydraulic conductivity for Na solution decreased well with increasing pH (Fig. 2). At lower pH, the 2:1 type clay minerals such as vermiculite and illite have positive charges at the edges. The edges are attracted by the permanent negative charges on the clay faces. Then, the clay particles keep stable card house structures. For the 1:1 type clay mineral, kaolinite, the negative variable charge decreases at lower pH. Therefore, the clay particles are flocculative and the saturated hydraulic conductivity decreases little at lower pH.

At higher pH, the variable charges at the edges of the 2:1 type clays become negative. Because negative charges of humic substances and kaolinite also increase, the electrical repulsive forces generate among the clays and humic substances. Therefore, the particles dispersed well and the saturated hydraulic conductivity decreased significantly.

Saturated Hydraulic Conductivity for Ca Solution—In the case of Ca solution, the saturated hydraulic conductivity decreased only a little because the electrical repulsive force among the particles was small. The saturated hydraulic conductivity at pH 7 was almost the same as that at pH 5. That at pH 9 was the smallest. However, that at pH 11 was larger than that at pH 7 and close to those at pH 5 and pH 7. At pH 11, silicate lime hydrate (mainly $CaOSiO_2H_2O$) and alumina lime hydrate (mainly $CaOAl_2O_3H_2O$) were probably generated with chemical reaction and the stable structures were made [8]. Therefore, the saturated hydraulic conductivity was also stable.

Change of the Sediment Length and the Saturated Hydraulic Conductivity—In general, the saturated hydraulic conductivity decreased more as the sediment length decreased (Figs. 2 and 3). Because all the sediment lengths decreased, there was no swelling by electrical repulsive force. The decrease of the saturated hydraulic conductivity was supposed to occur because of the sediment particle dispersion caused by the electrical repulsive force. The bulky flocculated sediment structure at higher concentration rearranged after the dispersion and the sediment volume decreased during the rearrangement; the larger pores decreased and the saturated hydraulic conductivity decreased. In the case of the Na solution at pH 5 and the Ca solutions, the sediment length decreased a little and the structure was stably flocculated, because the electrostatic repulsive force was smaller than the attractive force.

Dispersion Flocculation Experiment and the Saturated Hydraulic Conductivity—When the sediment showed dispersive in the dispersion flocculation experiment, the saturated hydraulic conductivity decreased. The result of the dispersion flocculation experiment explained the change of the saturated hydraulic conductivity qualitatively. However, the saturated hydraulic conductivity did not necessarily decrease well when the sediment showed dispersion. The sediment was mixed well with a solution in the dispersion flocculation experiment. However, the sediment stood still during the saturated hydraulic conductivity experiment. Lack of quantitative exact agreement probably resulted from these different experimental conditions.

Saturated Hydraulic Conductivity Experiment for Application of Hydrated Lime and Gypsum

In the Case of Gypsum Application—The sediment kept flocculative when Ca adsorbed in the sediment because electrical repulsive force decreased. This effect was observed in the case of gypsum application. The hydraulic conductivity kept the largest order of 10^{-4} cm/s for the solution infiltration method with 0.3 and 1 mol/kg applications as mentioned before. The larger hydraulic conductivity was maintained probably because Ca was well diffused in the sediment pores and maintained the flocculated condition for the solution infiltration method. The effluent EC decreased fastest for the mixing method. This result indicates that Ca discharged rapidly for the mixing method. This caused the smallest hydraulic conductivity for the mixing method. In the case of 0.1 mol/kg application, the highest hydraulic conductivity was not maintained although the applied Ca amount was not much larger than the CEC. Probably, Ca discharged gradually and the sediment became dispersive.

In the Case of Hydrated Lime Application—Different from the case of gypsum application, the chemical reaction which produced silicate lime hydrate and alumina lime hydrate affected the sediment structure and the saturated hydraulic conductivity because hydrated lime application increased the sediment pH. The chemical reaction was recognized from the effluent EC value. For the solution infiltration method, the effluent EC became smaller than the influent EC of hydrated lime solution even after much application more than the CEC, because Ca was chemically reacted with the sediment and some Ca amount was not discharged. Generally, the saturated hydraulic conductivity maintained a higher value with larger Ca application. Especially, the saturated hydraulic conductivity was largest for the mixing method except 0.1 mol/kg application. In the case of 0.1 mol/kg application, the hydraulic conductivity became smallest for the mixing method probably because Ca discharged fastest for the method. For the mixing method, hydrated lime was distributed inhomogeneously in the sediment; that probably caused heterogeneous pore structures: larger pores and smaller pores. Then, the hydraulic conductivity maintained larger value. On the other hand, for the solution infiltration method and the surface application method, hydrated lime diffused well in the sediment pores evenly and the pore structure probably became homogeneous after the chemical reaction; larger pores decreased.

Conclusions

The characteristics of the saturated hydraulic conductivity of high water content of Lake Kojima sediment were clarified experimentally. The predominant clay minerals were non-swelling vermiculite, kaolinite, and illite. The influence of pH on the saturated hydraulic conductivity was different between that for the Na solutions and that for the Ca solutions. The decrease of the saturated hydraulic conductivity for the Ca

solutions was little even when the dilute solution was percolated. The difference among that at pH 5, pH 7, and pH 11 was little for the Ca solutions. However, the saturated hydraulic conductivity at pH 9 became smallest. The sediment length also became the smallest at pH 9 among them. The saturated hydraulic conductivity at pH 11 was the most stable among those different pH conditions for the Ca solutions. The chemical reaction between Ca and the sediment probably made a stable sediment structure at the highest pH.

On the other hand, when the Na solutions were percolated, the saturated hydraulic conductivity significantly decreased with increasing pH. It resulted because the pH-dependent charge at the edge of the clays changed from positive to negative with increasing pH; the electrical interaction among sediment particles changed from attraction to repulsion as pH increased. The sediment became dispersive at higher pH. Then the dispersed particle clogged larger pores and the saturated hydraulic conductivity decreased.

In order to restrict the decrease of the saturated hydraulic conductivity, gypsum and hydrated lime were examined with different application methods. Hydrated lime has been used for soil stabilization for a long time. In such a case, the hydraulic conductivity usually decreased because they compacted the soil to stabilize it. However, the saturated hydraulic conductivity for the mixing method with the sediment and hydrated lime maintained larger values the same as or more than those for gypsum application. The inhomogeneously dispersed hydrated lime chemically reacted to the sediment and it probably caused the permeable structure. On the other hand, the solution infiltration method brought the highly permeable result for gypsum application. In the case of gypsum, a decrease of electrical repulsive force with Ca adsorption resulted in flocculative condition.

A large amount of hydrated lime application brings a pH increase. The pH change must be taken care for the use. Lime has been used for the pH amendment of acidic soils in agriculture. Therefore, hydrated lime is useful when acidic soils are concerned.

References

[1] Bolt, G. H. and Bruggenwert, M. G. M., *Soil Chemistry A. Basic Elements*, Elsevier, 1978.

[2] Nakagawa, T. and Ishiguro, M., "Hydraulic Conductivity of an Allophanic Andisol as Affected by Solution pH," *J. Environ. Qual.*, 23, 208–210 (1994).

[3] Matsukawa, S., Tomita, H., Suzuki, S., and Katoh, H., "Relation Between Soil Dispersion, Hydraulic Conductivity and pH of Soil Water for Allophanic Soils During Acid Solution leaching," (in Japanese with English summary) *Soil Physical Conditions and Plant Growth Japan*, 77, 3–9 (1991).

[4] Ishiguro, M. and Nakajima, T., "Hydraulic Conductivity of an Allophanic Andisol Leached with Dilute Acid Solutions," *Soil Sci. Soc. Am. J.*, 64, 813–818 (2000).

[5] Ishiguro, M., Nakaishi, K., and Nakajima, T., "Saturated Hydraulic Conductivity of a Volcanic Ash Soil Affected by Repulsive Potential Energy in a Multivalent Anionic System," *Colloids Surf., A*, 230, 81–88 (2003).

[6] Suarez, D. L., Rhoades, J. D., Lavado, R., and Grieve, C. M., "Effect of pH on Saturated Hydraulic Conductivity and Soil Dispersion," *Soil Sci. Soc. Am. J.*, 1984, Vol. 48, pp. 50–55.

[7] Iwata, S., Tabuchi, T., and Warkentin, B. P., *Soil-Water Interactions*, Marcel Dekker, 1995.

[8] Ariizumi, A., "Soil Stabilization with Lime," in *Fundamentals and Applications of Chemistry in Soil Mechanics and Foundation Engineering* (in Japanese), Japanese Society of Soil Mechanics and Foundation Engineering, 1978, pp. 164–177.

Journal of ASTM International, Vol. 3, No. 6
Paper ID JAI13316
Available online at www.astm.org

Mark Dyer[1]

Optical Tests on the Slow Release of Biogenic Gas Bubbles in Sediment

ABSTRACT: The anaerobic decomposition of organic matter in marine or fresh water sediments can generate methane, carbon dioxide, hydrogen sulphide, and hydrogen as biogenic gases. In addition, innovative technologies are being used to remediate contaminated sediments and groundwater by releasing biogenic gases from the fermentation of carbon substrates as electron donors. Both scenarios can result in large discrete gas bubbles being present in sediment, which can affect aqueous permeability and mechanical strength. Furthermore the movement of gas bubbles can affect bioavailability as electron donors. In order to investigate bubble dispersion and movement in sediments, a series of novel optical experiments were carried out to observe the release and movement of discrete bubbles in artificial coarse-grained sediment. The results showed that buoyancy-induced movement depended on the clustering together of individual bubbles to achieve a critical depth of gas pocket to overcome the capillary force acting across the pore throat between sediment grains.

KEYWORDS: biogenic gas, discrete bubbles, buoyancy-induced movement, sediments

Introduction

The anaerobic decomposition of organic matter in marine or fresh water sediments can generate methane, carbon dioxide, hydrogen sulphide, and hydrogen as biogenic gases (Singleton 1999). In addition, innovative technologies are being used to remediate contaminated sediments and groundwater by releasing biogenic gases from the fermentation of carbon substrates as electron donors (Dyer et al. 2000; Dyer et al. 2003; Suthersan 1997). Both scenarios can result in large discrete gas bubbles being present in sediment, which can affect aqueous permeability and mechanical strength. Furthermore the movement of gas bubbles can affect bioavailability as electron donors.

It has been recognized for sometime that the presence of discrete gas bubbles can have a significant effect on the permeability and mechanical behaviour of marine sediments (Corey 1957; Sills et al. 1991; Wheeler 1988; Wheeler 1990). However there has been little research into actual movement of slowly released biogenic gas bubbles in sediments and the corresponding mass transfer from gaseous to aqueous phases and potential consumption by indigenous bacteria. As part of a program of research into the movement and mass transfer of gas bubbles, a series of optical tests were carried out to directly observe discrete gas bubbles in granular sediment.

Experimental Technique and Apparatus

The optical technique used crushed borosilicate glass as substitute sediment immersed in light grade liquid paraffin, which has a similar refractive index and so rendered the medium transparent. The borosilicate glass was crushed using a mechanical mortar and pestle and wet sieved before being air dried. The majority of tests were carried out using coarse sand sized particles (0.6–2.0 mm) with a subangular shape. Earlier plane strain and direct shear box tests by Drescher (1976) and Dyer (1986) have already shown the mechanical properties of the crushed glass to be similar to coarse-grained sediment. A sample of crushed glass is shown in Fig. 1.

The laboratory tests were carried out in a modified 100 mm diameter Perspex cylinder previously used

Manuscript received May 3, 2005; accepted for publication September 13, 2005. Presented at ASTM Symposium on Contaminated Sediments: Evaluation and Remediation Techniques on 23–25 May 2006 in Shizuoka, Japan; M. Fukue, K. Kita, M. Ohtsubo, and R. Chaney, Guest Editors.
[1] Professor of Civil Engineering, University of Strathclyde, UK.

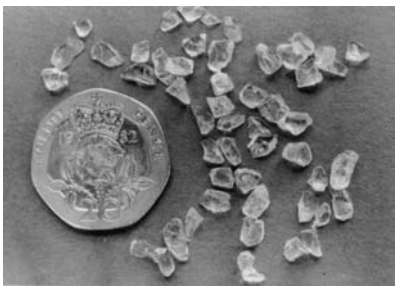

FIG. 1—*Samples of crushed borosilicate glass (0.6 to 2.0 mm).*

for constant head permeability tests. Pore pressure was applied using compressed air via a liquid/air interface. The pore pressure was controlled by a pressure regulator, which operated between 2–30 psi (13.8–207 kPa). Air was released into the base of the cell using a peristaltic pump, which pumped against the backpressure. The pump was capable of working at pressures of up to 200 kPa and flow rates between 0.23 and 20.77 ml/min. The pore liquid pressure and air entry pressure were measured using pressure transducers.

Although the use of liquid paraffin as a pore fluid allowed the sample to be rendered transparent, the difference in surface tension (σ_t) and dynamic viscosity from water would have affected size of air bubbles. The different physical properties are shown in Table 1. The effect on bubble size can be calculated using the capillary equation where the difference in pore fluid and gas pressure ($u_g - u_f = 2\sigma_t/R$) can be related to surface tension (σ_t) and radius of curvature (R) of an air bubble between sediment grains. Using this expression, there would be a 56 % reduction in bubble size in light grade paraffin compared with water, where surface tension is 0.032 and 0.0728 N/m, respectively. This agrees with observations made by Zhang and Burns (2000) on the effect of surfactants on air bubbles in a porous media. The use of surfactants in deionized water reportedly reduced air bubble diameter from 1.4 to 0.6 mm in an idealized porous media of silica beads (14.5 to 27 mm diameter).

Entrapped Bubbles

The experimental results illustrated several different features about the size, stability, and movement of gas bubbles in a coarse-grained sediment, which can be related to the slow release of biogenic gases. It should be noted that in each case the results represent assemblies of entrapped gas bubbles and not continuous gas channels.

The first set of tests provides an insight into the movement of gas bubbles as shown by the close-up photographs in Fig. 2. The photographs are of entrapped gas bubbles within a saturated sample of coarse sand sized crushed glass (0.6 to 2.0 mm size). The photographs were taken along the same portion of the test column over a 24-min period. The gas bubbles where generated by releasing air into the base of the column at a flow rate of 0.23 ml/min under a pore liquid pressure of 50 kPa. The photographs allow the movement of individual bubbles to be monitored. As a result it could be seen that that individual bubbles clustered together over the 24-min period. Circles B and C have been drawn around the same portion of column to highlight the clustering of bubbles at the same location.

In comparison with these close-up photographs, images of entrapped gas bubbles along the length of the column are shown in Fig. 3 for two different samples. The first sample shown in Fig. 3(*a*) was prepared using a single sized grading of coarse sand sized particles of crushed glass. In the second sample shown in Fig. 3(*b*) a layer of medium sized sand particles was introduced in the middle section of the sample to act

TABLE 1—*Properties of liquid paraffin (light grade) and water.*

Fluid	Surface Tension, σ_t (N/m)	Dynamic Viscosity, η (mPa-s)	Density, ρ (kg/m^3)
Liquid paraffin	0.032	110	880
Water	0.0728	10	1000

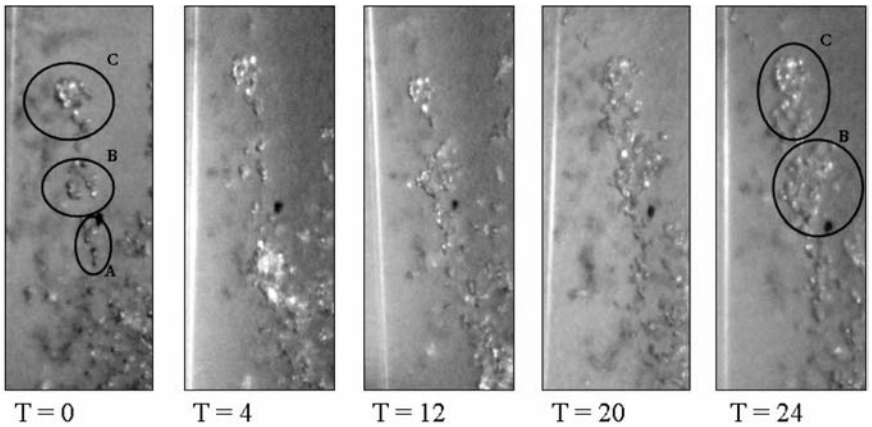

FIG. 2—*Close-up images of entrapped gas bubbles at different times (T minutes) in column tests released at 0.23 ml/min at 50 kPa pore pressure.*

as a potential barrier to the movement of gas bubbles. The gas was released from a lance (1 mm internal diameter) at sample midheight at a pore pressure of 50 kPa at a rate of 0.23 ml/min. The first test results in Fig. 3(*a*) shows clustering of entrapped bubbles at different locations along the height of the sample. Rectangles have been drawn around clusters of bubbles with the thickness of clusters written alongside. The clusters were identified where there was a clear localized grouping of gas bubbles at individual locations in the sample. The measurements show that gas bubbles typically grouped into clusters of between 12 and 18 mm thicknesses before triggering movement. The result confirms the earlier observation that migration of gas bubbles at low rates of release in coarse-grained sediments was characterized by clustering in order presumably to obtain sufficient buoyancy. In comparison with bubble movement in a

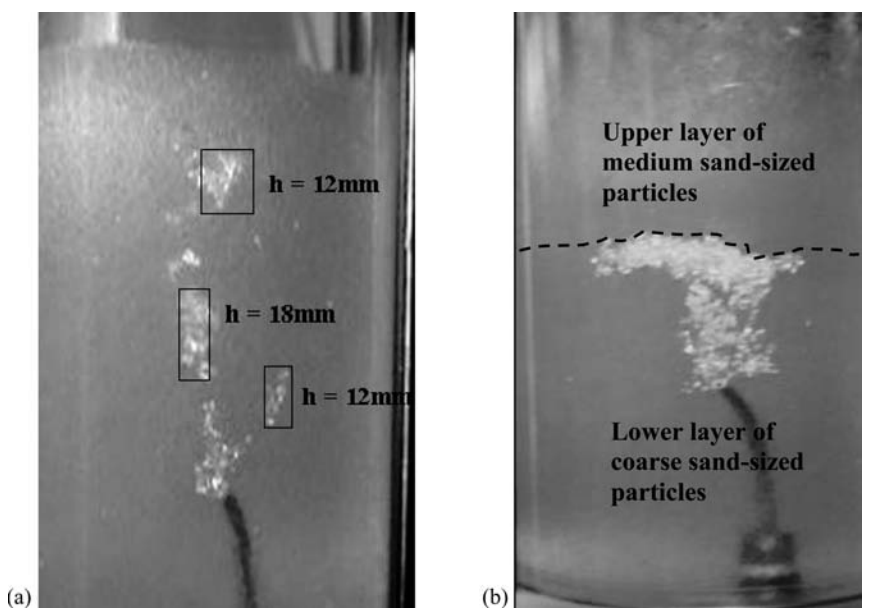

FIG. 3—*Distribution of bubbles in (a) uniform and (b) layered sample of crushed glass.*

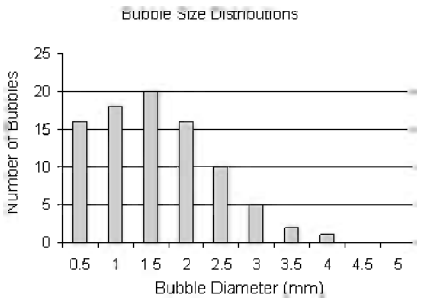

FIG. 4—*Distribution of gas bubbles diameters.*

uniform sample, Fig. 3(*b*) shows the effect of including a layer of medium-sand sized glass particles into the column after gas has been released over a 60-min period. The image shows a column of bubbles migrating upward through the coarse-sand size particles until a layer of medium-sand size particles was encountered. The slight change in particle size was sufficient to halt the movement of gas bubbles and create a pocket of gas bubbles that would significantly reduced the aqueous permeability of the sediment as demonstrated by Corey (1957). Yet the layering corresponds to slight changes in geological facies in coarse-grained sediments that would be difficult to detect.

With regard to the size of individual bubbles, the distribution of bubble diameters produced by injection from sample mid-height is shown in Fig. 4. The measurements were made after 30 min of injection at 0.23 ml/min with a pore-pressure of $50 kN/m^2$. The resulting distribution is skewed toward the smaller diameter bubbles with the majority of bubbles between 0.5 and 2.0 mm diameters.

Buoyancy-Induced Bubble Movement

Buoyancy-induced bubble movement is not a new concept but has already been proposed as a mechanism to explain the movement of large individual bubbles in very soft clay sediments. Using plasticity theory to determine limiting pressures on a long cylinder and alternatively cavity expansion/contraction theory, Wheeler (1990) calculated that an excessively large bubble (greater than 10 mm radius) would be required for buoyancy-induced movement to occur in fine-grained sediment with shear strength greater than 10 Pa. In comparison, the optical column tests on saturated crushed glass showed that buoyancy forces were often insufficient to move individual bubbles upward in the column. Instead it appeared that the necessary buoyancy force was achieved by the clustering of bubbles to form a pocket of gas. The clusters or pockets of gas appeared to provide a critical buoyancy force to allow intermittent movement to occur over short distances of several centimetres. Furthermore bubble movement was blocked by a slight reduction in particle size from a coarse-sand size (0.6 to 2.0 mm) to medium-sand size particles (200 to 600 μm), which indicated that a change in pore throat between particles had a major influence on buoyancy-induced bubble movement. It would appear that an increase in buoyancy force was needed due to clustering of bubbles to overcome the capillary force across individual pore throats.

In order to investigate the mechanism for buoyancy-induced movement in coarse-grained sediments further, a supplementary set of tests were carried out using a closed-ended conical tube with a central aperture as shown in Fig. 5. The experimental results are shown in Fig. 6 and compared with predicted values based on the calculation of the critical thickness (h_{crit}) of gas pocket required to cause buoyancy-induced movement determined. The critical thickness (h_{crit}) of the gas pocket was determined by equating the capillary force resisting movement due to surface tension (σ) across the meniscus against the buoyancy-induced force to give the following expression:

$$h_{\text{crit}} = 2\sigma_t \cos\theta / r(\gamma_l - \gamma_g)$$

where the parameter (r) is the radius of the pore throat, ($\gamma_l - \gamma_g$) is the difference in density between air and liquid paraffin, the wettability contact angle (θ) for the paraffin liquid. The predicted values assume a perfectly wetting liquid, which means that the contact angle was conservatively assumed to be zero. In

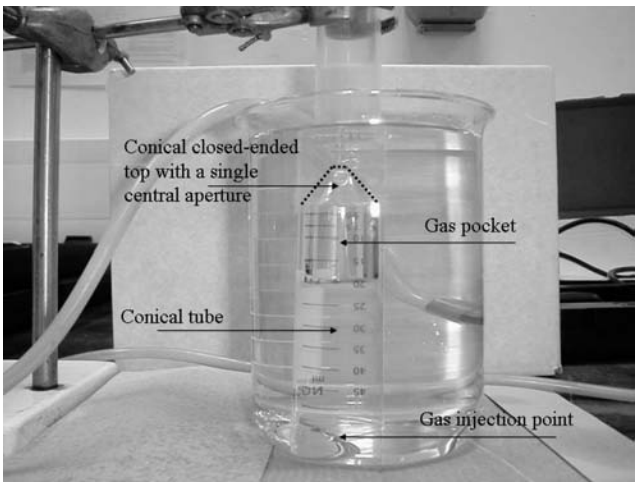

FIG. 5—*Apparatus for conical tests on buoyancy induced-movement of gas pockets in liquid paraffin.*

practice the contact angle would be in the order of 20 deg, which would give a 6 % reduction in the theoretical critical thickness (h_{crit}). Allowing for this slight overestimate the results show good agreement between predicted and experimental values for aperture diameters of 0.7 to 1.5 mm for this relatively simple theory. In each case the contact angle should be independent of the slope of the conical top of the tube.

In comparison, the clusters of bubbles observed in a uniform sample of coarse-sand sized particles in Fig. 3(*a*) measured between 12 and 18 mm. According to Fig. 6, the cluster of gas bubbles corresponds to a pore throat diameter of typically 0.7 mm, which is feasible for a sample of particle sizes measuring between 0.6 and 2.0 mm.

The predicted critical thickness (h_{crit}) of gas pocket shown in Fig. 6 also illustrates how a reduction in pore aperture below 0.7 mm would have rapidly increased the required thickness of the gas pocket to trigger buoyancy-induced movement. This observation explains how the layer of medium-sized sand particles effectively blocked the upward migration of gas bubbles as shown in Fig. 3(*b*). In practice, tortuosity in a granular media could also influence the critical thickness of cluster required to overcome capillary force resisting movement.

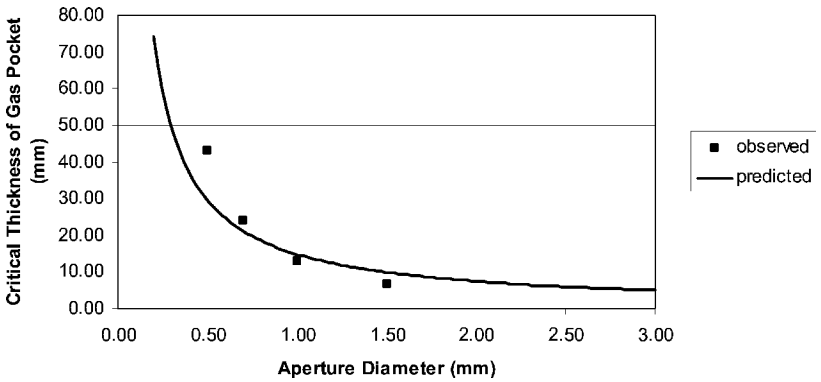

FIG. 6—*Comparison of observed and predicted critical thickness (H_{crit}) of gas pocket to cause buoyancy-induced movement for different size apertures in liquid paraffin.*

Conclusions

The experimental results provided an unusual insight into the release and movement of biogenic gas bubbles in a saturated coarse-grained sediment. The results showed that gas bubbles movement depended on the clustering of individual bubbles to promote buoyancy-induced movement, where the buoyancy force acting across a pore throat would exceed the force from surface tension acting across the meniscus.

Buoyancy-induced movement of bubbles was explored further in closed-end tube tests, where the critical buoyancy force required inducing gas movement through a single aperture could be related to the critical thickness of the gas pocket beneath the aperture. Based on these results an expression was derived for the critical thickness (h_{crit}) of a gas pocket or a cluster of gas bubbles required for buoyancy-induced movement in coarse-grained sediment. In coarse-sand sized sediment gas pockets of between 12 and 18 mm lead to buoyancy-induced movement. However the reduction in pore diameter for a medium-sand sized particle of crushed glass effectively blocked the upward migration of gas bubbles. Furthermore, tortuosity in a granular media could also influence the critical thickness of cluster required to overcome capillary force resisting movement.

In conclusion, the experimental results have provided a valuable insight into the movement and distribution of biogenic gas bubbles released at a slow rate in marine sediment. This information can be further used to study the rate of mass transfer and dissolution from bubbles into the aqueous phase.

References

Corey, A. T., "Measurement of Water and Air Permeability in Unsaturated Soil," *Soil Science Society Proceedings*, 1957.

Drescher, A., "An Experimental Investigation of the Flow Rules for Granular Material Using Optically Sensitive Glass Particles," *Geotechnique* 26(4), 591–601 (1976).

Dyer, M. R., "Observation of Stress Distribution in Crushed Glass with Application to Sediment Reinforcement." DPhil. Thesis, Oxford University, 1986.

Dyer, M. R., Van Heiningen, E., and Gerritse, J., "In-Situ Bioremediation of 1,2-Dichloroethane Under Anaerobic Conditions," *Geotech. Geologic. Eng.* 18(4), 313–334 (2000).

Dyer, M. R., Van Heiningen, E., and Gerritse, J., "A Field Trial for In-Situ Bioremediation of 1,2-DCA," *Eng. Geol. (Amsterdam)* 70, 315–320 (2003).

Sills, G. C., Wheeler, S. J., Thomas, S. D., and Gardner, T. N., "Behavior of Offshore Sediments Containing Gas Bubbles," *Geotechnique*, 41(2), 227–241 (1991).

Singleton, P., *Bacteria in Biology, Biotechnology and Medicine*, John Wiley and Sons, England, 1999.

Suthersan, S. S., *Remediation Engineering Design Concepts*, CRC Lewis, New York, 1997.

Wheeler, S. J., "A Conceptual Model for Sediments Containing Large Gas Bubbles," *Geotechnique* 38(3), 389–397 (1988).

Wheeler, S. J., "Movement of Large Gas-Bubbles in Unsaturated Fine-Grained Sediments," *Mar. Geotech.*, 9(2), 113–129 (1990).

Zhang, M. and Burns, S. E., "Surfactant Effects on the Transport of Air Bubbles in Porous Media," *Environmental Geotechnics—Proceedings of Sessions of Geo-Denver 2000, Geotechnical Special Publication*, No. 105. ASCE.

SECTION III: HEAVY METALS

Journal of ASTM International, Vol. 3, No. 6
Paper ID JAI13341
Available online at www.astm.org

M. Ohtsubo,[1] *T. Morishita,*[2] *L. Li,*[3] *T. Higashi,*[4] *and S. Yamaoka*[2]

Effects of Salt on the Sorption of Lead by Marine Clay in Column Tests

ABSTRACT: In recent years incinerated municipal solid waste has been disposed of in landfill sites near the coastal area in Japan where the underlying marine clay deposits are expected to serve as a natural clay barrier. In this study, marine clay from Japan is examined for the effects of salt on sorption of lead using column leaching tests with deionized water, sea water, and bottom ash leachate spiked with 100 mg/L lead as permeants, and then selective sequential extraction (SSE) was employed to assess the retention mechanism of lead onto marine clay. Lead concentration in the effluent was less than 5 MG/L throughout the column leaching tests with the deionized water, whereas it exceeded Pb concentration in influent below one pore volume leaching for the sea water. Lead in pore water accumulated in the top layer of the column soil for the deionized water whereas it was distributed throughout the depth for the sea water and ash leachate. The SSE indicated that carbonate, exchangeable, and hydroxides phases are predominant for Pb retention.

KEYWORDS: heavy metal, lead, clay barrier, sorption, marine clay, salt

Introduction

Municipal solid waste (MSW) has recently been disposed of in coastal landfill sites because of the shortage of suitable landfill sites in mountainous areas of Japan. In the coastal landfill sites underlying marine clay deposits are expected to serve as a natural clay barrier that attenuates contaminant transport through various sorption processes. About 70 % of municipal solid waste is incinerated in Japan (Hanashima and Furuichi 2000), and much of the resulting bottom and fly ash is dumped in the coastal landfill sites (Kamon 1997). The bottom and fly ash contain various contaminants, which pose threats to aquatic environment if the underlying marine clay does not have sufficient capacity to attenuate the contaminants via sorption. Leaching tests of the bottom and fly ash have indicated that heavy metal and salts are major contaminants in ash leachate, and lead is predominantly present (Kanaya et al. 1994; Ohsako et al. 2001; Abbas et al. 2003; Ohtsubo et al. 2004). Lead is a very toxic element, which causes a variety of health effects at low dose levels. Chronic (long term) exposure to lead in humans results in effects on the blood (anemia), central nervous system, blood pressure, kidneys, and vitamin D metabolism (ATSDR 1993).

A number of studies have been conducted regarding the possible use of natural soils as liner materials. These studies have indicated that heavy metals commonly found in leachate from landfills can be effectively attenuated by various soil liner materials (Griffin et al. 1976; Yanful et al. 1988; Mohamed et al. 1994; Li and Li 2001; Yong et al. 2001). Heavy metal adsorption onto clay particles may, however, be reduced due to competition with heavy metals with cations in salt. In MSW ash leachate containing high concentrations of salts and when this leachate permeates through the underlying marine clay in the coastal landfill sites, the migration of heavy metals may increase. Studies have indicated that the presence of salts inhibit metal sorption to particulates through competition with metals for particulate binding sites of the soils (Amrheim and Strong 1990; Kookana and Naidu 1998; Warren and Zimmerman 1994; Ohtsubo et al. 2005). Very few studies have been conducted on the validity of heavy metal sorption in the presence of

Manuscript received March 29, 2005; accepted for publication September 16, 2005. Presented at ASTM Symposium on Contaminated Sediments: Evaluation and Remediation Techniques on 23–25 May 2006 in Shizuoka, Japan; M. Fukue, K. Kita, M. Ohtsubo, and R. Chaney, Guest Editors.

[1] Professor, Faculty of Agriculture, Kyushu University, Fukuoka, Japan.
[2] Graduate student, Faculty of Agriculture, Kyushu University, Fukuoka, Japan.
[3] Associate Professor, Department of Civil Engineering, The University of British Columbia, 6250 Applied Science Lane, Vancouver, B.C., Canada V6T 1Z4.
[4] Associate Professor, Faculty of Agriculture, Kyushu University, Fukuoka, Japan.

TABLE 1—*Properties of marine clay from Ariake-cho, Japan.*

Water content (%)	130.0	Dominated clay minerals (%)	
Liquid limit (%)	133.2	Smectite	48
Plastic limit (%)	46.6	Illite	26
Particle size distribution (%)		Kaolinte	11
Clay	70.0	Chlorite	10
Silt	29.8		
Sand	0.2		
pH	4.8	Pore water salinity (g/L)	
Organic matter (%)	3.2		24
CEC ($cmol_c$/kg)	38.5	Ions in pore water (g/L)	
		Na	14.49
		K	0.59
		Ca	1.56
		Mg	1.80
		Cl	3.30
		SO_4	12.45

salts in the marine clay. In the present study, the effects of salts on sorption of lead for marine clay were examined using column tests, and the retention mechanisms of lead were examined based on selective sequential extraction (SSE).

Materials

In this study, marine clay was collected from the sediment in the channel of reclaimed area in Ariake-cho, Saga Prefecture, Kyushu, Japan. The chemical and physical properties of the sample are shown in Table 1. Clay mineral composition was determined based on the procedure described by Ohtsubo et al. (2002). The major clay minerals identified are smectite, illite, kaolinite, and chlorite. The smectite present in the sample is classified as low-swelling smectite, commonly found in marine clay throughout Japan (Egashira and Ohtsubo 1982). The pore fluid of the marine clay was measured for its salinity, and soluble cation and anion concentrations. The pore fluid of the marine clay was extracted using the 10 % soil suspension by weight soil/solution prepared by adding deionized water to the clay sample. The concentrations thus determined were converted to those in the pore water of the sample at its natural water content, as summarized in Table 1.

Methods

Column Leaching Tests

Column leaching tests were conducted on marine clay slurry samples with lead solutions at different salinity. Figure 1 shows a schematic diagram of the column test equipment. Three kinds of spiked lead solutions (100 mg/L of Pb) were used for this study including deionized water, sea water, and bottom ash leachate at pHs 3 and 6. The sea water was prepared artificially using chloride solutions of Na^+ (14.6 g/L), K^+ (0.6 g/L), Ca^{2+} (1.4 g/L), and Mg^{2+} (3.1 g/L). The bottom ash leachate was prepared by leaching 700 g of bottom ash placed in a column leaching cell (Fig. 1) with 8 L deionized water. The bottom ash was obtained from a municipal solid waste incineration plant in Fukuoka, Japan. The chemical composition of the ash leachate is Na^+ (5 g/L), K^+ (5.5 g/L), Ca^{2+} (1.2 g/L), Mg^{2+} (0.18 g/L), Cl^- (13.5 g/L), and SO_4^{2-} (1.53 g/L).

Each slurry soil sample with a water content of 130 % was placed in a leaching cell with a diameter of 60 mm and a height of 100 mm. The lead solutions permeated through the samples from the top of the column at a constant air pressure of 50 kPa, equivalent to a hydraulic gradient of 50. Each leaching test was terminated when the volume of the effluent solution reached five pore volumes. The number of pore volumes p is defined as $v_d t/\alpha L$, where v_d is Darcy's velocity, α is the water-filled porosity of the soil material (Kirkham and Powers 1971). During the initial permeation process (at the early stage, below one pore volume of effluence collected), the marine clay was consolidated by ~6 to 10 % of the initial volume

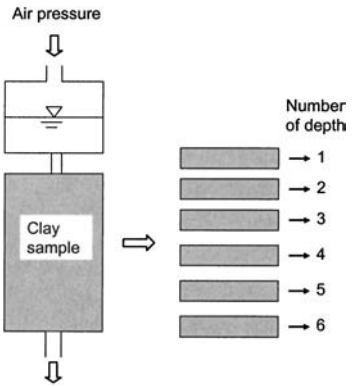

FIG. 1—*Schematic diagram of the column leaching cell.*

due to the high hydraulic gradient. This induced differences in the water content of the sample. The water content, for instance, changed from 128 % at the top to 109 % at the bottom for the sample permeated with deionized water (pH 3). The samples permeated with other solutions exhibited similar changes in water content.

Hydraulic conductivity was determined as a function of time by measuring the amount of effluent from the column. The pH, Pb concentration, and salt concentration of the effluent were also analyzed. After the permeation was complete, the sample in the column was sliced into six equal pieces. Pore water was extracted from each slice of material with pore water pressure equipment, and the pH of the pore water was determined. The Pb retained by the soil material was analyzed for each slice by selective sequential extraction.

Selective Sequential Extraction (SSE)

The SSE methods were adopted from Tessier et al. (1979), Li and Li (2001), and Yong et al. (2001). The basic utility of SSE is its use of appropriate reagents to release different heavy metal fractions from soil solids by progressively destroying the binding agents between the metals and the soil solids and permitting the metal species to be detected at each stage.

The clay samples sliced into six equal slices (Fig. 1) were used for SSE analysis: (1) Initial rinse: To remove the heavy metals dissolved in the pore water, 8 mL of distilled water were added to the soil sample and centrifuged; (2) Exchangeable cations extraction: 8 mL of 1 M potassium nitrate (KNO_3) with pH 7 were added to the samples, agitated for 1 h in a rotary shaker at 22 rpm and centrifuged; (3) Carbonate: 8 mL of 1 M sodium acetate (NaOAc), adjusted to pH 5.0 using acetic acid (HOAc) were added to the sample to release metals precipitated with carbonates. After agitation for 5 h, the sample was centrifuged at 2200 rpm; (4) Oxides and hydroxides: 20 ml of 0.004 M hydroxylamine hydrochloride ($NH_3OH \cdot HCl$) in 25 % (v/v) HOAc was added to the sample, agitated occasionally at 96±2°C for 6 h, and centrifuged to extract all metals precipitated as hydroxides and/or adsorbed on the oxides or the amorphous hydroxides; (5) Organics: Heavy metals bound to organic constituents in soil via complexation, adsorption, and chelation. This extraction was divided into three phases: Phase (i): via 3 mL of 0.02 M nitric acid (HNO_3) and 5 mL of 30 % H_2O_2 adjusted to pH 2.0 with HNO_3 occasionally agitated at 85±2°C; Phase (ii): with 3 mL of 30 % H_2O_2 (at pH 2.0), intermittently, agitated for 3 h at 85±2°C; and Phase (iii): by 5 mL of 3.2 M ammonium acetate (NH_4OAc) in 20 % (v/v) HNO_3, diluted to 20 mL, and continuously agitated at room temperature for 30 min; (6) Residual fractions: Metals bound to the soil solids via specific adsorption in soil mineral lattice were extracted by digestion. The residue (after previous four stages) was digested with HNO_3 and centrifuged. In each of the above procedures, the supernatant collected by centrifugation was analyzed for lead concentration.

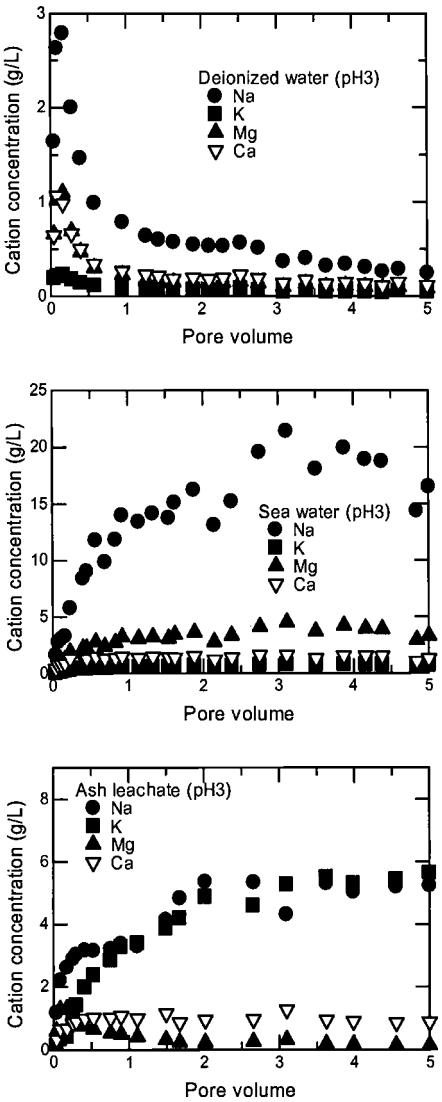

FIG. 2—*Change in cation concentration with permeation of various solutions (pH 3).*

Results and Discussion

Change in Salt Concentration, pH, and Permeability

Figure 2 shows changes in cation concentration in column leaching tests using deionized water, sea water, and ash leachate at pH 3. The leached cation concentrations were almost a constant amount at approximately two to three pore volumes (pv) for the sea water and ash leachate samples, whereas the leached concentrations decreased to 0.25, 0.049, 0.114, and 0.084 g/L for Na, K, Ca, and Mg for the sample leached with deionized water. Similar results were obtained for pH 6 solutions (not shown here). The concentration ratio of divalent cations ($Ca^{2+}+Mg^{2+}$) to total cation ($Na^{+}+K^{+}+Ca^{2+}+Mg^{2+}$) was in the range 0.3 to 0.4 for pH 3 and 0.4 to 0.5 for pH 6 (Fig. 3), probably due to the effect on the hydraulic

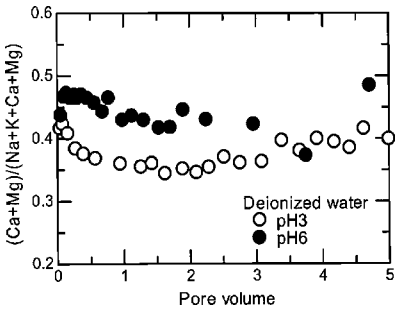

FIG. 3—*Ratio of divalent cation to total cation concentration for pure water permeation.*

conductivity of the marine clay as described in the next section. Figure 4 shows the pH profile of the pore water at different pore volume for deionized water, sea water, and ash leachate. The pH exceeded 4.5 for the deionized water and sea water samples, whereas the pH of the pore fluid using ash leachate was less than 4.5.

Figure 5 shows changes in hydraulic conductivity (k) during the permeation of deionized water, sea water, and ash leachate at pH 3 and 6. The results indicate that after one pv, k was almost constant with pH 6 (sea water and ash leachate), whereas it slightly decreased with increasing pore volume for the deionized

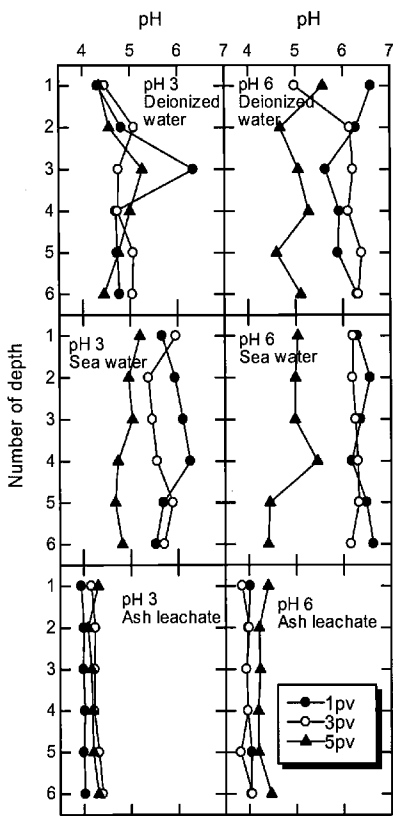

FIG. 4—*Profile of pore water pH for various permeates.*

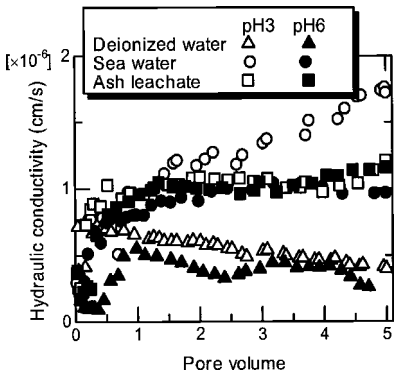

FIG. 5—*Change in hydraulic conductivity with permeation of various solution.*

water sample. When a sample was permeated with sea water at pH 3, there was a continuous increase in k. The increase in k for the sea water and ash leachate samples could result from the development of a flocculated structure at high cation concentrations (van Olphen 1977). For the deionized water sample, k was expected to decrease with decreasing concentrations of cation due to an increase of diffuse double layer thickness. However, k for the marine clay using deionized water exhibited only a slight decrease (Fig. 5). This could be because, as indicated by the result shown in Fig. 3, that the ratio of divalent cations to total cations in deionized water is between 0.3 and 0.5, which is also true for reduced cation concentrations (Fig. 3). The presence of divalent cations could be a controlling factor in determining the diffuse double layer thickness even at reduced cation concentrations (Bolt 1956), which in turn controls the k.

Pb Migration Behavior

Figure 6 shows changes in Pb concentration in the effluent (C_e) during permeation of the deionized water, sea water, and ash leachate. The C_e of the deionized water sample was less than 5 mg/L for both pH 3 and 6 permeates throughout leaching process. The heavy metal concentration in the effluent is closely related to the solubility of heavy metals in the pore solution of soil material. The solubility of Pb in the solution changes with pH. The lead was present mostly as soluble Pb^{2+} below pH 5, but above this pH the solubility decreased with increasing pH. (Marani et al. 1995). The low Pb concentration in the effluent for the deionized water sample with pH 3 permeates can be attributed mainly to the adsorption of Pb onto clay particles, since the pH of the pore water ranged from 4.2 to 5.3 (Fig. 4). For the deionized water sample with pH 6 permeate, having a pore water pH of 4.5 to 7 (Fig. 4), both adsorption and precipitation of Pb

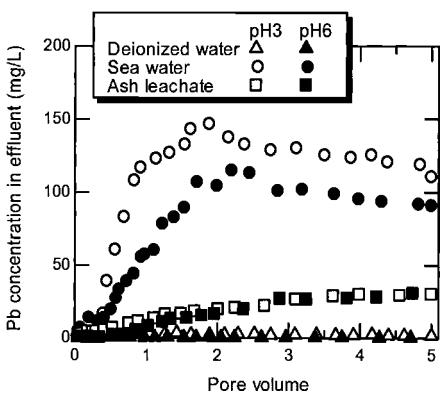

FIG. 6—*Breakthrough curve of Pb for various permeates.*

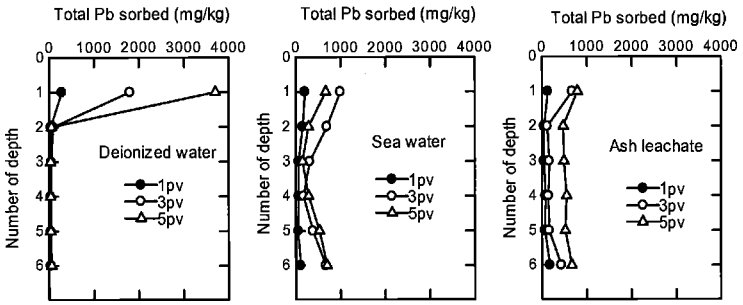

FIG. 7—*Profiles of total Pb retained at 1, 3, and 5 pv for the samples subjected to leaching with pH 3 permeates.*

contributed to the low Pb concentration in the effluent. Cerussite ($PbCO_3$) and hydrocerussite [$Pb_3(CO_3)_2(OH)_2$] have been proposed as predominant Pb precipitates in this pH range (Marani 1995; Ponizovskii and Mironenko 2001; Pierrand et al. 2002).

In Fig. 6 the sea water sample exhibited higher Pb concentrations in the effluent than in the deionized water. This is ascribed mainly to the interference of Pb adsorption on clay particles due to competition of Pb with other cations such as Na, K, Ca, and Mg in sea water (Kookana and Naidu 1998; Warren and Zimmerman 1994; Ohtsubo et al. 2005). The Pb concentration in the effluent for pH 3 and 6 permeates both exceeded the Pb concentration of the influent (100 mg/L) below one pore volume (pv) leaching, reaching 150 and 120 mg/L at the maximum respectively at ~2 pv leaching. The higher Pb concentrations in the effluent than in the influent can be attributed to the dissociation of Pb originally retained in the soil sample, due to replacement of Pb by other cations in the sea water. The soil sample originally contained 40 mg/kg Pb, equivalent to ~40 mg/L when the Pb retained is all dissociated into pore water under a water content of 100 %. The higher maximum Pb concentration for the pH 3 than for the pH 6 permeates is due to the higher solubility of Pb in pore water for the pH 3 permeate with lower pore water pH (Fig. 4). For the ash leachate sample, the maximum Pb concentrations in the effluent for pH 3 and 6 permeates were identical because of a similar solubility of the two permeate samples due to the pore water pHs $<$ 4.5 (Fig. 4).

Pb Sorption Characteristics

Sequential selective extraction was performed on six portions sliced from the soil sample in the column (Fig. 1). The sum of Pb determined for the phase of exchangeable, carbonate, hydroxide, organic, and residual is shown in Fig. 7 against the depth. The data include the total Pb retained at three leaching stages of 1, 3, and 5 pv for the samples subjected to permeation with pH 3 solutions for different types of permeate. For the deionized water sample, the highest retention of Pb occurred in the top layer of the soil column. The Pb accumulated as permeation progressed, and Pb retention reached 3700 mg/kg after 5 pv leaching. Thus, under continued exposure of the soil to Pb solution, Pb retention was maintained at the top layer even after 5 pv leaching. This continues until such time when the saturation limit is reached, i.e., when the buffering capacity of the soil has been fully utilized. Accumulation of Pb in the top layer reflected in the low Pb concentration in the effluent at 5 pv in Fig. 6. For the sea water sample, Pb retention at the top layer for 1 pv leaching was almost the same as for the deionized water sample, but exhibited less increase for further permeation compared to the deionized water sample (Fig. 7). This results from competition of the spiked Pb (100 mg/kg) with other cations present at greater concentrations in the sea water (Table 1). The Pb that was not retained at the top layer descended and was partially retained in lower layers, while the rest was leached out of the bottom of the soil column. Similar results were observed for the ash leachate sample.

The sequential selective extraction results for 5 pv leaching, presented in Fig. 8, offer insight on how the heavy metals are sorbed onto clay particles. For the deionized water sample (both pH 3 and 6), three phases of carbonate, exchangeable and hydroxides predominated in the top layer. Similar results were

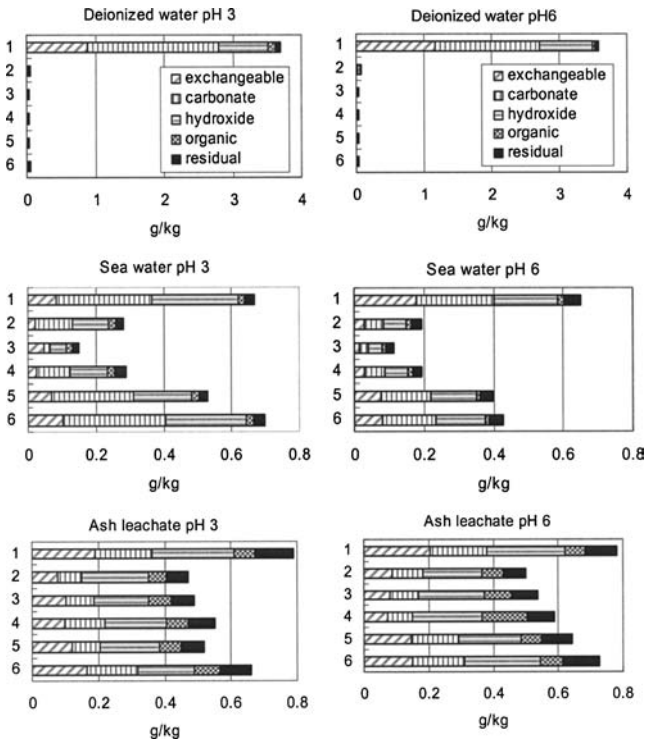

FIG. 8—*SSE results for 5 pv permeation.*

obtained for illite soil (Yong 2000), where the amount of Pb retained through carbonate and hydroxide phase was predominant above pH 4 and increased with increasing pH. Sorption through ion exchange occurred through the whole pH range of 2 to 7.

By replacing the deionized water to permeate with the sea water and ash leachate, the Pb in the top layer retained only through the exchangeable phase was expected to decrease due to competition of Pb with other cations in the sea water and ash leachate. However, the Pb retained through the carbonate and hydroxide phase also decreased to a great extent. This could be explained in terms of a change in soil structure during permeation of salt solutions; preferential pathways have been formed due to flocculation of clay particles in the presence of salts (Li and Li 2001), which decreased the surface area exposed to Pb solution, leading to a decrease in the Pb retained thorough exchangeable, carbonate, and hydroxide phases. Decreases of Pb in carbonate phase could be explained partly by reduction in the formation of cerussite ($PbCO_3$) and hydrocerussite $[Pb_3(CO_3)_2(OH)_2]$ because Pb competes with other cations in salt solutions for available carbonates.

Summary and Conclusions

The hydraulic conductivity was almost constant or slightly decreased during leaching depending on the pH of permeates for the deionized water sample, whereas it increased initially and then became constant for the sea water (pH 6) and ash leachate samples.

The sea water sample exhibited higher Pb concentration in the effluent compared with the deionized water. This is ascribed mainly to the interference of Pb adsorption on clay particles due to competition of Pb with other cations in the sea water such as Na, K, Ca, and Mg.

The highest retention of Pb occurred in the top layer of the soil column for the deionized water permeation after leaching by five pore volumes. For the sea water and ash leachate permeation, Pb not

fully retained in the top layer traveled downward and was partially retained in lower layers; the rest was leached out through the bottom of the soil column.

The selective sequential extraction indicated that three phases of carbonate, exchangeable, and hydroxides were predominant in Pb sorption for the deionized water. By replacing the deionized water with the sea water and ash leachate, the Pb retained through exchangeable, hydroxides, and carbonate phases all decreased considerably. This was explained in terms of a change of soil structure during permeation of the salt solutions.

References

Abbas, Z., Moghaddam, A. P., and Steenari, B. M., "Release of Salts from Municipal Solid Waste Combustion Residues," *Waste Manage.* 23, 291–305 (2003).

Amrheim, C. and Strong, J. E., "The Effect of Deicing Salts on Trace Metal Mobility in Roadside Soils," *J. Environ. Qual.* 19, 765–772 (1990).

ATSDR. "Agency for Toxic Substances and Disease Registry: Toxicological Profile for Lead." US Public Health Service, US Department of Health and Human Services, Atlants (1993).

Bolt, G. H., "Physico-Chemical Analysis of the Compressibility of Pure Clay," *Geotechnique*, 6(2), 86–93 (1956).

Egashira, K. and Ohtsubo, M., "Smectite in Marine Quick-Clays of Japan," *Clays Clay Miner.*, 30(4), 275–280 (1982).

Griffin, R. A., Shimp, J. D., Steele, J. D., Rugh, R. R., White, W. A., and Hughes, G. M., "Attenuation of Pollutants in Municipal Landfill Leachate by Passage through Clay," *Environ. Sci. Technol.*, 10, 1262–1268 (1976).

Hanashima, M. and Furuichi, T., "Landfill Sites in Japan 2000," Kanko-Sangyo Newspaper Company, 1–10 (2000).

Kamon. M., "Geotechnical Utilization of Industrial Wastes," *Environmental Geotechnics, Balkema, Proceedings of the 2nd International Congress on Environmental Geotechnics, Osaka, Japan*, 1996, 1293–1309.

Kanaya, K., Kashimoto, S., and Terashima, Y., "Effect of Acid Rain to Heavy Metal Leaching from Municipal Solid Waste Ash," *Environ. Technol.* 23(3), 35–40 (1994).

Kirkham, D. and Powers, W. L., *Advanced Soil Physics*, John Wiley & Sons New York, 1971, pp. 400–401

Kookana, R. S. and Naidu R., "Effect of Soil Solution Composition on Cadmium Transport Through Variable Charge Soils," *Geoderma*, 84, 235–248 (1998).

Li, L. and Li, F., "Heavy Metal Sorption and Hydraulic Conductivity Studies Using Three Types of Bentonite Admixes," *J. Environ. Eng.* 127(5), 420–429 (2001).

Marani, D., Macchi, G., and Pagano, M., "Lead Precipitation in the Presence of Sulphate and Carbonate: Testing of Thermodynamic Predictions," *Water Res.*, 29(4), 1085–1092 (1995).

Mohamed, A. M. O., Yong, R. N., Tan, B. K., Farkas, A., and Curtis L. W., "Geo-environmental Assessment of a Micaceous Soil for its Potential Use as an Engineered Clay Barrier," *Geotech. Test. J.*, 17(3), 291–304 (1994).

Ohsako, M., Yamada, M., Inoue, Y., Kim, Y. J., Park, J. K., Lee, D. H., Yoshida, T., and Nomura, T., "A Comparative Study on Leaching Characteristics of Heavy Metals from Municipal Solid Waste Incineration Bottom Ashes in Korea and Japan," *Waste Manage. Res.*, 12(6), 256–265 (1994).

Ohtsubo, M., Egashira, K., Tanaka, H., and Mishima, S., "Clay Minerals and Geotechnical Index Properties of Marine Clays in East Asia," *Marine Georesources & Geotechnology*, 20 (4), 22–35 (2002).

Ohtsubo, M., Li, L., Yamaoka, S., and Higashi, T., "Leachability of Metals from Municipal Solid Waste Fly-Ash and Bottom-Ashes at Different pH," *Geoenvironmental Engineering, Integrated Management of Groundwater and Contaminated Land*, edited by R. N, Yong and H. R., Thomas, 283–290 (2004).

Ohtsubo, M., Yamaoka, S., Li, L., and Higashi, T., "Effect of Salt Concentration on the Lead Sorption Characteristics of Clay Liner Material," *The 6th Geoenvironmental Engineering Symposium*, The Japanese Geotechnical Society, 225–230 (2005).

Pierrand, J. C., Rimbault, J., and Aplincourt, M., "Experimental Study and Modeling of Lead Solubility as a Function of pH in Mixtures of Ground Waters and Cement Waters," *Water Res.*, 36, 879–890 (2002).

Ponizovskii, A. A. and Mironenko, E. V., "Mechanisms of Lead (II) Sorption in Soils," *Eurasian Soil*

Science, 34(4), 371–381 (2001).

Tessier, A., Campbell, P. G. C., and Bison, M., "Sequential Extraction Procedure for the Speciation of Particulate Trace Metals," *Anal. Chem.*, 51, 844–850 (1979).

van Olphen, H., *An Introduction to Clay Colloid Chemistry*, 2nd Ed. John Wiley & Sons, New York (1977).

Warren, L. A. and Zimmerman, A. P., "The Influence of Temperature and NaCl on Cadmium, Copper and Zinc Partitioning Among Suspended Particulate and Dissolved Phases in an Urban River," *Water Resour.*, 28(9), 1921–1931 (1994).

Yanful, E. K., Quigley, R. M., and Nesbitt, H. W., "Heavy Metal Migration at a Landfill Site, Sarnia, Ontario, Canada-2: Metal Partitioning and Geotechnical Implications," *Appl. Geochem.* 3, 623–629 (1988).

Yong, R. N., *Geoenvironmental Engineering, Contaminated Soils, Pollution Fate, and Mitigation*, CRC Press, 169–189 (2000).

Yong, R. N., Yaacob, W. Z. W., Bentley, S. P., Harris, C., and Tan, B. K., "Partitioning of Heavy Metals on Soil Samples from Column Tests," *Eng. Geol. (Amsterdam)* 60, 307–322 (2001).

Journal of ASTM International, Vol. 3, No. 7
Paper ID JAI13313
Available online at www.astm.org

Dimitris Dermatas,[1] *Rudoeph Bonaparte,*[2] *Maria Chrysochoou,*[1] *and Deok Hyun Moon*[1]

Chromite Ore Processing Residue (COPR): Hazardous Contaminated Soil or Solid Waste?

ABSTRACT: Chromite ore processing residue (COPR), which contains hexavalent chromium (Cr^{6+}) at concentrations typically in the range of thousands of milligrams/kilograms, was deposited over a timeframe of 50 years as fill at a site referred to as SA7 in New Jersey. Significant surface heaving associated with COPR weathering-induced mineralogical expansion has been observed at the site over time. The current site owner is being required to remediate the site to mitigate both human health risks associated with the Cr^{6+} and site redevelopment problems associated with COPR heave. The owner is presently required to remediate the COPR by excavation and off-site disposal at a licensed hazardous waste landfill. This is a very expensive remediation option, one that may not be financially sustainable at other COPR impacted sites. The owner has undertaken a major investigation to better characterize the nature of COPR and to develop on-site treatment technologies to reduce Cr^{6+} concentrations and mitigate COPR heave potential. As one part of the investigation, the characteristics of COPR were evaluated with respect to the definitions of hazardous contaminated soil and hazardous solid waste under the toxicity characteristic waste provisions of the U.S. Resource Conservation and Recovery Act (RCRA). Remediation clean-up standards, and thus the potential costs and applicable methods associated with site remediation, under these two definitions are significantly different. This paper explains these differences and evaluates the COPR for conformance with each definition. This evaluation includes comparison of sampling, logging, and laboratory testing techniques for COPR compared to soil, geotechnical parameter comparisons, and mineralogical and total metals comparisons. Based on these comparisons, the authors conclude that COPR should classify as a hazardous contaminated soil from both regulatory and scientific perspectives. The bases for this conclusion are provided in the paper. The methodology presented herein to evaluate COPR classification may have applicability to other contaminated soil-like media from industrial processes that are potentially subject to the requirements of RCRA hazardous waste regulations or similar regulations in other countries.

KEYWORDS: chromium contamination, chromium remediation, COPR, hazardous waste, contaminated soil, soil classification, RCRA

Introduction

This paper describes the scientific and engineering aspects of material classification as it pertains to the applicable regulatory definition for a contaminated site involving chromite ore processing residue (COPR). About 1.5 million tons of COPR were deposited over a span of 50 years as a fill at a site designated as Study Area 7 (SA7) in New Jersey. COPR is an alkaline industrial process residual that contains significant amounts of hexavalent chromium (Cr^{6+}). The current site owner has been required to design and implement a site remediation program involving COPR excavation, transport, and disposal at an off-site hazardous waste landfill facility. As this removal and off-site disposal option is very expensive (more than $200 per ton of material remediated) and potentially not financially sustainable at other COPR impacted sites, the owner has undertaken an extensive investigation to better characterize the nature of COPR and a major development effort for potential on-site treatment technologies to reduce COPR Cr^{6+} concentrations and mitigate COPR heave potential.

Solid Waste and Contaminated Soil

An important step in developing a remediation plan for COPR, or for any other contaminated media, involves defining the required remediation endpoints. Most commonly, a target concentration of the chemi-

Manuscript received March 31, 2005; accepted for publication May 26, 2005. Presented at ASTM Symposium on Contaminated Sediments: Evaluation and Remediation Techniques on 23–25 May 2006 in Shizuoka, Japan; M. Fukue, K. Kita, M. Ohtsubo, and R. Chaney, Guest Editors.

[1] W.M. Keck Geoenvironmental Laboratory, Stevens Institute of Technology, Castle Point on Hudson, Hoboken, NJ 07030.
[2] GeoSyntec Consultants, 2002 Summit Blvd., NE, Suite 885, Atlanta GA 30319.

cal of concern in the contaminated media, or in a leachate extracted from the media, represents the required endpoint. In the United States (U.S.), the regulatory determination of treatment requirements for a material that exhibits the toxicity characteristic under the Resource Conservation and Recovery Act (RCRA) [1] is critically dependent on the classification of that material as a "hazardous solid waste" or a "hazardous contaminated soil." Under RCRA, a solid waste is any discarded, abandoned, or recycled material that is not excluded by specific variance [Title 40 of the U.S. Code of Federal Regulations (CFR), Sec. 261.2]. Under RCRA, both solids and liquids may carry the regulatory classification of solid waste; When considering solids, "nonwastewater" treatment standards apply. The United States Environmental Protection Agency (USEPA) has defined soil for the purpose of evaluating the Land Disposal Restrictions (LDR) of "contaminated soil" as [1] "unconsolidated earth material composing the superficial geologic strata (material overlying bedrock), consisting of clay, silt, sand, or gravel size particles as classified by the U.S. Natural Resources Conservation Service, or a mixture of such materials with liquids, sludges, or solids which is inseparable by simple mechanical removal processes and is made up primarily of soil by volume based on visual inspection."

If a material is classified as a solid waste under RCRA and it exhibits a toxicity characteristic leaching procedure (TCLP) chromium concentration of more than 5 mg/L, the material is a characteristic hazardous solid waste with a D007 waste code [2]. This hazardous solid waste may only be disposed in a licensed hazardous waste landfill if it meets the universal treatment standard (UTS) for nonwastewaters under the LDR of RCRA, as detailed in Sec. 268.48 [1]. The UTS for D007 waste is 0.60 mg/L total chromium in the TCLP extract. If a material classifies as a contaminated soil under RCRA, if it exhibits a TCLP chromium concentration of more than 5 mg/L, and if the material is "generated" for purposes of landfill disposal as discussed in the next paragraph, the material is a hazardous contaminated soil. This hazardous contaminated soil may only be land disposed if it meets the LDR treatment standard of 40 CFR Sec. 268.49 [1] which requires reduction of the TCLP hazardous constituent concentration to not more than 10 % of the original TCLP concentration, or reduction to not more than 10 times the UTS concentration, whichever is greater. As noted above, the nonwastewater UTS for chromium is 0.60 mg/L (Sec. 268.48) [1]. Thus, for contaminated soil, the treatment standard for TCLP chromium in a hazardous contaminated soil is no less than 6 mg/L, and the treatment standard will be higher than this value if the untreated TCLP chromium concentration is higher than 60 mg/L. Typical COPR TCLP chromium concentrations are in the range of 10 to 100 mg/L. Thus, COPR treatment requirements to meet LDR prior to hazardous waste landfill disposal will depend on the regulatory classification of the material as a hazardous contaminated soil versus hazardous solid waste.

LDR treatment standards apply to hazardous solid waste or hazardous contaminated soil when the material is "generated" and "placed in a land disposal unit" (63 FR 28617) [3]. In situ contaminated soil is only "generated" when it is removed from the land; thus, LDR treatment standards do not apply to in situ contaminated soil. In addition, under certain circumstances, hazardous contaminated soil may be managed or treated on-site within an area of contamination (AOC) or a corrective action management unit (CAMU), as defined in RCRA, without triggering the LDR treatment standards. If a contaminated soil is treated within an AOC or CAMU prior to "generation" to below the TCLP threshold of 5 mg/L and the applicable contaminated soil treatment standard, that soil will never "become" a hazardous waste and may, depending on local requirements and other regulations, be allowed to remain on site as a treated material, often with other engineering or institutional controls, or alternatively, the material may be allowed to be disposed of in a municipal solid waste or nonhazardous industrial waste landfill at considerably lower cost than hazardous waste landfill disposal.

For the SA7 site, an extensive field investigation and COPR sampling program was undertaken in 2003. The associated laboratory analyses of the sampled COPR resulted in mean, mean plus sigma, and maximum TCLP chromium concentrations of 51, 94, and 180 mg/L, respectively [4]. The corresponding LDR treatment standards for a contaminated soil material with these TCLP chromium concentrations would be 6, 9.4, and 18 mg/L. In comparison, the LDR treatment standard for a characteristic hazardous waste with those same TCLP chromium concentrations is 0.60 mg/L. The contaminated soil treatment standards are from 10 to 30 times higher than the solid waste treatment standards. This comparison does not consider the possibility of obtaining a LDR treatability variance for either material classification. Based on the foregoing, the regulatory classification of COPR as a hazardous solid waste versus a hazardous contaminated soil under U.S. RCRA regulations for the toxicity characteristic is an important issue

with respect to both landfill disposal of that material and the potential for on-site treatment and placement back on the site. The type of treatment and/or disposal and the treatment standard have significant implications with regard to the design, implementation, and cost of remediating a COPR contaminated site. The remainder of this paper further considers this question of COPR material classification.

It should also be mentioned that the contaminated soil provisions of RCRA were developed by the U.S. Environmental Protection Agency (USEPA) to be both protective of human health and the environment and to account for the large volumes and heterogeneous nature of contaminated soil media found in the U.S. [5]. Prior to the promulgation of contaminated soil provisions, large volumes of soils containing relatively low levels of contaminants might have required incineration rather than landfill disposal, because soil treatment could not achieve the nonwastewater UTS for solid waste. One of USEPA's goals in promulgating the contaminated soil provision was to incentivize responsible parties to undertake soil remediation projects by making them more feasible and economical, while, at the same time still protecting human health and the environment.

In considering the question of whether a material is a solid waste or contaminated soil, USEPA [6] addressed the issue of solid waste and soil mixtures. The agency indicated that to be considered a contaminated soil, the material should be made up predominantly of soil and that other materials in the mixture should be inseparable from the soil using simple physical or mechanical means. These could include, for example, physical separation or screening. Chemical analysis for soil properties in order to differentiate precisely between solid waste and soil is not required.

It is also useful to consider textbook definitions of soil when evaluating the question of waste classification. The book *Fundamentals of Soil Behavior* [7] makes the point that the solid particles in soil may vary in size from boulders to clay size particles, with most particles being crystalline, but with noncrystalline and organic constituents commonly found, and with particle shapes ranging from nearly spherical to bulky, flat, and needlelike. This same book indicates that the most abundant soil elements are oxygen, silicon, hydrogen, and aluminum, and that along with calcium, sodium, potassium, magnesium, and carbon, comprise over 99 % of the solid mass of soils worldwide. The book *An Introduction to Geotechnical Engineering* [8] contains many of the same points in defining and describing soils.

Based on the above, the following questions will be discussed with respect to the characterization of COPR as a contaminated soil versus solid waste:

1. How was COPR generated and what was the history of placement and site use?
2. How is COPR sampled, logged, and tested in the laboratory and how do these compare to the methods used to sample and characterize soil?
3. What are the physical characteristics of COPR and how do these compare with the physical characteristics of soil?
4. To what extent is COPR intermixed with native soil and how does its mineralogy compare with other soil and nonsoil matrices?
5. What are the geochemical and geotechnical characteristics of COPR and how do these interact with the environment?

COPR Origin and History of the SA7 Site

From 1905 to 1954, the Mutual Chemical Company of America operated a sodium dichromate manufacturing facility east of the SA7 site across Route 440 in Jersey City, New Jersey. COPR was generated by the extraction of chromium as soluble sodium chromate from chromite ore of the general formula $(Mg,Fe)(Cr,Al,Fe)_2O_4$ by means of a high-temperature roasting process [9]. Addition of lime at 1200°C led to the formation of oxides such as brownmillerite (Ca_2FeAlO_5) and periclase (MgO), that incorporated trace compounds such as Si and Cr. The resulting solid contains residual chromium in concentrations of 3–5 %, up to 30 % of which is in its hexavalent form.

The timeframe of plant operations (1905–1954) predates the timeframe for environmental laws regulating the management and disposal of COPR (as well as most other industrial manufacturing residuals). During that timeframe, COPR resulting from plant operations was transported and placed hydraulically on 34 acres of Hackensack River tidelands at the site now designated as SA7 [4]. Land grants permitting fill placement were issued from 1900 to 1925. In 1954, Mutual Chemical stopped processing chromium ore. After hydraulic deposition, the COPR was spread mechanically across the site, graded, and covered with

soil for the purpose of commercial site development. A drive-in theater was constructed at the site and then an adjacent large department store (1966). A furniture depot and a car wash facility were also constructed at the site. All structures but the furniture depot ultimately had to be demolished due to the pronounced surface heaving caused by the delayed volumetric expansion of the COPR. During this commercial development period, the site was occasionally reworked to eliminate the heave features.

The history of the site highlights the fact that during the timeframe of development, COPR was considered to be an appropriate material to use as a fill for construction of commercial structures. In other words, it was considered equivalent to soil as a foundation material. The heaving phenomenon observed at the site revealed that COPR, at the prevalent geochemical state at the time, was not appropriate as a foundation material, as its expansion lead to structural failures of timber and concrete foundation elements. Similar phenomena have been widely reported for lime-stabilized clays used as foundation material for road and pavement construction; swelling of the lime-treated clays lead to the formation of cracks in the asphalt in numerous cases [10].

Materials and Methods

Sampling and Logging

An extensive subsurface investigation and field sampling program was conducted at SA7 in 2003 [4]. The program included the drilling of shallow and deep soil borings, in order to delineate the depth and condition of COPR and underlying strata, as well as to obtain samples from the upper zones that contained COPR. Hollow-stem augers and split spoon samplers, which are customarily used for geotechnical and geoenvironmental investigations of soils [11], were used to obtain the COPR samples. Cone penetrometer testing (CPT) was also performed and monitoring wells were installed. These too represent conventional methods for the investigation of soils. A total of 92 discrete disturbed samples were obtained from different depths in 38 soil borings, while a further 25 relatively undisturbed samples were obtained from tube samplers and one block sample was obtained from a trench excavation. The boring logs from all of these sources describe the SA7 COPR material in the conventional terminology used to describe the engineering characteristics of soil as presented by the American Society of Testing and Materials (ASTM). The boring logs also contain standard penetration test (SPT) blow counts obtained using an ASTM standard test for soils. The ASTM soil standards utilized in developing the boring logs include [12]:

- D 2487–"Classification of Soils for Engineering Purposes (Unified Soil Classification System)."
- D 2488–"Description and Identification of Soils (Visual–Manual Procedure)."
- D 1586–"Penetration Test and Split-Barrel Sampling of Soils."

Laboratory Methods

The following laboratory analysis techniques were employed in order to evaluate COPR physicochemical and mineralogical properties:

1. Visual description was performed in accordance with ASTM method D 2488 [12], as stated above.
2. Grain size distribution was determined following standard practice set forth in ASTM D 421 [12] and a modified form of ASTM D 422 [12]. ASTM D 422 was modified to control the amount of deaggregation of COPR grain agglomerations produced by the test procedure.
3. Atterberg limits were measured in accordance with ASTM D 4318 [12].
4. The water content was measured in accordance with method ASTM D2216-98 [12].
5. pH: The laboratory pH of the COPR samples was evaluated in accordance with ASTM D4980-89 [12].
6. X-ray powder diffraction (XRPD): Samples were air-dried for 24 h and pulverized to pass a U.S. standard 400 sieve (38 μm). Step-scanned XRPD data were collected using a Rigaku DXR 3000 computer-automated diffractometer using Bragg-Brentano geometry. The diffractometry was conducted at 40 kV and 30 mA using diffracted beam graphite-monochromator with Cu radiation. The data were collected in the range of two-theta values between 5° and 65° with a step size of 0.05° and a count time of 5 s per step. The qualitative analysis of the XRPD patterns was performed using the Jade software [13]. The reference databases for powder diffraction and crystal structure

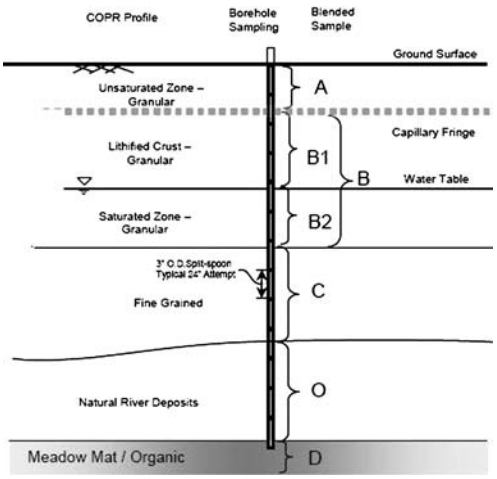

FIG. 1—*Vertical profile of COPR stratigraphy at SA7.*

data were the PDF-2 set of the International Center for Diffraction Data database [14] and the Inorganic Crystal Structure Databases [15], respectively.

7. Total metal analyses: The total content of individual metals was measured by acid digestion [16] and Inductively Coupled Plasma/ Atomic Emission Spectrometry [17].

Results and Discussion

COPR Physical Description and Stratigraphy

Several distinct horizons of COPR and non-COPR material were identified during the subsurface investigation of the SA7 site. A classification system was developed to designate the different horizons, based on their physical description and their location with respect to the groundwater table. The designations of the horizons are shown in Fig. 1.

The upper in situ horizons were all found to contain granular material. Zone A, the uppermost horizon located in the unsaturated zone, was found to consist of gray/black/brown medium sand with some silt. Zones B1 and B2 were found to consist of coarse sand with some silt and gravel; many particles were observed to be cemented together to form larger agglomerations of COPR. The color of the material was observed to be similar to zone A, with occasional green particles or particle agglomerations. Zone B was divided into zone B1, located above the groundwater table, and Zone B2, located in the saturated zone. COPR found in the underlying zone C horizon was observed to be physically distinct from the other COPR horizons in that it consists mainly of fine-grained, gray, brown, green yellow fine sand and silt with some clay and trace to some gravel size particles. Based on visual observation, fine grained soil seams and lenses appear to be contained within the C horizon, particularly closer to the west side of the site, nearer the adjacent Hackensack River. Native soil deposits underlie the COPR horizons. These native deposits consist of an upper layer of silty fine sand and clay of light brown color and floodplain depositional origin, and an underlying layer of dark brown organic clay and peat termed as meadow mat (layers O and D in Fig. 1). Granular river alluvium underlies the meadow mat.

Geotechnical Parameters

Following the identification of distinct material horizons, composite samples were prepared to represent each horizon for the purpose of characterizing geotechnical and other parameters representative of the horizon. Five soil borings from across the SA7 site were chosen to prepare the composite samples. Equal amounts of COPR were obtained from each horizon in each soil boring, mixed, and homogenized; the

TABLE 1—*Selected geotechnical properties of COPR composite samples.*

	Water content	Soil pH	Gravel[a] %	Sand[a] %	Fines[a] %	Liquid[a] limit	Plasticity[a] index	USCS[a] symbol
Composite B1	27.7	12.5	16.5	65.6	17.9	NP	NP	SM
Composite B2	34.4	12.5	7.2	72.9	19.9	NP	NP	SM
Composite C	74.9	12.5	2.3	34.1	63.6	65	17	CH

[a](Sieve opening) for gravel: (75–4.75 mm), Sand: (4.75 mm–75 μm), Fines: (<75 μm). S: sand; M: silt; CH: clay; NP: nonplastic.

homogenized samples were designated as composites B1, B2, and C. Table 1 shows the pH, water content, grain size distribution, and placticity characteristics of the three composite samples, along with their classification according to the Unified Soil Classification System (USCS).

The composite B1 and B2 samples both classified as silty sands (SM), while the composite C sample, which contained high amounts of fines and exhibits significant plasticity and strength upon drying, classified as inorganic clay with significant plasticity (CH). The ASTM terminology used to classify COPR does not, therefore, distinguish it from natural soil.

The water content of COPR is also within the range of water content values encountered in natural soils. Das [18] provides a range of moisture content values of 16–30 % for in situ sands, while the range of values for most clayey soils is 20–120 %. The water content characteristics of COPR are, thus, similar to those of natural soils.

The pH analysis showed that COPR is a highly alkaline material (Table 1). This highly alkaline condition is not common to natural soils, in which the pH regime is usually neutral (pH 7) to slightly alkaline (pH 7.4 to 7.8) or acidic (pH$<$6) [19]. However, the pH of contaminated soil is sometimes alkaline, depending on the type of contamination. Moreover, contaminated soils that are treated with pozzolanic reagents become highly alkaline due to the nature of the binders used, e.g., lime and cement. The pH of saturated lime water is 12.4 [20], so that the pH regime of soils following lime or cement treatment is in the highly alkaline region (pH$>$12). The pH analysis of discrete samples of COPR (as opposed to the bulk samples) showed that there is significant pH variability between individual samples. The average value of 103 pH analysis results is 12.0, with a standard deviation of 0.8 pH units. The maximum value encountered was 12.9 and the minimum 8.1. The authors originally hypothesized that a low pH regime would be indicative of the presence of natural soil in the sample; however, subsequent mineralogical analyses showed that while this was sometimes true, a few samples that contained only soil-like minerals had high pH ($>$11), while several low pH samples were found to contain traces of COPR Based on these observations, it became apparent that the chemical interaction between COPR and natural soil at the SA7 site is complex and pH alone cannot be used to distinguish between natural soil and deposited COPR material.

Overall, the geotechnical characterization of COPR, as established by conventional soil analysis methods, resulted in geotechnical material descriptions and parameters consistent with those applicable to natural nonimpacted and contaminated soils. COPR was classified as silty sand or inorganic clay according to the USCS in the two predominant horizons encountered at the SA7 site; the measured COPR water content values were consistent with this classification. The pH regime, while outside the range for natural soils, is not uncommon to soils treated with pozzolanic reagents such as lime and cement.

Mineralogical Analyses

One hundred eighteen (118) samples obtained from the SA7 site were analyzed by qualitative and quantitative XRPD. The identified phases were classified into three categories:

1. *COPR mineral phases:* These include minerals that were originally generated by the roasting process, i.e., brownmillerite [Ca_2FeAlO_5], periclase [MgO], and portlandite [$Ca(OH)_2$] and their transformation products: hydrogarnets (katoite [$(CaO)_3Al_2O_3(H_2O)_6$] being the main phase), hydrotalcites (quintinite [$Al_2Mg_4(OH)_{12}(CO_3)(H_2O)_3$] is a representative compound), and calcium-aluminum-chromium-oxide-hydrates (CACs–[$Ca_4Al_2O_6(CrO_4)\cdot nH_2O$]) are the main weathering products derived from brownmillerite, while brucite [$Mg(OH)_2$] is the main periclase hydration product next to the hydrotalcites that scavenge part of the magnesium. Ettringite [$Ca_6Al_2(SO_4)_3(OH)_{12}\cdot 26H_2O$] and calcite [$CaCO_3$] are present when sulfate and carbonate are introduced to the system by means of water and/or air infiltration.

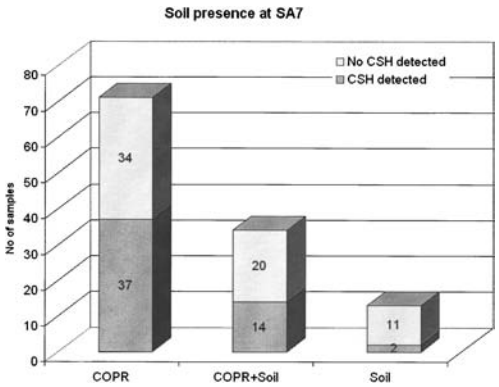

FIG. 2—*Distribution of COPR phases, soil mineral phases, and CSH in SA7 samples, as determined by XRPD analysis.*

2. *Soil mineral phases:* Silicate minerals identified in the SA7 site XRPD patterns that are commonly found in soils are quartz [SiO_2], albite [$(Na,Ca)Al(Si,Al)_3O_8$], muscovite [$(K,Na) \times (Al,Mg,Fe)_2(Si_{3.1}Al_{0.9})O_{10}(OH)_2$], chlorite-serpentine [$(Mg,Al)_6(Si,Al)_4O_{10}(OH)_8$] sodium mica [$NaAl_3Si_3O_{11}$], and mullite [$Al_4Si_2O_{10}$]. These were not considered to be part of the original COPR mineralogy, as they are not stable at the high temperature ($>1200\,^{\circ}C$) of the roasting process (the crystallization temperature of silicate minerals begins at 1200°C and decreases down to 573°C for quartz [7]).
3. *Calcium Silicate Hydrates (CSH):* These are products of COPR-soil interaction. The solubility of silica increases with pH, so that silicic acid [H_4SiO_4] is released from silicate-bearing phases in the highly alkaline COPR environment and reacts with the abundant calcium present in COPR to form CSH, in what is a common pozzolanic reaction encountered in lime- and cement-stabilized soils [10]. Although there is some silicon inherently present as a trace element in the original chromite ore, it cannot account for the high amounts of CSH encountered in some SA7 samples. It is therefore considered to be a product of soil-COPR geochemical interaction and an indication of soil present in the COPR that dissolved to provide the silica source for CSH formation. A significant problem for CSH identification by means of XRPD is that it is commonly present as amorphous material; a crystalline component, afwillite [$Ca_3(HSiO_4)_2(H_2O)_2$] belonging to the ettringite/thaumasite group was, however, identified in numerous XRPD patterns. As the positive identification of amorphous CSH is not possible by XRPD, afwillite will be reported as CSH in the following discussion.

Figure 2 shows the distribution of COPR phases, soil minerals, and CSH in the 118 COPR samples analyzed by XRPD.

Thirteen (13) out of 118 (11 %) samples evaluated by XRPD contained only soil minerals, while 34 samples (29 %) were a mixture of COPR and soil phases. Seventy-one (71) (60 %) samples contained only COPR phases. However, the presence of CSH in 37 of these samples indicates the former presence of soil minerals that provided a silica source for CSH formation, as discussed above. In summary, 84 out of 118 samples, or 71 % percent, contained a mixture of COPR and soil-derived mineral phases. Moreover, the authors note that some of the COPR mineral phases identified by XRPD are conventionally considered soil. These include, for example, periclase, brucite, and calcite. Furthermore, portlandite, hydrotalcite, hydrogarnet, and ettringite are not uncommonly found in cement- and lime-treated contaminated soils, as they are derived from pozzolanic reactions between these reagents and soils. Ettringite is also commonly found in lime-stabilized clays [10].

The authors believe that the above findings fulfill the RCRA requirement that "the definition of soil includes the concept that mixtures of soil and other materials are to be considered soil provided the mixture is made up predominantly of soil and that other materials are inseparable using simple physical and mechanical means." While the presence of soil and soil minerals in COPR at the SA7 site is not

TABLE 2—*Total analyses (in* mg/kg*) results of COPR samples and two lead-contaminated soils.*

	Al	Ca	Fe	Mg	Mn	Cr	Pb
Composite B1	42,540	214,620	103,640	46,240	1,118	20,430	-
Composite B2	42,450	227,317	97,967	57,400	1,283	16,217	-
Composite C	29,508	247,700	55,654	47,196	731	28,488	-
Soil 1 [22]	43,151	33,186	30,980	20,105	660	-	3,165
Soil 2 [22]	2,247	235,044	5,562	17,010	252	-	49,228
Range in Soils [19]	10,000 - 300,000	700 - 500,000	2,000 - 550,000	50 - 100,000	20 - 10,000	1 - 2,000	<10-700

predominant as a percentage, it is significant and pervasive. Furthermore, the bulk soil materials and individual soil minerals within the COPR agglomerates cannot be separated from the COPR using simple physical and mechanical means.

The presence of surface heaving and foundation structural failures has been linked to the presence of ettringite in lime-stabilized clays [21]. The goal of lime treatment of expansive clay is to form calcium-alumina-hydrate (CAH) and CSH compounds that act as cementing agents and prevent swelling of clays due to water permeation. However, the formation of ettringite upon sulfate influx has led to substantial surface heave and pavement and foundation failure in the case studies reported in the cited literature [10,21]. Interestingly, the presence of ettringite in COPR at the SA7 site is also linked to a heaving phenomenon observed at the site. This observation points to common geochemical and geotechnical mechanisms in lime-treated clays and SA7 COPR. The authors note, however, that other mineral hydration and carbonation reactions as previously described (e.g., brownmillerite to katoite, periclase to brucite) may also contribute to the observed heave phenomenon in COPR at the SA7 site.

In summary, the results of the mineralogical analyses of SA7 COPR samples show that there is an extensive presence of natural soil minerals at the site. These minerals provide a source of soluble compounds, mainly silica, that react with COPR constituents, namely, calcium, to form pozzolanic reaction products (CSH) that are commonly found in cement- and lime-treated contaminated soils. Most COPR mineral phases are also commonly found in natural or treated soils. Overall, natural soil and COPR comprise an inseparable geochemical system at the SA7 site, with characteristics and interactions that cannot be isolated.

Total Metal Analyses

Table 2 shows the total analysis results for major metals in the COPR composite samples, as compared to the total contents of these metals in another study of lead-contaminated soils [22] and to the range of concentrations found in analysis results for soils from throughout the world, as reported by Sparks [19]. The following observations are drawn from Table 2:

- The concentrations of major metals for the two soils contaminated with lead [Pb] are highly variable, reflecting variability in mineralogy, origin, and environmental conditions for the soils. This observation highlights the fact that there are substantial ranges in total metals concentrations when the definition of soil comes into question. This observation is also consistent within the reported wide range in metals concentrations in soils from around the world [19]. Both the COPR samples and the samples from Dermatas et al. [22] have total metals concentrations with the ranges for soils worldwide. The only exceptions are for Cr (COPR) and Pb [22], which exceed the concentrations in natural soils because they are in fact contaminated, rendering these materials "contaminated soil."
- The presence of high concentrations of a contaminant, as in the case of Pb in soil 2, does not alter the nature of the soil to a degree that it would fall outside of the RCRA definition of contaminated soil. In the case that a heavy metal is present, one simply speaks of "contaminated soil" instead of "natural soil."
- The concentrations of the major contaminant in COPR and in the two soils are of comparable order of magnitude, the difference consisting in the contaminant species (chromium in COPR and Pb in the two soils). In other words, one cannot distinguish between COPR and soil on the basis of the specific heavy metal constituent of concern.

Summary and Conclusions

This paper has described the scientific and engineering aspects of material classification as it pertains to the applicable regulatory definition for a COPR contaminated site in New Jersey. COPR is an alkaline industrial process residual that contains significant amounts of Cr^{6+}. The current site owner has been required to design and implement a site remediation program involving COPR excavation, transport, and disposal at an off-site hazardous waste landfill facility. As this removal and off-site disposal option is very expensive and potentially not financially sustainable at other COPR impacted sites, the owner has undertaken an extensive investigation to better characterize the nature of COPR and a major development effort for potential on-site treatment technologies to reduce COPR Cr^{6+} concentrations and mitigate COPR heave potential.

As described in the paper, the regulatory determination of treatment requirements for a material such as COPR that exhibits the toxicity characteristic under RCRA is critically dependent on the classification of that material as a hazardous solid waste or a hazardous contaminated soil. If a material is classified as a solid waste under RCRA and it exhibits TCLP chromium concentration of more than 5 mg/L, the material is a characteristic hazardous solid waste with an LDR UTS of 0.60 mg/L total chromium in the TCLP extract. If a material classifies as a contaminated soil under the RCRA definition, if it exhibits a TCLP chromium concentration of more than 5 mg/L, and if the material is "generated" for purposes of landfill disposal, the material is a hazardous contaminated soil. The LDR treatment standard for contaminated soil requires reduction of the TCLP hazardous constituent concentration to not more than 10 % of the original TCLP concentration, or reduction to not more than 10 times the UTS concentration, whichever is greater.

For COPR at the SA7 site, an extensive sampling and analysis program resulted in mean, mean plus sigma, and maximum TCLP chromium concentrations of 51, 94, and 180 mg/L, respectively. The corresponding LDR treatment standards for a contaminated soil material with these TCLP chromium concentrations would be 6, 9.4, and 18 mg/L. These treatment standards are from 10 to 30 times higher than the solid waste UTS. Based on the foregoing, the regulatory classification of COPR as a hazardous solid waste versus a hazardous contaminated soil under RCRA regulations is an important issue with respect to both landfill disposal of that material and the potential for on-site treatment and placement back on the site. The type of treatment and/or disposal and the treatment standard have significant implications with regard to the design, implementation, and cost of remediating COPR contaminated sites.

In this paper, the authors developed a methodology for evaluating the regulatory and scientific basis for considering COPR as hazardous contaminated soil versus hazardous solid waste. The evaluation considered the regulatory definition of contaminated soil, the methods used to sample, log, and analyze COPR from the SA7 site, the results of geotechnical parameter testing of COPR, and the results of mineralogical and total metals analyses of COPR.

Based on the presented information, the authors conclude that COPR should classify as hazardous contaminated soil and not hazardous solid waste. While any final decision on this classification rests with the jurisdictional regulatory agency and not the authors, the authors do believe that the bases for the conclusions presented herein are sound:

- COPR was considered as an appropriate structural material and constituted historical fill until heaving phenomena, similar to those observed in stabilized soils and in concrete, rendered the geotechnical use of the material unacceptable for commercial development.
- COPR is sampled and logged using the same geotechnical methodologies used to sample and log soils; the physical descriptions of COPR in boring logs prepared in accordance with applicable ASTM standards contain the same conventional terminology applied to soil boring logs.
- Laboratory testing techniques used to characterize the physical/mechanical properties of COPR are the same as those used to characterize soils; such tests, when applied to COPR, yield results similar to those produced from the same laboratory tests on soils; the geotechnical characterization of COPR, as established by conventional soil analysis methods, results in geotechnical material descriptions and parameters consistent with those applicable to soils; of note, COPR at the SA7 site classifies predominantly as a silty sand (SM) or inorganic clay (CH) according to the USCS.
- The alkaline pH regime of COPR, while outside the range for natural soils, is common to both nonimpacted and contaminated soils treated with pozzolanic reagents such as lime and cement.
- COPR is intermixed with significant and pervasive percentages of soil, soil minerals, and soil

artifacts (i.e., silica that formed CSH in situ after deposition); the soil components of COPR are inseparable by simple physical or mechanical means from the COPR mineral phases; in addition, several of the COPR mineral phases (periclase, brucite, calcite) are considered soil minerals when they occur within the range of grain sizes for soils, as they do at the SA7 site; other COPR mineral phases (portlandite, hydrotalcite, hydrogarnet, and ettringite) are not uncommonly found in cement- and lime-treated soils, as they are derived from the pozzolanic reactions between these reagents and soils.

- Comparison of total metals analyses for COPR with total metals analyses for lead-impacted soils and total concentrations of metals in soils worldwide show compositional similarities amongst these materials.

In closing, the authors note that the methodology presented herein to evaluate COPR classification may have applicability to other contaminated soil-like media from industrial processes that are potentially subject to the requirements of RCRA hazardous waste regulations or similar regulations in other countries.

Acknowledgments

The authors wish to thank Honeywell International Inc. for the financial support of the COPR investigation at SA7 and the analyses at Stevens Institute of Technology.

References

[1] *Code of Federal Regulations*, Sections 268 and 269.
[2] *Code of Federal Regulations*, Title 40, Section 261, Part 261.24.
[3] *Federal Register*, Vol. 63 No. 100 p. 28617, Tuesday May 26, 1998, Rules and Regulations.
[4] Mueser Rutledge Consulting Engineers, January 2004, "2003-2004 Subsurface Investigation Study Area 7 (Daylin Grace site), Jersey City, New Jersey," Draft report.
[5] U.S. EPA, "Land Disposal Restrictions: Summary of Requirements," *EPA 530-R-01-007*, 2001.
[6] *Federal Register*, Vol. 63 No. 100 p. 28620, Tuesday May 26, 1998, Rules and Regulations.
[7] Mitchell, J. K., *Fundamentals of Soil Behavior*, John Wiley & Sons, New York, 1993.
[8] Holtz, R. D. and Kovacs, W. D., *Introduction to Geotechnical Engineering*, Prentice Hall, New Jersey, 1982.
[9] Allied Signal, 1982, Process Descriptions Baltimore Plants.
[10] Dermatas, D., "Ettringite-Induced Heaving in Soils: State-of-the-Art," *Appl. Mech. Rev.* Vol. 38, No. 10, pp. 659–672 (1995).
[11] Danied, D. E., *Geotechnical Practice for Waste Disposal*, Chapman and Hall, London, 1993.
[12] American Society for Testing and Materials, *Annual Book of ASTM Standards*, ASTM, 2003
[13] Materials Data Inc., 2004, *Jade version 7.1*, California.
[14] "Powder Diffraction File, PDF-2 Database Release 1998," announcement of new database release, International Centre for Diffraction Data (ICDD).
[15] *Inorganic Crystal Structure Database*, 2004, Fachinformationszentrum Karlsruhe, Germany
[16] U.S. EPA, *SW-846*, Method 3015A, "Microwave Assisted Acid Digestion of Aqueous Samples and Extracts."
[17] U.S. EPA, *SW-846*, "Method 6010B, Inductively Coupled Plasma–Atomic Emission Spectrometry."
[18] Das, B. M., *Principles of Geotechnical Engineering*, PWS Publishing Company, Boston, 1998.
[19] Sparks, D. L., *Environmental Soil Chemistry*, Academic Press, New York, 2003.
[20] Hausmann, M. R., *Engineering Principles of Ground Modification*, McGraw-Hill, New York, 1990.
[21] Mitchell, J. K., "Practical Problems from Surprising Soil Behavior," *J. Geotech. Eng.*, Vol. 112, No. 3, 1986.
[22] Dermatas, D., Shen, G., Chrysochoou, M., Grubb, D., Menounou, N., Xu, X., and Cao, X., "Lead speciation vs. TCLP release in army firing range soils," Journal of Hazardous Materials, in press.

Journal of ASTM International, Vol. 3, No. 6
Paper ID JAI13309
Available online at www.astm.org

Deok Hyun Moon, Ph.D.,[1] *Dimitris Dermatas, Ph.D.,*[1] *Maria Chrysochoou, M.Sc.,*[1] *and Gang Shen*[1]

An Investigation of the Heaving Mechanism Related to Chromite Ore Processing Residue

ABSTRACT: Significant heaving has been observed over time at chromite ore processing residue (COPR) deposition sites in Maryland and New Jersey. Confined swell tests were employed in order to investigate the geochemical mechanisms that lead to the manifestation of heave in COPR. Ettringite, a known heave culprit in cement and soil-related literature, was identified in numerous samples across the sites and was therefore considered as the primary heaving mechanism in COPR. In addition, other possible mechanisms, such as brownmillerite hydration to hydrogarnets, carbonation reactions, calcium aluminum chromium oxide hydrate (CAC) formation, and change of hydration state were also investigated. The confined swell tests were conducted under wet/dry cycles. Sulfate, carbonate, and chromate solutions were introduced to the samples during wet cycles in order to validate the different heaving hypotheses associated with phase transformations. The test results showed that swell development occurred only in COPR upon 0.7 mole/l sulfate addition. Furthermore, x-ray diffraction analyses confirmed the formation of ettringite in the COPR sample following the addition of sulfate. Conversely, carbonation reactions led to no height change or even to consolidation, while the formation of hydrogarnets and CACs could not be established. It was, therefore, demonstrated that ettringite formation is a thermodynamically powerful reaction and also a viable expansion and failure mechanism in COPR.

KEYWORDS: COPR, ettringite, heaving, confined swell tests, sulfate

Introduction

Chromite ore processing residue (COPR) is the solid residue generated by a high-lime process for Cr extraction [1]. Specifically, chromite ore mixed with soda ash and lime was heated in a rotary kiln at ~1200°C to produce soluble sodium chromate. COPR was widely used as structural fill material in several countries including England, Japan, West Germany, and the United States [2]. The major COPR deposition sites in the United States are located in Maryland, New Jersey, Ohio, and New York [3]. About 1.5 million tons of COPR were deposited over a 34-acre area at Study Area 7 (SA7), located in Hudson Country, New Jersey, and a significantly larger amount was deposited over an 85-acre area at Dundalk Marine Terminal, located in Baltimore, Maryland. Extensive heaving was observed over time at these COPR deposition sites, resulting in high cost pavement regrading maintenance operations, limited site use, and in the case of SA7, no site use at all.

Brownmillerite (Ca_2FeAlO_5), periclase (MgO), and quicklime (CaO) are considered to be the COPR "parent" materials, i.e., the compounds that comprise COPR when it comes out of the roasting process. Hydrogarnets [katoite $(CaO)_3Al_2O_3(H_2O)_6$ being the main phase], hydrotalcites [$Al_2Mg_4(OH)_{12}(CO_3)(H_2O)_3$ is a representative compound], calcium aluminum chromium oxide hydrates [CACs $-Ca_4Al_2O_6(CrO_4)\cdot nH_2O$] are the main pozzolanic products derived from brownmillerite, while brucite [$Mg(OH)_2$] is the main periclase hydration product next to hydrotalcites that scavenge part of the magnesium, and hydrated lime [$Ca(OH)_2$] is the product of quicklime hydration. Ettringite [$Ca_6Al_2(SO_4)_3(OH)_{12}\cdot 26H_2O$] and calcite ($CaCO_3$) will form when sulfate and carbonate are introduced to the system by means of water and/or air infiltration.

In view of the COPR mineralogy and transformation reactions described above, the potential heaving mechanisms are summarized as follows:

Manuscript received April 19, 2005; accepted for publication July 12, 2005. Presented at ASTM Symposium on Contaminated Sediments: Evaluation and Remediation Techniques on 23–25 May 2006 in Shizuoka, Japan; M. Fukue, K. Kita, M. Ohtsubo, and R. Chaney, Guest Editors.

[1] W. M. Keck Geoenvironmental Laboratory, Center for Environmental Systems, Stevens Institute of Technology, Castle Point on Hudson, Hoboken, NJ 07030.

- Brownmillerite hydration to hydrogarnets
- Periclase hydration to brucite
- Carbonation reactions, i.e., calcite formation
- Formation of pozzolanic products (ettringite, CACs, hydrotalcites, etc)

In this study, periclase to brucite hydration was ruled out as the main COPR heaving mechanism due to the low amounts of periclase and brucite identified by x-ray powder diffraction (XRPD) in both SA7 and DMT samples. Moreover, it has been reported that brucite formation can suppress swell in high porosity systems similar to COPR, such as active clays [4]. Consequently, only the other three mechanisms were considered for the experimental design in this investigation. The first mechanism studied was the brownmillerite hydration to hydrogarnets, as this transformation leads to a net volume increase, reflected in the decrease of the specific gravity of brownmillerite (3.76) to katoite (2.76). This mechanism has not been reported in the literature as responsible for expansion and/or failure of concrete or soils; it was, however, considered as a possible mechanism due to the high amount of brownmillerite available in COPR. The second mechanism tested was carbonation reactions; these reactions are triggered by the influx of CO_2 and form calcite as their main product. It is unclear whether or not the bulking effect caused by carbonation can be accommodated in the existing voids of the COPR material and therefore this mechanism was also considered in this study. Pozzolanic reactions were the third mechanism investigated. Ettringite is a pozzolanic product forming in cementitious systems, such as COPR, upon presence of sulfate. It has widely been reported as an expansion-inducing phase both in the cement and the soil-related literature. Specifically, the expansion and failure of concrete by mainly delayed ettringite formation (DEF) has been established [5]. In addition, ettringite has been reported as a heaving culprit in lime-stabilized clays [6,7]. Ettringite was observed in abundant quantities in several locations, spread both vertically and horizontally across the two sites (DMT and SA7). It is, therefore, considered, that ettringite formation is possibly a main driver for the development of swell pressures and manifestation of heaving phenomena at the COPR deposition sites. Furthermore, it is considered possible that CACs may play a role in COPR swelling, as they have been observed in high amounts in heaved areas, both at SA7 and DMT. The platy morphology of monophases, i.e., CACs, does not favor the development of swell pressures adequate to overcome media restraint and thus lead to failure. There is only one literature reference that refers to the formation of monosulfates (monophases similar to CACs with sulfate instead of chromate) as a possible heaving mechanism in cements [8]. The role of CAC formation was included in this present study in order to elucidate the viability of such an expansion mechanism in COPR.

In order to investigate experimentally the heaving mechanisms described above, confined swell tests were employed, using different geochemical conditions in order to simulate COPR reactions and the geotechnical properties that correlate to swell development. The samples were subjected to wet and dry cycles with the introduction of different permeants such as deionized water, sulfate, chromate and carbonate solutions to evaluate the heaving hypotheses related to hydrogarnet, calcite, ettringite and CAC formation.

Experimental Methodology

COPR Samples and Reagents

There are two types of COPR materials identified at SA7 and DMT: One type of COPR is a granular sand-size, grey black material (designated as GB) while the other type of COPR is a fine-grained material of orange to reddish brown color with high degree of lithification (designated as HB). These two materials are mineralogically distinct, in that HB samples have very low brownmillerite content and a high amount of transformation products (hydrogarnet, hydrotalcites, and CACs), indicating a highly advanced reaction state, whereas GB samples contain abundant brownmillerite (initial-reaction state) and low amounts of transformation products. A total of four COPR samples were used for the confined swell experiment. Three out of the four samples, namely, GB1, GB2, and HB were obtained from SA7. Samples GB1 and HB were deemed to be undisturbed COPR specimens since these samples were extruded from tube samplers. Sample GB2 was trimmed from an original block sample obtained from trenching activities conducted at SA7 and is also thought to be relatively undisturbed. The fourth sample, namely, GB3, originated from DMT and was reconstituted from a disturbed grab sample by compaction to the original field density. The

TABLE 1—*Description of COPR samples.*

Sample ID	Site	Sampling method	Depth	Physical description
GB1	SA7	Tube	3-5.8 ft	Gray black
GB2	SA7	Trench, block	2.2 ft	Gray black
GB3	DMT	Trench, grab	3-4 ft	Gray black
HB	SA7	Tube	6-8.7 ft	Hard brown

COPR sample descriptions including the sampling method, depth, and physical appearance are presented in Table 1. Sand control samples were also set up in order to identify possible system deformations caused by changes to the ambient environment such as temperature and vibration, which would affect the sample displacement reading.

Deionized (DI) water was used as permeant, while sodium sulfate (Na_2SO_4), sodium carbonate (Na_2CO_3), and potassium chromate (K_2CrO_4) salts dissolved in DI water were used as sulfate, carbonate, and chromate sources for COPR reactions, respectively. These chemicals were obtained from Fisher Scientific (Suwanee, GA). Compressed atmospheric air was used as drying agent for the dry cycles.

Test Apparatus

The one-dimensional (1D) confined swell test device was designed by Geosyntec Inc. (Kennesaw, GA). The schematic drawing is presented in Fig. 1.

As illustrated in Fig. 1, the COPR material was placed in a stainless steel chamber with an effective diameter of 7.24 cm and a height of 7.62 cm. Filter paper covered both the top and bottom of the sample, followed by a pair of porous stones. A stainless steel top cap, circled with a plastic O ring, was used to provide a platform for the steel frame. The steel frame transferred the applied dead load onto the tested specimen. Bottom and top inlets of the chamber were used for the injection of the permeant and air, respectively. Any height change, in terms of sample swell or consolidation, was measured by the linear vertical displacement transducer (LVDT) on a minute basis. All the readings were automatically transferred and recorded to a Geolog Box that was connected to a computer.

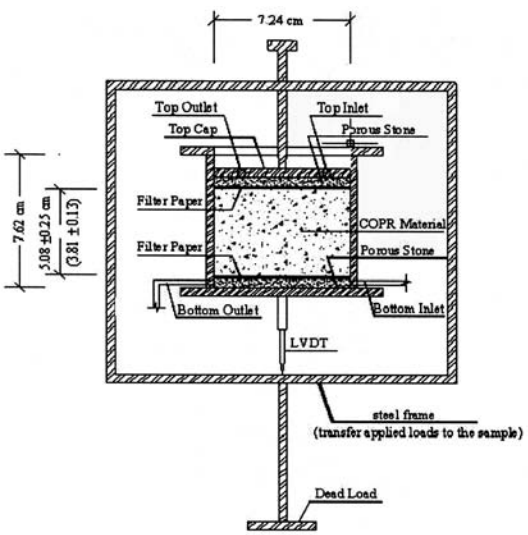

FIG. 1—*1D confined swell test apparatus.*

TABLE 2—*Swell test matrix.*

Sample ID	Sample description	Temperature (°C)	Chemical addition	Mechanism tested
Control 1	Sand	25	Water	···
Control 2	Sand	50	Water	···
GB1	Pitcher barrel sample	25	Sodium carbonate (1.26 mole/l)	Carbonation
GB2	SA7 trench block sample	25	Sodium sulfate (0.7 mole/l)	Brownmillerite to ettringite
GB3	DMT disturbed sample	50	Water	Brownmillerite to hydrogarnets (katoite)
HB	Pitcher barrel sample	25	Potassium chromate (0.64 mole/l)	Hydrogarnets to CACs

Testing Conditions and Swell Test Matrix

A confined swell test with wet and dry cycles was employed in this study, as it is considered that a lithified sample state can thus be achieved. Lithification is thought to be an essential (but not sufficient) precondition for the manifestation of heave, as it provides the media restraint that cannot accommodate swell pressures within the matrix and thus leads to an overall volume expansion. In order to validate the hypothesized COPR heaving mechanisms, different permeants such as sulfate, chromate, and carbonate solutions were prepared and introduced to the sample through the bottom inlet of the chamber during the wet cycle. The chemicals were added during the fourth or fifth wet cycle, in order to achieve stability in the experimental conditions, in a concentration based on the dry weight of the sample as follows: 0.7 mole of sulfate, 1.26 mole of carbonate, and 0.64 mole of chromate in 1 L of deionized (DI) water. The permeant was continuously provided until the entire sample was saturated and the solution came out from the top inlet of the chamber. The inlets were then closed and the saturated sample was considered to be in a closed system for a period of 2 to 3 days. During the dry cycle, compressed air was continuously introduced to the specimen from the top inlet of the device at the pressure of 14 kPa for 2 to 3 days. Four samples were tested at a constant temperature of 25°C to simulate field conditions and two samples were installed at 50°C in order to accelerate the brownmillerite hydration reaction, which is very slow under field conditions. The swell test matrix in Table 2 summarizes the testing conditions for all the samples. The determination of the tested swell mechanism was done according to the initial mineralogical composition of the samples, determined by XRPD, which will be presented in the results and discussion section.

Confined Swell Test Sample Preparation

The undisturbed samples GB1 and HB were directly extruded from the pitcher barrel tubes to achieve a sample height of ~5 cm. The GB2 specimen was trimmed to fit the cylindrical testing chamber with a diameter of 7.2 cm and a height of ~5 cm. Disturbed bulk sample GB3 was gently compacted at ~0.8 cm per layer using a rubber pestle (diameter 3.2 cm) until the ultimate density of each compacted sample reached its field density. A total sample height of 4.2 cm was achieved for the GB3 sample. Furthermore, a dead load of 2.27 kg was applied on top of all the samples throughout the entire testing period to establish a confined condition since all the COPR samples were located at varying depths. Finally, the top and bottom surfaces of each sample were gently smoothed so that the LVDT could be read properly and to facilitate filter paper and porous stone installation.

X-ray Powder Diffraction (XRPD) Analyses

XRPD samples were collected from the top and bottom surfaces of the swell samples after test completion. Prior to XRPD analyses, all the samples were air dried for 24 h and then pulverized to pass through a U.S. standard #400 sieve (38 μm). Step-scanned x-ray diffraction patterns were collected by the Rigaku DXR-3000 computer-automated diffractometer using Bragg-Brentano geometry. XRPD was performed at 50 kV and 40 mA using a diffracted beam graphite monochromator with Cu radiation. The data were collected in the range of 5° to 65° 2θ with a step size of 0.02° and a count time of 5 s per step. The qualitative analyses of the XRPD patterns were performed using the Jade software version 7.1 [9]. The whole pattern-fitting function of Jade, which is based on the Rietveld method [10], was used in order to quantify the identified crystalline phases. The quantification analyses rely on calculated XRD patterns produced by refining known crystal structures and calculating their reflections based on x-ray diffraction algorithms. The produced calculated patterns are then fitted to the observed patterns by means of a least-squares-model [11].

TABLE 3—*Sample properties.*

Sample ID	Sample weight (g)	Volume (cm^3)	Initial w/c (%)	Moist unit weight[a] (g/cm^3)	Dry unit weigh[a] (g/cm^3)	Estimated Gs[b]	Estimated e[b]	Saturated w/c (%)[b]	Dry unit weigh[c] (g/cm)	pH
Sand control 1	297.0	183.2	0	1.62	1.62	2.60	0.62	24	1.62	⋯
Sand control 2	236.7	150.3	0	1.58	1.58	2.72	0.76	28	1.58	⋯
GB1	335.6	184.8	28	1.82	1.42	2.50	0.78	31	1.42	11.75
GB2	305.1	208.3	28	1.46	1.14	2.21	0.93	42	1.15	11.26
GB3	294.1	176.2	19	1.67	1.40	2.57	0.69	27	1.40	11.95
HB	410.8	202.9	36	2.02	1.49	2.77	0.86	31	1.49	10.98

[a]Before the confined swell tests.

[b]Values were computed based on 100% saturation.

[c]After the confined swell tests.

The reference databases for powder diffraction and crystal structure data were the PDF-2 set of the International Center for Diffraction Data database [12], and the Inorganic Crystal Structure Database [13], respectively.

Physicochemical Analyses

The pH measurements of the COPR materials were performed in accordance with the method, ASTM D 4972-89 [14], and the water content was determined employing the method, ASTM D 2216-92 [14].

The moist unit weight of the samples was calculated by dividing the mass (measured as weight) by the total volume of the sample. The dry unit weight, void ratio, and specific gravity of the samples were then calculated for 100 % saturation based on the following equations [15].

$$\gamma_d = \left[\frac{\gamma}{1 + w} \right] \tag{1}$$

$$e = \left[\frac{\gamma_d \times w}{\gamma_d \times w - S \times \gamma_\omega} \right] \tag{2}$$

$$Gs = \left[\frac{S \times e}{w} \right] \tag{3}$$

where γ_d=dry unit weight; γ=moist unit weight; γ_w=unit weight of water; w=water content; S=degree of saturation; e=void ratio; Gs=specific gravity.

Results and Discussion

Geotechnical Properties

The geotechnical properties of the samples, including weight, volume, moist unit weight, water content, degree of saturation (S), void ratio (e), and specific gravity (Gs) are presented in Table 3.

The initial water content of the undisturbed GB1 and HB samples was close to the saturated water content value, indicating that these samples were in the saturated zone in the field. The pH values showed highly alkaline conditions for all COPR samples. Based on the initial water content, the water content at saturation, and the dry weight of the sample, the amount and concentration of the solution to be added to each sample was calculated. The dry unit weight of the COPR material prior to and after testing did not change significantly. This may be due to the transformation of phases with similar specific gravity such as portlandite (2.23) and CAC (2.5) into calcite (2.71). This indicates that while the void ratio may decrease the dry unit weight may keep the same value.

TABLE 4—*Comparison of COPR sample mineralogy before and after swell tests.*

Mineral	GB1 initial	GB1 top	GB1 bottom	GB2 initial	GB2 top	GB2 bottom	GB3 initial	GB3 top	GB3 bottom	HB initial	HB top	HB bottom
Brownmillerite	11	16.8	18.3	35	31.8	25.7	55	36	35	5.1	3.3	3
Periclase	⋯	⋯	⋯	0.6	0.4	0.4	3.3	1.8	1.6	1.1	2.0	1.2
Brucite	2.1	2.0	2.3	8.5	10.3	9.6	5.3	3.6	3.2	10.5	6.5	7.5
Portlandite	20	4.4	13.8	1.6	⋯	⋯	3.4	0.4	⋯	⋯	⋯	⋯
Calcite	24	46.7	34.1	9.7	14.3	38.3	10	33	36.2	2.7	11.2	11.3
Hydrotalcite	3.8	6.1	4.5	5	4.3	3.7	3.7	5.2	4.5	26	28.9	26.9
Hydrogarnets	18	19	22	13	13.9	10.7	18	20	19.9	26	37.1	38.6
Ettringite	2.8	2.1	3.8	3.3	12.6	3.2	⋯	⋯	⋯	⋯	⋯	⋯
CAC	14	2.5	1.4	12	4.2	1.3	1.3	⋯	⋯	28	11	11.4
Afwillite	4.1	⋯	⋯	12	8.2	7.1	⋯	⋯	⋯	⋯	⋯	⋯

Initial COPR Sample Mineralogy and Mechanisms Tested

The initial mineralogy of the four samples is presented in Table 4. The GB1 sample was found to contain a relatively high amount of portlandite $[Ca(OH)_2]$ and was therefore chosen to be tested for carbonation reactions, as portlandite readily converts to calcite upon CO_2 influx. The GB2 sample was found to contain a relatively high amount of brownmillerite, so that its transformation to ettringite was tested by the addition of sodium sulfate solution. Crystal growth of existing ettringite could also be an expansion mechanism in GB2. The GB3 sample was at a less advanced reaction state as is indicated by the higher brownmillerite content; therefore hydration of brownmillerite to hydrogarnets was evaluated in GB3 by addition of DI water. Finally, by addition of potassium chromate, the transformation of hydrogarnets to CAC was expected in the HB sample because of its elevated content of hydrogarnets. The hydration and dehydration of CACs could also be a contributing mechanism for expansion in this sample.

Height Change Results

The height change readings of the sand control samples showed that no displacement occurred due to the experimental conditions, i.e., the LVDT reading was stable throughout the duration of the experiment.

The height change as a percentage of the total height of the sample is plotted against time for GB1 samples in Fig. 2. The plot shows that there was little change in height for this sample during the first cycles, while a 0.5 % consolidation was registered during the last cycles, both prior to and following the

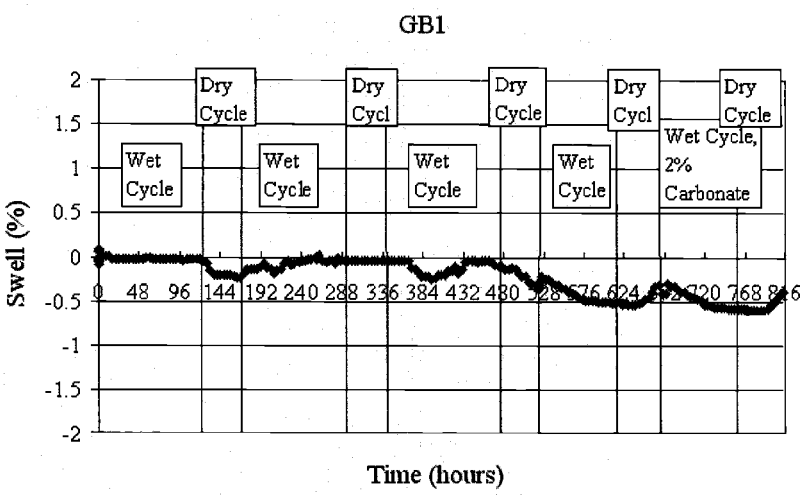

FIG. 2—*Height change in percent for the GB1 sample.*

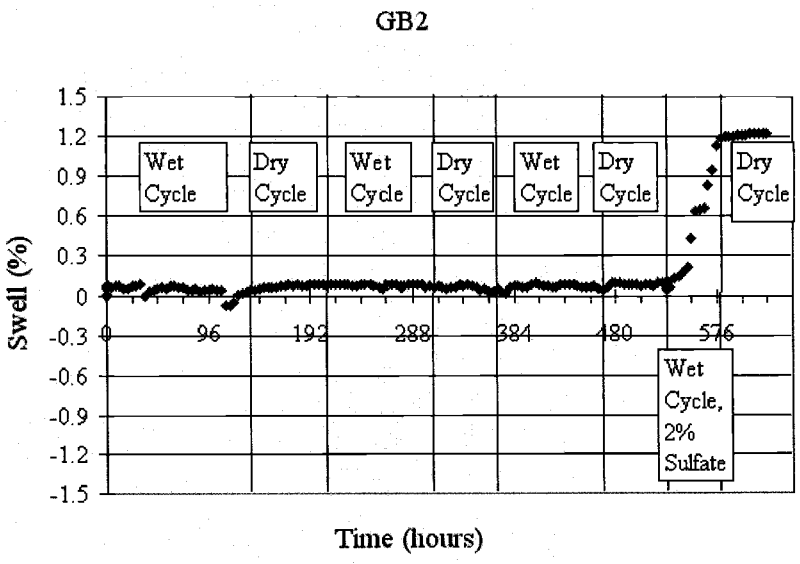

FIG. 3—*Height change in percent for the GB2 sample.*

carbonate addition. It seems that the consolidation occurred during the fourth wet cycle upon application of a dead load. It is not clear whether portlandite was transformed to calcite since no x-ray data were available.

Figure 3 shows the height change in percent for the GB2 sample in which sulfate was added to test ettringite formation. It was observed as the only sample to exhibit a height increase of 1.3 %, which is significant considering that the sample was tested under the application of a dead load. The height increase was observed in the wet cycle, in which the sulfate solution was applied, indicating that a fast reaction triggered the swell development. The formation of ettringite is favorable thermodynamically at pH conditions of the experiment [16–18]. Geochemical modeling results also showed that ettringite formation is favorable upon sulfate influx [19]. Moreover, ettringite was observed within 1 h upon the addition of even very small amounts of sulfate 5.2×10^3 mole/l [20]. Again, no significant height change was recorded in the initial wet and dry cycles with DI water as permeant.

Figure 4 shows the height change in percent for sample GB3 where brownmillerite hydration was tested at 50°C. No significant height change in this sample was recorded throughout the experiment. Similarly, no significant height change was recorded in the HB sample both prior to and following the chromate addition (Fig. 5).

Overall, it is true that both calcite and ettringite formations could fill voids in the sample. But, samples which have a high content of calcite did not provide swell development whereas samples that contain a high content of ettringite showed a significant swell development. The needlelike structure of ettringite favors the buildup of high swell pressures that may overcome media restraint even in high-porosity systems. The values of specific gravity for portlandite, calcite, and ettringite are 2.23, 2.71, and 1.8, respectively. Therefore, portlandite consumption to form calcite leads to an increase in the specific gravity, i.e., to a probable consolidation of the sample, rather than to swelling. A similar tendency was reported by Fukue et al. [21] who observed consolidation of marine sediments due to carbonation.

Final XRPD Results of Tested Samples

COPR sample mineralogy at the end of the presented testing period was determined by XRPD and compared with the initial COPR mineralogy in order to elucidate the geochemical mechanism that leads to the observed behavior in height change. The samples were obtained from the top and bottom surfaces of

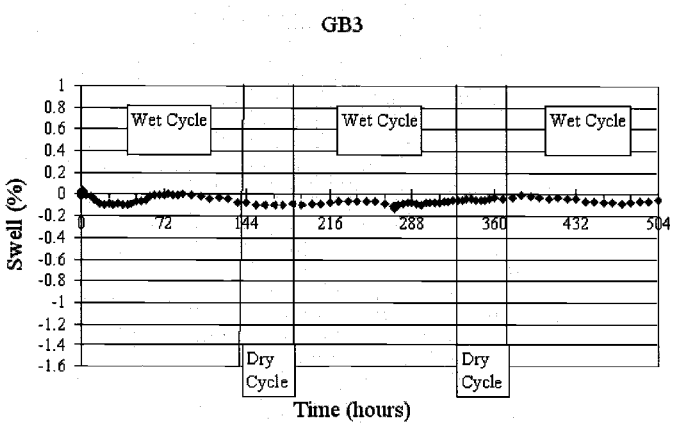

FIG. 4—*Height change in percent for the GB3 sample.*

the samples, in order to keep the specimens as undisturbed as possible and to be able to continue the experiments. The quantitative analyses of the obtained data are presented in Table 4. In general, carbonation was the major reaction in all samples tested. It seems that the influx of atmospheric air during the dry cycle resulted in significant carbonation of the top layers, as the highly alkaline pH of the COPR samples renders CO_2 sequestration a fast and powerful reaction. Carbonation reactions seemed to "attack" CACs first, resulting in their partial or complete dissolution in all samples. Portlandite dissolved in the top layer of the GB1 sample while it was present in higher amounts in the lower layer, indicating that carbonation reactions were still ongoing at the end of the fifth cycle despite the soluble carbonate influx. Brownmillerite also dissolved partially in the GB3 sample as a result of carbonation, while no hydrogarnets formed according to XRPD. These results indicate that, although calcite formation is a pronounced COPR reaction, it does not lead to volume increase; on the contrary, it will lead to consolidation, depending on the initial geotechnical properties of the sample (lithification, void ratio). The 25°C sample did not present

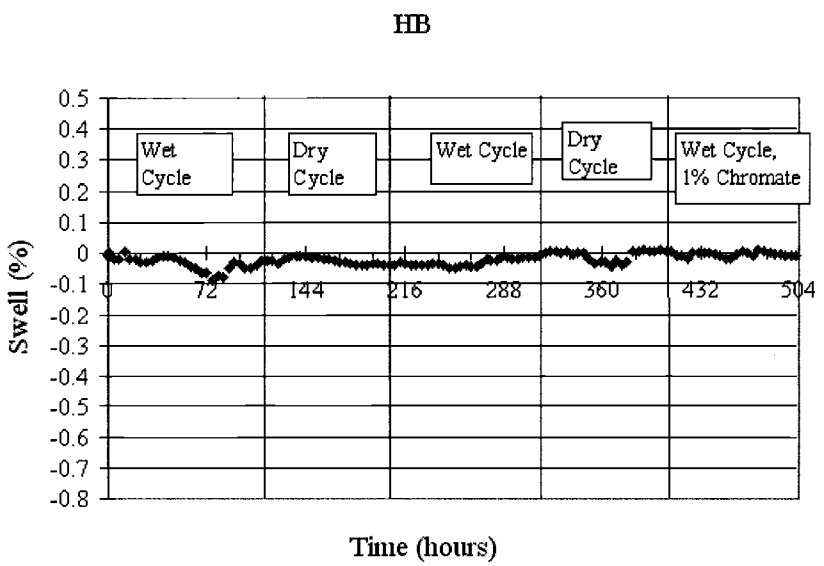

FIG. 5—*Height change in percent for the HB sample.*

significant lithification and therefore consolidated, while the 50°C sample lithified to some extent during the wet and dry cycles and accommodated calcite within the existing voids, with no apparent change in volume. Similar observations with the GB3 sample hold also for the HB sample. No additional CACs formed upon addition of chromate as carbonation seems to dominate as the prevalent geochemical mechanism.

Conversely, ettringite formation proved to be a powerful thermodynamic reaction in sample GB2, as it formed despite the influx of CO_2 and the competitive formation of calcite. These were the only mineral formations observed in this sample, with brownmillerite and CACs (with some afwillite, a calcium silicate hydrate also partially dissolving), their dissolution acting as a calcium and aluminum source. As calcite formation was ruled out as a heaving mechanism on the basis of the remaining three swell samples, ettringite formation seems to be the only viable heaving mechanism to explain the height change observed in sample GB2 upon sulfate addition.

Conclusions

Confined swell tests were performed in order to investigate the heaving phenomena in COPR. Samples were obtained from different zones at COPR deposition sites in New Jersey and Maryland, and were selected to represent different heaving mechanisms formulated on the basis of COPR mineralogy. The identified expansion mechanisms in COPR tested in this investigation were: (a) brownmillerite hydration to hydrogarnets; (b) carbonation reactions and calcite formation; (c) ettringite formation; and (d) formation of calcium aluminum chromium oxide hydrates (CACs). The detailed observations obtained from the confined swell tests can be summarized:

1. Carbonation reactions were pronounced in all samples tested, due to the rapid CO_2 sequestration during the dry cycle. Calcite form in the existing voids, and it produced no net volume increase or even led to consolidation, depending on the sample's respective geotechnical properties (degree of lithification and void ratio).
2. Upon 2 % sulfate addition, up to 1.3 % swelling was observed in the respective COPR sample under the confinement imposed by a 2.27 kg dead load. The quantity of ettringite significantly increased immediately after the addition of sulfate, based on XRPD analyses at the beginning and the end of the testing period.
3. No hydrogarnet formation was observed in the sample with high brownmillerite, tested at higher temperature (50°C), which was employed in order to accelerate the slow dissolution of brownmillerite. No correlation between hydrogarnet formation could, therefore, be established between brownmillerite hydration and volume expansion.
4. Similarly, no CAC formation was observed upon addition of chromate to a COPR sample, as carbonation dominated the geochemical reactions in this case as well. The viability of the CAC-related expansion mechanism remained, therefore, inconclusive.

Overall, the present investigation verified that ettringite is a viable expansion and heaving mechanism in COPR; its formation is a thermodynamically favorable [15–17] when sulfate is introduced into the system. The manifestation of heave is associated, however, with the overall geotechnical properties of the matrix, i.e., the expansion was observed in a sample that was highly lithified, providing the necessary media restraint. Carbonation was excluded as an expansion mechanism in COPR, while the contribution of other hydration and pozzolanic products remained inconclusive as their formation was shown to be less favored compared to ettringite and was thus suppressed by carbonation reactions. Further investigation will address the viability of these mechanisms and their relative contribution to COPR expansion.

Acknowledgments

This research was sponsored by Honeywell International Inc. The authors wish to thank Nick Muto and Adriana Sanchez for their assistance with the test preparation and monitoring.

References

[1] Hiller, S., Roe, M. J., Geelhoed, J. S., Fraser, A. R., Farmer, J. G., and Parterson, E., "Role of Quantitative Mineralogical Analysis in the Investigation of Sites Contaminated by Chromite Ore Processing Residue," *Sci. Total Environ.* 308, 195–210 (2003).

[2] McKee, T., "Chromate Chemical Production Industry: Waste Treatment Past and Present," Report to the New Jersey Department of Environmental Protection, Trenton, NJ, 1988.

[3] Public Health Service, "The Chromate-Producing Industry. In: Health of Workers in Chromate Producing Industry—A Study," *Federal Security Agency*, Public Health Service, Publication No. 192, 1953.

[4] Xeidakis, G. S., "Stabilization of Swelling Clays by $Mg(OH)_2$: Changes in Clay Properties after Addition of Mg-Hydroxide," *Eng. Geol. (Amsterdam)* 44, 107–120 (1996).

[5] Taylor, H. F. W., Famy, C., and Scrivener, K. L., "Review Delayed Ettringite Formation," *Cem. Concr. Res.* 31, 683–693 (2001).

[6] Dermatas, D., "Ettringite-Induced Swelling in Soils: State-of-the Art," *Appl. Mech. Rev.* 48(10), 659–673 (1995).

[7] Puppala, A. J., Intharasombat, N., and Vempati, R. K., "Experimental Studies on Ettringite-Induced Heaving in Soils," *J. Geotech. Geoenviron. Eng.*, 131(3), 325–337 (2005).

[8] Chatterji, S., and Jeffery, J. W., "A New Hypothesis of Sulphate Expansion," *Mag. Concrete Res.*, 15(44), 83–86 (1963).

[9] Materials Data Inc., 2004, Jade Version 7.1, California.

[10] Rietveld, H. M., "A Profile Refinement Method for Nuclear and Magnetic Structures," *J. Appl. Crystallogr.*, 2, 65–71 (1969).

[11] Dermatas, D. and Chrysochoou, M., "The Rietveld Method as a Tool for Assessing Heavy-Metal Immobilization in S/S Treatment Investigations," *International Conference on Stabilisation/ Solidification Treatment and Remediation*, University of Cambridge, UK, April 12–13, 2005, pp. 97–106.

[12] "Powder Diffraction File, PDF-2 Database Release 1998," Announcement of New Database Release, International Centre for Diffraction Data (ICDD), 1998.

[13] Inorganic Crystal Structure Database (ICSD) Fachinformationszentrum Karlsruhe, Germany, 2004

[14] ASTM Standard *DH4972-89 Annual Book of ASTM Standards*, American Society for Testing and Materials, Soil and Rock, Vol. 4.08, 2000.

[15] Das, B. M., *Principles of Foundation Engineering*, PWS Publishing Company, Boston, MA, 4th Ed., 1999.

[16] Chrysochoou, M., and Dermatas, D., "Evaluation of Ettringite and Hydrocalumite Formation for Heavy Metal Immobilization: Literature Review and Experimental Study," *J. Hazard. Mater.*, in press.

[17] Dermatas, D., "Ettringite-Induced Swelling in Soils: State-of-the-Art," *Appl. Mech. Rev.*, 48(10), 659–673 (1995).

[18] Palmer, C. D., "Precipitates in a Cr(VI)-Contaminated Concrete," *Environ. Sci. Technol.* 34, 4185–4192 (2000).

[19] Chrysochoou, M., Dermatas, D., Moon, D. H., Christodoulatos, C., Wazne, M., French, C., Morris, J., and Kaouris, M., "Investigation of Barium Treatment of Chromite Ore Processing Residue (COPR)," *The 3th International Symposium on Contaminated Sediments*, Shizuoka, Japan, May 23–25, 2006.

[20] Moon, D. H., Chrysochoou, M., Dermatas, D., Christodoulatos, C., Kaouris, M., and Morris, J., "Investigation of Ettringite Formation in Chrome Ore Processing Residue, *The 8th International In Situ and On-Site Bioremediation Symposium*, Baltimore, Maryland, June 6-9, 2005.

[21] Fukue, M., Nakamura, T., Kato, Y., and Yamasaki, S., "Degree of Pollution for Marine Sediments," *Eng. Geol. (Amsterdam)* 53, 131–137 (1999).

Journal of ASTM International, Vol. 3, No. 6
Paper ID JAI13314
Available online at www.astm.org

Maria Chrysochoou, M.Sc.,[1] *Dimitris Dermatas, Ph.D.,*[1] *Deok Hyun Moon, Ph.D.,*[1] *Christos Christodoulatos, Ph.D.,*[1] *Mahmoud Wazne, Ph.D.,*[1] *Chris French,*[2] *John Morris,*[2] *and Maria Kaouris*[2]

Investigation of Barium Treatment of Chromite Ore Processing Residue (COPR)

ABSTRACT: Barium addition to chromite ore processing residue (COPR) was investigated in order to address (a) the pronounced heaving phenomena that are associated with mainly the presence of ettringite and (b) hexavalent chromium leaching. Sulfate was added to representative samples of grey-black (GB) and hard-brown (HB) COPR to simulate worst-case conditions of sulfate influx and ettringite formation. Both the X-ray powder diffraction (XRPD) and the modeling results showed that ettringite is a thermodynamically favored reaction in COPR. The subsequent addition of barium lead to the formation of both barite and barium chromate, observed as solid solution between the two phases. Modeling results confirmed that barium sulfate is the more stable species that will dissolve ettringite and that barium chromate will also dissolve COPR chromate phases when sulfate is depleted. The Toxicity Characteristic Leaching Procedure (TCLP) test on GB samples showed that the optimal stoichiometry to maintain Cr and Ba TCLP concentrations below the U.S. Environmental Protection Agency regulatory limit of 5 and 100 ppm, respectively, lies between 1:1 (Ba to sulfate plus chromate ratio) and 1.5:1. The respective optimal stoichiometry for the HB COPR was found to be higher, between 2:1 and 5:1. Considering that COPR is actually a Cr-contaminated cement form, a further area of research is the identification of barium-containing wastes (i.e., heavy-metal sludges, contaminated soils, etc.) that would be suitable for combination with COPR; in this way, an environmentally sustainable yet cost-effective treatment application can be realized.

KEYWORDS: COPR, chromate, hexavalent chromium, ettringite, heaving, barium

Introduction

Chromite ore processing residue (COPR) is generated as a by-product of the chromite ore $[(Mg,Fe)(Cr,Al,Fe)_2O_4]$ processing to isolate and extract chromium. The ore is mixed with quicklime and soda ash and roasted at high temperature ($\sim$1200°C)) [1]. The end products of the process are soluble sodium chromate and a residue that consists of primarily brownmillerite $[Ca_2(Al,Fe)_2O_5]$, periclase [MgO], excess hydrated lime $[Ca(OH)_2]$ and various impurities, including chromium in both its trivalent and hexavalent form. Millions of tons of COPR have been deposited in urban environments, with Hudson County, N.J., being a characteristic example of an area with several COPR deposition sites [2]. Extensive heaving phenomena have been observed in various deposition sites, rendering their use as construction sites for either industrial or urban redevelopment purposes unacceptable. The presence of heaving phenomena, as well as the presence of hexavalent chromium in COPR deposition sites, has been a cause for major attention in the past years and has resulted in extensive investigations with regard to the geochemical mechanisms that lead to swell development and to possible chromate migration. The Dundalk Marine Terminal (DMT) in Baltimore, Maryland, is a characteristic COPR deposition site, at which trenching activities were conducted in June, 2004, to identify COPR geochemistry and elucidate the heaving mechanism at the site.

The findings of the trenching investigation at DMT, including the physical description of COPR, trench stratigraphy, physicochemical characteristics, and mineralogy, are presented in Dermatas et al. [3]. In summary, the trenching activities led to the identification of two distinct types of COPR: A grey-black

Manuscript received March 31, 2005; accepted for publication June 29, 2005. Presented at ASTM Symposium on Contaminated Sediments: Evaluation and Remediation Techniques on 23–25 May 2006 in Shizuoka, Japan; M. Fukue, K. Kita, M. Ohtsubo, and R. Chaney, Guest Editors.
[1] Stevens Institute of Technology, Castle Point on Hudson, Hoboken, NJ 07030.
[2] Honeywell International Inc., 101 Columbia Road, Morristown, NJ 09762.

granular material (designated as GB) and a hard-brown lithified material (designated as HB). GB COPR was found to contain high amounts of COPR "parent" phases, i.e., brownmillerite and periclase, while HB was dominated by hydration and pozzolanic products, including brucite [$Mg(OH)_2$], hydrogarnets (katoite [$(CaO)_3Al_2O_3(H_2O)_6$] being the main phase), hydrotalcites ([$Al_2Mg_4(OH)_{12}(CO_3)(H_2O)_3$] is a representative compound), and calcium aluminum chromium oxide hydrates [$CACs-Ca_4Al_2O_6(CrO_4)\cdot nH_2O$]. The latter are concluded to be major sink for hexavalent chromium in COPR [4]. Ettringite [$Ca_6Al_2(SO_4)_3(OH)_{12}\cdot 26H_2O$] was also identified in several samples, at concentrations that reached ~70 % by weight (w/w) in an area below the heaving bulge in one trench. Ettringite presence and its relation to the heaving phenomena at DMT are also discussed in Dermatas et al. [3].

In order to mitigate ettringite-induced heaving observed in lime-stabilized clays, Dermatas [5] used barium salts, as barium forms insoluble barite ($BaSO_4$) and scavenges the available sulfate at the expense of ettringite. The addition of 15 %(w/w) barium hydroxide [$Ba(OH)_2\cdot 2H_2O$], barium chloride [$BaCl_2\cdot 2H_2O$], or barium carbonate [$BaCO_3$] successfully eliminated ettringite formation and swell development in lime-treated kaolinite and montmorillonite specimens [5]. Moreover, barium also forms highly insoluble barium chromate [$BaCrO_4$]. The barium addition to COPR was therefore investigated in the present study as a possible treatment to bind both sulfate and chromate in highly insoluble salts, eliminating both ettringite formation and chromate leaching potential. Geochemical modeling was also performed in order to investigate the reaction pathway of the two types of COPR (GB and HB) and the system response to an influx of sulfate and barium.

The investigation on barium-based treatment of COPR was pursued in the frame of identifying both environmentally and economically sustainable treatment options. COPR is essentially a contaminated cement form, as its mineralogy is similar to ordinary cements, with elevated levels of chromium, which render it contaminated. As cements are commonly used in stabilization/solidification (S/S) applications to immobilize contaminated media, such as heavy-metal sludges and soils, the combination of COPR with a barium-containing waste could result in a stabilized matrix similar to those produced in S/S applications.

Materials and Methods

Sampling

COPR samples were collected as disturbed bulk samples from various depths in the excavated trenches. Two representative samples of GB and HB COPR were chosen to conduct the treatability studies, as these two materials present different mineralogical and chemical characteristics. The GB sample was located at 6 ft depth, while the HB sample was located at 4 ft depth; the samples were chosen on the basis of their mineralogical characteristics, as ettringite was not present in the original sample, while their mineralogy represented the average mineralogy of the respective layers (GB and HB). Moreover, no soil admixtures from the surface cover (extending to 1–2 ft depth) were detected in these samples.

Experimental Methodology

The original samples were characterized by the following analysis methods:

- pH: ASTM D4980-89 [6] was used to measure the pH of the solid.
- Total analyses: The Cr(VI) content was measured by alkaline digestion and colorimetric analysis (EPA method 3060A [7] and 7196A [8]).
- X-ray powder diffraction (XRPD): Samples were air-dried for 24 h and pulverized to pass a U.S. standard #400 sieve (38 μm)). Step-scanned XRPD data were collected using a Rigaku DXR 3000 computer-automated diffractometer using Bragg-Brentano geometry. The diffractometry was conducted at 40 kV and 30 mA using diffracted beam graphite monochromator with Cu radiation. The data were collected in the range of two-theta values between 5° and 65° with a step size of 0.05° and a count time of 5 s per step. XRPD patterns were analyzed by the *Jade Software Version 7.1* [9] and reference to the patterns of the International Centre for Diffraction Data database [10], as well as the Inorganic Crystal Structure Database [11].

Samples were homogenized and air dried for 24 h prior to the initiation of the experiments. Air-dried samples were pulverized manually to pass a #100 U.S. standard sieve (0.15 mm opening) in order to

TABLE 1—*Testing matrix for Ba treatment of COPR samples.*

Stoichiometry	Dry sample (g)	Sulfate (g)[a]	Chromate (g)[a]	Ba (g)	$Ba(OH)_2$ (g)
0.5:1	3	0.15	0.07	0.12	0.16
1:1	3	0.15	0.07	0.25	0.31
1.5:1	3	0.15	0.07	0.37	0.47
2:1	3	0.15	0.07	0.5	0.62
5:1	3	0.15	0.07	1.25	1.56

[a]Sulfate was calculated as 5 %w/w, chromate as 1 %w/w Cr(VI) of the dry solid.

ensure homogeneity and to provide enough surface area for reactions to occur homogeneously within the sample. Sulfate was added to all samples in the form of sodium sulfate (Na_2SO_4) on a 5 %w/w basis, in order to simulate worst-case conditions of sulfate influx and thus ettringite formation. 50 000 mg/kg was the highest sulfate concentration observed in the bulk HB COPR samples obtained at DMT, located in an area below a heaving feature in the excavated trenches [12]. A liquid-to-solid (L:S) ratio of 2 was employed, to provide enough water for reactions to occur, while staying close to the actual field conditions. A curing time of one week was provided to reach operational equilibrium. The samples were then air dried, in order to establish uniform moisture conditions for the subsequent barium addition.

Barium was added as $Ba(OH)_2$ solution, considering five stoichiometries of the ratio $Ba:(SO_4^{2-}+CrO_4^{2-})$ and employing the same L:S ratio of 2. Duplicate samples were tested for the 1:1 stoichiometry. Table 1 presents an overview of the testing matrix, which was identical for the GB and HB materials.

The curing time for the barium reaction was, again, one week.

The samples were then subjected to the Toxicity Characteristic Leaching Procedure (TCLP) test [13]. Cr(VI) was measured by the colorimetric method [8] and the total Ba, S, and Cr in the TCLP leachate were determined by Inductive Couple Plasma/Atomic Emission Spectrometry (ICP/AES) [14]. XRPD analysis was performed on the TCLP residues, in order to determine the mineralogical changes imposed by the reactions and the TCLP testing.

Modeling

Geochemical modeling of COPR was performed using the EQ3/6 software package [15].

The EQ3/6 thermodynamic database was modified to include the following solid phases:

- CAC [$Ca_4Al_2O_6(CrO_4)\cdot 15H_2O$]: Data were obtained from Perkins and Palmer [16];
- Cr(VI)-ettringite [$Ca_6[Al(OH)_6]_2(CrO_4)_3 26\ H_2O$]: data were obtained from Perkins and Palmer [17].

The purpose of the modeling employment was not to precisely predict aqueous concentrations and distribution of solid phases at this stage of the research, but rather to observe the tendencies in the relative stability of the mineral phases and their response to the influx of sulfate and barium. In other words, the qualitative and not the quantitative reaction pathway was attempted, as the current treatability study aimed at the initial screening of the Ba treatment; ongoing and future research focuses on the quantification of individual reaction steps and their modeling, as well as on the refinement of the treatment conditions.

Modeling included three steps:

1. Modeling of the initial COPR reaction pathway, in order to simulate the HB material: Brownmillerite, periclase, and lime, the COPR "parent" minerals, reacted with water, chromate, and carbonate. The stoichiometries of the parent minerals were chosen to represent the average chemical composition of COPR. The aqueous concentrations were chosen based on groundwater data, but they were not significant as any precipitates were removed from the system prior to the initiation of the reaction, i.e., an equilibrium solution of aqueous species was the input to the reaction pathway.
2. Modeling of sulfate influx in the HB equilibrium COPR of the previous run: The sulfate addition was calculated as 5 %w/w of the initial reactants.
3. Modeling the addition of BaO at 1:1 stoichiometry on the total amount of sulfate and chromate. Barium oxide was used as it was the only entry in the EQ3/6 database. It is, however, very soluble (log K_{sp}=47.8 for the dissolution reaction), so that the results are equivalent with the addition of barium hydroxide.

TABLE 2—*Modeling input to simulate HB COPR and its reaction with sulfate and barium.*

Reactants	Mol/kg H_2O	Aqueous species	mg/L
Brownmillerite	0.16	Ca^{2+}	582
Periclase	0.2	Al^{3+}	1.34
Lime	0.05	Fe^{3+}	0.05
CrO_4^{2-}	0.03	Mg^{2+}	0.09
HCO_3^-	0.05	CrO_4^{2-}	1.4
SO_4^{2-}	0.05	SO_4^{2-}	2.4
BaO	0.08	HCO_3^-	5
		Ba^{2+}	0.09

The input is shown in Table 2. The initial pH was 12 and the initial L:S ratio 10:1. Redox reactions were suppressed.

Results and Discussion

Initial Characterization and TCLP Results

The results of the initial characterization of the two samples (GB and HB) are presented in Table 3.

Table 3 shows that both materials are highly alkaline, favoring the formation of pozzolanic products, such as CAC and ettringite. The latter was not detected in the original XRPD patterns, indicating that the samples were "clean" prior to the initiation of the experiments. The Cr(VI) content varied greatly in the two materials, as it was 0.36 % in the GB and 1.67 % in the HB COPR. Both values deviated from the 1 %w/w assumption that was employed in order to calculate the barium stoichiometries (Table 1). The variation is, however, small, compared to the addition of 5 %w/w sulfate and is taken into account in the interpretation of the results.

The XRPD results confirmed that the two materials were distinct in mineralogy; the GB sample contained very high amounts of brownmillerite and relatively high amounts of periclase, while the HB sample was dominated by calcite, hydrogarnets, and CACs. CACs were a major Cr(VI) sink in both materials, as was previously established [4].

Table 4 presents the TCLP results for the various stoichiometries.

The post-tumbling TCLP pH regime was different in the two materials: The pH in the HB material remained at relatively high values, in the range of 10–11, while the pH in GB dropped to values in the range of 8.4–9.5. This is a result of the different mineralogy, which contributes to a different behavior in the buffering capacity of the two COPR materials. The HB sample is dominated by pozzolanic products that tend to dissolve when the pH drops below 11, thus contributing to the buffering capacity while the pH is still high; the addition of increasing amounts of $Ba(OH)_2$ is the reason why the pH increases with increasing stoichiometry of the barium hydroxide addition. Conversely, the brownmillerite that dominates the GB COPR dissolves at much lower pH values (6 or lower), so that its alkalinity is not released in the high pH regime of the GB CORP. The relative contribution of COPR minerals and barium hydroxide is not straightforward, in this case.

TABLE 3—*pH, Cr(VI) content, and mineralogy of the initial COPR samples.*

	GB	HB
pH	12.4	12.0
Cr(VI)mg/kg	3590	16700
XRPD (%w/w)		
Brownmillerite	66.5	3.6
Periclase	5.3	-
Brucite	5.1	4.8
Calcite	41.3	41.5
Katoite	10.2	14.6
CAC	7.5	14.4
Hydrotalcite	1.2	13.0
(Cr,Al)O(OH)	-	6.1

TABLE 4—*TCLP results for the two COPR materials and the five employed stoichiometries.*

	TCLP pH	Cr(VI) (mg/L)	Cr (mg/L)	Ba (mg/L)	S (mg/L)	SO_4^{2-} (mg/L)[a]
GB						
0.5:1	8.5	n.a.	105	2.58	328.1	1005
1:1	8.4	46	41	2.74	134.4	412
1:1 (b)	8.9	n.a.	42	2.84	153.4	470
1.5:1	9.5	n.a.	0.13	170.4	36.5	112
2:1	9.1	0.3	0.19	292.9	48.4	148
5:1	8.4	n.a.[b]	0.23	1098.7	42.5	130
HB						
0.5:1	10.0	570	588	15.8	113.9	349
1:1	10.3	345	374	3.39	62.7	192
1:1 (b)	10.4	317	333	3.02	54.3	166
1.5:1	10.5	151	157	2.95	64.9	199
2:1	10.8	26	23	3.29	25.9	79
5:1	10.9	0.016	0.25	1344	19.5	60

[a]Sulfate was calculated from the S concentration assuming that it was all present as sulfate.
[b]n.a.: not available.

Cr(VI) leaching in the GB TCLP leachate could not be directly established in four of the GB samples due to experimental uncertainties in the colorimetric method. However, the total Cr concentration may be regarded as equivalent to the Cr(VI) concentration, as Cr(III) precipitates as insoluble hydroxide at this pH regime [18] and should not thus be present in the TCLP solution in considerable amounts. This is also illustrated in the case of the HB material (Table 4), as the Cr(VI) and total Cr concentrations are very close.

The TCLP regulatory limit established by USEPA for Cr is 5 mg/L. Table 4 shows that the barium treated GB material exceeds the limit for the 0.5:1 and 1:1 stoichiometries, while the 1.5:1 stoichiometry yields a TCLP Cr concentration (0.13 mg/L) that lies far below the 5 mg/L threshold. This indicates that the optimal stoichiometry for Ba treatment of COPR lies between 1:1 and 1.5:1. Conversely, the optimal stoichiometry for the HB material is between 2:1 and 5:1, most probably due to the significantly higher Cr(VI) concentration in this type of COPR.

It should be noted that the Ba concentration in the TCLP leachate is also important from the regulatory point of view, as the TCLP limit for Ba is 100 mg/L. In the GB material, the TCLP Ba concentration is very low (3 mg/L) up to the 1:1 stoichiometry and then increases suddenly to 170 mg/L at the 1.5:1 ratio. As the optimal stoichiometry is assessed between 1:1 and 1.5:1, it is most probable that Ba leachability will not be a problem upon treatment optimization. The Ba concentration is also low around 3 mg/L in the HB COPR and only increases to >1300 mg/L for the very high stoichiometry of 5:1. Again, a stoichiometry close to 2:1 to optimize Cr(VI) leaching, would also probably keep the Ba concentration below the regulatory limit. Overall, the data point to the existence of a solubility controlling phase for Ba, as its concentration is constant at 3 mg/L for most of the stoichiometries and then suddenly increases above a threshold ratio. The mechanisms behind this behavior will be explored further in the following discussions and the modeling section.

In order to obtain a more accurate picture of the relative release of hexavalent chromium, barium, and sulfate, the leachability ratio was calculated by normalizing the TCLP concentrations multiplied by the L:S ratio (20) over the total concentration of the compounds in the solid. The values are presented (in percent) in Table 5. In the case of the GB material, the total Cr concentrations were used, as discussed above.

According to Table 5, barium presents a very low leaching ratio for all the stoichiometries, which becomes extremely low (0.1%) for the 0.5:1 and 1:1 ratios in GB and all ratios but the 5:1 in HB. This indicates that the formation of barium precipitates are thermodynamically powerful reactions; the TCLP Ba concentration becomes high only when the system is oversaturated with Ba.

The comparison between the Cr(VI) and SO_4^{2-} leachability ratios shows that sulfate uptake by barium is more favored compared to chromate. This observation is supported by thermodynamic data, as the solubility product for barite is $\log K_{sp} = -9.98$, while the respective value for barium chromate is $\log K_{sp} = -9.67$ [19], indicating that the latter is more soluble. Moreover, mass action due to the high sulfate content also leads to comparatively more sulfate forming barite, to comply with equilibrium requirements.

TABLE 5—*Leachability ratio (in percent) for hexavalent chromium, barium and sulfate.*

	TCLP pH	Cr(VI) leached (%)	Ba leached (%)	SO_4^{2-} leached (%)
GB				
0.5:1	8.5	59	0.13	40
1:1	8.4	23	0.07	16
1:1 (b)	8.9	24	0.07	19
1.5:1	9.5	0.07	2.76	4
2:1	9.1	0.11	3.51	6
5:1	8.4	0.13	5.27	5
HB				
0.5:1	10.0	68	0.79	14
1:1	10.3	41	0.08	8
1:1 (b)	10.4	38	0.07	7
1.5:1	10.5	18	0.05	8
2:1	10.8	3	0.04	3
5:1	10.9	0.002	6.45	2

The introduction of sulfate generally increases the solubility of chromate, as it forms thermodynamically more stable compounds and tends to displace chromate out of the solid matrix, as evidenced previously in COPR matrices [20]. The leachability ratios of both chromate and sulfate decrease with increasing barium addition, as would be expected; the optimization of the treatment would indicate the point of balance, in which all concentrations would comply with regulatory requirements.

XRPD Results

In order to investigate the speciation of the three compounds in the solid, as well as to evaluate mineral transformations due to treatment, XRPD was conducted on selected TCLP residues.

Figure 1 shows the XRPD pattern of the original GB sample, overlaid by the pattern obtained from the 1:1 treated sample. The formation of high amounts of barite is clear, along with formation of calcite and possibly some hydrotalcites. CACs dissolved due to the low pH (8.4) of the TCLP residue, which renders pozzolanic phases unstable. No ettringite was detected in any of the patterns, which would also be unstable under the TCLP conditions. However, no gypsum was observed either. As gypsum is the dissolution product of ettringite, it is hypothesized that no ettringite formed in the solid prior to the TCLP. The

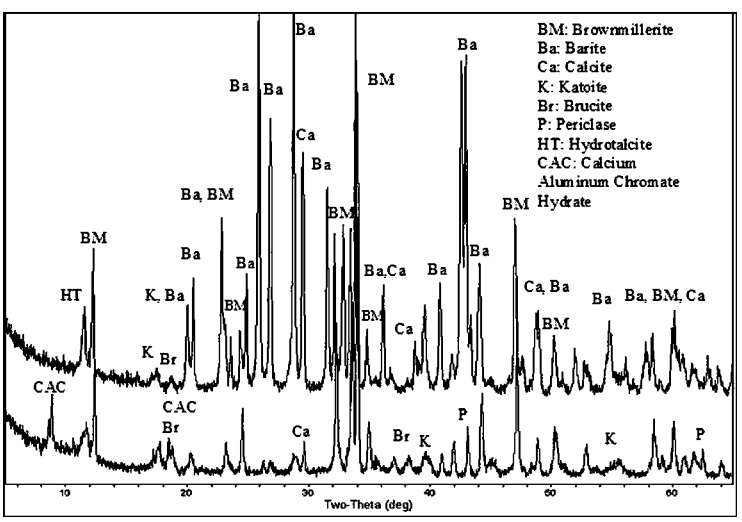

FIG. 1—*XRPD pattern of GB samples - original (below) and 1:1 treated sample after TCLP (above).*

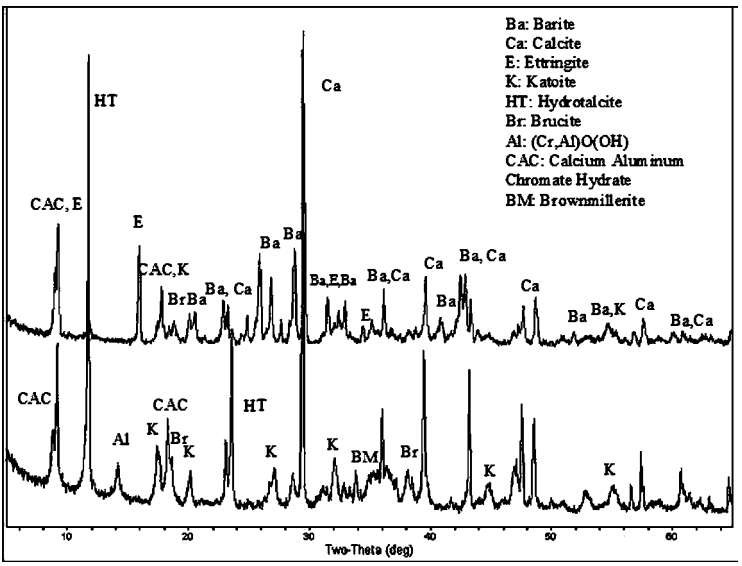

FIG. 2—*XRPD pattern of HB samples - original (below) and 1:1 treated sample after TCLP (above).*

formation of ettringite in GB is kinetically inhibited due to the slow dissolution of brownmillerite at ambient conditions, which constitutes the main alumina source in GB COPR. Consequently, the elimination of ettringite formation is relatively easy with lower amounts of barium in the GB material.

Figure 2 shows the original and the 1:1 ratio XRPD patterns of the HB material. The influx of sulfate resulted, in this case, to significant formation of ettringite; the "parent" materials, i.e., the calcium and aluminum sources, seem to have been CAC and katoite, as well as the phase (Cr,Al)O(OH), which is similar to boehmite [AlO(OH)], as their peak intensities appear diminished or vanished in the case of the (Cr,Al)O(OH). The addition of barium on a 1:1 basis resulted to significant formation of barite, which was however, not sufficient to eliminate ettringite formation. Ettringite was present with very high peaks in the 0.5:1 pattern as well, despite the fact that the pH was 10.0, which is theoretically outside the ettringite pH stability domain (10.5-13 in most of the studies in the literature [21]). Ettringite was still present in the 2:1 XRPD pattern of the HB material and disappeared only in the 5:1 stoichiometry. These results indicate that ettringite formation in the HB COPR is a thermodynamically favored reaction, with favorable kinetics for rapid reactions to occur.

Barium chromate was not directly observed in the XRPD patterns of the TCLP residues. This was, however, due to the fact that barite and barium chromate have similar crystal structures and thus produce XRPD patterns with similar peak positions. Fernandez-Gonzalez et al. [22] studied the solid solution series between $BaSO_4$ and $BaCrO_4$ by X-ray diffraction and found that the lattice constants of barite shift to higher values upon incorporation of chromate, due to its larger radius. Table 6 shows the Rietveld refine-

TABLE 6—*Unit cell parameters and peak broadening of barite (theoretical and calculated according to Rietveld refinement).*

	A	b	c	FWHM
$BaSO_4$[a]	8.881	5.454	7.157	···
$Ba(SO_4)_{0.73}(CrO_4)_{0.27}$[a]	8.940	5.470	7.200	···
GB 1:1	8.895	5.455	7.171	0.13
GB 2:1	8.889	5.447	7.168	0.13
HB 1:1	8.935	5.470	7.200	0.28
HB 2:1	8.935	5.460	7.210	0.28

[a]From Fernandez-Gonzalez et al. [22].

TABLE 7—*Precipitated phases in* mol/KgH_2O *at each equilibrium step of the COPR reaction pathway.*

		First step	Second step	Third step
pH		12.8	13.1	13.1
Hematite	Fe_2O_3	0.16	0.16	0.16
Hydrotalcite	$Mg_4Al_2(OH)_{14}:3H_2O$	0.05	0.05	0.05
Katoite	$(CaO)_3Al_2O_3(H_2O)_6$	0.08	0.064	0.10
Portlandite	$Ca(OH)_2$	0.32	0.27	0.35
Calcite	$CaCO_3$	0.005	0.005	⋯
CAC	$Ca_4Al_2O_6(CrO_4)\cdot 15H_2O$	0.03	0.029	0.004
Ettringite	$Ca_6Al_2(SO_4)_3(OH)_{12}\cdot 26H_2O$	⋯	0.017	⋯
Witherite	$BaCO_3$	⋯	⋯	0.005
Barite	$BaSO_4$	⋯	⋯	0.05
Barium chromate	$BaCrO_4$	⋯	⋯	0.026

ment results for the lattice constants of barite in the GB and HB XRPD patterns, as well as the full width half maximum (FWHM) of the respective peaks.

The comparison between the theoretical and refined values for the unit cell parameters of barite show that there is very little shift in the GB patterns, while the peak width corresponds to the intrinsic peak broadening of the instrument. In other words, there is only one phase corresponding to the barite peaks, which agrees very well with the barite crystal structure. This observation agrees with the fact that the amount of Cr(VI) in the GB COPR is relatively low (0.35 % w/w), so that substitution for sulfate in barite is either absent or nondetectable. Conversely, the high Cr(VI) concentration in the HB material (1.67 % w/w) results in significant solid solution between barium sulfate and barium chromate. This is reflected both in the peak width, which corresponds to two phases sharing the same peaks, and in the shift in the unit cell parameters, as predicted in the study by Fernandez-Gonzalez et al. [22]. The refined values for barite correspond to a chromate substitution ~25 % for sulfate. The total chromate-to-sulfate ratio is about 1:3, the chromate affinity for barium is, however, lower than the sulfate, as discussed previously. Overall, the agreement between the experimental observations and the theoretical premises for the formation of barium sulfate and chromate is very good.

The phase transformations in the present experiments were also investigated by means of geochemical modeling, employing a reaction pathway code to monitor phase equilibria upon influx of sulfate and then barium in the COPR system.

Geochemical Modeling

Geochemical modeling was conducted in three subsequent steps: (1) dissolution of COPR "parent" materials, brownmillerite, periclase and lime, and reaction with chromate and carbonate anions, (2) reaction of the equilibrium system with sulfate, and (3) reaction of the equilibrium system generated by the second step with barium oxide.

The type and amount of precipitated phases at the equilibrium of each step are shown in Table 7.

The composition of HB COPR is predicted relatively accurately by the model, with a few exceptions:

- The presence of hematite corresponds to amorphous iron phases, which are abundant in the HB COPR [3].
- Hydrotalcite scavenges all the available magnesium released by periclase, at the expense of brucite [$Mg(OH)_2$], according to the model. This, however, does not affect the equilibria of the chromate and sulfate pozzolanic phases, i.e., it does alter the results of the second and third steps.
- Portlandite is predicted in high amounts. The comparison between Table 7 and the HB Rietveld results (Table 3) shows that this is due to the low amount of carbonate that restricted calcite formation. This, however, does not affect the overall results. COPR carbonation is a complex process the study of which is not the purpose of this paper; it will, therefore, not be considered further at this stage. The pH regime, which is generally affected by carbonation, is highly alkaline both in the actual conditions and the modeling results; the geochemistry of other phases is not significantly affected by the portlandite-calcite equilibrium in the pH range 12–13.

Overall, the results of the first step show that the model reflects, within its limitations, the actual geochemical processes in COPR. Figure 3 shows the reaction progress for selected compounds, in order to illustrate the phase equilibria during the three modeling steps.

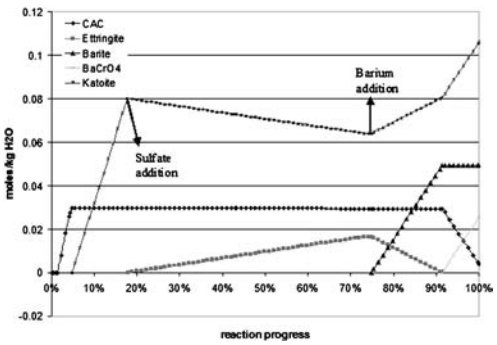

FIG. 3—*Reaction pathway for selected COPR phases.*

During the first step, katoite starts to form when all available chromate has reacted to form CAC and increases until the brownmillerite dissolution is complete. When sulfate is introduced into the system, katoite dissolves to form ettringite, with portlandite also contributing as a calcium source. Other phases remain unaffected, as was assumed in the XRPD discussion.

The addition of barium during the third step results first in the gradual dissolution of ettringite. Barite scavenges the sulfate, while calcium, and aluminum reform katoite. When ettringite is exhausted, CACs start to dissolve and form barium chromate and additional katoite. In other words, the model predicts that chromate will only be bound to barium, when no sulfate is available. This was not the case, however, in the HB experiments; the simultaneous formation of barite and barium chromate was observed as a solid solution in the 1:1 XRPD pattern; ettringite was therefore, still present at this stoichiometry. The model also predicts that some of the barium forms barium carbonate (witherite), dissolving the existing calcite. This transformation was not observed in the 1:1 XRPD pattern, it was only in the 5:1 stoichiometry that witherite formed in ample amounts dissolving the existing calcite, both in the GB and HB XRPD patterns of the TCLP residues. The different pH regime of the TCLP, which was 8 to 9 in the GB and 10 to 11 in the HB, whereas it was 13 in the modeling results, may be the reason for this observation.

Overall, the modeling results accurately reflect the geochemical transformations observed by XRPD, i.e., katoite is the parent material to form ettringite, which is then dissolved to form barite. CACs also dissolve to form barium chromate. The difference between the modeling and the experimental results is that the model predicts a subsequent formation of the two barium salts, i.e., barium chromate forms only when sulfate is depleted, while the experimental results show that these occur in solid solution toward the sulfate end member. Ettringite is still present in the 1:1 stoichiometry in the experiment, while the model predicts that it completely dissolves.

Summary and Conclusions

Barium addition to chromite ore processing residue (COPR) was investigated in order to address the two environmental and geotechnical issues associated with COPR deposition as a structural fill at numerous sites: (a) the pronounced heaving phenomena that are associated with mainly the presence of ettringite and (b) hexavalent chromium leaching. Barium forms highly insoluble complexes with both sulfate and chromate and is therefore a favorable candidate to effectively immobilize both anions.

Two types of COPR were encountered at Dundalk Marine Terminal (Maryland) that were different in texture, color, and mineralogy; one (grey-black (GB) COPR) resembled the parent COPR material that came out of the chromite ore roasting process, while the other (hard-brown (HB) COPR) was dominated by COPR hydration and pozzolanic reaction products.

Sulfate was added to representative samples of the two types of COPR to simulate worst-case conditions of sulfate influx and ettringite formation. Both the XRPD and the modeling results showed that ettringite is a thermodynamically favored reaction in COPR.

The subsequent addition of barium led to the formation of both barite and barium chromate, observed as solid solution between the two phases in the XRPD patterns of the HB COPR that had high Cr(VI)

concentrations; the low amount of chromate in GB COPR did not allow the detection of barium chromate by XRPD. Modeling results confirmed that barium sulfate is the more stable species that will dissolve ettringite and that barium chromate will also dissolve COPR chromate phases when sulfate is depleted.

The TCLP test on GB samples showed that the optimal stoichiometry to maintain both Cr and Ba TCLP concentrations below the EPA regulatory limit of 5 and 100 ppm, respectively, lies between 1:1 (Ba to sulfate plus chromate ratio) and 1.5:1. The respective optimal stoichiometry for the HB COPR was found to be higher, between 2:1 and 5:1.

The elimination of ettringite formation seemed to be successful in the GB material; this is probably due to kinetic limitations, as brownmillerite dissolves slowly to form ettringite. Conversely, in the HB material, ettringite formed from hydrogarnet, the HB predominant phase and remained persistent in the XRPD patterns of the TCLP residues up to the 2:1 stoichiometry; it was absent only in the 5:1 XRPD pattern. It should be stressed, however, that the sulfate addition was chosen on the basis of worst-case conditions; further research will address average scenarios of sulfate presence in order to optimize treatment for ettringite formation. Considering that COPR is actually a Cr-contaminated cement form, a further area of research is the identification of barium-containing wastes (i.e., heavy-metal sludges, contaminated soils, etc.) that would be suitable for combination with COPR; in this way, an environmentally sustainable and cost-effective treatment application can be realized.

Acknowledgments

The authors wish to thank Honeywell International Inc. for the financial support of the COPR trenching investigation and the analyses at Stevens Institute of Technology.

References

[1] Allied Signal, 1982. Process Descriptions Baltimore Plants.
[2] Lioy, P. J., Freeman, N. C. G., Wainman, T., Stern, A. H., Boesch, R., Howell, T., and Shupack, S. I., "Microenvironmental Analysis of Residential Exposure to Chromium-Laden Wastes In and Around New Jersey Homes," *Risk Anal.*, 12, pp. 287–299 (1992).
[3] Dermatas, D., Chrysochoou, M., Moon, D. H., and Christodoulatos, C., "Mineralogical Characterization of Chromite Ore Processing Residue at Dundalk Marine Terminal area 1800," *In situ and on-site Bioremediation Symposium*, Battelle, Columbus, Ohio, 2005.
[4] Chrysochoou M., Dermatas D., Moon, D. H., and Wazne M., "The Role and Properties of Calcium Aluminum Chromate Hydrates in Chromium Waste Stabilization,"*1st International Conference on Environmental Science and Technology*, American Academy of Sciences, 2005.
[5] Dermatas D., "An Experimental Study to Elucidate and Eliminate Ettringite-Induced Swelling in Lime-stabilized, Sulfate-Bearing Clayey Soils," Ph.D. Thesis, University of California, Berkeley, 1992.
[6] ASTM Standard *D 4980-89*, "Standard Test Methods for Screening of pH in Waste," *D Annual Book of ASTM Standards*, ASTM International, West Conshohocken, PA.
[7] U.S. EPA, *SW-846*, Method 3060A, "Alkaline digestion for hexavalent chromium."
[8] U.S. EPA, *SW-846*, Method 7196A, Chromium, hexavalent (colorimetric).
[9] Materials Data Inc., Jade Version 7.1, California, 2004.
[10] "Powder Diffraction File, PDF-2 Database Release 1998," announcement of new database release, International Centre for Diffraction Data (ICDD), 1998.
[11] Inorganic Crystal Structure Database (ICSD) Fachinformationszentrum Karlsruhe, Germany, 2004.
[12] Stevens Institute Technology, Final Report on trench investigation and COPR analysis at Dundalk Marine Terminal area 1800, 2005.
[13] U.S. EPA, *SW-846*, Method 1311, "Toxicity Characteristic Leaching Procedure."
[14] U.S. EPA, *SW-846*, Method 6010B, "Inductively Coupled Plasma–Atomic Emission Spectrometry."
[15] EQ3/6, A Software Package for Geochemical Modeling Version 8.0, The Regents of the University of California, Lawrence Livermore National Laboratory 2002.
[16] Perkins R. B., and Palmer, C. D., "Solubility of Chromate Hydrocalumite ($3CaOAl_2O_3CaCrO_4nH2O$) at 5-75°C," *Cem. Concr. Res.*, 31, 983–992 (2001).

[17] Perkins, R. B., and Palmer, C. D., "Solubility of $Ca_6[Al(OH)_6]_2(CrO_4)_3$ $26H_2O$, the Chromate Analog of Ettringite at 5-75 oC," *Appl. Geochem.*, 15, 1203–1218 (2000).
[18] Dermatas, D., and Meng, X., "Utilization of Fly-Ash for Stabilization/Solidification of Heavy Metal Contaminated Soils," *Eng. Geol.* 70, 377–394 (2003).
[19] Gustafsson, J. P., Visual MINTEQ ver. 2.30, KTH (Royal Institute of Technology), Sweden, 2004.
[20] Geelhoed, J. S., Meeussen, J. C. L., Roe, M. J., Hillier, S., Thomas, R. P., Farmer, J. G., and Paterson, E., "Chromium Remediation or Release? Effect of Iron(II) Sulfate on Chromium(VI) Leaching from Columns of Chromite Ore Processing Residue," *Environ. Sci. Technol.* 37, 3206–3213 (2003).
[21] Chrysochoou, M., and Dermatas, D., "Evaluation of Ettringite and Hydrocalumite Formation for Heavy Metal Immobilization: Literature Review and Experimental Study," *J. Hazard. Mater.* (in press).
[22] Fernandez-Gonzalez, A., Martin-Diaz, R., and Prieto, R., "Crystallization of $Ba(SO_4,CrO_4)$ Solid Solutions from Aqueous Solutions," *J. Cryst. Growth*, 200, 227–235 (1999).

Journal of ASTM International, Vol. 3, No. 7
Paper ID JAI13326
Available online at www.astm.org

Masashi Kamon,[1] *Huyuan Zhang,*[2] *Takeshi Katsumi,*[3] *and Toru Inui*[4]

Biochemical Effects on the Long-Term Mobility of Heavy Metals in Marine Clay at Coastal Landfill Sites

ABSTRACT: In coastal landfill facilities that are constructed to contain municipal and industrial wastes in Japan, natural marine clay layers serve as bottom liners to prevent pollutant migration. Leachates from landfills are rich in dissolved organic carbon (DOC) that can be used by micro-organisms. Biological processes could lead to redox reactions that change the pH and Eh. These biochemical factors may strongly influence the behavior of pollutants leached from landfills, particularly heavy metals. In this paper, modified batch tests were conducted to investigate the effects of pH and Eh and to simulate both chemical and biochemical reactions on zinc mobility in a marine clay layer. To examine the effects of pH and Eh, the pH and Eh were controlled by adding acid or base, respectively, and a reducing agent. To study the zinc mobility, biochemical reactions were enhanced by cultivating native micro-organisms, which gradually changed the pH and Eh conditions. Batch tests with different DOC concentrations were also conducted to evaluate the effect of DOC on zinc mobility. In addition, biochemical processes in the bottom clay liners at coastal landfill sites that receive municipal solid waste (MSW) incinerator ash were simulated by batch tests using a solution of MSW incinerator ash mixed with seawater along with cultivating native micro-organisms found in marine clay. The experimental results indicated that microbial activities in closed soil-water systems result in strongly reduced conditions compared to that controlled by a strong reducing agent, and that the zinc mobility is lowered through the formation of sulfides. Although microbial activity was initially limited under highly alkaline conditions due to MSW incinerator ash, the pH gradually decreased mainly due to the formation of organic acids from microbial activity. Under the oxidized conditions, the solubility of zinc was controlled by pH and the Eh had a negligible effect on the zinc concentration. DOC in the leachate served as a bioavailable carbon source for microbial activities, which promoted anaerobic conditions in the soil-water system and the immobilization of zinc. However, DOC also formed soluble complexes with heavy metals, which increased the zinc concentration. These observations confirmed that heavy metals in the leachates became immobilized under the conditions found at landfill bottom liners when estimated in terms of pH, Eh, and DOC.

KEYWORDS: heavy metals, clay, pH, dissolved organic carbon, redox reaction, landfill

Introduction

Engineered landfills are commonly used as the final disposal technology for municipal solid waste (MSW) and its incinerator ashes in Japan. Due to the potential impact on the nearby environment, leakage of landfill leachates is minimized in modern landfill sites by designing an impermeable cover, a bottom liner system, and a leachate collection system. Heavy metals are major pollutants contained in MSW, particularly in MSW incinerator ash. However, most of the available monitoring data shows that their concentrations in leachates are normally very low (Kjeldsen et al. 2002). This implies that heavy metals are attenuated or immobilized in landfill sites and bottom clay liners. With respect to the mobility of heavy metals in a landfill clay liner, Kamon et al. (2002) investigated the influence of microbial activities. They attributed the effective attenuation of heavy metals to low redox potentials and neutral to basic pH conditions that predominantly prevail in the stabilization processes. However, oxygen will eventually intrude into the landfills and switch the anaerobic decomposition into an aerobic one, which will decrease the pH. Zhang et al. (2004) investigated the long-term mobility of heavy metals in a landfill clay liner by focusing on the acid neutralization capacities of the leachate-liner soil system. They concluded that both

Manuscript received April 12, 2005; accepted for publication September 15, 2005. Presented at ASTM Symposium on Contaminated Sediments: Evaluation and Remediation Techniques on 23–25 May 2006 in Shizuoka, Japan; M. Fukue, K. Kita, M. Ohtsubo, and R. Chaney, Guest Editors.

[1] Professor, Kyoto University, Yoshida-honmachi, Sakyo-ku, Kyoto 6068501, Japan.
[2] Professor, Hohai University, 1, Xikang Road, Nanjing 210098, China.
[3] Associate Professor, Kyoto University, Yoshida-honmachi, Sakyo-ku, Kyoto 6068501, Japan.
[4] Assisstant Professor, Kyoto University, Yoshida-honmachi, Sakyo-ku, Kyoto 6068501, Japan.

the landfilled wastes and liner system possess sufficient acid buffering capacity to consume the protons produced in organic oxidation reactions. Hence, high levels of remobilization of heavy metals should not occur even in the long-term (Zhang et al. 2004).

MSW landfill leachates contain a high content of dissolved organic carbon (DOC). Native micro-organisms can use the DOC as a carbon source for metabolism, which leads to a series of reduction-oxidation (redox) reactions (e.g., Lovley and Phillips 1988) that, in turn, control the mobility of heavy metals (e.g., Lyngkilde and Christensen 1992; Rugge et al. 1995). To investigate the effects of pH and Eh on the heavy metal mobility, both chemical and biochemical methods were employed in various tests. For example, the pH is controlled by adding acids or bases, while the Eh is controlled by adding reducing agents. When a biochemical method is used, the native micro-organisms in soil-water systems must be cultivated. These enhanced biochemical reactions should gradually change the pH and Eh conditions. The extent that the chemical and biochemical effects are similar remains unknown. Thus, in this research, various batch adsorption tests were designed to compare the pH and Eh effects derived from chemical and biochemical reactions. In particular, the changes in pH and Eh derived from biochemical processes in the bottom clay liner of coastal landfill sites that receive MSW incinerator ash and their effects on heavy metal mobility were evaluated by cultivating native micro-organisms found in marine clay. In addition, batch adsorption tests with different DOC levels were designed to evaluate the effects of DOC on heavy metals since, in theory, DOC can complex with heavy metals and mobilize them.

Background

Waste disposal in coastal areas is an emerging topic due to limited inland space in Japan, particularly for metropolitan areas. In addition, the types of waste materials have changed. Since the 1980's, incinerator ash and incombustible matter have become the main components discarded into landfill sites. Compared to the United States and many European countries, incineration has been a major intermediate treatment technology for MSW in Japan.

Bottom clay liners are the most important barriers used in solid waste disposal facilities. For coastal landfill facilities, natural marine clay layers are regarded as the clay layer that prevents pollutant migration. Bottom clay liners at landfill sites, especially at coastal landfill sites, may be under moderate to strong reduction conditions. In addition, leachates from landfills are rich in dissolved organic matter that micro-organisms can utilize. Therefore, microbial activities are most important events that occur in MSW landfills during decomposition. On one hand, temporal variations in the leachates, pH, and Eh, provide basic conditions for microbial activities, but on the other hand, microbial activities alter the pH and Eh of the leachates. Besides serving as a carbon source for microbial activities, organic matter in landfills can influence the mobility of heavy metals in other ways, such as adsorption, and complexation, etc. Reactions between organic matter and metals may exhibit different, even opposite, effects on a metal's mobility. For example, the association with insoluble organic compounds tends to reduce the availability of metals, whereas organic chelates tend to mobilize metals from insoluble minerals (Tate 1987). Schulin et al. (1995) and Christensen et al. (1996) reported that dissolved organic matter increases the mobility of heavy metals by forming metal-organic carbon complexes. It is obvious that a better evaluation of the natural attenuation of heavy metals in landfill clay liners is dependent on a thorough understanding of the relationship between pH, Eh, TOC, and microbial activities. In addition, many nonbiological processes, in particular the adsorption-desorption processes and the precipitation-dissolution processes, that are responsible for the mobility of heavy metals in landfills and landfill clay liners are significantly affected by changes in the pH and Eh. Table 1 lists processes of relative importance for several mechanisms of heavy metal attenuation in soil.

Other aspects that require redox effects to be considered are the type of containment facility and the nature of the waste materials received. Disposing incinerator ash in coastal landfill sites has recently become a common practice in Japan, which may affect the microbial activities along with the pH, Eh, and TOC.

TABLE 1—*Attenuation mechanisms of heavy metals in soil (Kamon et al. 2002, modified from Hutchison and Ellison 1992).*

	Chemical species	Attenuation mechanism												
		Physical				Physico-chemical		Chemical					Biological	
		Filtration	Dispersion	Dilution	Volatilization	Adsorption	Fixation	Precipitation	Hydrolysis	Complexation	Oxidation	Reduction	Bacterial reaction	Cellular uptake
Increasingly attenuated	Chromium (III)	●	○	○				●	●		○	○		○
	Lead		○			●	○	○	○					
	Mercury	●	○		○	●		○			○	○		○
	Copper		○	○		●	●		○	○	○	○		
	Nickel		○	○		○	○	○	○					
	Zinc		○	○		●	○	●	○			●	●	
	Cadmium		○	○		○			○	○				
	Cobalt		○	○		●	○			○				

●: primary attenuation mechanism; ○: secondary attenuation mechanism

Experimental Methods and Analysis

Test Design and Materials

A modified batch adsorption test procedure is adopted since it allows microbial cultivation to enhance the microbial activities and the biochemical reactions among soil-water-pollutant systems to be highlighted.

Three types of soil are used in this research: (1) Gifu soil, an alluvial sediment, sampled from Gifu Prefecture, Japan; (2) Kyoto soil sampled from farmland owned by the Graduate School of Agriculture, Kyoto University, Kyoto, Japan; and (3) Osaka marine clay dredged at the depth of almost 10 m in Osaka Port, Japan. All the soils are sieved through a 2-mm screen (see Table 2 for basic soil properties). Zinc is the target pollutant since it is a heavy metal commonly encountered in leachates from both hazardous and municipal solid waste landfill sites. Zn is an amphoteric element that has increasing mobility under both acidic and alkaline conditions. Thus, it should be considered from a geoenvironmental viewpoint. Similar to other heavy metals found in landfills like Pb or Cu, the mobility of Zn is affected by pH and Eh (Forstner et al. 1988). Therefore, the results of this study will be helpful for evaluating the mobility of these elements.

Table 3 details the five series of adsorption tests, Series A, B, C, D, and E. A subobjective is determined for each testing series. Series A is designed to investigate the influence of Eh on Zn solubility. Thus, a strong reducing agent, dithionite ($Na_2S_2O_4$), is added to control the Eh. Series B examines the influence of pH on Zn solubility. Hence, an alkaline, sodium hydroxide (NaOH), is added to control the pH. Series C probes the effects of both Eh and pH on Zn solubility, where the microbial activities of native microorganisms found in the soil samples gradually change the pH and Eh of the soil suspensions. Series D explores the influence of dissolved organic carbon on the adsorption of Zn onto the surface of soil particles. Series E studies the effects of microbial activities on Zn solubility at the bottom of the coastal landfill sites that receive MSW incinerator ash. Thus, a solution of MSW incinerator ash mixed with the seawater (L/S=10) is used as the solvent for the batch test.

In all cases, 100 g of dry soil is mixed with the solvent in a constant solid-to-liquid ratio of 1:10. The solvent in Series A, B, and C is distilled water, while the solvent in Series D is 200 mL of distilled water mixed with 800 mL of landfill leachates. The landfill leachates are collected from an offshore landfill site

TABLE 2—*Basic properties of the soils used.*

Parameters	Gifu soil	Kyoto soil	Osaka marine clay
Liquid limit (%)	60.4	49.4	40.4
Plastic limit (%)	32.9	32.1	23.7
Grain size distribution			
2 mm–75 μm (%)	0	36.3	54.8
<75 μm (%)	100	63.7	45.2

TABLE 3—*Testing cases.*

	A Series	B Series	C Series	D Series				E Series			
Test Case	A1-A7	B1-B7	C1-C6	D1-D3	D4-D6	D7-D9	D10-D12	E1	E2	E3	E4
Soil	Gifu	Gifu	Kyoto	Gifu	Gifu	Gifu	Gifu	Osaka	Osaka	Osaka	Osaka
Solvent											
Distilled water (mL)	1000	1000	1000	200	200	200	200	⋯	⋯	⋯	⋯
Landfill leachate (mL)	⋯	⋯	⋯	800	800	800	800	⋯	⋯	⋯	⋯
Seawater (mL)	⋯	⋯	⋯	⋯	⋯	⋯	⋯	1000	⋯	⋯	⋯
Seawater+MSW[a] (mL)	⋯	⋯	⋯	⋯	⋯	⋯	⋯	⋯	1000	1000	1000
$C_6H_{12}O_6$ (mg/L)	3000	3000	3000	⋯	150	600	1500	⋯	⋯	3000	⋯
$NH_4H_2PO_4$ (mg/L)	30	30	30	30	30	30	30	300	300	⋯	⋯
CH_3COONa (mg/L)	⋯	⋯	⋯	⋯	⋯	⋯	⋯	3000	3000	⋯	⋯
$Na_2S_2O_4$ (mg/L)	⋯	⋯	⋯	⋯	⋯	⋯	⋯	1000	1000	1000	⋯
$ZnCl_2$ (mg/L)	1000	1000	1000	1000	1000	1000	1000	⋯	1000	1000	1000
Shaking time (hour)	20	20	20	20	20	20	20	20	20	20	20
Further amendment	$Na_2S_2O_4$ N_2 gas	NaOH N_2 gas	None	None	None	None	None	N_2 gas	N_2 gas	N_2 gas	N_2 gas
Initial pH	4.6∼6.5	4.7∼6.5	3.5∼6.4	2.9∼4.5	2.9∼4.1	2.9∼4.1	2.9∼4.1	10.0	9.8	10.2	9.8

[a]Solution prepared by mixing MSW incinerated ash with seawater (L/S=10, 6 h), followed by filtration.

that receives MSW incineration ash in Osaka Bay (Zhang et al. 2004). One thousand millilitres of a solution that simulates leachates in an offshore landfill that receives MSW incineration ash is used in Series E. The solution is a mixture MSW incinerated ash (collected from a MSW incineration plant) and seawater in a solid-to-liquid ratio of 1:10 that is shaken for 6 h on a shaking table and then filtered. If the microbes are provided with carbon, nitrogen, and phosphorous to enhance the microbial activities, they are added as glucose ($C_6H_{12}O_6$), dihydrogenphosphate ($NH_4H_2PO_4$), and/or sodium acetate (CH_3COONa).

Prepreparation and Temporal Maintenance of Soil Suspensions

All the soil suspensions are shaken for 20 h to reach an equilibrium state between the solid and liquid phases. Before shaking, two types of prepreparations are conducted on the suspensions to obtain different initial Eh and pH conditions. One is to adjust the initial pH value by adding 0.1 M chloride acid (HCl), and the other is to bubble the soil suspensions with N_2 or O_2 gas for 30 min. After prepreparing the samples, all the soil suspensions are shaken for 20 h. Then the first set of data is collected using 15–20 mL of the soil suspension from each reactor. The pH, Eh, and other chemical parameters are analyzed. This concludes the tests on Series D and samples in Series A, B, C, and E are further amended as described below. Then data sets are periodically collected for Series A, B, C, and E to create a temporal sequence for each sample. Prepreparation and temporal maintenance for samples in each series are detailed below.

Series A is divided into two subseries A1-A4 and A5-A7 for comparison. The former is bubbled with O_2 gas for 30 min, while the latter is bubbled with N_2 gas for 30 min in the prepreparation. Both subseries A1-A4 and A5-A7 are prepared in the same way with respect to pH. That is, the same volume of HCl is added to the corresponding pairs. After collecting the first data set, Series A is further amended by continuously bubbling the suspensions with N_2 gas. After a specific incubation period, e.g., 1, 3, 7, and 14 days, 15–20 mL of the suspension is regularly sampled from an outlet tube by an airtight syringe. Two weeks later, 0.1 M dithionite ($Na_2S_2O_4$), a reducing agent, is added to the suspensions (10 mL for A1–A4 and 20 mL for A5–A7). Then regular data sets are collected 1, 3, 7, and 14 days later. Then more dithionite is added and a final data set is collected 1, 3, 7, and 14 days afterward.

Similar to Series A, prepreparation and temporal maintenance are conducted on Series B. Samples B1–B3 are bubbled with O_2 gas, while samples B4–B7 are bubbled with N_2 gas for 30 min. The pH is adjusted in the same manner for B1–B3 and B4–B7. In the temporal maintenance of Series B, sodium hydroxide (NaOH), a strong base, is used instead of dithionite.

In the prepreparation of Series C and D, all of the soil suspensions are only bubbled with N_2 gas for 30 min. The pH adjustment in Series C is divided into two pH pairs, e.g., C1–C3 and C4–C6, while Series D is divided into four pH pairs, e.g., D1–D3, D4–D6, D7–D9, and D10–D12. The organic carbon levels are also varied in Series D. The soil suspensions in Series C are contained in closed bottles throughout the experiment. On a time interval similar to Series A, 15–20 mL of the suspension is collected.

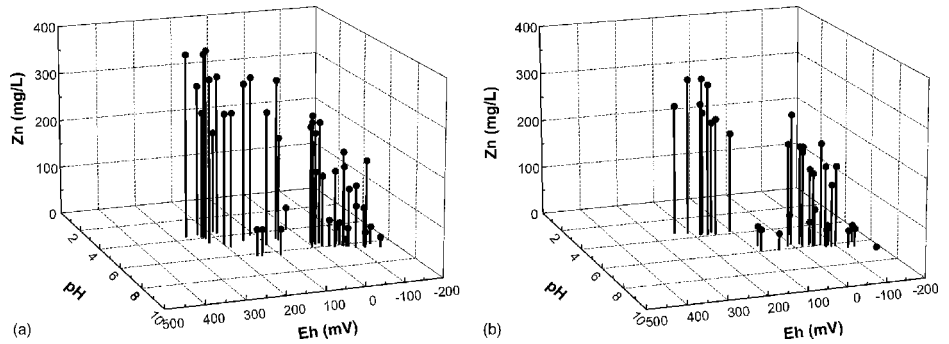

FIG. 1—*Eh and pH effects on soluble Zn concentration in Series A (Eh is controlled by adding reducing agent, (a) Cases A1–A4, (b) Cases A5–A7).*

Various concentrations and nutrients are used in the prepreparation for Series E to influence microbial activity. The pH and Eh are not adjusted. Regulatory sampling (1, 3, 7, 10, 13, 17, and 38 days later) is conducted using the method adopted in Series A, along with continuously bubbling the suspensions with N_2 gas.

Measurements and Chemical Analysis

The pH and Eh are measured immediately after collecting the sample. Then the suspensions are centrifuged at 3000 rpm for 20 min and the supernatants are filtered through syringe filter with a 0.45 μm pore size. The total organic carbon (TOC) and Zn concentration of the filtered solutions are analyzed by a Total Organic Carbon Analyzer (TOC-5050A, Shimadzu) and an inductively coupled plasma spectrometry (ICPS-8000, Shimadzu), respectively. The total adenosine triphosphate (ATP) concentration in the soil suspension of Series E is determined by regressing from the RLU (relative light unit) value measured with ATP analyzing system (Uni-Lite®, Biotrace International). ATP is the energy molecule for microorganisms and a higher value indicates a higher microbial activity under aerobic conditions.

Test Results and Analysis

Effects of Eh through Addition of a Reducing Agent on Zn Mobility

In Series A, dithionite is employed as a reducing agent to gradually lower the redox potentials of the soil suspensions. In fact, several researchers have used this method to maintain a low Eh in soil systems (Chen et al. 1987; Stucki 1988). The dithionite ion, $S_2O_4^{2-}$, may be conceptualized as two sulfoxyl (SO_2^-) radicals joined by a S-S bond. Due to a weak link of the S-S bond, the $S_2O_4^{2-}$ ion reversibly dissociates to form two SO_2^- radicals that are highly reactive reductants.

Figure 1 shows the soluble Zn concentrations against Eh and pH in samples A1–A4 and A5–A7. As previously mentioned, the former suspensions (A1–A4) are subjected to 30 min of oxygen gas, while the latter (A5–A7) are exposed to 30 min of nitrogen gas before 20 h of shaking. Consequently, the difference in the initial pH and Eh conditions and the initial Zn concentrations are established as indicated by the bars in the left-back corners of Fig. 1.

Figure 1 indicates that soluble Zn tends to decrease as the pH increases and the Eh decreases. The Eh-pH diagram analysis (not shown) indicates that the decrease in the Zn concentration is due to the formation of zinc hydroxides and sulfides, mainly generated by acid-base reactions and redox reactions, respectively. Comparing the correlation of the Zn concentration against the pH and Eh among different suspensions determined that the concentration of soluble Zn initially depends on the change in pH, and then depends on the change in Eh. This is consistent with the fact that the initial pH values determine the initial Zn concentrations. The variations in the pH significantly influence the Zn concentration, while the variations in Eh only moderately affect the Zn concentration.

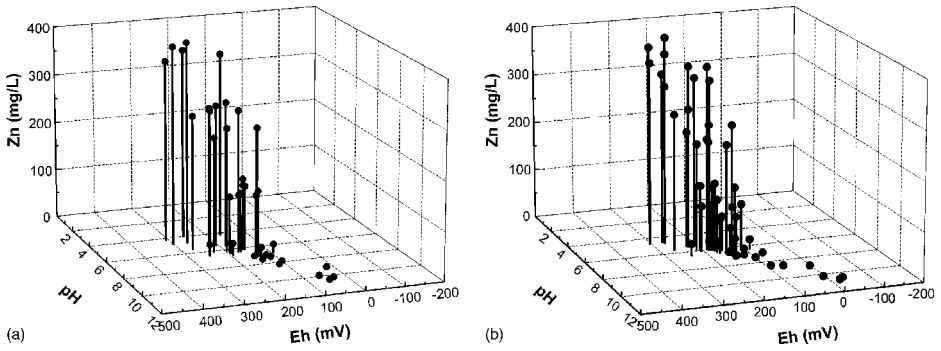

FIG. 2—*Eh and pH effects on soluble Zn concentration in Series B (pH is controlled by adding sodium hydroxide, (a) Cases B1–B3, (b) Cases B4–B7).*

The addition of a reducing agent to the soil suspensions simultaneously decreases the Eh and increases the pH since the redox reaction consumes hydrogen, which shifts the pH from a lower to a higher value. Thus, the decreased Zn concentration upon adding a reducing agent is due to both redox and pH effects, although the redox effect dominates the process.

Effects of pH through Addition of Base on Zn Mobility

Figure 2 show the relationship between the soluble Zn and pH and Eh for samples B1–B3 and B4–B7, when the pH is increased stepwise by adding an alkaline solution, sodium hydroxide, to the soil suspensions. As shown in Fig. 2, when the pH increases above 7, the Zn concentration decreases to zero due to the formation of zinc hydroxide precipitates in the soil suspensions. Figure 3 replots the data shown in Fig. 2 when the Eh data is ignored. The Zn-pH points shown in Fig. 3 are distributed in a narrow area, which reveals that under oxidized conditions, the solubility of Zn is mainly controlled by pH and the influence of Eh is negligible. This is consistent with the result of Kamon et al. (2002), who conducted similar batch adsorption tests using Osaka marine clay.

Leachates from MSW incineration residuals are reported to have a pH as high as 10. The test results from Series B suggest that the formation of zinc hydroxide is mainly responsible for the attenuation of Zn in landfills that receive MSW incineration residuals.

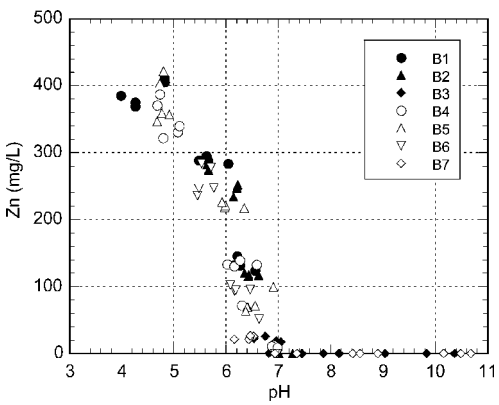

FIG. 3—*Changes in soluble Zn concentration with pH in Series B (pH is controlled by adding sodium hydroxide).*

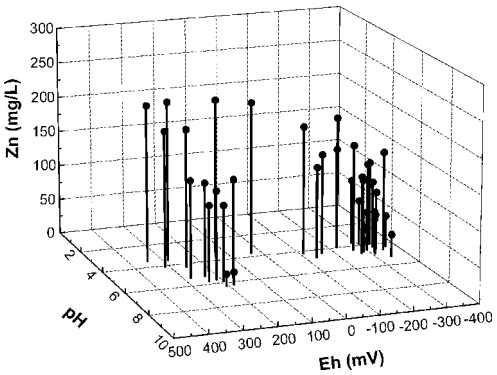

FIG. 4—*Eh and pH effects on the soluble Zn concentration in Series C (pH and Eh is gradually changed by the microbial activities of native micro-organisms).*

Effects of Eh and pH due to Microbial Activities on Zn Mobility

Although nutrients are added to the soil suspensions in Series A and B in order to support microbial activities (see Table 3), obvious changes in the total organic carbon (TOC) are not observed (data not shown). Therefore, it is concluded that microbial activities do not contribute to the reactions in Series A and B. This is probably due to an insufficient supply of microbes in the Gifu soil.

To highlight the influence of microbes on the solubility of Zn in a soil-water system, soil collected from farmland owned by Kyoto University is used in Series C since it is believed to contain numerous active microbes. After the initial pH adjustment and 20 h of shaking, the soil suspensions in Series C are kept in bottles that are closed from the atmosphere. The bottles are only disturbed when data is collected for regular analyses.

Figure 4 shows the effects of Eh and pH on the soluble Zn concentrations for C1–C6. The most important phenomenon observed from Series C is that the Eh values decrease from the initial values between 211–346 mV to as low as −282−−364 mV within the 22-day cultivation period. Figure 5(*a*) shows the results for sample C2 as a representative of the Series C and the concentration of soluble Zn decreases from 223.6 to 92.1 mg/L when the Eh decreases from 346 mV to −282 mV and pH increases from 3.49 to 3.74. Both the increased pH and decreased Eh are responsible for the decrease in Zn concentration. However, the redox reaction plays a more important role in the Zn decrease since the pH varies in the strong acidic area and the increment of change is only 0.25 pH values. Figure 5(*b*) indicates that over 22 days the total organic carbon (TOC) decreases from 1207 to 857.1 mg/L, while the inorganic carbon (IC) increases from 0 to 162.9 mg/L. This is reasonable due to the microbial turnover of organic

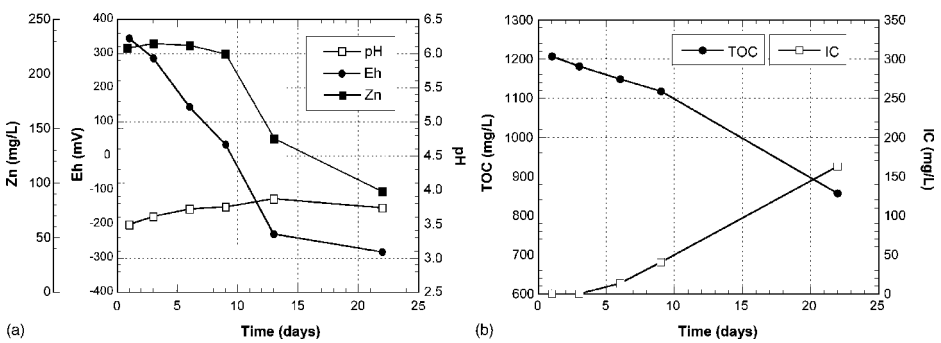

FIG. 5—*Changes in (a) Eh, pH, and soluble Zn and (b) TOC and IC with incubation time for Kyoto soil sample C2 (pH and Eh is gradually changed by the microbial activities).*

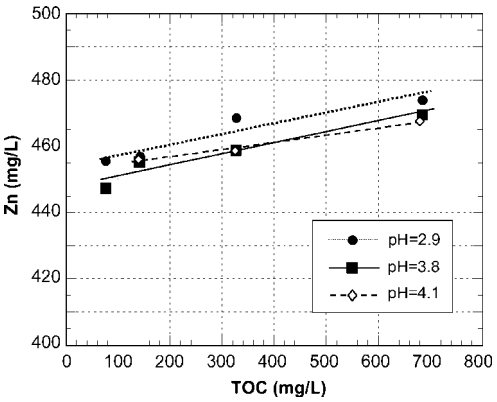

FIG. 6—*Effect of TOC on soluble Zn at different pH values in Series D (DOC concentration is controlled by adding glucose).*

carbon to inorganic carbon. Therefore, it is concluded that the microbial activities cause the variations in pH and Eh, which, in turn, reduce the concentration of soluble Zn. Although Zn is not directly subjected to a redox transformation due to its single valence state, its soluble levels are influenced by a number of processes that are regulated by the redox potential. Under oxidizing conditions, Zn is associated with Fe(III) and Mn(IV) oxides and soluble phases. However, under reducing conditions, Zn tends to be associated with insoluble sulfides, large molecular humic compounds, and carbonates, which all decrease the mobility (Guo et al. 1997).

It is interesting to compare the results from Series C to Series A. In the former, biochemical reactions dominate, while chemical reactions dominate in the latter. The available data supports the hypothesis that anaerobic respirations in a closed soil-water system might attenuate Zn as effectively as a strong reducing agent. However, quantitatively comparing the chemical and biochemical effects on Zn attenuation using the results from Series A and C is inadequate since different soils are used in Series A and C and the microbes themselves have the ability to adsorb heavy metals.

Effects of Dissolved Organic Carbon (DOC) on Zn Mobility

The objective of Series D is to investigate the interaction between heavy metals and dissolved organic carbon and possible influences on Zn solubility. It is determined from Series B that under oxidized conditions, the solubility of Zn is mainly controlled by pH and the Eh has a negligible influence. Therefore, for analytical simplicity, Series D only investigates the pH and dissolved organic carbon (DOC), and ignores the Eh. The definition of DOC is operational and includes all of the dissolved organic materials that pass through a 0.45 μm filter (Buffle et al. 1992). Since a simple organic compound (glucose) is used in Series D, the dissolved organic carbon (DOC) is referred to as total organic carbon (TOC).

Figures 6 and 7 show representative data from Series D. Figure 6 reveals that at the given pH levels, pH 2.9, 3.8, and 4.1, the Zn concentration in solution linearly increases with the TOC. For example, the soluble Zn increases from 450 to 470 mg/L as the TOC increases from 100 to 700 mg/L. Figure 7 shows the influence of both pH and TOC on the Zn concentration.

The results from Series D support the hypothesis that the mobility of Zn is enhanced, to some degree, by increasing the TOC. This is probably due to the formation of metal-organic carbon complexes. Organic molecules with more than one electron-donating functional group may form polydenatate complexes with the same cation, which are called chelates. Due to the high stability and compensation of the positive charge, dissolved chelate complexes can increase the mobility of metal ions (Schulin et al. 1995).

Similar to these results, Christensen et al. (1996) also reported an increased heavy metal solubility as the DOC increased. It has been concluded that dissolved organic carbon from landfill polluted groundwater do complex with heavy metals such as Cd, Ni, and Zn, but the effect has only minor practical implications on heavy metal mobility (Christensen et al. 1996).

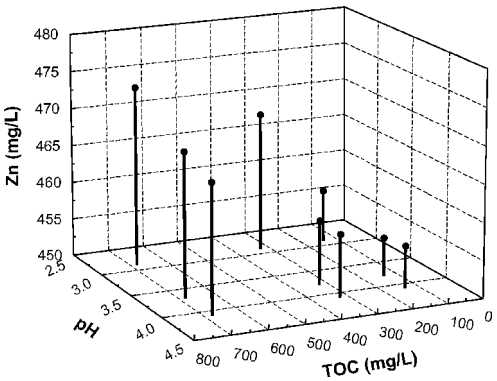

FIG. 7—*Effects of TOC and pH on soluble Zn in Series D (DOC concentration is controlled by adding glucose).*

Since the pH area investigated ranges from 2.9 to 4.1, which is too narrow, it is difficult to make conclusive remarks about the TOC-pH correlation. Richards et al. (2000) explained that the contribution of DOC on metal transport should be magnified as pH increases, but the overall mobility is greater at low pH due to the increased solubility of DOC and the very low solubility of metals in neutral to alkaline pH soils.

Zn Mobility in Offshore Landfill Sites that Receive MSW Incinerated Ash

The objective of Series E is to investigate the biochemical effects on Zn solubility at offshore landfill sites. Therefore, seawater or a solution that has a 1:10 solid-to-liquid ratio of MSW incinerated ash and seawater as well as Osaka marine clay is used in the modified batch leaching tests.

E1 is designed to evaluate the microbial activities in clay deposits at the bottom of offshore landfill sites and their effects on the chemical conditions. Figure 8 shows the temporal changes in pH, Eh, TOC, ATP, and sulfide concentration with incubation time for E1. Along with a gradual decrease in TOC, the ATP concentration continuously increases for the first five days and then rapidly decreases to approximately 0.01 μM. Along with the rapid reduction in ATP concentration, Eh also decreases like in Series C from about 0 mV to lower than −400 mV. These changes in ATP and Eh imply that the initial aerobic respiration is transformed to anaerobic respiration since the amount of ATP generated by the microbial activity under anaerobic conditions is significantly reduced compared to aerobic conditions. Another important finding in Fig. 8 is that under strongly reduced conditions, the sulfide concentration increases with incubation time ($Eh < -400$ mV). This sulfide generation will immobilize the heavy metals by forming insoluble sulfides.

The results for E1 indicate that if native micro-organisms in the marine clay are active, then the clay-leachate system is in strongly reduced conditions and the Zn mobility is reduced by forming insoluble sulfides. However, when MSW incinerator ash is involved, the high alkalinity caused by the MSW incinerator ash could significantly influence both the microbial activity and heavy metal mobility. Therefore, E2, E3, and E4 probe the effects on related biochemical processes and Zn mobility under alkaline conditions using a solution that is a mixture of MSW incinerated ash and seawater with a liquid-to-solid ratio of 10 for the modified batch test.

E3 represents Series E in Fig. 9, which shows that the pH constantly decreases from 10.2 to 6.7 during the first 17 days of incubation and the TOC also gradually decreases from 700 to 570 mg/L. Although the ATP concentration is low, about 1×10^{-3} μM, during the first three days, it drastically increases up to 5×10^{-3} μM over the next four days (seven days total) and then rapidly decreases to approximately 2×10^{-3} μM. Figure 10 shows the relationship between the ATP concentration and pH and Eh for samples E2–E4, which has various kinds and concentrations of nutrients. Figure 10 also shows that the ATP concentrations increase, but their values depend on the concentration of nutrients (lowest in E4), as the pH decreases. Another tendency is that the ATP concentration is higher the lower pH when Eh ranges from −100 to 100 mV. Figures 9 and 10 both imply that aerobic respiration, which is indexed by the ATP

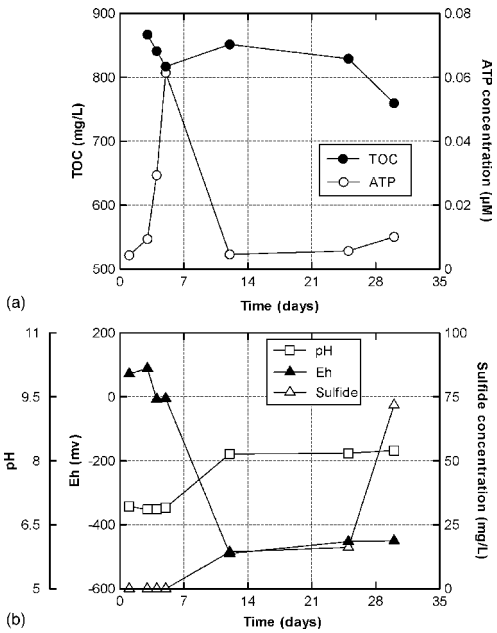

FIG. 8—*Changes in (a) TOC and ATP concentrations and (b) pH, Eh, and sulfide concentration with incubation time for sample E1 (microbial activity is enhanced in the seawater).*

concentration, is initially enhanced as the pH decreases. This could be due to (1) the alkaline attenuation by the seawater and the clay and (2) the formation of organic acids by the microbial activity. Then as the Eh gradually begins to decrease, and the ATP concentration drastically decreases, the aerobic respiration changes into anaerobic respiration. However, the ATP concentrations are one order of magnitude lower and Eh values are much higher than those in E1. These results indicate that microbial activity is reduced by alkali and other chemical components leached from MSW incinerated ash.

Figure 11 shows the soluble Zn concentrations that are affected by pH in E2-E4 when the pH gradually decreases with incubation time due to microbial activity. Before incubation, the initial pH values for E2–E4 are near 10 and the soluble Zn concentration is extremely low due to the formation of zinc hydroxide. However, Figure 11 shows that the soluble Zn concentration increases as the pH decreases, but the pH of the solution is much lower than the other series. In particular, when pH is lower than 7.5, drastically higher Zn concentrations are observed. This result is almost consistent with Fig. 3 where the pH is controlled by adding chemical agents.

The results in Fig. 11 imply that under alkaline conditions where Zn exists as a hydroxide, the microbial activity has an adverse effect on the stabilization of Zn since it dissolves the zinc hydroxide. However, in the long term, the bottom clay layers may provide moderate to strong reduction conditions as observed in E1. Thus, the related biochemical processes may reduce the Zn mobility by forming insoluble Zn complexes such as zinc sulfide. Therefore, long-term, experimental studies and in situ monitoring of the biochemical parameters will be useful for examining the immobilization of heavy metals implicated from the results for E1.

Conclusions

In this research, modified batch tests were conducted to investigate the effects of pH and Eh, derived from both chemical and biochemical reactions, on Zn mobility in bottom clay liners of coastal landfill sites. The following conclusions are drawn.

1. Microbial activities in closed soil-water systems result in a strongly reduced environment similar

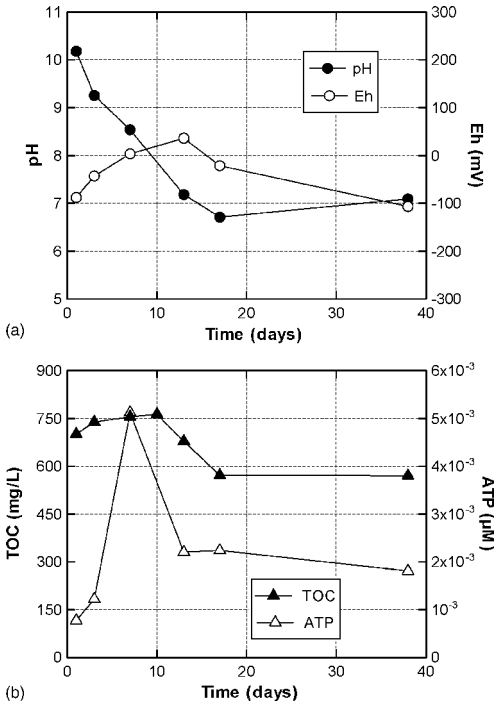

FIG. 9—*Changes in Eh, pH, ATP, and TOC with incubation time for sample E3 (microbial activity is enhanced in a solution of MSW incinerator ash mixed with the seawater).*

to that controlled by a strong reducing agent. Both the reducing conditions effectively attenuate Zn by forming sulfides, but the high alkalinity induced by municipal solid waste incinerator ash leads to a relatively lower microbial activity and less reduced conditions.

2. Dissolved organic carbon in leachates mainly serves as a sufficient bioavailable carbon source for microbial metabolism. These microbial activities promote anaerobic conditions in landfills, which dominate most of the landfill life and establish a chemical framework that effectively immobilizes most heavy metals.

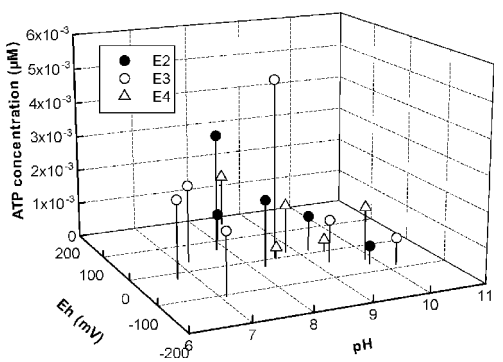

FIG. 10—*Effects of Eh and pH on ATP concentration for Osaka marine clay samples E2 to E4 (microbial activity is enhanced in a solution of MSW incinerator ash mixed with the seawater).*

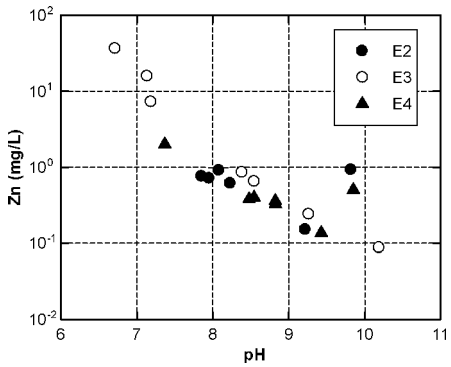

FIG. 11—*Changes in soluble Zn concentrations with pH values in E2 to E4 (microbial activity is enhanced in a solution of MSW incinerator ash mixed with the seawater).*

3. Dissolved organic carbon can form soluble complexes with heavy metals, which increases the concentration of the metals and is responsible for the leaching of heavy metals in the acidification stage along with lowering the pH. The formation of metal-organic carbon complexes has a minor significance on heavy metal leaching compared to lowering the pH.
4. The microbial activity effectively contributes to the long-term immobilization of heavy metals by forming insoluble complexes such as sulfides. However, when heavy metals precipitate as hydroxides under highly alkaline conditions induced by disposing of incinerator residues, organic acids are formed by the microbial activity and may lead to the dissolution of the hydroxides.

Acknowlegments

Financial support from the Japan Society for the Promotion of Science for this study is greatly acknowledged. The laboratory experiments were conducted with the cooperation of K. Yajima and Y. Maeda, graduate students at Kyoto University.

References

Buffle, J., Peret, D., and Newman, M., "The Use of Filtration and Ultrafiltration for Size Fractionation of Aquatic Particles, Colloids, and Macromolecules," *Environmental Particles*, edited by J. Buffle and H. P. van Leeuwen, Lewis Publishers, Inc., Boca Raton, FL, 1992, pp. 171–230.

Chen, S. Z., Low, P. F., and Roth, C. B., "Relation between Potassium Fixation and Oxidation State of Octahedral Iron," *Soil Sci. Soc. Am. J.* 51, 82–86 (1987).

Christensen J., Jensen, D. L., and Christenson, T. H., "Effect of Dissolved Organic Carbon on the Mobility of Cadmium, Nickel and Zinc in Leachate Polluted Groundwater," *Water Res.* 30, 3037–3049 (1996).

Forstner, U., Kerstern, M., and Wienberg, R., "Geochemical Processes in Landfills," *The Landfill: Reactor and Final Storage*, edited by P. Baccini, Springer-Verlag, Berlin, 1988, pp. 39–82.

Guo, T., DeLaune, R. D., and Patrick, W. H., Jr., "The Influence of Sediment Redox Chemistry on Chemically Active Forms of Arsenic, Cadmium, Chromium, and Zinc in Estuarine Sediment," *Environ. Int.* 23, 305–316 (1997).

Hutchison, I. P. and Ellison, R. D., *Mine Waste Management*, Lewis Publishers, Inc., Chelsea, MI, 1992.

Kamon, M., Zhang, H., and Katsumi, T., "Redox Effects on Heavy Metal Attenuation in Landfill Clay Liner," *Soils Found.* 42, 115–127 (2002).

Kjeldsen, P., Barlaz, M. A., Rooker, A. P., Baun, A., Ledin, A., and Christensen, T. H., "Present and Long-Term Composition of MSW Landfill Leachate: A Review," *Critical Reviews in Environmental Science and Technology* 32, 297–336 (2002).

Lovley, D. R. and Phillips, E. J. P., "Novel Mode of Microbial Energy Metabolism: Organic Carbon

Oxidation Coupled to Dissimilatory Reduction of Iron and Manganese," *Appl. Environ. Microbiol.* 54, 1472–1480 (1988).

Lyngkilde, J. and Christensen, T. H., "Redox Zones of a Landfill Leachate Pollution Plume (Vejen, Denmark)," *J. Contam. Hydrol.* 10, 273–289 (1992).

Richards, B. K., Steenhuis, T. S., Peverly, J. H., and McBride, M. B., "Effect of Sludge-Processing Mode, Soil Texture and pH on Metal Mobility in Undisturbed Soil Columns under Accelerated Loading," *Environ. Pollut.* 109, 327–346 (2000).

Rugge, K., Bjerg, P. L., and Christensen, T. H., "Distribution of Organic Compounds from Municipal Solid Waste in the Groundwater Downgradient of a Landfill (Grindsted, Denmark)," *Environ. Sci. Technol.* 29, 1395–1400 (1995).

Schulin, R, Geiger, G., and Furrer, G., "Heavy Metals Retardation by Soil Organic Matter under Changing Environmental Condition," *Biogeodynamics of Pollutants in Soils and Sediments—Risk Assessment of Delayed and Non-Linear Responses*, edited by W. Salomons and W. M. Stigliani, Springer, Berlin, 1995, pp. 53–85.

Stucki, J. W., "Structural Iron in Smectites," *Iron in Soils and Clay Minerals*, edited by J. W. Stucki, B. A. Goodman, and U. Schwertmann, 1988, pp. 625–675.

Tate, R. L., *Soil Organic Matter: Biological and Ecological Effects*, John Wiley & Sons, Inc., New York, 1987.

Zhang, H., Kamon, M., and Katsumi, T., "Effect of Acid Buffering Capacity on the Long-Term Mobility of Heavy Metals in Clay Liner," *Soils Found.* 44(6), 111–120 (2004).

Journal of ASTM International, Vol. 3, No. 7
Paper ID JAI13332
Available online at www.astm.org

Loretta Y. Li,[1] *Gevan Mattu,*[2] *Don McCallum,*[3] *Ken Hall,*[4] *and Min Chen*[5]

The Temporal and Spatial Dynamics of Trace Metals in Sediments of a Highly Urbanized Watershed

ABSTRACT: The Brunette watershed (7200 ha) is located in the urbanized metropolitan area of Greater Vancouver, Canada. It is an area of high traffic density and extensive impervious surfaces (paved roads and roof tops). This watershed provides an excellent area for the study of the spatial and temporal trace metal contamination in sediments. Street surface, stream, and lake sediments were collected over a 25-year period and analyzed for total and acid-extractable trace metals (Cu, Fe, Mn, Pb, and Zn). Lead concentrations in all areas have decreased dramatically, directly as a result of the discontinuation of lead addition to fuels in the 1970s. The mean concentration of total lead in stream sediments has decreased from 230 in 1973 to 134 and 36–66 mg/kg in 1993 and 1997–1998, respectively. Manganese, especially the acid extractable fraction, increased during the early 1990s when MMT replaced tetraethyl lead as an antiknock compound. The 0.5 M HCl extractable manganese in stream sediments has increased from 18 in 1973 to 545 in 1993 and 162–273 mg/kg in 1997–1998. Burnaby Lake, a shallow (Z_{av}=1.0 m, 140 ha) lake, has acted as a sink for trace metal contaminated sediments. Highest trace metal levels are found in surface sediments at the east end of the lake (where Cu, Pb, and Zn were 159, 179, and 529 mg/kg) containing more silt (24 %) and higher organic matter (32.5 %). The sandy delta of Still Creek (silt<4 %, organic matter 5.6 %), which contributes over 50 % of the flow to the lake, has lower trace metal levels (Cu, Pb, and Zn were 72, 77, and 207 mg/kg) even though the creek is the predominant source of trace metals transported to the lake.

KEYWORDS: watershed, sediment, trace metals, traffic, land use

Introduction

The growth of population and intensive human activities are causing increasing pollution in our urban watersheds. Industrial enterprises constitute the major point sources of pollution, whereas roadways and the transportation network in general, with their associated impervious surfaces, leading to surface runoff to our urban streams, comprise the major distributed source of pollution in urban watersheds. The runoff from roadways and the transportation network may contain high concentrations of metals, in particular lead, zinc, iron, chromium, cadmium, nickel, and copper, resulting from the continuous wear of brakes, tires, and other vehicles parts (FHWA 1998). Surface water such as lakes and streams are particularly vulnerable because they are directly exposed to contaminants released into the air and to direct discharges from point and non-point sources (Young et al. 1996). Roadway runoff sediments tend to be heavily contaminated with Zn, Cu, and Pb (Albasel and Cottenie 1985; Mikkelsen et al. 1996; Norrstrom and Jacks 1998; Pagotto et al. 2000).

Trace metals are of particular importance due to their potential toxic effects on aquatic organisms. The association of trace metals with suspended solids and bed sediments, and the dynamic nature of the stream environment, have generated interest in the past three decades in determining the accumulation and concentrations of key trace metals in sediments (e.g., Yousef et al. 1990; Xanthopoulos and Hahn 1990;

Manuscript received March 31, 2005; accepted for publication May 27, 2005. Presented at ASTM Symposium on Contaminated Sediments: Evaluation and Remediation Techniques on 23–25 May 2006 in Shizuoka, Japan; M. Fukue, K. Kita, M. Ohtsubo, and R. Chaney, Guest Editors.

[1] Associate Professor, Department of Civil Engineering, The University of British Columbia, 6250 Applied Science Lane, Vancouver, B.C. Canada V6T 1Z4.
[2] Engineer, Environmental Protection Branch, Environment Canada, 201-401 Burrard Street, Vancouver, B.C. Canada V6S 3S5.
[3] Engineer, Gartner Lee Ltd., 490-6400 Roberts Street, Burnaby, B.C. Canada V5G 4C9.
[4] Professor, Department of Civil Engineering, The University of British Columbia, 6250 Applied Science Lane, Vancouver, B.C. Canada V6T 1Z4.
[5] Graduate Assistant, Department of Chemical and Biological Engineering, The University of British Columbia, 2216 Main Mall, Vancouver, B.C. Canada V6T 1Z4.

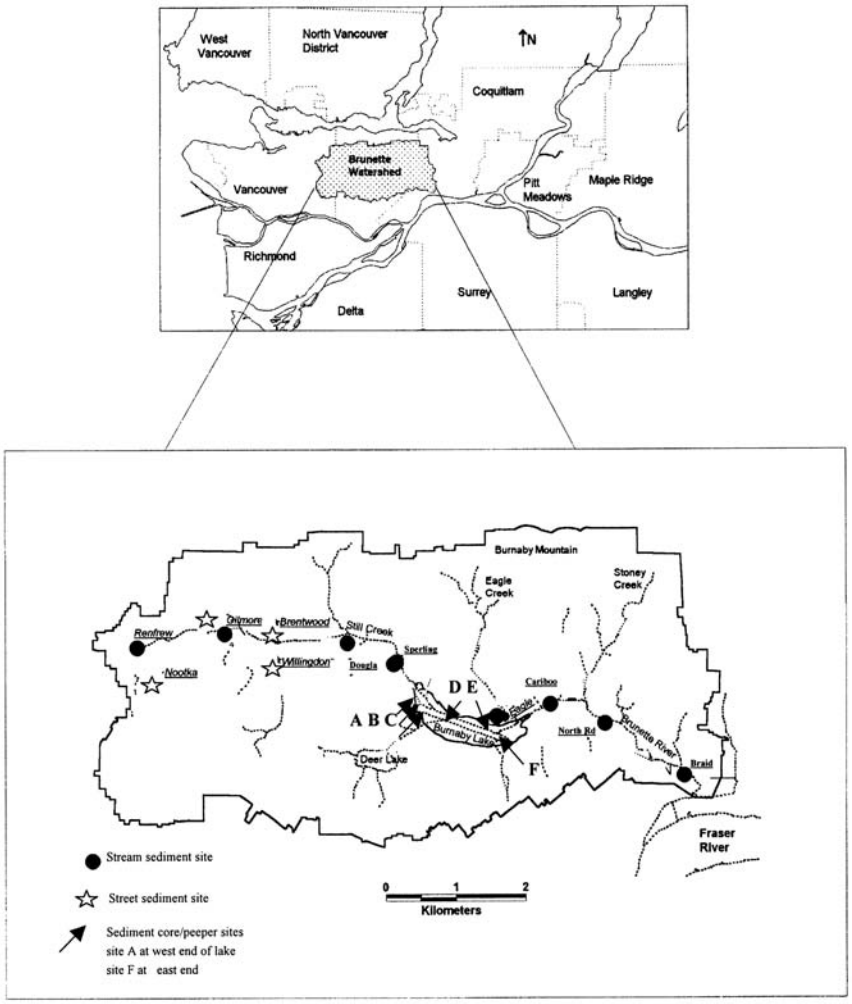

FIG. 1—*Location of the Brunette River watershed and sampling sites.*

Grottker 1990; Lee et al. 1997; MacDonald et al. 1997; Kayhanian et al. 2003). Others have sought to determine whether or not these contaminants are available to aquatic organisms (Morrison and Revitt 1987; Revitt et al. 1990; Bindra and Hall 1977).

The Brunette River watershed (7200 ha) is an area of high traffic density and extensive impervious surfaces (paved roads and roof tops) located in the urbanized metropolitan area of Greater Vancouver, British Columbia, Canada (Fig. 1). Two lakes—Burnaby and Deer Lakes—and a number of streams, including Still Creek and the Brunette River, are located in the watershed. Still Creek provides 50 % of the flow into the lake, whereas the Brunette River discharges the runoff from the watershed to the Fraser River. The watershed serves as an important transportation corridor with two major highway transportation corridors passing through it, including Highway 1 and the Lougheed Highway. Its trace metal pollution has been studied since the 1970s. Considerable data on water quality, urban hydrology, and trace metals, both in water and in sediment, have been collected over an almost 30-year period (McCallum 1995; Yuan 2000). This watershed provides an excellent area to study the spatial distribution and temporal dynamics

of trace metal contamination in sediment. The objectives of this study include: (1) Identification of the extent and severity of trace metal contamination in streambed and lakebed sediments in the watershed; (2) Quantification of changes in sediment trace metal concentrations over the last 25 years; (3) Assessment of changes in land activity, land cover, and traffic density in the watershed over the same period; (4) Identification of relationships between land use (land activity, land cover, and traffic) and trace metal contamination in sediments; and (5) Determination of correlations among the trace metals in the stream sediments.

Methodology

Sampling

Sampling sites on streets and in streams were chosen in April 1998 to correspond with sites sampled in May 1973 (Hall et al. 1976) and July 1993 (McCallum 1995), shown in Fig. 1. Street samples were collected along curbed areas with a plastic scoop, whereas stream samples were collected with an aluminum pot affixed to a 3 m wooden pole. Lake sediment cores of approximately 300 mm were taken with a 1 m piston corer, extruded in the laboratory, and cut into 2 cm segments. All sediment samples were placed in plastic bags and frozen at -20°C until analysis. Thawed samples were wet sieved (180 μm stainless steel sieve). Sieved sediments were dried at 104°C for 24 h and disaggregated.

Digestion and Trace Metal Analysis

One to two gram samples of dried sediment were digested on a hot plate using either nitric acid or aqua regia, as described in Method 3030 of Standard Methods (APHA 1989) for total metals. For extractable trace metals, 2 g of dried sediment were extracted at room temperature with 20 mL of 0.5 M HCl in screw cap tubes on a mechanical shaker overnight. Samples were filtered and the extract made up to 40 mL with distilled water. Digested samples were analyzed by atomic absorption spectroscopy (Thermo Jarrell Ash Video 22 AA). In 1998, the acid extractable metals were analyzed with a Thermo Jarrell Ash ICAP 61 instrument operated in the ICP-AES mode. The precision of the methodology was determined by performing duplicate analysis on duplicate or triplicate grab samples from each station, whereas the accuracy was evaluated by analyzing a certified reference soil during each analytical period.

Statistical Analysis

Nonparametric statistics were used to detect differences in the sample populations since the data were not normally distributed. The Wilcoxon signed-rank test and Friedman test were employed to detect significant changes in one sampling area over time. The Wilcoxon signed-rank test detects the differences in the distributions of two related variables while the Friedman test was applied to detect the differences of $k(k>2)$ related variables. Relationships between trace metals were analyzed using Spearman rank correlation coefficients (Iman and Conover 1983). The data are displayed using box-whisker plots.

Results and Discussion

Street Sediments

The total concentrations of trace metals (Cu, Mn, Pb, and Zn) in street surface dirt are presented in Fig. 2. These results indicate that copper concentrations in street sediments have decreased since 1973, even though urbanization has increased in the watershed. This decrease appears to be attributable to the phasing out of several metal foundaries in the Still Creek sub-watershed.

Manganese increased dramatically in 1993 and then returned to 1973 levels by 1998. This appears to be attributable to the replacement of lead with manganese [in the form of (MMT), i.e., methylcyclopentadienyl manganese tricarbonyl, a manganese-based gasoline additive] as an antiknock agent in gasoline in the 1980s. In the late 1990s many fuel suppliers started removing MMT from gasoline due to environmental contamination concerns (Loranger et al. 1994; Lytle et al. 1995; Brault et al. 1994). Over the same period, lead decreased dramatically between 1973 and 1993 and remained low as it was phased out of gasoline as an antiknock additive.

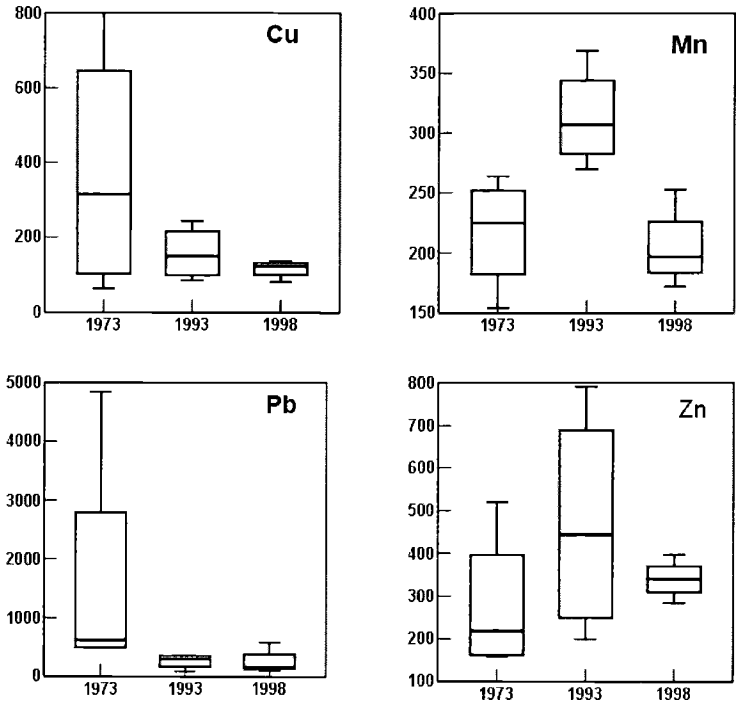

FIG. 2—*Changes of total metal concentration in street sediments from 1973 to 1998 illustrated using box-whisker plots (units in* mg/kg*) n=4 stations.*

Zinc has increased in street surface contaminants between the 1970s and 1990s, most likely as a result of larger volumes of traffic in the watershed. Corrosion of galvanized components on vehicles is believed to be a major source of zinc contamination on roadways (Ward 1990).

Surface Stream Sediments

The total and acid extractable levels of Cu, Mn, Pb, and Zn in surface stream sediments are presented in Fig. 3. Total copper has followed the street surface Cu contamination, with the range of concentrations decreasing dramatically since the 1970s. The extractable copper is usually less than half of the total copper. Median copper concentrations are below the probable effects level (PEL) for the protection of freshwater aquatic life, but are usually higher than the threshold effects level (TEL).

The manganese in stream sediments has followed the street contamination profile, with much higher levels in 1993. The extractable manganese was almost negligible in 1973, but increased to over 50 % of the total Mn in 1993. The high level of manganese in the Brunette water system may be a consequence of MMT combustion products, possibly in the forms of manganese phosphates, oxides, and sulphates (Ethyl 1997). These would certainly contribute to the acid-extractable fraction of manganese. They are deposited on the urban impervious surfaces and discharged into the water by surface runoff. The manganese oxides could also act as scavengers to absorb other trace elements from the water.

The lead in stream sediments remained relatively high up to 1993 but decreased dramatically in 1998. Thus changes have lagged behind the decrease in street sediments by several years. Median values of both total and extractable lead exceeded the PEL in 1993 but fell below this level in 1998. However, median levels of lead still exceeded the TEL.

Similar results were observed by Lee et al. (1997) during the sampling period between 1993 and 1995,

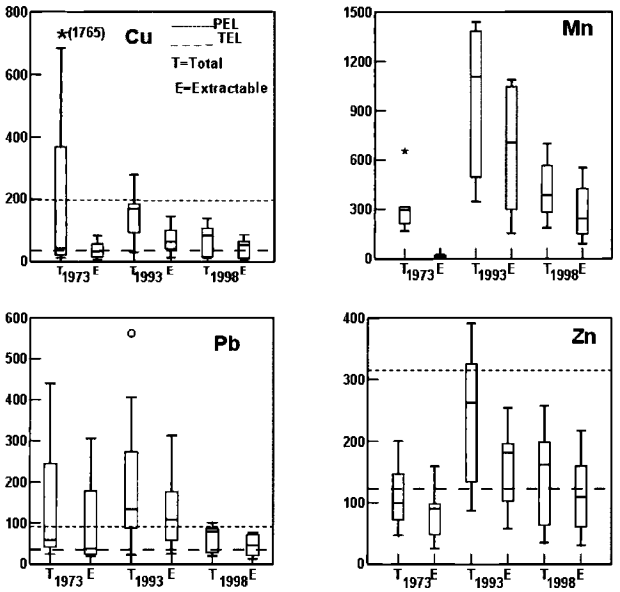

FIG. 3—*Changes of metal concentration in stream sediments from1973 to 1998 illustrated using box-whisker plots (units in* mg/kg*). Thresheld effects level (TEL) and probable effects levels (PEL) for fresh-water sediments also presented, n*=8 *stations.*

where the settling particles in the highway retention pond had concentrations of 55.4 μg/g for Pb and 681.7 μg/g, for Mn. The high manganese concentration and the comparatively low lead concentrations could be due to the change in fuel additives.

Zinc stream sediment concentrations have followed the same temporal pattern as the street dirt contamination. The acid extractable or potentially available zinc is usually >50 % of the total zinc. Zinc concentrations are well below the PEL, but total zinc concentrations exceeded the TELs in the 1990s.

Lake Sediments

The average total and acid extractable trace metals in the top 300 mm of lake sediment appear in Fig. 4. These data are presented as concentrations in the mineral matter of the sediment since the organic matter from aquatic macrophytes (pond lilies) and a beaver lodge near site/station D tend to distort the spatial distribution of the lake trace metals. These data are presented from the upstream end of the lake, where Still Creek enters, to the discharge eastern end of the lake at the Brunette River outlet. Still Creek provides more than 50 % of the flow to Burnaby Lake and is the most highly urbanized subwatershed in this drainage.

The upper three stations (A, B, and C) in the lake are highly influenced by Still Creek. Sediments from these three stations represent deposits of sandy sediments from this sub-watershed. The highest concentrations of the more toxic trace metals—Cu, Pb, and Zn—were found at the two stations at the eastern end of the lake. The finer silt and clay fractions of sediment, which usually contain higher concentrations of trace metals, appear to be transported along the lake before being deposited in the lake sediment. During major rainfall events, Burnaby Lake with an average depth of <1 m, can have a residence time of less than one day, allowing finer more contaminated sediments to be transported along the lake.

The lake sediments appear to be acting as a sink for trace metal accumulation since the concentrations of Cu, Pb, and Zn, especially in the eastern end of the lake, are higher than in the stream sediments, and all exceed the PEL. This represents very unfavorable conditions for organisms associated with the sediments, especially if one considers the cumulative effects of these toxic metals.

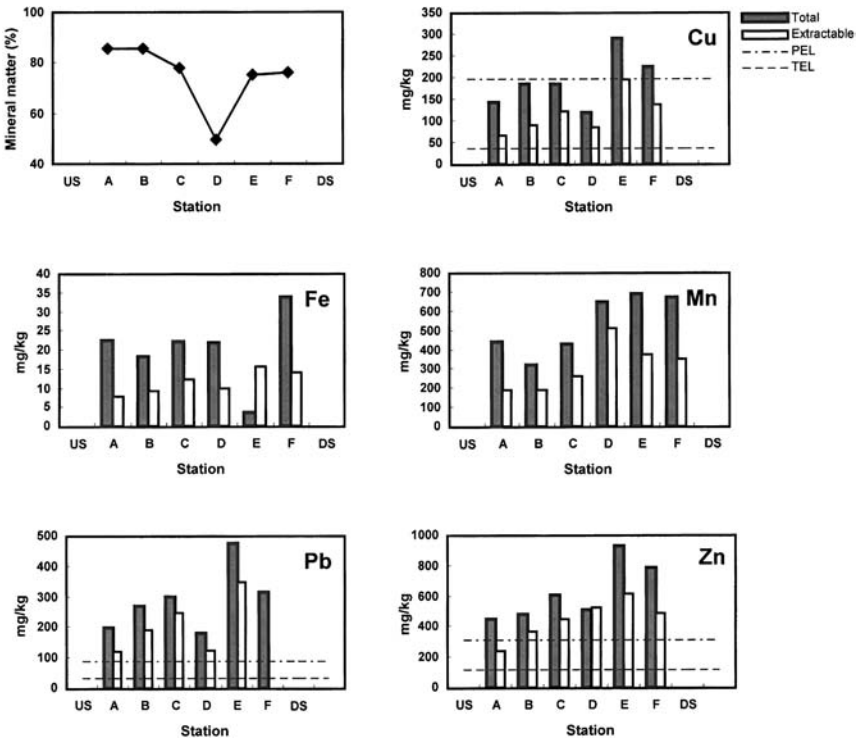

FIG. 4—*Trace metal in mineral component of Lake Sediments (1998). Data are presented from upstream (US) (Still Creek inlet) to downstream (DS) (Brunette R. outlet) in the lake. Thresheld effect levels (TEL) and probable effect levels (PEL) for freshwater aquatic sediments presented.*

Relationships of Land Use and Activity with Trace Metal Concentrations in Stream Sediments

The effects of land use and land activity (traffic intensity) on trace metal levels found in the stream sediments of the subwatersheds are portrayed in Figs. 5 and 6. The impervious surface area (paved streets and roofs) in the Still Creek subwatershed exceeds 50 %, almost twice as high as in the Eagle Creek subwatershed. The traffic intensity is also twice as high in the Still Creek subwatershed. As a result of this difference in land use, the average trace metal concentrations of Cu, Pb, and Zn in the stream sediments of Still Creek are 2–5 times higher than in Eagle Creek.

However, Eagle Creek, which originates on Burnaby Mountain, slopes much more steeply than Still Creek. Therefore there may be less opportunity for contaminated sediment deposition along Eagle Creek.

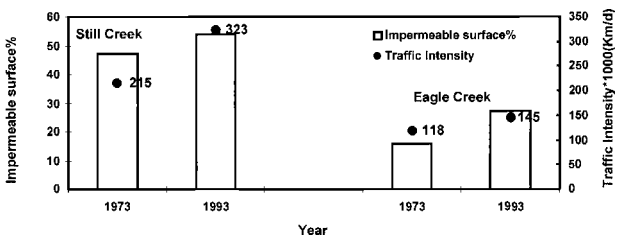

FIG. 5—*Land use (impermeable surface and traffic intensity) in the subwatershed (Still Creek and Eagle Creek) of the Brunette R. Basin.*

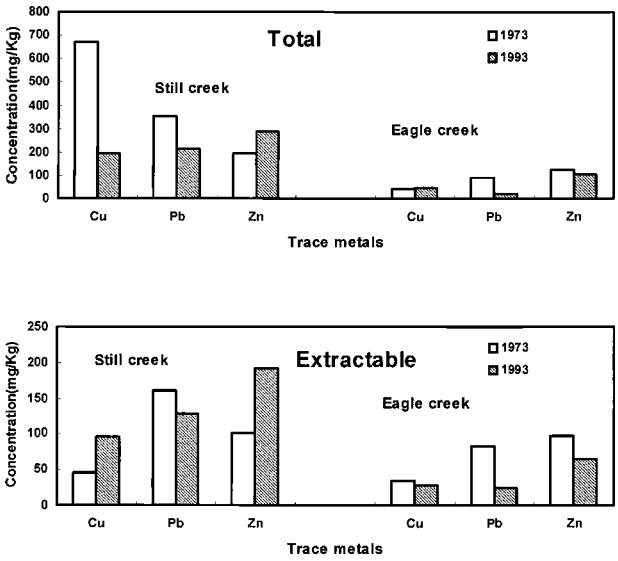

FIG. 6—*Comparison of trace metals (total and extractable) in the stream sediments of Still and Eagle Creek.*

The impervious surfaces and traffic volume have increased in both sub-watersheds over the 20-year period under consideration (Fig. 5) as the population of the Greater Vancouver region has grown. The total and extractable zinc have also increased considerably over this period in the Still Creek watershed, likely as a direct result of corrosion of zinc from higher traffic volumes which have also increased by 50 % over this period.

While total copper and lead in Still Creek have decreased considerably over the 20-year period as noted above, the proportion of extractable copper has increased greatly, implicating a different source. This source could well be copper from the wear of brake linings, accentuated by significantly higher traffic volume (FHWA 1998; Kayhanian 2003). On the other hand, total and extractable Cu, Pb, and Zn have either decreased or changed very little in the Eagle Creek watershed from 1973 to 1993, reflecting the considerably smaller change in traffic intensity (an increase of only about 10 %.)

Statistical Analysis of Trace Metals in Stream and Street Sediments

Tables 1 and 2 show that a statistical correlation of the total and extractable stream sediment trace metals over the three sampling periods indicates that contamination from copper, lead, and zinc are highly correlated (R=0.73–0.85). This correlation probably reflects the importance of watershed imperviousness and traffic intensity as controlling factors for nonpoint source trace metal contamination in this highly urbanized watershed. The poor correlations of iron and manganese to the other trace metals (Cu, Pb, and Zn) likely reflects the high natural levels of these two elements in most soils. The increased levels of manganese from MMT do not appear to have affected the levels of other trace metals.

TABLE 1—*Spearman rank correlation matrix for total metal concentrations in streambed sediments (data from 1973, 1993, and 1998) (nitric acid digestion, n=24).*

	Cu	Fe	Mn	Pb	Zn
Cu	1.00				
Fe	0.47	1.00			
Mn	0.09	0.41	1.00		
Pb	**0.85**	0.65	0.13	1.00	
Zn	**0.77**	0.66	0.28	**0.80**	1.00

TABLE 2—*Spearman rank correlation matrix for extractable metal concentrations in streambed sediments (data from 1973, 1993, and 1998) (cold 0.5 M HCl acid extraction, n=23).*

	Cu	Fe	Mn	Pb	Zn
Cu	1.00				
Fe	0.02	1.00			
Mn	0.18	0.07	1.00		
Pb	**0.77**	0.07	−0.02	1.00	
Zn	**0.82**	0.01	0.26	**0.73**	1.00

The Friedman statistical test only showed a significant statistical difference ($p=0.05$) for total manganese in street sediments over the period of study (1973–1998). This demonstrates the influence of the fuel additive MMT on street dirt contamination.

Total copper ($p=0.04$) extractable manganese ($p=0.002$) and extractable lead ($p=0.05$) in stream sediments over the study period demonstrated a significant temporal difference (Friedman statistical test). The Friedman test results of stream sediments indicate that Mn increased in 1993 and decreased in 1998, whereas Pb decreased in 1998. These changes are no doubt related to the change in fuel additives, as discussed above. The lack of significant temporal variation over this 25-year period that appears qualitatively obvious from the whisker-box plots of some of the other trace metals, demonstrates the high degree of variability that can occur even within one sampling period. This can be attributed to the dynamic nature of stormwater runoff and its ability to transport and deposit sediment associated contaminants.

A grouping of Burnaby lake sediment sampling sites into western end (A–D) and eastern end (E–F) did not show a statistically significant difference that is obvious for most trace metals from the bar graphs (Fig. 4), using the Wilcoxon test ($p=0.05$).

The mean rank analysis (Wilcoxon test) of the stream sediments between Still Creek and Eagle creek subwatersheds over the three sampling periods demonstrated that both total and extractable copper, lead, and zinc were higher in Still Creek and total and extractable manganese higher in Eagle Creek although none of these spatial trends were highly significant at $p=0.05$.

To put the sediment contamination in the Brunette watershed into context it is compared to other investigations into nonpoint source pollution associated with street and urban storm water runoff (Tables 3 and 4). The copper contamination of street dirt in the Brunette watershed is higher than reported for motorways in England, comparable to many areas in Germany, but has a very high area of contamination attributable to industrial activity in the watershed (Table 3). The iron for all watersheds is comparable to values reported for many soils. Manganese on the English motorways was an order of magnitude higher than found in a German and the Brunette Watershed. The Brunette watershed contained very high levels of lead in the 1970s but values since then (1993–1997) are more comparable to other areas studied (Table 3). Zinc street dirt contamination in the Brunette watershed is similar to many of the values reported for the European watersheds, but is only half the higher values reported (1400–1600 mg/kg).

Trace metal sediment contamination in various sediment traps (detention ponds, gully pots) from European studies are very similar to the levels found in both the stream and lake sediments of the Brunette watershed (Table 4). An exceptionally high level of copper (1765 mg/kg) was found in the Brunette watershed during the early years of this investigation (1973) which exceeds the reported literature values.

TABLE 3—*Trace metals in street dirt from different investigations.*

	Trace metal[a]				
Study Area	Cu	Fe	Mn	Pb	Zn
Hildeshein, Germany[b]	76	2.34	…	362	187
Motorways (M1, M6, M25), England[c]	60–72	2.4–3.1	3760–5097	…	955–1472
Hamburg, Germany[d]	90–237	2.2–3.7	225–304	188–224	408–523
Karlsrube, Germany[e]	122	…	…	193	1675
Brunette Watershed, Canada[f]	81–800	1.06–2.54	154–369	90–4840	160–791

[a]All values as total trace metals in milligrams/kilograms dry weight, except Fe as percent.
[b]Muschack (1990).
[c]Ward (1990).
[d]Dannecker et al. (1990).
[e]Xanthopoulos and Hahn (1990).
[f]This investigation for three periods–1973, 1993, 1997.

Again this is attributable to an industrial source which was phased out in the early 1980s. Considerably higher zinc levels for a detention pond (Stotz 1990) and the gully pots (Grottker 1990) in Germany exceeded any zinc contamination in stream and lake sediments of the Brunette watershed.

This comparison illustrates the high level of contamination from trace metals in our urbanized watersheds. Since many of these trace metals exceed levels considered safe for aquatic organisms and the cumulative effects of several trace metals are unknown the management of these nonpoint source contaminants presents a difficult challenge.

Conclusions

- Lead concentrations in lake, stream, and street sediments have decreased dramatically over the past three decades as a result of the removal of the lead additive—tetraethyl lead—from gasoline in the

TABLE 4—*Trace metals in sediments in catchment areas.*

	Trace metal[a]				
Catchment Area/Device	Cu	Fe	Mn	Pb	Zn
Detention Pond (Germany)[b]	204–330	1.8–2.4	…	723–840	1340–2175
Detention Pond (Florida)[c]	4–73	…	…	30–1025	27–538
Gully Pots (Germany)[d]	170–515	3.3–5.23	…	…	895–2905
Detention Ponds (France)[e]	…	2.05	195	57	130
Sediment (Germany)[f]	40	1.38	…	184	330
Stream Sediments (this study)[g]	6–1765	0.2–2.93	90–1334	7–840	44–408
Lake Sediments (this study)[g]	59–218	1.07–2.72	272–517	89–357	252–697

[a]All values as total trace metals in mg/kg dry weight, except Fe as percent.
[b]Stotz (1990).
[c]Yousif et al. (1990).
[d]Grottker (1990).
[e]Lee at al. (1997).
[f]Muschack (1990).
[g]This investigation, stream sediments 1973, 1993, 1997; lake sediment 1998.

  1970s. The mean concentration of total lead in stream sediments decreased from 230 mg/kg in 1973 to 134 mg/kg in 1993 and 36–66 mg/kg in 1997–1998.
- Manganese, especially the acid extractable fraction, increased during the early 1990s when tetraethyl lead was replaced by MMT as an antiknock compound. The 0.5 M HCl extractable manganese in stream sediments increased from 18 mg/kg in 1973 to 545 mg/kg in 1993, before falling to 162–273 mg/kg in 1997–1998.
- Lake sediment contaminant profiles and spatial patterns of stream and street sediment contamination indicate that traffic has contributed a large proportion of the Pb, Cu, and Zn loading to the watershed.
- Burnaby Lake, a shallow (Zav=1.0 m, 140 ha) lake has acted as a sink for trace metal contaminated sediments. The highest trace metal levels have been found in surface sediments at the east end of the lake (where Cu, Pb, and Zn were 159, 179, and 529 mg/kg) containing more silt (24 %) and higher organic matter (32.5 %). The sandy delta of Still Creek (silt $<$ 4 %, organic matter 5.6 %), which contributes over 50 % of the flow to the lake, has lower trace metal levels (Cu, Pb, and Zn concentrations of 72, 77, and 207 mg/kg), even though the creek is a predominant source of trace metals transport to the lake.
- The total and extractable stream sediment trace metals copper, lead, and zinc are highly correlated (0.73–0.85) over the three sampling periods in 1973, 1993, and 1997–1998, probably reflecting the importance of watershed imperviousness and traffic intensity as controlling factors in nonpoint source trace metal contamination in this highly urbanized watershed.
- To protect the aquatic habitats, two alternatives to complete treatment of urban runoff are suggested. The first option is to identify the pollutant source and eliminate it before it is released. The second is to identify areas which contribute the bulk of contaminants, and collect and treat the storm water from those areas only. Dredging could be instituted to remove contaminated sediments

from Burnaby Lake to restore the quality of this aquatic environment and protect aquatic life.

References

APHA (American Public Health Association), 1989, *Standard Methods for the Examination of Water and Wastewater*, 17th ed., Washington, D.C.: American Public Health Association.

Albasel, N. and Cottenie, A., "Heavy Metal Contamination near Major Highways, Industrial and Urban Areas in Belgian Grassland," *Air and Soil Pollution*, 24, 103–109 (1985).

Bindra, K. S. and Hall, K., 1977, "Geochemical Partitioning of Trace Metals in Sediments and Factors Affecting Bioaccumulation in Bethic Organisms," Draft research paper, Dept. of Civil Engineering, The University of British Columbia, Canada.

Brault, N., Loranger, S., Courchesne, F., Kennedy, G., and Zayed, J., 1994, "Bioaccumulation of Manganese by Plants: Influence of MMT as a Gasoline Additive," *Sci. Total Environ.*, 153, 77–84 (1994).

Dannecker, W., Au, M., and Stechmann, H., "Substance Load in Rainwater Runoff from Different Streets in Hamburg," *Sci. Total Environ.*, 93, 385–392 (1990).

Ethyl, 1997, *Characterization of Manganese Particulates from Vehicles Using MMT Fuel–A Compilation of Results from Studies*, Ehtyl Corp., Richmond, VA.

FHWA, 1998, Is Highway Runoff a Serious Problem?, Office of Infrastructure R&D. Turner-Fairbank Highway Research Center. McLean, VA, http:/www.fhwa.dot.gov/terp/prog.htm#I129

Grottker, M., "Pollutant Removal by Gully Pots in Different Catchment Areas," *Sci. Total Environ.*, 93, 515–522 (1990).

Hall, J. K., Yesaki, I., and Chan, J., Trace Metals and Chlorinated Hydrocarbons in the Sediments of a Metropolitan Watershed, Tech. Report No. 10, Westwater Research Center, The University of British Columbia, B.C., Canada, 1976.

Iman, R. L. and Conover, W. J., *A Modern Approach to Statistics*, John Wiley & Sons, New York.

Kayhanian, M., Singh, A., Suverkropp, C., and Borroum, S., 2003, "Impact of Annual Average Daily Traffic on Highway Runoff Pollutant Concentrations," *J. Environ. Eng.*, Vol. 129, 975–990 (1983).

Lee, P. K., Baillif, P., and Touray, J.-C., "Geochemical Behaviour and Relative Mobility of Metals (Mn, Cd, Zn and Pb) in Recent Sediments of a Retention Pond along the A-71 Motorway in Sologne, France," *Environ. Geol.*, 32 (2), 142–152 (1997).

Loranger, S., Zayed, J., and Forget, E., "Manganese Contamination in Montreal in Relation with Traffic Density," *Water, Air and Soil Pollution*, 74, 385–396 (1994).

Lytle, C. M., Smith, B. N., and McKinnon, C. Z., "Manganese Accumulation along Utah Roadways: a Possible Indication of Motor Vehicle Exhaust Pollution," *Sci. Total Environ.*, 162, 105–109 (1995).

MacDonald, R., Hall, K. J., and Schreier, H., Water Quality and Stormwater Contaminants in the Brunette River Watershed, British Columbia, 1994/95, Research report, Westwater Research Center, The University of British Columbia, Canada, 1997.

McCallum, D. W., An Examination of Trace Metal Contamination and Land Use in an Urban Watershed, M.Sc. thesis, Dept. of Civil Engineering, The University of British Columbia, Canada, 1995.

Mikkelsen, P. S., Häfliger, M., Ochs, M., Tjell, J. C., Jacobsen, P., and Boller, M., "Experimental Assessment of Soil and Groundwater Contamination from Two Old Infiltration Systems for Orad Run-off in Switzerland," *Sci. Total Environ.*, 189/190, 341–347 (1996).

Morrison, G. M. P. and Revitt, D. M., "Assessment of Metal Species Bioavailability and Geochemical Mobility in Polluted Waters," *Environ. Technol. Lett.*, 8, 361 (1987).

Muschack, W., "Pollution of Street Runoff by Traffic and Local Conditions," *Sci. Total Environ.*, 93, 419–431 (1990).

Norrström, A. C. and Jacks, G., "Concentration and Fractionation of Heavy Metals in Roadside Soils Receiving De-icing Salts," *Sci. Total Environ.*, 218, 161–174 (1998).

Pagotto, C., Remy, N., Legret, M., and Le Cloirec, P., "Heavy Metal Pollution of Road Dust and Roadside Soil near a Major Rural Highway," *Environ. Technol.* 22, 307–319 (2000).

Revitt, D. M., Hamilton, R. S., and Warren, S., "The Transport of Heavy Metals within a Small Urban Catchment," *Sci. Total Environ.*, 93, 359–373 (1990).

Stotz, G., "Decontamination of Highway Surface Runoff in the FRG," *Sci. Total Environ.*, 93, 507–514 (1990).

Ward, N. I., "Multielement Contamination of British Motorway Environments," *Sci. Total Environ.*, 93, 393–401 (1990).

Xanthopoulos, C. and Hahn, H. H., "Pollutants Attached to Particles from Drainage Areas," *Sci. Total Environ.*, 93, 441–448 (1990).

Young, G. K., Stein, S., Cole, P., Kammer, T., Graziano, F., and Bank, F., *Evaluation and Management of Highway Runoff Water Quality*, GKY and Associates, Incorporated, FHWA, 1996.

Yousef, Y. A., Hvitved-Jacobsen, T., Harper, H. H., and Lin, L. Y., "Heavy Metal Accumulation and Transport through Detention Ponds Receiving Highway Runoff," *Sci. Total Environ.*, 93, 433–440 (1990).

Yuan, Y., The Bioavailability of Trace Metal Contaminants in the Brunette River Watershed, M.A.Sc. thesis, The University of British Columbia, Dept. of Civil Engineering, Canada, 2000.

Journal of ASTM International, Vol. 3, No. 7
Paper ID JAI13337
Available online at www.astm.org

Behnaz Dahrazma[1] *and Catherine N. Mulligan*[2]

Evaluation of the Removal of Heavy Metals from Contaminated Sediment in Continuous Flow Tests with Selective Sequential Extraction

ABSTRACT: Solutions to heavy metal-contaminated sediment require the understanding of the availability of heavy metals, interaction of the contaminants with soil and sediment particles, and metal retention mechanisms, which are complicated phenomena. The objective of this investigation was to study the removal of heavy metals (copper, zinc, and nickel) from the sediments by employing a biosurfactant rhamnolipid in continuous flow tests. Continuous flow of the biosurfactant in a column was applied to evaluate the feasibility of this type of setup since the configuration simulates the process of soil flushing. In the case of heavy metals, the flowing washing agent is believed to reduce the possibility of readsorption of the metals on to the soil and sediment. In addition, since the distribution of heavy meals between soil and solute is the key to evaluating the environmental impact of the metals, to determining the mobility of metals and to recommending reliable removal techniques, selective sequential extraction tests were used to determine the portion of sediment from which the metal was removed. This method is based on extracting metals with solutions of increasing strengths from different fractions of soils or sediments. Exchangeable, carbonate, reducible oxide, and organic fractions responded to washing techniques while residually bound contaminants are not economical or feasible to remove. This information is vital in proposing the most appropriate conditions for sediment washing.

KEYWORDS: contaminated sediments, rhamnolipid, continuous flow tests, selective sequential extraction, heavy metals

Introduction

For centuries, heavy metals along with other metals and minerals have been released from their natural chemical compounds through industrial activities and processes, but there were no codes or regulations to restrict their return to the environment. In 1988, the Canadian government launched the St. Lawrence Action Plan for protection, conservation, and remediation of the river. The study performed by Environment Canada (EC) shows that in 1992 the average level of heavy metals in the harbor of Montreal was more than five times more than the toxic level (EC 1993). According to the Ministry of Environment of Quebec, within the Montreal Island alone, there are 48 sites contaminated with nickel, 167 sites contaminated with zinc, and 182 sites contaminated with copper. This number in most cases has an overlap of two or three metals although the level of toxicity is not the same for all cases (EQ 2004).

Measurement of the mobility and availability of metals is required to predict and interpret their behavior. Trace metals can be found in numerous sediment and soil components in different ways (Krishnamurthy et al. 1995). Metals in river sediments can be bound to different compartments: adsorbed onto clay surfaces or iron and manganese oxyhydroxides; present in the lattice of secondary minerals like carbonates, sulphates, or oxides; attached to amorphous materials such as iron and manganese oxyhydroxides; and complexed with organic matter or in the lattice of primary minerals such as silicates (Tessier et al. 1979; Schramel et al. 2000; Gismera et al. 2004). To determine the speciation of metals in soils, various methods are used. One method is to use specific extractants. By sequentially extracting with solutions of

Manuscript received March 30, 2005; accepted for publication June 3, 2005. Presented at ASTM Symposium on Contaminated Sediments: Evaluation and Remediation Techniques on 23–25 May 2006 in Shizuoka, Japan; M. Fukue, K. Kita, M. Ohtsubo, and R. Chaney, Guest Editors.

[1] Ph.D., Department of Building, Civil, and Environmental Engineering, Concordia University, 1455 de Maisonneuve Blvd. W., Montreal, Quebec, Canada H3G 1M8.

[2] Research Chair in Environ. Eng., Department of Building, Civil, and Environmental Engineering, Concordia University, 1455 de Maisonneuve Blvd. W., Montreal, Quebec, Canada H3G 1M8.

increasing strength, a more precise evaluation of the different fractions can be obtained (Tessier et al. 1982). A soil or sediment sample is shaken over time with a weak extractant, centrifuged and the supernatant is removed by decantation. The pellet is washed in water and the supernatant removed and combined with the previous supernatant. A sequence of reagents is used following the same procedure until finally, mineral acid is used to extract the residual fraction. Heavy metal concentrations are then determined in the various extracts by atomic absorption or other means. Numerous techniques and reagents have been developed and have been applied to soils (Shuman 1985), sediments (Tessier et al. 1982), sludge-treated soils (Petrozelli et al. 1983) and sludges.

None of the extractions is completely specific. However the extractants are chosen in an attempt to minimize solubilization of other fractions and provide a distribution of the partitioning of the heavy metals. The chemical agents are used to destroy the bonds of the heavy metals to the various sediment components. The extracting agents increase in strength throughout the sequence (Yong 2000). As an example, Koeckritz et al. (2001) proposed an equivalent step to simplify the sequential extraction procedure designed by Zeien and Brummer (1989). They reduced four initial steps in the procedure to one with no significant change in the results.

To extract the exchangeable fraction, ammonium acetate, barium chloride, or magnesium chloride at pH 7.0 is generally used (Lake 1987). They cause the displacement of the ions in the soil or sediment matrix bound by electrostatic attraction. Other agents such as calcium chloride, potassium nitrate, and sodium nitrate can also be used (Yong 2000). The reducible phase (iron and manganese oxides) is extracted with hydroxylamine hydrochloride with acetic acid at pH 2.0. The hydroxylamine hydrochloride reduces the ferrous and manganese hydroxides to soluble forms (Tessier et al. 1979). The carbonate phase (calcite and dolomite) is extracted at pH 5.0 with sodium acetate acidified with acetic acid. This solubilizes the carbonates, releasing carbonate-entrapped metals (Yong and Mulligan 2004). Hot hydrogen peroxide in nitric acid is used to oxidize the organic matter. The oxidized organic matter then releases metals that are complexed, adsorbed, and chelated. These agents are used so that the silicates are not affected by this treatment (Yong 2000). In the final step, strong acids at high temperatures dissolve the silicates and other materials. This residual fraction is usually used to complete the mass balances for the metals.

Yong et al. (1999) reported that through selective sequential extraction techniques (SSE), they found that precipitation of heavy metal with carbonates and amorphous materials (oxides and hydroxides) is higher than heavy metals retention by exchangeable mechanisms. The study indicates that the strength of retention mechanisms of heavy metals by the phases of soil solids decreased in the following order:

$$\text{Carbonates} > \text{Amorphous} > \text{Organics} > \text{Exchangeable}$$

Previous studies showed that several washing steps improved the performance of soil washing and metal extraction by biosurfactants (Mulligan 1998; Dahrazma and Mulligan 2004). The idea of using continuous flow for sediment and soil washing is based on batch tests. Since the batch tests showed that metal removal from sediments was possible (Mulligan and Dahrazma 2003; Mulligan 2005; Mulligan et al. 2001), another configuration was used to study the effect of flow on the removal process to simulate in situ soil treatment. Beneficial results by this method will open a new horizon in in situ sediment and soil remediation.

The objective of this research was to determine the speciation of metals in the sediments and also to find the fractions of sediment which respond to rhamnolipid treatment in column tests under different conditions using sequential extraction techniques. The removal tests were performed in a continuous flow configuration with varying the concentration of rhamnolipid. The effect of time was also investigated through a time course study.

Methods and Materials

Characterization of the Sediments

The metal-contaminated sediment sample was obtained from the Lachine Canal area which is surrounded by metal and steel industries. The canal passes through residential and industrial areas and the area is known as a contaminated site by Environment Canada (EC 1993). To proceed with the experiment, the sample was air dried and mixed fully to obtain a homogenous sample. X-ray analysis indicated the

TABLE 1—*Characterization of the sediment sample*

Parameter	Value
Chromium	145 mg/kg
Copper	140 mg/kg
Nickel	76 mg/kg
Lead	572 mg/kg
Zinc	4854 mg/kg
Organic matter content	20 %
Cation exchange capacity	14.55 meq/100 g
pH	6.4
Fe_2O_3	17 800 mg/kg
Al_2O_3	11 200 mg/kg
SiO_2	23 400 mg/kg
Specific surface area	174.82 m^2/g

presence of 33.5 % quartz, 38 % feldspar, 5.4 % chlorite, 18.5 % amphibole, and 4.5 % illite. The grain size distribution was as follows: 15 % sand, 65 % silt, and 20 % clay. The sediments were digested by the method recommended by Environment Canada (1990) and then analyzed by a Perkin Elmer Atomic Absorption Aanalyst 100 Spectrophotometer for heavy metal content. The organic matter content was measured based on the method involving digestion by hydrogen peroxide. Cation exchange capacity was measured using the method proposed by Chapman (1965). The pH was measured based on EPA SW-846 Method 9045. For determining the amorphous content (Fe_2O_3, Al_2O_3, and SiO_2) the method recommended by Segalen (1968) was used. The specific surface area was measured by the method proposed by Carter et al. (1965). The results are summarized in Table 1.

Rhamnolipid

The rhamnolipid is an anionic biosurfactant (JBR215) that was obtained as a 15 % solution (w/v) from Jeneil Biosurfactant, Saukville, WI. It is produced from sterilized and centrifuged fermentation broth. Two major types of rhamnolipids, RLL (R1) and RRLL (R2), are present in the solution. The molecular weight of RLL ($C_{26}H_{48}O_9$, rhamnolipid type I) is 504 and of RRLL ($C_{32}H_{58}O_{13}$, rhamnolipid type II) is 650 as determined by the supplier. The critical micelle concentration (CMC) of the rhamnolipid was determined through conductivity and surface tension measurement to be 0.035 g/L.

Sediment Washing Procedure

To perform the continuous flow tests, a Teflon PFA Holder cylindrical test section (column) of 47 mm outer diameter and 42 mm inner diameter was used. The total length of the sediment sample was 6 mm. Both inlet and outlet tubing had the same diameter. The connecting tubings were Masterflex PharMed Pump Tubing and PTFE Tubing with outer diameters (OD) of 6.35 mm and inner diameters (ID) of 4.7625 mm. A cartridge pump (6 Masterflex Model 7519-15) was used to provide the dynamic head for the flow.

The biosurfactant solution was placed in a tank and the suction tubing was placed close to the bottom to prevent air entry. The temperature was 25°C (room temperature) and pH was adjusted to 6.5. In the solution of rhamnolipid and 1 % NaOH, the pH was elevated to 11. The flow was pumped and entered the column from its lowest level. This ensured the exhausting of air from the column. The column was filled from bottom to top by: 0.2 g of Pyrex Brand Wool–Filtering Fiber, 22 g of 4 mm Pyrex Brand solid glass beads, 0.2 g of glass wool, 10 g sediment and 0.5 g of glass wool.

The flow rate of 0.5 mL/min was maintained by a valve downstream of the column section. A three-way stopcock polypropylene with Teflon TFE 4 mm plug was used to measure the flow rate through counting of drops. The washing solution was collected in another tank. Each 24 h, when all 720 mL of the rhamnolipid solution was passed the sample, the collecting, and feeding tanks were switched. Under this configuration, the volume of sediment was 8.31 mL and the flow rate was 0.05 mL per gram of sediment per minute. The samples from the solvent were taken and in order to release the heavy metals trapped in the biosurfactant samples were digested. The concentrations of copper and other metals in each sample were measured by the atomic absorption spectrophotometer.

TABLE 2—*Sequential extraction process (Adapted from Yong et al. 1993)*

Sequence	Chemical reagents	Fraction
1	Extraction of metals by surfactants and controls	Soluble
2	Extraction of metals with 8 mL of 1 M $MgCl_2$ (pH 7) for 1 h.	Exchangeable
3	Extraction of metals with 8 mL of 1 M NaOAc[a] adjusted to pH 5 with acetic acid for 5 h.	Carbonates
4	Extraction of metals with 20 mL of 0.04 M $NH_2OH.HCl$ in 25 % (v/v) acetic acid (pH 2.5) at 96°C for 6 h	Oxides and hydroxides
5	Extraction with 3 mL of 0.02M HNO_3 and 5 mL of 30 % H_2O_2 (pH 2) for 2 h at 85°C, followed by 3 mL of 30 % H_2O_2 (pH 2) at 85°C for 3 h and then 5 mL of 3.2 M NH_4OAc in 20 % (v/v)HNO_3 diluted to 20 mL at room temperature for 30 min	Organic matter
6	Digestion at 90°C with 25 mL of dilute aqua regia (50 mL HCl, 200 mL HNO_3 and 750 mL water) for 3 h	Residual fraction

[a]Ac denotes acetate

Procedure for Selective Sequential Extraction (SSE)

The procedure used for the sequential extraction was similar to that of Yong et al. (1993) shown in Table 2. Sediment samples (10 g) were washed with the biosurfactant solutions and controls in a continuous flow configuration to determine the soluble fraction. Each of the fractions was collected and the concentrations of heavy metals were determined by atomic absorption spectrometry (Perkin Elmer Atomic Absorption Aanalyst 100 Spectrophotometer). Samples were washed with distilled water to prepare samples for the next step after each step. The amounts of copper, zinc, and nickel extracted from each of the extractants were then calculated.

Results

Speciation of Heavy Metals in the Sediment before Washing

Sequential extraction procedures were used on the sediments to determine the speciation of the heavy metals (Cu, Zn, and Ni) before surfactant washing. The exchangeable fractions of all metals were small. The carbonate and oxide fractions accounted for over 60 % of the zinc present in the sediments (Table 3). The organic fraction constituted over 80 % of the copper. A major proportion of nickel was found in the residual fraction. Similar to the results of the present study, Chartier et al. (2001) reported that in their sample of sediment, 65 % of copper was found in organic matter and 50 % of nickel was in the residual fraction. Jenne (1968) stated that the fraction of soil in which zinc exists is dependent on the Fe and Mn oxide content.

SSE of the Sediment after Washing with Different Agents in Continuous Flow Configuration

Sequential extraction of the sediments was performed after washing with the biosurfactant in a column configuration for three days. The flow rate was kept at 0.5 mL/min. The results of these experiments for copper, zinc, and nickel are shown in Figs. 1, 2, and 3, respectively.

Rhamnolipid, as in the batch configuration (Mulligan and Dahrazma 2003), removes copper from the organic fraction when NaOH was added while without NaOH in the solution, the oxide fraction was the most affected fraction in copper removal. Comparing the SSE results for copper washed by 1 % NaOH

TABLE 3—*Sequential extraction characterization of metal contaminants in sediment before washing with the biosurfactant (Mulligan and Dahrazma 2003).*

Metal	Fraction (% of total)				
	Exchangeable	Carbonate	Oxide	Organic	Residual
Copper	1	1	4	86	12
Nickel	0	9	23	29	39
Zinc	4	18	46	22	10

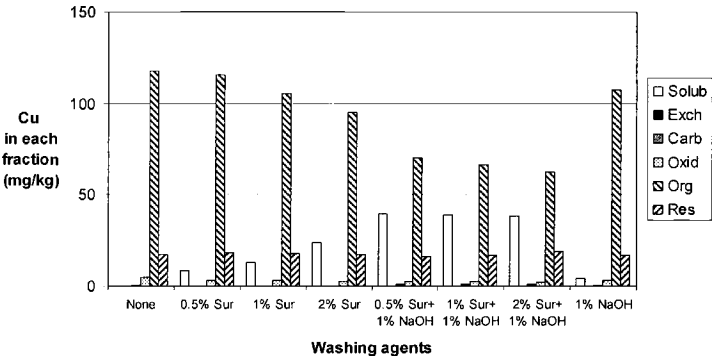

FIG. 1—*Sequential Extraction of Cu after washing sediments with each agent, 0.5, 1, and 2 % rhamnolipid, with and without 1 % NaOH and 1 % NaOH in a continuous flow configuration of* 0.5 mL/min. *The fractions are indicated as Solub for Soluble, Exch for Exchangeable, Carb for Carbonate, Oxid for Oxide, Org for Organic, and Res for Residual.*

with the other solutions of rhamnolipid and NaOH, indicates the proficiency of NaOH in association with the rhamnolipid for solubilizing the organic associated copper in the sediment since the removal of copper from the organic fraction by 1 % NaOH is not as significant as by the others (Fig. 1).

For zinc, a major decrease in the carbonate fraction for the solution with no NaOH was detected. A smaller decrease of zinc in the exchangeable fraction of sediment was also observed. Although in the presence of NaOH and the biosurfactant, there was removal from the organic and oxide fractions of zinc, the most influenced fraction was the exchangeable fraction where the zinc was almost completely removed (Fig. 2).

In the case of nickel, the reduction of the metal in the oxide and carbonate fractions was proportional to the concentration of the biosurfactant (Fig. 3). There were also significant reductions in the organic fraction, upon addition of 1 % NaOH to the 0.5 % surfactant solution. The same result was obtained from the SSE tests for the two other metals.

SSE of the Sediment after Washing over Time in the Continuous Flow Configuration

SSE tests were performed to study the sensitivity of the removal of each fraction over time. Samples underwent the SSE tests before as well as after washing with a solution of 2 % rhamnolipid for 3 days and

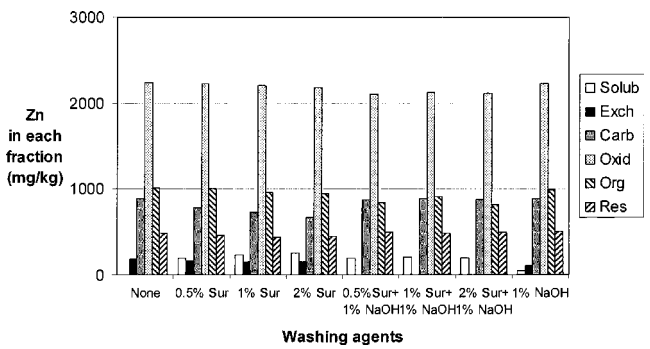

FIG. 2—*Sequential extraction of Zn after washing sediments with Each Agent, 0.5, 1 and 2 % rhamnolipid (Surf), with and without 1 % NaOH and 1 % NaOH in a continuous flow configuration of* 0.5 mL/min. *The fractions are indicated as Solub for Soluble, Exch for Exchangeable, Carb for Carbonate, Oxid for Oxide, Org for Organic, and Res for Residual.*

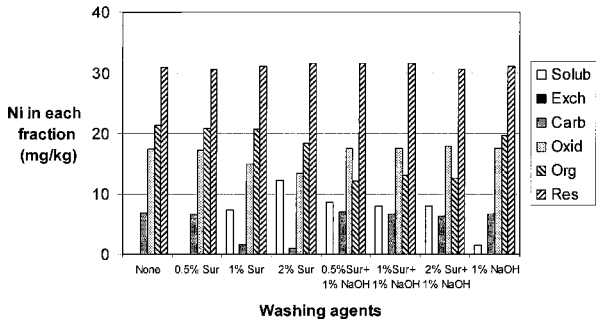

FIG. 3—*Sequential extraction of nickel after washing sediments with each agent, 0.5, 1 and 2 % rhamnolipid (Surf), with and without 1 % NaOH and 1 % NaOH in a continuous flow configuration of* 0.5 mL/min. *The fractions are indicated as Solub for Soluble, Exch for Exchangeable, Carb for Carbonate, Oxid for Oxide, Org for Organic, and Res for Residual.*

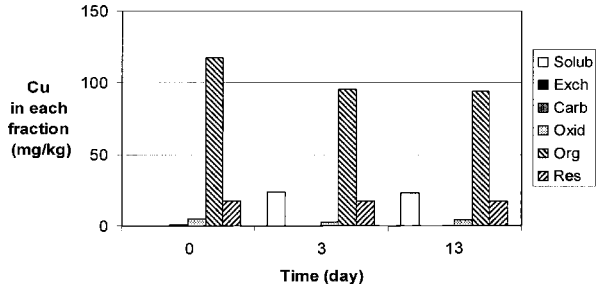

FIG. 4—*Sequential extraction of Cu after washing sediments for different periods of time with the solution of 2 % rhamnolipid in a continuous flow configuration. The flow rate was* 0.5 mL/min *and samples were taken on days 0, 3, and 13. The fractions are indicated as Solub for Soluble, Exch for Exchangeable, Carb for Carbonate, Oxid for Oxide, Org for Organic and Res for Residual.*

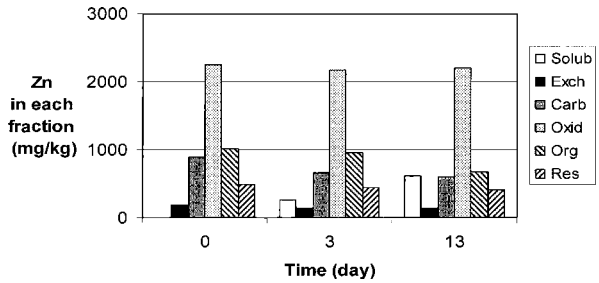

FIG. 5—*Sequential extraction of zinc after washing sediments for different periods of time with the solution of 2 % rhamnolipid in a continuous flow configuration. The flow rate was* 0.5 mL/min *and samples were taken on days 0, 3, and 13. The fractions are indicated as Solub for Soluble, Exch for Exchangeable, Carb for Carbonate, Oxid for Oxide, Org for Organic, and Res for Residual.*

13 days. Figures 4, 5, and 6 show the results of these tests for Cu, Zn, and Ni, respectively. The results of the SSE tests for copper after 3 days and 13 days support the results of the test of removal of copper from the sediment which showed that the removal of copper remained constant after 3 days. It indicates that not only the total removal of copper from the sediment after 3 days remains constant, but also the concentration of copper in each fraction will be the same after 13 days in comparison with 3 days (Fig. 4).

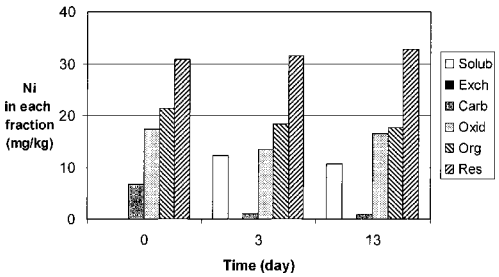

FIG. 6—*Sequential extraction of nickel after washing sediments for different periods of time with the solution of 2 % rhamnolipid in a continuous flow configuration. The flow rate was* 0.5 mL/min *and samples were taken on days 0, 3, and 13. The fractions are indicated as Solub for Soluble, Exch for Exchangeable, Carb for Carbonate, Oxid for Oxide, Org for Organic, and Res for Residual.*

Figure 5 shows the outcome of the SSE tests for zinc removal over time. The noticeable result of the SSE test for zinc in this part of investigation is the behavior of the exchangeable fraction interacting with the rhamnolipid. The concentration of the metal in the exchangeable fraction changed in the first three days but remained constant after this period while the concentration of zinc in carbonate and organic fraction continuously decreased during the period of the test. The major effect was seen for the organic fraction, where the concentration of zinc decreased remarkably over time.

Nickel showed a different behavior over time. The concentration of nickel in the soluble fraction increased and then declined over time, which means that the removed nickel returned to the sediment when the removal rate was lower than the readsorption rate. By using the results of the SSE tests, this behavior can be interpreted. The returning nickel to the sediment, the readsorbed nickel, was not evenly distributed over the fractions of sediment. As shown in Fig. 6, the concentration of nickel in carbonate and organic fractions declined over time although the concentration of nickel decreased in the soluble fraction at the same point in time. The reason for this decrement can be explained by the accumulation of the readsorbed nickel in the oxide and hydroxide fraction, which was at a higher rate than the rate of nickel removal from the other fractions. According to Yong and Mulligan (2004), carbonate minerals are more soluble than aluminum/iron oxides, hydroxides, and oxyhydroxides; thus nickel that was removed from oxide and carbonate fractions of the sediments, preferentially readsorbs to the oxide fraction which is less soluble.

Discussion

The contamination of sediments with heavy metals and the required removal measures are complicated phenomenon and require further investigation. As Kabala and Singh (2001) stated, the mobility and availability of heavy metals depends on the ways that metals are associated with different soil components. Krishnamurti et al. (1995) and Gismera et al. (2004) have also indicated that the measurement of mobility and availability of heavy metals is needed to predict the behavior of heavy metals in the soil. To determine the speciation of metals in sediments (the distribution of elements among chemical forms or species), specific extracts are used in a process called selective sequential extraction. This method can be used to determine if heavy metals are removable by remediation techniques or to predict removal efficiencies. Sequential extraction can be employed for the evaluation of the most appropriate sediment remediation technology and for monitoring remediation procedures. Exchangeable, carbonate, reducible oxide, and organic fractions are amenable to washing techniques, and residually bound contaminants are not economical or feasible to remove. This information is not only important in designing the most appropriate conditions for sediment washing, but also, as Gismera et al. (2004) mentioned, even a slight variation in metal availability may make trace metals toxic to animals and plants. With due attention to the importance of the SSE, these tests were performed in a variety of manners by different researchers (Tessier et al. 1979; Yong et al. 1993; Ho and Evans 2000; Chartier et al. 2001; Koeckritz et al. 2001; Elass et al. 2004).

In this study, SSE tests were performed for different samples of sediment with regard to the procedure proposed by Yong et al. (1993). The sediment samples were subjected to SSE before and after washing

TABLE 4—*Heavy metal affinity for various fractions in the sediments (Mulligan and Dahrazma 2003).*

Heavy metal	Affinity for each fraction
Copper	Organic > residual > oxide > carbonate, exchangeable
Nickel	Residual > organic > oxide > carbonate > exchangeable
Zinc	Oxide > organic > carbonate > residual > exchangeable

with the agents during a short time (three days) in both batch and continuous flow configurations. The purpose of this part of the present research was to investigate if the configuration can change the share of each fraction in heavy metal removal process. To be able to predict and interpret the soil washing technique (continuous flow configuration), SSE tests were performed for different samples that were washed with a variety of agents and over time.

The affinity of the heavy metals for various fractions in the sediment was determined through the SSE tests for the sediment before applying any washing agent (Table 4). Similar to these results, Chartier et al. (2001) reported that 65 and 73 % of total copper existed in the sediments detected in the organic matter and sulfide fractions respectively while 50 and 80 % of nickel and chromium were found in the residual fractions. Ho and Evans (2000) reported that copper and lead mostly existed in oxidizable organic matter and zinc was found in all soil fractions. Jenne (1968) stated that Fe and Mn oxides determine the fractions of soil in which Zn exists. The present study has also found that 46.2 % of Zn exists in oxide fraction of the sediments. Karam et al. (2003) stated that humic substances (HS) have a high affinity to form stable complexes with copper. As a result, copper is usually immobile in organic soil. Kabata-Pendias (2001) indicated that copper and HS interaction could be a result of complexation, ion exchange, precipitation, and dissolution.

Comparing the results of SSE after washing the sediment with different washing agents in batch (Mulligan and Dahrazma 2003) and continuous flow setups, one can conclude that regardless of the quantity of metal removal, each fraction follows the same pattern in interaction with an individual agent.

The results of the SSE for the samples that were washed with different agents in batch (Mulligan and Dahrazma 2003) and continuous flow column configurations show that the organic phase-associated metals can be mostly removed by rhamnolipid with sodium hydroxide. Conditions without NaOH addition were effective for removing the zinc and nickel in the carbonate and oxide phases. Residual fractions, the most difficult to remove, were not affected during the surfactant washing studies. It was shown that copper could be removed mostly from the oxide-bound fraction and zinc from the carbonate-bound fraction during washing with the rhamnolipid biosurfactant.

This information is important in designing the appropriate conditions for soil washing. A combination of acidic and basic conditions, therefore, would increase the amounts of metals removed in the case of carbonate, oxide, and organic-associated metals. Sequential extraction procedures can provide indications but not specific information on the chemical binding of metals. This information can then be used to determine remediation procedures and to monitor the procedures during the treatment phase. Knowing the fraction(s) in which heavy metals exist, the engineer is able to conclude the degree of mobility of heavy metals and consequently the environmental impact of the contaminated soil. In the case that removal becomes necessary, the SSE guides the selection of the right treatment techniques based on the fractions in which heavy metal should be removed.

It has also become known that copper removal from each fraction remained constant throughout the tests over time (between 3 to 13 days). Zinc removal from each fraction is time dependant. Exchangeable Zn is available for removal in the short time (3 days), while organic fraction releases more Zn as time goes. Nickel shows a high degree of dependency with time. According to the SSE and removal tests, the removable nickel was available in carbonate, oxide, and organic fractions. If the removal was applied over a short time (3 days), all of these fractions participated in the release of metal to the solution but over an extended time (13 days) the oxide fraction acted differently. Accumulation of readsorbed nickel can be observed in the oxide and hydroxide fractions as illustrated in Fig. 6.

Conclusions

By summarizing the results of selective sequential extraction tests, it becomes more reasonable to employ such tests before designing any treatability protocol. Ho and Evans (2000) mentioned that SSE results help

in understanding the feasibility of remediation and the ecological significance of contamination by metals. Flow rate, time, and the type of washing agent can be optimized according to the type of contaminant and the fraction in which the heavy metal exists. To illustrate the above statement, one can say for a zinc-contaminated sediment, an extended time period will not be helpful in removing the zinc if the metal exists mostly in the exchangeable fraction. Also, it can be added that if the contamination is by nickel in the carbonate fraction in the presence of the oxide fraction, removal shows a remarkable deficiency if the time is extended because of readsorption. With the same analogy, it can be said that copper removal is more sensitive to the washing agent than time.

As indicated earlier, SSE can be used as a basis for designing a sediment washing protocol depending on the metal, the fraction with which the metal is associated, and the type of washing as well as other physical and chemical conditions.

References

Carter, D., Heilman, T., and Gonzalez, J., "Ethylene Glycol Monoethyl Ether for Determining Surface Area of Silicate Minerals" *J. Soil Sci.*, 100, 356-361 (1965)

Chapman, H. D., "Cation Exchange Capacity: Methods of Soil Analysis" *J. Am. Soc. Agron.* 9, 891–901 (1965).

Chartier, M., Mercier, G., and Blais, J. F., "Partitioning of Trace Metals Before and After Biological Removal of Metals From Sediments," *Water Resour.* 6, 35 1435–1444 (2001).

Dahrazma, B., and Mulligan, C. N., "Extraction of Copper From a Low Grade Ore by Rhamnolipids," *Pract. Period. Hazard., Toxic, Radioact. Waste Manage.*, 8, 166–172 (2004).

Elass, K., Laachach, A., and Azzi, M., "Three-Stage Sequential Extraction Procedure for Metal Partitioning in Polluted Soils and Sediments," *Ann. Chim. (Rome)* 94(4), 325–332 (2004).

Environnement Canada, Service de conservation et protection Region Quebec *Methode d'analyse des metaux dans sediments, les boues et les sols*, 1990.

Environment Canada, "Sediment Contamination in Montreal Harbor," 1993 Ottawa, Canada.

Environment Quebec, "Bilan-2001," 2004, Quebec, QC, Canada.

Gismera, M. J., Lacal, J., Da Silva, P., Garcia, R., Sevilla, M. T., and Procopio, J. R., "Study of Metal Fractionation in River Sediments. A Comparison Between Kinetic and Sequential Extraction Procedures," *Environ. Pollut.* 127, (2), 175–182 (2004).

Ho M. D., and Evans G. J., "Sequential Extraction of Metal Contaminated Soils with Radiochemical Assessment of Readsorption Effects," *Environ. Sci. Technol.* 6(34), 1030–1335 (2000).

Jenne, E., "Controls on Mn, Fe, Cu, Ni and Zn Concentrations in Soil and Water," *Trace Inorganics in Water Hdv. Chim. Ser.* 73, 227–387 (1968).

Kabala, C., and Singh, B. R., "Fraction and Mobility of Copper, Lead, and Zinc in Soil Profiles in the Vicinity of a Copper Smelter," *J. Environ. Qual.*, 30, 485–492 (2001).

Kabata-Pendias, A., *Trace Elements in Soils and Plants* 3rd ed., CRC Press, Boca Raton, FL, 2001.

Karam, A., Côté C., and Parent, L. E., "Retention of Copper in Cu-Enriched Organic Soils," *Organic Soils and Peat Materials for Sustainable Agriculture*, edited by Parent L. E. and Ilnicki P. CRC Press LLC. Boca Raton, FL, 2003.

Koeckritz, T., Thoming, J., Gleyzes, C., and Odegard, K. E., "Simplification of a Sequential Extraction Scheme to Determine the Moblisible Heavy Metal Pool in Soil," *Acta Hydrochim. Hydrobiol.* 29, (4), 197–205 (2001).

Krishnamurthy, J. S. R., Huang, P. M., Van Rees, K. C. J., Kozzak L. M., and Rstad, H. P. W., "Speciation of Particulate-Bound Cadmium of Soils and its Bioavailability," *Analyst (Cambridge, U.K.)*, 120, 659–665 (1995).

Lake, D. L., "Chemical Speciation of Heavy Metals in Sewage Sludge and Related Matrices," *Heavy Metals in Wastewater and Sludge Treatment Processes. I: Sources, Analysis, and Legislation*, edited by Lester, J. N., 1987, CRC Press, Boca Raton, FL, 1987.

Mulligan, C. N., "On the Capability of Biosurfactants for the Removal of Heavy Metals from Soil and Sediments," Ph.D. thesis, McGill University, 1998, Montreal, Canada.

Mulligan, C. N., "Environmental Applications for Biosurfactants," *Environ. Pollut.* 133, 183–198 (2005).

Mulligan C. N. and Dahrazma, B., "Use of Selective Sequential Extraction for the Remediation of Con-

taminated Sediments," ASTM STP 1442, 2003, 208–223.

Mulligan, C. N., Yong, R. N., and Gibbs, B. F., "Heavy Metal Removal from Sediments by Biosurfactants," *J. Hazard. Mater.*, 85, 111–125 (2001).

Petrozelli, G., Giudi, G., and Lubrano, L., *Proc. Int. Conf. Heavy Metals in the Environment*, Heidelburg, FRG, 1983, p. 475.

Schramel, O., Michalke, B., and Kettrup, A., "Study of the Copper Distribution in Contaminated Soils of Hop Fields by Single and Sequential Extraction Procedures," *Sci. Total Environ.* 263, 2000, 11–22.

Segalen, P., "Note sur un Methode de Determination des Produits Mineraux Amorphes Dans Certains sols a Hydroxides Tropicaux," *Cah. Orstom Ser. Pedol*, 6, 105–126 (1968).

Shuman L. M., "Fractionation Method for Soil Microelements," *Soil Sci.*, 140, 11–22 (1985).

Tessier, A., Campbell, P. G. C., and Bisson, M., "Sequential Extraction for the Separation of Particulate Trace Metals," *Anal. Chem.* 51, 844–851 (1979).

Tessier, A., Campbell, P. G. C., and Bisson, M., "Particulate Trace Speciation in Stream Sediments and Relationships with Grain Size: Implication for Geochemical Exploration," *J. Geochem. Exploration* 16(2). 77–104 (1982).

Yong, R. N., *Geoenvironmental Engineering: Contaminated Soils, Pollutant Fate and Mitigation*," CRC Press, Boca Raton, FL, 2000.

Yong, R. N., Bentley, S. P., Harris, C., and Yaacob, W. Z. W., "Selective Sequential Extraction Analysis (SSE) on Estuarine Alluvium Soils," *Proc. 2nd BGS Conference on Geoenvironmental Engineering*, Thomas Telford, London, 1999, pp. 118–126.

Yong, R. N., Galvez-Cloutier, R., and Phadingchewit, Y., "Selective Extraction Analysis of Heavy-Metal Retention in Soil," *Can. Geotech. J.*, 30(5), 834–847 (1993).

Yong, R. N. and Mulligan, C. N., *Natural Attenuation of Contaminants in Soils*, CRC Press, Boca Raton FL, 2004.

Zeien H. and Brummer G. W., 1989, "Chemische Extrakionen zur Bestimmung von Schwermetallbindungsformen," *Boden. Mitt. Dtsch. Bodenkd. Ges.* 59(1), 505–510 (1989).

Journal of ASTM International, Vol. 3, No. 7
Paper ID JAI13338
Available online at www.astm.org

Catherine N. Mulligan[1] *and Raymond N. Yong*[2]

Overview of Natural Attenuation of Sediments

ABSTRACT: Natural attenuation involves the use of the natural processes with the soil and groundwater to remediate contamination by physical, chemical, and biological processes to reduce the risk to human health and the environment. Although the use of natural attenuation as a treatment process is increasing for remediation of contaminated groundwater, much less research has focused on contaminated soils and sediments. Industrial effluents, agricultural runoff, and sewage discharges are major sources of contaminants for the sediments. In addition, benthic organisms can transport contaminants through bioturbation and there is considerable variability at sites. Organic materials, a particularly important component of the sediments, can sequester the contaminants. Sediment-water partitioning controls the release of the contaminants into pore water and benthic organisms. Fate and transport mechanisms for both organic and inorganic contaminants within the sediments need to be understood to establish protocols for the monitoring and use of natural attenuation.

KEYWORDS: natural attenuation, sediments, contaminant transport, protocols, mechanisms

Introduction

Approximately 0.9 billion m^3 of sediment are contaminated which are a risk to fish, humans, and animals that eat the fish, according to the United States Environmental Protection Agency (USEPA) (1998). The contaminants that are left in the sediment environment without intervention can undergo naturally occurring processes. It is often more cost effective than dredging, capping, or treatment or combinations thereof, of the contaminated sediments and can be appropriate for low risk areas. Like natural attenuation of soil and groundwater, monitoring is a key element in determining the success and applicability of this remediation method. The natural processes include biological degradation, volatilization, dispersion, bioturbation, dilution, radioactive decay, sorption of the contaminant onto the organic matter and clay minerals in the sediments, and natural capping processes. These mechanisms will be discussed further later on.

Natural attenuation is mainly used for benzene, toluene, ethyl benzene, and xylene (BTEX) and more recently for chlorinated hydrocarbons. Other contaminants that could potentially be remediated by natural attenuation include pesticides, polychlorinated biphenyls (PCBs), and inorganic compounds (Yong and Mulligan 2004). The success of natural attenuation depends on the site conditions, sediment characteristics, and microbiology. In this paper, the mechanisms involved and case studies of natural attenuation of various pollutants at contaminated sediment sites will be examined.

Natural Attenuation Processes of Sediments

Abiotic Processes

Natural capping is one of the dominant mechanisms in sediments. This involves the covering of the contaminated sediments with clean sediments (Cardenas and Lick 1996), thus forming a barrier between the contaminated sediments and the aquatic environment. Sediment deposit rates will thus determine the rate of attenuation in this case.

Adsorption reactions or processes involving organic chemicals and soil fractions are governed by: (a)

Manuscript received March 30, 2005; accepted for publication June 30, 2005. Presented at ASTM Symposium on Contaminated Sediments: Evaluation and Remediation Techniques on 23–25 May 2006 in Shizuoka, Japan; M. Fukue, K. Kita, M. Ohtsubo, and R. Chaney, Guest Editors.

[1] Research Chair in Environmental Engineering, Concordia University, Montreal, Canada.
[2] North Saanich, B.C., Canada.

the surface properties of the soil fractions; (b) the chemistry of the porewater; and (c) the chemical and physical-chemical properties of the pollutants. In general, organic chemical compounds develop mechanisms of interactions which are somewhat different from those given previously for inorganic contaminants. If the transport of organic chemicals in soils is considered, interactions between the contaminant and soil surfaces are important in predicting the retention capacity of the soil and the bioavailability of the contaminant. The interaction mechanisms are influenced by soil fractions, the type of and size of the organic molecule, and the presence of water. As in the case of inorganic contaminant-soil interaction, the existence of surface active fractions in the soil such as soil organic matter (SOM), amorphous noncrystalline materials, and clays can significantly enhance oil retention in soils significantly because of large surface areas, high surface charges, and surface characteristics.

The distribution of organic chemical pollutants between soil fractions and porewater is generally known as *partitioning*. By this, chemical pollutants are partitioned such that a portion of the pollutants in the porewater (aqueous phase) is removed from the aqueous phase. From the study of partitioning of heavy metals, it seems that this assumption of sorption by the soil fractions may not be totally valid. This is because precipitation of the heavy metals will also serve to remove the heavy metals from solution. Precipitation mechanisms for organic chemical pollutants do not occur so, it is generally assumed that the total "partitioned" organic chemicals are sorbed or attached to the solids. The partitioning or distribution of the organic chemical pollutants is described by a coefficient identified as k_d. As defined previously, this coefficient refers to the ratio of the concentration of pollutants "held" by the soil fractions to the concentration of pollutants "remaining" in the porewater (aqueous phase), i.e., $C_s = k_d C_w$, where C_s refers to the concentration of the organic pollutants sorbed by the soil fractions and C_w refers to the concentration remaining in the aqueous phase (porewater) respectively.

The linear constant k_d, partition coefficient, used in the retardation coefficient R which is represented as $(1+[\rho^*/n]/k_d)$, implies that adsorption by the soil fractions is infinite. The factors ρ^* and n are bulk density of the soil divided by the density of water and the soil porosity, respectively. As the concentration of contaminants increases, the sorption also increases. K_d is strongly related to f_{oc} (fraction of organic carbon) and this relationship is often shown as $k_d = f_{oc} k_{oc}$ where k_{oc} is the soil/sediment-water distribution coefficient. Although it is not always linear adsorption with soil organic matter (SOM), k_{oc} is important in fate and transport modeling.

K_{oc} estimations have been through one-parameter linear free energy relationships over many decades. Quantitative structure-activity relationships (QSARs) have been developed. Correlations between $\log k_{oc}$ and $\log k_{ow}$ (the octanol-water partition coefficient) and between $\log k_{oc}$ and $\log S_w$ (water solubility) have also been utilized. Recently, polyparameter linear free energy relationships for estimating k_{oc} have been developed as the one parameter linear relationships are not accurate for polar chemicals (Nguyen et al. 2005). Various factors can influence the k_{oc}. For the sorption of oils, the concentration of the oil and the weathering state must be accounted for (Jonker et al. 2003).

For the Dover site (Witt et al. 2002) where the organic fraction is low ($f_{oc}=0.00025$), R values for perchloroethylene (PCE), trichloroethylene (TCE), and dichloroethylene (DCE) were determined as 1.3, 1.2, and 1.1, respectively. At $R=1.3$, transport across the site would take about 49 years. Polycyclic aromatic hydrocarbons (PAHs) with increasing molecular weights exhibit higher low k_{ow} and are thus bound more strongly to organic matter.

Organic matter exists as dissolved and suspended forms and on the bottom sediments. The functional groups of the organic matter interact with heavy metals. The affinities of these groups for heavy metals in decreasing order are

$$\text{enolates} > \text{amines} > \text{azo compounds} > \text{ring N} > \text{carboxylates} > \text{ethers} > \text{carbonyls}.$$

On the other hand, however, organic matter may lead to the extraction of the heavy metals via mineral dissolution and solubilization of metal sulfides and carbonates.

Volatilization may be an important attenuation mechanism for volatile organic contaminants. Freshly spilled petroleum products such as gasoline can exhibit high rates of volatilization that can occur from the free phase or dissolved phase. Henry's constant law describes volatilization from the dissolved phase. The rate of volatilization slows as the age of the spill increases. As a general guideline, a dimensionless

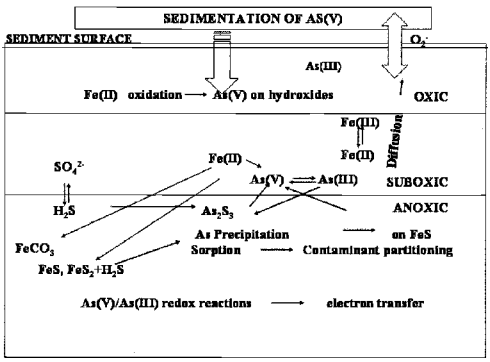

FIG. 1—*As cycling mechanisms in sulfidic environments (adapted from Bostick et al. 2004).*

Henry's constant greater than 0.05 means that volatilization or off gassing is likely, while if it is less than 0.05, volatilization would be negligible. In sediments, this mechanism is not a dominant one due to the depth of the sediments in the water column.

The abiotic reactions and transformations are sensitive to at least two factors: (a) the physicochemical properties of the pollutant itself, and (b) the physico-chemical properties of the soil (i.e., soil fractions comprising the soil). Similar to inorganic contaminants, abiotic chemical reactions with organic compounds occur and include (a) hydrolysis, (b) formation of a double bond by removal of adjacent groups, and (c) oxidation/reduction, dehydrohalogenation, or hydrolysis reactions. For example, hydrolysis half-lives for PCE and TCE have been estimated as 9.9×10^8 and 1.3×10^6 years (Jeffers et al. 1989).

Chemical mass transfer is responsible for partitioning of contaminants in the fate and transport of contaminants. Reduction-oxidation reactions can also play an important role in the fate of the contaminants. Assessment of the retention or retardation processes is required to understand partitioning and the attenuation of contaminants within the sediment. If potential pollution hazards and threats to public health and the environment are to be minimized or avoided, we must ensure that the processes for contaminant attenuation are irreversible and the levels of contaminants are below allowable limits or levels.

For example, for arsenic, two models exist in respect to possible mechanisms for release of arsenic from the arsenic-bearing materials: (a) reduction mechanisms and (b) oxidation processes. In the former process, it is reasoned that reductive dissolution of arseniferrous iron oxyhydroxides releases the arsenic responsible for pollution of the groundwater. The other model for arsenic release from the alluvium relies on oxidation of the arsenopyrites as the principal mechanism. This occurs when oxygen invades the groundwater because of the lowering of the groundwater from the abstracting tubewells. The sorption of arsenic(III) by anoxic estuarine sediments has been studied by Bostick et al. (2004). Although sorption was apparent at all pH values, it was more significant at $pH > 7$. Sorption conformed to Langmuir isotherms. Iron sulfide fractions led to most of the sorption. In addition, over time, the FeAsS-like precipitates reacted to form As_2S_3 and when combined with the drop in redox potential stabilized the arsenic as shown in Fig. 1. The sorbed species of arsenic were determined by extended x-ray absorption fine structure (EXAFS) spectroscopy.

Biotic Processes

Understanding the types of chemicals that can be biodegraded or transformed, and the pathways of conversion, are important and will be discussed, as well as the toxicity and availability of several chemicals since this will serve as the foundation of knowledge required for determining the potential for natural attenuation. These concepts are described in further detail in Yong and Mulligan (2004).

Microorganisms, the key to the biological treatment of contaminants, include bacteria, protozoa, fungi, algae, and viruses (Mulligan 2002). A wide variety of hydrocarbons can be degraded by microorganisms through electron transfer by various mechanisms. Most of the knowledge related to natural attenuation is related to the degradation of BTEX compounds. The availability of oxygen and other electron acceptors such as nitrate, sulfate, and iron (III) determine the rate of biodegradation. However, anaerobic methano-

genic degradation of benzene in aquifer sediments has been shown despite the lack of the electron acceptors (Weiner and Lovley 1998). Other factors include the presence of water and mineral nutrients. Although the rate of aerobic biodegradation is higher than anaerobic, the latter type may be more dominant. Products of aerobic degradation are carbon dioxide and water while the products of anaerobic degradation include carbon dioxide, water, methane, hydrogen, nitrogen, and others. For chlorinated compounds (PCE and TCE), the reductive dehalogenation products of cis-DCE, vinyl chloride (VC), and ethane are indicators of degradation.

The fuel oxygenate (methyl tert butyl ether, MTBE) has been found in various surface water sources from atmospheric deposition, stormwater runoff, industrial releases, recreational activities, and discharge of groundwater. Microorganisms, however, within the stream and lake sediments are able to biodegrade the MTBE (Bradley et al. 2001). Increasing the silt and clay content decreased MTBE degradation almost completely, most likely due to a decrease in oxygen permeability into the sediments. Increasing the organic content also slightly correlated with a decreased in biodegradation. There may have been competition between the organic substrates.

Heavy metals are also subject to microbial conversions. Sediment samples, near a mining area in Spain of the largest producer of mercury (Hg), indicated concentrations of 2300 $\mu g/g$ of Hg and 82 ng/g of methyl-Hg (Gray et al. 2004). These elevated methyl-Hg levels are an indication that microbial methylation is highly likely to occur in the wet, anoxic sediments with high organic contents. Rittle et al. (1995) showed in the laboratory that arsenic could precipitate by bacterial sulfate reduction, thus immobilizing the arsenic on the sediments.

Microcosm studies, polymerase chain reaction analysis (PCR) and site data can be used to determine the potential for natural attenuation at a site. Samples from both the groundwater and sediment are required. Microcosms are useful for identifying degradation potential under various nutrient and electron-donor conditions. For example, PCR analysis can provide information on the presence and spatial distribution of dechlorinating bacteria on site (Fennell et al. 2001).

Although the remediation of most sites is in temperature climates, the feasibility of natural attenuation at subarctic sites has been evaluated (Richmond et al. 2001). Although TCE and TCA degradation products were found and reductive dechlorination conditions were likely, rates of degradation were slow and thus dilution not biodegradation was the dominant attenuation mechanism. BTEX biodegradation was likely in the past. In situ sediment microcosm studies with organic acid measurement may be helpful in determining natural attenuation biodegradation mechanisms in dilute systems.

Bioattenuation and Bioavailability

Determination of the capacity for bioattenuation has not received a great deal of attention in assessment of the natural attenuation of organic chemical pollutants. Substrates can become less bioavailable via interaction with negatively charged clay particles and organic material (Alexander 1982). Sorption and sequestration can be influenced by pH, organic matter content, temperature, and pollutant characteristics. The biodegradation of PAHs is particularly affected by sorption.

Bioavailability of contaminants can influence microbial activity and biological responses. There exist many definitions of bioavailability, depending on the discipline. The National Research Council (NRC) (2002) in a recent report indicated that "bioavailability processes as the individual physical, chemical, and biological interactions that determine the exposure of organisms to chemicals associated with soils and sediments." Ehlers and Luthy (2003) recently attempted to define the terms, bioaccessibility, and bioavailability to improve risk assessment and remediation technology selection. Bioavailable contaminants are immediately available to an organism for storage, transformation, or biodegradation. However, bioaccessible chemicals could be available to an organism after release from soil organic matter or other physical constraints after a short or lengthy time period. This is indicated in Fig. 2.

Therefore, determination of sediment or soil contents could be used to indicate biodegradation potential. Changes in porosity can also occur as a result of dissolution processes. Excessive carbon dioxide produced can also increase porosity because of calcite and dolomite dissolution under acidic conditions (Bennett et al. 2000). Other reactions under anoxic conditions such as carbonate and bicarbonate saturation with calcite can plug pore spaces and decrease permeability.

A variety of other products from bacteria can also influence the desorption of hydrocarbons and metals from the soil and sediments. Due to their anionic and hydrophilic/hydrophobic nature, biodegradable

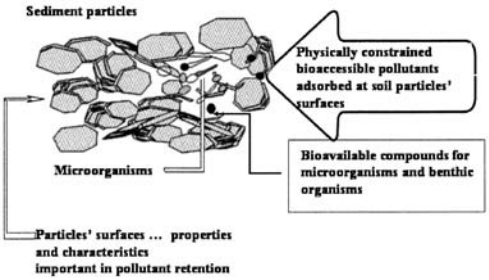

FIG. 2—*Bioavailability and bioaccessibility of contaminants in sediments.*

surfactants including rhamnolipids, surfactin, and sophorolipids, by-products of bacteria or yeast, have been able to remove metals and hydrocarbons from an oil-contaminated soil by disruption of the pollutant/soil bonds (Mulligan 2005).

Bioturbation

Burrowing, feeding, and ventilation activities of benthic organisms are known as bioturbation. Deposit feeders ingest sediment, move sediments toward the surface, and irrigate porewater. Banta and Andersen (2003) reviewed the mechanisms of the interaction of bioturbating organisms with sediment contaminants. Recalcitrant organic matter can be moved from anoxic to oxic zones, thus stimulating biodegradation. Insoluble metal complexes may also be oxidized which can then serve as electron acceptors for biodegradation. The focus of the review was on the polychaetes *Arenicola marina* and *Nereis diversicolor. A. marina* affects transportation via particle mixing, pore water flushing through irrigation, and degradation of organic pollutants via stimulation of microbial activity. *N. diversicolor* stimulates biodegradation directly through metabolism of the contaminants and affects biodiffusive mixing. It can also stimulate microbial activity. This study has indicated the complicated effects that bioturbation has on the fate and transport of contaminants in the sediment. Models should be mechanistically correct to predict the effect of bioturbation on the fate of pollutants such as shown by the model by Forbes and Kure (1997). This model was coupled with a adsorption-degradation model by Timmermann (2001).

The effect of the burrowing of the polychaete on sediment contaminated with 3, 3′,4, 4′ tetrachlorobiphenyl was evaluated (Gunnarsson et al. 1999). Bioturbation enhanced the release of the contaminant and organic matter enhanced the release of the contaminant in the water column by 280% compared to the control. The enhanced release of the contaminant by the organic matter is contrary to other studies.

Zinc fluxes in the presence of bioturbating organisms with and without capping were studied (Simpson et al. 2002). Without capping, zinc fluxes were in the order of 10 to 89 mg Zn/m^2-day. Removal of benthic organisms decreased bioturbation. Capping with clean sediment (5 mm thickness) was effective in reducing zinc fluxes by forming anoxic environments for the formation of metal sulfides. Capping materials were disturbed by the organisms and therefore it was recommended that depths of the capping material must be greater than 30 cm. Overall, the mechanisms for natural attenuation in sediments can be seen in Fig. 3.

Selective Sequential Extraction

To determine the speciation of metals in soils and sediments, various methods are used. The speciation enables evaluation of the solubility, transport, and bioavailability of the components and can be effective for designing treatments. One method is to use specific extractants. By sequentially extracting with solutions of increasing strengths, a more precise evaluation of the different fractions can be obtained (Tessier et al. 1979). A soil or sediment sample is shaken over time with a weak extractant, centrifuged, and the supernatant is removed by decantation. The pellet is washed in water and the supernatant removed and combined with the previous supernatant. A sequence of reagents is used following the same procedure until, finally, mineral acid is used to extract the residual fraction. Heavy metal concentrations are then

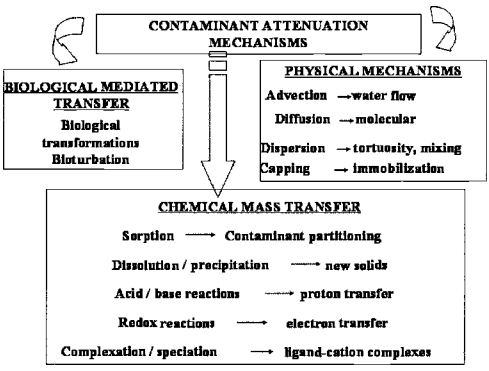

FIG. 3—*Mechanisms of natural attenuation of sediment (adapted from Yong and Mulligan 2004).*

determined in the various extracts by atomic absorption, inductively coupled plasma (ICP), or other means. Numerous techniques and reagents have been developed and have been applied to soils (Shuman 1985), sediments (Tessier et al. 1979), sludge-treated soils (Petrozelli et al. 1983) and sludges.

Metal speciation of solid-state sediments may be obtained by spectroscopic methods such as X-ray absorption fine structure in sediments (XAFS) (Helz et al. 1996). Detection limits as low as microgram/gram can be achieved at ambient atmospheric temperatures for wet sediments. Since synchotron radiation is required for XAFS, only a few researchers have access to this type of equipment. X-ray absorption near-edge structure (XANES) or extended X-ray absorption fine structure (EXAFS) can be used to determine the valence states of elements.

Both solid state and chemical extractions were used for mercury speciation (Kim et al. 2003). 100% of the Hg was in the form of insoluble cinnabar, and metacinnabar were identified by XAFS removed from the strongly complexed fraction (12 N HNO_3) and the aqua regia extraction of a marine sediment. Reducing conditions could increase the mercury sulfides that could be removed by concentrated HCl. Bloom et al. (2003) determined the methylation potential of anoxic sediments. The F3 fraction (extracted with 1 M KOH, organochelated) exhibited the greatest potential for methylation. This fraction and the F5 (aqua regia extraction) were the most commonly found in the sediment samples. Multiple analytical techniques can improve predictions of availability and the design of potential remediation techniques.

This method can be used to determine if heavy metals are removable by remediation techniques or to predict removal efficiencies (Mulligan and Dahr Azma 2003). Sequential extraction can be employed for the evaluation of the most appropriate sediment remediation technology and for monitoring remediation procedures. A biosurfactant, rhamnolipid, was used to remove organic-bound copper and carbonate-bound zinc. Exchangeable, carbonate, reducible oxide and organic fractions are amenable to washing techniques, and residually bound contaminants are not economical or feasible to remove. This information is important in designing the most appropriate conditions for sediment washing.

Protocols Developed for Natural Attenuation

Various technical protocols have been established such as the *Designing Monitoring Programs to Effectively Evaluate the Performance of Natural Attenuation* by the Air Force Centre for Environmental Excellence (Weidemeier and Haas 1999). Sampling type, frequency and location, and analyses required for NAPL contaminants are described. The *Technical Protocol for Evaluation Natural Attenuation of Chlorinated Solvents in Ground Water* (Weidemeier et al., 1998) was established to demonstrate mechanisms of chlorinated solvent natural attenuation. The USEPA (2001) points out, however, that field information can be substantially different from laboratory research, particularly regarding dechlorination rates and product concentrations. For chloromethane, chloroethanes, chlorinated benzenes, and chlorinated ethers, the reductive dechlorination rates need to be compared in the laboratory and field. Field information is not available for many processes and their reaction rates. There are other uncertainties related to interactions with other

contaminants, high concentrations at the source area, and other mechanisms for degradation than reductive dechlorination.

To demonstrate that natural attenuation is taking place, lines of evidence are established to indicate decreases in contaminant concentrations (NRC 1993). They include:

- Decreases in contaminant concentration and/or plume size over time. This is used to indicate that biodegradation is occurring faster than plume size increases.
- Geochemical and biochemical indicators of microbiological activity in the groundwater chemistry such as consumption of oxygen, nitrate, and sulphate and production of Fe(II), Mn(II), and methane.
- Laboratory microcosm studies are used to simulate aquifer conditions to determine if bacteria at the site can biodegrade the contaminants and at what rate. This step is mainly used if neither of the first two clearly indicates significant trends.

Of the three lines of evidence suggested by the NRC (1993), it is suggested that primary lines are usually required. Secondary or tertiary are required only if primary lines are insufficient. Site specific attenuation rates can be used as a secondary line of evidence showing that attenuation is occurring and the rate at which is occurring. Monitoring frequency is according to the potential impact on receptors, ability to meet remedial goals, plume behavior, and institutional controls used. Contingency plans are necessary only if the goals cannot be met.

Protocols have been reviewed by the NRC (2000). The number of samples, parameters to be monitored and contaminant concentrations to be obtained can vary substantially among the protocols. For example, in addition to those mentioned above, 14 federal, state, profession and industry protocols were evaluated. Community concerns, scientific and technical issues, and implementation issues were considered. Only seven have been peer reviewed.

The USEPA (2001) has recommended the establishment of procedures for evaluating the natural attenuation of inorganics. Natural attenuation mechanisms for arsenic and other inorganics should be determined. The effect of geochemical conditions on remobilization must be established. The effect of organics on inorganic contaminant behavior and vice versa should be studied. Guidelines need to be developed to understand immobilization processes based on laboratory and field data and the use of models. Uncertainty needs to be incorporated.

The majority of the available protocols address only fuel hydrocarbons or chlorinated solvents. Other organic contaminants such as PAHs, PCBs, explosives, and pesticides are not addressed while metals, inorganics, and radionuclides are infrequently discussed. Therefore, there are major shortcomings in these protocols.

One aspect not considered by the NRC, since their focus was groundwater, was that most protocols are designed for groundwater natural attenuation and not for soil natural attenuation or sediments. Few protocols exist for soil with the exception of the USEPA (1998) and those by the Department of Energy (DOE). Sediments have not received much attention at all. Sediments differ from soils since they can be transported. Organisms can transport contaminants and there is considerable variability at sites. Technical protocols have not been developed for sediments. The USEPA (2001) has recommended that research be expanded to determine natural attenuation mechanisms in sediments, monitoring methods need to be developed for quantifying natural attenuation, the contaminant transport and bioaccumulation for analysis and assessment. Research specific for fresh water, coastal, and marine aquatic environments is also required. A protocol adapted from Yong and Mulligan (2004) for sediments can be seen in Fig. 4.

Witt et al. (2002) demonstrated the use of a lines of evidence approach in indicating natural attenuation for groundwater and aquifer sediment remediation. The first line of evidence was a loss of 40% of PCE and TCE at field scale. The second line of evidence was the presence and distribution of biogeochemical indicators including low and higher concentrations of dissolved oxygen, low concentrations of iron (II), low concentrations of sulfate, and the presence of elevated levels of methane and hydrogen, presence of cis-DCE, VC, and TCE and elevated chloride levels. The presence of catabolic genes of mono- and di-oxygenases indicated co-oxidation of PCE and TCE and decreasing cis-DCE, VC, and methane levels. Finally, the third line of evidence was that microbiological data supported biodegradation. Indigenous bacteria were capable of degrading PCE and TCE.

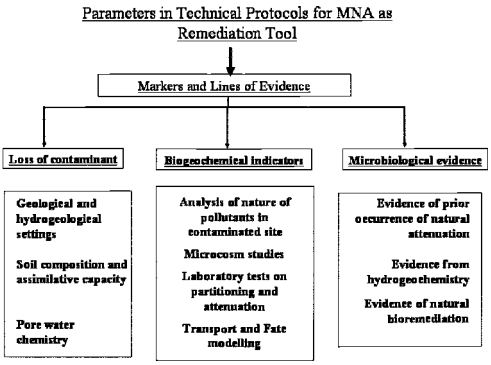

FIG. 4—*Protocol for natural attenuation of sediments (adapted from Yong and Mulligan 2004).*

Case Studies

In this section, various case studies of natural attenuation will be examined. For example, in Germany, levels of nitrate as high as 250 mg/L, aluminium as high as 0.64 mg/L and potassium up to 60 mg/L have been found in the groundwater in agricultural areas (Houben 2002). Acid rain has decreased the pH of the soil to 2.75 and the groundwater to 3.4. The soil buffering capacity has also diminished. Cation exchange and autotrophic denitrification (reaction of nitrate with FeS_2) natural attenuation mechanisms have restricted the movement of the pollutants. Modeling including determination of the groundwater age, mass balances, and reactive transport was performed using hydrochemical and geochemical data. The PHREEQC-2 model was used for the hydrochemical equilibrium modeling. Sorption and desorption column experiments with undisturbed samples of sandy sediments for magnesium, sodium, potassium, and aluminium ions were performed. Modeling was accurate for most ions with the exception of potassium. Competition cannot be accounted for in the mass balance approach. Due to the high velocity in the columns, there was not even time for the nitrate to react with the pyrite. The models indicated that the contaminants move a few centimeters per year.

The ability of sediments to retain organic contaminants is one of the keys to natural attenuation. At another site in Germany, a lignite seam accumulated aliphatic and aromatic chlorinated hydrocarbons downstream from a chemical plant (Dermietzel and Christoph 2002). A two-compartment model was shown to approximate the experimental results. An initial fast desorption based on transfer from the outer surface of the sediment was followed by a slower diffusion controlled released from the interior of the sediment.

In 1998, sediment samples at Lake Harwell, SC were taken at five places to determine the occurrence of natural attenuation of polychlorinated biphenyls (PCB) (Pakdeesusuk et al. 2005). The mole percentage of each congener of PCB and/or changes in the total of meta, para, and ortho chlorines and total chlorines per biphenyl were determined and compared to 1987 sediment samples. Solubilization and desorption were negligible according to mass balances. It was concluded that in situ dechlorination was occurring at a slow rate since 1987, after an initial rapid rate. Microcosm studies supported the findings. Lack of information on organic matter and electron acceptors such as nitrate, sulfate, iron, and manganese make it difficult to predict optimal dechlorination conditions. Capping with fresh sediment may need to be increased to decrease the risk of bioaccumulation in fish.

Trichloroethene contamination in the groundwater was first detected in 1982 at a Michigan National Priorities List site (An et al. 2004). Samples were monitored in 1991, 1992, 1994, 1995, and 1998, 100 m from the shore and later, 3 m from the shore. Products of dichloroethene (DCE), vinyl chloride (VC), ethene, and methane were found, indicating anaerobic degradation. Degradation rates were estimated using a two-dimensional (2D) model. Analysis of the water in the lake sediments indicated natural attenuation.

Although most protocols indicate the dominance of the biological degradation, other mechanisms may also be significant. Ferrey et al. (2004) indicated that although there was no evidence of biodegradation cis-dichloroethylene (cis-DCE) and 1,1 DCE, iron minerals such as magnetite removed these compounds

from sterilized sediments by reductive dechlorination. Sorption, particularly to organic matter, did not appear to be responsible for the loss.

At the Columbus Air Force Base, Columbus, MS, 60 sediment samples were taken to evaluate the fate and transport jet fuel contaminants (Stapleton and Sayler 1998). DNA probes were used to determine the genes for the following degradative enzymes: alkane dioxygenase, toluene monooxygenase, naphthalene dioxygenase, toluene dioxygenase, toluene monooxygenase, xylene monooxygenase, carbon monoxide dehydrogenase, and methyl coenzyme reductase. 10^7 to 10^8 organisms per gram of sediment were found, compared to 10^4 to 10^6 organisms per gram by traditional methods. Degradation of BTEX and naphthalene were also indicated, particularly after five to seven days. More than 40% of these ^{14}C-labeled compounds were mineralized in the sediments, without nutrient addition. Correlations of laboratory assay and field analyses are required and thus further field tests will be performed.

At the Dover Air Force Base, Dover, DE, contaminated with chlorinated ethenes, a characterization of the microbial community was performed (Davis et al. 2002). Low biomass levels ($<10^7$ bacteria per gram sediment) were found. Mineralization of vinyl chloride and cis-DCE was occurring and 16 S rRNA gene sequence indicated the presence of anaerobic microorganisms that were capable of anaerobic halorespiration and iron reduction. The data showed that the microorganisms were the major mechanism for reductive and oxidative attenuation of the chlorinated ethenes.

The weathering of PAH contaminated sediments was monitored by Brenner et al. (2002) at the Wyckoff/eagle Harbor Superfund Site near Seattle, Washington. Three PAH sources were determined (creosote, urban runoff, and natural background). Urban runoff was found to contribute to the contamination over the past 50 to 70 years. Unweathered and pure-phase creosote deposits were found below 30 cm in depth. However, surface sediments (upper 20 to 30 cm) were a mixture of weathered creosote and urban runoff. Lower molecular weight PAHs in particular were lost in creosote-contaminated weathered sediments. Capping of 1 to 3 m of clean sand was performed since the deposit of clean sediments was not extensive due to continuous contamination from urban runoff.

Moser et al. (2003) evaluated a "freeze core" sampling method for determining the geochemistry and microbiology of sediments contaminated with chromium (VI). Liquid nitrogen was used to freeze the cores. Significant numbers of sulfate, nitrate, and iron-reducing bacteria in addition to amounts of acid-volatile sulfide were found but the freezing decreased the numbers viable bacteria. This indicated the potential for a combination of anaerobic microbial and chemical processes to contribute to the natural attenuation of chromium at the Hanford site. Reduction of chromium (VI) to chromium (III) decreases its solubility and toxicity.

Arias et al. (2003) also studied Cr (VI) natural attenuation in sediments by laboratory mesocosms to mimic environmental conditions. Cr accumulated in the upper 5 mm of the sandy sediments. However, Fe, Mn, and total organic contents did not correlate with total Cr levels. PCR of 16S rRNA genes were used to analyze microbial populations and indicated that the microbial population were inhibited and therefore little information regarding the bacteria present if natural attenuation is to be employed.

A study of heavy metals was conducted in Port Philip Bay, Australia as there were indications of toxic metals in fish and shell fish (Fabris et al. 1999). The objective was to determine the partitioning of heavy meals in dissolved and particulate species in the bay waters. Despite a flushing time of 10 to 16 months in the bay, concentrations in the near shore and estuarine areas were not higher than those in the coastal marine waters. Most of the mechanisms for partitioning were related to precipitation of iron and manganese oxyhydroxides that coprecipitate with dissolved heavy metals. There was a strong correlation of iron with chromium, nickel and zinc in the particulates. Contrary to the metals, arsenic concentrations [as As (III)] increased in depth in the sediments and thus did not seem to be the result of anthropogenic activity. Near the surface layer of sediments, arsenic is oxidized to As (V) and leaves the sediments. Fe (III) can co-precipitate some of the arsenic and become trapped in the sediments.

Evaluation of the Natural Attenuation of Sediments

As with soil, the application of natural attenuation requires the understanding of the sediment-contaminant interactions, in addition to the environmental conditions. Much less information exists regarding the natural attenuation of heavy metals than for organic chemicals, although there are numerous partitioning mechanisms that can play a role. Dredging, however, can disrupt these conditions by increasing the

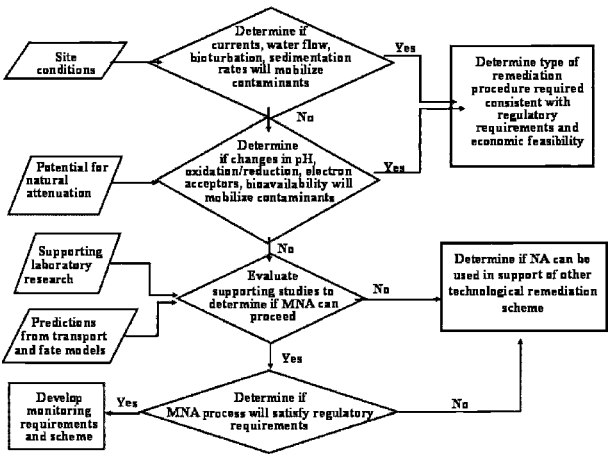

FIG. 5—*Schematic for determining the applicability of natural attenuation for sediments (adapted from Yong and Mulligan 2004).*

oxidation conditions which can lead to increased mobility and bioavailability of heavy metals. Zinc, copper, lead, cadmium, nickel, and mercury have all increased in mobility during dredging (Darby et al. 1986).

However, unlike soil, special environmental conditions in lakes, streams, rivers, estuaries, seas, and oceans can potentially lead to the mobilization of contaminants. Some of these include flowing water and currents which enhance mixing, dilution, and diffusion of contaminants. Storms and other high wave events may resuspend sediments. Bioturbation can cause particle mixing and solute transport which can also influence pollutant movement. Knowledge on the presence and distribution of the infauna and their mechanisms of bioturbation will be required to predict the behavior of the contaminants in the sediments (Banta and Andersen 2003). Natural capping through sedimentation of clean sediments can maintain the reducing conditions.

Changes in pH, oxidative/reduction conditions, inorganic and organic complexation, and microbial populations can influence adsorption, absorption, sedimentation, and precipitation. The factors must be understood to determine the potential of natural attenuation for remediation of the contaminated sediments. Techniques such as selective sequential extraction can assist in evaluating the potential for heavy metal mobilization. For organic contaminants, knowledge of the k_{oc} and k_{ow} partition coefficients provide information on the contaminant characteristics. The strength of the bonding mechanisms and the age of the contamination in the sediments must be known.

Figure 5 shows the general protocol for considering monitored natural attenuation (MNA) as a remediation of contaminated sediments. Site specific data must be evaluated. Laboratory tests and predictive models are also necessary to provide information on the ability of the site materials and conditions to attenuate the contaminants. Insufficient conditions for natural attenuation would require technological remediation such as capping with clean sediments, sand, or other materials or other methods including dredging.

Monitoring is essential in determining the success of natural attenuation in reaching the remediation goals and thus, the use of the terminology, MNA. The pollutants both in the water and sediments need to be tested to ensure that the environmental conditions (pH, redox changes) have not changed and that the pollutants are not released into the environment. In addition, the laboratory tests and models used for prediction can be confirmed by the monitoring. Human and other receptors must be protected from exposure to the contaminants.

Conclusions

There are various advantages regarding the natural attenuation of sediments including the possibility of destroying the contaminant completely, potentially for reduction in remediation costs and limited site

disruption. Potential disadvantages, however, include longer remediation times compared to other technologies, a lack of knowledge concerning mechanisms for remediation particularly with regard to inorganic contaminants, substantial requirements for monitoring, and the potential for desorption or resolubilization of contaminants.

Although there are many similarities between existing protocols and guidelines for natural attenuation, particularly concerning lines of evidence and data requirements, very few consider the sediments in their protocols and most have been adapted for hydrocarbon and chlorinated solvent contamination. The natural attenuation of many other contaminants has been limited for PAHs, PCBs, pesticides, and inorganic contaminants. The interaction of organic and inorganic contaminants with the soil components may also be an important factor in natural attenuation processes. Some of the natural attenuation processes that are specific for sediments are sediment deposition and resuspension, mixing due to wave action, and bioturbation and thus are not included in groundwater protocols.

In addition, there is little information available regarding the comparison of the natural attenuation processes in the various sediment environments (rivers, estuaries, lakes, and coastal seas and oceans). The processes are site specific and therefore, the evaluation of these processes must also be.

References

Alexander, M., "Aging, Bioavailability and Overestimation of Risk from Environmental Pollutants," *Environ. Sci. Technol.* 34, 4259–4265 (1982).

An, Y-J., Kampbell, D. H., Weaver, J. W., Wilson, J. T., and Jeong, S-W., "Natural Attenuation of Trichloroethene and its Degradation Products at a Lake-Shore Site," *Environ. Pollut.*, 130, 325–335 (2004).

Arias, Y. M., Obraztsova, A., and Green-Ruiz, C., "Natural Attenuation of Cr(VI) Contamination in Laboratory Mesocosms," *Geomicrobiol. J.*, 20, 389–401 (2003).

Banta, G., and Andersen, O., "Bioturbation and the Fate of Sediment Pollutants—Experimental Case Studies of Selected Infauna Species," *Vie et Mileu.* 53, 233–248 (2003).

Bennett, P. C., Hiebert, F. K., and Roger J. R., "Microbial Control of Mineral-Groundwater Equilibria: Macroscale to Microscale," *Hydrogeol. J.*, 8, 47–92 (2000).

Bloom, N. S., Preuss, E., Katon, J., and Hitlner, M., "Selective Extractions to Assess the Biogeochemically Relevant Fraction of Inorganic Mercury in Sediments and Soils," *Anal. Chim. Acta* 479, 233–248 (2003).

Bostick, B. C., Chen, C., and Fendorf, S., "Arsenite Retention Mechanisms with Estuarine Sediments of Pescadero, CA," *Environ. Sci. Technol.*, 35, 3299–3304 (2004).

Bradley, P. M., Landmeyer, J. E., and Chapelle, F. H., "Widespread Potential for Microbial MTBE Degradation in Surface-Water Sediments," *Environ. Sci. Technol.*, 35, 658–662 (2001).

Brenner, R. C., Magar, V. S., Ickes, J. A., Abbott, J. E., Stout, S. A., Crecelius, E. A., and Bingler, L. S., "Characterization and FATE of PAH-Contaminated Sediments at the Wyckoff/Eagle Harbor Superfund Site," *Environ. Sci. Technol.*, 36, 2605–2613 (2002).

Cardenas, M., and Lick, W., "Modeling the Transport of Sediments and Hydrophobic Contaminants in the Lower Saginaw River," *J. Great Lakes Res.*. 22, 669–682 (1996).

Darby, D. A., Adams, D. D., and Nivens, W. T., "Early Sediment Changes and Element Mobilization in a Man-Made Estuary Marsh," *Sediment and Water Interactions*, edited by P. G. Sly, Springer, Berlin, 343–351 (1996).

Davis, J. W., Odom, J. M., DeWeerd, K. A., Stahl, D. A., Fishbain, S. S., West, R. J. Klecka, G. M. and DeCarolis, J. G., "Natural Attenuation of Chlorinated Solvents at Area 6, Dover Air Force Base: Characterization of Microbial Structure," *J. Contam. Hydrol.*, Vol. 57, 41–59 (2002).

Dermietzel, J., and Christoph, G., 2002, "The Release of Pollutants from Aged Field Sediments. IAHS Publications," *IAHS Publications-Series of Publications and Reports, Internal. Assoc. Hydrological Sciences.* Vol. 275, 147–151.

Ehlers, L. J., and Luthy, R. G., "Contaminant Bioavailability in Soil and Sediment," *Environ. Sci. Technol.*, 37, 295A–302A (2003).

Fabris, G. J., Monahan, C., and Batley, G. E., "Heavy Metals in Waters and Sediments of Port Philip, Australia," *Mar. Freshwater Res.*, 50, 503–513 (1999).

Fennell, D. E., Carroll, A. B., Gossett, J. M., and Zinder, S. H., "Assessment of Indigenous Reductive Dechlorinating Potential at a TCE-Contaminated Site Using Microcosms, Polymerase Chain Reaction Analysis and Site Data," *Environ. Sci. Technol.*, 35, 1830–1839 (2001).

Ferrey, M. L., Wilkin, R. T., Ford, R. C., and Wilson, J. T., "Nonbiological Removal of Cis-Dichloroethylene and 1,1-Dichloroethylene in Aquifer Sediment Containing Magnetite," *Environ. Sci. Technol.*, Vol. 38, 1746–1752 (2004).

Forbes T. L., and Kure, L. K. 1997, "Linking Structure and Function in Marine Sedimentary and Terrestrial Soil Ecosystems: Implications for Extrapolation from the Laboratory to the Field," *Ecological Risk Assessment of Contaminants in Soil*, edited by N. M. Van Straalen and H. Lokke, Chapman and Hall, London.

Gray, J. E., Hines, M. E., Higueras, P. L., Adatto, I., and Lasorsa, B. K., "Mercury Speciation and Microbial Transformation in Mine Wastes, Stream Sediments, and Surface Waters at the Almaden Mining District," *Environ. Sci. Technol.*, 38, 4285–4292 (2004).

Gunnaersson, J. S., Hollertz, K., and Rosenberg, R., "Effects of Organic Enrichment and Burrowing Activity of the Polychaete *Nereis diversicolor* on the Fate of Tetrachlorobiphenyl in Marine Sediments," *Envir. Toxicol. Chem.*, 18, 1149–1156 (1999).

Helz, G. R., Mille, C. V., Charnock, J. M., Mosselmans, J. F. W., Pattrick, R. A. D., Garner, C. D., Vaughan, D. J."Mechanism of molybdenum removal from the sea and its concentrations in black shales: EXSFS evidence," *Geochimica et Cosmochimica Acta.* 60, 3631–3642 (1996).

Houben, G. J., "Flow and Transport Modeling-Natural Attenuation of Common Agricultural and Atmospheric Pollutants: Reactive Transport of Nitrate, Potassium and Aluminium," *IAHS Publications*, Vol. 275, 519–524 (2002).

Jeffers, P. M., Ward, L. M., Woytowitch, L. M., and Wolfe, N. L., "Homogenous Hydrolysis Rate Constants for Selected Chlorinated Methanes, Ethanes, Ethenes, and Propanes," *Environ. Sci. Technol.*, 23, 965–969 (1989).

Jonker, M. T. O., Sinke,. A. C., Brils, J. M., and Koelmans, A. A., "Sorption of Polycyclic Aromatic Hydrocarbons to Oil Contaminated Sediment: Unresolved Complex?" *Environ. Sci. Technol.*, 37, 5197–5203 (2003).

Kim, C. S., Bloom, N. S., Rytuba, J. J., and Brown, Jr, G. E., "Mercury Speciation By X-Ray Absorption Fine Structure Spectroscopy and Sequential Chemical Extractions: A Comparison of Speciation Methods, *Environ. Sci. Technol.*, 37, 5102–5108 (2003).

Moser, D. P., Fredrickson, J. K., Geist, D. R., Arntzen, E. V., Peacock, A. D., Li. S.-M. W., Spadoni, T., and Mckinley, J. P., "Biogeochemical Processes and Microbial Characteristics Across Groundwater-Surface Water Boundaries of the Hanford Reach of the Columbia River," *Environ. Sci. Technol.*, 37, 5127–5134 (2003).

Mulligan, C. N., *Environmental Biotreatment*, Government Institutes, Rockville, MD, 2002.

Mulligan, C. N., "Environmental Applications for Biosurfactants." *Environmental Pollution*. 133, 183–198 (2005).

Mulligan, C. N. and Dahr Azma, B., "Use of Selective Sequential Extraction for the Remediation of Contaminated Sediments," *Contaminated Sediments: Characterization, Evaluation, Mitigation/Restoration, and Management Strategy Performance, ASTM STP 1442*, J. Locat, R. Galvez-Cloutier, R. C. Chaney, and K. Demars, Eds., ASTM International, West Conshohocken, PA, 2003, pp. 208–223.

NRC (National Research Council), *In Situ Bioremediation: When Does it Work?* Washington, D.C., National Academic Press, 1993.

NRC (National Research Council), 2000, Natural Attenuation for Groundwater Remediation, Committee on Intrinsic Remediation, *Water Science and Technology Board and Board on Radioactive Waste Management, Commission on Geosciences, Environment and Resources*, Washington, D.C., National Academy Press, 2000.

National Research Council, *Bioavailability of Contaminants in Soils and Sediments: Processes, Tools and Applications*. National Academies Press, Washington, D.C., 2002.

Nguyen, T. H., Goss, K-U, and Ball, W. P., "Polyparameter Linear Free Energy Relationships for Estimating the Equilibrium Partition of Organic Compounds Between Water and the Natural Organic Matter in Soils and Sediments," *Environ. Sci. Technol.*, 39, 913–924 (2005).

Pakdeesusuk, E., Lee, C. M., Coates, J. T., and Freedman, D. L., "Assessment of Natural Attenuation Via

In Situ Reductive Dechlorination of Polychlorinated Biphenyls in Sediments of the Twelve Mile Creek Arm of Lake Hartwell, SC," *Environ. Sci. Technol.*, 39, 945–952 (2005).

Petrozelli, G., Giudi, G., and Lubrano, L., *Proc. Int. Conf. Heavy Metals in the Environment*, Heidelberg, FRG, p. 475. 1983.

Richmond, S. A., Lindstrom, J. E., and Braddock, J. F., "Assessment of Natural Attenuation of Chlorinated Aliphatics and BTEX in Subarctic Groundwater," *Environ. Sci. Technol.*, 35, 4038–4045 (2001).

Rittle, K. A., Drever, J. I., and Colberg, P. J. S., "Precipitation of Arsenic During Bacterial Sulfate Reduction," *Geomicrobiol. J.*. 13, 1–11 (1995).

Shuman, L. M., "Fractionation Method for Soil Microelements," *Soil Sci.*, 140, pp. 11–22 (1985).

Simpson, S. L., Pryor, I. D., Mewburn, B. R., Batley, G. E. and Jolley, D., "Considerations for Capping Metal-Contaminated Sediments in Dynamic Estuarine Environments," *Environ. Sci. Technol.*, 36, 3772–3778 (2002).

Stapleton, R. D., and Sayler, G. S., "Assessment of the Microbiological Potential for the Natural Attenuation of Petroleum Hydrocarbons in a Shallow Aquifer System," *Microb. Ecol.*. 36, 349–361 (1998).

Timmermann, K., "Effect and Fate of Pyrene in Bioturbated Sediment-Development, Verification and Use of Diagenetic Models," M.Sc. Department of Life Science and Chemistry, Roskilde Univ. Roskilde 2001.

Tessier, A., Campbell, P. G. C., and Bisson, M., "Sequential Extraction Procedure for the Speciation of Particulate Trace Metals," *Anal. Chem.*, 51, 7, 844–851 (1979).

U.S. Environmental Protection Agency 1998, EPA's Contaminated Sediment Management Strategy, *EPA-823-R-98-001*, U.S. EPA Office of Water, Washington, D.C.

USEPA, Science Advisory Board, Monitored Natural Attenuation; *USEPA Research Programme—An EPA Science Advisory Board Review, Science Advisory Board (1400A)*, Washington, D.C., 2001.

Weidemeier, T. H., and Haas, P. E., *Designing Monitoring Programs to Effectively Evaluate the Performance of Natural Attenuation*, U.S. Air Force Center for Environmental Excellence, San Antonia, TX, 1999.

Weidemeier, T, Swanson, M. A., Moutoux, D. E., Gordon, E. K., Wilson, J. T., Wilson, B. H., Kampbell, D. H., Haas, P. E., Miller, R. N., Hansen, J. E., and Chapelle, F. H., *Technical Protocol for Evaluating Natural Attenuation of Chlorinated Solvents in Ground Water*, EPA/600//R-98/128, September, EPA Office of Research and Development, Washington, D.C., 1998.

Weiner, J. M., and Lovley, D. R., 1998, "Rapid Benzene Degradation in Methanogenic Sediments from a Petroleum-Contaminated Aquifer," *Appl. Environ. Microbiol.* 64, pp. 1937–1939 (1998).

Witt, M. E., Klecka, G. M., Lutz, E. J., Ei, T. A., Grosso, N. R. and Chapelle, F. H., "Natural Attenuation of Chlorinated Solvents at Area 6, Dover Air Force Base: Groundwater Biogeochemistry," *J. Contam. Hydrol.*. 57, 61–80 (2002).

Yong, R. N., and Mulligan, C. N., *Natural Attenuation of Contaminants in Soils*, CRC Press, Boca Raton, FL, 2004.

SECTION IV: REMEDIATION TECHNOLOGIES

Journal of ASTM International, Vol. 3, No. 6
Paper ID JAI13334
Available online at www.astm.org

Christine S. Manhart[1] *and Ronald C. Chaney*[2]

Modeling TPH Desorption in Unconsolidated Dune Sand during Remediation Using Dual-Equilibrium Desorption (DED) Model

ABSTRACT: The verification of the cleanup of dune sands from a dissolved phase petroleum hydrocarbon plume at an active service station site undergoing ozone treatment is being accomplished through soil and groundwater sampling. We hope to use modeling by the dual-equilibrium desorption (DED) model in order to determine when remedial goals negotiated with the regulatory agencies have been met. The site is located in the harbor area of Crescent City, California in an area underlain by dune sands of marine origin. During remediation of sorbed-phase gasoline and diesel range organics (GROs and DROs) and dissolved-phase methyl tertiary butyl ether, target compounds, intrinsic indicators, by-products, and bacterial composition were monitored in the area groundwater and soil. At present, this monitoring has been employed to establish the degree of cleanup of the sands. In this paper the use of the DED model to verify the degree of cleanup of the sands is presented. Results indicate rapid degradation of the target compounds from the dissolved phase with gradual degradation from the sorbed phase. Degradation of the sorbed phase GROs and DROs was indicated by periodic spikes in dissolved-phase concentrations, which are interpreted as representing desorption events. Co-located soil and groundwater samples were collected at intervals of approximately six to nine months. Results from this verification sampling were modeled using the DED. We hope to find a tool that an investigator at a typical underground storage tank site can use to gauge the success of remediation systems. So far, the DED appears to correlate with samples collected using standard field techniques. The use of this methodology has application in establishing the degree of cleanup of contaminated sandy dredge sediments.

KEYWORDS: dual-equilibrium, desorption, sands, dredge sediments, petroleum hydrocarbons, ozone, remediation, model

Introduction

As sites contaminated with petroleum hydrocarbons are being remediated, there remains a need for a contaminant desorption model that project scientists can use to determine the efficacy of cleanup methods. There are various models available to demonstrate the rate of desorption of various chemicals from either the aquifer matrix or sediment/water interface; however, most models assume either Langmuir or linear desorption rates and are valid for pure chemicals only. The average consultant working in the field will have data for the most common mixtures of gasoline or diesel range organics (GROs and DROs) in the form of results from Total Petroleum Hydrocarbons as gasoline or diesel (TPHg and TPHd) analyses. Determining the physical-chemical constants for mixtures is difficult at best.

In addition, most models assume that adsorption and desorption are similar, but opposing processes that occur at similar rates. Several recent studies, however, indicate that adsorption and desorption most likely occur in a biphasic manner, with a rapid initial response characterized by high concentrations and a second more resistant response characterized by relatively low concentrations (Zhang 2003, Chen et al. 2002, Kan et al. 1998). What this implies is that while adsorption may happen at a rapid rate, desorption, once past the initial rapid phase, is likely to proceed slowly. There may even be a portion of material in this second "compartment" that is irreversibly sorbed (i.e., combined in some sort of organic matrix from which the reaction processes are different from the pure chemical and occur at a much slower rate). This

Manuscript received March 30, 2005; accepted for publication June 27, 2005. Presented at ASTM Symposium on Contaminated Sediments: Evaluation and Remediation Techniques on 23–25 May 2006 in Shizuoka, Japan; M. Fukue, K. Kita, M. Ohtsubo, and R. Chaney, Guest Editors.

[1] Associate Geologist, LACO ASSOCIATES, 21 W. 4th Street, Eureka, CA 95501.
[2] Professor Emeritus, Department of Environmental Resources Engineering, Humboldt State University, 1 Harpst Street, Arcata, CA 95521.

may be leading to the common hysteresis effect observed in many treatment technologies and the persistence of contaminants in both groundwater plumes and water bodies.

Chen et al. (2002) published a dual-equilibrium desorption (DED) model to demonstrate this biphasic nature in the hope of providing a more accurate representation of the desorption process. The basic precepts of the model are that the two compartments have fundamental differences in the patterns of adsorption and desorption that have long-term implications as to remediation goals and the efficacy of remedial technologies. However, as is frequently the case, the model was developed looking only at pure substances and not the mixtures that are most commonly dealt with in a field situation.

Typically, regulators choose concentrations of the contaminants of concern in groundwater as project goals for regulatory closure. Few desorption models can help predict when these remedial goals have been met for concentrations of mixtures such as GROs and DROs given the limitations of the data that are typically collected. Typical data available are limited aquifer and sediment matrix characteristics such as organic carbon and metals content. Our site is an active fueling station located in a coastal area of Crescent City, California. The underlying geology is approximately 40 ft of unconsolidated dune sand comprising the Battery formation overlying the Plio-Plistocene St. George formation, which consists of poorly consolidated silt- and sandstone. In situ chemical oxidation by the sparging of ozone through microporous sparge points began in November 2002. To date, approximately 100 kg of an ozone/air mixture have been injected. The site had been contaminated with approximately 700 kg of sorbed and dissolved-phase TPHg, TPHd, the gasoline constituents benzene, toluene, ethylbenzene, and xylenes (BTEX), and the fuel oxygenates methyl tertiary butyl ether (MtBE), tertiary butyl alcohol (TBA), and tertiary amyl methyl ether (TAME) as well as small volumes of nonaqueous phase liquid (NAPL). These constituents formed the contaminants of concern.

In the program run by the State of California under which this site is being remediated, goals are considered to be met when all of the monitoring wells associated with the project have achieved the agreed-upon concentrations and can remain below them for four consecutive quarters of monitoring after the system is shut down. As petroleum hydrocarbons in groundwater/pore water are remediated fairly quickly, the question becomes at what point the sorbed contaminants are reduced to where rebound will stay below the remedial goals. Rebound is generally the process by which contaminant desorption and diffusion from fine-grained sediments, or passage of a contaminated plume through the treatment area results in an increase in concentrations following remedial treatment. The mode of desorption is directly relevant to the lifetime of the remediation and to the associated costs incurred.

Description of Dual-Equilibrium Desorption Model

DED Model

The dual-equilibrium desorption (DED) model (Chen et al. 2002) assumes that the sorption and desorption processes are biphasic, occurring in two discrete "compartments" with varying rates and behaviors. The derivation of the model is in Chen et al. (2002); however, the general model can be expressed by

$$q = K_{oc}^{1st} f_{oc} C + \frac{K_{oc}^{2nd} f_{oc} q_{max}^{2nd} C}{q_{max}^{2nd} + K_{oc}^{2nd} f_{oc} C} \tag{1}$$

where K_{oc} is the organic carbon partition coefficient and is represented by the commonly used relationship $K_{oc}^{1st} = 0.63 K_{ow}$ for the first coefficient (Karickhoff et al. 1979), K_{ow} is the octanol water solubility coefficient, K_{oc}^{2nd} is the organic carbon partition coefficient for the second compartment that has been shown to be represented for a wide range of compounds by $K_{oc}^{2nd} = 10^{5.92 \pm 0.16}$ (Kan et al. 1998), f_{oc} is the fractional organic carbon (unitless), C_{sat} is a measure of the highest concentration of a specific chemical species that can remain in a soluble state, and C is the aqueous concentration. The typical range of C_{sat} for hydrocarbons is from 100 to 300 milligrams per liter or mg/L. The final term, q_{max}^{2nd} can be quantitatively derived on a site-specific basis, or calculated by

$$q_{max}^{2nd} = [f_{oc} K_{ow} C_{sat}]^{0.534} \tag{2}$$

The relationship between log q and log C is a curve comprising of three parts. These parts are an initial inclined linear curve in the low aqueous concentration range followed by a plateau which in turn

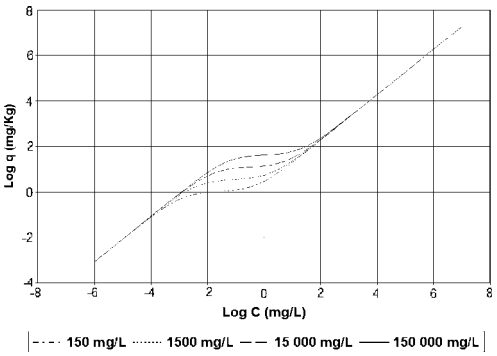

FIG. 1—*Log q versus log C as a function of* C_{sat}, $f_{oc} = 0.001$, $K_{oc}^{1st} = 1\ 862$ *L/kg.*

becomes a linear inclined curve again in the high aqueous concentration range, Fig. 1. Corrections can be made for the presence of NAPL or cosolvents, both of which have the effect of shifting predicted aqueous concentrations toward lower or higher values, respectively.

Using the DED Model in Typical UST Investigation

During a typical underground storage tank investigation, the type of data that a project scientist is commonly able to obtain is fairly limited. This data are commonly restricted to concentration data only for TPH mixtures such as "gasoline" and "diesel" (*both of which have definitions that differ by laboratory*), BTEX constituents, and some of the fuel oxygenates, such as MTBE, TBA, and TAME. Because none of these compounds are present alone, but instead are found in a soup with varying amounts of other compounds, using any of the desorption models developed to date has been difficult. Research into the chemical constants required for models is not performed on gasoline due to its inherent variations during production, let alone during weathering. However, for a model to be useful to a field worker, it does not necessarily need to provide high precision. A prediction precise to an order of magnitude is typically adequate to calculate the lifespan of a remediation project.

In evaluating the degree to which the DED model would be applicable given the data limitations described above, an evaluation of parameter sensitivity is necessary. To do this, the predicted DED desorption isotherm is calculated keeping all variables constant except for the one being tested. In all, three of the variables were tested; K_{oc}^{1st}, f_{oc}, and C_{sat}. K_{oc}^{1st} and C_{sat} are the least well-defined for gasoline and diesel mixtures. Fractional organic carbon (f_{oc}) is an easily measured parameter; however, during some remedial technologies (such as in situ chemical oxidation) it is probably not constant. Figures 1–3 demonstrate the effects of varying these parameters. It is apparent that the model is most sensitive to changes in f_{oc}.

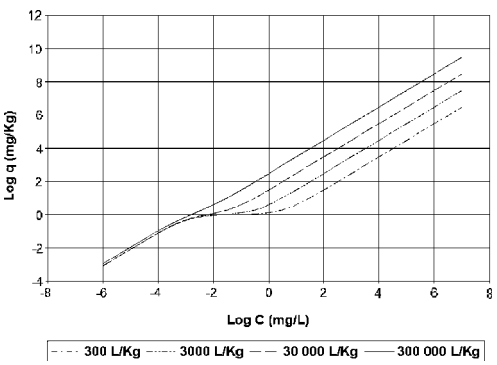

FIG. 2—*Log q versus log C as a function of* K_{oc}^{1st}, $f_{oc} = 0.001$, $C_{sat} = 150$ *mg/L.*

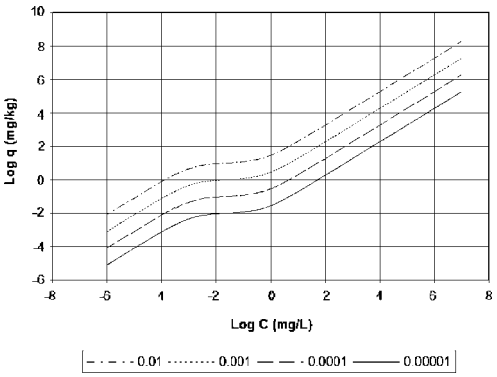

FIG. 3—*Log q versus log C as a function of* f_{oc}, C_{sat} *= 150 mg/L,* K_{oc}^{1st} *= 1 862 L/kg.*

The amount of contaminant sorbed to the soil/sediment is represented by q (in units of milligram contaminant per milligram soil) while C is the concentration present in groundwater/pore water (in units of milligrams contaminant per liter water). The groundwater/pore water sample is the quantity typically measured during remediation. The variation of log q versus log C as a function of C_{sat} is presented in Fig. 1. The f_{oc} and K_{oc}^{1st} are held constant. A review of the figure indicates that the effect of varying C_{sat} is limited to a range of log C from −4 to +2 for the conditions studied. Within this range of log C the effect of increasing C_{sat} from 150 to 150 000 mg/L results in decreased desorption from the sediment into the pore water in the plateau range of the curve for a constant q. As C_{sat} for gasoline is generally thought to be close to 150 mg/L and certainly less than 1 500 mg/L (Methanol Institute 2005), the actual variability in log q expected to be encountered in the field is probably between 0 and something less than 1. The effect of varying the organic carbon partition coefficient from the first compartment (K_{oc}^{1st}) on the amount of desorption occurring in sediment is shown in Fig. 2. A review of Fig. 2 shows that as K_{oc}^{1st} increases, the DED relationship becomes more linear with the disappearance of the plateau. This represents a decrease in the rate of desorption of the contaminant from the sediment and into the groundwater/pore water. As K_{oc}^{1st} reaches a maximum at 300 000 litres per kilogram or L/kg, the desorption relationship becomes linear; however, as the partition coefficient decreases, the desorption isotherm becomes increasingly biphasic. The effect of increasing f_{oc} concentration translates the DED curve upwards (Fig. 3). This results in a decrease in desorption of a chemical species from the sediment and into the pore fluid/groundwater for a constant q. This is expected given the function of organic carbon as an organic contaminant sorption site.

Based on this sensitivity analysis, the parameter that most effects the prediction of desorption of a contaminant from a sediment is f_{oc}.

Field Program

General Description

Monitoring during this remediation project involved an intensive program of groundwater and soil sampling. Groundwater samples were collected bimonthly for the first six months, monthly for the following 18 months, and quarterly thereafter. In addition to the contaminants of concern, periodic analyses were run for oxidation by-products such as chromium IV (CrVI) and tertiary butyl formate (TBF). Pre- and in-treatment samples were collected for the analysis of oxidation indicators such as: chemical oxidation demand; dissolved and total iron, chromium and selenium; bromide and bromate; free carbon dioxide; and alkalinity. The field intrinsic parameters temperature, pH, oxidation-reduction potential, conductivity, and dissolved oxygen were collected with every groundwater sample.

Colocated soil and groundwater samples were collected from two locations on site using a GeoProbe® 6600[3] direct push rig at approximately 6 to 9-month intervals to gauge the degradation of sorbed-phase

[3]GeoProbe Systems, Salina, Kansas.

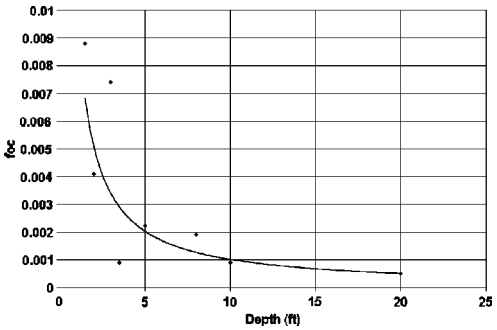

FIG. 4—*f_{oc} as a function of depth.*

contaminants. Soil samples from approximately 6 in. intervals were analyzed for the contaminants of concern and total organic carbon. Depth-discrete groundwater samples were collected at approximately 0.5 to 1-ft intervals from across the same zone. Both of these samples were analyzed for the contaminants of concern. The GROs and fuel oxygenates were analyzed by EPA Method 8260B modified for VOCs by GC/MS.

Operation of Ozone Sparge System

Sixteen sparge points were installed in nine wells and were connected to two Kerfoot Technologies C-Sparge® control panels.[4] Air was converted into approximately 95 % oxygen by passing through AirSep® molecular sieve filters, which removes nitrogen from the air stream. After concentrating oxygen from the air stream, it is converted to ozone by passing the stream through a corona discharge ozone generator. An air compressor mixes the ozone with ambient air for distribution to individual sparge points, which is controlled through a manifold and a series of solenoids. Discharge is determined by a programmed timer allowing flow to each sparge point for a predetermined length of time. Air flows to each point is at the rate of 0.11 m^3/s (4 scfs) and delivers approximately 5 g ozone per hour per panel. To date, approximately 85 kg of ozone have been injected.

The pretreatment fractional organic carbon (f_{oc}) versus depth below the ground surface is presented in Fig. 4 along with a polynomial best-fit curve (solid line). A review shows that the f_{oc} drops off with depth in the soil column from 0.01 to approximately 0.002 at 5 ft below ground surface (bgs). The variation of percent passing the 0.074 mm sieve (#200 sieve) versus depth is shown in Fig. 5 along with a polynomial best-fit curve (solid line). While the data are highly variable, the percent passing is shown to vary from

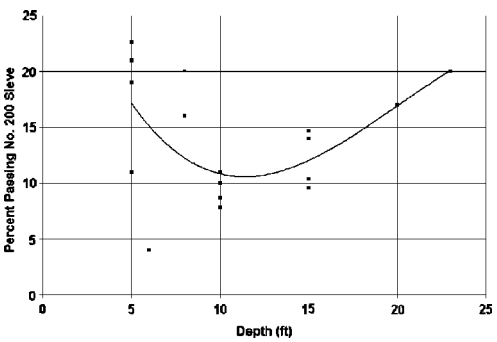

FIG. 5—*Percent passing No. 200 sieve as a function of depth.*

[4]Kerfoot Technologies, Mashpee, Massachusetts.

TABLE 1—*Changes in f_{oc} during ozone sparing.*

Boring	7/22/2003	2/12/2004	1/27/2005
B12	0.0009	0.0007	0.0009
B13	0.0009	0.0010	0.0004

approximately 18 % at 5 ft bgs dropping to 10 % at 11 ft and then increasing to 20 % at 23 ft bgs. This fits field observations of silty surficial beds overlying the medium sands that make up the bulk of the formation.

Ozone is an indiscriminant oxidizer in that it will oxidize organics and metals with which it comes into contact. Typically, it is assumed that since chemical oxidants destroy soil organic carbon ozone acts the same way, releasing previous sorbed hydrocarbons into solution after destruction of the sorption sites. However, field data are less clear on the relationship between soil organic carbon destruction, desorption, and the slow input of low concentrations of ozone, especially in a soil naturally depleted in organic carbon. While the data in this study are fairly limited, the reduction in f_{oc} seems insufficient to account for the sorbed mass reduction observed to date (Table 1, Fig. 6). Therefore, it is likely that mass reduction is occurring through some combination of processes such as destruction of the organic carbon and or sequestration of contaminants in organic ligands and other complexes. There are insufficient data at this point to determine the mode. In addition, the inherent heterogeneity in the analysis of soil samples leads to difficulties in interpretation.

Mass reduction was determined by comparing the results of the soil samples collected during the consecutive boring installations described above and calculating changes in the resulting mass. Two locations in the core of the source were sampled repeatedly in order to track the changes in contaminant mass. Approximately 85 % of the initial contaminant mass, or nearly 500 kg, has been destroyed to date. Although soil concentrations are always highly variable due to the heterogeneous nature of the medium, when the masses from the two areas were compared over time, the trend was clear.

Using site values of C_{sat}=150 mg/L, f_{oc}=0.01, K_{oc}^{1st}=1 862 L/kg a dual equilibrium desorption curve along with field data are presented in Fig. 7. The data presented in Fig. 7 are further subdivided into poorly graded sand to silty sand (SP-SM) and silty sand (SM) material and show reasonable agreement between the theory and field results. In addition, any differences in desorption behavior between SP-SM and SM materials cannot be distinguished based on the field results.

Discussion and Conclusions

The dual equilibrium desorption (DED) model was originally developed using pure substances and not mixtures that are most commonly dealt with in field situations. In this study the model has been utilized to evaluate its ability to predict the amount of sorbed hydrocarbon contaminant remaining on dune sand based on a groundwater/pore water field sampling program. Variation between field data and model prediction can possibly be explained by considering the differences in volumes of material sampled for

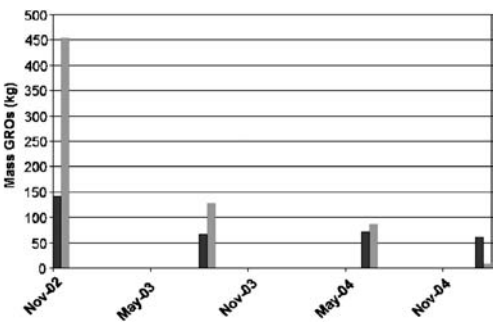

FIG. 6—*Reduction in contaminant mass (in kilograms) in two borings over time.*

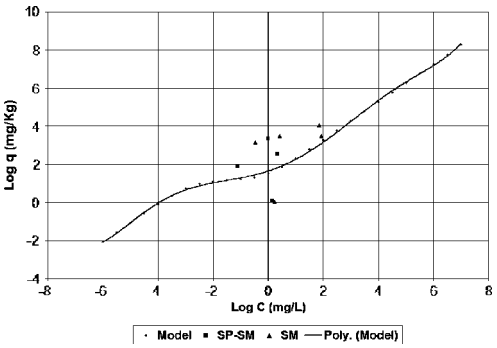

FIG. 7—*Log q versus log C model compared with field data,* C_{sat} *= 150 mg/L,* f_{oc} *= 0.01,* K_{oc}^{1st} *= 1 862 L/kg.*

determining the contamination of sediments as compared to contaminated pore water/groundwater. As an approximation, in the case of sediment contamination 5 g of material are used as compared to 40 ml (or approximately 40 g) of liquid.

In addition, a parametric study was performed to evaluate the sensitivity of the DED model to various sediment input parameters. Based on this study it was found that the parameter that most affects the amount of desorption is the fractional organic carbon (f_{oc}). Specific conclusions are as follows:

1. Results from the case study indicate that the DED model using site-specific parameters provides an estimate on the amount of contamination left in the sediment based on measurements of the contaminant mass in groundwater. This is based on a comparison between field data and model predictions.
2. Based on lab and field results, the behavior differences between SP-SM and SM materials cannot be distinguished.
3. The DED desorption model can potentially provide a means to evaluate the effectiveness of different remediation techniques.

References

Chen, W., Kan, A. T., Newell, C. J., Moore, E., and Tomson, M. B., 2002, "More Realistic Soil Cleanup Standards with Dual-Equilibrium Desorption," *Ground Water*, 40(2), 153–164 (2002).

Kan, A. T., Chen, W., and Tomson, M. B., "Irreversible Adsorption of Neutral Organic Hydrocarbons—Experimental Observations and Model Predictions," *Environ. Sci. Technol.*, 32, 892–902 (1998).

Karickhoff, S. M., Brown, D. S., and Scott, T. A., "Sorption of Hydrophobic Pollutants on Natural Sediments," *Water Resour.*, 13, 241–248 (1979).

Methanol Institute. 2005. "A Summary of Physical and Chemical Properties of Methanol, Gasoline (BTEX), and Benzene." http://www.methanol.org/methanol/fact/sumprop.cfm

Zhang, C., "Characterization and Desorption Kinetics of PAHs from Contaminated Sediment in Houston Ship Channel," *Environmental Institute of Houston - 2003 Annual Report*, 2003, pp. 39–41.

Journal of ASTM International, Vol. 3, No. 6
Paper ID JAI13321
Available online at www.astm.org

Rosa Galvez-Cloutier,[1] *Serge Leroueil,*[1] *Delphine Allier,*[2] *Jacques Locat,*[3] *and S. Arsenault*[4]

A Combined Method: Precipitation and Capping, to Attenuate Eutrophication in Canadian Lakes

ABSTRACT: Eutrophication is a natural phenomenon, unfortunately amplified and accelerated by human activities. Phosphorus and nitrogen are the principal nutrients responsible for eutrophication. Their excess in the environment, of domestic and agricultural origins, represents an important toxicological risk for the users of water. These excessive nutrients cause algae overgrowth and excess oxygen consumption, which leads to anoxic waters, production of toxins (such as those produced by cyanobacteria), and the production of pollutant gases. Excess nutrients and dead biomass settles at the bottom of the lake together with other trace contaminants such as toxic metals that are trapped within bottom sediments. Seasonally, the sediments release nutrients and contaminants that need to be mitigated in order to prevent eutrophication and overall water contamination. In Quebec and in Canada several lakes suffer from this problem and solutions have been divided in preventive practices (better runoff controls, protection of shores, elimination of leaking domestic septic tanks) and rehabilitating practices (oxygenation of water, precipitation of nutrients, dredging of sediments or capping). This paper will present recent advances in the development of a combined rehabilitating technique: Precipitation of phosphorous and capping of contaminated sediments. The paper includes: a recent literature review; phosphorous precipitation experiments using alum under optimized parameters; capping design considerations and theory; as well as the results of an experimental simulation of capping using a composite liner calcite/sand.

KEYWORDS: eutrophication, phosphorous, heavy metals, capping, coagulation

Introduction

Effluents from industrial/municipal sources and polluted urban/agricultural runoffs have carried contaminants to water bodies causing contamination of water and sediments in rivers, lakes, estuaries, and bays. Pollutants, often considered indefinitely locked within sediments pose threats because of mechanisms that trigger their release: particle resuspension, burrowing by bioturbators, upward groundwater flow through contaminated sediment layers and diffusion due to concentration gradients. Today, 43 areas in the Great Lakes, five ports along the St. Lawrence River, Champlain Lake (at the U.S. border), and numerous Canadian lakes contain bottom sediments that are considered polluted (IJC 2002; Tuchman et al. 1997). Since 1998, fish consumption advisories have been issued for more than 2506 bodies of water in Canada and the United States. Typical contaminants found in bottom sediments are excess nutrients (P and N) and metals (e.g., Pb, Cd, Cr, Hg). These contaminants become available to benthic organisms and disrupt the food chain through bioaccumulation, biomagnification, and reduce biodiversity. They also pose a risk to human health through water or fish consumption or contact with contaminated water and they accelerate eutrophication which causes specific algae blooms (e.g., cyanobacteria), oxygen depletion, anoxic conditions and production of toxins. As citizens lose water uses and become aware of health and ecological risks associated with contaminants and the negative impacts on regional economy, governments have recognized that restoring water quality and use are unattainable without Watershed Restoration Plans (WRPs), which very often include Sediment Restoration Actions (SRAs) (IJC 2002). Typically, WRPs require mandatory control and reduction of external sources of pollution such as better agricultural practices, reducing surface runoff, and restoring vegetation buffers (Exxep 2002, 2004; Klapper 2003). These are

Manuscript received May 24, 2005; accepted for publication September 28, 2005. Presented at ASTM Symposium on Contaminated Sediments: Evaluation and Remediation Techniques on 23–25 May 2006 in Shizuoka, Japan; M. Fukue, K. Kita, M. Ohtsubo, and R. Chaney, Guest Editors.

[1] Department of Civil Engineering, Laval University, Quebec.
[2] ENTPE, Lyon, France.
[3] Department of Geology and Geological Engineering, Laval University, Quebec
[4] Génivar, Quebec.

preventive actions that need to be prioritized. The longevity and success of any in-lake remediation action, such as the one proposed here, will depend on the achievement of source pollution reduction. In-lake remediation constitutes a curative approach where preventive measures are proven insufficient. Indeed, research studies (Bishop 1997; Klapper 2003; Simoneau 2004) show that water bodies may require long periods of time for recuperation (from decades to centuries) after input sources were stopped.

Missisquoi Bay (in Champlain Lake) and St. Augustin Lake sites include SRAs as part of in-lake pollution controls. Both sites present high metal and P content within sediments. Extreme eutrophication conditions occur each summer. Both sites have been controlling external sources of pollution for the last 10 to 15 years without measurable water quality improvement (Simoneau 2004; Exxep 2004). Both sites are well oxygenated and phosphorus is considered to be an internal source. The first site is the subject of an U.S.-Canada agreement and is a strategic issue in Canadian/Quebec international politics. St. Agustin Lake is the unique remaining natural lake in the urbanized Quebec region. These two sites, for their importance, location, history, and representative conditions constitute excellent sites to be studied and used as models for the development of an original and innovative restoration technique consisting of the integration of "*active capping*" with "*enhanced coagulation*."

Literature Review

Traditional capping is the controlled placement of a covering cap of clean isolating material (usually gravel, sand, or silt) over contaminated sediments at an open-water site. Until today, capping layers have been designed to serve two primary physical functions: (a) physical isolation of the contaminated sediments from the benthic environment and (b) stabilization of contaminated material, preventing resuspension and transport to other sites. Considerations in evaluating the feasibility of capping include: site bathymetry, water depth, currents/waves, climate, physical characteristics of contaminated sediments, capping placement technique and capping material availability (Palermo et al. 1998). It should also include site hydrogeology and input water quality but are seldom considered. With respect to capping layer design, height and consolidation have been the master designing parameters.

Because multicontaminant retention and overall environmental performance and long-term stability of the cap are of concern today, new design considerations need to be included. In this project we have aimed to add two new considerations: (1) capping material chemical characteristics and functions and (2) incoming contaminant loadings from all contaminated water fluxes. By doing so, the new and original capping method will offer a sustainable technically superior solution that combined with pollution prevention will give permanent results.

Capping Material Characteristics and Functions—"Active Capping"

Recent research (Klapper 2003) indicates that much thinner caps (clay, geomembranes) can be successful in sequestering contaminants for long periods of time but at higher costs due to expensive material and placement techniques. Clay caps have been used in Europe in connection with control of eutrophication, but they cannot be used in lakes under artesian pressures. Our recent studies (Galvez et al. 2003, 2004; Ize 2003) have shown that other active materials such as calcareous and oxides minerals can be effective capping materials due to their high sorption/precipitation capacities. When treated before use (e.g., grinding and washing), calcite has shown a high retention capacity for phosphorus and heavy metals (Galvez et al. 2003, 2004). In the case of groundwater transporting nutrients in an upward flow, the "active layer" will precipitate these contaminants until this source fades out. Fresh sorption sites in a calcareous "active cap" will greatly reduce if not stop the rate at which heavy metals and phosphorus move through the cap both during consolidation and long-term diffusive processes. In addition, calcite offers a high pH buffering action that will attenuate lake acidification. Other considerations in favor of the use of a calcareous cap include: (1) placement techniques of noncohesive materials are far easier than for clays, organic rich fine materials or silt are more likely to require armouring; (2) calcareous silt gravel is stable at steeper slopes than fine grained materials, the footprint of a fine grained cap will be larger than a calcareous cap; (3) more fine material is needed to cap the same deposit as with a coarser cap, and finally; (4) a calcareous cap may present high potential to improve water physico-chemical characteristics more suitable for benthic recolonization.

Contaminant Charges in Water Fluxes—"Enhanced Flocculation"

Active capping will stop or limit contaminant flux from the bottom sediments to the water column (internal loadings) and may cause some phosphorus coagulation during cap placement, but it may still be necessary to further remove P from water column in order to attain quality limits to stop eutrophication [Quality Criteria (QC) Total Phosphorus (TP) <20 μg/L, MDDEP 2005a]. Enhanced selective coagulation preceeding capping will result in P precipitation, floc formation, and settlement which can then be trapped by the calcite cap. "Alum" (aluminum sulfate) is a nontoxic compound commonly used in water treatment and is increasingly studied as an efficient coagulant to reduce phosphorus in the water column Exxep 2004; Klapper 2003; Szmelter 1999). Alum binds with phosphorus to form aluminium phosphate, insoluble in water under most conditions, so that phosphorus can no longer be used as food by algae. The floc also tends to collect suspended particles in the water and carry them down to the bottom, leaving the water noticeably clearer. In the United States, few P flocculation projects have been fully documented but various cases report long term results (Szmelter 1999), though coagulant dispersion efficiency, fragility, and mobility of floc have been issues that need to be solved. Last year, alum dosages where calculated based on enhanced jar test experiments, using geochemical information (P speciation) and water characteristics (pH and alkalinity) to minimize water chemical manipulations (ban of pH adjustments and additives) (Parant 2004; Allier 2004). This preliminary study, run with water samples from Missisquoi Bay and St. Augustin Lake, showed that low alum dosages (10–20 mg/L) plus calcite addition could precipitate TP up to a final concentration of 15 μg/L which fall under QC. Residual Al levels fall under 0,05 mg/L which is below 0,087 mg Al/L, the concentration reported as showing no toxic effect on rainbow trout or salmon (MDDEP 2005a).

Aim and Objectives

This project aims at developing an original and integrative active capping method. The method will mitigate contamination and will stop eutrophication in Canadian shallow lakes where preventive measures and source reduction have been proven insufficient.

- To determine an optimal alum dosage and application technique (in water and/or close to sediments, in solid or liquid form) in order to attain high coagulant dispersion, stronger, and stable flocs, and to increase phosphorus and metal retention.
- To maximize/optimize contaminant retention characteristics of calcite by pretreating and grinding (manipulation of surface area). To evaluate and assess retention mechanisms using microanalysis and analytical speciation tools.
- To validate and calibrate two hydrogeochemical models and to use them in order to determine an initial "active layer" thickness. To compare results and recommend one model for design purposes.
- To use the recommended model, to simulate large column results, and to predict hydraulic and geochemical behavior of the "active calcite layer" for evaluation of long term performance.

Methods and Materials

Phase I—Coagulation/Capping Design

Preliminary *Alum coagulation* experiments were carried last year (Allier 2004), low dosages of alum have been calculated based on phosphorus forms to be neutralized (TP, SP, orthophosphates). During this project, coagulation-flocculation process and P removal were studied using jar tests and geochemical microanalysis. The role of calcite when combined with alum has shown various positive effects: (1) no need of addition of buffers; (2) final pH falls within good ranges for protection of fauna and flora; and (3) phosphorus precipitation during calcite deposition, which allows certain reduction of alum dosages.

Calcite retention capacity was assessed using precipitation and adsorption batch experiments after manipulations of calcite surface area (by grinding and sieving). Adsoprtion mechanisms where studied using microanalysis (scanning electron microscope) and analytical speciation tools (SSE) according to the methods described in (Galvez-Cloutier 2003; MDDEP 2005b). These results serve to assess the stability

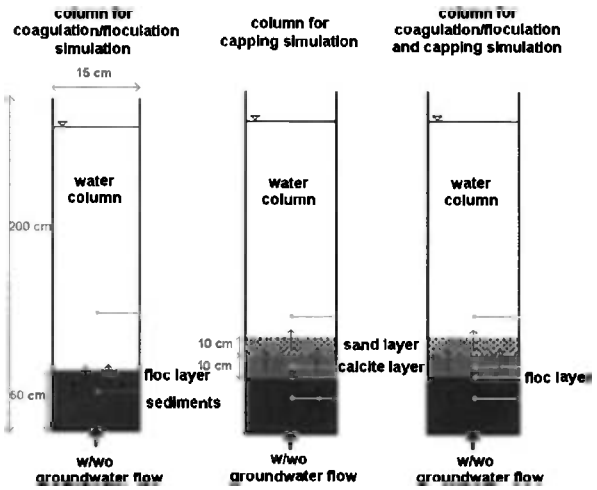

FIG. 1—*General column experimental layout (w/wo = with or without).*

and strength of contaminant bonding, the speciation of contaminants, and to calculate an initial minimum cap thickness.

The "active cap" was designed integrating calcite retention capacity batch results with column simulations and mathematical modeling. Figure 1 shows the general layout of the column experimental setup. Four, 3 m vertical columns will simulate the following profile: a given thickness of contaminated sediments (20–50 cm), a 10–15 cm depth of calcite layer, 15 cm of sand, and a 2 m water column. The systems to be modeled are: upward continuous groundwater flow (for St. Augustin Lake).

The desired function of the active cap is to chemically isolate the contaminants in the long term and to reduce the flux of contaminants such that a water or sediment quality standard level can be maintained. Thus, both advective and diffusive processes will be considered in determining the cap design parameters for isolation. If ground water/surface water interaction indicates that advection is not significant, the cap design may only need to address diffusion mechanisms ignoring colloidal transport due to advection. Since the objective of the cap is the attainment of a given contaminant flux, two mathematical models will be used to back calculate an effective "active cap" thickness.

Results

Table 1 shows the initial water column conditions of St. Augustin Lake before coagulation with alum. It can be noticed that the pH is very high varying between 8.5 and 8.9. Turbidty is also very high (between 2.5 and 3.2 NTU).

Optimization of Alum Application

Table 2 presents the results of four different Jar tests. Due to the high pH of the lake, lower alum dosages failed flocculation and required dosages higher than 15 mg/L.

Figure 2 also shows the failure of flocculation for alum concentrations lower than 25 mg/L. Indeed, one notes no reduction of turbidity (about 2 NTU) before adding 30 mg/L of alum. It can be noticed in

TABLE 1—*Initial water conditions.*

pH	8.6
Temperature (°C)	15
Turbidity (NTU)	3.2
Filtered Turbidity (NTU)	0.3

TABLE 2—*Optimization of alum concentration.*

			Water Analysis	
Jar n°	Alum dose (ppm)	Flocculation	Final pH	Final Turbidity (NTU)
1	0	raw water	8.9	1.9
2	5	Failure	8.3	2.55
3	10	Failure	8.2	1.95
4	15	Failure	8.1	2.07
5	20	Failure	7.9	2.02
6	25	Failure	7.8	2.02
7	30	Good	7.7	0.98
8	35	Very Good	7.6	0.67
9	40	Good	7.6	0.74

Fig. 3 a strong reduction in the final pH (reduction of two units of pH for an alum concentration of 30 ppm). To compensate for this fall of pH, one can add soda, but a reduction in pH can be desirable in this case given the initial high pH.

Figure 4 shows residual P as a function of alum dosages. An interesting fact shows that even if flocculation failed for a concentration of 25 alum ppm, the residual phosphorus concentration of the treated water decreased under remedial objective concentrations.

Thus, the optimal alum concentration was chosen as 30 mg/L of alum. During this study other coagulants such as ferrous sulphate were tested, but alum gave the best results.

Optimization of pH

The goal of these tests is to find an optimal pH to obtain a good flocculation with an alum concentration of 20 ppm. Table 3 shows the results of flocculation and highlights the optimal pH at 6.

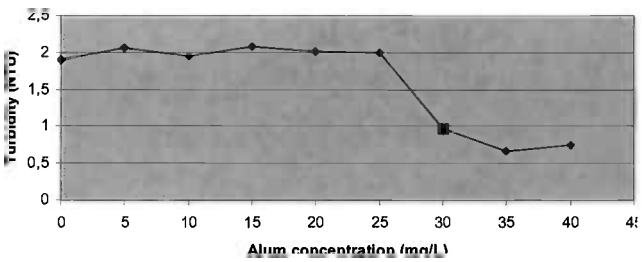

FIG. 2—*Optimization of alum as function of turbidity.*

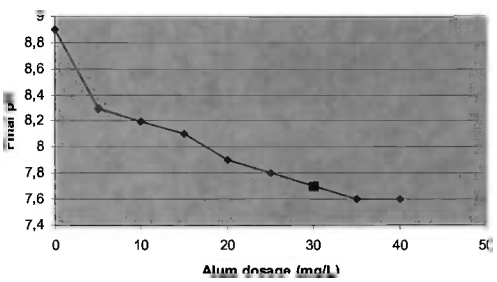

FIG. 3—*Final pH after alum addition.*

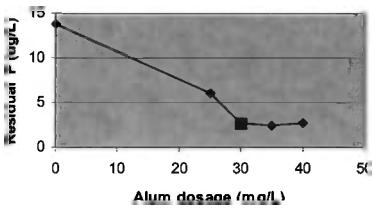

FIG. 4—*Residual P as function of alum dosage.*

Optimization of Coagulation Time and Mixing Gradient

Table 4 and Figs. 5 and 6 shows various coagulation times and mixing gradients as function of phosphorus removal. Thus, the most effective agitations were those carried on Jar no 1: one minute of rapid mixing at 230 RPM and slow mixing of 20 min at 40 RPM and 20 min at 20 RPM.

Figure 7 shows the phosphorus leaching and adsorption results. The histograms show the phosphorus retained by calcite rock which fell between 30 and 70 mg; P/kg of calcite. Leached phosphorus into the water column (solid curves) always surpassed the background concentration of P in groundwater, thus P was leached out from bottom sediments. Phosphorus concentrations leached form sediments into the water column were always higher than the eutrophication limits given by MDDEP and equal to 20 $\mu gP/L$. Figure 8 shows SEM results on calcite after percolation time ended. The analysis showed particles of Cu and Zn carbonates validating the results on heavy metal adsorption.

TABLE 3—*Optimal pH.*

Jar n°	Alum dosage	Initial pH	Flocculation results
1	20	8.6	Failure
2	20	7.4	Failure
3	20	7.6	Failure
4	20	6.9	Failure
5	20	6.5	Failure
6	20	6.4	Very good
7	20	4.8	Failure

TABLE 4—*Coagulation and flocculation times and mixing gradients.*

Jar	1	2	3	4
Alum dosage (ppm)	30	30	30	30
Coagulation time	1 min at 230 RPM	45 s at 230 RPM	30 s at 230 RPM	1 min at 150 RPM
Flocculation time	20 min at 40 RPM +20 min at 20 RPM	10 min at 40 RPM +10 min at 20 RPM	30 min at 30 RPM	50 min at 20 RPM

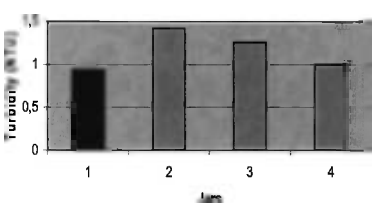

FIG. 5—*Final turbidity.*

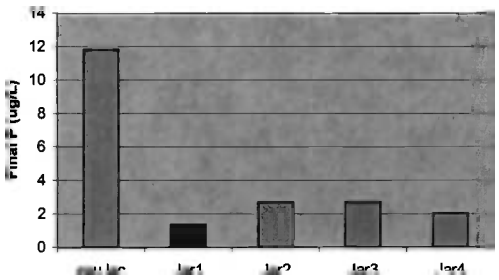

FIG. 6—*Final phosphorus (Eau du lac = Lake water).*

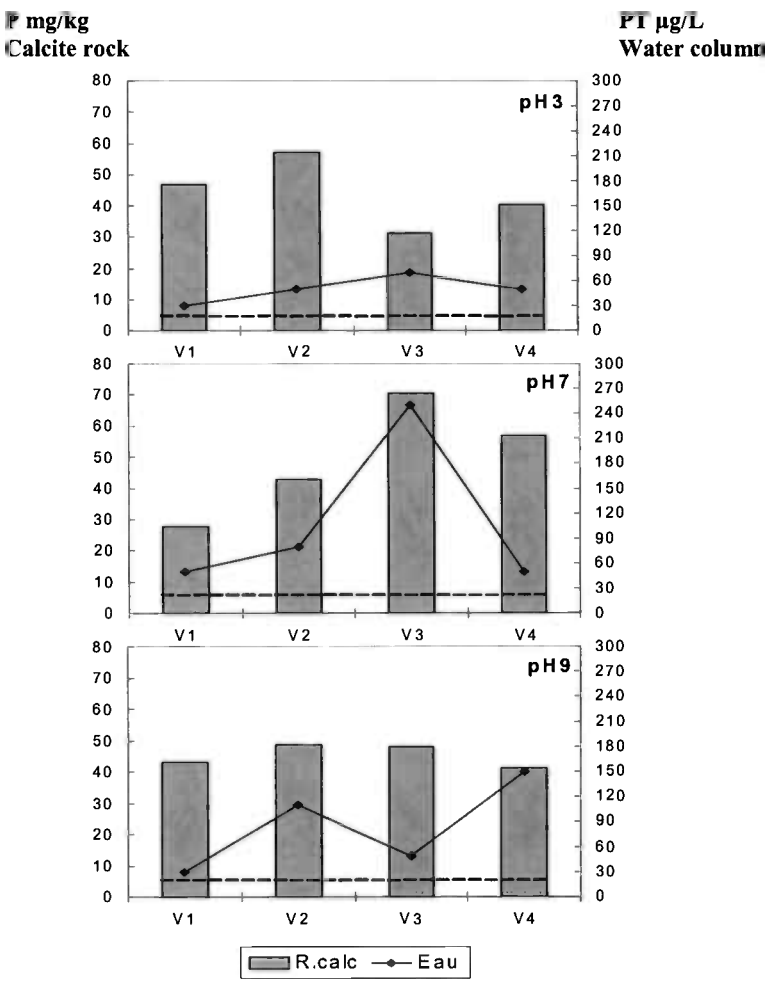

FIG. 7—*Phosphorous leaching/adsorption column results.*

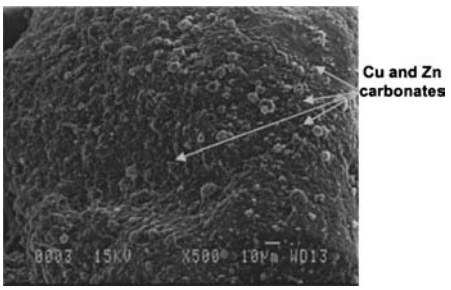

FIG. 8—*Metal adsorption results.*

Conclusions

- The results showed that heavy metals are well retained within the sediment matrix or within the calcite rock, thus there is low potential for solubilisation.
- On the contrary, phosphorus is highly mobile and was easily leachable from sediments. The calcite rock retained large amounts of phosphorus between 30 and 70 mg·P/kg of calcite. Since the P leachable concentrations were higher than the eutrophic limit the pre-coagulation step appears necessary.
- Coagulation with alum concentration between 15 and 25 mg/L of alum gave the best results in term of removal of orthophosphates.

References

Allier, D., "Al Coagulation of Missisquoi Bay and St-Augustin Lake Waters," Technical Report. U. Laval, 2004.

Bishop, D., "Perspective on Remediation and Natural Recovery of Contaminated," 1997.

Exxep, Diagnose Écologique du Lac Saint-Augustin, 2002.

Exxep, "Gestion de la Qualité de L'eau à la Baie Missisquoi: Regards sur les Solutions," 2004.

Galvez-Cloutier, R. et al., *Quality Evaluation of Eutrophic Sediments at St-Augustin Lake*, ASTM STP 1442, ASTM International, West Conshohocken, PA, 2003.

Galvez-Cloutier, R. et al., (2004). "Étude d'une Solution de Confinement de Polluants dans les Sédiments du lac St-Augustin," in *Proc. GEOQUEBEC 2004*.

Groupe des gens d'affaires Lac Champlain, "Impact Économique—Perte des Usages d'eau," 2003.

International Joint Commission, *11th Report*, 2002, Great Lakes Water Quality, United States, Canada.

Ize, S., "Étude de la Retention des Contaminants Inorganiques par une Mélange Sable Bentonite Enrichi en Carbonates," Thèse de maîtrise. U. Laval, 2003.

Klapper, H., "Technologies for Lake Restoration," *J. of Limnology*, 62, 73–90 (2003).

MDDEP, http://www.menv.gouv.qc.ca/eau/flrivlac/criteres.htm, 2005a.

MDDEP, http://www.ceaeq.gouv.qc.ca/methodes/chimie_inorg.htm, 2005b.

Palermo, M. et al., "Guidance for Subaqueous Dredged Material Capping," USACE, 1998.

Parant, M.-A., "Various Progress Reports of Masters Studies," 2003.

Simoneau, M., "Qualité des eaux du Bassin de la baie Missisquoi: Un Portrait," *Forum Qualité de l'eau et Santé*, Notre-Dame-de-Stanbridge, 2004.

Smeltzer, E. et al., "Long-term Water Quality and Biological effects of Alum Treatment of Lake Morey, Vermont.," *J. of Lake and Reservoir Management*, 15(3), 173–184 (1999).

Tuchman, M., et al., "Solving Great Lakes Contaminated Sediment Problems," *Proceedings National Conference on Management and Treatment Contaminated Sediments*, EPA/625/R-98/001, 1997.

Journal of ASTM International, Vol. 3, No. 7
Paper ID JAI13887
Available online at www.astm.org

Kazuo Murakami,[1] *Yuichiro Nobusawa,*[2] *and Yutaka Kameyama*[3]

The Lasting Effect of Sand Capping Techniques on Nutrient Release Reduction from Contaminated Sediments in Tokyo Bay

ABSTRACT: This paper describes the lasting effect of sand capping techniques on nutrient release reduction from contaminated sediments. Bottom sediments in Tokyo Bay are very contaminated as the results of eutrophication behavior. From the sediments, a large amount of nutrients are released into seawater bodies. In order to know the effect of the sand capping technique on nutrient release reduction and its lasting effect, we carried out the undisturbed sediment sampling at Yokohama Port. Then we carried out the laboratory tests to estimate the nutrient release rate. From the study, it is concluded that the sand capping technique has a still effect on nutrient release reduction from the contaminated sediments, and the effectiveness is dependent upon the thickness of mud layer accumulated on the capped sand.

KEYWORDS: contaminated sediments, nutrient release, sand capping, laboratory test, tokyo bay

Introduction

Water quality in enclosed coastal seas is generally contaminated because of the large amount of sewage loads discharged into the sea and small water exchange between polluted enclosed coastal water and clean ocean water. Especially in 1970s, the water quality in Tokyo Bay was very contaminated by eutrophication. Therefore, red tides and other environmental problems occurred very frequently in those days.

After establishment of the Environmental Agency of Japan in 1971, several water quality control regulations against water contamination were enacted. As the results of these regulations, the amount of sewage loads discharged into Tokyo Bay was decreased greatly. However, water quality in Tokyo Bay is still contaminated condition (Ministry of Land, Infrastructure and Transport 2003).

The reason why the water quality is still contaminated is because of a large amount of nutrient release loads from contaminated sediments. To cope with the nutrient release loads, the sand capping techniques to cover the contaminated sediments with clean sands were conducted in several coastal seas. Yokohama Municipal Government carried out the sand capping constructions at Yokohama Port in Tokyo Bay. It is known that the sand capping technique has considerable effect on nutrient release reduction from contaminated sediments (Murakami et al. 1996), however, the lasting effect of sand capping technique is not clarified yet. So in this paper, we studied the lasting effect of the sand capping technique on nutrient release reduction from contaminated sediments by field observations and laboratory tests. It is expected that the effect of nutrient release reduction by sand capping construction is maintained at least 20 years.

Field Observations of Sediment Quality and Executions of Sediment Sampling

Figure 1 shows the study site map of Yokohama Port, which is located in Tokyo Bay, Japan. Yokohama Municipal Government carried out the sand capping constructions at Yokohama Port. The construction around St. 2 was conducted in 1994, and around St. 3 was conducted in 1998. The area of St. 1, the sand

Manuscript received April 21, 2005; accepted for publication December 8, 2005. Presented at ASTM Symposium on Contaminated Sediments: Evaluation and Remediation Techniques on 23–25 May 2006 in Shizuoka, Japan; M. Fukue, K. Kita, M. Ohtsubo, and R. Chaney, Guest Editors.

[1] Professor, Musashi Institute of Technology, Tokyo, Japan158-8557, e-mail: kmuraka@sc.musashi-tech.ac.jp
[2] Research Engineer, Nishihara Co. Ltd., Tokyo, Japan108-0023, e-mail: n_yuichiro@nifty.com
[3] Research Engineer, Ministry of Land, Infrastructure and Transport, Yokohama, Japan221-0053, e-mail: kameyama-y83ab@pa.ktr.mlit.go.jp

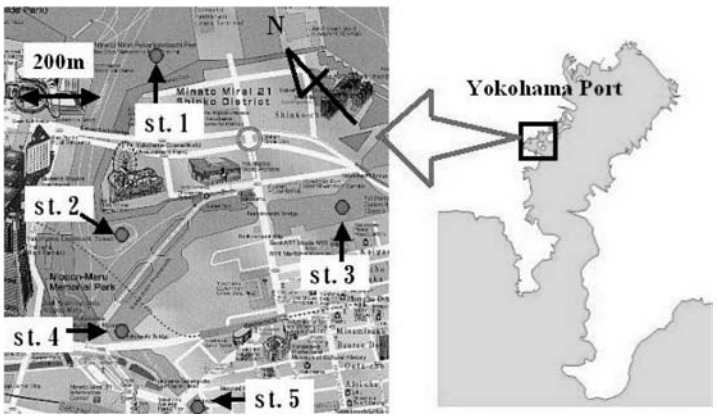

FIG. 1—*Study site map of Yokohama Port in Tokyo Bay (Site 1 is the site without sand capping, and Sts. 2 and 3 are the sites with sand capping).*

TABLE 1—*Results of water quality measurements at study sites in winter, 2004.*

	NO_2-N (mg/l)	NO_3-N (mg/l)	NH_4-N (mg/l)	T-N (mg/l)	PO_4-P (mg/l)	T-P (mg/l)
St. 1	0.0381	0.5519	0.0726	1.3204	0.0529	0.0530
St. 2	0.0357	0.4408	0.0808	1.2736	0.0672	0.0583
St. 3	0.0370	0.5710	0.0969	1.3925	0.0687	0.0618

TABLE 2—*Observation results of bottom surface sediments in winter, 2004.*

	St. 1	St. 2	St. 3	St. 4	St. 5
Temperature(C)	16.9	16.6	16.1	16.6	16.3
Smell	Hydrogen sulfide	No smell	No smell	Hydrogen sulfide	Hydrogen sulfide
Appearance	Silt	Sandy silt	Sandy silt	Silt	Silt
Color	Dark olive 5GY3/1	Dark olive 2.5GY3/1	Dark olive 5GY3/1	Dark green 7.5GY3/1	Dark green 10GY3/1
Mixture	Nothing	Shell	Shell	Shell, Woods	Shell, Cloths
ORP(mV)	−119	82	11	−59	−99

TABLE 3—*Sediment qualities of bottom surface sediments in winter, 2004.*

Items		Unit	St. 1	St. 2	St. 3	St. 4	St. 5
T-N		mg/g(dry)	3.10	0.86	0.80	2.80	4.50
T-P		mg/g(dry)	0.74	0.27	0.25	0.89	1.10
COD		mg/g(dry)	22.0	5.3	5.5	22.0	37.0
Water content		%	73.8	35.8	35.5	63.2	72.1
Ignition loss		%	9.2	2.9	2.5	9.7	13.9
Grain size	Gravel	%	0	9	0	1	0
	Sand	%	11	69	79	17	6
Distribution	Silt	%	59	15	14	55	64
	Clay	%	30	7	7	27	30

TABLE 4—*Observation results of bottom surface sediments in summer, 2004.*

	St. 1	St. 2	St. 3
Temperature(C)	23.7	25.4	23.7
Smell	Hydrogen sulfide	Hydrogen sulfide	Hydrogen sulfide
Appearance	Silt	Silt	Silt
Color	Black	Black	Black
	N2/0	N2/0	N2/0
Mixture	Shells, woods	Shells	Shells, plants
ORP(mV)	−160	−121	−149

capping construction was not conducted yet. Sites 4 and 5 are located in the Ohoka River, where is also not the area of sand capping construction.

We carried out field measurements of water quality at Sts. 1 to 3, the sampling of bottom surface sediments at Sts. 1 to 5 for sediment quality measurements, and the undisturbed core sampling of bottom sediments at Sts. 1 to 3 for nutrient release laboratory tests in winter, 2004. The sampling of bottom surface sediments was carried out by using the Ekman Birge type sediment sampler, and the core sampling of undisturbed sediments was carried out by using two types of acrylic pipes which are 20 cm diameter and 50 cm length for laboratory tests and 10 cm diameter and 150 cm length for observation on the boat.

Table 1 shows the results of water quality of nitrogen compounds and phosphate compounds at Sts. 1 to 3. For example, the values of total nitrogen at all stations exceed the fifth class of environmental quality standard value, that is, the worst class. From the results, it is shown that the water quality at Yokohama Port is the state of eutrophication.

Table 2 shows the observation results of bottom surface sediments. The sediments at Sts. 1, 4, and 5 have a strong odor of hydrogen sulfide, because these sediments are very contaminated fine silts materials. On the other hand, at Sts. 2 and 3, the smells of the sediments are odorless, and the sediment materials are mixture of silt and sand. The values of ORP (oxidation reduction potential) of the sediments at Sts. 1, 4, and 5 are negative, but the values of sediments at Sts. 2 and 3 are positive. The negative ORP value means the state of reduction of the sediment. Therefore hydrogen sulfide is generated from the sediment. This is the reason why the bad smell of the sediments is noticed at Sts. 1, 4, and 5.

Sediment quality at each measuring stations is shown in Table 3. From the table, it is shown that the sediment qualities at Sts. 1, 4, and 5 show a high concentrations of T-N (total nitrogen), T-P (total phosphorus), sediment COD (chemical oxygen demand), and large values of water content and ignition loss. The particle size distributions of sediments at Sts. 1, 4, and 5 contain a high percentage of fine silt and clay. On the contrary, sediment qualities at Sts. 2 and 3 show a low concentrations of T-N, T-P, and COD, and small values of water content and ignition loss. This means that the sediment quality of bottom surface sediment on the sand capping area is relatively clean.

Tables 4 and 5 show the same results of sediment quality at Sts. 1 to 3, when measurements were carried out in the summer of 2004 by the Ministry of Land, Infrastructure and Transport. The sediment qualities obtained in both summer and winter show similar properties, but the values of water content and ignition loss obtained in winter are smaller than the values obtained in summer. The results say that the sediment quality of bottom surface sediments in winter is slightly improved in comparison with the sediment quality in summer. We do not know the reason for the difference, so we intend to study the reason in the future.

TABLE 5—*Sediment qualities of bottom surface sediments in summer, 2004.*

Items		Unit	St. 1	St. 2	St. 3
T-N		mg/g(dry)	3.60	1.20	0.80
T-P		mg/g(dry)	0.84	0.37	0.30
COD		mg/g(dry)	23.0	8.9	6.9
Water content		%	339.0	83.2	67.6
Ignition loss		%	11	4	3
Grain size	Gravel	%	0	7	0
	Sand	%	6	68	76
Distribution	Silt	%	44	9	11
	Clay	%	50	16	13

Then undisturbed sediment core samplings were carried out at the same stations for observation of sediment quality and for laboratory tests of nutrient release. Photo 1 shows the pictures of undisturbed sediments taken in winter at Sts. 1 to 3, respectively. The property of the sediment at St. 1 shown in Photo 1 is a dark black color and occupied by contaminated fine silt for all layers. While the properties of the sediments at Sts. 2 and 3 are a gray colored silty sand covered with thin dark black sandy silt. The thickness of the dark black sandy silt layer accumulated on the capped sand at Sts. 2 and 3 are approximately 1 cm and 5 cm, respectively.

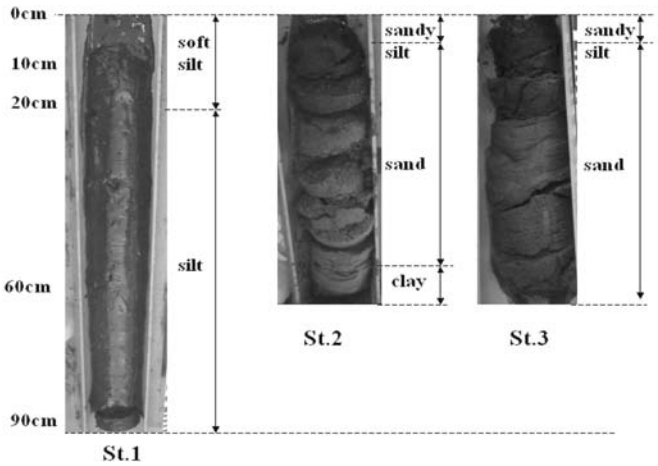

PHOTO 1—Undisturbed sediments taken from at Sts. 1, 2, and 3 in winter, 2004.

Similar undisturbed core samplings were carried out in summer at same stations. The properties of the sediments in the summer are relatively similar, but the thickness of the dark black sandy silt layer accumulated on the capped sand at Sts. 2 and 3 are 10 cm and 5 cm, respectively. The thickness of the mud layer accumulated on the capped sand is different between winter and summer. In general, it is said that the seasonal change of bottom sediment quality is small. From the field observations, however, seasonal change of bottom surface sediment quality is relatively large. The difference is very important to consider the lasting effect of sand capping techniques.

Laboratory Tests of Nutrient Release

In order to investigate the effect of sand capping on nutrient release reduction from contaminated sediments, we carried out the laboratory tests of nutrient release from the sediments. At Yokohama Port, undisturbed core sampling of bottom sediments were carried out. At each station, three sediment samples were collected for laboratory tests. Figure 2 shows the experimental apparatus for nutrient release test. The acrylic pipe for undisturbed sediment sampling is 50 cm in length and 25 cm in diameter. In the pipe, the thickness of the sediment layer is 25 cm and the remains are the water which was taken from the bottom layer just above the bottom sediment at each sampling station.

The experimental conditions for laboratory tests are shown in Table 6. Water temperature in the tank, which covers the experimental apparatus, is controlled as 20°C. And the condition of dissolved oxygen in water above the sediment is aerobic supplied of air or anaerobic supplied of nitrogen gas. After the laboratory test starts, a small amount of water is picked up by siphon in order to know the nutrient release rate from the sediments at the fixed time intervals as shown in Table 6.

Figures 3–8 show the laboratory test results of nutrient release such as nitrite nitrogen (NO_2-N), nitrate nitrogen (NO_3-N), ammonium nitrogen (NH_4-N), total nitrogen (T-N), phosphate phosphorus (PO_4-P), and total phosphorus (T-P). From the figures, it is shown that the release rates of ammonium nitrogen, total

TABLE 6—*Experimental conditions of nutrient release tests.*

Items	Conditions
Test duration	72 h
Sampling time	0, 2, 4, 6, 10, 24, 48, 72 h after test starts
Water temperature	20°C
Dissolved oxygen	Aerobic and anaerobic conditions
Light condition	Dark condition

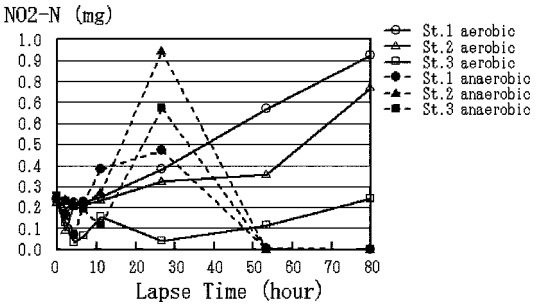

FIG. 3—*Experimental results of* NO_2-N *release from sediments.*

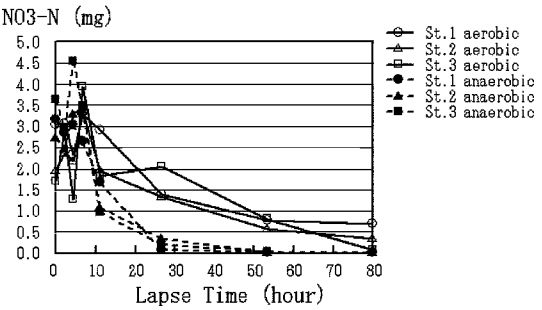

FIG. 4—*Experimental results of* NO_3-N *release from sediments.*

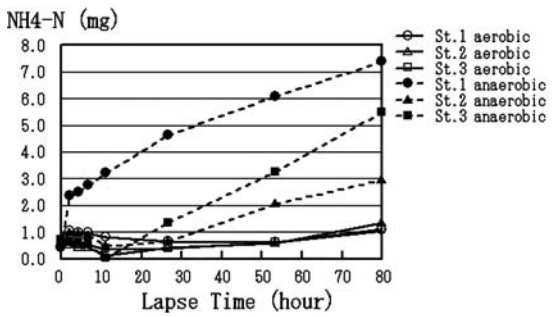

FIG. 5—*Experimental results of* NH_4-N *release from sediments.*

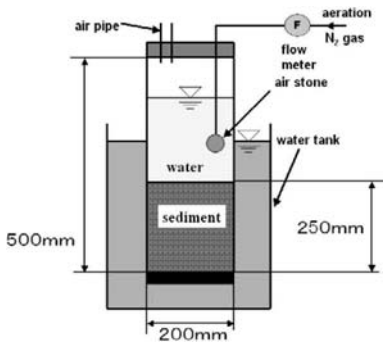

FIG. 2—*Laboratory test apparatus for nutrient release.*

nitrogen, phosphate phosphorus, and total phosphorus from bottom sediments under the anaerobic condition are larger than the ones under the aerobic condition.

The order of release rate is Sts. 1, 3, and 2. This means that the release rate from sediment without sand capping is larger than the rate from sediment with sand capping. The nutrient release rate is dependent upon the thickness of the mud layer, which is accumulated on the capped sand. The result says that the lasting effect of sand capping techniques on nutrient release reduction from contaminated sediments still maintains after ten years of the construction. But the effectiveness of the sand capping construction is relatively decreased by the accumulation of fluid mud on the capped sand.

From the figures, it is shown that there are some different properties of the concentrations of nutrients between before 10 h and after 10 h from the laboratory test starts. By considering above results, the nutrient release rates of phosphate phosphorus are estimated by using the results of before 10 h and after

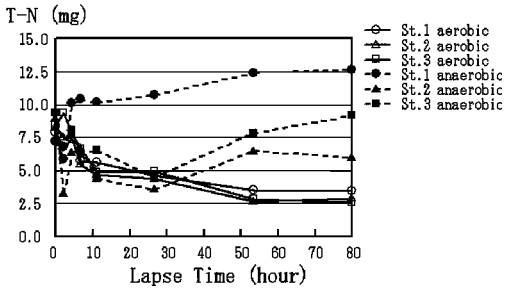

FIG. 6—*Experimental results of T-N release from sediments.*

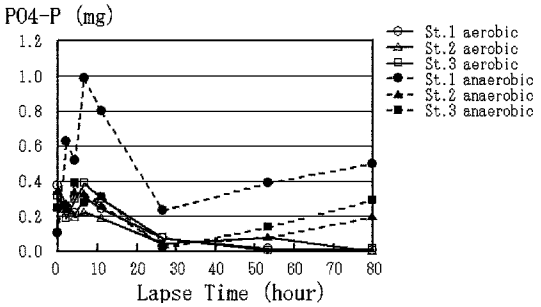

FIG. 7—*Experimental results of* PO_4-P *release from sediments.*

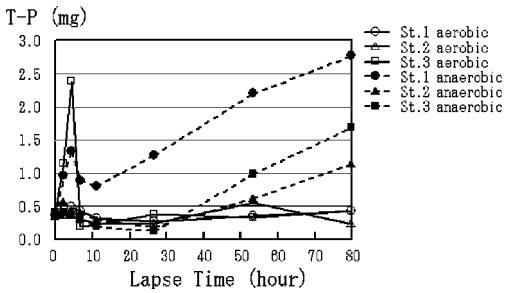

FIG. 8—*Experimental results of T-P release from sediments.*

10 h, respectively, as shown in Table 7. From the table, in the case of after 10 h, the nutrient releases from the sediment only under anaerobic condition. This result says that the concentration of dissolved oxygen in bottom layer is a very important factor to consider the nutrient release reduction.

Concluding Remarks and Discussion

In the study, we carried out field observations of water and sediment qualities, bottom sediment sampling, and laboratory tests in order to know the lasting effect of sand capping techniques on nutrient release reduction from contaminated sea bottom sediments at Yokohama Port. From the study, the following conclusions are obtained.

1. By undisturbed sediment core sampling, it is shown that the dark mud of 1 cm thickness is accumulated on the sand capping materials at St. 2, and the mud of 5 cm thickness is accumulated at St. 3.
2. By laboratory tests for nutrient release, it is shown that the nutrient release rate from the contaminated sediment without sand capping is larger than the rate from the sediment with sand capping. And the nutrient release rate is dependent upon the thickness of mud layer accumulated on the capped sand and the concentration of dissolved oxygen of bottom water.
3. The sand capping techniques has a still effect on nutrient release reduction, but the effectiveness of the sand capping is decreased due to the accumulation of dark fluid mud on the capped sand in sea bottom.

Similar sediment core samplings were carried out by Ministry of Land, Infrastructure and Transport (2004) in the summer. According to the report, the thickness of the dark mud layer was about 10 cm at St. 2 and about 5 cm at St. 3. The sediment qualities between in winter shown in Table 3 and in summer shown in Table 5 are relatively different. These results say that the thickness and sediment quality of the mud accumulated on the bottom at St. 2 varied from summer to winter. Two reasons are considered to vary the thickness and sediment quality of the mud. One reason is the weather condition. In 2004, there were several typhoons that attacked Japanese islands, so strong currents and/or strong waves would be generated. Then the mud would be transported by current and/or wave actions. Therefore, we have to consider the movement of bottom mud by current and wave actions in order to know the lasting effect of sand capping. Another reason is water quality difference between winter and summer. There were big differences of water quality such as the concentrations of dissolved oxygen and chlorophyll-a. Due to the big

TABLE 7—*Experimental results of* PO_4-P *release rate for before and after* 10 h *data. (Unit:* $mg/m^2/day$*).*

Station	DO condition	before 10 h	after 10 h
St. 1	Aerobic	−6.80	−1.07
St. 2	Aerobic	−5.50	−0.69
St. 3	Aerobic	4.05	−0.99
St. 1	Anaerobic	49.99	4.28
St. 2	Anaerobic	−3.06	2.52
St. 3	Anaerobic	4.25	4.36

difference of water quality between winter and summer, the variance of the thickness of fluid mud layer would be generated. We intend to study the behavior of mud accumulation or transport on the sea bottom in the near future.

Acknowledgments

This observational study was carried out by the Kanto Regional Development Bureau, Ministry of Land, Infrastructure and Transport, and Kokudo Kankyo Ltd. The authors express their greatest thanks to the persons in charge of field measurements.

References

Ministry of Land, Infrastructure and Transport, 2003, "Report of Environmental Survey of Water Quality at South-Central District in Chiba Port," (in Japanese).

Ministry of Land, Infrastructure and Transport, 2004, "Report of the Study on Improvement of Marine Environment in Artificial Seaweeds Beds," (in Japanese).

Murakami, K., Hosokawa, Y., and Horie, T., 1996, "Field Experiments on Improving of Bottom Sediments Quality by Sand Capping in Mikawa Bay," *Clean Sea in Toyohashi*, Int. Workshop and Symposium on Environmental Restoration for Enclosed Coastal Seas, pp. 122–134.

Journal of ASTM International, Vol. 3, No. 6
Paper ID JAI13342
Available online at www.astm.org

James T. Olsta,[1] *Charles J. Hornaday,*[2] *and Jerald W. Darlington*[3]

Reactive Material Options for In Situ Capping

ABSTRACT: Environmental dredging creates challenges in finding areas to construct confined disposal facilities and typically results in residual contamination. In situ capping (either in place of dredging or for capping residual contaminants) can be limited by concerns regarding navigation, uniform cap placement, biointrusion and geotechnical stability. A potential solution for many in situ capping concerns is the use of a reactive material cap. A reactive material cap could greatly reduce the thickness required for the cap compared to conventional sand caps. Various reactive materials (e.g., activated carbon, apatite, organo-clay, zeolite, zero-valent iron) are used for removal of organics and metals in wastewater and groundwater treatment and may be applicable to in-situ capping. There are several ways that could be used for in-situ capping with reactive materials. A layer of reactive material could be placed in bulk using a clamshell or pumped through a tremie pipe. Another option is a reactive material filled geotextile mat. A reactive material mat would have several advantages over loose placement of reactive materials, including: (1) uniform and verifiable mass per area placement of reactive or adsorptive material; (2) ability to mix reactive or adsorptive materials in defined proportions; (3) geotextiles provide separation of the reactive material from the contaminated sediment and cover material; (4) geotextiles provide a barrier to biointrusion; (5) multiaxial strength of the geotextiles provides resistance to uplift and differential settlement; and (6) geosynthetic reinforcement provides stability on sloped areas. In the United States, a carbon-based geotextile mat was constructed and successfully deployed. A barge with a crane was used to deploy the material off shore. Other deployment methods have also been used for installing geosynthetics in waterways from shoreline and would be applicable to a reactive material mat.

KEYWORDS: capping, reactive, adsorption, sequestration

Introduction

Dredging has evolved into a highly sophisticated process drawing from some of the latest technology. The methods of navigational dredging range from clamshell buckets to sophisticated hydraulic dredges. More recently, these techniques have evolved into the processes used for environmental dredging applications.

High concentrations of certain contaminants in sediments pose human heath and ecological risks. Dredging of contaminated sediment provides a method of removal of these contaminants of concern (COC). One of the most obvious benefits of environmental dredging is the fact that contaminated sediments are permanently removed from the water body. These sediments are typically disposed of in an upland containment facility or landfill. In some cases, disposal of contaminates may not be permitted or the costs to transport them to a permitted facility may be very high. Alternate uses for the contaminated sediments may be considered and may help to reduce or eliminate risks. The cost of these alternate treatment and use methods must be evaluated against other permissible disposal options.

Of paramount concern when dredging is the ability of the process to remove the COCs to a level that is below the regulated concentration. Although dredging techniques have been demonstrated to reduce sediment contaminant concentrations, it appears that these techniques can result in residual contamination. This residual contamination may be the result of re-suspension of contaminates into the water column or sloughing of adjacent materials into the dredged areas. Concern over these residual concentrations may lead to subsequent passes or other means to minimize risk from the residuals.

The impacts of the cleanup activity to the surrounding area need to be evaluated regarding the impact of the operation or long-term disturbance of an area. A dredging operation will typically require some sort

Manuscript received April 3, 2005; accepted for publication July 14, 2005. Presented at ASTM Symposium on Contaminated Sediments: Evaluation and Remediation Techniques on 23–25 May 2006 in Shizuoka, Japan; M. Fukue, K. Kita, M. Ohtsubo, and R. Chaney, Guest Editors.

[1] Technical Manager, CETCO, 1500 W. Shure Dr., Arlington Heights, IL 60004.
[2] Group Manager, CETCO, 1500 W. Shure Dr., Arlington Heights, IL 60004.
[3] Research & Development Director, CETCO, 1350 W. Shure Dr., Arlington Heights, IL 60004.

of sediment dewatering process. After removal of the solids, the associated water may have to be treated before it can be discharged back into the waterway. Because of these facts a dredging operation typically requires onshore support facilities. Construction of these facilities will likely impact the area surrounding the dredged area.

In Situ Capping

An alternate solution to dredging contaminated sediments is to cap them in place. In situ sediment caps are typically designed to take into consideration stabilization and physical isolation of the sediments as well as contaminate transport mechanisms (Palermo et al. 1998). Laboratory treatability testing and computer modeling is used to predict long-term movement of contaminants into or through the cap. The U.S. Environmental Protection Agency (EPA) has developed a model that considers both diffusive and advective fluxes, the thickness of the sediment layers, physical properties of the sediments, concentrations in the sediments and other parameters (Reible 1998)

Due to a limited set of information on many mechanical processes that can affect the long-term stability of the cap some uncertainty exists over this issue. Concerns exist over the effects of ice heaving, currents, tides, wave action, propeller, and thruster wash on the cap. Caps may be limited for areas where concerns over these erosion forces may not exist. Alternatively, these concerns are typically addressed by increasing the cap thickness to the point that it exceeds the thickness of material that may be affected by such forces. Additional research in this area may provide a more clear understanding of these forces on a cap design. Another alternative is to include a component in the cap design that would act to minimize the effect of these erosion forces.

A proper cap design should take into account the indigenous benthic community. To do so means to properly address the potential for biointrusion into the contaminated sediment. This is typically done by increasing the overall cap thickness to the point that it exceeds the depth of penetration of the local benthos. Another approach is to block biointrusion with some other layer in the cap design.

Construction processes have evolved to allow an accurate placement of the cover materials in a traditional sand cap. Although these processes have advanced, an allowance in the cap design is typically made to account for the spatial variability of the cover material placement. Once again this allowance usually entails adding more material to account for the variability of placement. Methods of ensuring uniform placement of materials are needed.

With all of the variability in the conditions which a cap may be in service, comes a degree of uncertainty. This uncertainty is typically compensated by adding more and more material to the cap design. For this reason cap designs may become impractical in water depths that do not even exceed the total cap thickness. Clearly, the impact to navigability must be assessed when evaluating whether a cap design is practical. From a practical point, if a thin cap can be designed that provides as good or better a performance than a traditional sand cap, then the capping alternative may become a practical solution for a wider range of applications.

Despite the variability in cap designs based on the range of considerations herein, in situ capping whether traditional or thin cap design does offer some inherent advantages over dredging. First, the cost to cap is typically only 30 % of the cost to dredge and dispose (Evison et al. 2004).

In addition to the cost advantage, typically a remediation of contaminated sediment can be completed faster by in situ capping than by dredging. This may be of significance to a heavily navigated area or an area where recreational use needs to be restored rapidly.

Finally, the impact to the surrounding area may be of importance. In an urban setting the shoreline may not be conducive to the operation of a dewatering facility. Or, the impact of having sustained dredging operations to the area may be financially significant. These impacts are generally less if capping is chosen as the remedial option.

Reactive Materials

Various reactive materials (e.g., activated carbon, apatite, organoclay, zeolite, zero-valent iron) are used for water, wastewater, and groundwater treatment and can be applied to in situ capping. Activated carbon is a widely used adsorptive media for water treatment removal of phenol, halogenated compounds and pesti-

FIG. 1—*Deployment of Organoclay Cap at Willamette River.*

cides. Activated carbon is made by the thermal decomposition of various carboneous materials followed by an activation process. Raw materials include woods, rice hulls, and nutshells. The resulting activated carbon is amorphous and contains complex networks of interconnected micropores. (Thomas and Crittenden 1998). Apatite, $Ca_{10}(PO_4)_6(OH,F)_2$, is a commercially available mineral that has been shown to be effective at sequestration of lead. Apatite removes contaminants from water through three mechanisms: ion exchange, isomorphic substitution, and precipitation (Gardner and Stern 2004).

Organoclays are surface-modified clays that have been shown to be effective adsorbents for insoluble and partially insoluble compounds. The production of organoclays replaces the surface cation of bentonite or hectorite clay with an organic molecule. Quaternary amines based upon tallow are the most commonly used organic compound. The resulting organoclay is oleophilic, hydrophobic, and permeable. A properly compounded organoclay will exhibit minimal swelling upon organic adsorption and maintain high permeability. Several manufacturing quality control tests have been developed using x-ray diffraction and thermo gravimetric analysis to assure proper compounding. In treatment of produced water from off-shore crude oil production organoclays have removed polyaromatic hydrocarbons to non-detect levels (Darlington 2002).

Zeolites are porous crystalline aluminosilicates. Both natural and synthetic zeolites are used commercially for their adsorption, ion exchange, molecular sieve, and catalytic properties. Zeolites are used in water treatment for removal of nitrates and metals such as lead, zinc, and copper (Thomas and Crittenden 1998). Zero-valent iron, Fe(0), is a strong reductant and has been used successfully in permeable reactive barriers for the dechlorination of chlorinated hydrocarbons and the reductive precipitation of chromate (Cr^{+6} as CrO_4^{-2} (Powell et al. 2002). Reductive precipitation involves the transfer of electrons from Fe(0) to the hexavalent chromium and transforming the chromium to a less soluble form, $Cr(OH)_3$.

Bulk Deployment

A layer of reactive material can be placed in bulk using a clamshell, pouring from super sacks or pumped through a tremie pipe. At the Anacostia River Demonstration Project in Washington, D.C. apatite material was placed in bulk over sediments using a clamshell. The clamshell was opened just above the surface and the material settled over the sediments. The target thickness was 150 mm. Core samples indicated that the actual thickness was 130 mm±45 mm. A sand layer approximately 150 mm thick was placed over the apatite to allow for colonization by benthic organisms. Operator experience and a global positioning system on the crane were critical for controlling the thin lifts. In the Willamette River in Oregon, a 600 mm thick organoclay bulk layer was placed over hydrocarbon nonaqueous phase liquid (NAPL) seeps using 1800 kg heavy duty woven polypropylene bags, referred to as super sacs. The super sacs were positioned over the area with a backhoe and then the bottom of the sacs were opened above the surface allowing the organoclay to pour out and settle over sediments (Fig. 1). An articulating concrete mat was placed over the organoclay cap for protection.

Reactive Material Mat

A system has been devised that encapsulates reactive materials within a geotextile composite that can be easily deployed as an in situ capping material over sediments. Geotextiles are textiles that are manufac-

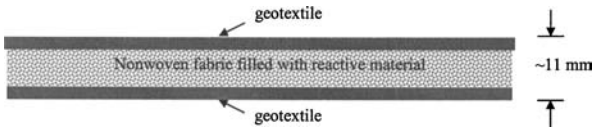

FIG. 2—*Cross section of laminated reactive core mat.*

tured into flexible, porous fabrics with synthetic fibers. Synthetic fibers are resistant to biodegradation. Geotextiles have varying properties based upon the type of polymer, the type of fiber, and fabric style. The four main functions of geotextiles are separation, reinforcement, filtration, and drainage. Geotextiles are used in civil engineering, and particularly in coastal work. Some early uses of geotextiles were in the late 1950s behind precast concrete seawalls and under large riprap (Koerner 1998).

Reactive mats have been constructed by CETCO using two methods. The first method is by needlepunching. This method has been used since the late 1980s to manufacture geosynthetic clay liners. In the needlepunching operation a layer of geotextile, either woven or nonwoven, is fed onto the line. A hopper disperses an even layer of the reactive material onto the geotextile. A top nonwoven geotextile is then unrolled on top of the reactive material. The material is then fed through a loom where nonwoven fibers are needlepunched through the reactive material and into the lower geotextile. Typical thickness of the needlepunched mat is 6 mm. The reactive mat is rolled onto a core tube and then wrapped in a polyethylene bag.

The second method is a laminating method (Fig. 2). This method allows a higher mass per unit area than needlepunching and the ability to use abrasive reactive materials that cannot be needlepunched. In the laminating method a nonwoven core is bonded either by needlepunching or adhesive to a geotextile. The bonded material is then fed core side up through the line. Reactive material is fed onto the core from a hopper. The core has an apparent opening size (AOS) that is larger than the maximum particle size of the reactive material. The reactive material is worked into the core openings by suction and/or vibration. A cap geotextile is then bonded to the top of the core by heat or adhesive. Typical thickness of the laminated mat is 11 mm. The reactive mat is rolled onto a core tube and then wrapped in a polyethylene bag.

Certain reactive materials, such as activated carbon, are buoyant. The reactive mat may be engineered with a geotextile with a high specific gravity and/or a fraction of sand mixed with the reactive material to counteract the buoyancy.

Benefits

An advantage of a reactive cap over a sand cap is reduced cap thickness. Lab column testing and modeling illustrate that a thin layer of highly adsorptive material such as activated carbon can have over 100 times the adsorption capacity for polychlorinated biphenyls (PCBs) as sand or organically rich soil containing 3.8 % carbon fraction (Murphy and Lowry 2004). Project specific conditions and adsorptive material properties will affect results. However, a 10 mm thick reactive mat can theoretically replace 1 m of sand or soil. This can help maintain navigable depths and flow capacity of waterways.

One factor with using reactive materials is their cost. By constructing a mat encapsulating the reactive materials within geotextiles they can be used in a controlled and potentially cost-effective manner. The reactive mat also combines the benefits of reactive materials and geotextiles. Activated carbon reactive mat for a recent project cost $\sim$US\$16.5/m^2. The reactive mat properties included permeability per ASTM D2434 $\geqslant 1$ by 10^{-2} cm/s and grab tensile strength per ASTM D4632 $\geqslant 660$ N.

The U.S. EPA program on Assessment and Remediation of Contaminated Sediments (ARCS) has developed guidance on the design of in situ caps that includes laboratory tests and models of the following key processes; advective/diffusive contaminant flux, bioturbation, consolidation and erosion. The potential functions of geotextiles in in situ cap designs include: (1) providing a bioturbation barrier; (2) preventing mixing of cap materials with underlying sediments; (3) reducing contaminant flux; (4) promoting uniform consolidation; (5) stabilizing the cap; and (6) reducing erosion of the capping materials (Palermo et al. 1998). Since the reactive mat is constructed with two geotextiles the composite mat can be designed to perform multiple cap functions.

Hampton et al. (2002) showed that geotextiles can greatly reduce movement of benthic invertebrates

FIG. 3—*Reactive material mat being prepared for deployment on the Anacostia River.*

in sediments. As previously stated, a geotextile with a proper AOS can contain the cap material and prevent mixing into the underlying sediments. The multiaxial tensile strength of the geotextiles can provide stabilization to the cap. At the Anacostia River Demonstration Project the reactive mat was installed over soft sediments with 0.6 kN/m^2 undisturbed shear strength (at 600 mm depth) per field vane shear ASTM D2573 test results. The geotextile, along with appropriate armoring, can also help reduce erosion of the capping material.

Mat Deployment

Reactive mats may be deployed in a number of ways. The Anacostia River demonstration project was a successful demonstration of a barge based deployment technique (Fig. 3). In this demonstration, a barge mounted crane was used to position the rolls and unroll the reactive mat underwater. The mats were first submerged to allow them to absorb water and displace entrained air. Then the rolls were positioned 450 mm above the river bottom and anchored with sand at one end. The crane was able to swing across and unroll the mat. The installation was assisted by a global positioning system and coordinated by a diver in radio communication with the crane operator. A sand layer approximately 150 mm thick was placed over the reactive mat for protection and to allow for colonization by benthic organisms (Horne Engineering Services 2004).

Land based deployment techniques may also be used to deploy reactive mats. Rolls may be positioned on shore suspended by a spreader bar system with a clamp connected to the leading edge of the roll. The material is then pulled off of the roll using a winch that is either mounted on a barge or on the opposite side of the waterway.

Deployment techniques may also take advantage of temporary buoyancy before the mat absorbs water and displaces air to allow the material to "float" into position and subsequently sink as it takes on water. This technique is planned for capping approximately four hectares of hydrocarbon contaminated sediment with an activated carbon reactive mat in a Minnesota bay in early 2006.

Conclusions

The environmental remediation community is seeking innovative methods to remediate contaminated sediments. Reactive materials and geotextiles have been used extensively in civil engineering for water treatment and coastal applications, respectively. The use of reactive materials for in situ capping of contaminated sediments has many potential benefits. A reactive material mat combines the benefits of reactive materials and geotextiles in addressing concerns with in situ capping. Several techniques have been used or planned for deployment of reactive material mats. It is likely that as the reactive material mat technology develops, the methods of deployment will also evolve.

References

Darlington, J. W., "New Technology Achieves Zero Discharge of Harmful Alkyl Phenols and Polyaromatic Hydrocarbons from Produced Water," *Proceedings of ONS 2002 Conference*, Offshore Northern Seas Foundation, Stavanger, Norway, 2002.

Evison, L., Grosso, N., and Stansbury, J., "Dollars and Sense in Risk Management Decision Mak-

ing," *Addressing Uncertainty and Managing Risk at Contaminated Sediment Sites: USACE/USEPA/SMWG Joint Sediment Conference*, SMWG, Detroit, MI, 2004.

Gardner, K. and Stern, E., "Status of Ex-Situ and In-Situ Treatment Methods," *Addressing Uncertainty and Managing Risk at Contaminated Sediment Sites: USACE/USEPA/SMWG Joint Sediment Conference*, SMWG, Detroit, MI, 2004.

Hampton, D. R., Cassidy, D. P., Beck, D. R., and Kohler, S. L., "In-Situ Remediation of Contaminated Sediments in Groundwater-Fed Streams and Lakes," *Abstract Book of AGWSE 2002 Annual Conference*, National Ground Water Association, Westerville, OH, 2002, pp. 40–41.

Horne Engineering Services 2004, "Revised Draft, Cap Completion Report for Comparative Validation of Innovative 'Active Capping' Technologies, Anacostia River, Washington D.C.," www.hsrc-ssw.org/pdf/cap-completion-rpt.pdf

Koerner, R. M., *Designing with Geosynthetics*, 4th Ed., Prentice Hall, Upper Saddle River, NJ, 1998.

Murphy, P. J. and Lowry, G. V., "In Place Management of PCB-Contaminated Sediments: Performance Evaluation and Field Placement of Sorbent-Amended Sediment Caps." *Proceedings of Environmental Chemistry Division 228th ACS National Meeting*, pp. 629–636. American Chemical Society, Columbus, OH, 2004.

Palermo, M., Maynord, S., Miller, J., and Reible, D., *Guidance for In-Situ Subaqueous Capping of Contaminated Sediments*, U.S. Environmental Protection Agency, *EPA 905/B-96/004*, Great Lakes National Program Office, Chicago, IL, 1998.

Powell, R. M., Powell, P. D., Puls, R. W., and Burden, D. S., *Economic Analysis of the Implementation of Permeable Reactive Barriers for Remediation of Contaminated Ground Water*, U.S. Environmental Protection Agency, *EPA 600/R-02/034*, National Risk Management Research Laboratory, Cincinnati, OH, 2002.

Reible, D., *Guidance for In-Situ Subaqueous Capping of Contaminated Sediments, Appendix B: Model for Chemical Containment by a Cap*, U.S. Environmental Protection Agency, *EPA 905/B-96/004*, Great Lakes National Program Office, Chicago, IL, 1998.

Thomas, W. J. and Crittenden, B. D., *Adsorption Technology and Design*, Butterworth-Heinemann, Oxford, Great Britain, UK, 1998.

Journal of ASTM International, Vol. 3, No. 6
Paper ID JAI13344
Available online at www.astm.org

Krishna R. Reddy[1] *and Prasanth R. Ala*[2]

Electrokinetic Remediation of Contaminated Dredged Sediment

ABSTRACT: This paper investigates the feasibility of electrokinetic remediation of contaminated sediment at Indiana Harbor, Indiana. The sediment is a fine-grained material with high moisture content of 78 % and high organic content of 19 % and it is contaminated with a wide range of polycyclic aromatic hydrocarbons (PAHs) and heavy metals. Four bench-scale electrokinetic experiments were conducted at 2.0 VDC/cm of constant voltage gradient using two surfactants (5 % Igepal CA-720 and 3 % Tween 80), a cosolvent (20 % *n*-butylamine), and a cyclodextrin (10 % HP-β-CD) as flushing solutions for the solubilization/desorption of PAHs. The mobility and removal of heavy metals was also investigated while flushing these solutions. The experimental results show that 20 % *n*-butylamine and 5 % Igepal 720 systems are effective for the partial solubilization of the PAHs in the sediments; however, both 3 % Tween 80 and 10 % HP-β-CD systems are found to be ineffective for desorption/solubilization of PAHs in the sediment. None of the selected flushing agents is found to be effective for the removal of heavy metals from the contaminated sediment. The low removal of PAHs and heavy metals is attributed to the high organic content and high acid buffering capacity of the sediment.

KEYWORDS: electrokinetics, sediments, PAHs, heavy metals, remediation

Introduction

Contaminated sediments are of great concern to humans and wildlife who live within the Great Lakes Basin. Over the decades, heavy metals and toxic organic chemicals mixed with the particles of rock, soil, and decomposing woods have contaminated the sediments and are deteriorating the quality of rivers and harbors in the Great Lakes Basin. Evidence now supports that pollutants trapped in sediment can adversely impact humans and the environment. The USEPA (1998) reports the locations of different sites in the Great Lakes Basin where large quantities of contaminated sediments are found. These sediments contain both organic (e.g., polychlorinated biphenyls (PCBs), polycyclic aromatic hydrocarbons (PAHs), 2,3,7,8-tetrachlorodibenzo-p-dioxin, and hexachlorocyclohexane), and inorganic (such as mercury, lead, and arsenic) contaminants (Mulligan et al. 2001).

It is critical that the concentrated deposits of contaminated sediment be addressed quickly, because over time they may be transported from a river or harbor to the Great Lakes. Once dispersed into the lakes, cleanup is virtually impossible (Nobbs and Chipman 2003). The most common remediation method has been dredging the contaminated sediments followed by disposal in permitted confined disposal facilities (CDFs). However, disposal of dredged sediments in CDFs can create potential concerns such as contaminant exposure, slow dewatering and consolidation, high costs, and long-term liability. The USEPA created the Assessment and Remediation of Contaminated Sediment (ARCS) Program to evaluate different technologies that may be used to remediate the contaminated sediments. Sediment treatment refers to the use of physical, chemical, or biological processes to remove or degrade contaminants or immobilize the contaminants within the sediment. Different techniques to remediate contaminated sediments include thermal desorption, washing, and bioremediation. The available processes and approaches for design and implementation of treatment have been well documented (USEPA 2001). In addition, field pilot studies

Manuscript received April 1, 2005; accepted for publication September 16, 2005. Presented at ASTM Symposium on Contaminated Sediments: Evaluation and Remediation Techniques on 23–25 May 2006 in Shizuoka, Japan; M. Fukue, K. Kita, M. Ohtsubo, and R. Chaney, Guest Editors.

[1] Associate Professor, Department of Civil and Materials Engineering, University of Illinois at Chicago, 842 West Taylor Street, Chicago, Illinois 60607, USA, e-mail: kreddy@uic.edu

[2] Graduate Research Assistant, Department of Civil and Materials Engineering, University of Illinois at Chicago, 842 West Taylor Street, Chicago, Illinois 60607, USA.

TABLE 1—*Properties of dredged sediment.*

Property	Test method[a]	Value
Moisture content	ASTM D 2216	78.60 %
Specific gravity	ASTM D 854	1.25
Grain size distribution	ASTM D 422	% gravel=0.1 % sand=8.4 % fines=91.5
Atterberg limits	ASTM D 4318	Liquid limit=45% Plastic limit=32% Plasticity index=13%
Maximum dry density	ASTM D 698	1.35 g/cm^3
Optimum moisture content	ASTM D 698	24.0 %
Hydraulic conductivity	ASTM D 5084	3.3×10^{-7} cm/s
pH	ASTM D 4972	7.0
Organic content	ASTM D 2974	19.20 %
USCS classification	ASTM D 2487	OL

[a]ASTM (2003).

using promising treatment technologies have been conducted under USEPA programs including the ARCS program. Many treatment technologies have proven to be effective, but cleanup cost is the major constraint to the wider application of treatment for sediment remediation projects. Treatment costs can range from around $50US per cubic meter for a process such as stabilization to over $1000US per cubic meter for high temperature thermal processes. As of 1998, over 2 million cubic yards of sediment have been remediated at a total expense of over 360 million dollars (USEPA 1998).

It is necessary to develop a simple, safe, and cost-effective cleanup process for contaminated sediments. This study investigates the feasibility of using electrokinetic remediation process to cleanup contaminated sediments. Electrokinetic remediation can be implemented as an ex situ or in situ process to remediate both heavy metals and organic compounds. Essentially, electrokinetic remediation involves the installation of electrodes into the contaminated sediments (ex situ or in situ). After the electrodes are installed, a low electric potential is applied across the anodes (positively charged electrodes) and the cathodes (negatively charged electrodes). Application of electric potential induces the following three major transport processes in the sediment: (1) electroosmosis, the movement of interstitial water toward cathode; (2) electromigration, the movement of ionic species to the oppositely charged electrode; and (3) electrophoresis, the movement of charged colloids and particles to the oppositely charged electrode. In addition, electrolysis reactions occur at the electrodes which generate H^+ ions at the anode and OH^- ions at the cathode. The electromigration of H^+ and OH^- ions can reduce the sediment pH near anode and increase the sediment pH near cathode (Reddy and Parupudi 1997).

Electrokinetic remediation can remove dissolved contaminants from fine grained, low permeability sediments. However, contaminants with limited solubility or that sorb to sediment surfaces cannot be remediated by electrokinetic remediation. In order to increase dissolution, solubilization, or desorption of the contaminants, flushing of different selected solutions such as surfactants, cosolvents, and chelants through the sediments during electrokinetic remediation is often required.

This study investigates the efficiency of electrokinetic remediation of contaminated sediment obtained from Indiana Harbor of Great Lakes Basin. Dredged sediment samples were obtained and characterized for different physical and chemical properties. The sediment was found contaminated with a wide range of polycyclic aromatic hydrocarbons (PAHs) and heavy metals. A series of bench-scale electrokinetic experiments was conducted using different flushing solutions for the removal of these contaminants. Efficacy of two surfactants (namely, 5 % Igepal CA-720 and 3 % Tween 80), a cosolvent (20 % *n*-butylamine) and a cyclodextrin (10 % HP-β-CD) were investigated to enhance the solubilization of PAHs from the sediments. The experimental results are used to evaluate the relative performance of these flushing agents to enhance the electrokinetic removal of PAHs and heavy metals from the sediment.

Experimental Methodology

Sediment Characterization

The sediment samples were obtained from Indiana Harbor, Indiana. The sediment was homogenized and characterized for physical and chemical properties (Table 1). The results revealed that sediment possesses

TABLE 2—*Contaminants found in dredged sediment.*

(*a*) Total metals (USEPA Method 6020/7471A)[a]		(*b*) Polycyclic aromatic hydrocarbons (USEPA Method 8270/8270C)[a]	
Chemical	Concentration (mg/kg-dry)	Chemical	Concentration (mg/kg-dry)
Aluminum	5400	Acenaphthene	23
Antimony	1.7	Acenaphthylene	9.6
Arsenic	42	Anthracene	27
Barium	92	Benz(a)anthracene	52
Beryllium	0.94	Benzo(a)pyrene	36
Cadmium	9.5	Benzo(b)fluoranthene	23
Calcium	26,000	Benzo(g,h,i)perylene	23
Chromium	530	Benzo(k)fluoranthene	25
Cobalt	9	Carbazole	58
Copper	200	Chrysene	34
Iron	110,000	Dibenz(a,h)anthracene	11
Lead	570	Fluoranthene	94
Mercury	1.1	Fluorene	31
Magnesium	8,900	Indeno(1,2,3-cd)pyrene	24
Manganese	1,800	Naphthalene	66
Nickel	67	Phenanthrene	100
Potassium	680	Pyrene	66
Selenium	<0.99		
Silver	2.4		
Sodium	150		
Thallium	3.5		
Vanadium	17		
Zinc	3700		

[a]USEPA (1986).

high moisture content of 78 % and high organic content of 19 %. The sediment constitutes over 90 % of fines, but exhibits low plasticity. The sediment possesses low hydraulic conductivity of 3.3×10^{-7} cm/s. The pH of the sediment is found to be 7.0. As shown in Table 2, the sediment was contaminated by heavy metals and PAHs. The toxic heavy metals found in high concentration include zinc (3700 mg/kg), lead (570 mg/kg), chromium (530 mg/kg), copper (200 mg/kg), barium (92 mg/kg), and arsenic (42 mg/kg). Several carcinogenic PAHs exist in the sediment at relatively high concentrations.

The acid buffering capacity of the sediment as determined by titration method using 0.5 M HNO_3 is shown in Fig. 1. The results of control test on deionized water are shown for comparison purposes. The results reveal high acid buffering capacity of the sediment, possibly due to high carbonate content.

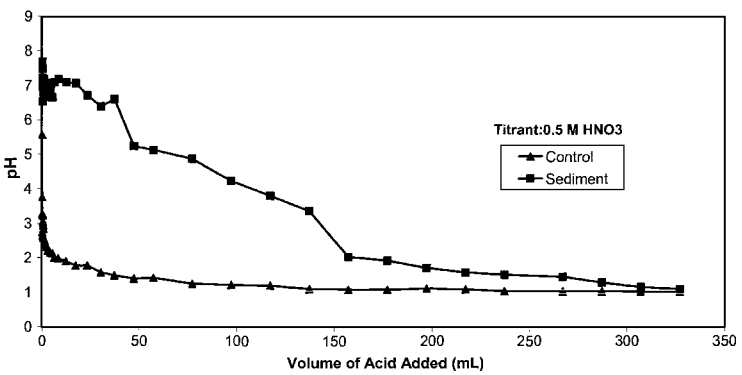

FIG. 1—*Acid buffering capacity of dredged sediment.*

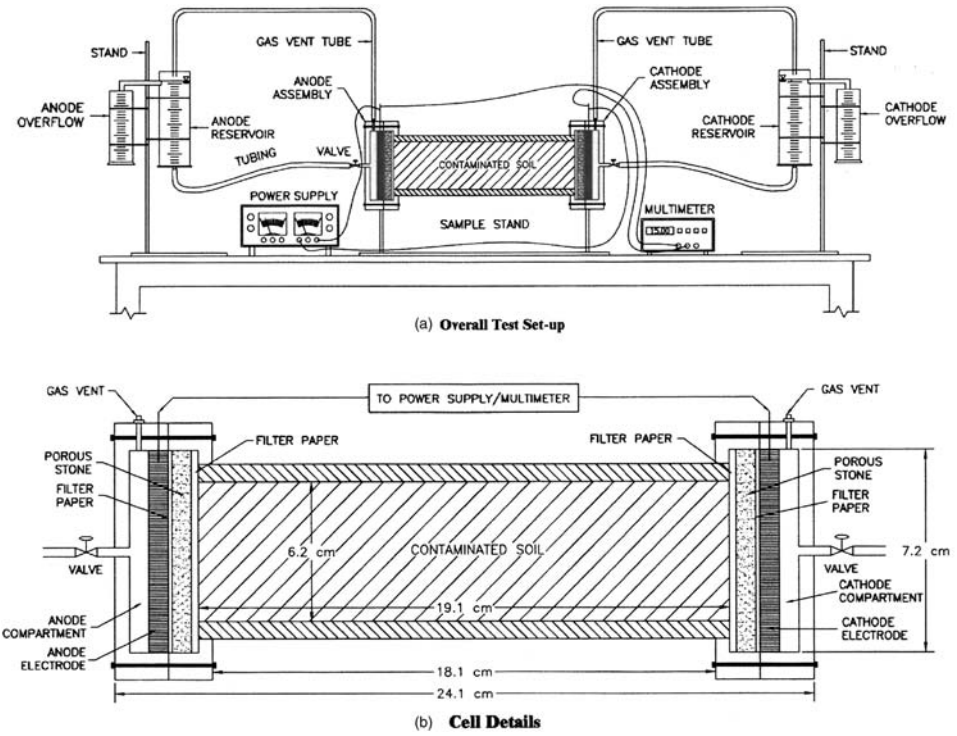

FIG. 2—*Electrokinetic test setup.*

Electrokinetic Test Setup

Figure 2 shows the schematic of the electrokinetic test setup used for this study. Reddy and Parupudi (1997) have described this setup in detail. The setup consists of an electrokinetic cell, two electrode compartments, two electrode reservoirs, a power source, and a multimeter. Plexiglas[3] cells having an inside diameter of 6.2 cm and a total length of 19.1 cm were employed in this study. Each electrode compartment consisted of a valve to control the flow into the cell, a slotted graphite electrode, and a porous stone. The electrode compartments were connected to the either end of the cell using screws. The electrode reservoirs were made of 3.2 cm inner diameter Plexiglas tubes and were connected to the electrode compartments using Tygon[4] tubing. Exit ports were created in the electrode compartments, and the tubing was attached to these ports to allow the gases generated due to the electrolysis of water to escape. The other end of these gas tubes was connected to the reservoirs to collect any condensable liquid that was removed along with the gases. A power source was used to apply a desired constant voltage to the electrodes, and a multimeter was used to monitor the voltage and measure current during the test.

Test Variables

As shown in Table 2, quality of the sediment is largely deteriorated by the presence of carcinogenic PAHs as compared to heavy metals. Keeping this in view, the testing program was first aimed to determine the feasibility of removing PAHs from the contaminated sediment. Because of the hydrophobic characteristics of PAHs, different flushing solutions were investigated to enhance solubilization of PAHs. The flushing solutions selected were two different surfactants, 5 % Igepal CA-720 and 3 % Tween 80; a cosolvent, 20

[3]Trademark of Rohm & Haas Company.
[4]Trademark of Norton Company.

TABLE 3—*Electrokinetic testing program using dredged sediment.*

Test number	Voltage gradient (VDC/cm)	Hydraulic gradient (cm/cm)	Flushing solution
1	2.0	1.5	5 % Igepal CA-720
2	2.0	1.0	3 % Tween 80
3	2.0	1.0	20 % *n*-Butylamine
4	2.0	1.5	10 % HP-β-CD (HPCD)

% *n*-butylamine; and a cyclodextrin, 10 % HP-β-CD. Surfactants and cosolvents were selected mainly to enhance the removal of PAHs, but the mobility/transport of heavy metals while observing the removal of PAHs was also examined. Cyclodextrins were employed to determine their efficiency in the removal of both PAHs and heavy metals simultaneously. These flushing solutions and their concentrations were determined based on batch experiments conducted on different soils contaminated with PAHs and heavy metals (Maturi 2004). Table 3 lists the details of the four experiments conducted in this study. All the experiments were conducted under a constant voltage gradient of 2.0 VDC/cm. All the tests were conducted using different flushing solution. Based on the elevation difference between the liquid levels in the anode and cathode reservoirs, the maximum hydraulic gradient was either 1.0 or 1.5 (Table 3). These hydraulic gradients were not significant enough to generate substantial hydraulic flow because of the low permeability of the sediment.

Testing Procedure

The sediment (as received from the field) was placed in the electrokinetic cell in layers and each layer was gently compacted uniformly using a hand compactor. The electrode compartments were then connected to the electrokinetic cell. In each electrode compartment, filter papers were inserted between the electrode and the porous stone as well as between the porous stone and the sediment. The electrode compartments were connected to the anode and cathode reservoirs using Tygon tubing. The anode reservoir was then filled with selected flushing solutions and the cathode reservoir was initially filled with deionized water. The electrokinetic cell was then connected to the power supply and a constant voltage gradient of 2.0 VDC/cm was applied to the sediment sample. Throughout the test duration, the elevation of solution/water in both reservoirs was monitored and adjusted to maintain a constant hydraulic gradient across the specimen. The electric current and voltage across the sediment sample as well as the outflow or inflow at the anode and cathode reservoirs was measured at different time periods throughout the duration of the experiment. Effluent from the cathode reservoir was collected at different time intervals.

After completion of each test, aqueous solutions from the anode and cathode reservoirs and electrode assemblies were collected and the volumes were measured. Then, the reservoirs and electrode assemblies were disconnected, and sediment specimen was extruded from the cell using a mechanical extruder. The sediment specimen was sectioned into three equal parts: S-1 (near anode), S-2 (middle), and S-3 (near cathode). Each part was weighed and preserved in a glass bottle. From each sediment section, 10 g of sediment was taken and mixed with 10 mL of a 0.01 M $CaCl_2$ solution in a glass vial. The slurry was shaken thoroughly by hand for several minutes and the solids were allowed to settle for an hour. This slurry was then used for measuring the sediment pH. The pH of the aqueous solutions from the electrodes was also measured. The moisture content of each sediment section was determined in accordance with ASTM D 2216 (ASTM 2003).

Chemical Analyses

Representative samples from both reservoir solutions, sediment sections, and the initial sediment for each test were analyzed for total metals and PAHs. The total metals were analyzed using the USEPA Method SW6020/SW7471A and the PAHs were analyzed using the USEPA Method SW8270/SW8270C (USEPA 1986). The chemical analysis of all the samples was performed with stringent quality control by the STAT Analysis, Inc., Chicago, Illinois (an USEPA certified laboratory). To ensure accuracy of the test results, new electrodes, porous stones, and tubing were used for each experiment, and the electrokinetic cell and compartments were washed thoroughly and then rinsed first with tap water and finally with deionized water to avoid cross contamination between the experiments.

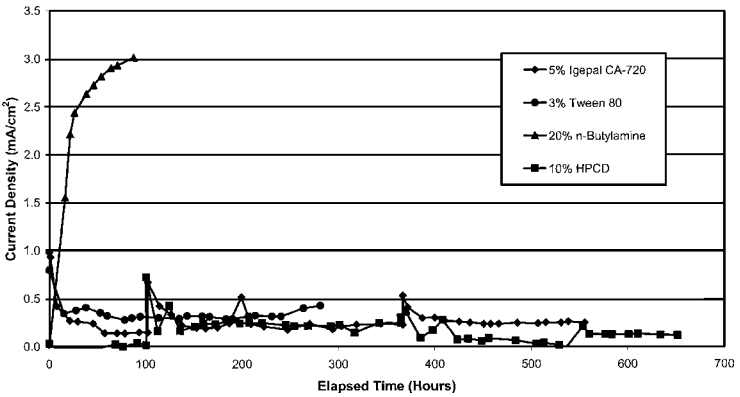

FIG. 3—*Measured electric current density during electric potential application.*

Results and Analysis

Electric Current Density

Figure 3 compares the current density variation with time for all tests. Current density values were calculated by dividing measured current values (recorded during experiments) by the cross-sectional area of the sediment specimen. The results show that when surfactants are employed, initially current density is high (0.8–1 mA/cm^2) and then it decreases and stabilizes at about 0.4 mA/cm^2 as the experiments proceed. Experiment with HPCD showed that current density increases slowly to 0.7 mA/cm^2 in 100 h, then decreases and stabilizes at 0.2 mA/cm^2. In general, current density remained less than 1 mA/cm^2 for all tests conducted with surfactants and HPCD. However, the current density values show an interesting trend for the test conducted with 20 % *n*-butylamine. Results reveal that current density increases rapidly to 2.5 mA/cm^2 value within 20 h and continues to increase gradually to 3 mA/cm^2 in 80 h when the test was terminated. The high current values generated in the *n*-butylamine system indicates introduction of substantial mobile ions to the pore water. A slow initial current increase in the HPCD test may be due to low/partial contaminant dissolution/desorption from the sediment minerals. The current generated in the surfactant systems is similar due to the formation of micelles in both the Igepal system and the Tween 80 system.

Electroosmotic Flow

Figure 4 shows the electro-osmotic flow data for all tests in terms of cumulative number of pore volumes with elapsed time. In all tests, the flow occurred from anode to cathode. The results suggest that flow behavior was dependent on the type of flushing solutions employed to extract contaminants from the sediment. Typically, the flow increases with time for all the tests. Maximum flow was observed in the cosolvent system, i.e., 20 % *n*-butylamine system, while the lowest flow was observed with the HPCD system. A similar flow behavior was observed in both surfactant systems. The flow variation in all the tested systems correlates with the measured current densities.

During the beginning of the test, when the current is high, the transfer of momentum to the surrounding fluid molecules may be substantial. This often corresponds to a significant volume of electroosmotic flow. A high ionic strength, however, can also be detrimental for electro-osmotic flow, because it reduces the thickness of the diffuse double layer and, thereby, constricts the electro-osmotic flow. The electro-osmotic flow depends on the properties of flushing solutions such as dielectric constant and viscosity. The electro-osmotic flow is proportional to the dielectric constant and inversely proportional to the viscosity.

Contaminant Removal

Outflow samples collected periodically at the cathode were analyzed for metals and PAHs. Figure 5(*a*) shows the cumulative metal removal per pore volume of the flow, and Fig. 5(*b*) shows the cumulative total

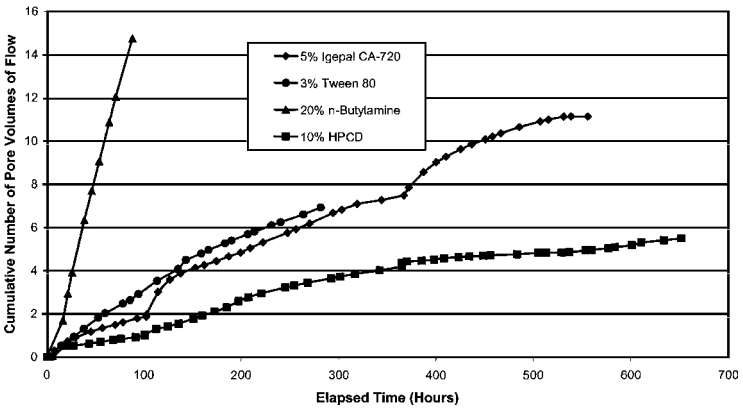

FIG. 4—*Measured pore volumes during electric potential application.*

PAHs removal per pore volume of the flow. These results show that several metals are removed during the application of electric potential; however, the removal of toxic metals was found to be low in all tests. It is pertinent to mention here that the flushing solutions employed in these studies were selected mainly for solubilization of PAHs and thus they have an insignificant removal capacity for the metals. Approximately 50 mg of total PAHs were removed with HPCD, while the PAHs removal was less than 10 mg with cosolvent and surfactants. The reason for this may be the sorption of PAHs and flushing solutions to the organic fraction of the sediment.

Moisture Content and pH

The initial moisture content of the sediment was 78 %. Figure 6(*a*) shows the variation of moisture content with normalized distance from the anode after the completion of electrokinetic treatment. The normalized distance is defined as the distance to the specific location from the anode divided by the total distance from the anode to the cathode. In general, moisture content decreased throughout the sediment in all the tests except near the anode in 5 % Igepal test. These changes in moisture contents may be attributed to the variations in the electro-osmotic flow that occurred as a result of the physicochemical changes occurring within the sediment due to increased ionic strength, conductivity, and/or electrical gradient. These results suggest that the electro-osmotic flow may not be uniform and there may be changes in pore pressures (Eykholt 1997). Nevertheless, it appears that the sediment moisture content remained higher than 50 % in all the tests. It is possible that regions where the electro-osmotic flow was high created a pressure gradient so that the solution was pulled from regions where the electro-osmotic flow was lower. Since the solution was continuously transported throughout sediment, the moisture content did not substantially decrease.

The electrolysis of water results in the formation of H^+ ions (low pH solution) at the anode and OH^- ions (high pH solution) at the cathode, and, primarily due to electromigration, these ions tend to migrate toward the oppositely charged electrode(s). However, because of high acid buffering capacity of the sediment, the H^+ ions are neutralized and the H^+ ions are not migrated through the sediment. However, OH^- ions migrate through the sediment toward the anode. Figure 6(*b*) shows the variation of sediment pH versus normalized distance from the anode for all the tests. The initial pH of the sediment was 7.0. Figure 6(*b*) showed a slight decrease in the sediment pH in the first section near the anode in the systems flushed with surfactants and HPCD. This may be due to slow migration of acidic front into sediment due to the high acid buffering capacity of the sediment. The sediment pH of the second section ranges from 6.2 to 7.0 and remains approximately the same as initial pH of 7.0. The third section, which is closest to the cathode, variation in sediment pH was slightly pronounced. For surfactants flushed tests maximum sediment pH was found to be 8.8 and 7.2 for 3 % Tween 80 and 5 % Igepal CA-720 system, respectively. However, in the HPCD flushed system, the sediment pH remains a slightly low value of 6.8. A uniform higher sediment

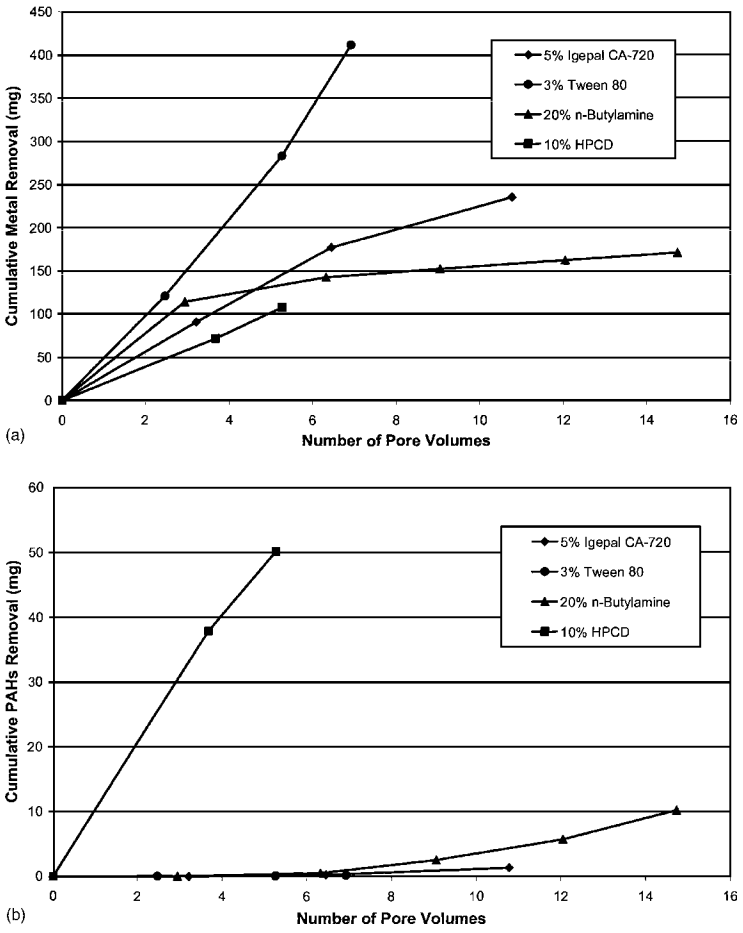

FIG. 5—*(a) Measured total metal removal during electric potential application. (b) Measured total PAHs removal during electric potential application.*

pH (ranging from 11.5 to 11.9) was recorded for all three sections of the sediment that was flushed with 20 % *n*-butylamine cosolvent solution. The high pH in the cosolvent test was due to very alkaline nature (pH greater than 12) of the cosolvent solution.

Residual Contaminant Distribution

After the completion of testing, the sediment samples were sectioned into three equal parts: S-1 (near anode), S-2 (middle), and S-3 (near cathode). The contaminant concentrations determined for each of these sections are plotted together in order to elucidate the migration behavior of the contaminants. Figures 7(*a*) and 7(*b*) show residual distribution of total metals, and PAHs concentrations, respectively, in the sediment treated with 5 % Igepal CA-720. As seen from Fig. 7(*a*), all the metals are found to be evenly distributed throughout the sediment. But sodium concentration was found to be higher at anode, i.e., section S1 while thalium was in excess at cathode section S3. This may be due to their respective migrations toward electrode or heterogeneous distribution of the contaminants in the sediment. These results also indicate because of high pH, toxic metals existed in unfavorable forms (sorbed/precipitated) that do not allow removal by the surfactant flushing. Figure 8(*b*) shows that Igepal CA-720 has potential to remove a wide

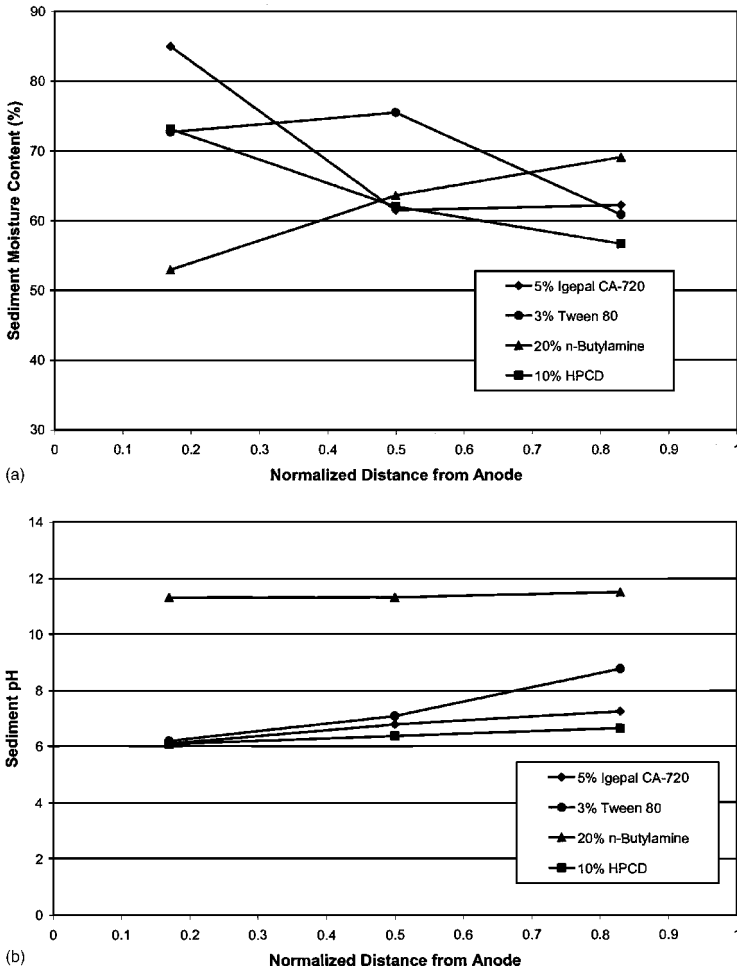

FIG. 6—*(a) Sediment moisture content distribution after testing. (b) Sediment pH distribution after testing.*

array of PAHs from the sediments. The results show that the concentration of all the PAHs in the sediment was appreciably low near anode (i.e., Section S-1), indicating the migration of PAHs from anode toward cathode. These results also confirm that hydrophobic character of the PAHs increases with the number of rings, as the concentration of higher ringed PAHs was found to be considerably high in S-1 section, indicating that these PAHs were strongly attached to the sediments.

Figures 8(*a*), 9(*a*), and 10(*a*) show the residual metal concentrations in different sections for tests conducted with 3 % Tween 80, 20 % *n*-Butylamine, and 10 % HPCD, respectively. Based on these results, it can be observed that there are no significant changes in the metal concentrations of different sections. This implies that the metals are not migrated toward the electrodes under the influence of flushing solutions used. This indicates that flushing solutions used were not effective for desorption and/or dissolution of metals in the sediment. This may be due to a significant amount of organic matter that strongly adsorbed metals. In addition, the high pH of the sediment may have caused some metals to precipitate. Thus, strong adsorption and precipitation of metals resulted into low migration and low removal of metals in all experiments.

The residual concentrations of PAHs in different sections are shown in Figs. 8(*b*), 9(*b*), and 10(*b*), for

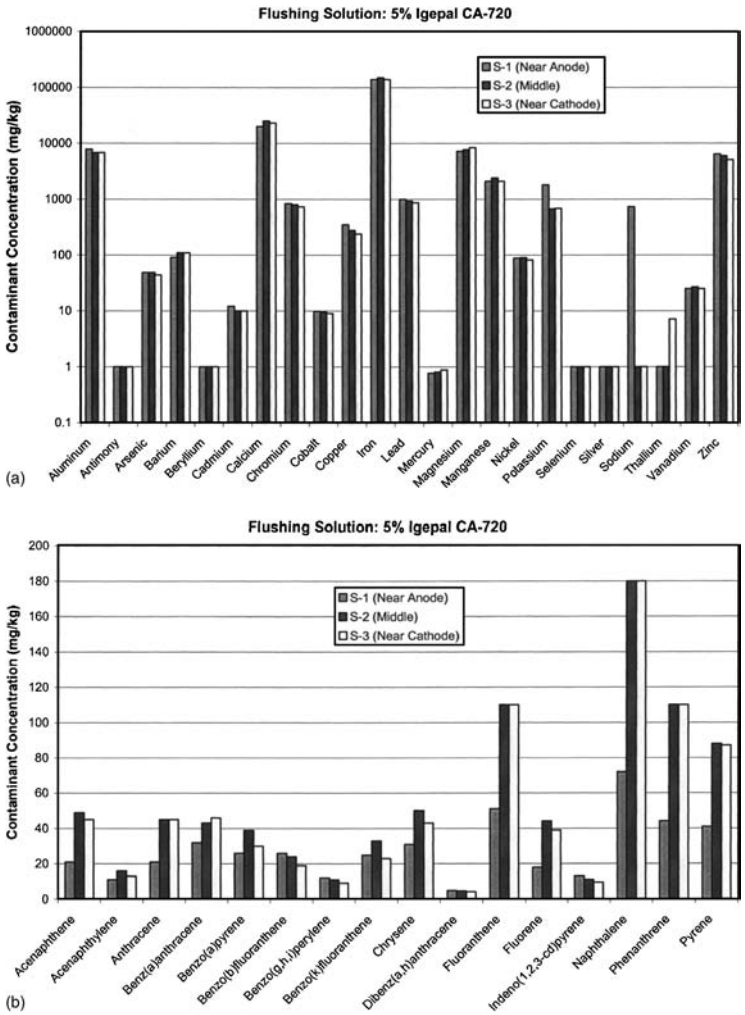

FIG. 7—*(a) Metal concentrations in sediment sections from anode to cathode in 5 % Igepal CA-720 test. (b) PAHs concentrations in sediment sections from anode to cathode in 5 % Igepal CA-720 test.*

the tests conducted with Tween 80, *n*-butylamine, and HPCD, respectively. Figure 8(*b*) shows low concentration of PAHs at anode indicating the migration of PAHs from anode to cathode. Further the concentration of all the PAHs was found to be higher in the middle section (S-2). This reflects that the flushing solution Tween 80 partially solubilized PAHs and caused migration toward the cathode. Similarly, Fig. 9(*b*) shows that PAHs were partially solubilized by 20 % *n*-butylamine and migrated toward the cathode. Figure 10(*b*) shows low solubilization of PAHs and there is no evidence of significant migration of PAHs toward the cathode. However, it should be noted that PAHs were removed in the effluent in HPCD flushing test [Fig. 5(*b*)]. This indicates that the HPCD may have formed inclusion complexes with some of the PAHs initially and these complexes were removed by the electro-osmotic flow. The reduced electro-osmotic flow at later stages in this test may have prevented PAHs removal from the sediment.

In general, the concentration of PAHs increases from Section S-1 to Section S-3 in all the studied systems. This shows that PAHs partially solubilized and migrated toward the cathode. The cosolvent, i.e.,

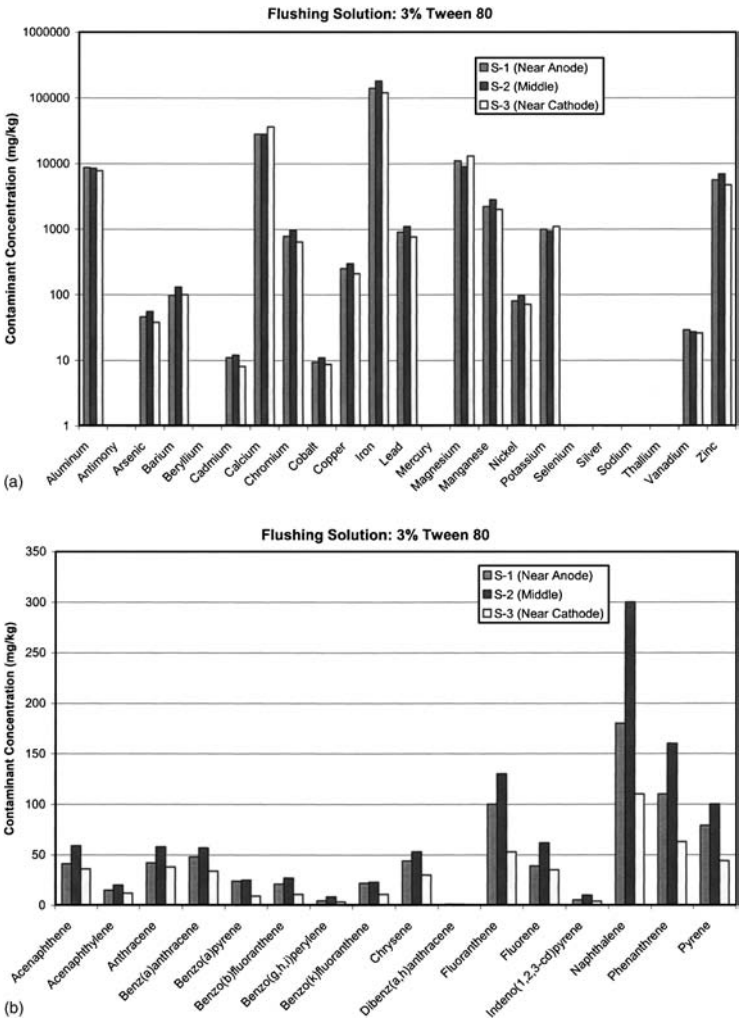

FIG. 8—*(a) Metal concentrations in sediment sections from anode to cathode in 3 % Tween 80 test. (b) PAHs concentrations in sediment sections from anode to cathode in 3 % Tween 80 test.*

20 % *n*-butylamine had contributed to the solubilization/desorption of the PAHs from the sediment resulting in their migration toward the cathode. The variation in the concentrations of PAHs in the three sections may also be contributed to heterogeneous distribution of the contaminants in the sediment. Among the surfactants used 5 % Igepal CA-720 was found to be more effective for the solubilization of the PAHs indicating formation of stable micelles. It is important to mention here that below the critical micelle concentration (CMC), surfactants exist solely as monomers and have minimal effect on the solubility of most contaminants of interest. Above the CMC, the surfactant monomers aggregate to form micelles. Micelles in aqueous systems have a hydrophilic exterior and a hydrophobic interior, with the latter acting as a phase to which low polarity contaminants can partition. This partitioning produces an increase in apparent solubility, thereby increasing the dissolution and desorption of the contaminants. In Tween 80 system, mobilization of contaminants due to the reduction in interfacial tensions seems to be the dominant mechanism. The HPCD system showed poor affinity for the solubilization of the contaminants from the

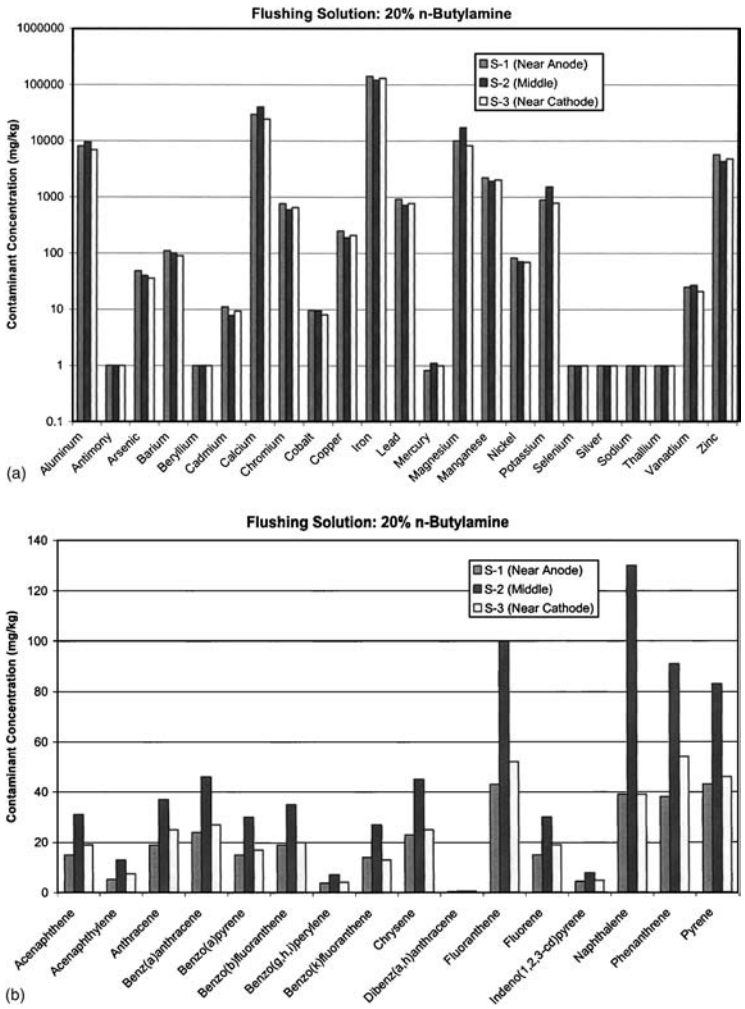

FIG. 9—*(a) Metal concentrations in sediment sections from anode to cathode in 20 % n-butylamine test. (b) PAHs concentrations in sediment sections from anode to cathode in 20 % n-butylamine test.*

sediments. Generally, cyclodextrins form inclusion complexes with the low polarity contaminants that fit in their relatively nonpolar cavity. But in this study it appears that the inclusion complexes formed during the treatment process may have adsorbed to the minerals and organic contents of the sediments that resulted in the reduced removal efficiency of the tested system. Metals are readily precipitated under the tested conditions and PAHs were not efficiently solubilized by the flushing solutions under the experimental conditions. Although substantial electro-osmotic flow can be induced in the sediment using different flushing solutions, the removal of contaminants is difficult to achieve. Since the contaminants are not easily desorbed or solubilized, the risk posed by the contaminants to the environment and public may be minimal and should be assessed based on the site-specific conditions.

Conclusions

The sediment obtained from Indiana Harbor, Indiana, was found contaminated with heavy metals and PAHs. Under the applied electric potential, substantial electro-osmotic flow was induced in the sediment.

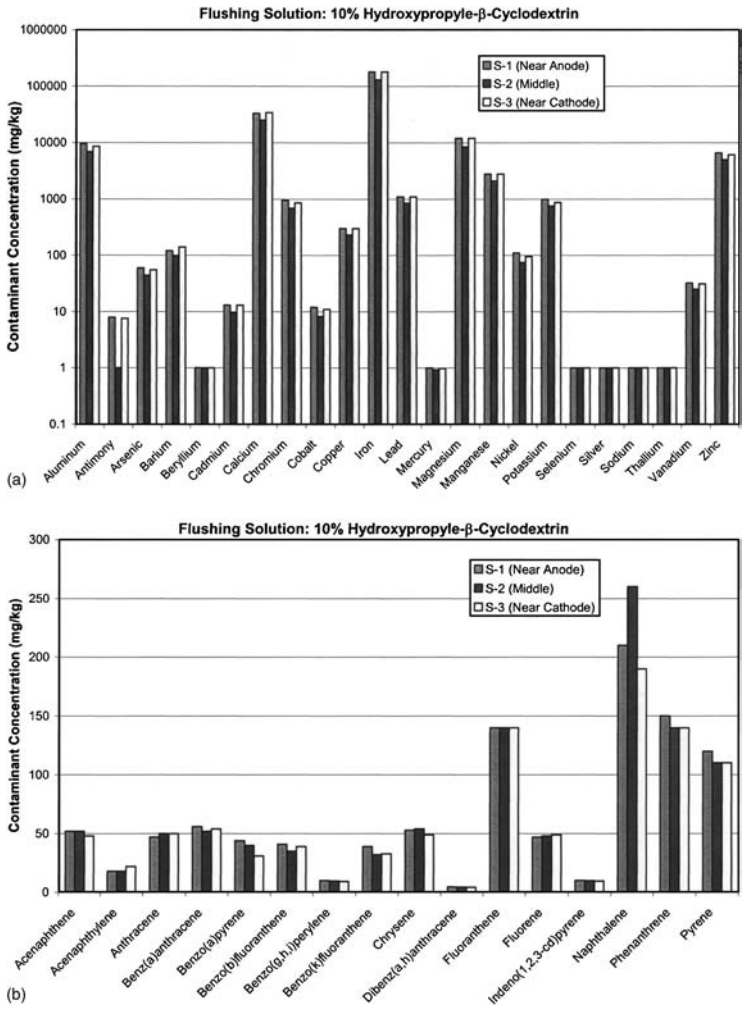

FIG. 10—*(a) Metal concentrations in sediment sections from anode to cathode in 10 % HPCD test. (b) PAHs concentrations in sediment sections from anode to cathode in 10 % HPCD test.*

The sediment pH increased significantly and remained the same throughout the sediment sections for the cosolvent systems. However, the surfactant and HPCD systems did not induce substantial change in the sediment pH.

Heavy metals remained strongly adsorbed/precipitated due to high sediment pH conditions before and after the treatment. Only a small extent of metal transport and removal was observed in the Tween 80 system, but in all other tested systems the metal transport was negligible. Overall, the removal of heavy metals from the sediment for all flushing solutions used in this study was insignificant.

The removal of PAHs from the sediments depends upon the type of flushing solution. PAHs were partially solubilized by the flushing solutions and then they migrated from anode toward the cathode. However, PAHs remained strongly adsorbed to the sediment. Among the flushing agents used 5 % Igepal CA-720 and 20 % *n*-butylamine systems were found to be more effective than Tween 80 and HPCD in partial solubilization/desorption of the PAHs. The PAHs may be strongly sorbed to the organic content in the sediment, leading to low removal efficiency.

Acknowledgments

The financial support for this project was received from the State of Illinois (Technology Challenge Grant) and STAT Analysis Corporation, and this support is grafully acknowledged. The authors are thankful to Saurabh Sharma, Kranti Maturi, Surendra Kumar, and Craig Chawla for their assistance in this project.

References

ASTM Standard D2216, Soil and Rock, *Annual Book of ASTM Standards*, Vol. 04.08, American Society of Testing and Materials, Philadelphia, PA, 2003.

Dzenitis, J. M., "Steady State and Limiting Current in Electroremediation of Soil," *J. Electrochem. Soc.* 144, 1317–1322 (1997).

Eykholt, G. R., "Development of Pore Pressures by Nonuniform Electroosmosis in Clays," *J. Hazard. Mater.* 55, 171–186 (1997).

Maturi, K., "Electrokinetic Remediation of Soils Contaminated with Co-existing PAHs and Heavy Metals," M.S. Thesis, University of Illinois at Chicago, 2004.

Mitchell, J. K., *Fundamentals of Soil Behavior*, John Wiely and Sons, Inc., New York, NY, p. 437, 1993.

Mulligan, C. N., Yong, R. N., and Gibbs, B. F., "An Evaluation of Technologies for the Heavy Metal Remediation of Dredged Sediments" *J. Hazard. Mater.* 25, 145–163 (2001).

Nobbs, D. and Chipman, G., "Contaminated Site Investigation and Remediation of Chlorinated Aromatic Compounds," *Sep. Purif. Technol.* 31, 37–40 (2003).

Reddy, K. R. and Parupudi, U. S., "Removal of Chromium, Nickel, and Cadmium from Clays by In-Situ Electrokinetic Remediation," *J. Soil Contaminat* 6, 391–407 (1997).

USEPA, "Test Methods for Evaluating Solid Waste," *Volume 1A: Laboratory Manual, Physical/Chemical Methods, SW-846*, 3rd Ed., Office of Solid Waste and Emergency Response, Washington, D.C.

USEPA, "Realizing Remediation: A Summary of Contaminated Sediment Remediation Activities in the Great Lakes Basin," Great Lakes National Program Office, Chicago, 1998.

USEPA, "Guide to Great Lakes Program Office Assessment and Remediation of Contaminated Sediments (ARCS) Program." http://www.epa.gov/glnpo/arcs/arcshome.html, 2001

Journal of ASTM International, Vol. 3, No. 6
Paper ID JAI13305
Available online at www.astm.org

Ha Ik Chung[1] *and Masashi Kamon*[2]

Electrokinetic Dewatering and Sedimentation of Dredged Contaminated Sediment

ABSTRACT: This research focuses on electrokinetic dewatering and settling of contaminated sediment. A series of laboratory experiments with different magnitudes of applied voltage is performed with artificially made contaminated sediment mixed with contaminant. Investigated parameters in experiments are settlements of the slurry specimen, volumes of water extracted from the slurry specimen, and the changes in fluid content of the specimen. The results show that the sedimentation rate and velocity are varied and controlled by the applied voltage. From the test results, a significant investigation is derived for the mechanisms associated with dewatering and sedimentation of contaminated sediment. A coupled effect of electrokinetic dewatering and settling processes is investigated.

KEYWORDS: electrokinetics, electroosmosis, electrophoresis, slurry, waste, settlement

Introduction

There are many engineering applications that demand dewatering and settling acceleration, volume reduction, and contaminant extraction of contaminated fine solid suspensions and sediments existing in river and seashore environments. These suspensions and sediments contain significant clay, colloidal fraction, and contaminants. This small sized clay and fraction can result in very high water content and void ratio, and very soft strata. Its potential hazards exist in subsurface environments. It is important to improve the reduction of thickness as well as the extraction pore water and contaminant because settling acceleration of dredged soil decreases the scale of industrial process and volume reduction, and the extraction of contaminant from dredged soil decreases environmental challenges to disposal sites and treatment processes.

Direct electric current induces the movement of fine solid particles suspended in water and the transport of water molecules in soil. Upon formation of a soil structure, the current further induces the movement of water and contaminant in the soil skeleton. These phenomena are known as electrokinetics (Acar at el. 1993; Lockhart 1993). This study investigates the viability of using the technique of electrokinetic dewatering to dredge sediments for settling acceleration and volume reduction, and analyzes the efficiency of using the technique of electrokinetic migration of contaminants during dewatering from contaminated dredged soil (Shang 1997; Chung and Kamon 2000; Chung 2001). Simulated dredged sediments on the bottom of the river and seashore were used for the laboratory test specimen. Laboratory electrokinetic dewatering and settling tests were carried out. The height and volume of specimens, the quantity and concentration of dewatered outflow, and current density were measured during electrokinetic tests. Aspects such as dewatering rate, sedimentation velocity, volume reduction of soil specimen, and water content are also discussed. The solid particles in sediments were moved to the anode part by electrophoresis, and the water in sediments was moved to the cathode part by electrosomosis. From the test results, a significant investigation is derived for the mechanisms associated with dewatering and settling on dredged contaminated sediments.

Manuscript received April 19, 2005; accepted for publication July 12, 2005. Presented at ASTM Symposium on Contaminated Sediments: Evaluation and Remediation Techniques on 23–25 May 2006 in Shizuoka, Japan; M. Fukue, K. Kita, M. Ohtsubo, and R. Chaney, Guest Editors.

[1] Research Fellow,Geotechnical Engineering Department, Korea Institute of Construction Technology 2311 Daehwa-dong, Ilsan-gu, Goyang-shi, Gyeonggi-do, 411-712, Korea, e-mail: hichung@kict.re.kr
[2] Professor,Graduate School of Global Environmental Studies, Kyoto University Yoshida-Honmachi Sakyo-ku 606-8501, Japan, e-mail: kamon@geotech.gee.kyoto-u.ac.jp

TABLE 1—*The physical and chemical properties of Korean Daemyung Kaolin.*

Items	Values
Type	Korean Daemyung Kaolin
Visual appearance	White color (%)
Clay fraction	42.6
SiO_2	48.35
Al_2O_3	30.88
Fe_2O_3	0.97
CaO	11.13
K_2O	0.42
Na_2O	2.70
Loss on ignition	5.14

Experiments

Materials

Korean Daemyung Kaolin spiked with organic substance was used to simulate contaminated waste slurry. Kaolin ensured homogeneity of the specimens and consistency between tests. Table 1 contains the physical and chemical properties of he Kaolin used in this experiment. The percent of clay fraction finer than 2 μ is 42.63 %. The organic matter content is 5.14 %. The mineralogical composition is as follows: SiO2, 48.35 %, Al2O3, 30.1 %, Fe2O3, 0.97 %, etc. The study waste slurry is artificially contaminated with organic substance, ethylene glycol (C2H6O2). Ethylene glycol is a colorless and odorless liquid completely miscible with water and many organic liquids.

Testing Programs

A schematic diagram and photograph of the electrokinetic sedimentation and dewatering system is shown in Fig. 1. This system consisted mainly of an electrokinetic cell, power supply, and electrodes. The electrokinetic cell was a cylindrical tube 200 mm in length and 100 mm in diameter. A stainless steel electrode was used to prevent production of corrosion.

Testing Procedure

The electrokinetic settling and dewatering experiments were conducted in electrokinetic cells. To prepare a sample, predetermined quantities of dry soil and organic solution were blended to slurry of gravimetric solid content of 28 % and organic solution of 78 %. The organic solution was a mixture of 80 % distilled water and 20 % ethylene glycol. The mixture was poured into an electrokinetic cell. The initial fluid content of the mixture was about 250 %. The cell was assembled to the electrokinetic test system. One stainless steel electrode was placed at the bottom of the cell and the other at the top of the sample, consisting of a parallel plate arrangement. The top electrode was removable for the convenience of sample preparation.

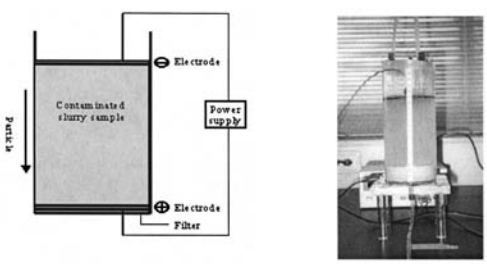

FIG. 1—*A schematic diagram and photograph of the electrokinetic testing system.*

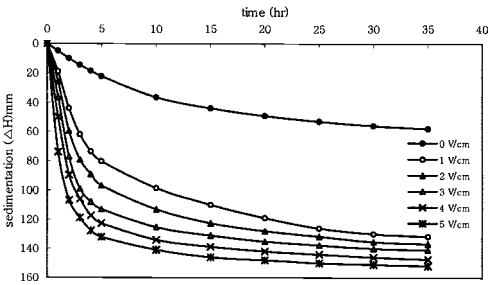

FIG. 2—*Sedimentation height with time.*

The tests were conducted in electrokinetic sedimentation condition. A regulated constant voltage was applied on the testing sample, directed upward, top cathode (–) and bottom anode (+). In this case, negatively charged clay particles will be attracted toward the bottom resulting in accelerated sedimentation. The phenomenon is known as electrophoresis (Shang 1996).

The time-dependant settlement due to electrophoresis was measured on an hourly basis. The settlement with time was recorded through reading the mudline from the scales installed on the cells. After an electrokinetic test, the cell was disassembled from the electrokinetic system and the soil specimen was extruded and sliced into three parts as upper, middle, and lower. The value of pH and the fluid content were measured in each slice to assess the change of chemical and physical properties in the slurry specimen.

Results and Discussion

Sedimentation Rate

Figure 2 shows the results of sedimentation of contaminated waste slurries versus time. Settlement was increased with time elapsed in all cases. The sedimentation heights in the cases of 0, 1, 2, 3, 4, and 5 V/cm were about 58, 132, 137, 141, 147, and 152 cm respectively. Applied voltage denotes the upward electric gradient for electrophoretic sedimentation using top cathode (-) and bottom anode (+). Clay particles are negatively charged, so the movement of clay particles is developed downward due to electrophoresis. The electrophoretic sedimentation was developed in a first short time, and then sedimentation was constant. Figure 3 represents the time to reach 50 and 100 % maximum sedimentation. The time to reach 50 % maximum sedimentation was 12, 9, 7, 6, and 5 h and the time to reach 100 % maximum sedimentation was 25, 19, 15, 12, and 11 h with the applied voltage of 1, 2, 3, 4, and 5 V/cm, respectively. The time to reach maximum sedimentation is short in the case of higher applied voltage compared with lower applied voltage.

The settlement rate in Fig. 4 is presented as $\Delta H/H$, the amount of sedimentation divided by the initial sample height. The initial sample height was $H=200$ mm. At the end of the test, the final heights of the

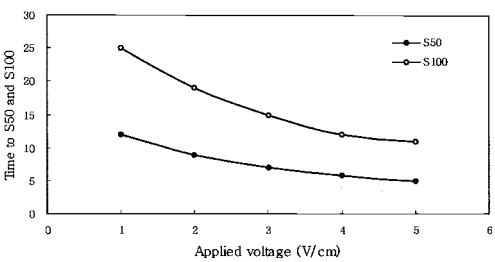

FIG. 3—*Time to reach 50 and 100 % of maximum sedimentation.*

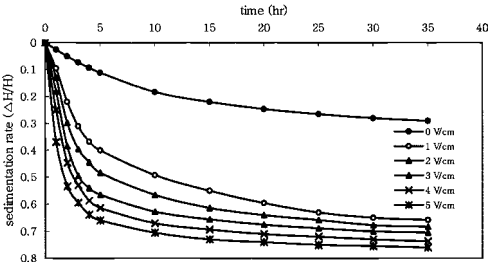

FIG. 4—*Sedimentation rate with time.*

samples were about 142, 68, 63, 59, 53, and 48 mm corresponding to 0.29, 0.66, 0.68, 0.71, 0.74, and $0.76\Delta H/H$ in the case of 0, 1, 2, 3, 4, and 5 V/cm respectively. The settlement rate is increased with time elapsed and constant after about 20 h. After this time, the electrokinetic and gravitational sedimentation was completed. The settlement rate is high and rapid in the case of higher applied voltage compare with lower applied voltage. The volume reduction of waste slurries achieved was 29, 66, 68, 71, 74, and 76 % in the test conditions of 0, 1, 2, 3, 4, and 5 V/cm by electrokinetic processing.

Sedimentation Velocity

The variation of sedimentation velocity with time and applied voltage can be observed in Fig. 5. As seen, the sedimentation velocity increased within the first short time. The sedimentation velocity was clearly increased in the first stage; on the other hand, the sedimentation velocity was decreased in the later stage and reached nearly zero after 25, 19, 15, 12, and 11 h with the applied voltage 1, 2, 3, 4, and 5 V/cm, respectively. The reason for rapid sedimentation of the specimen in a short time after voltage applied is that the clay fraction of the specimen is lower and electrical power is applied to the specimen. Sedimentation was attributed to both gravitational and electrophoretic effects. As the electrokinetic sedimentation proceeds, the sedimentation velocity is gradually decreased.

Quantity of Dewatering

In the first stage, the negatively charged solid particles are moved to the anode part by electrophoresis, and the water is moved to the cathode part by electroosmosis. In the second stage, the water is moved to the cathode part by electroosmosis. Thus, the solid particles are moved downward and the water is moved upward. At the same time, the contaminants in the pore water and on the solid particles are moved upward with water in first stage. On the other hand, the water and the contaminants downward in the second stage.

Figure 6 shows the volume of dewatering from the sample. In this figure, we note that the volume of dewatering is increased with time elapsed and constant after 25, 19, 15, 12, and 11 h with applied voltage 1, 2, 3, 4, and 5 V/cm. The final volume of dewatering was reached at 4553, 10 338, 10 731, 11 069, 11 571, and 11 932 ml in the case of 0, 1, 2, 3, 4, and 5 V/cm applied voltage density. The contaminant that

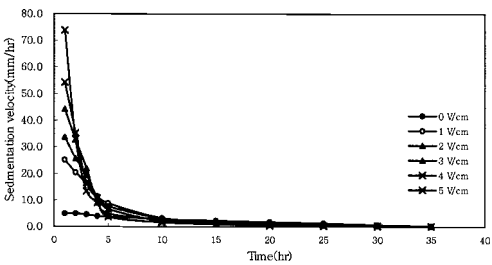

FIG. 5—*Sedimentation velocity with time.*

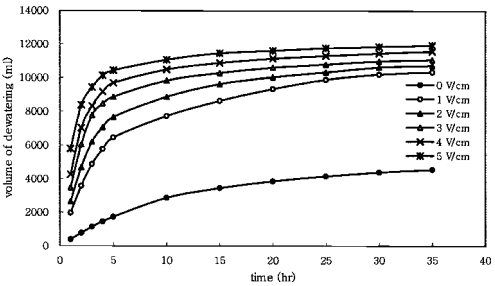

FIG. 6—*Volume of dewatering with time.*

existed in water of the soil pore was removed by extraction of pore water. The water that accumulated at the top can be evaporated by solar radiation and drained by a hydraulic or pumping system in the field application.

Fluid Content Changes

At the end of the electrokinetic experiments, the soil fluid contents in the three sliced samples were measured, as shown in Fig. 7. The initial fluid content was 250 % and final fluid content was about 150, 70, 65, 55, 51, and 48 % with applied voltage of 0, 1, 2, 3, 4, and 5 V/cm respectively. Thus the final fluid content was decreased 100, 180, 185, 195, 199, and 202 %, respectively, compared with the initial fluid content. The reason is that the water and organic substance are moved out of the specimen by electroosmosis.

Conclusions

Electrokinetic settling and dewatering to simulate the rapid volume reduction and water extraction on contaminated slurry-type wastes with high water and void were investigated in an experimental study. From the results of the experiments, the following conclusions were reached:

1. The effectiveness of electrokinetic settling and dewatering technology for stabilization of contaminated waste slurries can be evaluated. Effects on settlement, reduction of volume and fluid content, extraction of porewater, and contaminant were achieved.
2. The rate of sedimentation and volume reduction calculated from sample heights measured before and after electrokinetic tests were about 29, 66, 68, 71, 74, and 76 %, respectively, in applied voltage of 0, 1, 2, 3, 4, and 5 V/cm.
3. The sedimentation velocity was increased in the first stage and decreased in the later stage. The

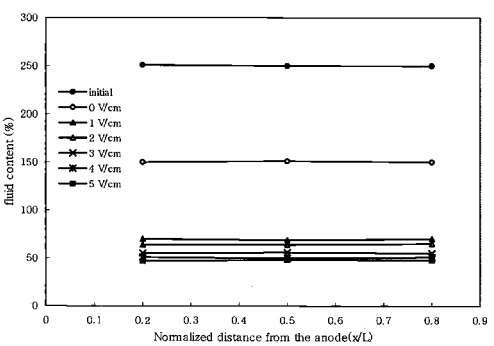

FIG. 7—*Fluid content distribution in specimen.*

solid particles were moved to the anode part by electrophoresis, and the water was moved to the cathode part by electroosmosis.

References

Acar, Y. B. and Alshawabkeh, A. N., "Principles of Electrokinetic Remediation," *Environ. Sci. Technol.*, 27,(13), pp. 2638–2647 (1993).

Chung, H. I. and Kamon, Masashi, "Electrokinetic Sedimentation and Remediation of Contaminated Slurry Wastes," *5th International Symposium on Environmental Geotechnology and Global Sustainable Development*, Brazil, 2000, Vol. **9**, pp. 70–77.

Chung, H. I., "Enhancement of Sedimentation and Remediation of Contaminated Sediments by Electrokinetics," *The Proceedings of the 1st Korea-Japan Joint Seminar on Geoenvironmental Engineering*, Korea, 2001, Vol. **4**, pp. 71–77.

Chung, H. I. and Kamon, M., "Sedimentation and Remediation of Contaminated Waste Slurries by Electrokinetics," *Creation of New Geo-Environment, Fourth Kansai International Geotechnical Forum*, Japan, 2000, Vol. **5**, pp. 217–220.

Lockhart, N. C., "Electroosmotic Dewatering of Clays: Influence of Voltage," *Colloids Surf., A* 6, 229–238 (1993).

Shang, J. Q., "Electrokinetic Dewatering of Clay Slurries as Engineered Soil Covers," *Can. Geotech. J.*, 34, 78–86 (1997).

Journal of ASTM International, Vol. 3, No. 6
Paper ID JAI13307
Available online at www.astm.org

Ha Ik Chung,[1] *Gilliance C. Sills,*[2] *and Masashi Kamon*[3]

Electrokinetically Enhanced Settlement and Remediation of Contaminated Sediment

ABSTRACT: Electrokinetic technique has been used in sedimentation at mining applications as a volume reduction for slurry tailing wastes. This technique has been used in remediation for environmental application as a potential in-situ remediation method for contaminated soils and wastes. Thus electrokinetic technique can be used in sedimentation and remediation of sediments. A regulated constant voltage was applied on the testing sample, directed upward, top cathode (−) and bottom anode (+) during electrokinetic sedimentation process. On the other hand, constant voltage was applied on the testing sample, directed downward, top anode (+) and bottom cathode (−) during electrokinetic remediation process. This means that the polarity reversal was employed. The time dependent settlement and concentration due to electrophoresis and electro-osmosis was measured on an hourly basis. The sedimentation rate of specimen and removal rate of contaminant in contaminated sediment were increased with increasing of applied voltages.

KEYWORDS: electrokinetic, sedimentation, remediation, contaminant, sediment

Introduction

The quantity of sediments such as river and seashore sediments is increasing significantly by the growth in industrialization and population all over the world. If these sediments are to be contained in impoundment and landfill, they are usually placed hydraulically as slurry by open dumping. Design problems associated with these impoundments and landfills include storage capacity, densification of filling materials, embankment stability, migration of contaminated pore fluid, and final land use. These sediments contain significant clay, colloidal fraction, and contaminants. This small-sized fraction can result in soft strata with high initial void, and its potential hazards in subsurface environments are existing. In these cases, it is needed to sediment the slurry-type waste for volume reduction and to remediate the contaminated waste for pollutant extraction.

Electrokinetic technique has been used in sedimentation at mining applications as a volume reduction for slurry tailing wastes. This technique has been used in remediation for environmental application as a potential in situ remediation method for contaminated soils and wastes (Acar et al. 1989; Yakawa et al. 1976). Thus electrokinetic technique can be used in sedimentation and remediation of sediments (Been and Sills 1980; Chung and Kamon 2000; Chung 2001; Shang 1997). Electrokinetic technique was developed for improvement of soft soil using electro-osmotic consolidation and dewatering mechanism, and recently this technique was extended for remediation of contaminated soil using electro-osmosis and electromigration mechanism. In this research, the coupled effects of sedimentation and remediation of contaminated sediments are focused on using electrokinetic sedimentation and remediation techniques. Electrokinetic sedimentation and remediation is discussed from experimental aspects.

The contaminated sediments in rivers, lakes, and harbors contain significant clay, colloidal fraction, and contaminants. This small-sized fraction can result in soft strata with high initial void and high water content, and its potential hazards in subsurface environments are existing. In these cases, it is needed to

Manuscript received April 19, 2005; accepted for publication September 13, 2005. Presented at ASTM Symposium on Contaminated Sediments: Evaluation and Remediation Techniques on 23–25 May 2006 in Shizuoka, Japan; M. Fukue, K. Kita, M. Ohtsubo, and R. Chaney, Guest Editors.

[1] Research Fellow, Geotechnical Engineering Department, Korea Institute of Construction Technology, 2311 Daehwa-dong, Ilsan-gu, Goyang-shi, Gyeonggi-do, 411-712, Korea, e-mail: hichung@kict.re.kr
[2] Professor, Department of Engineering Science, Oxford University, Parks Road Oxford OX1 3PJ United Kingdom, e-mail: gilliane.sills@eng.ox.ac.uk
[3] Professor,Graduate School of Global Environmental Studies, Kyoto University, Yoshida-Honmachi Sakyo-ku 606-8501, Japan, e-mail: kamon@geotech.gee.kyoto-u.ac.jp

FIG. 1—*Photograph of river basin sampled natural sediment.*

settle the slurry-type waste for volume reduction and to remediate the contaminated waste for pollutant extraction. A series of laboratory experiments including two cases of applied voltage are performed with the contaminated sediment specimens dredged at the river basin. The electrokinetic experimental apparatus consisted of electrokinetic sedimentation and remediation units with direct current power supply. Investigated parameters in experiments are volumes of water extracted from and through the specimen, the variation of electric current, and the changes of concentration level in the specimen. From the test results, the variation of settlement and concentration of contaminated sediments in which simultaneous sedimentation and remediation processes are involved by electrokinetics is investigated with different solid content, applied voltage, and concentration level. The coupled effects of slurry soil densification and contaminant transport are analyzed.

Experiments

Materials

The materials used in this experiment were contaminated natural sediment and artificial sediment. Two types of sediments such as natural and artificial sediments were used as test samples in this study. In the case of natural sediment, which was sampled in the river basin, various types of contaminants originally existed in the sediment section. In the case of artificial sediment, ethylene glycol was artificially mixed with water, and the mixtures were blended with Kaolin, so ethylene glycol existed in the sediment section. The contaminated sediment sampled at the river basin in Korea as shown in Fig. 1 was used to simulate contaminated natural sediment. The Kaolin called Speswhite fine china clay, produced in the United Kingdom admixed with organic substance (ethylene glycol, $C_2H_6O_2$) was used to simulate contaminated artificial sediment. Commercial Kaolin ensured homogeneity of the specimens and consistency between tests. The index properties of Speswhite Kaolin are specific gravity 2.61, liquid limit 62–69 %, plastic limit 32–38 %, and the percent finer than 2μ is 82 %. The organic matter content is 13.14 %. The mineralogical composition is as follows: SiO_2 46.2 %, Al_2O_3 38.7 %, Fe_2O_3 0.56 %, etc.

Ethylene glycol is a colorless, odorless liquid completely miscible with water and many organic liquids. The ethylene glycol cannot represent a real field contamination in dredged sediments. The simulation of contaminated sediment that has pollutants was required in this test. A chemical agent that is completely miscible with water and is non-hazard for safe handling of the specimen during the test was needed. The ethylene glycol was one of the proper chemical agents in organic substances for this, so ethylene glycol was selected as a contaminant in this test. In the case of natural sediment, which was sampled in river basin, various types of contaminants originally existed in the sediment section. In the case of artificial sediment, ethylene glycol was artificially mixed with water, and the mixtures were blended with Kaolin, so ethylene glycol existed in the sediment section.

Testing Program

In this study, 13 tests were conducted by using one-dimensional electrokinetic test apparatus for sedimentation and remediation of contaminated waste slurries. Two tests using natural sediment with variation of

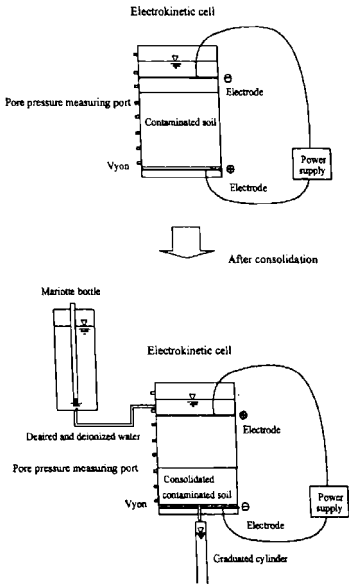

FIG. 2—*A schematic diagram of the electrokinetic testing system.*

applied voltage (1 V/cm, 3 V/cm) and eleven tests using artificial sediment with variation of initial solid content concentration level, and applied voltage were conducted. Eleven tests can be divided into three groups: (1) tests EK1-EK4 for the effect of initial solid content (15, 25, 40, and 50 %, respectively) conducted under the same electric field intensity of 3 V/cm and the same concentration level of 25 % of ethylene glycol; (2) tests EK2 and EK5-EK8 for the effect of concentration level in specimen (25, 0, 50, 75, and 100 %, respectively) conducted under the same applied electric field intensity of 3 V/cm and the same initial solid content of 25 % mass/mass; (3) tests EK2, EK9, EK10, and GR for the effect of applied electric field intensity (30, 10, 20, and 0, respectively) conducted under the same initial solid content of 25 % mass/mass and the same of concentration level of 25 % of ethylene glycol.

Test GR was the control test by gravitational sedimentation not applied electric field intensity. The solid contents chosen are 15, 25, 40, and 50 %, and these solid contents are the same as 560, 300, 150, and 100 % of water content, respectively. Normally, the water content of sediment dredged from river and seashore has a range of 100–500 %. Thus, the chosen solid content and water content were reasonable to simulate the condition of real field sediment.

Constant voltage conditions were used in all tests. Investigated were the changes of settlement, the volume of dewatering and outflow, the electric current, and contaminant transport with the variation of each parameter.

Testing Methods

A schematic diagram of the electrokinetic sedimentation and remediation system is shown in Fig. 2. The aim of this study is to enhance and accelerate the volume reduction and dewatering of the slurry-type sediment and removal of contaminant from contaminated sediment after volume reduction. If electrokinetic remediation with the water supply was implemented from the start of the experiment, the settlement effect of the specimen due to a continuous supply of water and a constant water content of the sample was not occurring and only the migration of the contaminant was occurring, so only remediation effect was occurring at the whole test time and volume reduction effect was not occurring. This result deviates from the original aim of this paper. Thus electrokinetic sedimentation was implemented at the first stage and

electrokinetic remediation was implemented at the second stage. The water accumulated at the top of the soil after electrokinetic sedimentation can be evaporated by solar radiation and drained by hydraulic gradient or a pumping system in a typical field application.

The contaminant transported back and forth due to the difference of water movement direction and polarity reversal during electrokinetic sedimentation and remediation stages. In this study, a downward water outlet system toward the bottom of the cell was selected in electrokinetic remediation stage for getting an electro-osmosis effect coupled with a gravitation effect to increase water and contaminant movements. On the other, if an upward outlet system toward the top of the cell was selected in the electrokinetic remediation stage, a gravitation effect could not couple to the electro-osmosis effect, so water and contaminant movements would be decreased some compared to the downward system.

The selected system mainly consisted of electrokinetic cell and power supply. The electrokinetic cell was a cylindrical tube with 100 mm in length and 100 mm in diameter. To prepare a test sample for simulation of natural sediment, predetermined quantities of natural sediment were stirred and poured in an electrokinetic cell. To prepare a test sample for simulation of artificial sediment, dry soil and organic solution were blended and poured in an electrokinetic cell. Organic solution was a mixture of deionized distilled water and ethylene glycol. The cell was assembled to the electrokinetic test system. One stainless steel electrode was placed at the bottom of the cell and the other at the top of the sample, consisting of a parallel plate arrangement. The top electrode was removable for the convenience of sample preparation.

The tests were conducted in two phases, namely, sedimentation and remediation. In the first phase, a regulated voltage was applied on the testing sample, directed upward, top cathode (−) and bottom anode (+), to induce the movement of clay particles to downward due to electrophoresis. This is the electrokinetic sedimentation process. On the other hand, in the second phase, a regulated voltage was applied on the testing sample, directed downward, top anode (+) and bottom cathode (−), to induce the movement of water and organic substance downward due to electro-osmosis. This is the electrokinetic remediation process. In this phase, the polarity reversal employed and the bottom drainage channels were open. The time dependent settlement and concentration due to electrophoresis and electro-osmosis was measured on an hourly basis. The settlement or interface height with time was recorded through reading the slurry line from the scales installed on the cell. The concentration of outflow with time was measured by a liquid densiometer. The electrical current with time was measured using current meter.

Results and Discussion on Natural Sediment

Settlements

Figures 3(*a*) and 3(*b*) show the results of settlement and settlement rate of contaminated natural sediment with elapsed time under the applied voltage of 1 and 3 V/cm. Settlement is increased with time elapsed in all tests. Settlement is rapidly increased to about 10 h in the applied voltage of 3 V/cm and 15 h in the applied voltage of 1 V/cm and then constant to the end of experiment. The maximum settlement were 57.4 mm in 1 V/cm and 67.7 mm in 3 V/cm comparing with an initial height of 100 mm.

The electrophoretic sedimentation accelerated in the first and middle stages, and lasted to the last stage for the electrokinetic sedimentation process even though some differences were happened with experimental conditions. Clay particles are negatively charged, so the movement of clay particles is developed downward due to electrophoresis in the electrokinetic sedimentation process. Settlement is attributed to both gravitational and electrophoretic effects.

Dewatering and Outflows

The solid particles are moved toward the anode part by electrophoresis and the water is moved toward the cathode part by electro-osmosis and the drained water is remained over solid particles. Thus, the solid particles are moved downward and the water is moved upward in the electrokinetic sedimentation process. At the same time, the contaminant in the pore water is moved upward with water.

Figure 4 shows that the accumulated quantity of dewatering during the electrokinetic sedimentation process and the accumulated quantity of outflow during the electrokinetic remediation process with time. The quantity of dewatering is increased with time elapsed in all tests. At the end of the electrokinetic

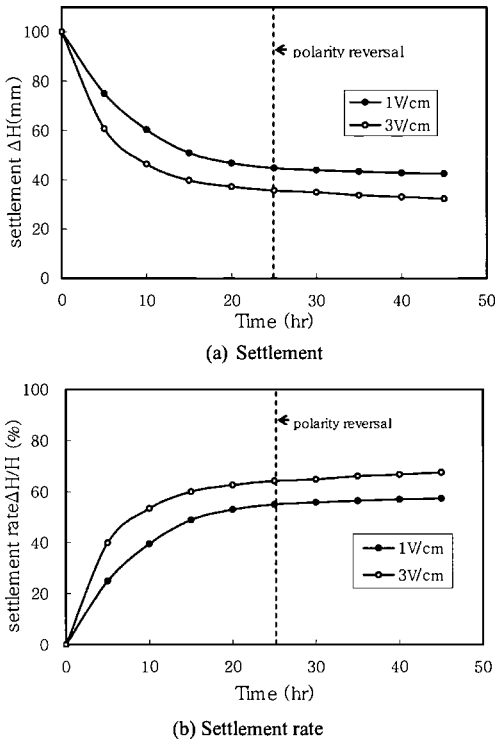

FIG. 3—*Settlement characteristics.*

sedimentation test, the final quantities of dewatering are about 433 and 505 ml for 1 and 3 V/cm, and at the end of the electrokinetic remediation test, the final quantities of dewatering are about 912 and 987 ml for 1 and 3 V/cm, respectively. The accumulated quantity of dewatering and outflow is high with increasing of the applied voltage.

Current Density

Figure 5 shows the variation of the applied voltage and current density with time. Positive voltage and current density denote the upward electric gradient using the top cathode and bottom anode for electroki-

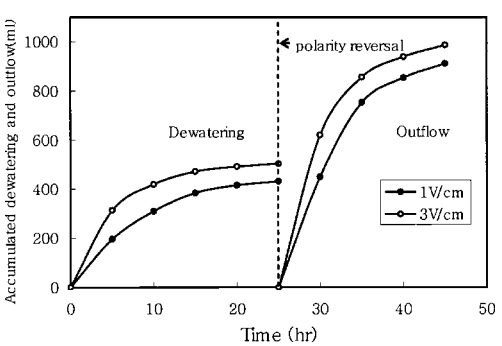

FIG. 4—*Dewatering and outflow.*

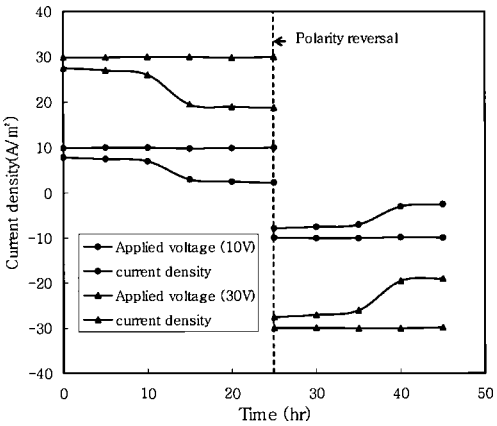

FIG. 5—*Current density.*

netic sedimentation process, and the negative voltage and current density denote the downward electric gradient using the top anode and bottom cathode for the electrokinetic remediation process. The polarity was reversed after 25 h for electrokinetic remediation. The constant voltage of 1 and 3 V/cm and the approximate current density of 5 and 20 A/m^2 was decreased with test time.

The current generally decreases due to increasing of resistance by volume and pore space reduction at the electrokinetic sedimentation process, and the current generally decrease due to the decreasing of the current conductor by a depletion of ions in pore water at the electrokinetic sedimentation process. As shown in Fig. 5, the current is decreased due to a reduction of volume and pore space during the electrokinetic sedimentation stage and also decreased due to a depletion of ions in pore water during the electrokinetic remediation stage.

Contaminant Transport

In the electrokinetic sedimentation process, the solid particles are moved downward and the water is moved upward. At the same time, the contaminant in the pore water is moved upward with water. In the electrokinetic remediation process, deionized distilled water is continuously supplied from the mariotte bottle with a constant head on the anode. The contaminated pore water passed through soil specimen downward toward the cathode by electroosmoosis and contaminated pore water replaced with deionized distilled water.

The results of chemical analysis for dewatering and outflow water are shown in Fig. 6 and Table 1. Chemical analysis was carried out at 0, 10, and 20 h on the water sample collected at the upper part of the electrokinetic cell during the electrokinetic sedimentation process, and at 30 and 40 h on the water sample collected from the drainage channel during electrokinetic remediation process. Data at 0 h represent the initial pore water concentration.

The pH of initial pore water in specimen and fresh water supplied by mariotte bottle is 6.5–7.0. The pH of dewatering and outflow water was measured and the pH of the sliced specimen section was not measured in this experiment. The pH of the dewatering water from the specimen increased to 10.4–11 at 10 h elapsed and 10.7–11.3 at 20 h elapsed due to the cathode reaction ($H_2O \rightarrow H_2\uparrow + OH^-$) at the upper part of the specimen in the electrokinetic sedimentation process as shown in Table 1 and Fig. 6. On the other hand, the pH of outflow water passing through the specimen remained at 10.6–11.2 at 30 h elapsed (10 h elapsed from the start time of the electrokinetic remediation process) due to the cathode reaction at the lower part of the specimen and decreased 8.0–8.5 at 40 h elapsed (20 h elapsed from the start of the electrokinetic remediation process) due to the dilution of high pH by intrusion of low pH generated by the anode reaction ($H_2O \rightarrow O_2\uparrow + H^+$) at the upper part of the specimen and intrusion of fresh water from the upper mariotte bottle toward the lower part of the specimen in the electrokinetic remediation process as shown in Table 1 and Fig. 6. The pH difference at the upper and lower parts of the specimen for the

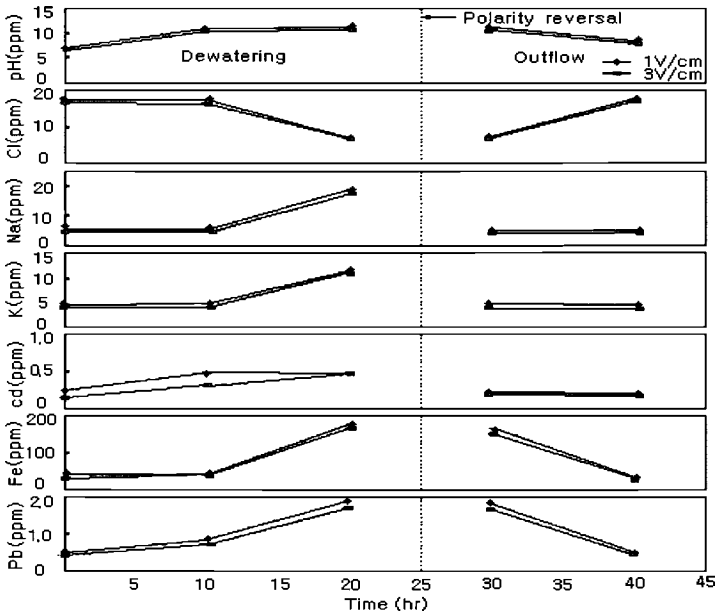

FIG. 6—*Chemical analysis of dewatering and outflow.*

electrokinetic sedimentation process and electrokintic remediation process varied from 6.5 to 11.3; it appears that the electromigration of products from the electrolysis reactions (H+ and OH^-), the dilution of anode and cathode products, and the introduction of fresh water were the main causes of pH changes.

The dewatering concentration of sodium, potassium, iron, cadmium, and lead cations gradually increased due to electromigration and transportation of cations with water movement upward in the electrokinetic sedimentation process; on the other hand, the outflow concentration of these cations gradually decreased with time due to transportation of cations downward by electro-osmosis and electromigration in electrokinetic remediation. The contaminant was transported with dewatering outflows from the sediment section at the electrokinetic sedimentation stage, and the contaminant was transported by electrokinetic soil flushing effects from the sediment section at the electrokinetic remediation stage. In the stage of electrokinetic sedimentation, the settlement of specimen is dominant and the migration of contaminant due to going up of water and going down of a soil particle by electrophoresis and electro-somosis effects is a little. In the stage of electrokinetic remediation after electrokinetic sedimentation, the migration of contaminant due to the electrokinetic soil flushing effect with fresh water is dominant. Contaminant transport effect continuously occurs in both stages as illustrated in Fig. 6.

TABLE 1—*Chemical analysis data of dewatering and outflow.*

	Concentration of ions with applied voltage and elapsed time									
	Applied voltage, 1 V/cm					Applied voltage, 3 V/cm				
Param-eters	0 h	10 h	20 h	30 h	40 h	0 h	10 h	20 h	30 h	40 h
pH	7	11	11.3	11.2	8.5	6.5	10.4	10.7	10.6	8
Cl	17.2	17.3	7.2	7.4	17.6	16.5	16.4	6.8	7	16.9
Na	5.2	5.3	18.6	4.9	5	4.7	4.6	17.2	4	4.2
K	1.8	1.9	4.5	1.9	1.8	1.62	1.63	4.4	1.5	1.45
Cd	0.25	0.48	0.492	0.231	0.198	0.15	0.32	0.47	0.21	0.18
Fe	40	42	176	165	35	32	40	165	151	30
Pb	0.51	0.84	1.87	1.8	0.524	0.43	0.71	1.71	1.65	0.45

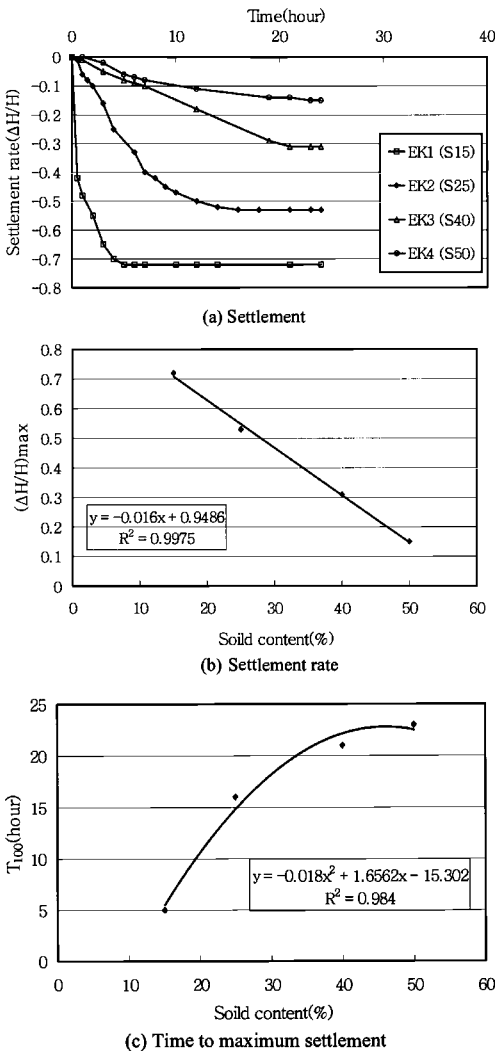

FIG. 7—*Settlement characteristics with solid content.*

Results and Discussion on Artificial Sediment

Settlement Characteristics by Solid Content in Electrokinetic Sedimentation Process

Figure 7(*a*) shows the results of the settlement rate of contaminated waste slurries with time by solid content 15, 25, 40, and 50 % for EK1, EK2, EK3, and EK4 test under the same applied voltage and concentration level. Settlement is increased with time elapsed in all tests by a variation of solid content. Clay particles are negatively charged, so the movement of clay particles is developed downward due to electrophoresis in electrokinetic sedimentation process. The electrophoretic sedimentation accelerated in the first and middle stages, and lasted to the last stage for the electrokinetic sedimentation process even though some differences happened with experimental conditions. Settlement is attributed to both gravitational and electrophoretic effects.

The sedimentation rate is presented as $\Delta H/H$, the amount of sedimentation divided by the initial sample height in Fig. 7(*b*). The initial sample height was $H=10$ cm. At the end of the test, the final height ratios of the samples are about 0.72, 0.53, 0.31, and $0.15\Delta H/H$ for EK1, EK2, EK3, and EK4, respectively. This means that the initial height was reduced 72, 53, 31, and 15 %, respectively. The volume reduction of waste slurries was achieved 72, 53, 31, and 15 %, respectively, compared with initial volume by the electrokinetic sedimentation processing. The settlements of specimen are in the order: EK1, EK2, EK3, and EK4. This means that the settlement rate is high and rapid with a decreasing of the solid content, otherwise the settlement rate is low and slow with an increasing of the solid content. The length and volume of the specimen is reduced due to the extraction of pore water and the settlement of the specimen in the proceeding of electrokinetic sedimentation tests.

Figure 7(*c*) shows the relationship between maximum settlement rate and solid content under the same applied voltage and concentration level. The corelative equation between maximum settlement rate, so-called final settlement rate, and solid content is derived from regression analysis and can be expressed as follows:

$$(\Delta H/H)\max = -0.016S + 0.9486 \tag{1}$$

$$t_{100} = -0.018S^2 + 1.6562S - 15.302 \tag{2}$$

where:

ΔH = settlement,
H = initial sample height,
S = solid content, and
t_{100} = time to reach final settlement.

Settlement Characteristics by Applied Voltage in Electrokinetic Sedimentation Process

Figure 8 shows the results of the settlement rate of contaminated waste slurries with time by applied voltage 0, 10, 20, and 30 V, that is 0, 1, 2, and 3V/cm, for GR, EK9, EK10, and EK2 tests under the same solid content and concentration level. Settlement is increased with time elapsed in all tests by a variation of applied voltage. The final sedimentation rates are 0.23, 0.45, 0.47, and 0.53 $\Delta H/H$ for GR, EK9, EK10, and EK2, respectively. This represents that the initial sample height was reduced 23, 45, 47, and 53 %, respectively, by electrokinetic sedimentation processing. It can be recognized that the settlement rate of specimen is increased with an increasing of applied voltage; on the other hand, the settlement rate is decreased with a decreasing of applied voltage. The regressive equation between final settlement rate and time to final settlement versus applied voltage can be expressed as

$$(\Delta H/H)\max = -0.0004V^2 + 0.0212V + 0.242 \tag{3}$$

$$t_{100} = 0.05V^2 - 2.36V + 42.9 \tag{4}$$

where:

V = applied voltage.

Settlement Characteristics by Concentration Level in Electrokinetic Sedimentation Process

Figure 9 shows the relationship of the settlement versus the concentration level. It is very difficult and complicated to investigate and we suggest the regression equations regarding relationships between settlement and concentration level are due to diversity of contaminant and concentration. Settlement rate is increased with a decreasing of the concentration level. It is attributed from that the current decreases and settlement decrease in the higher concentration than lower concentration due to increase of resistance by nonionic characteristics of ethylene glycol.

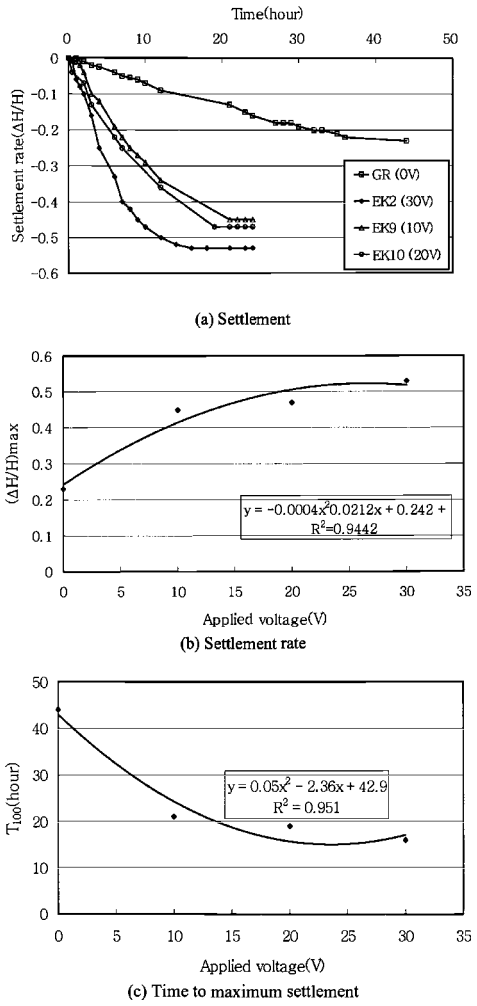

FIG. 8—*Settlement characteristics with applied voltage.*

Concentration of Outflow in Electrokinetic Remediation Process

The specific gravity of ethylene glycol is 1.13 and pure water is 1.0. Pore water in specimen is mixtures of ethylene glycol and pure water, so the density of initial pore water is higher than pure water. The density of pore water is varied with time and outflow. The density of outflow liquid was measured by precision densiometer. The density of initial pore water is decreased with time and outflow and finally reached the same density as pure water because mixed liquid with ethylene glycol and pure water migrate from the specimen and replaced with pure water during electrokinetic remediation stage. Where the difference of liquid density has the same meaning as the difference of liquid concentration. The concentration ratio can be obtained from the ratio of final and initial ethylene glycol density instead of ethylene glycol concentration due to difficulty of chemical analysis for ethylene glycol. Concentration profile in Figs. 10(*a*) and 11(*a*) was obtained by this method.

The contaminant in specimen is transported with water flow downward to the cathode by advection due to electro-osmosis and by diffusion due to concentration difference. The concentration of ethylene

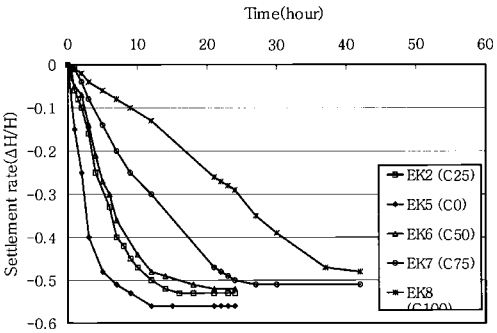

FIG. 9—*Settlement characteristics with concentration level.*

glycol was measured from the outflow. The normalized ethylene glycol concentration profile with the elapsed time of four experiments is shown in Fig. 10(*a*) for the electrokinetic remediation process. Ethylene glycol removal rate which is the inverse of concentration profile with elapsed time is shown in Fig. 10(*b*). The normalized ethylene glycol concentration profile with outflow rate is shown in Fig. 11(*a*). Ethylene glycol removal rate that is the inverse of concentration profile with outflow rate is shown in Fig. 11(*b*). The concentration of the contaminant in outflow is normalized by the initial concentration of the contaminant in soil prior to electrokinetic treatment. Where, C is the ethylene glycol concentration of outflow and Co is the initial ethylene glycol concentration in specimen.

As observed from the figures of concentration profile and removal rate, contaminated specimens are fully cleaned by introducing of electrokinetic remediation technique. The ethylene glycol concentration in

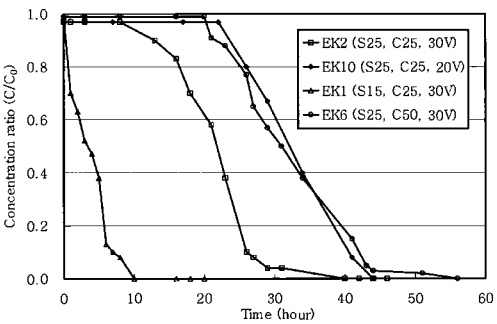

(a) Concentration profiles of outflow

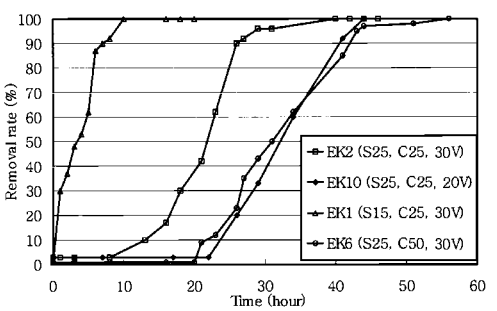

(b) Removal rate of contaminant

FIG. 10—*Concentration profiles and removal rate with time.*

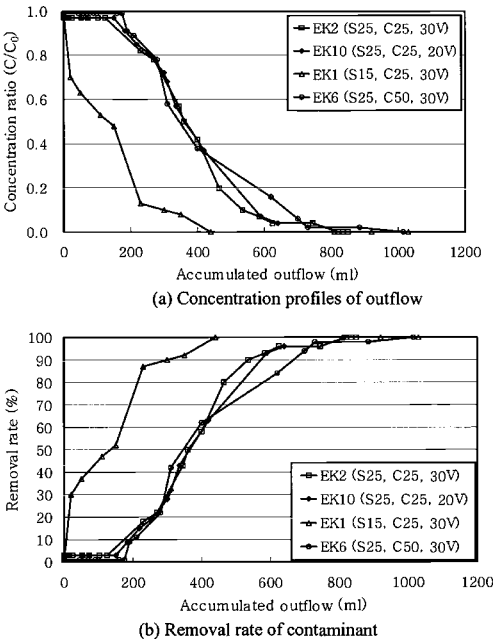

FIG. 11—*Concentration profiles and removal rate with outflow.*

the effluent collected at the cathode is not detected for some time in the initial stage. After that, the ethylene glycol concentration is detected with time. The concentration ratio decreased rapidly in the middle stage and decreased slightly before the experiment stopped. The 50 % removal times of contaminant in specimen are 27 h for EK1 test, 46 h for EK2 test, 55 h for EK6 test, and 56 h for EK10 test, respectively. The 100 % removal times of contaminant in specimen were 34 h for EK1 test, 65 h for EK2 test, 79 h for EK6 test, and 68 h for EK10 test, respectively. The contaminant diluted in pore water in the sample was removed as extraction of pore water by the electrokinetic flushing mechanism. From the above results, the contaminant in the specimen was almost fully removed from the specimen, and the removal speed and time of contaminant was shortened with an increasing of applied voltage, and with a decreasing of solid content and contamination level.

Summary

In this research, the coupled effects of sedimentation and remediation of natural sediment contaminated with various substances and artificial sediments contaminated with ethylene glycol are focused using electrokinetic sedimentation and remediation techniques. From the test results, the variation of settlement and concentration of contaminated sediments in which simultaneous sedimentation and remediation processes are involved by electrokinetics is investigated with different solid content, applied voltage, and concentration level. The coupled effects on densification and decontamination for contaminated slurry-type sediment are analyzed. Limited to these conditions, the following results can be summarized:

1. The current at the electrokinetic sedimentation process decreased due to an increasing of resistance by volume and pore space reduction, and the current at the electrokinetic sedimentation process decreased due to a decreasing of current conductor by depletion of ions in pore water.
2. The outflow pH at the electrokinetic sedimentation process increased to 10.4–11 at 10 h and 10.7–11.3 at 20 h due to the cathode reaction; on the other hand, the outflow pH at electrokinetic remediation process remained 10.6–11.2 at 10 h due to the cathode reaction and decreased 8.0–8.5

at 20 h due to the dilution of high pH by intrusion of low pH generated by the anode reaction and intrusion of fresh water supplied from mariotte bottle.

3. The corelative equation between maximum settlement and solid content (S) was derived from regression analysis. Settlement rate and time to maximum settlement (t_{100}) could be expressed as $(\Delta H/H)\max = -0.016S + 0.9486$, $t_{100} = -0.018S^2 + 1.6562S - 15.302$ for ethylene glycol contaminated sediment.
4. The corelative equation between maximum settlement rate and applied voltage (V) was derived from regression analysis. Settlement rate and time to maximum settlement (t_{100}) could be expressed as $(\Delta H/H)\max = -0.0004V^2 + 0.0212V + 0.242$, $t_{100} = 0.05V^2 - 2.36V + 42.9$ for ethylene glycol contaminated sediment.
5. The particle settlement rate at the electrokinetic sedimentation process was increased with an increasing of applied voltage and a decreasing of solid content and a concentration (ethylene glycol) level.
6. The cations and organic substances such as sodium, potassium, iron, cadmium, lead, and ethylene glycol were transported and extracted by electrophoresis and electro-osmosis mechanisms at the electrokinetic sedimentation process, and electro-osmosis, electromigration, and soil flushing mechanisms at electrokinetic remediation process.
7. The contaminant removal time at the electrokinetic remediation process was shortened with an increasing of applied voltage, and with a decreasing of solid content and contamination (ethylene glycol) level.
8. The rapid and simultaneous volume reduction and contaminant removal from contaminated sediments with high initial void and water content were achieved by the coupled effects of electrokinetic sedimentation and electrokinetic remediation techniques suggested in this research.

References

Acar, Y. B., Gale, R. J., Putnam, G., and Hamed, J., "Electrochemical Processing of Soils: Its Potential Use in Environmental Geotechnology and Significance of pH Gradients," *2nd International Symposium on Environmental Geotechnology*, Shanghai, China, May 14–17, Envo Publishing, Bethlehem, PA, 1989, Vol. 1, pp. 25–38.

Been, K. and Sills, G. C., "Self-Weight Consolidation of Soft Soils: An Experimental And Theoretical Study," *Geotechnique*, 31(4), 519–535 (1980).

Chung, H. I., "Enhancement of Sedimentation and Remediation of Contaminated Sediments by Electrokinetics," *The Proceedings of the 1st Korea-Japan Joint Seminar on Geoenvironmental Engineering*, Korea, 2001. 4, pp. 71–77.

Chung, H. I. and Kamon, Masashi, "Electrokinetic Sedimentation and Remediation of Contaminated Slurry Wastes," *5th International Symposium on Environmental Geotechnology and Global Sustainable Development*, Brazil, 2000. 9, pp. 70–77.

Shang, J. Q., "Electrokinetic Dewatering of Clay Slurries as Engineered Soil Covers," *Can. Geotech. J.*, 34, 78–86 (1997).

Yukawa, H., Yoshida, H., Kobayashi, K., and Hakoda, M., "Fundamental Study on Electro-Osmotic Dewatering of Sludge at Constant Electric Current," *J. Chem. Eng. Jpn.*, 9(5), 402–407 (1976).

Journal of ASTM International, Vol. 3, No. 6
Paper ID JAI13322
Available online at www.astm.org

Toshiro Hata, PhD,[1] *Futoshi Kurisu, PhD,*[2] *Osami Yagi, PhD,*[3] *Hirotoshi Mori,*[4] *Reiko Kuwano, PhD,*[5] *and Hidetoshi Kohashi, PhD*[6]

Development of an In Situ Biodegradation Technology by Using Anaerobic Micro-Organisms for Sediment Contaminated with Dioxins

ABSTRACT: In this paper, an in situ bioremediation method is proposed for dioxin contaminated sediments and its efficiency is assessed in laboratory tests including microbial analysis. The main outcomes of this research are (1) Proposal of an in situ bioremediation method using anaerobic micro-organisms monitored by molecular microbial techniques. (2) It was shown that the proposed method can reduce dioxin concentrations and can increase populations of the dehalogenating micro-organism (*Dehalococcoides* sp.). (3) It was further shown that the dioxin degradation processes can be monitored using polymerase chain reaction (PCR) denaturing gradient gel electrophoresis and real-time PCR. Microbial analysis using molecular techniques was useful for the monitoring and management of the sediment remediation process.

KEYWORDS: Contaminated sediments, Dioxins, Bioremediation, PCR, DGGE

Introduction

In Japan, increasing evidence of dioxin contamination of sediments led to a "Law Concerning the Special Measures against dioxins" being enacted in 1999. The law defines "dioxins" as a general term for polychlorodibenzo-p-dioxins (PCDDs), polychlorodibenzo furans (PCDFs), and coplanar PCBs (Co-PCBs). Dioxins are highly toxic to human beings and animals even at low concentration and are suspected of affecting the reproductive, thyroid, and immune systems. Although remediation methods, such as thermal treatment, have been developed to treat small quantities of highly concentrated wastes, dioxin pollution in sediments is generally at low concentrations and widely dispersed. Moreover, the environmental standard for sediments is stricter than that for wastes and soil, and accordingly the amount of sediment to be treated is extremely large. Thus, conventional methods are difficult to apply in terms of both costs and facilities and new technologies urgently need to be developed for sediment remediation. In this research a new enhanced natural attenuation technology for safe and in situ treatment of sediments contaminated with dioxins was developed. This paper describes the method and assesses its effectiveness through laboratory testing using environmental samples.

The objectives of this study are to (1) effect the dechlorination of highly chlorinated congeners in naturally contaminated sediments and (2) to elucidate the dehalogenation mechanisms involved. Batch slurries were incubated with added nutrient salts and carbon source under anaerobic conditions. Slurry samples were taken at various times over a one-year period and were analyzed for evidence of dehalogenation by High-resolution mass spectrometer (JMS-700D, JEOL).

Manuscript received March 30, 2005; accepted for publication June 29, 2005. Presented at ASTM Symposium on Contaminated Sediments: Evaluation and Remediation Techniques on 23–25 May 2006 in Shizuoka, Japan; M. Fukue, K. Kita, M. Ohtsubo, and R. Chaney, Guest Editors.

[1] Researcher, Research Center for Water Environment Technology, The University of Tokyo.
[2] Assistant Professor, Research Center for Water Environment Technology, The University of Tokyo.
[3] Professor, Research Center for Water Environment Technology, The University of Tokyo.
[4] Researcher, Materials and Geotechnical Engineering Research Group, Public Works Research Institute.
[5] Senior Researcher, Materials and Geotechnical Engineering Research Group, Public Works Research Institute.
[6] Head of Division, Material and Geotechnical Engineering Research Group, Public Works Research Institute.

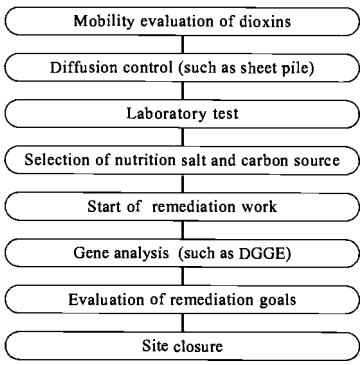

FIG. 1—*Process of the remediation method.*

Overview of the Proposed Remediation Techniques

Reductive dechlorination of dioxins and PCBs by micro-organisms has been reported in sediments at the bottom of lakes and rivers (Barkovskii and Adriaens 1996, Ballerstedt et al. 2004). Recently, a strain of *Dehalococcoides* sp. CBDB1 was found to dechlorinate highly chlorinated PCDD (Bunge et al. 2003). The dechlorination rate by the strain CBDB1 is slow but can be accelerated by improving its environment using engineering methods. The process of the proposed remediation method is shown in Fig. 1, and a schematic diagram of the remediation system is shown in Fig. 2. Before initiating this type of remediation project the mobility of dioxins should be evaluated. When contaminants are located near groundwater, contaminated sediment must be separated by sand caps and sheet piles to prevent dioxins from spreading due to factors such as groundwater flow. A treatability test should then be conducted to evaluate the decomposition performance in a laboratory with various combinations of nutrients and carbon sources. Along with the monitoring of dioxin concentrations, microbial monitoring was conducted to evaluate whether the soil conditions remain appropriate for continued reductive dechlorination. The microbial monitoring included both community analysis and the enumeration of *Dehalococcoides* sp. strain CBDB1 and its lineage. A combination of nutrients and a carbon source (selected according to the treatablity test) is injected into the ground through the injection well to accelerate the remediation activities of microorganisms. During remediation, microbial monitoring was also conducted to ensure optimal conditions for the entire microbial community in general and the dehalogenation microorganisms in particular.

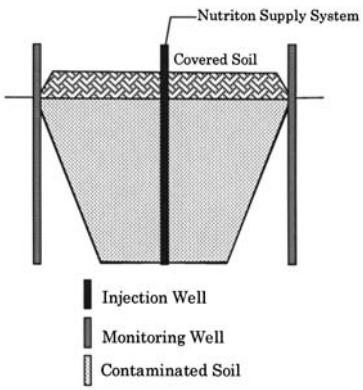

FIG. 2—*Schematic diagram of the remediation site.*

TABLE 1—*Physical properties of the soil sample.*

Item	Unit	Measured value	Testing method
Dioxin Concentration	pg−TEQ/g	28,000	…
Hydrogen ion concentration	…	7.4	JGS 0211-2000
Moisture content	%	27.3	JGS 0122-2000

Materials and Methods

Sediment Collection

Approximately 20 kg sediment (0–20 cm) was collected using an acetone-rinsed shovel from the actual site contaminated with dioxins. Sediments were stored at room temperature in an airtight container until use.

Characterization of Sediment Sample

The physical properties of the soil samples are shown in Table 1. Dioxin isomer concentrations were measured with a high-resolution mass spectrometer (JMS-700D, JEOL). The dioxin concentrations were converted to the TEQ (Toxicity Equivalence Quantity) value by using the TEF (Toxic Equivalency Factor) Value. Hydrogen ion concentration (pH) and moisture content were measured with The Japanese Geotechnical Society (JGS) standard method (The Japanese Geotechnical Society, 2000a).

Treatability Tests

Acetic acid, lactic acid, and molasses were used as carbon sources. Samples for the tests were prepared as follows: (1) The contaminated sediment was air-dried; (2) sediment pH was adjusted to nominal value of 7.0 by the addition of 30 mM sodium phosphate; (3) 15g of the dried sediment, 15g of nutrient salts (Table 2), and 1000 mg/L of the carbon source either acetic acid, lactic acid, or molasses were put into 70 mL vials; (4) the headspace of the vials was purged with N_2 gas; and (5) the vials were rapidly sealed with viton rubber caps.

The vials were incubated for 12 months at 30°C and shaken at 120 rpm. Samples were taken after 1, 3, 6, and 12 months. Duplicate vials were prepared for each sampling time so that the whole sample could be used for analysis.

Analytical Methods

Sampling and pH Measurement—Two grams of the sediment slurry were collected from the vial for microbial analysis. Then, the remaining 28 g of residual slurry was continuously stirred for 1 min before measuring pH using a pH electrode. The rest of the sample was used for the dioxin analysis.

Dioxin Concentration—The cultivated slurry samples were sampled at 1, 3, 6, and 12 months and analyzed for Octachlorodibenzo-p-dioxon (OCDD) and other toxic dioxin isomers. The slurry sample was

TABLE 2—*Composition of nutrient salts.*

Culture medium			Trace element solution			Vitamin solution		
NH_4Cl	10	MM	$FeCl_2$	10	mM	biotin	20	nM
KH_2PO_4	1	MM	$CoCl_2$	1	mM	4-aminobenzoic acid	20	nM
$MgCl_2 \cdot 6H_2O$	1	mM	$MnCl_2 \cdot 4H_2O$	1	mM	pantothenate	20	nM
$CaCl_2 \cdot 2H_2O$	1	mM	$ZnCl_2$	1	mM	pyridoxine	20	nM
$NaHCO_3$	30	mM	H_3BO_3	0.1	mM	nicotinamide	20	nM
$Na_2S \cdot 9H_2O$	1.5	mM	$NiCl_2$	0.1	mM	thiamine	20	nM
Cystein-HCl	1.5	mM	$AlCl_3$	0.1	mM	lipoic acid	20	nM
Trace elements solution	1	ml/L	$Na_2MoO_4 \cdot 2H_2O$	0.1	mM	folic acid	20	nM
Vitamin solution	1	ml/L	Na_2SeO_3	0.01	mM	vitamin B12	20	nM
			$Na_2WO_4 \cdot H_2O$	0.01	mM	riboflavin	20	nM
			$CuCl_2$	0.01	mM			

TABLE 3—*Primers and probes for PCR detection and real-time PCR.*

Analysis method	Name	Alignment	References
PCR detection	DET730	GCGGTTTTCTAGGTTCTC	Bunge et al. (2003)
	DET1350	CACCTTGCTGATATGCGG	Bunge et al. (2003)
Real-time PCR	FW-Primer	CTGGAGCTAATCCCCAAAGCT	He et al. (2003)
	RV-Primer	CAACTTCATGCAGGCGGG	He et al. (2003)
	Probe	CCTCAGTTCGGATTGCAGGCTGAA	He et al. (2003)

divided into the solid phase and liquid phase.

The solid phase was extracted in a Soxhlet extractor by using toluene for over 16 h. The liquid phase was extracted using liquid-liquid extractors using dichloromethane for 30 min by 3 times. Samples were analyzed on a Hewlett Packard 6890 gas chromatograph with a JEOL JMS-700D high-resolution mass spectrometer, using a SP-2331 column (60 m by 0.25 mm i.d., film thickness 0.2 μm, SUPELCO, SIGMA-ALDRICH). The injector and detector temperatures were 270°C. The oven temperature was held at 100°C for 1 min, ramped at 20, and then 3°C/min to 261°C, and held for 12 min, ramped at 3°C/min to 273°C, and held for 1.5 min. The dioxin isomer concentrations were calculated in accordance with the measurement result of solid phase and liquid phase. The dioxin concentrations were converted to the TEQ (Toxicity Equivalence Quantity) value by using the TEF (Toxic Equivalency Factor) Value.

Microbial Community Analysis by PCR-DGGE (Polymerase Chain Reaction-Denaturing Gradient Gel Electrophoresis)—Microbial DNA was extracted from the 2 gs of slurry samples by using ISoil DNA extraction kits (Nippon Gene, Tokyo). The DNA extracts were used for all the microbial analysis. Partial 16S rDNA was amplified by the universal PCR pair GC-341f&534r for DGGE analysis. The PCR conditions were as follows: 95°C for 10 min. 94°C for 1 min. and 53°C for 1 min 72°C for 1 min (32 cycles), and 4°C for 20 min. The reactions were conducted with Thermal Cycler PERSONAL (TaKaRa TP240). DGGE was performed by the D-CODE system (Bio-Rad Lab, CA.). The denaturing gradient gel was prepared to obtain 8 % acrylamide gel with denaturant gradient of 30 to 60 %. The electrophoresis conditions were at 130 V for 5 h.

Detection and Enumeration of Dehalococcoides sp.—Dehalococcoides sp. CBDB1 lineage was detected by using the nested PCR method (Bunge et al. 2003). The almost complete 16SrDNA was first amplified with the universal PCR pair fD1&rP2. Then, *Dehalococcoides* sp. CBDB1 lineage targeted PCR was done with a specific primer (DET730, 1350). The primer sequences are shown in Table 3. The PCR conditions were as follows: 95°C for 10 min, 94°C for 1 min, 55°C for 1 min, 72°C for 1 min, (40 cycles), and 4°C for 20 min. The reactions were conducted with a Thermal Cycler PERSONAL (TaKaRa TP240).

Quantification of oligonucleotides targeting 16SrRNA gene sequences of *Dehalococcoides* sp. was performed by a real time PCR method (Jianzhong He et al. 2003). Primers and probes used are shown in Table 3. Each MicroAmp optical tube had a 30-μL reaction volume containing 1×TaqMan Universal PCR Master Mix (including DNA polymerase, deoxynucleoside triphosphates, and $MgCl_2$); forward primer, reverse primer, and TaqMan probe (300 nM each); and a series of tenfold-diluted DNA templates.

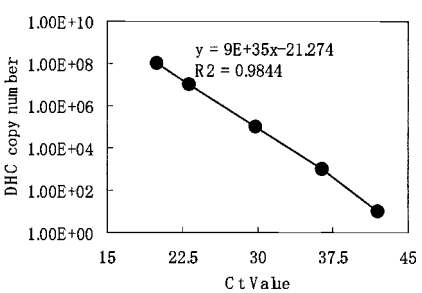

FIG. 3—*Calibration curve of Dehalococcoides sp.*

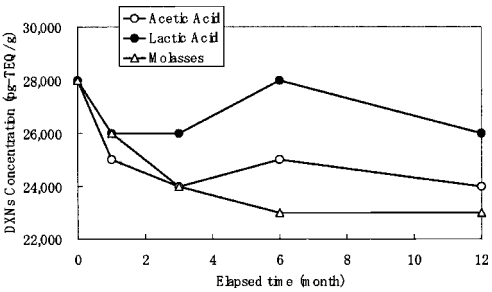

FIG. 4—*Dioxins concentration change as TEQ equivalent.*

The PCR conditions were as follows: 2 min at 50°C and 10 min at 95°C, followed by 45 cycles of 15 s at 95°C and 1 min at 60°C. PCR was carried out in a spectrofluorimetric thermal cycler (ABI Prism 7700, Applied Biosystems). Standard *Dehalococcoides* DNA fragments were prepared by PCR amplified with primer sets of DET730 and DET1350. A calibration curve was obtained by using serial dilutions of DNA of known concentration (Fig. 3). The Ct (threshold value) values for each sample were compared with the standard curve to determine the template DNA concentration. With a sample size of 2 g used for DNA extraction, the lower limit of quantification is 10^2 copies/g-soil.

Results and Discussion

Trend of Dioxin Concentrations and pH

Changes in the TEQ value during the test period are shown in Fig. 4. After one month of incubation, the largest reduction in the TEQ value was shown in the sample with acetic acid. After three and six months of incubation, increases in the TEQ concentration were observed in the sample with lactic acid. This was most probably due to the production of more toxic dioxins by the dechlorination. After twelve months of incubation, decreases in the TEQ concentration were observed in the samples with lactic acid and acetic acid. The sample with molasses showed continuous decreases in TEQ concentration and the greatest decrease over twelve months.

The rates of changes in PCDDs, in the sample with molasses are shown in Fig. 5. Dechlorination of highly chlorinated dioxins was observed. Among tetra chlorinated DDs, 1,3,6,8-T4CDD and 1,3,7,9-T4CDD decomposed rapidly, but 2,3,7,8-T4CDD, which is the most toxic, was found to have accumulated after one month. The concentration decreased thereafter and the initially observed increase is most likely due to a temporary accumulation of dechlorination products from higher chlorinated DDs.

The rates of changes in PCDFs in the sample with molasses are shown in Fig. 6. Dechlorination of octachlordibenzofuran (OCDF) was observed. Among tetrachlorinated DFs, 2,3,7,8-T4CDF decomposed fast, but 1,2,7,8-T4CDD, which is the nontoxic, was found to have accumulated after one and three months. Pentachlorinated DFs, 2, 3, 4, 7, 8-T5CDF and 1, 2, 3, 7, 8-T5CDF were not found to have

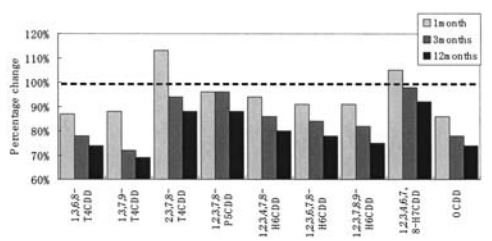

FIG. 5—*PCDDs concentration in sample with molasses.*

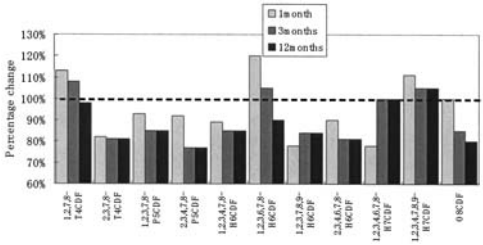

FIG. 6—*PCDFs concentration in sample with molasses.*

accumulated. The concentration decreased thereafter and thus it seems to be caused by the temporal accumulation of the dechlorination products like 1, 2, 3, 6, 7, 8-H6CDF from higher chlorinated DFs.

Other main results were as follows. Acetic acid samples showed increases in the 2, 3, 7, 8-T4CDD isomer after six months. Lactic acid samples showed an increase in concentrations of the 2, 3, 7, 8-T4CDD isomer after three and six month. Therefore, the increase in TEQ concentration is caused by accumulation of high toxicity PCDDs isomers.

The pH changes in each sample during the test period are shown in Fig. 7. The pH rose to about 8.2 at the first month and then gradually lowered to become neutral in all samples. Thus, the addition of carbon sources does not change the pH significantly.

Changes in Microorganism Community Structure

The result of the PCR-DGGE analysis is shown in Fig. 8. Each unique band suggests the existence of a different species of microorganisms. The number of bands increased notably from the beginning of the experiment, which shows proliferation of the micro-organisms. A comparison between bands at one and three months of incubation showed a shift of the bacterial community. It has been documented that changes in the microbial community can result in different dechlorination patterns. Thus, the genetic diversity revealed in the DGGE assays may be attributable to the different dechlorination patterns observed in three carbon sources. The micro-organism structure is scheduled to be analyzed through the base sequence decision of each band in the future.

Detection of the Dehalococcoides sp. Strain CBDB1 Lineage

PCR detection of *Dehalococcoides* sp. CBDB1 lineage in the one month sample is shown in Fig. 9. The specific primer for the strain CBDB1 detected the lineage of the strain in the sample with acetic acid, which showed the sharpest reductions in dioxin concentrations among the three conditions tested. Since the strain was not detected in the samples before incubation, the strain reached detectable levels through incubation with acetic acid and the nutrients. The CBDB1 lineage was not detected in the sample with lactic acid and molasses, though reductions in TEQ concentration were observed. This suggests that the

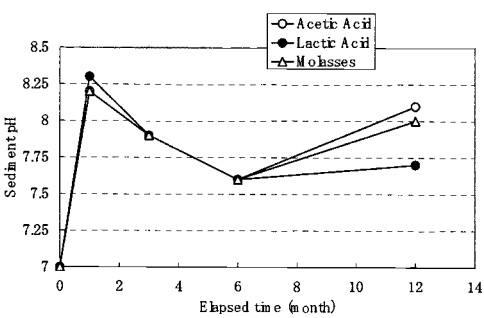

FIG. 7—*pH trends.*

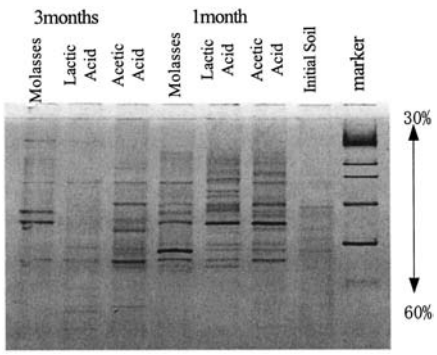

FIG. 8—*Gel image of PCR-DGGE analysis.*

CBDB1 lineage might be active even at undetectable levels or that microorganisms other than the CBDB1 lineage were involved in the decomposition of dioxins.

Quantification of Dehalococcoides sp.

The results of the quantification of *Dehalococcoides* sp. by real-time PCR are shown in Fig. 10. The concentration of the organisms in the sediment before incubation was below the detection limit (10^2 copies/g−soil). Growth of *Dehalococcoides* sp. was observed in all samples incubated with nutrients and carbon sources after one month.

Dehalococcoides sp. were detected in the specimens cultured in a nutrient salt medium with acetic acid, which showed rapid decomposition at the start of incubation. The number of micro-organisms as well as the concentration of dioxins decreased along with the incubation. Slight growth of *Dehalococcoides* sp. was observed in the sample with lactic acid after one month. However, no *Dehalococcoides* sp. were detected in the specimens cultured for three months and thereafter.

The sample incubated with molasses, which showed the largest reduction of dioxins after six months, showed growth of *Dehalococcoides* sp. after one and three months. However, no *Dehalococcoides* sp. was detected after six months, even though the dioxin concentrations continued to drop. This suggests that micro-organisms other than *Dehalococcoides* sp. might be involved in the decomposition of dioxins. The relationship between the degraded concentration of dioxins and *Dehalococcoides* sp. was investigated in

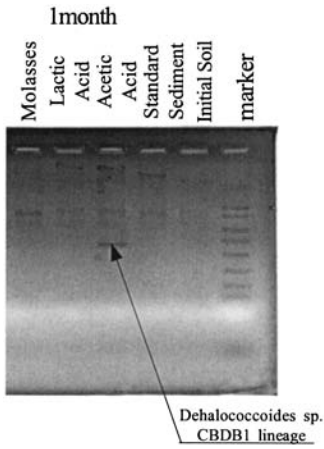

FIG. 9—*PCR detection of Dehalococcoides sp. CBDB1 lineage.*

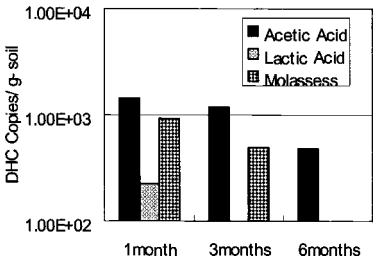

FIG. 10—*Quantification of Dehalococcoides sp. by real-time PCR.*

the acetic acid specimens, in which *Dehalococcoides* sp. were detected. The relationship between the degraded concentration of dioxins and the number of *Dehalococcoides* sp. copies is shown in Figure 11. The acetic acid specimens showed a trend of reduced dioxin concentration as the number of the copies of *Dehalococcoides* sp. increased. The trend was notable at the start of culture and after three months of culture. From three to six months of culture, the number of the copies of *Dehalococcoides* sp. was stable but the TEQ concentration rose.

Conclusion

Laboratory tests were conducted to verify the effects of nutrient and carbon source addition to biodegradation of dioxins in sediments. The major conclusions of this study are as follows:

1. The TEQ concentration of sediments contaminated with dioxins can be reduced by activating the endogenous microorganisms in the sediments.
2. A maximum reduction of 5000 pg-TEQ/g in twelve months was attained by adding 1000 ppm of molasses with nutrients.
3. The addition of 1000 ppm of acetic acid and nutrients enhanced the growth of the known PCDDs dechlorinator, *Dehalococcoides* sp. strain CBDB1 lineage.
4. The number of *Dehalococcoides* sp. appeared to have some correlation with the dioxins dehalogenation when acetic acid was added as a carbon source, but the relationship was not obvious with molasses.

Future research should attempt to determine optimal conditions for limiting the accumulation of dehalogenated intermediate products and further identify the bacteria which are actually involved in the dioxins' reduction.

References

Ballerstedt, H., Hantke, J., Bunge, M., Werner, B., Gerritse, J., Andreesen J., and Lechner, U., Properties of a Trichlorodibenzo-p-Dioxin Dechlorinating Mixed Culture with a Dehalococcoides as Putative

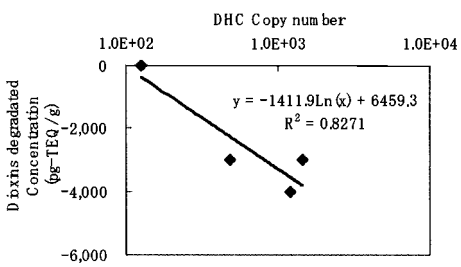

FIG. 11—*Relationship between the numbers of Dehalococcoides sp. and the dioxins' degraded concentration.*

Dechlorinating Species," *FEMS Microbiology Ecology* 47, 223-234 (2004).

Barkovskii A L., and Adriaens, P., "Microbial Dechlorination of Historically Present and Freshly Spiked Dioxins and Diversity of Dioxin Dechlorinating Populations," *AEM* 62(12), 4556-4562 (1996).

Bunge, M., Adrian, L., Kraus, A., Opel, M., Lorenz, W. G., Andreesen, J. , Gorischi, H., and Lechner, U., "Reductive Dehalogenation of Chlorinated Dioxins by an Anaerobic Bacterium," *Natre (London)* 421, 357-360 (2003).

The Japanese Geotechnical Society, "Test Method for pH of Suspended Soils," *JGS 0211-2000*, 2000a.

The Japanese Geotechnical Society, "Test Method for Water Content of Soils by the Microwave Oven," *JGS 0122-2000*, 2000b.

He, J., Ritakahti, K., Aiello, M. , and Loffler, F. , "Complete Detoxification of Vinyl Chloride by Anaerobic Enrichment Culture and Identification of the Reductively Dechlorinating Population as a Dehalococcoides Species," *AEM* 69, (2), 996-1003 (2003).

Journal of ASTM International, Vol. 3, No. 6
Paper ID JAI13340
Available online at www.astm.org

Taku Nishimura,[1] *Hiroyuki Shirato, B. Ag.,*[1] *Miyuki Hayashi, B. Ag.,*[2] *and Makoto Kato*[1]

Effect of Dispersivity of Filling Material on Performance of Contaminant Barrier

ABSTRACT: The performance of pollution barriers is discussed using solute soil dispersion parameters. Masa sandy loam and Toyoura sand, with dispersivities of 0.21 and 0.17 cm at saturation, respectively, were used as barrier material. 2.5 wt.% of the synthetic P-type zeolite was mixed with the soil to control the adsorption capacity of the barrier without changing soil structure. Soils were packed into an acrylic plastic column to form model barriers with different thicknesses. Adsorption capacity of the columns was between 6.1 and 7.5 $mmol_c$ per column. 42 $mg \cdot dm^{-3}$ Cd as nitrate solution was applied to the column under water saturated conditions, and effluent was collected at the bottom of the column. A relatively thin barrier, i.e., five times greater than the dispersivity, resulted in the detection of Cd with only 0.075 $mmol_c$ load of Cd, while a thicker barrier, 30 times greater than dispersivity, showed no leak of Cd with a 0.9 $mmol_c$ load of Cd added to the column.

KEYWORDS: dispersivity, dispersion coefficient, synthetic zeolite, pollution barrier

Introduction

Heavy metals are released to the environment through atmospheric deposition, fertilizer impurities, sewage sludge, and wastes from stockbreeding. Understanding the processes of solute transport through and chemical adsorption by sediments is important for the design of counter measures, such as isolation and remediation. Static physicochemical properties, cation exchange capacity and equilibrium constant are often used to express the performance of chemical barriers (Selim et al. 1992; Hinz and Selim 1994), and predict the release of contaminants from polluted soils (Boekhold and van der Zee 1992; Oste, Lexmond, and Van Riemsdijk 2002). However, soil layers with similar adsorption characteristics do not always show similar responses to pollution loads, including the release or adsorption of contaminants (Voegelin et al. 2003).

Previous studies have omitted several important factors. The column experiments of most previous studies assumed the columns as homogeneous reactors. The adsorption capacity and kinetics of the fill material are often considered in describing the behavior of contaminants in porous media, while travel time is the only physical factor taken into account. Relatively little attention has been paid to the transport behavior of contaminants (Seuntjens et al. 2001). Parameters of solute transport, such as the dispersion coefficient and dispersivity or dispersion length (Jury and Horton 2004), are important parameters to describe contaminant transport through porous media, and thus design contaminant isolation and release. Most previous heavy metal remediation and prevention studies did not adequately consider transport processes. Proper consideration of both transport and adsorption properties of soil is necessary to design pollution reduction procedures.

Convection dispersion equation (CDE) is a model of chemical transport through soils that has been successfully applied to the transport of soluble salts (Simunek et al. 1999) and heavy metals (Kookana and Naidu 1998). The results of these studies suggested that CDE modeling can be utilized to help interpret heavy metal behavior in soils. CDE assumes chemicals moving through a soil migrate, repeatedly mixing, as well as adsorbing and desorbing (Jury and Horton 2004). Dispersivity is the parameter that describes the extent of instance of mixing event of flowing pollutants. If a porous material having high adsorption

Manuscript received March 31, 2005; accepted for publication September 16, 2005. Presented at ASTM Symposium on Contaminated Sediments: Evaluation and Remediation Techniques on 23–25 May 2006 in Shizuoka, Japan; M. Fukue, K. Kita, M. Ohtsubo, and R. Chaney, Guest Editors.

[1] Department of International Environmental and Agricultural Sciences, Tokyo University of Agriculture and Technology.
[2] Ministry of Agriculture Forestry and Fishery.

TABLE 1—*Specific surface area (SSA) and cation exchange capacity (CEC) of materials.*

	Toyoura sand	Masa sandy loam	Synthetic zeolite (R-107)
SSA ($m^2 \cdot g^{-1}$)	2.8	39.0	211.3
CEC ($mol_c \cdot kg \cdot soil^{-1}$)	0.0	0.15	3.0
Charge density ($mol_c \cdot m^{-1}$)	...[a]	3.85×10^{-6}	1.42×10^{-5}
pH	...[a]		

[a]Toyoura sand is assumed to have no charge.

capacity also has a thick macropore, most of the polluted liquid may flow through the macropore and the high adsorption capacity cannot show its whole performance. This is similar to a porous material having a large dispersivity for mixing of flowing solution.

In the present study, authors tried to use the physical parameter of CDE, dispersivity, as an index of the mixing process in soil, to discuss the performance of pollution barriers.

Materials and Methods

Soils

Masa sandy loam (10 % clay, 10 % silt, and 80 % sand) from Fukushima prefecture and Toyoura sand ($0.075\ mm < d < 0.0425\ mm$) from Yamaguchi prefecture, Japan, were used in this experiment. Masa sandy loam is derived from weathered granite and Toyoura sand is sediment at a former sea shore in Yamaguchi, Japan. Soils were sieved through a 3-mm-mesh screen. Additionally, only Toyoura sand was washed with distilled water to remove fine and reactive materials such as clay particles. Packing dry bulk density was 1.30 and 1.60 $g\text{-}cm^{-3}$ for the Masa sandy loam and the Toyoura sand, respectively. To prevent segregation of soil particles during packing, soils were moistened, 10 wt% and 5 wt-% for Masa sandy loam and Toyoura sand, respectively, prior to packing. Soils were packed into an acrylic plastic cylinder with a 4-cm-inner diameter. Compacting of the soil sample was conducted using a rod that was fitted to the inner diameter of the plastic cylinder. Packing of each 5-mm-thick soil layer was completed to form the whole soil column. Following the packing, the soil column was saturated from the bottom, and the experiment was carried out under saturated conditions.

The P-type synthetic zeolite synthesized from coal ash of an electric power plant by sodium hydroxide treatment was used in this study. 2.5 wt-% of the synthetic zeolite (R-107 from Plantec Inc., Osaka, Japan) was mixed with the soils to enhance adsorption capacity. Cation exchange capacity (CEC) determined by ammonia acetate adsorption, specific surface area (SSA) by ethylene glycol monoethyl ether (EGME) adsorption, and pH by 1:5 soil-water ratio are shown in Table 1.

Solute Displacement Experiment

A solute displace experiment was conducted to measure solute transport parameters. Soils were packed into an acrylic plastic cylinder with a 4-cm-inner diameter and 14-cm length using the procedure described above. The column had four-probe electrical conductivity sensors at depths of 2.5 (EC1), 5.5 (EC2), 8.5 (EC3), and 11.5 (EC4) cm from the top (Rhoades and Schilfgaarde 1976; Inoue and Shiozawa 1994) and measured bulk electrical conductivity (EC) using a CR10X data logger (Campbell Sci. Inc., Utah, USA). The top of the column was connected to a solution supply reservoir and the bottom of the column was connected to a drainage pipe. The flow velocity of the solution was controlled by manipulating the heights of the reservoir and drainage outlet.

The soil column was first saturated from the bottom with 10-mmol-L^{-1} calcium chloride ($CaCl_2$) solution and then the top inlet was connected to the reservoir having the same solution, and downward solute transport started. The 10-mmol-L^{-1} $CaCl_2$ solution flow was maintained until all the sensors showed an EC value appropriate to the corresponding solute concentration and flow velocity reached steady state. Then, 10-mmol-L^{-1} $CaCl_2$ solution was replaced with 100-mmol-L^{-1} $CaCl_2$ solution. During the displacement experiment, EC inside the column was monitored using four-probe electrical conductivity sensors.

TABLE 2—*Cation adsorption capacity of each column.*

Soil	Masa sandy loam (2.5 cm in thick)	Masa sandy loam-zeolite mixture (2.0 cm in thick)	Toyoura sand-zeolite mixture (5 cm in thick)
Cation adsorption capacity ($mmol_c$-$column^{-1}$)	7.2	6.1	7.5
Saturated hydraulic conductivity ($cm\text{-}s^{-1}$)	$3.62 \pm 1.0 \times 10^{-3}$	$3.62 \pm 1.0 \times 10^{-3}$	$7.33 \pm 0.07 \times 10^{-3}$

Occasionally, EC of effluent solution was measured. The experiment was completed when EC of the effluent solution was identical to that of the inlet solution. pH of the flowing solution was 5.5 to 6.0. Two to four replicates were created for each condition.

Cadmium (Cd) Transport Experiment

A Cd transport experiment was conducted to examine potential performance of synthetic zeolite-soil mixed barrier to isolate Cd pollution. The same acrylic plastic cylinder as used for the displacement experiment was used for this experiment. Different thickness barriers, 2.0, 2.5, 5.0 cm, with similar adsorption capacity, were prepared. The barriers consisted of Masa sandy loam (2.5-cm thick), mixture of Masa sandy loam and 2.5-wt-% synthetic zeolite (2.0-cm thick), and Toyoura sand and 2.5-wt-% synthetic zeolite mixture (5-cm thick) and were constructed in the acrylic plastic cylinder. The cation adsorption capacity of each barrier is shown in Table 2.

The column was saturated with 10-$mmol\text{-}L^{-1}$ $CaCl_2$ solution and then 42-$mg\text{-}dm^{-3}$ $Cd(NO_3)_2$, which was equivalent to 0.48-$mmol_c\text{-}L^{-1}$, was applied from the top of the column. pH of the solution was 5.5 to 6.3. The drainage outlet of the column was connected to a fraction collector and took effluent samples periodically. Cd concentration of collected samples was measured by an atomic adsorption spectrometer. Two to three replicates were created for each condition.

Theory of Solute Transport Parameters

One-dimensional solute transport through homogeneous adsorbing media at constant water content is described here using the convection dispersion equation (CDE) (Jury and Horton 2004).

$$R\frac{\partial C}{\partial t} = D_s\frac{\partial^2 C}{\partial z^2} - v\frac{\partial C}{\partial z} \tag{1}$$

where t is time (s), z is distance (cm), C is concentration of chemical, D_s is dispersion coefficient, and R is retardation factor. Retardation factor and dispersion coefficient are defined as follows:

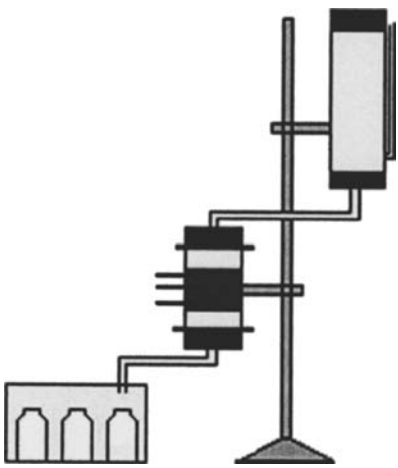

FIG. 1—*Schematics of column experiment.*

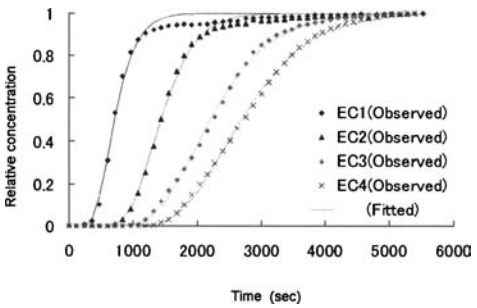

FIG. 2—*Measured and fitted breakthrough curves of Masa sandy loam. EC1 to EC4 in the figure denote position of the sensor.*

$$R = 1 + \left(\frac{\rho}{\theta}\right) K_d \tag{2}$$

$$D_S = D_m + \lambda v \tag{3}$$

where ρ is dry bulk density, θ is volumetric water content of the media, K_d is partition coefficient of ion exchange (kg-L^{-1}), D_m is molecular diffusion coefficient (cm^2-s^{-1}), λ is dispersivity or dispersion length (cm), v is average pore water velocity (cm-s^{-1}). Numerical solution of Eq (1) is coupled with nonlinear optimization as provided by the CXTFIT code (Toride et al. 1999) to optimize the dispersion coefficient, mean pore water velocity, and retardation factor. D_m in water is an order of 10^{-5} cm^2-s^{-1} and often negligible when there is water flow through the media. In this case dispersivity λ can be derived using Eq (3) by linear regression of D_s with various pore water velocity (v). STANMOD software (Simunek et al. 1999), which is implemented with the CXTFIT, was used for data analysis in presenting study.

Cation Adsorption

Cation selectivity of the synthetic zeolite was measured by batch experiment. 0.1 g of airdry zeolite was equilibrated with several different concentration electrolyte solutions (0.01, 0.1, and 1 mol-L^{-1}). Then the cation concentration of a supernatant solution was measured by atomic adsorption spectrometry. The measured supernatant concentration was subtracted from the initial concentration, and was assumed to give the amount of adsorption of the synthetic zeolite. During the batch experiment, pH of the testing solution was between 5.8 and 6.6.

Results and Discussions

Solute Transport Parameters

Figures 2 and 3 show breakthrough curves (BTC) of the Masa sandy loam and synthetic zeolite-Masa sandy loam mixture column. Marks in the figures denote measured concentrations and lines show fitted results. Both figures show a strong agreement with experimental and numerical results except the results of EC1, which were 2.5-cm deep from the top of the column. The position of EC1 was too shallow to assure complete dispersion phenomena. In addition, some disturbance could occur at the surface to shallow depth, in the top 2.5-cm soil layer during application of solutions.

Except EC1, the numerical solution of CDE by STANMOD could represent solute transport through a soil column with and without synthetic zeolite fairly well. According to the nonlinear optimization by STANMOD, mean pore water velocity, the dispersion coefficient, and the retardation coefficient were determined to represent the solute transport observed in each experiment. Figure 4 shows the results of the relationship between sample mean pore water velocity (v) and dispersion coefficient (D_s). The slope of the linear regression of the v-D_s relationship may give the dispersivity of the soil. Toyoura sand showed dispersivity similar to the Masa sandy loam.

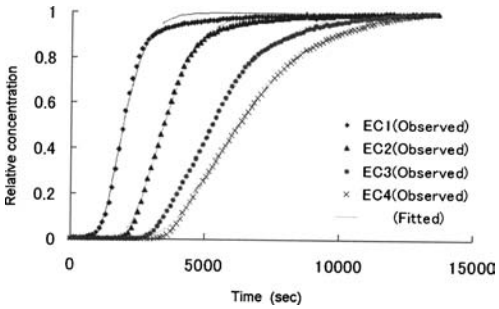

FIG. 3—*Measured and fitted breakthrough curves of 2.5-wt-% synthetic zeolite-Masa sandy loam mixture. EC1 to EC4 in the figure denote position of the sensor.*

The mixing of fine material may cause changes in the structure of a soil and thus change its transport characteristics. In the present study, incorporating 2.5 wt-% of zeolite did not change the saturated hydraulic conductivity of Masa soil, suggesting a pore structure, and, as shown in Table 3, the transport characteristics of both soils were consistent. Masa sandy loam showed a small increase in dispersivity following mixing 2.5 wt-% of synthetic zeolite, however, Toyoura sand showed dispersivity decreasing with the addition of 2.5 wt% synthetic zeolite (Table 3). However, those changes were small, around 0.1 cm. It is concluded that the mixing of a small amount of synthetic zeolite, 2.5 wt-% in the present study, did not cause significant changes in the soil transport characteristics.

Adsorption Characteristics of Soil Materials

The synthetic zeolite used in the present study had a high CEC, 20 times higher than that of the Masa sandy loam, however the synthetic zeolite had a large specific surface area, as well. Thus, the charge density of the synthetic zeolite was only four times greater than the charge density of Masa sandy loam.

The batch experiment designed to measure the cation exchange isotherm showed that the synthetic zeolite used in the present study showed linear adsorption for the concentration range of 0.01 to 1 mol-L^{-1} electrolyte solution (Fig. 5). The slope of the linear regression 6.66 was assumed to be the partition coefficient K_d of synthetic zeolite for cation exchange. The K_d of Masa sandy loam was determined using the estimated retardation factor by STANMOD and Eq (2). It was assumed that K_d for the soil-zeolite mixture can be estimated using the weighted average of K_d of the Masa sandy loam and the

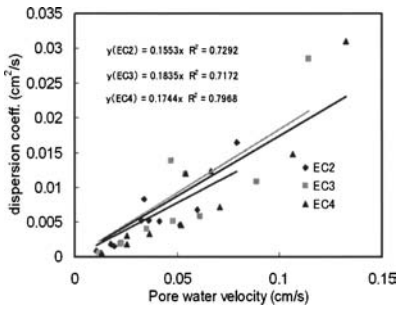

FIG. 4—*v-D_s relationship with Toyoura sand.*

TABLE 3—*Dispersivity of soil materials.*

	Toyoura sand	Toyoura sand with 2.5-wt-% zeolite	Masa sandy loam	Masa sandy loam with 2.5-wt-% zeolite
Dispersivity (cm)	0.17	0.09	0.21	0.31

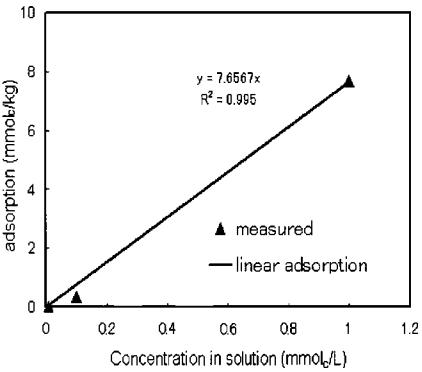

FIG. 5—*Adsorption isotherm of the synthetic P-type zeolite (R-107).*

synthetic zeolite. Results are shown in Table 4. K_d of synthetic zeolite was 100 times greater than that of Masa sandy loam. The retardation factor of the zeolite-Toyoura sand mixture and the zeolite-Masa sandy loam mixture was similar. Calculated retardation factors using K_d for the materials tended to be smaller than those estimated by STANMOD alone.

Breakthrough of Cadmium through Pollutant Barrier

Figure 6 shows the relationships between amount of polluted (Cd) solution input and the concentration of effluent from the column. Pore volume is a nondimensional variable, which was derived as cumulative drainage divided by the volume of all the pores in the soil column. As shown in Table 2, the cation adsorption capacity of each barrier was similar, independent of the barrier thickness. However, during the Cd load experiment, the synthetic zeolite-Masa sandy loam mixture barrier showed quick penetration of Cd with a small application of Cd solution. The Masa sandy loam barrier showed breakthrough of Cd second, and the synthetic zeolite-Toyoura sand mixture barrier was most tolerant of the Cd load. It showed no breakthrough of Cd when 50 pore volumes of Cd solution was applied. The Cd pollutant load was 0.1 $mmol_c$ when there was a breakthrough of Cd through the synthetic zeolite-Masa sandy loam mixture barrier. This load was 1.6 % of the barrier's adsorption capacity. No penetration of Cd through the Masa sandy loam barrier (d=2.5 cm) and the synthetic zeolite-Toyoura sand mixture barrier (d=5.0 cm) occurred until the load was less than 0.6 and 0.9 $mmol_c$, respectively. This was 8.3 and 12 % of the barriers' cation adsorption capacities, respectively. A thin barrier showed pollutant breakthrough with a smaller load of Cd than predicted by the barrier's adsorption capacity.

It is questionable why the barriers with a similar adsorption capacity showed differences in tolerance to the application of Cd contaminated solution. This may be due to the process of solute transport through the column. As shown in the miscible displacement experiment, Figs. 2 and 3, CDE can represent solute transport in the present study. The CDE solute transport model employs the dispersion coefficient to represent the mechanical behavior of solute. The dispersion coefficient is a function of the multiplication

TABLE 4—*Retardation factor and partition coefficient of the soil materials.*

	Zeolite	Zeolite-Toyoura sand mixture	Masa sandy loam	Masa sandy loam-zeolite mixture
R	···	2.2	1.25	2.4
K_d[a]	7.65	···	0.077[b]	···
R^{*c}	···	1.8	···	1.7

[a]slope of linear adsorption isotherm.

[b]Estimated by using Eq (2) and retardation factor

[c]Estimated by using Eq (2) and weight averaged K_d.

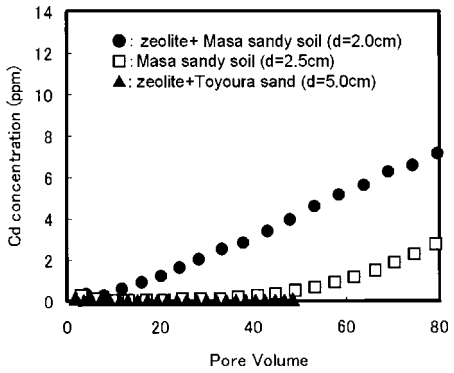

FIG. 6—*Breakthrough of Cd-contaminated solution through barriers. "d" in the figure denotes thickness of the barrier.*

of mean pore water velocity and dispersivity. Dispersivity is a scale upon which solute convection is averaged (Jury and Horton 2003). The solute moves through the soil with repeated mixing, and the interval of the mixing is conceptually expressed as dispersivity.

Dispersivity, or dispersion length, is the measurement of the mixing process frequency for chemicals flowing through porous media. One conceptual mixing process can be expected to occur when solute flows down for a distance equivalent to dispersion length. As shown in Table 3, the dispersivity of the synthetic zeolite-Masa sandy loam barrier was 0.31 cm. This suggests that Cd solution could approximately encounter six mixing instances during its flow through the 2.0-cm-thick barrier, while 12 mixing events could occur in the 2.5-cm-thick Masa sandy loam barrier, and 55 consecutive mixing events were expected during flow through the 5-cm-thick synthetic zeolite-Toyoura sand mixture barrier.

Cation exchange capacity is a static property of a soil, however cation exchange capacity can not contribute to the capture of pollutants unless the pollutants have a chance to access adsorption sites in the soil. The number of mixing occasions can be an index showing the extent of accessing adsorption sites by pollutants. A lower mixing frequency may lead to a lower chance of adsorption, thus a higher adsorption capacity cannot be demonstrated. This may indicate the reason for the thin synthetic zeolite-Masa sandy loam mixture barrier did not show the characteristic of capturing Cd similar to that of the thicker synthetic zeolite-Toyoura sand mixture barrier, which had a similar adsorption capacity.

Conclusion

In the present study, soil barriers having similar adsorption capacity did not show similar Cd capture performance in a column experiment. The results suggested that not only chemical properties of the fill materials but also the solute transport process in the column played an important role in capturing contaminants. Interpretation of the dispersivity of the fill materials indicated that the synthetic zeolite-Toyoura sand mixture barrier had smaller dispersivity, in which a larger number of consecutive mixing events could be expected, and showed higher performance in capturing Cd pollutants. In contrast, the synthetic zeolite-Masa sandy loam mixture barrier had greater dispersivity and fewer mixing occasion, which led to quick breakthrough of Cd after the application of a Cd-contaminated solution.

The present study suggests that the physical process of solute transport is also an important factor in evaluating the performance of a contaminate isolation barrier and discusses the release of pollutants from porous materials.

Acknowledgments

The current study was supported by a joint research project between Tokyo University of Agriculture and Technology and Plantec Inc. The author would thank to Ms. Ishizaki, Ms. Nakajima, and Mr. Tamura for their help in conducting the experiment.

References

Boekhold, A. E. and Van der Zee E. A. T. M., "Significance of Soil Chemical Heterogeneity for Spatial Behavior of Cadmium in Field Soils," *Soil Sci. Soc. Am. J.*, 56, 747–754 (1992).

Hinz. C. and Selim, H. M., "Transport of Zinc and Cadmium in Soils: Experimental Evidence and Modeling Approaches," *Soil Sci. Soc. Am. J.*, 58, 1316–1327 (1994).

Inoue, M. and Shiozawa, S., "Measurement of Electrical Conductivity in Soil Columns by the Four-Electrode Method and its Application," *Soil Physical Condition and Plant Growth, Jpn*, 70, 23–28 (1994).

Jury W. A. and Horton, R., "Chap. 7 Chemical Transport in soil," *Soil Physics*, John Wiley and Sons Inc., New Jersey, 2004.

Kookana, R. S. and Naidu, R., "Effect of Soil Solution Composition of Cadmium Transport through Variable Charge Soils, *Geoderma*, 84, 235–248 (1998).

Oste, L. A., Lexmond, T. M., and Van Riemsdijk, W. H., "Metal Immobilization in Soils Using Synthetic Zeolites," *J. Environ. Qual.* 31, 813–821 (2002).

Rhoades, J. D. and van Schilfgaarde, J., "An Electrical Conductivity Probe for Determining Soil Salinity," *Soil Sci. Soc. Am. J.* 54(1), 46–54 (1976).

Selim, H. M., Buchter, B., Hinz, C., and Ma, L. "Modeling the Transport and Retention of Cadmium in Soils: Multireaction and Multicomponent Approaches," *Soil Sci. Soc. Am. J.* 56, 1004–1015 (1992).

Seuntjens, P., Tirez, K., Simunek, J., van Genuchten, M. Th., Cornelis, C., and Geuzens, P., "Aging effects on cadmium transport in undisturbed contaminated sandy soil columns," *J. Environ. Qual.* 30, 1040–1050 (2001).

Simunek, J., van Genuchten, M. Th., Sejna, M., Toride, N., and Leij, F. J., *The STANMOD Computer Software for Evaluating Solute Transport in Porous Media Using Analytical Solutions of Convection-Dispersion Equation. Versions 1.0 and 2.0*, IGWMC - TPS - 71, International Ground Water Modeling Center, Colorado, 1999.

Toride, N., Leij, F. J., and van Genuchten, M. Th., "The CXTFIT Code for Estimating Transport Parameters from Laboratory or Field Tracer Experiments." *Ver. 2.1. Research Report No. 137*, U.S. Salinity Laboratory, ARS-USDA, Riverside, CA. 1999.

Voegelin, A., Barmettler, K., and Kretzschmar, R., "Heavy Metal Release from Contaminated Soils: Comparison of Column Leaching and Batch Extraction Results, *J. Environ. Qual.*, 32, 865–875 (2003).

Journal of ASTM International, Vol. 3, No. 6
Paper ID JAI13306
Available online at www.astm.org

Motoyuki Asada, Dr.,[1] *Preeda Parkpian, Dr.,*[2] *and Sumio Horiuchi, Dr.*[1]

Remediation Technology for Boron and Fluoride Contaminated Sediments Using Green Plants

ABSTRACT: Phytoremediation is the direct application of green plants and their associated micro-organism to stabilize or absorb contaminants from soils, sludge, sediments, surface water, or groundwater. Boron and fluoride were listed to the soil standards a few years ago in Japan; however, few researches have been reported about phytoremediation on the above elements. In this paper, the authors report the experimental results of accumulation and tolerance ability of green plants focusing on the fluoride and boron contamination. In the pot laboratory tests, the growth rate of Chinese cabbage was not affected by low fluoride concentration (<15 mg/L) or low boron concentration (<5 mg/L). In the hydroponics tests, fluoride content in both stems+leaves and roots increased 3–10 times higher than control. Fluoride is easy to be concentrated in the roots. Boron content in both stems+leaves and roots increased 1.2–1.5 times higher than control. Boron is easy to be concentrated in the upper portion. Especially, *Phytolacca Americana, Ambrosia trifida* L., and *Commelina communis* can accumulate boron with higher efficiency. The boron content in soil was 480–550 mg/kg, and the boron content in these grasses was 2–3 times higher than that in soil. These results show they can accumulate boron and fluoride, and phytoremediation can be adopted for relatively lower contamination.

KEYWORDS: phytoremediation, boron, fluoride, contaminants, plant

Introduction

Large-scale redevelopment of the former factories is now active by reason of industrial restructure in Japan. In some cases, toxic substances left or spilled underground cause problems, and there are many sites to be cleaned up so far. However, there are some sites which have not been remediated by the increase of clean up cost due to the strict target standard, and long range period necessary for remediation works. Also in Southeast Asian countries, typically in Thailand, there are some problems of soil and groundwater contamination (Parkpian et al. 2004); however, few contaminated sites have been cleaned up yet mainly due to the financial problem. Clean up methods using microbes or green plants are developing and they will be the promising technologies to reduce the contaminated soil remediation cost.

Phytoremediation is the direct application of green plants and their associated micro-organism to stabilize or absorb contaminants from soils, sludge, sediments, surface water, or groundwater (USEPA 2001). The first attempt on actual sites was carried out in early 1990s, followed by more than 200 sites in the United States (USEPA 2004). Because of its harmony to nature, phytoremediation can be an effective remediation method at a variety of sites and on numerous contaminants. For phytoremediation, plant species of fast growth and large water uptake capacity, such as hybrid popular, is suitable for the sites contaminated by volatile organic hydrocarbons.

Boron and fluoride were listed to soil environmental standard in 2002 in Japan, and a few studies about phytoremediation for boron and fluoride contaminants have been carried out. Boron usually exists as boric acid salts with a high solubility (4.9 g/100 g-water at 20°C), and is easy to penetrate into the soil with water flow. On the contrary, fluoride usually exists as stable chemicals like calcium fluoride (0.0016 g/100 g-water at 18°C) and tends to stay on the ground surface. Soil standards for boron and fluoride in Japan are established by both leaching value and soil content, and they are 1.0 mg/L and 4000 mg/kg for boron and 0.8 mg/L and 4000 mg/kg for fluoride.

Manuscript received April 12, 2005; accepted for publication September 16, 2005; published online March 2006. Presented at ASTM Symposium on Contaminated Sediments: Evaluation ad Remediation Techniques on 23–25 May 2006 in Shizuoka, Japan; M. Fukue, K. Kita, M. Ohtsubo, and R. Chaney, Guest Editors.
[1] Shimizu Corporation, Institute of Technology, 3-4-17 Echujima, Koto, 135-8530 Tokyo, Japan.
[2] Asian Institute of Technology, P.O. Box 4, Klong Luang, Pathumthani 12120, Thailand.

FIG. 1—*Hydroponics apparatus.*

Katsumi (1984) reported the experiments of fluoride influence as an air pollutant to the plants. Yamada (1980) studied the absorption of fluoride by *Theaceae* trees from soils and the chemical state of absorbed fluoride in relation to absorption of aluminum by the plants. Arnesen (1997) reported two pot experiments to study uptake of fluoride in clover and grasses from soil. Fluoride concentrations in white clover and ryegrass were highly collated with the amounts of H_2O- and 0.01 M $CaCl_2$-extractable F in soil. On the other hand, there are few investigations about boron phytoremediation as the contaminated pollutants, although plenty of studies on plant growth affects of boron have been reported (Fujiwara et al. 2004).

In this paper, the authors report the experimental results of tolerance and accumulation ability using green plants to investigate the efficiency and limitation of phytoremediation technology for cleaning fluoride and boron contamination. The laboratory tests were conducted both in Japan and Thailand, and the field survey was conducted in Japan.

Procedure

To investigate the tolerance of plants against boron and fluoride, pot tests and hydroponic tests were conducted in the laboratory scale. Fluoride and boron content in upper portion (leaves and stems), and roots were measured in the hydroponics tests. Also, at boron contained areas in the former factory site, plant phase and flora was investigated to examine the suitable species for boron phytoremediation. Pot tests and field survey were conducted in Japan. Hydroponic tests were conducted in Thailand using Thai native species.

Laboratory Pot Tests

Chinese cabbage (*Brassica campestris*) was selected for the laboratory pot tests to clarify the maximum leaching value and content for the limitation of plants growth. Twenty five seeds sowed in one pot (d =11.3 cm, H=6.5 cm) with 500 ml of soil. The seeds were bought in the market. The soil was diluvial clay loam and was sampled from the test field where there was no contamination of fluoride and boron at Hiroshima, Japan. Fluoride concentration was adjusted from 200 mg/kg to 4000 mg/kg using sodium fluoride, and boron concentration was adjusted from 42 mg/kg to 4000 mg/kg using boric acid.

TABLE 1—*Germination rate in fluoride contaminated soil.*

F-Content (mg/kg)	Leaching value (mg/L)	Germination (%)				
		2 days	3 days	4 days	5 days	10 days
200 (control)	0.4	15	78	85	85	85
500	6.6	12	72	83	85	77
750	15.9	25	77	95	92	82
1000	21.0	30	80	92	85	77
1500	48.0	8	47	67	65	62
2000	54.9	12	33	63	60	52
4000	120.0	2	7	7	7	5

TABLE 2—*Plant growth in fluoride contaminated soil.*

F-Content (mg/kg)	Leave length		Weight (20 days)	
	10 days (cm)	20 days (cm)	Weight (g/pot)	Weight index
200 (control)	1.5	4.7	3.6	100
500	1.5	4.5	3.1	86.0
750	1.5	4.5	3.6	102.3
1000	1.4	4.5	4.0	111.4
1500	0.9	3.2	2.0	57.2
2000	0.6	2.1	0.8	21.2
4000	…	…	…	…

The moisture content of the soil was kept at 25 wt-%. The plants were harvested after 20 days from seeding. Rate of germination was counted after 2, 3, 4, 5, and 10 days. Length of leaves was measured after 10 and 20 days, and weight of plants was measured after 20 days. This test procedure was based on the cultivation test for plant damage determined by the Ministry of Agriculture, Forestry and Fisheries, Japan (1984).

Laboratory Hydroponic Tests

Water mushroom (*Hydrocotyle unbellata* L.), Phakbung (*Ipomoea aquatica*), Silver fern (*Pityrogramma calomelanos*) were used for hydroponic laboratory tests. Aquatic plants, water mushroom, and phakbung were collected from the fields at Bangkok area and they were fixed directly in the hydroponics apparatus (Fig. 1). Silver fern was bought from the market and was fixed on the apparatus after the soil was removed from their roots. The plants were cultivated using Hoagland's nutrient solution for 30 days without additional fluoride or boron. After 30 days of plants acclimatized to hydroponics condition, the boron and fluoride concentration was increased from 3 to 50 mg/L for 80 days gradually. After the experiment, fluoride and boron content in upper portion (leaves and stems) and roots was measured.

Field Survey

The field survey was conducted in a former glass enamel factory site in Japan. Leaching value of boron was over the soil standard; it was 1.5 times higher than the soil standard 1.0 mg/L. All the names of plants were listed in the two designated areas (2 m × 6 m, 2.5 m × 6 m) and the plants were categorized into six groups; Dicotyledons, choripetalae, trees, and grasses, Dicotyledons, sympetalae, trees and grasses, and monocotyledons trees and grasses. Also the boron content was analyzed in the roots, stems, leaves and flowers of the collected plants.

Analytical Methods

Leaching method of the soil is as follows; (1) Put 50 g soil in the 500 mL pure water (pH5.8–6.3); (2) shake 6 h; (3) filter the liquid to make the analysis samples; and (4) analyze samples by absorbance

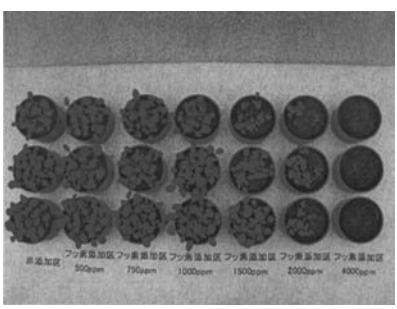

FIG. 2—*Plant growth after 20 days in fluoride contaminated soil.*

TABLE 3—*Germination rate in boron contaminated soil.*

B-Content (mg/kg)	Leaching value (mg/L)	Germination (%)				
		2 days	3 days	4 days	5 days	10 days
42 (control)	<0.1	15	78	85	85	85
75	1.7	37	75	90	85	82
150	6.6	10	60	82	88	85
250	17.1	8	48	67	70	80
500	38.8	7	12	23	27	18
1000	79.2	3	3	3	2	0
4000	323.0	0	0	0	0	0

method for fluoride and by inductivity coupled plasma method for boron. This was based on the test procedure for soil pollution standard determined by the Ministry of the Environment, Japan (1991).

HClO is used to extract hydrogen fluoride in the soil, and the concentration is measured by absorbance method. Alkali fusion is used for boron extraction, and the concentration is analyzed by inductivity coupled plasma method. This test procedure was based on the procedure determined by the Ministry of the Environment, Japan (2001).

Laboratory Pot Test Results

Table 1 shows the germination rate in fluoride contaminated pots. After ten days from seeding, 85 % of seeds germinated in control, germination rate was same until 1000 mg/kg as control. At 2000 mg/kg, 52 % germinated at ten days, and at 4000 mg/kg, germination rate decreased down to 5 % at ten days. Table 2 shows leaves length and plant weight in fluoride contaminated pots. Weight index shows the relative weight of each condition when the weight of control condition is calculated as 100. Figure 2 shows the plant growth in fluoride contaminated soil. After 20 days from seeding, leave length was 4.7 cm in control condition. Until 1000 mg/kg, leave length was the same as the control condition. At 4000 mg/kg, there was no growth of leaves. The weight index showed its maximum at 1000 mg/kg. Arnesen (1997) pointed out that with 400 mg/kg soil visible toxicity symptoms were found on the clover and Italian ryegrass grown. In this pot tests, Chinese cabbage showed higher tolerance clover and Italian ryegrass. The environmental standard of fluoride is 0.8 mg/L leachating value, and the growth rate was not affected by low fluoride concentration (<15 mg/L).

Table 3 shows the germination rate in boron contaminated pots. After ten days from seeding, 85 % of the seeds germinated in control, and until 250 mg/kg, germination rate was the same as control. At 500 mg/kg, 18 % germinated at ten days, and at 1000 to 4000 mg/kg, germination rate decreased down to 0–3 % at ten days. Table 4 show leaves length and plant weight in boron contaminated pots. Figure 3 shows the plant growth in boron contaminated soil. After 20 days from seeding, leave length was 4.7 cm in control. Until 75 mg/kg, leave length is the same as control. At more than 150 mg/kg, there was little growth of leaves. Weight index showed its maximum at 75 mg/kg. The environmental standard of boron is 1.0 mg/L leachate, and the growth rate was not affected by low boron concentration (<5 mg/L).

Laboratory Hydroponics Test Results

Figure 4 shows the growth of water mushroom in control, high fluoride, and boron concentration after 80 days. Roots in both fluoride and boron liquid grew worse than those in control. In fluoride liquid, leave

TABLE 4—*Plant growth in boron contaminated soil.*

B-Content (mg/kg)	Leave length		Weight (20 days)	
	10 days (cm)	20 days (cm)	Weight (g/pot)	Weight Index
42 (control)	1.5	4.7	3.6	100
75	1.5	4.5	3.7	104.1
150	0.8	1.1	0.5	14.0
250	0.7	⋯	⋯	⋯
500–4000	⋯	⋯	⋯	⋯

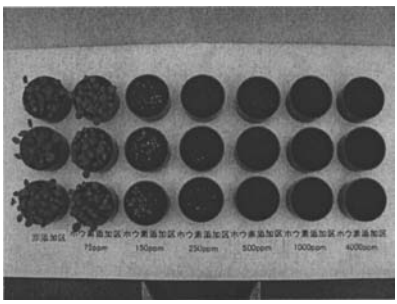

FIG. 3—*Plant growth after 20 days in boron contaminated soil.*

edge of aquatic plants like water mushroom and phakbung showed visible defects at more than 25 mg/L, however, silver fern can tolerate up to 50 mg/L without any visible defect. In boron liquid, aquatic plants showed their durability until 5 mg/L, but at more than 5 mg/L, the color of the edges of leaves changed to yellow or brown. Moreover, the leaves died at the higher concentration of boron. This result agrees with the test results of the above pot tests; leaching value affects the plant growth. Silver fern can grow until 50 mg/L of boron.

Figures 5 and 6 show the fluoride and boron content in the plant body after 80 days exposure of fluoride or boron. Fluoride content in both stems+leaves and roots increased 3–10 times higher than that in control. Fluoride is easily concentrated in the roots. Especially, silver fern can concentrate fluoride up to 120 mg/kg. This concentration ability is not the same as that of camellia, which is famous for hyperaccumulator of fluoride and can concentrate more than several hundred mg/kg (Yamada 1980); however, silver fern can concentrate much more than typical plants which can concentrate fluoride up to 30 mg/kg. Boron content in both stems+leaves and roots increased 1.2–1.5 times higher than that in control. Boron is easy to be concentrated in upper portion.

Field Test Results

There were 19 families and 24 types of choripetalae, 6 families and 13 types of sympetalae, and 5 families and 13 types of monocotyledons. In this survey, 30 families and 50 types of plants were found without any disorder growth. The ground was covered more than 90 % by grasses.

Table 5 shows the boron content in the collected plants. The boron content was analyzed in roots, stems, leaves, and flowers. The result shows that boron is easily concentrated in leaves. Grasses can concentrate more boron than trees in their body. Especially, *Phytolacca Americana, Ambrosia trifida L.*, and *Commelina communis* can accumulate boron with higher efficiency. The boron content in soil was 480−550 mg/kg (soil content standard 4000 mg/kg), and the boron content in grasses was more than that in soil. Boron hyperaccumulator was studied by Babaolu (2004) and caryophyllaceae can concentrate

FIG. 4—*Growth of water mushroom in control (left), fluoride (middle), and boron condition (right).*

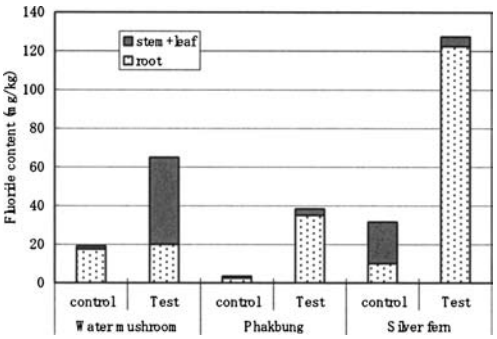

FIG. 5—*Fluoride content in the plant body after 80 days.*

boron with high content (more than 2000 mg/kg) in its above-ground parts. *Phytolacca Americana* can concentrate up to 1400 mg/kg in its leaves, and it can be a hyperaccumulator of boron.

Conclusions

In this paper, the authors report the experimental results and field survey of phytoremediation technology using green plants focusing on the fluoride and boron.

In the pot laboratory test, the growth rate of Chinese cabbage was not affected by low fluoride concentration (<15 mg/L) or low boron concentration (<5 mg/L). There is a possibility of phytoremediation contaminated by fluoride and boron with relatively lower concentration.

In the hydroponics tests, fluoride content in both stems+leaves and roots increased 3–10 times in the exposure condition more than in the control condition. Fluoride is easily concentrated in the roots. Especially, silver fern can concentrate fluoride up to 120 mg/kg. Boron content in both stems+leaves and roots increased 1.2–1.5 times in the exposure condition more than in the control condition. Boron is easy to be concentrated in upper portion.

In the field survey, *Phytolacca Americana, Ambrosia trifida* L., and *Commelina communis* can accumulate boron with higher efficiency. The boron content in soil was 480–550 mg/kg, and the boron content in grasses was more than that in soil. These results show they can accumulate boron and fluoride, and phytoremediation can be adopted for relatively lower contamination.

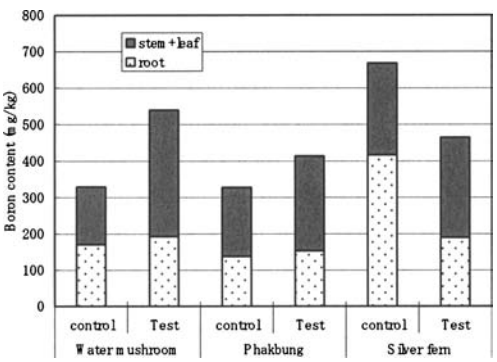

FIG. 6—*Boron content in the plant body after 80 days.*

TABLE 5—*Boron content in the plants at the survey area.*

Name	Boron content (mg/kg)			
	Roots	Stems	Leaves	Flowers
Dicotyledons, choripetalae, trees *Fatsia japonica, Celtis sinensis, Aphananthe aspera, Morus australis, Robiniapseudo-acacia*	49–77	47–75	230–610	···
Dicotyledons, choripetalae, grasses *Cayratia japonica, Achyranthes bidentata var. tomentosa, Phytolacca americana*	61–130	71–130	310–1400	630
Dicotyledons, sympetalae, trees *Nerium indicum, Sambucus nigra*	180	57–60	350–410	···
Dicotyledons, sympetalae, grasses *Datura stramonium, Solanum americanum, Erigeron canadensis, Ambrosia trifida* L.	54–86	56–76	160–990	···
Monocotyledons, trees *Trachycarpus fortunei*	79	83	140	···
Monocotyledons, grasses *Oplismenus undulatifolius var. japonicus, Zoysia japonica, Pleioblastus chino, Setaria viridis, Commelina communis*	110–240	41–230	70–600	67

Acknowledgments

The authors would like to acknowledge the support of the National Institute of Advanced Industrial Science and Technology, Japan, Osaka University, University of Yamanashi, InterRisk Research Institute and Consulting, Inc., Polytech Add, Co. Ltd.

References

Arnesen, A. K. M., "Availability of Fluoride to Plants Growth in Contaminated Soils," *Plant Soil*, 191, 13–25 (1997).

Babaolu, M., Gezgn, S., Topal, A., Sade, B., and Dural, H., "A Boron Hyperaccumulator Plant Species that May Phytoremediate Soils with Toxic B Levels," *Turk. J. Bot.*, 28, 273–278 (2004).

Fujiwara, T., Eguchi, S., Matsunaga, T., and Matoh, T., "Boron Nutrition of Crop Plants," *Japanese Soil and Nutrient Society Journal*, 75(3), 393–398 (2004).

Katsumi, H., "Studies on the Effect of Low-Concentration Atmospheric HF on Plants," *Fukui Agricultural Experiment Station Report (in Japanese)*, No. 8, 1984, pp. 12–24.

Parkpian, P., Tingsanchali, T., Polprasert, C., and Ozaki, H., "Soil and Groundwater Pollution Focusing on Toxic Elements and Pesticides in Thailand," *Proceeding of the Tenth Symposium on Groundwater and Soil Contamination and Remediation*, Geo-environmental Protection Center, Osaka, Japan, 2004, pp. 804–811.

U.S.EPA, "Brownfields Technology Primer: Selecting and Using Phytoremediation for Site Cleanup," Office of Solid Waste and Emergency Response, USEPA, 2001.

U.S.EPA, "Using Phytoremediation to Clean up Sites," U.S.EPA homepage (http://www.env.go.jp/superfund/phyto.htm), 2004.

Yamada, H., "Biogeochemical Studies on the Absorption of Fluorine by Plants," *Kyoto Prefectural University Report (in Japanese)*, No. 32, 1980, pp. 138–170.

Journal of ASTM International, Vol. 3, No. 7
Paper ID JAI13324
Available online at www.astm.org

Miah M. Hussainuzzaman[1] *and Hiroshi Yokota*[2]

Efficiency of Arsenic Removal Unit Working in Bangladesh and Cement Stabilization of Its Sludge

ABSTRACT: To supply safe water to the arsenic affected community, an arsenic removal unit, gravel sand filter (GSF), was developed by modifying the pond sand filter (PSF) so that it can be used to overcome the dry season low flow problem of it. Performance data of that arsenic removal unit shows that it can be the most suitable option to solve that problem of the PSF. GSF uses the naturally occurring iron to remove arsenic by coprecipitation. In this process it produces arsenic rich iron sludge. Disposal of this sludge to the nature may pose a risk of secondary contamination to the stratum. Leaching tests of the arsenic rich iron sludge and the solidified sludge with cement indicates that arsenic leaching ratio of sludge ranges between 3 and 13 % and that of cement stabilized sludge is between 1 and 6 %. This means that the arsenic has a strong bond with the iron sludge and its treatment may not be difficult.

KEYWORDS: arsenic, cement stabilization, leaching, sludge

Introduction

Arsenic contamination in the groundwater of Bangladesh is the most catastrophic arsenic poisoning in the history of water supply. According to the survey report conducted by the government and British Geological Survey, an estimated 35 million people are exposed to the risk of arsenic greater than 50 ppb concentration (Bangladesh standard for arsenic in potable water) in the drinking water (BGS, 2001) (Ahmed 2003). The arsenic containing sediments that formed this deltaic plain causes this pollution (Islam and Uddin 2003; Kinniburgh et al. 2003). The majority of the rural population of Bangladesh depend on groundwater for domestic water requirement (Ahmed 2003). Therefore, it is very important to find a way out to get safe water with arsenic below the acceptable concentration for drinking water. One alternative may be the use of surface water, but surface water is polluted by microbial contaminants, which also needs treatment. Besides, due to the increase of pisciculture in the ponds and other water bodies it is difficult to find a suitable source of surface water, because, those water are chemically and biologically loaded with fish feed. To find a sustainable solution to this problem, many government and nongovernment organizations are presently working in Bangladesh.

Background

Several laboratory researches have been conducted by the researchers aiming the use of naturally occurring iron for arsenic removal from iron-rich groundwater of Bangladesh. Mamtaz and Bache (2001) demonstrated that adsorption and coprecipitation with iron followed by settlement could remove significant amounts of arsenic provided that there is sufficient iron and a sufficient settling time ($>=3$d). They mentioned this method having considerable promise as a low-cost technique because of the total absence of added chemicals. Leupin and Hug (2005) showed that a few cycles of aeration of synthetic groundwater and subsequent filtration through quartz sands containing zero-valent iron fillings could bring arsenic down from 0.5 mg/L to below 0.05 mg/L. Along with arsenic, most of the added phosphate in the synthetic water was also removed by this process without an added oxidant.

The university of Miyazaki has been working on the cause and remediation of arsenic poisoning in

Manuscript received March 31, 2005; accepted for publication October 24, 2005. Presented at ASTM Symposium on Contaminated Sediments: Evaluation and Remediation Techniques on 23–25 May 2006 in Shizuoka, Japan; M. Fukue, K. Kita, M. Ohtsubo, and R. Chaney, Guest Editors.

[1] Ph.D. Student, University of Miyazaki, Miyazaki, Japan 889 2192.
[2] Professor, University of Miyazaki, Miyazaki, Japan 889 2192.

Bangladesh since 1997. Pond sand filter (PSF) has been developed and constructed in some severely arsenic affected villages to provide safe water to the villagers. Those PSFs were supplying safe water to the villagers with an excellent performance (Yokota et al. 2001). But in dry season these units cannot work properly due to the lack of water in the ponds. This situation compelled the users of those units to use the arsenic contaminated tube well (TW) water. Reexcavation of the ponds is expensive and might not be sustainable. So, it was necessary to find an alternative solution to this problem of the PSF.

The PSFs had a horizontal roughing filter attached to it as a pretreatment unit for the high turbid pond water. The interparticular spaces of the gravels in that roughing filters worked as a mechanical strainer as well as a bunch of mini settling basins to remove the turbidity. It was thought that settling basin property of the roughing filter could be utilized to remove the settable arsenic rich iron flocs, which can be produced as a result of oxidizing the iron rich ground water of Bangladesh. This hypothesis was tested in laboratory; later, batch tests in the rural Bangladesh showed positive results regarding arsenic removal from iron rich ground water by oxidizing it and passing it through the similar setting of the roughing filters (Hamabe et al. 2004). Based on those test results an arsenic removal unit, structurally similar to the PSF, has been developed to overcome the low flow problem encountered by it during dry season. It was constructed at Marua village of Chougacha upazila of Jessore district in eastern Bangladesh (near 23°15.25′N, 89°05′E as observed on the "small area atlas of Bangladesh" published by Bangladesh Bureau of Statistics, 1989).

The developed unit has operated about two years solely with groundwater to evaluate its long term performance as well as to adjust its setting for the finest performance. The groundwater contained arsenic conc.=0.217 mg/L, (Std. Dev.=0.038, averaged from 30 measurements, by atomic absorption spectrophotometer, Shimadzu AA 680) and total iron conc.=4.68 mg/L, (Std. Dev.=1.03, averaged from seven measurements by spectrophotometer Hach DR2010, Shimadzu UV-1600) but there is temporal variation of concentrations of these parameters (BGS 2001). In this paper, performance of GSF has been discussed briefly. The unit produces arsenic rich iron sludge in the process of arsenic removal, which is washed out periodically. The washed sludge is allowed to settle in an underground reservoir where other natural debris, i.e., washed soil particles, leaf, etc., also mixes up naturally. That sludge has been collected and tested for its arsenic leaching characteristics. The leaching test results have also been presented in this paper. But before going into that discussion, the working principle of the GSF will be discussed.

Gravel Sand Filter

The gravel sand filter (GSF) consists of four major units: inlet, gravel chambers, slow sand filter (SSF), and reservoir (Fig. 1). Water from the tubewell passes through gravel roughing filters and the sand filter before reaching the supply tap. Water flows from the pump to the inlet chamber and then flows to the gravel tank/chamber 1 through the bottom holes of the partition wall between them. Average diameter of gravel in the gravel chambers and outlet are about 5 mm but drain section at the bottom of the chambers contain larger gravels up to an average diameter of 20 mm. Water flows diagonally along the chamber to reach the holes, located near the upper part of the partition wall between gravel tank 1 and gravel tank 2. In gravel tank 2, water flows diagonally downward and enters into the outlet chamber of the roughing filters through the bottom holes in the partition wall. Then water spills over to the sand filter through a groove in the partition wall between them. In the sand filter water flows vertically down and is collected through the bottom drainage section consisting gravels and goes to the reservoir section. The users collect water by opening the tap of the reservoir/supply tank.

In this process, water gets aeration in the inlet chamber which helps chemically (Deutsch 1997) turning divalent iron (Fe^{2+}) and trivalent arsenic (As^{3+}) to their oxidized trivalent iron (Fe^{3+}) and pentavalent arsenic (As^{5+}) compounds respectively. In the prevailing pH range of the water, Fe^{3+} forms relatively insoluble ferric hydroxide [$Fe(OH)_3$] (Peavy et al. 1985). Arsenic ions have strong adhesion toward the $Fe(OH)_3$ particle surface and hence are adsorbed there (Ali and Ahmed 2003). Then, while flowing through the gravels in the roughing filters, the particles experience sudden constrictions, leading to flocculation, and then wider areas, leading to slower flow and hence, settling. Thus the arsenic containing iron sludge is being deposited in the inter-particular space of the gravels and relatively arsenic free water passes through the next sections. Thus arsenic is being removed from groundwater. In this process the gravel chambers gradually get clogged with accumulated arsenic rich iron sludge and eventually stops the flow. In such situations when flow rate falls, bottom drain valves of the gravel chambers are opened for some time to allow the sludge being washed out. The sludge is accumulated all over the gravels in the gravel

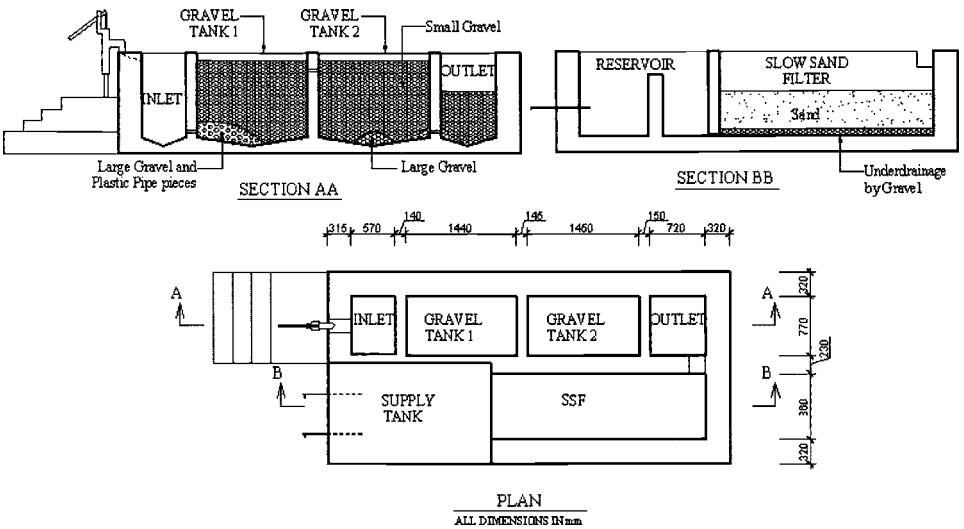

FIG. 1—*Diagram of the modified gravel sand filter (GSF).*

tank. Cleaning by backwashing is not enough to bring out all the sludge from all the parts of the gravel tank. Only sludge accumulated near the drain zone is being washed out. Majority of the sludge being accumulated near the bottom due to gravity force, so, small amount of sludge remains accumulated in the gravel after the backwashing. But after several backwashing the accumulated sludge in the upper part of the gravel tank becomes large enough to clog the flow. Therefore, thorough cleaning of the gravel, by taking them out of the tank and placing them inside after cleaning becomes necessary. In the field such severe clogging occurred almost once in every three months.

The washed sludge flows to an underground reservoir, where it settles down along with other debris that may fall in the drains and the reservoir from the surroundings. The supernatant water from that underground reservoir flows to a lined pond for expected further bioremediation (Stolz et al. 2002) before flowing to a natural pond. The method of monitoring and maintaining along with the data analysis has been provided in the following sections.

Methods

Field and laboratory measurements were performed for several parameters, i.e., dissolved oxygen content (DOC), oxidation-reduction potential (ORP), arsenic (As) and iron (Fe), from different sampling points throughout the unit. Sampling points in the gravel chambers were pre-installed vertical PVC tubes of 38 mm diameter reaching at different depths into the gravels. Before the measurements, tubes were purged to allow fresh water from the gravel inside the tube. The analysis of the collected data gave a better understanding of the processes going on inside the newly built unit during December 2003 to January 2004 period. During another field visit and measurements in January 2004, after one year of operation, some modification/rearrangements were made to solve some maintenance problems encountered by the users.

The modification is done because the users reported about clogging problem of the unit. To reduce clogging the pore volume of the bottom large gravels in the drain section is increased by introducing small pieces of polyvinyl chloride (PVC) plastic pipes (Fig. 1). PVC pipe of 18 mm diameter has been cut into 25 mm long pipe pieces; to make such cutting locally available cutter used for cutting PVC pipe strainer openings was used. Therefore, the 20–30 mm gravels, used at the bottom drain zone of the gravel tank, had similar sizes of those small pipe pieces. It was expected that a pipe piece would occupy almost same volume as large gravel, but would leave a considerable amount of empty space inside the hollow cylindrical piece helping an increase of pore volume of the drain zone. Any ratio of mix would increase the porosity by some degree and this presumption has been checked out by a simple test where equal volume

of cut pieces of PVC pipes has been mixed with gravel, all measured by buckets. The volume of water required to overflow a bucket filled with (a) only large gravels and (b) large gravel and pipe piece mix has been measured. After five trials the measured average water volumes required were 37.2 and 56.3 % of the bucket volume, respectively. A comparison of the porosity of coarse gravels (Todd 1980), which shows 28 % porosity for 16–32 mm sized gravels, ensures the justification of this measurement as the samples used here were more uniform in particle size. This test verified the expectation of porosity increase, which was hoped to solve the frequent clogging problem of the gravel filter. A longer clogging cycle was expected by this modification.

Periodical (twice a month) water samples were also collected from different parts of the unit and arsenic concentrations was checked to track the malfunctioning part as well as the efficiency of the unit. Data showed a malfunction of the unit causing increased arsenic concentration in the supply than the concentration of arsenic in water before it passed the sand filter. Investigation showed that it was due to the clogging of the sand bed with finer particles. Along with problems of lower flow it created a reducing situation inside the sand causing arsenic leaching back to the water. This problem was solved by periodical scraping of the sand surface (Hussainuzzaman et al. 2004). Among other parameters, total daily water consumption by the users is recorded from an attached water meter at the supply tap. During field measurements with the unit, a model pumping pattern, consisting of a two minute pumping followed by a three minute rest, was maintained with a view to mimic the actual stop-go-stop type flow experienced by the unit.

Besides these water samples for arsenic and flow data, samples were also collected from the accumulated sludge in the underground reservoir, once a month. The sludge tank is cleaned twice a year hence the collected sludge sample comprises of sludge from different months washouts. Sludge samples were then allowed to settle for 2/3 days in glass containers and the supernatant water had been spilled out. Then the semisolid compound has been stored in laboratory grade airtight plastic containers and brought back to the laboratory of the university of Miyazaki at Japan. The semisolid materials were air-dried and then oven dried for about 24 h in 105 °C. The dried material is then crushed in sieved to take out particles larger than 2 mm. Samples were then tested for total arsenic determination, leaching tests with and without cement solidification.

Cement stabilized sludge samples were prepared by hand mixing the dry sieved sludge with ordinary Portland cement at three different cement to sludge ratios (wt. cement/wt. dry sludge): 0.02, 0.1, and 0.2 respectively. Then distilled water was used to provide hydration water at a water to sludge ratio (wt. water/wt. dried sludge) of 0.2. They were mixed thoroughly with steel spatula and stored in airtight plastic containers for 28 days and then pulverized before leaching test. The leaching tests were done according to the Japanese standard procedure for leaching test (JLT 46[3]), which includes: oven drying sludge and smash it to take only that part having a maximum particle size of 2 mm; then put distilled water at a solid/water mass ratio of 0.1 and then put it into a shaker with 200 cycle/s, 4–5 cm shaking for 6 h; then the water is separated from the solid by centrifuging it at 3000 rpm for 20 min; then the liquid part is filtered by 0.45 μm filter paper to get the leachate; the leachate was tested with a Hydride-generation atomic absorption spectrophotometer (AAS, Shimadzu AA-6650).

Determination of total arsenic content of the sludge was performed following Japanese standard process of solid extraction (JLT 46). In this process digestion of the soil sample (2 g) was performed with concentrated nitric acid (15 ml) and 1:1 sulfuric acid (15 ml) on a hot plate (below 300 °C). More nitric acid (10 ml) was added when the liquid is decreased approximately to 15 ml. This process was repeated until white smoke came out following brown gas. Then for two or three times distilled water (15 ml) was added with the cooled liquid and heated again. The mix was then cooled at room temperature and was being filtered with a glass fiber filter (0.45 μm), volume adjusted to 100 ml with distilled water and stored for testing with AAS.

Sludge samples were tested for total arsenic content as well as for the leaching properties of arsenic. Leaching test data for sludge along with its stabilization experiments with cement has been presented in the following sections. Chronological arsenic removal performance data before and after increasing the gravel pore volume by applying PVC pipe pieces (as mentioned before) has also been presented and compared.

[3]Association for Environmental Measurement & Analysis in Japan. *The bottom sediment test methods* (as listed in the environmental agency notification no. 46; published in 2001, pp 1511–1514, in Japanese)

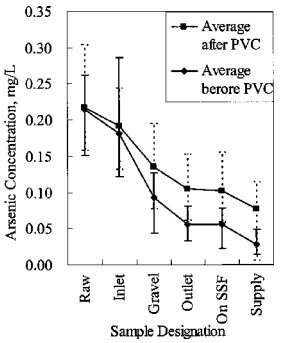

FIG. 2—*Comparison of arsenic removal performance before and after putting PVC pipe pieces at the drain section of the gravel tank 1; error bars indicate data range.*

Results and Discussions

Arsenic Removal Performance

Arsenic removal performance data is obtained from the periodical samples' test results by hydride-generation atomic absorption spectrophotometer (AAS; Shimadzu AA-660). Results show that the arsenic removal performance met the Bangladesh standard (concentration below 0.05 mg/L) before the application of the PVC pipe pieces. But after this modification to reduce clogging problem, the arsenic removal performance deteriorated (Fig. 2).

In Fig. 2, Raw indicates the raw water sample; Inlet indicates the sample obtained from the mid-depth section of the inlet chamber; Gravel indicates the sample obtained from gravel tank 1, near the holes through which water passes from gravel tank 1 to gravel tank 2; Outlet indicates the sample from the surface of the outlet section, just before overflowing to the SSF; and, Supply indicates samples collected from the supply tap. Average after PVC indicates the average arsenic concentration data of the samples collected after applying PVC pipe pieces, it comprises of 18 data points from February 14, 2004 to November 21, 2004. On the other hand, Average before PVC is developed from the average data before that modification with PVC pipe pieces; it comprises of 11 data from July 12, 2003 to January 13, 2004. The figure shows that the slope of the lines from outlet to supply remains the same before and after the modification. The deterioration is concentrated around gravel chambers, which have some influence over inlet and outlet sections.

The reason for this deterioration might be explained by the changed sludge accumulation pattern as observed during cleaning of gravel tank due to low flow situation. A thick, sticky mud like sludge cluster was observed in the gravels near the inlet holes, spreading about 20–50 cm from the holes as the gravel chambers were cleaned with the initial setting. In that situation, the passing water and oxidized iron flocs and arsenic were forced to pass through that sludge-packed region, which resulted high removal efficiency. On the other hand, when the clogged gravel tank was cleaned after applying PVC pipes, absence of such sticky mud like sludge cluster was noticed within the initial 0–15 cm from the inlet holes. Instead, thick sludge cluster was observed about 15 cm away from the inlet holes spreading along the drainage zone. This change of sludge accumulation pattern might have resulted from the difference of porosity between the small gravels and the large gravels in drain zone. Before applying the PVC pipes, the pore fraction of the large and small gravels were almost the same (measured average value, 35.2 % in small gravels and 37.2 % in large gravels). Therefore, sludge tended to settle at the vicinity of the entrance holes of the gravel tank 1. But with the new setting the drainage section near the bottom had more empty spaces for sludge accumulation. Therefore, most of the sludge bulk was flown to and being accumulated in that region leaving the entrance hole vicinity relatively clean. Water was not forced to pass through the gravels and thus chance of contact between arsenic and iron sludge became low resulting reduced removal and efficiency. Besides, channeling within the accumulated sludge in relatively large pore space might have played a role in this case (Ali et al. 2001).

TABLE 1—*Arsenic content test result for sludge.*

Sample ID	Source GSF No.	Collection date	pH	Arsenic content, mg/kg
1-6	GSF#1	28-Jun-2003	6.9	66.47
1-7	GSF#1	27-Jul-2003	6.7	48.16
1-8	GSF#1	30-Aug-2003	6.8	68.49
2-6	GSF#2	28-Jun-2003	7.0	10.19
2-7	GSF#2	27-Jul-2003	7.1	11.80
2-8	GSF#2	30-Aug-2003	6.9	18.97

Besides arsenic, total iron concentration of the treated water was below 0.01 mg/L (measured by Hach DR2010). In fact, almost all the iron is removed before water reaches the second gravel tank (in Fig. 1). Measured oxidation-reduction potential (ORP) of groundwater always was negative ($ORP < -100$) indicating a reducing state but treated water had positive ORP all the time. The ORP shifts from negative to positive indicating reducing to oxidizing state in the gravel tank 1 and continues rising along the water flow path at gravel tank 2. Dissolved oxygen content ($DOC = 1.3$ mg/L) showed a fall of its concentration along the water path through the gravel tanks as the DOC being used up by iron and arsenic as well (Hussainuzzaman et al. 2004). During these field measurements (December 02–January 03 and January 04) model pumping flow rate was approximately 720 litres/hour. The flow meter data (October 31, 2004 to November 21, 2004) reveals that average daily water consumption was about 1500 liters.

Arsenic Leaching Test from Sludge

The iron sludge accumulates arsenic and hence it may pose a risk of secondary contamination if not disposed properly. Generally the arsenic concentration of the soil stratum in Marua village is very small. Most of the arsenic is contained in a clay layer, where the highest arsenic concentration is about 20 mg/kg (Tanabe et al. 2001). Therefore, delivering this arsenic bearing iron sludge to the surrounding soil may not be a good option of disposal because of probable leaching of arsenic. Ali et al. (2003) checked the leaching of arsenic from some common arsenic treatment units operating in Bangladesh and found by the TCLP test that, in general, leaching of arsenic from the wastes was not significant and that none of the waste samples were "hazardous" as defined by the USEPA. But leaching with groundwater showed higher leachability of arsenic from some samples, by which, they suggested that TCLP test did not appear to be appropriate for assessing long-term leaching of arsenic from treatment wastes. Badruzzaman (2003) showed that in the field disposal conditions, as practiced by the users of arsenic removal systems in rural Bangladesh, a significant amount of arsenic is lost from sludge through biomethylation induced by the presence of organic matters.

Therefore the arsenic bearing sludge should be stabilized by some means. Jing et al. (2005) stated that cement treated arsenic sludge showed reduced leachability of As(III) in TCLP tests. They also showed that longer curing time of cement stabilized waste material reduces the As(III) leachability further. Phenrat et al. (2005) showed that arsenic can be chemically fixed into cementitious environment of solidified/stabilized matrices by three important immobilization mechanism; sorption onto C-S-H surface, replacing SO_4^{2-} or ettringite, and reaction with cement components to form calcium-arsenic compounds, the solubility limiting phases. Dermatas et al. (2004) checked the arsenic leachability of quicklime-fly ash stabilized field and artificial soil samples in a semidynamic leaching test by measuring the effective diffusion coefficient. They found that solidified/stabilized samples had lower leachability of arsenic. They also found that precipitation is the dominant mechanism of arsenic immobilization. Mollah et al. (2004) showed that the early hydration of cement inhibited by the presence of AsO_4^{3-}, and that the inhibition is mainly caused by the formation of highly insoluble $Ca_3(AsO_4)_2$ on the surface of hydrating cement particles. They concluded that Portland cement may be considered as a potential matrix to immobilize As(V) bearing wastes.

Therefore it can be expected that stabilizing the arsenic rich sludge with cement can reduce leaching of arsenic from it to the environment. To evaluate the possibility of arsenic leaching and its stabilization with the prevailing situation, leaching tests were performed with collected sludge and cement stabilized sludge. Test results are presented in Tables 1–3.

Table 1 shows the total arsenic content in the sludge along with its pH. Table 2 shows leaching of arsenic from the sludge, cement stabilized sludge (containing 2 and 10 % cement), pH of the leachate, and

TABLE 2—*Elution test result for arsenic sludge.*

Sample ID	Arsenic leaching							
	Sludge Only		sludge+2 % Cement			Sludge+10 % Cement		
	mg/kg	%	pH	mg/kg	%	pH	mg/kg	%
1-6	2.04	3.08	10.5	1.09	1.64	11.8	0.80	1.20
1-7	2.04	4.28	10.7	0.93	1.94	11.8	0.82	1.71
1-8	2.72	3.97	10.7	1.25	1.83	11.8	0.86	1.25
2-6	0.91	8.92	10.9	0.59	5.83	11.8	0.35	3.42
2-7	1.51	12.82	10.8	0.51	4.30	11.9	0.41	3.45
2-8	1.18	6.21	10.9	0.78	4.09	11.8	0.44	2.31

the percentage of total arsenic as shown in Table 1. Table 3 contains data of tests with a different set of samples. It contains the total arsenic content of the sample along with the leached arsenic from sludge without any cement and with 20 % cement.

GSF 1 refers to the GSF of this discussion and GSF 2 is another GSF located in the same village but with different design, input water quality and number of users than GSF 1. Results show wide variation of total arsenic content of the collected sludge. This variation is not easy to explain because in reality the sludge settles in the underground reservoir in an uncontrolled environment. Therefore, the amount of foreign materials, carried by runoff from its surrounding, varies with time and level of maintenance of the unit. Besides, the settled sludge may have spatial variation in concentration along the reservoir bed because of the point source with respect to the reservoir. Therefore two grab samples, collected simultaneously from different locations at the reservoir bed, may result in different concentrations of total constituents as well as leaching.

Result of the test (Table 2) shows that 3.8 to 12.82 % of the arsenic leaches out of the sludge. Therefore 85–95 % of the arsenic is confined into the sludge. The leaching figures ranging from 0.12 to 0.27 mg/L meet the criteria for industrial sludge disposal site in Japan but exceed the World Health Organization (WHO) guideline value for leaching (0.01 mg/L) by a wide margin.

The decreasing tendency of arsenic leaching with increasing amount of cement (Table 2 and Fig. 3) associates higher pH. In this condition calcium (source=Portland cement) arsenate solids may have formed, which are stable under this condition and hence prevent the release of arsenic (Khoe et al. 1997; Mollah et al. 2004). With a different batch of samples, an increased amount of cement has been used to further verify the stabilization effect. The results are very much in line with the previous results as shown in Table 3. Therefore, cement stabilization of sludge might be a very effective way for safe sludge disposal in the prevailing field condition. Carbonation of the cement-stabilized sludge in humid conditions might reduce this high pH associated with the use of Portland cement (Gervais et al. 2004).

Conclusions

This study shows the long term performance data of a community based arsenic removal unit which was developed to solve the low flow problem encountered by the existing PSFs during the dry season. The long-term data shows that the unit performs efficiently to remove arsenic from tubewell water (raw water arsenic=0.217 mg/L) and produces safe drinking water (arsenic concentration below 0.05 mg/L). This process is very cost efficient as no additional chemical is needed and it uses the naturally occurring iron of groundwater. The only problem associated with the system is maintenance, which includes clogging of the

TABLE 3—*Leaching test results for cement stabilized and nonstabilized arsenic sludge.*

Sample ID	Collection date	Total arsenic content, mg/kg	Leaching, mg/kg		Percent leaching		pH condition	
			Without cement	With 20 % cement	Without cement	With 20 % cement	Without cement	With 20 % cement
GSF-1	26-Jun-03	269	1.08	0.04	0.40	0.01	7.53	12.26
GSF-1	31-Jan-04	81	6.43	0.12	7.94	0.14	7.75	12.29
GSF-1	27-Mar-04	19	1.36	0.10	7.17	0.53	8.13	12.31
GSF-2	26-Jun-03	24	0.46	0.02	1.89	0.10	7.65	12.19
GSF-2	31-Jan-04	228	1.49	0.47	0.65	0.20	7.80	12.24
GSF-2	29-May-04	55	4.60	0.21	8.42	0.39	7.85	12.09

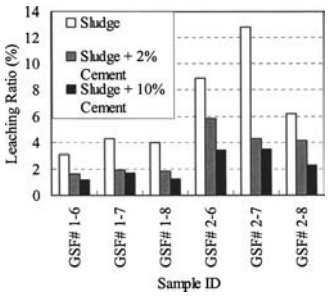

FIG. 3—*Comparison of arsenic leaching from stabilized sludge with different cement content.*

gravel filter requiring thorough cleaning of the gravels once about every three months. Therefore, to make the system more efficient and to use it solely as a good arsenic removal unit, this clogging problem should be solved or an easy maintenance system should be developed.

The unit produces arsenic rich iron sludge, which may pose a risk of secondary contamination of the environment by the leached arsenic if not disposed properly. This study also checked the possibility of cement stabilization of the sludge in the prevailing condition. Data shows that arsenic leaching has been reduced by solidification/stabilization with cement. An increase of cement amount in the stabilization process increased the stabilization efficiency as less arsenic is leached out in that case. The first batch experiments showed arsenic leaching between 3 and 13 % and for raw sludge while stabilization with 2 % cement reduced that to 1.5–6 % (Table 2). A further increase of cement to 10% has decreased leaching to 1–3.5 %. Use of 20 % cement for stabilization with a different sample set showed a decrease of leaching from the 0.4–8.5 % range to the 0.01–0.55 % range. Higher pH associated with the increase of cement for stabilization seems to be a common problem like any other material containing cement. Therefore it appears that safe disposal of arsenic rich sludge may not be a problem.

Acknowledgments

This research has received financial assistance from the scientific research fellowship grant from the government of Japan. Our gratitude to the local NGO (nongovernment organization) Asia Arsenic Network (AAN), and the Marua Arsenic Committee for providing support during the field visits/measurements.

References

Ahmed, M. F., "Arsenic Contamination Of Groundwater In Bangladesh," *Arsenic Contamination: Bangladesh Perspective*, edited by M. F. Ahmed, ITN-Bangladesh, Dhaka, Bangladesh, 2003, pp. 42–62.

Ali, M. A. and Ahmed, M. F., "Environmental Chemistry of Arsenic," *Arsenic Contamination: Bangladesh Perspective*, edited by M. F. Ahmed, ITN-Bangladesh, Dhaka, Bangladesh, 2003, pp. 21–41.

Ali, M. A., Badruzzaman, A. B. M., Jalil, M. A., Ahmed, M. F., Kamruzzaman, M., Rahman, M. A., and Masud, A. A., "Fate of Arsenic in Wastes Generated from Arsenic Removal Units," *Fate of Arsenic in the Environment*, edited by M. F. Ahmed, M. A. Ali, and Z. Adeel, ITN Centre, BUET on behalf of the Bangladesh University of Engineering and Technology and the United Nations University, Dhaka, Bangladesh, 2003, pp. 147–159.

Ali, M. A., Badruzzaman, A. B. M., Jalil, M. A., Hossain, M. D., Hussainuzzaman, M. M., Badruzzaman, M., Mohammad, O. I., and Akhter, N., "Development of low-cost technologies for removal of arsenic from groundwater," *Technologies for arsenic removal from drinking water*, edited by M. F. Ahmed, M. A. Ali, and Z. Adeel, The editors on behalf of the Bangladesh University of Engineering and Technology and the United Nations University, Dhaka, Bangladesh and Tokyo, Japan, 2001, pp. 99–120.

Badruzzaman, A. B. M., "Leaching of Arsenic from Wastes of Arsenic Removal Systems," *Fate of Arsenic in the Environment*, edited by M. F. Ahmed, M. A. Ali, and Z. Adeel, ITN Centre, BUET on behalf of the Bangladesh University of Engineering and Technology and the United Nations University, Dhaka, Bangladesh, 2003, pp. 161–179.

British Geological Survey (BGS), *Arsenic Contamination of Groundwater in Bangladesh*, Vol.1: Sum-

mary, February 2001.

Dermatas, D., Moon, D. H., Menounou, N., Meng, X., and Hires, R., "An Evaluation of Arsenic Release from Monolithic Solids Using a Modified Semi-Dynamic Leaching Test," *J. Hazard. Mater.* 116(1–2), pp. 25–38 (2004).

Deutsch, W. J., "Solution, Redox, and Gas Exchange Processes," *Groundwater Geochemistry: Fundamentals and Applications to Contamination*, Lewis Publishers, Florida, 1997, pp. 27–45.

Gervais, C., Garrabrants, A. C., Sanchez, F., Barna, R., Moszkowicz, P., and Kosson, D. S., "The Effects of Carbonation and Drying During Intermittent Leaching on the Release of Inorganic Constituents from a Cement-Based Matrix," *Cem. Concr. Res.* 34(1), pp. 119–131 (2004).

Hamabe, K., Yokota, H., Tanabe, K., RGAG, and NIPSOM, "Arsenic Contamination of Soil and Arsenic Removal from Groundwater in Bangladesh," *Sustainability of Water Resources*, edited by Professor Goen Ho and Dr. Kuruvilla Mathew, International Water Association, London, UK, 2004, pp. 41–48.

Hussainuzzaman, M. M., Setoyama, Y., Kataoka, D., and Yokota, H., "Performance and Mintenance of Arsenic Removal Unit Installed at Bangladesh," *Proceedings of the International Symposium on Lowland Technology*, edited by Norihiko Miura, Organizing body: International Association of Lowland Technology; Institute of Lowland Technology, Saga University; Faculty of Engineering, Kasetsart University; Asian Centrer for Soil Improvement and Geosynthetics, Asian Institute of Technology, Thailand, 2004, pp. 511–516.

Islam, M. N., and Uddin, M. N., "Hydrogeology and Arsenic Contamination in Bangladesh," *Arsenic Contamination: Bangladesh Perspective*, edited by M. F. Ahmed, ITN-Bangladesh, Dhaka, Bangladesh, 2003, pp. 101–133.

Jing, C., Liu, S., and Meng, X., "Arsenic Leachability and Speciation in Cement Immobilized Water Treatment Sludge," *Chemosphere* 59(9), 1241–1247 (2005).

Khoe, G. H., Zaw, M., and Emett, M. T., "Immobilisation of Arsenic and Stability of the Solid Waste," *Proc. Water Treatment and Residues Management-Conventional and Innovative Solutions, WISMUT-haus, Kirchoffstrasse 34–36, Chemnitz*, September 24 to 26 1997.

Kinniburgh, D. G., Smedley, P. L., Davies, J., Milne, C. J., Gaus, I., Trafford, J. M., Burden, S., Huq, S. M. I., Ahmad, N., and Ahmed, K. M., "The Scale and Causes of the Groundwater Arsenic Problem in Bangladesh," *Arsenic in Groundwater: Geochemistry and Occurrence*, edited by A. H. Welch and K. G. Stollenwerk, Kluwer Academic Publishers, Boston, 2003, pp. 211–257.

Leupin, O. X. and Hug, S. J., "Oxidation and Removal of Arsenic (III) from Aerated Groundwater by Filtration Through Sand and Zero-Valent Iron," *Water Res.* 39(9), pp. 1729–1740 (2005).

Mamtaz, R. and Bache, D. H., "Low-Cost Technique of Arsenic Removal from Water and its Removal Mechanism," *Technologies for Arsenic Removal from Drinking Water*, edited by M. F. Ahmed, M. A. Ali, and Z. Adeel, The editors on behalf of the Bangladesh University of Engineering and Technology and The United Nations University, Dhaka, Bangladesh and Tokyo, Japan, 2001, pp. 43–58.

Mollah, M. Y. A., Kesmez, M., and Cocke, D. L., "An X-Ray Diffraction (XRD) and Fourier Transform Infrared Spectroscopic (FT-IR) Investigation of the Long-Term Effect on the Solidification/Stabilization (S/S) of Arsenic(V) in Portland Cement Type-V," *Science of the Total Environment*, 325(1–3), 255–262 (2004).

Peavy, H. S., Rowe, D. R., and Tchobanoglous, G., "Engineered Systems for Water Purification," *Environmental Engineering*, edited by K. Verma, and D. A. Damstra, McGraw-Hill, Inc., Singapore, 1985, pp. 110–111.

Phenrat, E., Marhaba, T. F., and Rachakornkij, "A SEM and X-Ray Study for Study for Investigation of Solidified/Stabilized Arsenic-Iron Hydroxide Sludge," *J. Hazard. Mater.* 118(1–3), 185–195 (2005).

Stolz, J. F., Basu, P., and Oremland, R. S., "Microbial Transformation of Elements: The Case of Arsenic and Selenium," *International Microbiology*, 5(4), 201–207 (2002).

Tanabe, K., Yokota, H., Hironaka, H., Tsushima, S., and Kubota, Y., "Arsenic Pollution of Groundwater in Bangladesh," *Appl. Organomet. Chem.* 15, 241–251 (2001).

Todd, D. K., *Groundwater Hydrology*, 2nd Ed., John Wiley & Sons Pte. Ltd., Singapore, 1980, pp. 28–29.

Yokota, H., Tanabe, K., Sezaki, M., Akiyoshi, Y., Miyata, T., Kawahara, K., Tshushima, S., Hironaka, H., Takafuji, H., Rahman, M., Ahmad, S. A., Sayed, M. H. S. U., and Faruquee, M. H., "Arsenic Contamination of Ground and Pond Water and Water Purification System Using Pond Water in Bangladesh," *Eng. Geol. (Amsterdam)* 60, 323–331 (2001).

Journal of ASTM International, Vol. 3, No. 6
Paper ID JAI13319
Available online at www.astm.org

Masaharu Fukue,[1] *Taro Minato,*[2] *Koji Uehara,*[3] *Yoshio Sato,*[4] *Tomohiro Inoue,*[5] *and Shoichi Yamasaki*[6]

Development of Filtration System for Removal of Contaminated Suspended Solids in an Enclosed Sea Area

ABSTRACT: The quality of seawater can be improved by removing suspended solids (SS) that may adsorb hazardous substances, such as heavy metals, polycyclic aromatic hydrocarbons, bacteria, etc. In this study, two types of filtration systems are developed in order to remove SS from sea, lake, and pond water. The first filtration system is a larger system for the rapid reduction of SS, and the other can be used for a slower removal of SS. The features of the smaller system are that solar panels were used as the power source and clogging of the filter can be prevented by a reverse water flow with an automatic control. Long-term in situ experiments showed that SS were almost completely removed by filters made of granular materials. Removal capacity was dependent primarily on both the sectional area of the filter and the relationship between the permeability of filter materials and the size of the SS. With treatment, good water quality was obtained in terms of SS, chemical oxygen demand and concentrations of nutrients.

KEYWORDS: suspended solids, filtration, enclosed sea, eutrophication, heavy metals

Introduction

Various substances are discharged into the sea through anthropologic activities. Additionally, hazardous substances have accumulated in sea animals as a result of the pollution of seawater and its sediments.

Eutrophication has been described as one of the biggest environmental problems in enclosed sea areas (Suzumura et al. 2004; Sfriso and Marcomini 1999). Eutrophication results in the production of excessive phytoplankton that can trigger the occurrence of a red tide. Red tide causes a reduction of dissolved oxygen in water and may subsequently kill fish and shellfish.

Rehabilitation of marine environments can be achieved by the recovery of substances that have been released into the sea. To accomplish this recovery, bioaccumulation and sorption characteristics of solids can be conveniently used (Gifford et al. 2004). For example, nutrients released into seawater are first taken up by phytoplankton. Therefore, the removal of phytoplankton would directly prevent eutrophication.

In order to clean up polluted sea areas, both the sediments and seawater require treatment. The dredging of polluted sediments and sand capping of polluted sediments are used to decontaminate sediments. To preserve the environment after such artificial treatments, improvements in natural depuration are inevitably required. Therefore, complete rehabilitation of coastal environments can be achieved by the recovery of natural depuration, which consists of physical, chemical, biological, and/or combined treatments. To achieve improved recovery of contaminants by the use of a natural purification system, high quality seawater is required. For example, sea grass, which forms marine biomass, requires sunlight for photosynthesis. Algal (phytoplankton) blooms cloud the water and block sunlight, which causes underwater sea grasses to die. The dredging of sediments often causes a resuspension of sediment particles (Lohrer and Wetz 2003; Mulqueen et al. 2004). Since pollutants are adhered to sediment particles, the diffusion of

Manuscript received April 6, 2005; accepted for publication July 15, 2005. Presented at ASTM Symposium on Contaminated Sediments: Evaluation and Remediation Techniques on 23–25 May 2006 in Shizuoka, Japan; M. Fukue, K. Kita, M. Ohtsubo, and R. Chaney, Guest Editors.

[1] Professor, Department of Marine Civil Engineering, Tokai University, Shizuoka, 424-8610, Japan.
[2] Research Engineer, Aoki Marine Co., Kobe, 658-0026, Japan.
[3] Manager, Japan Industrial Land Development, Co., Tokyo, 108-8432, Japan.
[4] Professor, Tokai University, Shizuoka, 424-8610, Japan.
[5] Graduate Student, Ocean Engineering, Tokai University, Shizuoka, 424-8610, Japan.
[6] Manager, Aoki Marine Co., Osaka, 553-0003, Japan.

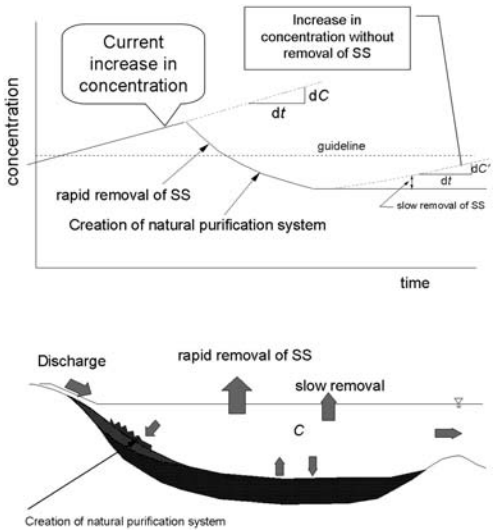

FIG. 1—*Concept of SS removal in enclosed sea areas.*

resuspended particles causes diffusion of the pollutants. To prevent this diffusion of pollutants, the suspended solids (SS) must be collected. Thus, an important treatment for the rehabilitation of coastal environments is water purification.

The primary objective of seawater purification is to remove SS. SS are either solid organic or solid inorganic particles that are held in suspension in a solution. The removal of SS, including phytoplankton, may prevent the occurrence of red tide. Nutrients, such as phosphorus and nitrogen, are generated from sediments when organic matter is decomposed by micro-organisms. The dissolution of nutrients into seawater again causes eutrophication. Therefore, removal of organic matter from seawater will result in a reduction of both the nutrients in seawater and also the organic matter. It is important to note that since SS contain pollutants as high or higher than contaminated sediments (Woitke et al. 2003; Sfriso and Marcomini 1999; Morrison et al. 2001), the removal of SS provides a reduction of hazardous substances from seawater. Thus, techniques for the removal of SS from seawater is a necessity for preservation of coastal environments.

The general concept of SS removal from an enclosed sea area is illustrated in Fig. 1. The final goal of SS removal is to maintain SS concentrations lower than the guidelines. In Fig. 1, "rapid removal of SS" is defined to mean to lower the concentrations of a hazardous substance or nutrient to an acceptable level as soon as possible, while "slow removal of substance" is defined as the maintenance of constant water quality. To achieve the slow removal of SS, substance removal must overcome the increasing rates of substance concentrations, dC/dt and dC'/dt, where C is the current concentration, C' is the concentration after SS removal, and t is time. A combination of the rapid and slow removal of SS is a filtering technique for the preservation of the environment. Bioaccumulation is another method used for the extraction of substances from enclosed sea areas (Sheng et al. 2004; Gifford et al. 2004).

SS Removal

In enclosed sea areas, the accumulation of toxic chemicals is a problematic phenomenon. First, seawater quality may be evaluated by the amount of SS present, where the amount of SS is defined as the dry weight of SS per unit volume of (sea) water. At present, SS retain hazardous substances, such as heavy metals, polycyclic aromatic hydrocarbons (PAHs), chlorinated organic compounds, and nutrients (Morrison et al. 2001). Bacteria, such as *Escherichia.coli* also adhere to SS. Therefore, SS removal provides:

1. Greater transparency

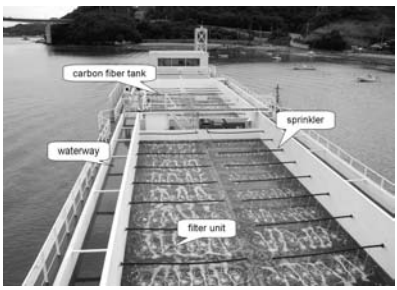

FIG. 2—*Purification vessel floating in Kasaoka Bay.*

2. Improved water quality for bathing
3. Lower frequency of eutrophication
4. Lower frequency of red tide
5. Improved sediment quality

Purification Vessel

Filtration is one of the most reliable techniques to remove SS. To treat a large volume of seawater using filtration, a barge (2350 t) was converted into a purification vessel (Minato et al. 2004). The barge had been used for the transportation of sandy materials for the reclamation of Kansai International Airport.

This purification vessel contained 38 filter units with a total area of 205 m^2. Each filter unit had an area of 1.5 m by 3.6 m and a height of 50 cm. The filter consisted of a steel slag layer with a thickness of 40 cm and a 5-cm-top layer of sea sand. The initial coefficient of permeability of the steel slag was 10^{-3} m/s. In contrast, the coefficient of permeability of the surface sand was 10^{-4} m/s. Thus, the permeability is lower for the upper layer and the filtration of seawater becomes an unsaturated flow in the slag layer. In fact, the steel slag was installed in baskets made from geotextile mesh. Since the steel slag layer has obvious ventilation, the filter units are maintained in an aerobic state during filtration. An outline of the barge is shown in Fig. 2. This purification system was composed of the following equipment:

a. Two pumps with a capacity to move 10 000 m^3 of seawater/day
b. Water tank to allow larger particles of sediment to settle
c. Carbon fibers and tank to collect organic matter
d. Two waterways with connection pipes
e. Filter units

Experimental Site

In July 2003, the vessel (barge) was towed by a tugboat into Kasaoka Bay as shown in Fig. 3. The present

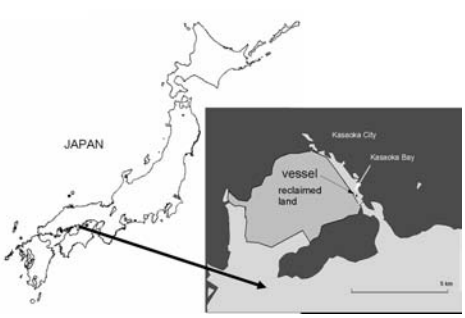

FIG. 3—*Experimental site in Kasaoka Bay.*

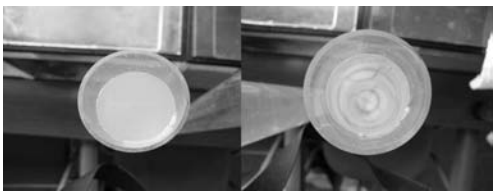

FIG. 4—*Differences in transparency between pumped and filtered seawater.*

geographical features of the bay were formed by environmental reclamation that began in 1972. The length of the bay is approximately 5 km and the width ranges from 50 to several hundred meters. Since the Kasaoka port is located at the northern part of the bay, many boats and ships navigate this narrow route. The bay area is approximately 2 500 000 m^2 and the water volume is 3 200 000 m^3. The range of the tide is approximately 4 m and it causes a rapid water velocity in the bay.

It may be important to note that a specified zone of Kasaoka Bay has been designated as a natural monument for the breeding of the Japanese horseshoe crab, which appears on the endangered list by the Ministry of the Environment of Japan. This experimental site is located in the northern limit of the habitat of this horseshoe crab, although at present, the horseshoe crab is rarely found in this region (Fukue et al. 2001).

Results and Discussion

The purification experiment described here was performed for 80 consecutive days, from August 1 to October 25, 2002. The water samples were pumped and the filtrates were analyzed. The variables measured included SS, dissolved oxygen (DO), chemical oxygen demand (COD), and pH.

Water Quality

The quality of seawater in Kasaoka bay is described as containing a concentration of SS of 30 mg/L. This value does not satisfy any standards for water quality. For example, the Japanese standards for SS at fisheries define Class 1 water as a SS concentration of 1 mg/L or less, Class 2 water as 2 mg/L or less, and Class 3 water as 3 mg/L or less. The SS value influences the transparency of water. Figure 4 shows the transparencies of both pumped and filtered seawaters, respectively. The height of the tube is 30 cm. Figure 4 shows that the filtered water is clear enough to see the bottom of the tube. The SS values that correspond to before and after filtration are approximately 20 and 1 mg/L, respectively. Details will be discussed later.

Water is sprinkled over the filters to provide aeration. The water is transferred from the filter unit to the sea surface in a drop-wise fashion, which causes an increase in the DO of the seawater. The results obtained for DO are shown in Fig. 5. This figure shows that the DO is relatively high for filtered seawater. The calculation of saturated DO with regard to water temperature indicates that filtered seawater contains

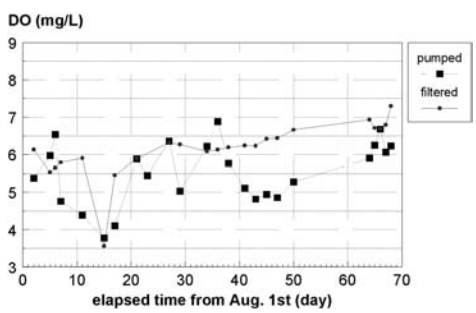

FIG. 5—*Changes in DO by filtration.*

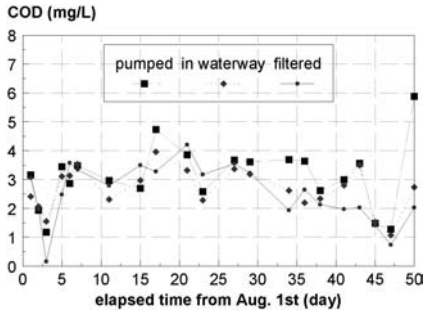

FIG. 6—*Changes in COD of seawater by filtration.*

sufficient oxygen. Furthermore, the filter unit was designed to not induce an anaerobic condition since the two filter layers are constructed with different permeabilities, as previously mentioned.

Chemical oxygen demand, COD, is defined as the measurement of the oxygen-consuming capacity of inorganic and organic matter present in water, which is expressed as the amount of oxygen consumed in milligrams per litre. Therefore, COD is an important index for water quality. The Japanese standards for COD at fisheries define Class 1 water as COD of 2 mg/L or less, Class 2 water as 2–3 mg/L, and Class 3 water as for 3–8 mg/L. The measured COD values of pumped and filtered seawaters are shown in Fig. 6. Figure 6 indicates that COD of filtered seawater is lower than that of pumped seawater and that these values vary with time. Thus, the filtering process acts to clean the seawater. The mean reduction rate of COD achieved was 16 %.

The steel slag used has a high pH, and thus, may have adverse effects on the environment. Figure 7 shows the change in pH values for both pumped and filtered seawater. The results show that there are no significant differences in pH values between them.

Volume of Filtration and Removed Solids

The SS remain on the surface of the sand filter. Since the size of SS are smaller than sand, the permeability of the filter decreases with filtration time, which causes a reduction of the filtration volume. The volume of filtration q, is given by Darcy's law

$$q = k\ A\ i \tag{1}$$

$$Q = k\ A\ i\ t \tag{2}$$

where

q: volume of filtered water per unit time (m^3/s),

Q: volume of filtered water (m^3),

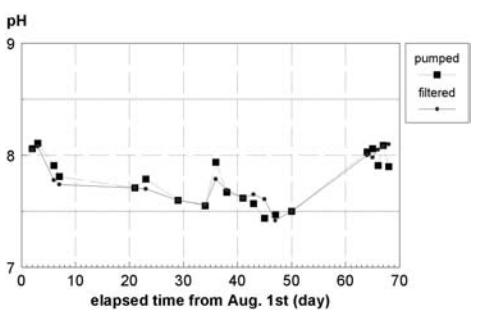

FIG. 7—*Changes in pH of seawater by passing through steel slag.*

FIG. 8—*Clusters of carbon fibers with organic matter.*

k: coefficient of permeability (m/s),
A: total sectional area of the filter (m^2),
i: hydraulic gradient, and
t: time (s).

The k of the filter unit was initially 1 by 10^{-1} cm/s, but decreased with time. The decrease in k to 1 by 10^{-3} cm/s was due to the clogging of the filter with SS after 700 h. When k is high, the water table is kept low, and the hydraulic gradient is relatively low under constant water supply. When the pore spaces of the filter are clogged, the k of the filter decreases. The average volume of purified water is given by the accumulation of treated water divided by the operating time. During the experiment, the average filtration volume was maintained at approximately 6000 m^3/day.

Before filtration of seawater, organic matter was removed with carbon fibers, as shown in Fig. 8. Three hundred bunches of carbon fibers were suspended in the carbon fiber tank that is installed just before the waterways. The basic idea is to allow micro-organisms to breed on the fibers because the organic matter will be adsorbed and consumed by the microorganisms. The amount of SS was decreased by, at most, 30% in the carbon fiber tank. However, it is noted that excessive breeding of micro-organisms increases the amount of SS because of bacterial waste. Therefore, the organic matter and micro-organisms had to be subsequently removed from the carbon fibers by washing.

A thick, drifting mud layer exists at the bottom of Kasaoka Bay, which is resuspended by the wakes from ferries and fishery boats. Therefore, the SS consist of these resuspended particles, phytoplankton, and particles discharged from existing rivers. The photomicrographs of SS that remain on the filter sand are shown in Fig. 9, which shows mostly silt-clay-sized inorganic particles, organic matter, diatoms, etc. The value of ignition loss of the SS ranges from approximately 4 to 12 %. In Kasaoka Bay, the resuspension of sediments is observed by the action of wakes induced by boats. The resuspended particles may occupy

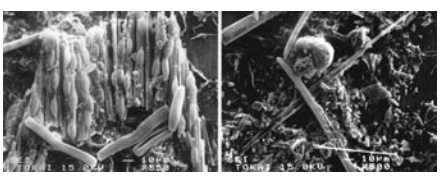

FIG. 9—*Photomicrographs of filtered SS.*

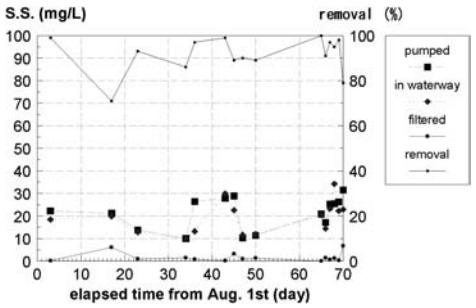

FIG. 10—*Changes in SS of seawater by filtration.*

50 % of the total SS or more. This reason may explain why the inorganic content of the SS is approximately 90 %. It is noted that the organic content is much lower than the value of ignition loss.

Figure 10 shows the changes in SS for pumped and filtered seawater. As seen in the figure, the SS change with time and day because the resuspension occurs easily by waves during low tide. Therefore, the amount of SS from pumped seawater depends on tides and waves from boats, and often exceeds 25 mg/L, as shown in Fig. 10. On the other hand, the SS of filtered seawater is generally lower than 2 mg/L (Fig. 10), suggesting that the amount removed is about 20 mg/L. The removal rate is also shown in Fig. 10, which appears to be as high as 90 % and contributes the improvements in seawater quality.

Removal of Chemicals

If we define the removal rate a, and calculate the removal amount divided by the volume of filtered seawater, then the removal of pollutants can be expressed by

$$R_n = Q\ a\ SS\ E_n \tag{3}$$

where

R_n: removed amount of pollutant n(mg),

Q: volume of filtered water (m^3),

SS: amount of SS(kg/m^3), and

E_n: concentration of element n (compound) in SS(mg/kg).

If we take that a is 0.8, E_n is 271 mg/kg, Q is 6000 m^3/day, and SS is 0.015 kg/m^3, the removed amount of the element is given by

$$R_n = Q\ a\ SS\ E_n = (6000)(0.8)(0.015)(271) = 19\ 512\ \text{mg/day}$$

Similarly, various elements, such as lead, copper, zinc, arsenic, etc., can then be calculated. If we assume that the above calculation is for zinc, the amount removed by filtration for two months may be comparable to the amount removed by an annual harvest of 10 000 kg of oysters (Gifford et al. 2004).

Table 1 shows the calculations of the amounts of pollutants removed by the purification vessel. The concentrations of pollutants were measured on SS of pumped seawater. For the calculation, a was assumed to be 0.8, which may be a little less than the actual value. From this point, the calculation of the removed amount is slightly underestimated. The calculations are based on the assumption that the concentration of the element is constant during filtration. This assumption may be invalid, because removal of the element will decrease the concentration of the element. From this point, the calculations are overestimated. However, the technique can be used in more contaminated sea areas, and the purification work lower contaminant concentrations to some extent. Since it is difficult to consider the actual effects of tidal currents, accurate calculations that consider decreasing concentrations may not be useful. Nevertheless, the results show that pollutants are effectively removed by the purification vessel, and that the technique is feasible for the preservation of enclosed sea area environments.

TABLE 1—*Estimation of pollutants removed by the purification vessel.*

Pollutant	Concentration E_n (mg/kg)	Amount removed per day (g) SS 0.01 kg/m^3	SS 0.03 kg/m^3
Al	42 000	2016	6048
Cu	360	17.2	51.6
Fe	23 400	1123	3369
Mn	2900	139.2	417
Pb	71	3.4	10.2
V	43	2.1	6.2
Ni	27	1.3	3.9
Zn	880	42.2	127
P	2880	138.2	415
Dry weight of SS		60 kg	180 kg
Pumped water		6000 m^3	

Small-Sized Filtration System

To maintain the environment after the rapid removal of SS, a smaller filtration system was developed. The system consists of a main body with a floater, three pumps, two float sensors, solar panels, and batteries. The sectional area of the small model is only 0.126 m^2. Filtration is achieved by drawing water with a pump, as shown in Fig. 11. The pump is operated continuously with batteries that can be charged in the daytime with the two solar panels. The dimension of the panel is 1580 mm by 802 mm by 50 mm (in length by width by thickness). The electric capacity supplied by the panels is 24 V, 180 W, and 5.05 A. Three pumps were used for upward and downward water flows, and for vacuuming the SS that accumulate on the bottom of the main body, respectively. An experiment using this model was carried out in a small pond in Shizuoka City, as shown in Fig. 12.

For the seepage force upward, measurements against quicksand are needed. In Fig. 11, such conditions can be written by

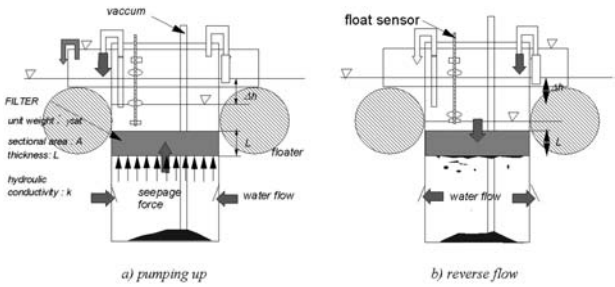

FIG. 11—*Schematic of a small filtration system.*

FIG. 12—*Purification experiment using a small-sized filtration system.*

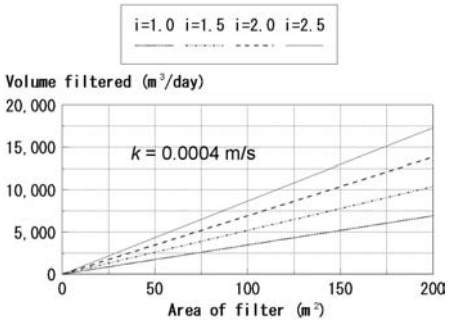

FIG. 13—*Relationship between area of filter and filtration volume, at a constant permeability and with various hydraulic constants.*

$$i\gamma_w < (\gamma_{sat} - \gamma_w) < \gamma' \tag{4}$$

$$0 < \gamma'/\gamma_w \tag{5}$$

where

i: hydraulic gradient,

γ_w: unit weight of water (kN/m^3),

γ_{sat}: unit weight of filter materials (kN/m^3), γ': submerged unit weight of filter materials, $(\gamma_{sat}-\gamma_w)\times$(kN/m^3).

However, Eq 5 is theoretical, and the weight of the filter should be adjusted empirically. If the conditions required are not satisfied, quicksand will develop and expected filtration results will not be achieved.

The upward water flow, shown in Fig. 11, can be given by Eq 6

$$Q = kAit \tag{6}$$

where $i = \Delta h/L$.

To recover the permeability that was lowered by the filter clogging with SS, downward water flow is used, as shown in Fig. 11. As the decrease in the permeability causes a drop in the water level above the filter, a float will drop down synchronous with the dropping water level. When the float drops down to a given level, the upward water pump will switch off. At the same time, the downward pump will operate. The downward flow washes away the materials that are clogging the filter and that have accumulated on the bottom.

The effect of small-system filtration is assumed to be similar to that of the purification vessel because of similar filter materials and the same principle. The volume of filtered water is proportional to the coefficient of permeability k and the sectional area A. The linear relationship between A and the volume of filtered water are given in Fig. 13. As seen in Eq 2, the volume of water is also proportional to the hydraulic gradient i. The amount of hazardous substances that can be removed is estimated by Eq 3. The basic idea for the use of this filtration system is that the amounts of hazardous substances should be maintained at levels below the standard or guideline.

Future Study

In this study, a full-scale, purification vessel and a very small filter model are developed. The size of the system is altered with respect to the area and water volume in considered sites. Therefore, the method of design is established. In principle, Eq 3 can be used for the design process.

In many cases, a huge amount of SS can be collected with the filtration system. The collected materials have to be disposed or utilized, and depend on the degree of contamination. If the collected materials are barely contaminated, they can be used as an organic fertilizer in the sea, although the concept of sea fertilizer should be established. In some sea areas, bottom trawling has made seabeds compacted and flat.

In such a situation, the fishery hauls have decreased. Solid fertilizers made of SS can be distributed to improve the bottom environment for microorganisms and benthos. The leachates from the fertilizer will increase marine basic production.

Conclusions

To remove SS from seawater, filtration systems were developed in this study. The results showed that filtration systems are quite effective at the removal of SS from water. The measurements that were performed showed that SS removal improved the quality of water in terms of transparency, COD, pH, DO, etc. Therefore, SS removal will provide a good impact on not only water, but also on bottom sediments. The amount of removed pollutants was calculated using the experimental data obtained. This calculation enables the design of filtration systems for future individual cases. Furthermore, SS removal can be used for various types of engineering work along coastal regions and lakes, including the prevention of red tide.

Acknowledgments

This study was done with the cooperation of Tokai University, Aoki Marine Co., Kasaoka City, National Institute for Rural Engineering, Nihon Kaiko, Co., Koa Kaihatsu, Co., and Japanese Land Development, Co. Ltd. The authors thank Dr. S. Tani and Mr. A. Nishihara for their cooperation.

References

Fukue, M. Sato, Y., Yanai, M., Nakamura, M., and Yamasaki, S., "Rehabilitation of Contaminated Marine Sediments in Relation to Living Things, Geoenvironmental Engineering, Geoenvironmental Impact Management," edited by Y. N. Yong and H. R. Thomas, Thomas Telford, London, pp. 198–203 (2001).

Gifford, S., Dunstan, H., O'Connor, W., and Macfarlane, G. R., "Quantification of In Situ Nutrient and Heavy Metal Remediation by a Small Pearl Oyster (*Pinctada imbricata*) Farm at Port Stephens, Australia," *Mar. Pollution Bull.*, in press.

Lohrer, A. M. and Wetz, J. J., "Dredging-Induced Nutrient Release from Sediments to the Water Column in a Southeastern Salt Marsh Tidal Creek," *Mar. Pollution Bull.*, 46, 1156–1163 (2003).

Minato, T., Yamasaki, S., Fukue, M., and Sato. Y., "Floating Vessel of Seawater Treatment for Rehabilitation of Marine Environment," *Journal of the Japanese Association of Coastal Zone Studies*, 16, 81–91 (2004).

Morrison, R. J., Narayan, S. P., and Gangaiya, P., "Trace Element Studies in Laucala Bay, Suva, Fiji," *Mar. Pollution Bull.*, 42 (5), 397–404 (2001).

Mulqueen, J., Rodgers, M., and Scally, P., "Phosphorus Transfer from Soil to Surface Waters," *Agric. Water Manage.*, in press.

Sfriso, A. and Marcomini, A., "Macrophyte Production in a Shallow Coastal Lagoon. Part II: Coupling with Sediment, SPM and Tissue Carbon, Nitrogen and Phosphorus Concentrations," *Mar. Environ. Res.*, 47, 285–309 (1999).

Sheng, P. X., Ting, Y-P., Chen, J. P., and Hong, L., "Sorption of Lead, Copper, Cadmium, Zinc, and Nickel by Marine Algal Biomass: Characterization of Biosorptive Capacity and Investigation of Mechanisms," *J. Colloid Interface Sci.*, 275, 131–141 (2004).

Suzumura, M., Kokubun, H., and Arata, N., "Distribution and Characteristics of Suspended Particulate Matter in a Heavily Eutrophic Estuary, Tokyo Bay, Japan," *Mar. Pollution Bull.*, 49, 496–503 (2004).

Woitke, P., Wellmitz, J., Helm, D., Kube, P., Lepom, P., and Litheraty, P., "Analysis and Assessment of Heavy Metal Pollution in Suspended Solids and Sediments of the River Danube," *Chemosphere*, 51, 633–642 (2003).

Journal of ASTM International, Vol. 3, No. 7
Paper ID JAI13317
Available online at www.astm.org

Espen Eek,[1] *Arne Pettersen,*[1] *Audun Hauge,*[2] *Gijs D. Breedveld,*[3] *Arve Solberg,*[4] *Sten U. Heines,*[5] *Kristian Solberg,*[6] *and Sverre O. Lie*[7]

Disposal of Dredged Material in a Local Confined Disposal Facility: Budgeting and Accounting of Contaminant Transport

ABSTRACT: Disposal of contaminated dredged material in local confined disposal facilities (CDF) has the advantages of reduced costs and reduced need for transport of the dredged material compared to many other disposal alternatives. CDFs can often be combined with land reclamation which can add considerable value to a dredging project. A local CDF has been constructed for Hg and HCB contaminated dredged material on a contaminated seabed close to one of Norway's largest industrial areas, Herøya. The construction has been completed with permeable barriers allowing transport of water from dewatering of dredged material and consolidation of sediment below the CDF. However, this design will also allow some transport of contaminants with the released pore water. The efficiency of the CDF was evaluated by making a budget of estimated contaminant emission from the disposal area before, during, and after construction and filling of the CDF. Laboratory tests and an analytical model were utilized for calculation of advective and diffusive transport of contaminants both from the dredged material and from the original contaminated seabed sediment at the disposal site. Our estimation of contaminant transport predicted that the leakage of contaminants from dredged material in the disposal facility would be orders of magnitude less than what was released from the seabed sediments at the disposal site before the realization of the CDF. Monitoring of contaminant transport, after realization of the CDF, has so far shown that the actual transport is much lower than the conservative estimate presented in our budget of contaminant transport. These results show that there can be a large and positive cost benefit from disposal of dredged material in CDFs constructed with permeable barriers in already contaminated areas. Sensitivity of calculated remediation efficiency to uncertainties in the estimated transport was found to be small in the case presented here. Our results also show that budgeting and accounting of contaminant transport can be a powerful tool both for impact assessments before realization of a project in contaminated sediments and for interpretation of monitoring data during and after the realization. Budgeting of contaminant transport also helps identifying the most critical transport mechanisms during the different phases of the project.

KEYWORDS: dredged material, confined disposal facility, environmental impact assessment

Introduction

Disposal of dredged material from areas with a long industrial history is an environmental and economical challenge. Disposal in local confined disposal facilities (CDF) has the advantages of reduced costs and reduced need for transport of the dredged material. A CDF for dredged materials consists of a confined volume with barriers often made from rock debris or other available clean fill material. When the CDF is filled with dredged material the function of the barrier is to keep contaminants inside the CDF. CDFs can be placed on land or in water with barriers extending above the water surface.

The dredged material placed in the CDF will replace the water that is inside the CDF. Excess water will also be released from the dredged material as it consolidates. This water, as well as infiltrating rain

Manuscript received April 19, 2005; accepted for publication September 28, 2005. Presented at ASTM Symposium on Contaminated Sediments: Evaluation and Remediation Techniques on 23–25 May 2006 in Shizuoka, Japan; M. Fukue, K. Kita, M. Ohtsubo, and R. Chaney, Guest Editors.

[1] Project Engineer, Norwegian Geotechnical Institute, 0806 Oslo, Norway.
[2] Division Director Environmental Engineering, Norwegian Geotechnical Institute, 0806 Oslo, Norway.
[3] Deputy Divison Director, Norwegian Geotechnical Institute, 0806 Oslo.
[4] Technical Director, Herøya Industrial Park, 3907 Porsgrunn, Norway.
[5] Technical Director, Grenland Harbour Authority, 3907 Porsgrunn, Norway.
[6] Survey Engineer, Geotek AS, 3900 Porsgrunn, Norway.
[7] HES-manager, Herøya Industrial Park, 3907 Porsgrunn, Norway.

water, can transport contaminants out of the CDF and therefore a strategy is necessary to handle this water. This can be done by constructing a drainage system from the CDF to the ambient water. Water drained directly from the CDF without a system for filtering particles from the effluent water can carry substantial amounts of contaminants (Price 2002). Therefore a water treatment system is often necessary as a part of such a drainage system. An alternative strategy is to use permeable barriers as a combined drainage and water treatment system. The barrier of the CDF is constructed to keep particulate materials from moving through it. Since only very small fractions of most contaminants are soluble in water, this effect alone can be enough to sufficiently clean the effluent pore water from the CDF. In addition, many barrier materials can act as a sorbent for contaminants that are dissolved in the effluent and thereby contribute further to cleaning the effluent.

In order to evaluate the environmental impact of the disposal of contaminated dredged material, comparison is often made with toxicity-based quality criteria for effluent water (Wiley et al. 2002; Burton et al. 2003). Direct biomonitoring outside the CDF has also been reported (Velleux et al. 1993). To do the evaluation of the potential impact in the design phase before construction, methods based on modeling of contaminant migration from the CDF are used (Velleux et al. 1993; Schroeder and Aziz 1999; Schroeder and Aziz 2002). However, none of these methods directly addresses the positive environmental impact of the CDF as a cap over existing contaminated sediments.

The Herøya peninsula near the city of Porsgrunn in southern Norway has been the site for one of Norway's major chemical industries during the major part of the last century. Herøya still hosts a variety of industries today. Although the release of contaminants from the industry has been reduced by orders of magnitude since the 1960's (Skei et al. 1989), sea bed sediments along the quays of the industrial harbor of Herøya and in the adjacent bay Gunneklevfjorden are still contaminated with mercury (Hg), dioxins, hexachlorobenzene (HCB), and polycyclic aromatic hydrocarbons (PAH) (Helland et al. 2004). In order to maintain navigational depths along the quays it was necessary to dredge about 18 000 m^3 of sediment. A predredging survey showed that all sediments to be dredged were contaminated (Pettersen 2003). In order to secure a safe and cost-efficient disposal of these sediments it was decided to build a local confined disposal facility (CDF) in the Gunneklevfjord. Creation of a new land area after completion of the CDF was also an important advantage that counted for the use of this disposal option for the dredged materials.

The location of the CDF on heavily contaminated sediments in the Gunneklevfjord has two important implications: (1) The impact of the CDF on contaminant migration both from the sediment at the CDF site and from the disposed dredged material in the CDF needs to be considered; (2) The CDF will act as a cap over the original sediments at the CDF site and reduce the migration of contaminants from these sediments to the water in the Gunneklevfjord. Therefore an environmental benefit from this disposal option can be expected in addition to the intended safe disposal of the dredged material.

This paper presents an alternative approach to environmental impact assessment of disposal of dredged materials. Estimates of the release of Hg and HCB, based on a site-specific conceptual model (SCM), were used to make a contaminant release budget of the planned project. Hg and HCB were chosen because Hg is the most important inorganic contaminant in this area and HCB is one of several chlorinated organic contaminants found in the sediment in this area. Contaminant release during construction, filling, and after completion of the disposal facility was calculated and compared to the background contaminant release at the CDF site before the CDF was constructed. Based on these estimates the environmental impact of the project was calculated as remediation efficiency (RE, relative reduction of contaminant release). Monitoring data from the construction phase were also utilized in the same model accounting for the actual contaminant release. A comparison was made between the estimated release (budget) and the measured release (accounts) to see how the accounts complied with the budget. We believe that this approach to impact assessment and evaluation of monitoring data could be helpful in the planning and evaluation of future dredging and remediation projects in contaminated sediments.

Methods

Concept of Remediation Efficiency

The basis for the evaluation of environmental impact in our system is a comparison of the release of contaminants to the local recipient before, during, and after realization of the planned project. Normally, a

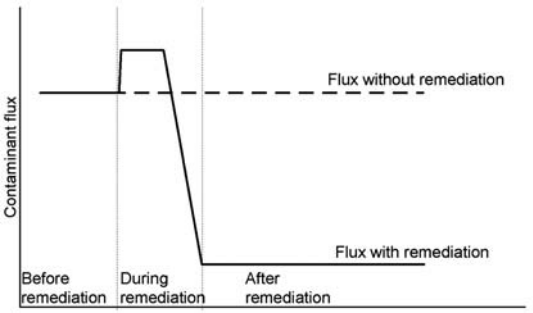

FIG. 1—*Conceptual illustration of contaminant flux before, during, and after remedial action.*

high release rate of contaminants from a sediment area, implying a potential environmental risk, will trigger remedial actions. During the remediation, handling of contaminated sediment and pore water can cause a preliminary increase in contaminant release. After a successful sediment remediation the release of contaminants to the environment will decrease. To achieve a net positive environmental effect from remediation, the increased release during the remediation must be outweighed by the reduced release after the remediation (Fig. 1). Fluxes from both the original location of the sediment and from the planned disposal area must be considered.

The efficiency of the remediation can be calculated from estimates or measurements of contaminant transport in the different phases of the project (Oen et al. 2003). Time (t) in formula 1 is years after the remediation is completed.

$$\mathrm{RE}(t) = 1 - \frac{\sum_{\text{begining of remediation}}^{t} \text{Release of contaminants}_{\text{during and after remediation}}}{\sum_{\text{begining of remediation}}^{t} \text{Release of contaminants}_{\text{without remediation}}} \tag{1}$$

In order to calculate the correct remediation efficiency (RE) it is important that the estimated or measured release of contaminants during and after remediation is as complete as possible.

For projects where the only motivation is to remediate contaminated sediments, the RE must be greater than zero within a reasonable time frame (5 to 20 years after the end of the remediation, depending on the project). This means that from the start of the remediation to the time of evaluation the overall contaminant release (sum of release during and after remediation) has to be less than without remediation. $\mathrm{RE} < 0$, means that the remediation has caused a net increase in release of contaminants rather than a reduction, and it means that no improvement has been achieved.

Even if remediation of contaminated sediments is not the main focus of a project, the concept of RE can be very useful. RE is then used to evaluate the impact of the project by evaluating the changes in contaminant release caused by the project. $\mathrm{RE} > 0$ means that the project has a benefit in reducing contaminant transport in addition to the direct benefits of the project, for example, greater sailing depth as a result of dredging. If the purpose of the project is sufficiently important, $\mathrm{RE} < 0$ can be tolerated.

CDF-Location, Construction, and Dredged Material

The CDF, to be evaluated in this case study, was constructed in the north part of the Gunneklevfjord (Fig. 2). The CDF covers a total area of 12 000 m^2 ($=A_{CDF}$) including sub-aqueous fills outside the barrier to improve geotechnical stability of the barrier. The area inside the CDF (A_{dm}) is 6 200 m^2. Below sea level the volume inside the CDF is 11 800 m^3 ($V_{CDF\ water}$); with barriers 1.9 m above sea level, the total volume reaches 23 000 m^3 (V_{CDF}).

The soil below the CDF consists of 25–35 m clayey silt and silty clay above bedrock. The upper 2 m consists of very soft contaminated clay with an average unit weight of about 15 kN/m^3. Table 1 shows concentrations of contaminants in two samples from the upper 10 cm of the soft clay in the sea bed sediment at the CDF location.

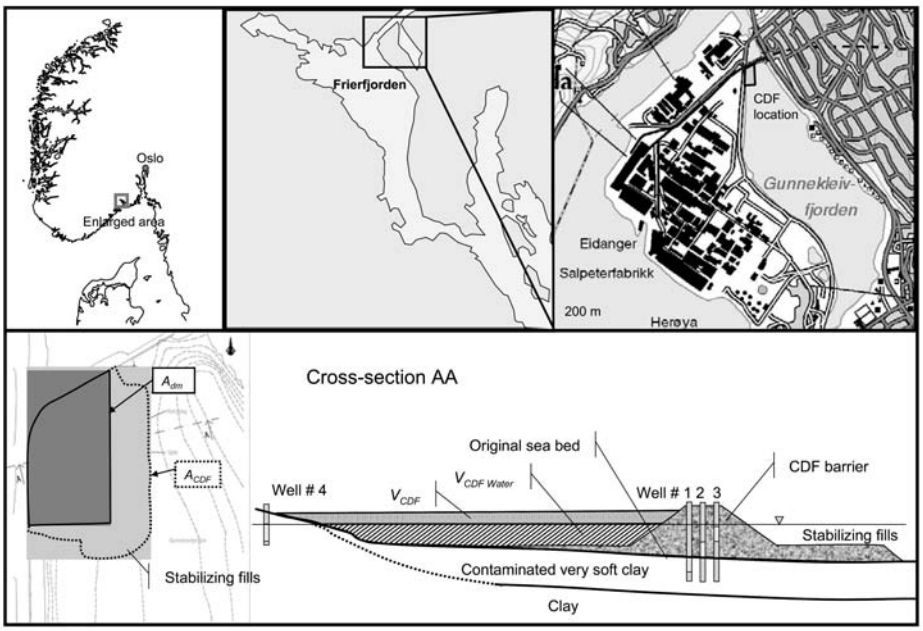

FIG. 2—*Location and design of CDF, showing also position of monitoring wells.*

The CDF was constructed and filled as follows: A geotextile (Geotex 300 g/m^2, polyester) were placed on the seabed in the area where barrier and geotechnical counter fills were to be placed. A stabilizing sand layer of 0.25 m was placed on top of the geotextile before the CDF barriers were constructed. The barriers were constructed from a silica-manganese-slag (amorphous SiO_2, CaO, Al_2O_3, MgO, MnO, and BaO pH=8.2–8.9 in water) available from a local company. Grain size distribution of this material (not shown) classifies it as a sandy gravel with d_{10}=0.32 mm. Table 1 shows concentrations of heavy metals in this slag.

TABLE 1—*Contaminants in sediments at the CDF location and in material used to construct the barrier (slag). All chemical analysis was done with standard methods and under a quality control system accredited according to EN ISO-IEC 17025.*

		Sediment at CDF site (N=2)	Dredged material (mixed sample from sediment at dredging site)	Slag material, used for construction of barrier
Water content	% of dw	132–230	121	0.1
Total organic carbon	% of dw	2.0	1.2	13
As	mg/kg dw	4.66–6.94	15	5.47
Cd	mg/kg dw	0.404–0.842	3.7	<0.05
Cr	mg/kg dw	21.8–37.5	28	31.8
Cu	mg/kg dw	53.7–66.8	47	12.6
Hg	mg/kg dw	60–67.4	6.4	<0.04
Ni	mg/kg dw	15.5–25.5	18	17.8
Pb	mg/kg dw	53.2–149	190	0.988
Zn	mg/kg dw	133–212	400	<2
HCB	mg/kg dw	6.2–8.9[b]	0.54	n.a.[c]
Dioxins	ng-TE[a]/kg dw	7740–9690	n.a.[c]	n.a.[c]

[a]TE=Toxicity equivalents (WHO).
[b]From Næs (1989).
[c]n.a.: not analyzed.

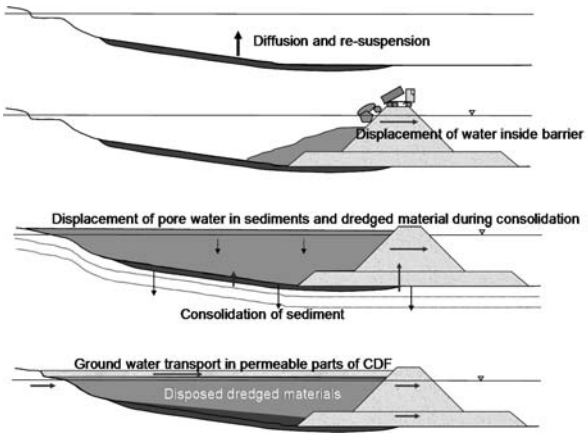

FIG. 3—*Mechanisms of migration of contaminated pore water from the CDF.*

When the barrier was completed monitoring wells (Ø 5 cm) were immediately installed (see Fig. 2). Three different wells were installed, one with filter in the clay below the original seabed, one with filter just above the original seabed, and finally one with filter just below the mean water level. It was assumed that the water in wells closest to the original sea bed (wells 1 and 2) will be mainly influenced by pore water from the sediment in the Gunneklevfjord. The water in well 3, in the upper part of the barrier wall, is on the other hand assumed to be representative of the water flowing from the CDF interior. The transport path for water through the barrier wall is shortest here and therefore will give the least resistance to water flow from the CDF interior. Ground water entering the CDF area was also monitored in a well up stream from the CDF (well 4).

The CDF was then filled with dredged material transported in barges from the dredging site. A total volume of 29 300 m^3 dredged material was placed in the CDF (V_{dm}). It is possible to place a larger volume of dredged material in the CDF than V_{CDF} because the dredged material consolidates significantly during the filling of the CDF. About 20 % consolidation of the dredged material was observed in this case. Construction and filling of the CDF presented in this paper was completed in nine months.

In order to increase the geotechnical stability of the area, stabilizing the dredged material with cement was considered.

Site-Specific Conceptual Model (SCM)

A site specific conceptual model (SCM) was developed to assist budgeting of contaminant release. The SCM follows many of the concepts of contaminant transport from CDFs presented by Martin and McCutcheon (1992). The SCM was also used to design the data acquisition program both for the experimental work for the preconstruction estimates and for the monitoring during and after construction. Within the SCM, release of contaminants to the environment was defined as contaminants released to the ambient water outside the CDF. The following fundamental transport mechanisms were considered: (1) diffusion from seabed without cover; (2) contaminants released from particles resuspended from the seabed during construction of the CDF-barriers; and (3) advection of contaminated water through the barrier.

Contaminants entering the water with resuspended particles and settling to the seabed, before the contaminants are desorbed from the particles, are not recognized as released to the environment. This is just considered a relocation of contaminated sediment within an already contaminated area. Figure 3 illustrates the most important mechanisms of transport of contaminants to ambient water in the Gunneklevfjord before, during, and after construction and filling of the CDF. Table 2 lists the transport mechanisms considered, data requirements, and methods used in data acquisition, both for the preconstruction estimates and for the monitoring during and after construction.

TABLE 2—*Transport mechanisms, data requirement, and acquisition within the SCM.*

Transport mechanism	Data requirement	Data acquisition for preconstruction impact assessment	Monitoring during and after construction
Background release of contaminants before construction of CDF			
1) Diffusion and natural resuspension	Flux caused by diffusion and resuspension from local sediments	Measured diffusion flux of Hg and HCB from sediments from Gunneklevfjorden (Skei et al. 1989)	
Release of contaminants during construction of CDF			
2) Resuspension during barrier construction	Influenced sea water volume ($V_{\text{resuspension}}$)		
	Sediment/water distribution=Leachate concentrations ($C_{\text{pw sed}}$)	Batch leaching test	Pore water concentration from monitoring wells
3) Displacement of contaminated water inside CDF during filling of dredged material	Volume of water in the CDF ($V_{\text{CDF water}}$)		
	Sediment/water distribution=Leachate concentration ($C_{\text{pw dm}}$)	Batch leaching test	Pore water concentration from monitoring wells
4) Rain water percolating through the CDF	Precipitation during construction phase	Precipitation data	Precipitation data
	Sediment/water distribution=Leachate concentrations ($C_{\text{pw dm}}$)	Batch leaching test	Pore water concentration from monitoring wells
5) Displacement of contaminated water inside CDF during consolidation of dredged material	Volume of water from de-watering of dredged material ($V_{\text{dm}}-V_{\text{CDF}}$)		Daily log of volume dredged material disposed
	Sediment/water distribution=Leachate concentration ($C_{\text{pw dm}}$)	Batch leaching test	Pore water concentration from monitoring wells
6) Displacement of contaminated pore water during consolidation of sediments below CDF	Consolidation of original sediment	Geotechnical analysis	
	Sediment/water distribution=Leachate concentration ($C_{\text{pw sed}}$)	Batch leaching test	Pore water concentration from monitoring wells
Release of contaminants after completion of CDF			
7) Groundwater transport through the permeable part of the CDF	Diffusion rate from surface of disposed dredged materials ($f_{\text{diffusion}}$)	Diffusion tests	Pore water concentration from monitoring wells

Calculation of Contaminant Release with the SCM for Budgeting and Accounting

1) Background Release of Contaminants before Construction of CDF—The area selected for the location of the CDF in the northern part of the Gunneklevfjord is heavily contaminated. Background flux of contaminants from this area will be dominated by biodiffusion and erosion from the sediment. As part of an environmental assessment, the Norwegian Institute for Water Research (NIVA) conducted in 1989 a study of diffusion flux of Hg and HCB from sediments from the Gunneklevfjord (Skei et al. 1989). The concentration of Hg in the sediment used in this test was 88 mg/kg, somewhat higher than the values of 60–67 mg/kg measured at the CDF site (Table 1). The diffusion flux from the Skei (1989) study, without resuspension, was assumed to be a modest estimate of the flux from the CDF site and was used as an estimate of the background flux from this area before realization of the CDF (F_{before}). The influence of different estimates of background flux on the calculated RE is discussed in the results and discussion section.

2) Resuspension during Barrier Construction—Before constructing the barrier walls of the CDF a geotextile and 25 cm sand layer were placed on the seabed to protect it during dumping of barrier material. It was assumed that these protective measures would reduce the resuspension considerable and that any resuspended particles would settle close to the CDF area. Transport out of the area is therefore only caused by contaminants desorbing from the resuspended particles. An estimate of the amount of contaminants released from resuspended particles ($M_{\text{resuspend}}$) was calculated from equilibrium concentrations of Hg and

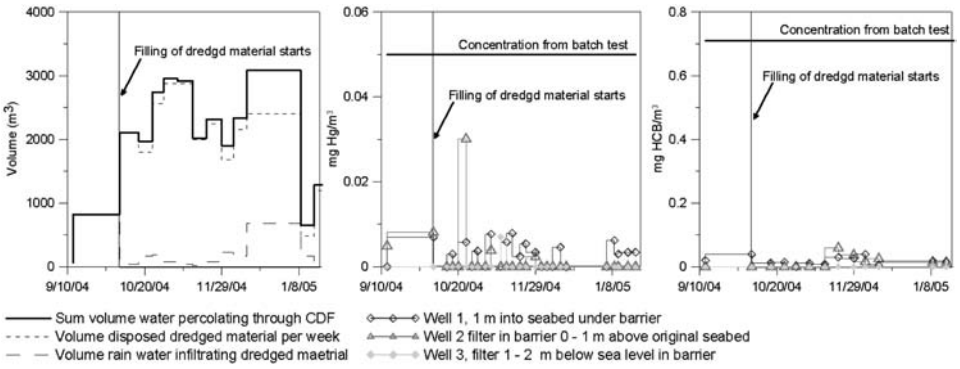

FIG. 4—*Local precipitation, volume of dredged material disposed in the CDF, and monitoring of Hg and HCB in barrier walls.*

HCB in water in contact with resuspended sediment ($C_{\text{pw sed}}$) and from the volume of water ($V_{\text{resuspension}}$) that is assumed to be influenced by resuspended particles during the time used for construction of the CDF barriers ($t_{\text{construction}}$=five weeks). $C_{\text{pw sed}}$ was determined as the leachate concentration from a batch leaching test based on the preliminary European standard prEN 12457. In this test, sediment and seawater was mixed 1:2 (based on dw.), after 24 h mixing concentrations of Hg and HCB in the water phase (leachate) were analyzed. All leachate concentrations were determined by standard analytical methods and under a quality control system accredited according to EN ISO-IEC 17025.

The resuspension was assumed to influence the water 2 m above the seabed in the entire CDF area (A_{CDF}). From modeling of water transport the retention time of the water in the Gunneklevfjord ($T_{\text{Gunneklev}}$) was assumed to be about four weeks (Hauge et al. 2002). From the monitoring data, $C_{\text{pw sed}}$ was taken as the average concentrations in well 1 (Fig. 4).

$$V_{\text{resuspension}} = A_{\text{CDF}} \cdot 2m \cdot \frac{t_{\text{construction}}}{\text{T}_{\text{Gunneklev}}} = 30\ 000\ \text{m}^3 \tag{2}$$

$$M_{\text{resuspension}} = V_{\text{resuspension}} \cdot C_{\text{pw sed}} \tag{3}$$

3) Displacement of Contaminated Water inside CDF During Filling of Dredged Material—When dredged material is filled into the CDF, water inside the CDF will be displaced and migrate through the barrier and out into the recipient. This water has been mixed with the dredged material leaching contaminants that can be transported with the water phase out of the CDF. The amount of Hg and HCB released with the displaced water ($M_{\text{CDF water}}$) was calculated from leachate concentration ($C_{\text{pw dm}}$, prEN 12457, as described above) and from the volume of water in the CDF before filling of dredged material ($V_{\text{CDF water}}$). $C_{\text{pw dm}}$ was taken as the average concentration measured in well 3 during filling of the CDF, (Fig. 4).

$$M_{\text{CDF water}} = V_{\text{CDF water}} \cdot C_{\text{pw dm}} \tag{4}$$

4) Transport with Infiltrated Rain Water—Precipitation registered at a local metrological station during the construction and filling of the CDF (P), the area covered with dredged material in the CDF (A_{dm}), and the average contaminant concentration in monitoring well 3 ($C_{\text{pw dm}}$) was used to calculate the amount of contaminants transported with rain water (M_{rain}).

$$M_{\text{rain}} = A_{\text{dm}} \cdot P \cdot C_{\text{pw dm}} = V_{\text{rain}} \cdot C_{\text{pw dm}} \tag{5}$$

5) Displacement of Contaminated Pore Water during Consolidation of Dredged Materials—The dredged material placed in the CDF contains extra water relative to the in situ water content. This water will be released from the CDF as the dredged material consolidates under its own weight. An estimate of

the volume of water from dewatering was made from the difference between the volume of dredged material placed in the CDF (V_{dm}) and the volume it occupies when the CDF was full (V_{CDF}). The amount of Hg and HCB released by this mechanism ($M_{CDF\ dewater}$) was calculated by

$$M_{CDF\ dewater} = (V_{dm} - V_{CDF}) \cdot C_{pw\ dm} \tag{6}$$

6) Displacement of Contaminated Pore Water during Consolidation of Original Sediments below the CDF—Under the vertical stress caused by the weight of the CDF barriers and the dredged material, the seabed soil will consolidate and release excess pore water. The pore water of the highly contaminated seabed below the CDF can carry contaminants out of the CDF. The released amount of Hg and HCB ($M_{consolidation}$) is estimated from leachate concentrations ($C_{pw\ sed}$) and a conservative estimate of the consolidation ($h_{consolidation}$=1.5 m) based on geotechnical analysis of the CDF (Eek and Nerland 2003).

$$M_{consolidation} = h_{consolidation} \cdot A_{CDF} \cdot C_{pw\ sed} = V_{consolidation} \cdot C_{pw\ sed} \tag{7}$$

7) Release of Contaminants after Completion of CDF—After filling and covering the CDF, ground water or rain water percolating the CDF are the major transport mechanisms for contaminants out of the CDF.

The permeability of the dredged material is very low and the flow of water through the dredged material will therefore be very small. In the more permeable material in the barrier and in the sand layer below and on top of the dredged material in the CDF, water will flow more easily. Although, these permeable parts of the CDF are made of clean materials, the water flowing here will also be in contact with the surface of the dredged material in the CDF. Diffusion of contaminants from this surface to the flowing water can be an important transport mechanism after the completion of the CDF. Stabilizing of the dredged material after placement in the CDF was considered during the planning of this project. The diffusion flux from the surface of the dredged material was therefore measured with a diffusion test using cement stabilized dredged material (according to Dutch standard NEN 7345). A monolith of cement stabilized dredged material was submerged in seawater. The seawater was changed at predefined times and analyzed for Hg and HCB. From the area of the monolith and the water concentrations at the different sampling times the diffusive flux from the monolith was calculated ($f_{diffusion}$). The flux measured in the last stage of the test multiplied with the surface area of the dredged material after disposal ($A_{surface\ dm}$) was used as the flux from the CDF (F_{after}) in the budget.

$$F_{after} = f_{diffusion} \cdot A_{surface\ dm} \tag{8}$$

The annual amount of water flowing through the CDF after its completion is assumed to be dominated by rain water as the ground water gradient in the area is low (0.002). After the completion of the CDF a large part of the area will be covered with impermeable surfaces like houses and asphalt, reducing the amount of rain infiltrating the CDF. It is assumed for the calculation of the annual flow through the CDF (Q_{CDF}) that 10 % of the annual rain fall (P) of about 910 mm/year is infiltrated. In the monitoring the concentration of this out flowing water was measured in well 3 ($C_{pw\ dm}$)

$$Q_{CDF} = 0.1 \cdot P \cdot A_{dm} \tag{9}$$

$$F_{after} = Q_{CDF} \cdot C_{pw\ dm} \tag{10}$$

By inserting the fluxes and released amounts resulting from the experimental work or monitoring in formula 1 we get the formula for the case specific RE as a function of time (t) after remediation.

$$RE(t) = 1 - \frac{M_{resuspension} + M_{CDF\ water} + M_{rain} + M_{CDF\ dewater} + M_{consolidation} + F_{after} \cdot t}{F_{before} \cdot t} \tag{11}$$

Results and Discussion

Results from the leaching tests (Table 3) were used according to the described model to make a budget of estimated release of contaminants during construction and filling of dredged materials in the CDF. Results from the monitoring of contaminant transport (Fig. 3) were used to account for the actual contaminant

TABLE 3—*Results from batch leaching tests of sediment and dredged material and diffusion test of stabilized dredged material.*

	Leached Hg	Leached HCB
Batch test sediment from the Gunneklevfjord	0.027–0.050 mg/m^3	n.a.
Batch test dredged material	0.041 mg/m^3	0.71 mg/m^3
Diffision test stabilized dredged material, long term leaching	0.003 mg-m^{-2}-year^{-1}	<0.018 mg-m^{-2}-year^{-1}

Note: n.a.: not analyzed.

release from the CDF. Table 4 shows the data from the experimental work and monitoring that are used in the calculations of the budgeting and the accounting of the contaminant release.

Results from Experimental Work And Monitoring

Monitoring of Hg and HCB in pore water from the wells in the CDF barrier showed that the concentration of Hg and HCB was significantly lower than estimated from the batch tests (Table 3 and Fig. 3). This discrepancy between results from the batch test and from the monitoring wells could be explained by an overestimation of the solubility of Hg and HCB by the batch test. The batch test is designed to measure contaminants in water in equilibrium with the solid phase of the dredged material. This assumption is conservative with respect to the complex processes actually taking place when contaminants are released from the dredged material in contact with water in the CDF (USACE 2003). Furthermore sorption of these contaminants in the barrier material before reaching the well could reduce the concentration in the water sampled from the wells further. The use of the results from the batch test to estimate the release of

TABLE 4—*Input values for modeling of contaminant release.*

Transport mechanism	Results from experimental work in design phase		Results from monitoring during construction and filling of CDF	
	Hg	HCB	Hg	HCB
Background release of contaminants before construction CDF				
1) Diffusion rate from CDF site[a]	0.91 mg-m^{-2}-year^{-1}	0.50 mg-m^{-2}-year^{-1}	0.91 mg-m^{-2}-year^{-1} (0.20–1.3)[b]	0.50 mg-m^{-2}-year^{-1} (0.19–1.2)
Release of contaminants during construction of CDF				
2) Resuspension during construction of barrier	A_{CDF}=12 000 m^3 $C_{pw\ sed}$= 0.050 mg/m^3	$C_{pw\ sed}$= 0.71 mg/m^3	$C_{pw\ sed}$= 0.003 mg/m^3 (0.002–0.030)	$C_{pw\ sed}$= 0.016 mg/m^3 (0.005–0.059)
3) Displacment of contaminated water inside CDF during filling of dredged material	$V_{CDF\ water}$=18 000 m^3 $C_{pw\ dm}$= 0.050 mg/m^3	$C_{pw\ dm}$= 0.71 mg/m^3	$V_{CDF\ water}$=11 800 m^3 $C_{pw\ dm}$= 0.0022 mg/m^3 (<0.002–0.007)	$C_{pw\ dm}$= 0.0062 mg/m^3 (<0.005–0.010)
4) Rain water percolating through the DCF	…	…	V_{rain}=2812 m^3 $C_{pw\ dm}$= 0.0022 mg/m^3 (<0.002–0.007)	$C_{pw\ dm.}$= 0.0062 mg/m^3 (<0.005–0.010)
5) Displacment of contaminated water during consolidation of dredged material	…	…	$V_{dm}-V_{CDF}$=6 300 m^3 $C_{pw\ dm}$= 0.0022 mg/m^3 (<0.002–0.007)	$C_{pw\ dm}$= 0.0062 mg/m^3 (<0.005–0.010)
6) Displacement of pore water during consolidation of sediments below CDF	$V_{consolidation}$=14 400 m^3 $C_{pw\ sed}$= 0.05 mg/m^3	$C_{pw\ sed}$= 0.71 mg/m^3	$V_{consolidation}$=18 000 m^3 $C_{pw\ sed}$= 0.0033 mg/m^3 (0.002–0.008)	$C_{pw\ sed}$= 0.016 mg/m^3 (0.50–1.9)
Release of contaminants after completion of CDF				
7) Ground water transport through CDF	$A_{surface\ dm}$=13 400 m^2 $f_{diffusion}$= 0.003 mg-m^{-2}-year^{-1}	$f_{diffusion}$= 0.02 mg-m^{-2}-year^{-1}	P=0.91 m/year $C_{pw\ dm}$= 0.0022 mg/m^3 (<0.002–0.007)	A_{dm}=6 200 m^2 $C_{pw\ dm.}$= 0.0062 mg/m^3 (<0.005–0.010)

[a]Data from Skei et al. (1989).

[b]Numbers in parenthesis are range of measured values

TABLE 5—*Contaminant budget and accounts.*

	Results from experimental work in design phase (budget)		Results from monitoring during construction (accounts)	
Transport mechanism	Hg	HCB	Hg	HCB
Background release of contaminants before construction of CDF				
1) Diffusion rate from CDF site	10 960 mg/year	5960 mg/year	10 960 mg/year (2400–15 360)[a]	5960 mg/year (2280–14 520)
Release of contaminants during construction of CDF				
2) Resuspension during construction of barrier	1500 mg	21 000 mg	139 mg (84–1264)	672 mg (210–2478)
3), 4), and 5) Displacement of contaminated water inside CDF during filling of dredged material	900 mg	12 780 mg	46 mg (42–146)	130 mg (105–209)
6) Displacement of contaminated pore water during consolidation of sediments below CDF	720 mg	10 224 mg	59 mg (36–540)	288 mg (90–1062)
Release of contaminants after completion of CDF				
7) Ground water transport through the CDF	40 mg/year	268 mg/year	1.2 mg/year (1.1–3.9)	3.5 mg/year (2.8–5.6)

[a]Numbers in parenthesis are range of measured or estimated values.

contaminants during the filling of the CDF will therefore result in an overestimation of this release. This provides extra safety when the design and permission from authorities relay on these estimates. A more elaborated analytical scheme, better reflecting field conditions (USACE 2003), could be used if needed to support a less conservative design.

The monitoring also showed that the concentration of Hg and HCB in the pore water during filling of dredged material into the CDF was similar to the concentration before filling the CDF. It seems therefore that mixing of dredged material with the water in the CDF does not result in elevated Hg or HCB concentrations in the water flowing out of the CDF.

The highest concentrations of both Hg and HCB were found in wells 1 and 2, installed just below and just above the original seabed. This is assumed to reflect a higher release of Hg and HCB from the sediment below the CDF than from the dredged material. The concentration of Hg and HCB in well 3 was below the limit of quantification (LOQ) during the whole period where the CDF was filled with dredged material except once (0.007 mg/m^3). Transport of Hg and HCB out of the CDF was calculated from the average concentrations measured in wells 3 and 1 ($C_{pw\ dm}$ and $C_{pw\ sed}$, respectively) and the volume of water from precipitation, replaced water, and consolidation.

Budget, Accounts and Remediation Efficiency (RE)

Table 5 shows the estimated contaminant release of Hg and HCB from experimental data (budget) and from monitoring data during and after construction (accounts). Since the concentrations of Hg and HCB were much lower in the monitoring wells than in the leachates the released amounts calculated from monitoring data are also much less than estimated from leaching tests. As discussed above, this discrepancy can be explained by adsorbtion to the barrier material or by an overestimation of dissolved fraction in the batch test.

The values in the budget and the accounts of the contaminant transport were used to calculate the remediation efficiency (RE) of this project using formula 11. This formula calculates the percentage reduction in release of contaminants after the remediation relative to the release before remediation. During the remediation work, release of contaminants usually increase temporally due to handling of contaminated sediment. The sum of this release and the release after remediation is used to calculate the relative reduction in contaminant release [=RE, see formula 11]. Since the release during the remediation is temporal and the release after the remediation is assumed constant per year, the release during remediation will have the largest negative impact on the RE for the years immediately after the remediation. This impact will diminish with time. RE will then asymptotically approach the relative reduction in release without the release during the remediation. Figures 5(*a*) and 6(*a*) shows RE calculated from the budget and the accounts as a function of time (number of years over which the contaminant release during the

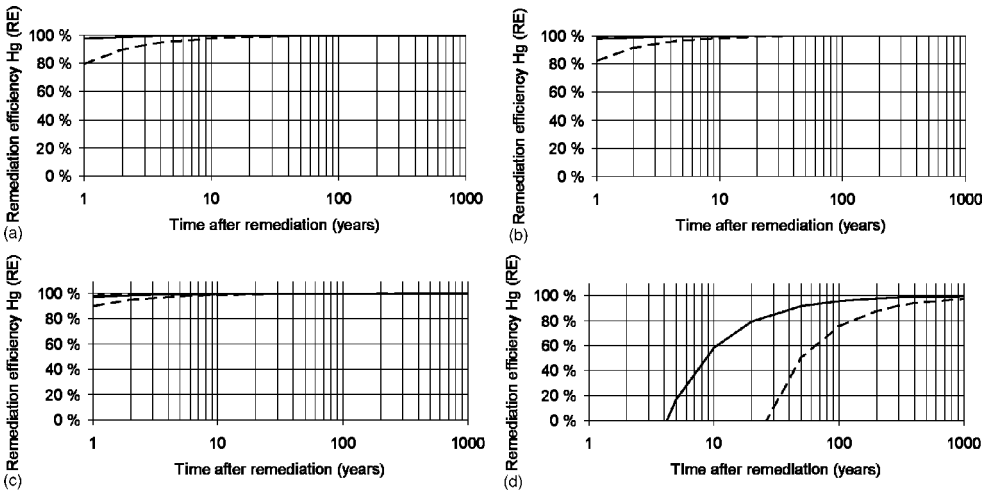

FIG. 5—*Remediation efficiency for Hg with different scenarios: (a) Budget (dashed line) and accounts (solid line), (b) RE from monitoring using average concentrations from well 3 (solid line), RE calculated with highest and lowest concentrations from well 3 (dashed lines), (c) RE calculated with average diffusion flux from original sediment (solid line), RE calculated from high and low diffusion flux (dashed lines), (d) RE calculated with release of water with SS concentration* 339 mg/l *(solid line), RE calculated with release of water with SS concentration 2128 mg/*l *(Price 2002) (dashed line).*

remediation is normalized) showing that the estimate of RE from the monitoring data (accounts) is much higher than the estimate made during the design phase (budget). This shows that the efficiency of the CDF was better than expected.

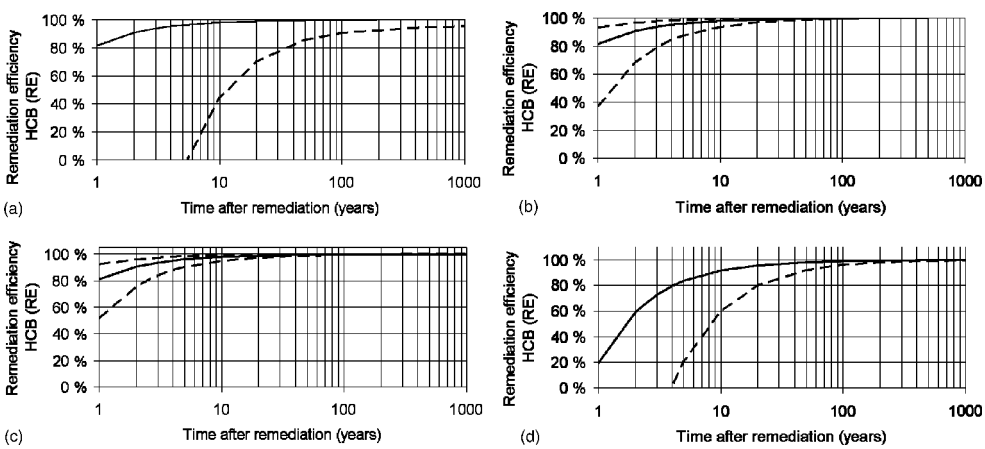

FIG. 6—*Remediation efficiency for HCB with different scenarios: (a) Budget (dashed line) and accounts (solid line); (b) RE from monitoring using average concentrations from well 3 (solid line), RE calculated with highest and lowest concentrations from well 3 (dashed lines); (c) RE calculated with average diffusion flux from original sediment (solid line), RE calculated from high and low diffusion flux (dashed lines); (d) RE calculated with release of water with SS concentration* 339 mg/l *(solid line); RE calculated with release of water with SS concentration 2128 mg/*l *(Price 2002) (dashed line).*

The RE calculated from the monitoring shows that the small increase in contaminant release caused by the construction and filling of the CDF is compensated by the reduced contaminant transport from the CDF area in less than one year resulting in a RE of more than 95 % for Hg and more than 80 % for HCB.

The models of contaminant transport and the input data used to make the contaminant budget and accounts will naturally be associated with uncertainties. The uncertainty in the budgeting based on leaching tests is accounted for by conservatism in the calculations. In order to estimate the uncertainties of the RE calculated from the monitoring, calculations were made assuming both the highest and lowest concentrations measured in the monitoring wells ($C_{\text{pw sed}}$ and $C_{\text{pw dm}}$). Figures 5(*b*) and 6(*b*) show the RE resulting from this sensitivity analysis. The ranges of measured concentrations of Hg and HCB in the monitoring wells in the CDF were both one order of magnitude (Table 4). However, since the amount of contaminant release calculated from the measured effluent concentrations was much less than the background release, the importance of variance in the release during the CDF construction was small. This resulted in the relatively narrow range of RE already one year after the realization of the CDF. Similarly, the greater range of RE for HCB than for Hg was explained by less difference between the background release and the release of HCB during the construction phase than what was observed for Hg.

Since the high background fluxes of Hg and HCB, in this case study, are able to reduce the sensitivity of the RE to the variability in the release during the construction phase, it could be expected that the RE is more sensitive to uncertainties in the estimate of the background flux. To investigate this, RE was calculated with the lowest and highest values of diffusion flux found in the study by Skei et al. (1989) (The values that are used are found in parenthesis in Table 4). RE from this calculation is plotted in Figs. 5(*c*) and 6(*c*). These results show, however, that the RE for Hg, after one year, changed only from 90 to 98 %, as a consequence of the variability of the background flux. For HCB the range of RE was larger (52–93 %). The variability of background flux was large enough to make a significant impact on the RE-value for HCB. However, even with the lowest background flux the RE was more than 90 % ten years after the realization of the CDF. To get RE values close to zero, the amount of contaminants released during the construction phase must be similar to or greater than the background flux. It is demonstrated that the release of contaminants with the water phase from the CDF in the present study is much lower than the estimated original flux from the sediment at the CDF site. By acting as a cap over these sediments, the CDF has reduced the Hg and HCB flux from this area by more than 95 %.

The permeable barrier in the CDF works as a huge particle filter. As both Hg and HCB are strongly associated with particles, dewatering of the CDF without particle control could result in a large transport of contaminants. Price (2002) monitored suspended solids (SS) in runoff from a CDF during rainfall. He found average values of 2128 mg SS/l in storm water from uncovered CDF areas and an average of 339 mg SS/l from areas with vegetation. If water with SS in this range were drained directly from the CDF it would increase the release of Hg and HCB to the recipient considerably. RE was recalculated with effluent concentrations during the construction phase assuming the above range of SS and Hg and HCB concentrations on the suspended particulate matter as in the dredged material (Table 1). The RE [Figs. 5(*d*) and 6(*d*)] was, as expected, much lower in the case of the particle facilitated transport than what was observed when effluent water is filtered through the barrier. In the worst case, RE is less than zero until 25 years after the construction, meaning that it could take 25 years to compensate for particle facilitated transport of this magnitude.

Conclusion

The use of leaching tests together with a conceptual model and analytical calculations of contaminant transport were successfully applied to make a conservative estimate of the transport of contaminants during and after the construction and filling of dredged material in a CDF. Monitoring presented in this study showed that the actual release of Hg and HCB during and after the construction phase was less than estimated, demonstrating the conservativeness of this approach to the impact assessment. We believe that the concept of remediation efficiency can be very useful as a part of impact assessments both in pure remediation projects and in other projects involving contaminated soil or sediment for the following reasons: (1) It can be used to evaluate both mechanisms causing increase and mechanisms causing reduction in contaminant release; (2) It can enable the user to evaluate which transport mechanisms cause the largest contaminant release; (3) The concept is simple and can be used with input from both simple analytical models and complex numerical simulations; and (4) Comparison of REs of alternative remedia-

tion strategies can be used to evaluate the cost-benefit of different remediation alternatives.

References

Burton, W., Farrar, J. S., and Pasquale, J., "Contaminant Sequestering and Water Quality Discharges at Confined Disposal Facilities," *Remediation of Contaminated sediments-2003*, edited by M. Pellei and A. Porta, Battelle Press, Columbus, OH..

Eek, E. and Nerland, Ø., "Confined Disposal Facility in the Gunneklevfjord-Environmental and Geotechnical Evaluations," in *Norwegian, NGI-report* 20031257-1, NGI, Oslo, Norway, 2003.

EN ISO-IEC 17025, "General requirements for the competence of testing and calibration laboratories," Norges Standardiseringsforbund, Oslo, Norway, 2000.

European Standard *prEN 12457*, "Characteristics of waste—Leaching—Compliance test for leaching of granular waste materials and sludges—Part 1: one stage batch test at a liquid to solid ratio of 2 l/kg with particle size below 4mm (without size reduction)," Draft, European committee for standardization, CEN, 1999.

Hauge, A., Nerland, Ø., and Holme, J. K., "Mass Disposal in the Gunneklevfjord, Feceability Study," in *Norwegian, NGI-Report* 20011556-1, Norwegian Geotechnical Institute, Oslo, Norway, 2002.

Helland, A., Olsen, M., Lindholm, O., Uriansrud, F., Traaen, T., and Rygg, B., "Remediation Plan for Contaminated Sediments in Telemark, Norway," in *Norwegian, NIVA-report* 4898-2004, Norwegian Institute for Water Research, Oslo, Norway, 2004.

Martin, J. L. and McCutcheon, S. C., "Overview of Processes Affecting Contaminant Release from Confinede Disposal Facilities," *Contract Report* D-92-1, US Army Engineer Waterways Experiment Station, Vicksburg, MS, 1992.

Næs, K., "Contaminants in the Gunnekleivfjorden. Sub-report 1: Concentrations and Amounts of Contaminants in the Sediments," in *Norwegian. NIVA-report 8806801 No.* 2192. NIVA Oslo, Norway, 1989.

NEN 7345, "Leaching characteristics of solid earthy and stony building and waste materials. Leaching tests. Determining of leaching of inorganic components from building and monolithic waste materials with the diffusion test," Nederlands Normalisatie-instituut, 1995.

Oen, A., Eek, E., Rudolph-Lund, K., Hauge, A., and Breedveld, G., "Evaluating Remediation Alternatives for Contaminated Sediments Based on Cost-Benefit Analyses," *Proceedings of the Second International Conference on Remediation of Contaminated Sediments* (Venice, Italy; 30 Sep-3 Oct 2003), edited by M. Pellei and A. Porta, Battelle Press, Columbus, OH, 2003.

Pettersen, A., "Environmental Survey of Harbour Sediments, Herøya Norway," in *Norwegian, NGI-report* 20031257-2, NGI Oslo, Norway, 2003.

Price, R. A., "Evaluation of Surface Runoff Water in a Freshwater Confined Disposal Facility-Effects of Vegetation," DOER Technical Notes Collection (ERDC TN-DOER-C28), U. S. Army Engineer Research and Development Center, Vicksburg, MS, 2002, www.wes.army.mil/el/dots/doer

Schroeder, P. R., and Aziz, N. M., "Contaminant Leaching Model for Dredged Material Disposal Facilities," *J. Environ. Eng.*, 125(9), 835–844 (1999).

Schroeder, P. R. and Aziz, N. M., "Effect of Vadose Zone Leachate Concentration," *Dredging '02 Key Technologies for Global Prosperity*, edited by S. Garbaciak, Jr, American Society of Civil Engineers, Orlando, Florida, 2002.

Skei, J., Pedersen, A., Bakke, T., and Berge, J. A., "Contaminants in the Gunnekleivfjorden. Sub-Report 4: Leaching of Mercury and Chlorinated Organic Compounds from the Sediments," in *Norwegian. NIVA-report 8806804 No.* 2196, NIVA Oslo, Norway, 1989.

U. S. Army Corps of Engineers (USACE), "Evaluation of Dredged Material Proposed for Disposal at Island, Nearshore, or Upland Confined Disposal Facilities—Testing Manual," *Technical Report* ERDC/EL TR-03-1, U. S. Army Engineer Research and Development Center, Vicksburg, MS, 2003.

Velleux, M. L., Rathbun, J. E., Kreis, Jr. R. G., Martin, J. L., Mac, M. J., and Tucman, M. L., "Investigation of Contaminant Transport from the Saginaw Confined Disposal Facility," *J. Great Lakes Res.*, 19(1), 158–174 (1993).

Wiley III, J. B., Tharwani, R. M., and Morgan, L. P., "Beneficial Use of Dredged Material in Brownfields," *Dredging '02 Key Technologies for Global Prosperity*, edited by S. Garbaciak, Jr, American Society of Civil Engineers, Orlando, Florida, 2002.

Journal of ASTM International, Vol. 3, No. 7
Paper ID JAI13323
Available online at www.astm.org

Jan K. Holme,[1] *Luke Dokter,*[1] *Espen Eek,*[1] *Tor Georg Jensen,*[1] *Tor Loken,*[1] *and Gijs D. Breedveld*[2]

Material Behavior of Dredged Contaminated Sediments from Simple Laboratory and Oedometer Tests

ABSTRACT: Contaminated sediments, near urbanized areas, usually have a high content of organic matter and therefore a high water content and low shear strength. During dredging, additional water is mixed with the sediment, increasing the water content even further. The resulting dredged material that has to be disposed will be very soft with a very low shear strength. As a result, capping of a disposal site with clean sediments will be a challenge and put restrictions on the thickness of the cap and the used placement technique. Simple laboratory tests have been conducted to evaluate the transition of newly dredged material from being a fluid to behaving like a continuum. The performed tests show that it is possible to put a sand layer on top of dredged material after a short initial consolidation phase. This indicates that dredged material at this stage is by definition a continuum. Results from special oedometer tests revealed that the time needed for primary consolidation for contaminated clay from the Bjørvika area in Oslo (Norway), was approximately 30 h. The undrained shear strength of dredged material after consolidation under the influence of a thin sand layer is difficult to measure using traditional methods. A simple laboratory test with a transparent cylinder and a tilting table was conducted to force a failure mechanism. From these results, the undrained shear strength can be back calculated. For Bjørvika clay, test results, using a 2–3 cm sand cap, indicated a shear strength of approximately 0.10–0.15 kPa after three days of consolidation. Thin sand layers will increase the shear strength of the dredged material and act as draining layers of excess pore pressure during disposal site operation. This will improve the stability of the final cap after site closure.

KEYWORDS: dredged material, shear strength, consolidation, capping, laboratory tests

Introduction

Sediments in urbanized areas are usually highly contaminated. Dredging and disposal of this material is a challenge. Sub-aqueous disposal often requires a protective cap of clean material to prevent uncontrolled spreading of contaminated sediments. Failure of a cap construction can have major environmental and economy consequences. Two different failure mechanisms can be identified; sliding failure (Fig. 1) and bearing failure (Fig. 2).

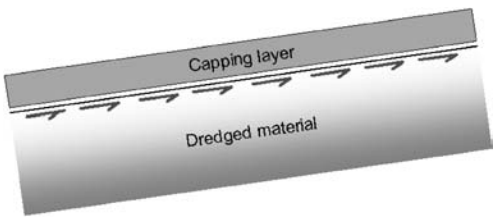

FIG. 1—*Sliding failure.*

Manuscript received May 23, 2005; accepted for publication January 5, 2006. Presented at ASTM Symposium on Contaminated Sediments: Evaluation and Remediation Techniques on 23–25 May 2006 in Shizuoka, Japan; M. Fukue, K. Kita, M. Ohtsubo, and R. Chaney, Guest Editors.

[1] Project Engineer, Norwegian Geotechnical Institute, 0806 Oslo, Norway.
[2] Technical Adviser, Norwegian Geotechnical Institute, 0806 Oslo, Norway.

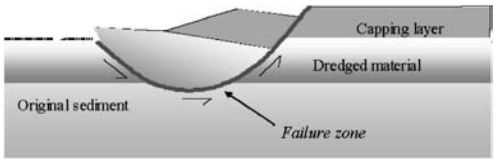

FIG. 2—*Bearing failure.*

Sliding Failure

One critical failure mechanism is the capping layer sliding on top of a very soft soil with hardly any shear resistance. Failure will be a function of slope angle and shear strength at the surface of the dredged material.

Bearing Failure

Another failure mechanism occurs if the capping layer has a higher weight than the bearing capacity of dredged material. The bearing capacity is a function of the shear resistance along the failure zone [1].

Both the sliding failure and bearing failure must be considered when a protective cap is to be constructed. Therefore, knowledge of the material behavior of dredged contaminated sediments is essential when making decisions on the thickness and placement technique of a protective cap.

Newly deposed dredged material can be very "fluffy" and it is relevant to question if this material should be considered as fluid or not. By definition, a fluid is a substance that deforms continuously under the action of an applied shear force or stress and it is able to flow [2]. It is important to emphasize that there will be a completely different failure zone for a fluid than for a continuum, and classical bearing capacity calculations for solids will not be true if the material is a fluid.

Classical in situ sediment investigation methods typically measure the shear resistance of a sediment. An example is the Cone Penetration Test [3] that is used frequently both offshore and onshore. The main objections to using in situ classical geotechnical investigation methods for dredged material are their inaccuracy at low shear strengths and the chance of overlooking an unclear transition zone between fluid and solid.

There are different standard laboratory tests that can be performed to measure the shear strength of clay. One example is the fall cone test that can be performed both for remolded and undisturbed clay. However, the accuracy of these results decreases with shear strengths below 1 kPa, and the results are not reliable for shear strength below 0.5 kPa [4].

This paper presents a simple laboratory test, "tilting table test," which has been conducted to demonstrate that it is possible to add sand on top of dredged material, shortly after dredging, and that dredged material has a measurable shear strength. In addition, a special oedometer test has been conducted to reveal the time needed for primary consolidation for contaminated clay from the Bjørvika area in Oslo, Norway.

Tilting Table Test

Background

If sand is added on top of newly deposed dredged material (capping), it is likely that the sand particles will fall through the fluffy material. Laboratory tests performed at NGI show that the time between deposal and capping is of great importance [5]. It was found that it took about one day before it was possible to add a 2–3 cm thick sand layer above the dredged material. One explanation is the increased strength in the dredged material simply because it was allowed to consolidate due to its own weight.

When the dredged material is allowed to consolidate, the excess pore pressure will decrease and the particle contact increase, resulting in increased shear strength. A typical shear strength profile of normally consolidated clay can be expressed as:

$$s_u^{DSS} = \alpha p_0' \tag{1}$$

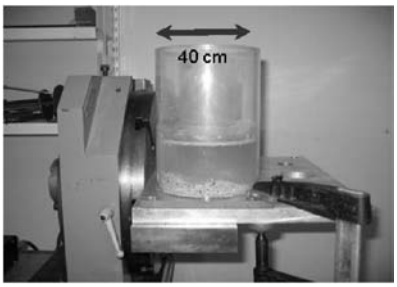

FIG. 3—*Cylinder connected to the tilting table (shell sand used as capping material).*

The parameter α is a constant with a typical range between 0.15 and 0.35. The effective vertical pressure p'_o is a function of density and depth. It is assumed that the same function also can be applied for contaminated dredged material, but that the range of α may differ.

Objective

Assuming that the shear strength of dredged material increases with depth and that sand has a higher friction angle than dredged clay, the tilting of dredged material with a capping layer on top of it, should give a failure mechanism as illustrated in Fig. 1, with the weakest layer just below the sand layer.

The objective of the tilting table test, was to find the angle where sliding occurs, then back calculate the undrained shear strength just below the capping layer. The tilting table test is not an alternative to any standard laboratory tests, and should be considered as a supplement to better understanding the soil behavior of very soft contaminated sediments.

Preparation

The sediment used in the tests originates from the Oslo Fjord and is highly polluted silty clay. It is very soft and pliable, with a total unit weight of about 16 kN/m^3 and water content (on dry weight basis) of around 150%.

A Ø400 mm cylinder of plexiglass with a height of 1.0 m was used. The tilting table and column are shown in Fig. 3.

The cylinder was attached to a base plate on a tilting machine that was connected to an electronic counter. The measurements were recorded by using a motor which turned at approximately 2.5° per minute (see Fig. 4).

Geometry effects that may have arisen from the size of the cylinder were considered. After consolidation, the sediment was about 130 mm thick, and the capping layer 20 mm thick. Using a cylinder diameter Ø400 mm geometry effects were assumed to be minimal. In addition, the cylinder was equipped with an internal wall at the height of the sediment, and placed along the inside of the cylinder (Fig. 5). This allowed the capping material to move freely. Three different tests were performed:

1. Capping layer on top of sediment above internal wall (Fig. 5)
2. Sediment without a cap above internal wall
3. Sediment and cap above internal wall

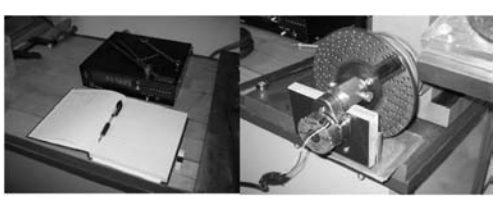

FIG. 4—*Motor and digital device for measuring the angle of the tilting table.*

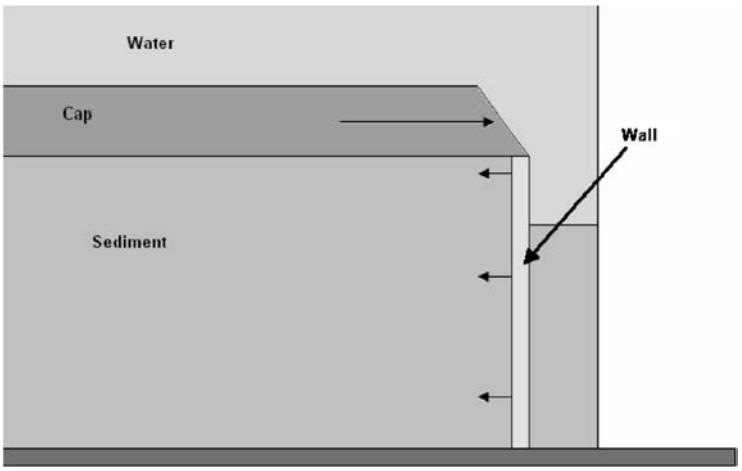

FIG. 5—*Schematic cross section of the test column, showing the internal wall.*

Initially the material was blended with sea water and allowed to settle. In order to obtain an even layer of sediment, the sediment was blended with around 16 l of sea water and then allowed to consolidate. Research on the consolidation of sediments, gave an "optimal" time (around 1000 min) at which we could apply the capping layer [5]. In the first test a capping layer of shell sand was applied around 1500 min after consolidation had begun. This can be seen in Fig. 6 along with the subsequent consolidation after the capping layer was applied.

The capping layer was quite well defined as a 20 mm thick layer on the surface of the sediment. The whole system was allowed to consolidate for a further three days, with only a minimal change in the height of the sediment over this period.

Results and Discussion, Tilting Table Test

Test 1: Capping Layer on Top of Sediment and Internal Wall

The cylinder was rotated to 10° with only a few small particles being dislodged. It was then tilted to 20° and still only a few particles fell from the face of the wall. The cylinder was then tilted at around 1° every 2–3 min and during this time small particles fell continuously from the front of the wall face, as can be seen in Fig. 7.

This gradual failure continued up until 40°, at which point a continual failure of the cap occurred. The

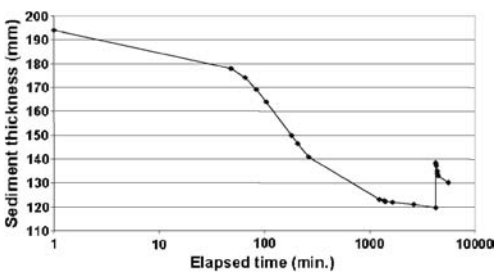

FIG. 6—*Consolidation curve of sediment and cap.*

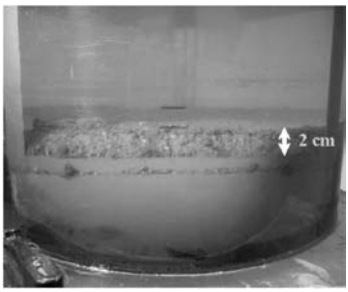

FIG. 7—*Particles falling from the face of the cap.*

cylinder was tilted a further 1° and then tilted back to horizontal. All water was drained and the resulting failure zone can be seen in Fig. 8. This failure was as deep as the capping layer itself but none of the sediment layer underneath was visible from the surface.

This failure mechanism was not as expected, since failure was believed to occur at a much lower inclination. Instead, the sand failed around its friction angle, the angle of repose, which is close to 40°.

In Fig. 9 the maximum shear strength in sand is shown as a function of submerged capping thickness (corresponding effective normal stress).

As seen in Fig. 9, the undrained shear strength at the top of the contaminated sediment must be greater than 0.1 kPa (corresponding to a 20 mm cap).

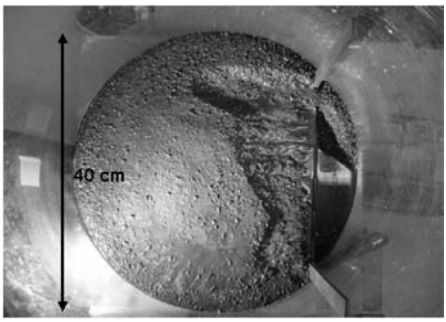

FIG. 8—*Failure zone of cap at 40°.*

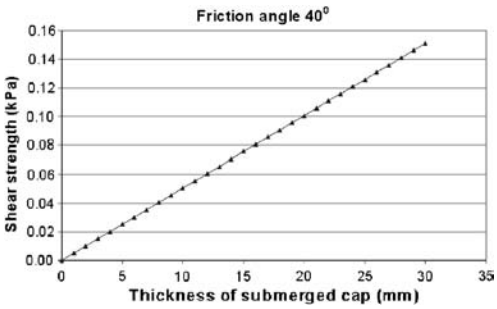

FIG. 9—*Maximum shear strength in sand.*

FIG. 10—*Fractures in sediment after the wall was removed.*

Test 2: Sediment Without a Cap Above Internal Wall

Based on the results from the previous test, test 2 was performed without a cap. However the sediment layer was higher than the internal wall. The sediment was mixed and allowed to consolidate about 1500 min. The temporary wall was then removed to allow the sediment to slump forward from the wall.

Figure 10 shows the fractures that formed in the sediment the moment the wall was removed, it must be said that at this point the exposed face of the sediment was still quite steep. The excess sediment that had fallen down into the front of the cylinder was removed to allow further erosion. The whole system was then allowed to stand for approximately 24 h, the resulting slope can be seen in Fig. 11. This slope was then measured and the cross section drawn to find the angle of the slope (see Fig. 14).

Test 3: Sediment and Cap Above Internal Wall

The third test was conducted similarly to test 2, although this time with a 3 cm capping layer of sand placed on the sediment. The sediment was permitted to consolidate after the application of the cap, the results can be seen in Fig. 12.

As in test 2, the system was placed onto the tilt table and the temporary wall was removed. The result was that the sand layer crumbed at the face but the sediment remained upright.

The system was allowed to stand for a further 24 h, although the face of the sediment failed around 3 h after the wall was removed. The resulting face can be seen in Fig. 13.

The angle of the face was measured and was found to be approximately 65° (see Fig. 14).

FIG. 11—*Slope in sediment after standing for* 24 h.

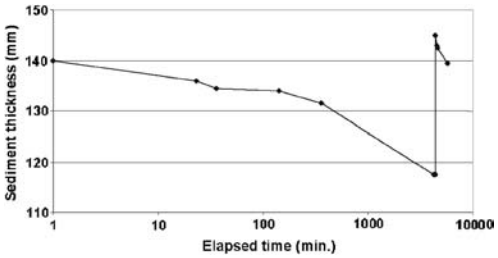

FIG. 12—*Consolidation curve of sediment and cap in test 3.*

A rough stability analysis has been performed assuming a circular critical failure zone illustrated in Fig. 15. Height H and average slope angle β is based on the profile in Fig. 14.

For test 2 the average shear strength is calculated to 0.11 kPa, and for test 3 the average shear strength

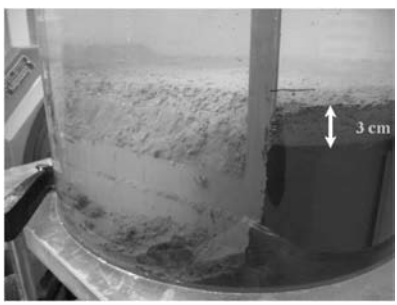

FIG. 13—*Resulting face of capping and sediment material.*

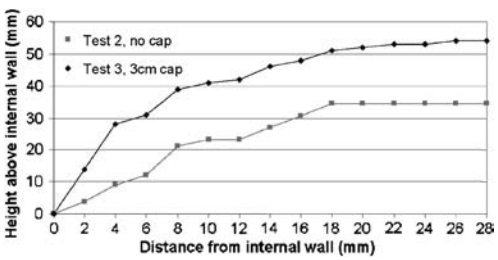

FIG. 14—*Cross section through center of column, test 2 and test 3.*

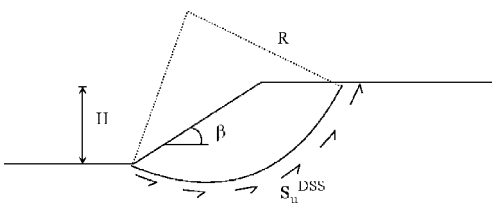

FIG. 15—*Stability analysis.*

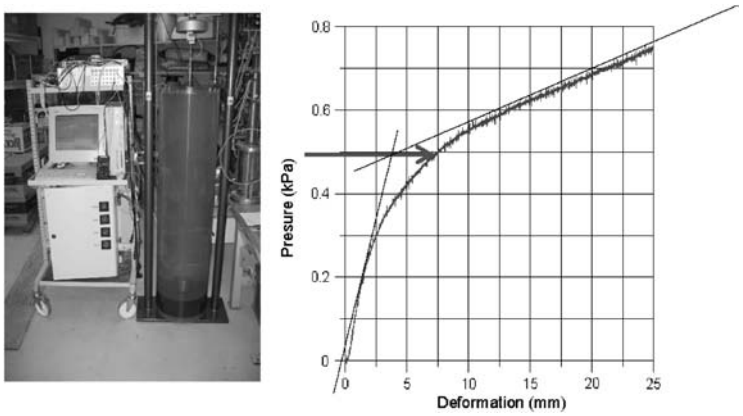

FIG. 16—*Preliminary plate-bearing test.*

is calculated to 0.14 kPa. The results must be considered as rough estimates, but we see the effect of a 3 cm cap giving an increased strength in test 3 compared to test 2 without capping. Both results exceed the value of 0.10 kPa indicated in Fig. 9.

The increase in shear strength from test 2 to test 3 could also be calculated by using Eq 1 with $\alpha = 0.2$ and

$$\Delta s_u^{DSS} = 0.2(p_0' + \Delta p_v') = 0.2[0 + 0.03(16 - 10)] = 0.035 \text{ [kPa]}$$

If the shear strength of the material is 0.10 kPa, the maximum bearing capacity of this material is approximately 0.5 kPa, which corresponds to a submerged capping thickness of 8 cm (total unit weight 16 kN/m^3).

A plate-bearing test was performed with a cylinder. A 2 cm capping layer of sand was placed on top of the same sediment as used for the tilting tests. The cylinder penetrated the cap with constant velocity and the resisting force was measured. Figure 16 shows picture of the setup and initial results from the test.

The results of the plate-bearing test indicate that the bearing capacity with a 2 cm capping layer with sand is about 0.5 kPa, and this compares well with the findings from the tilting test.

Special Oedometer Test

Three parallel tests were performed with the same sediments used in the tilting tests. The material was remolded and had an initial water content of 130%, void ratio 3.65, and salt content of the pore water about 35 g/l (equivalent NaCl). The specimen hight was 92.8 mm with diameter Ø40 mm. Measurements were taken for the following load steps: 1, 2, 3.9, 7.8, 15.7, and 31.4 kPa. The most interesting load step in relation to the tilting test is the first load step of 1 kPa.

Results and Discussion, Oedometer Tests

Figure 17 shows results for a load of 1 kPa. Time for primary consolidation was about 2000 min for the smallest load steps. For the first load step, the permeability coefficient k is calculated to 0.26 m/yr and the coefficient of consolidation c_v is found to be 0.69 m^2/yr. The permeability was decreasing with an increase in load steps. For the last load step, the permeability was found to be 0.05 m/yr.

Time for primary consolidation can be calculated from the following expression [1]:

$$t_p = \frac{H^2}{c_v} \tag{2}$$

where H is one-half of the consolidating stratum.

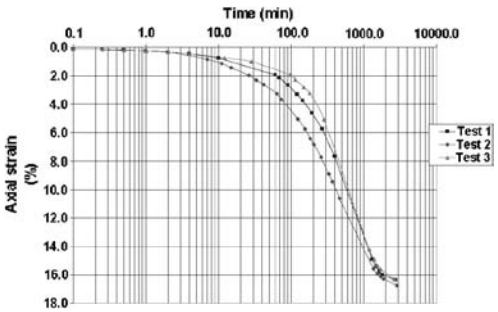

FIG. 17—*Results from oedometer test,* 1 kPa.

It should be mentioned that a thick layer of contaminated material will dissipate excess pore pressure much later than a thin layer. For test 1, the consolidating stratum is H=130 mm. Assuming c_v to about 0.69 m^2/yr, Eq 2 gives a time for primary consolidation of nine days. The sand was added after about one day.

Empirical correlation between compression index and in situ water content for clay and silt deposits and for peat is given in [6]. As can be seen in Fig. 18, results from the oedometer test show that the compression index is within the expected range but in the lower end of the reported data.

Conclusions

Simple tests were performed with dredged material mixed into columns with sea water to determine very low shear strengths. One very important finding is that it is possible to add a thin sand layer on top of a very soft and fluffy dredged material, if initial consolidation of the dredged material is allowed. At this stage the dredged material is by definition a continuum. If sand is added just after mixing, the sand particles will fall through the sediments.

A simple tilting table test indicated a possible shear strength range from 0.10–0.15 kPa in the upper part of the dredged material after capping with 2–3 cm of sand and three days of consolidation. This thin sand layer has two important functions. It will increase the shear strength after consolidation and it will act as a draining layer of excess pore pressure if more dredging material is added on top of it.

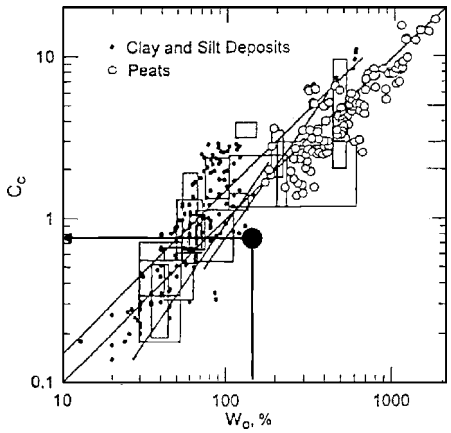

FIG. 18—*Empirical correlation between compression index and in situ water content [6] and compression index measured in oedometer tests.*

Oedometer tests show that the time for consolidation and strength increase can be very long if the dredged sediment thickness is high. The addition of a thin layer of sand in between deposing dredged material in a sub-aqueous disposal facility is therefore recommended.

References

[1] Lambe, T. W. and Whitman, R. V., *Soil Mechanics*, John Wiley & Sons, Inc., New York, 1969.

[2] Gerhart, P. M. and Gross, R. J., *Fundamentals of fluid mechanics*, Addison Wesley, Reading, MA, 1985.

[3] Lunne, T., Robertson, P. K., and Powell, J. J. M., *Cone Penetration Testing In Geotechnical Practice*, Blackie Academic & Professionals, London, 1997.

[4] Zreik, D. A., Ladd, C. C., and Germaine, J. T., "A New Fall Cone Device for Measuring the Undrained Strength of very weak cohesive soils," *Geotech. Test. J.*, Vol. 18, No. 4, 1995, pp. 427–482.

[5] Eek, E., Cappelen, P., Holme, J. K., Breedveld, G. D., and Hauge, A., "Subaqueous Disposal and Capping of Dredged Material: Sedimentation and Bearing Capacity," In: H. Tremblay, J. Locat, and R. Galvez-Cloutier, Eds., *Proceedings from the 2nd International Symposium on Contaminated Sediments*, 26–28 May 2003, Quebec City, Canada. pp. 229–332.

[6] Terzaghi, K., Peck, R. B., and Mesri, G., *Soil Mechanics in Engineering Practice*, Third Edition, John Wiley & Sons, New York, 1996.

Journal of ASTM International, Vol. 3, No. 7
Paper ID JAI13354
Available online at www.astm.org

Shigeru Tani,[1] *Shinji Fukushima,*[2] *Akira Kitajima,*[3] *and Koji Nishimoto*[2]

Applicability of Cement-Stabilized Mud Soil as Embankment Material

ABSTRACT: Although conventional improved soil using cement has high strength, a maximum strength can be induced by a small strain, causing cracks. Thus, such improved soil is not considered to be fit for core materials (i.e., impervious materials) for earth dam embankments. We have developed a method to repair embankments with crushed and compacted soil utilizing earth dam mud soil. This method enables embankments which rarely crack to be constructed. The improved soil was produced in the following manner. First, the stabilized soil was cured for a few days. The soil was then crushed, plowed, compacted, and re-stabilized, resulting in an improved soil that, although it had lower strength, at the maximum strength can only be generated by a large strain. In this paper, mechanical tests for soil specimens prepared in a laboratory and obtained from actual embankments were used to obtain the curing times till crushing, and the strength and deformation characteristics of the crushed-compacted soil. In addition, we carried out a dry-wet cycling test for endurance for the crushed-compacted soil, and examined the mechanical characteristics. Finally, we describe some actual examples where the present method has been applied.

KEYWORDS: earth dam, embankment, mud soil, improvement soil

Nomenclature

t_S = curing period at initial stabilizing process
$(q_u)_{IS}$ = unconfined compressive strength of initial stabilized soil
$(q_u)_{IS10}$ = unconfined compressive strength at $t_S=10$ days of initial stabilized soil
w = water content of mud soil before stabilization
$(w_0$ = water content at reference condition)
$(q_u)_{CC}$ = unconfined compressive strength of crushed and compacted soil
t_{CC} = curing period after crushing and compacting the initial stabilized soil
$t(=t_S+t_{CC})$ = total curing period after cement mixing
$(q_u)_{CC7}$ = unconfined compressive strength at $t_{CC}=7$ days of crushed and compacted soil
$(q_u)_{CC}$* = design strength of crushed and compacted soil
$(q_u)_{CCStability}$ = strength required to keep embankment stability
$(q_u)_{CCTrafficability}$ = strength required to achieve trafficability of construction vehicles
R = strength reduction rate in crushing and compacting process of initial stabilized soil (R_3: value of R at $t_S=3$ days)
ΔW_C = cement weight required to achieve design strength
ρ_{tCC} = wet density of crushed and compacted soil
α_{FL} = ratio of field strength to laboratory strength in stabilized soil

Manuscript received November 4, 2005; accepted for publication December 19, 2005. Presented at ASTM Symposium on Contaminated Sediments: Evaluation and Remediation Techniques on 23–25 May 2006 in Shizuoka, Japan; M. Fukue, K. Kita, M. Ohtsubo, and R. Chaney, Guest Editors.
[1] Program Coordinator, National Institute for Rural Engineering, Ibaraki, 305-8609, Japan.
[2] Engineer, Fujita.Co. LTD, Tokyo, 151-8570, Japan.
[3] Engineer, Fujita Technical Center, Kanagawa, 243-0125, Japan.

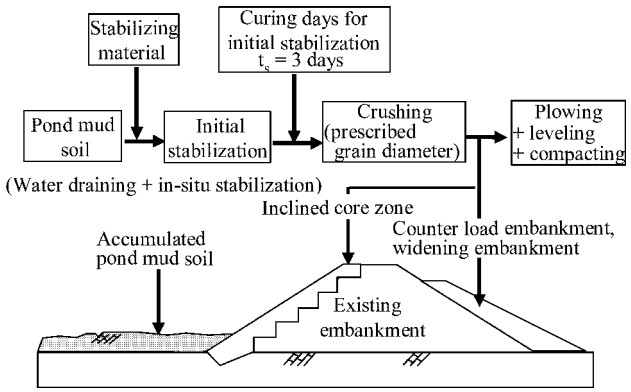

FIG. 1—*Schematic of construction method with crushed-compacted soil and application of improved soil.*

Introduction

In Japan, there are approximately 100 000 small-scaled earth dams (with a capacity to store 1000 tons of water) for irrigation called the "earth dams." These earth dams were constructed in ancient times, and thus are superannuated. In the areas that have become urbanized around the earth dams, nearly 20 000 earth dams need to be repaired immediately due to the problems of increasing water leakage and safety concerns. The following problems appear in such areas: (1) it is difficult to obtain embanking and core materials necessary for repairing and reinforcing the embankments and (2) mud soil often accumulates at the bottom of the earth dams, thus reducing the volume of water that can be stored and degrading the water quality. In addition, the construction needs to be executed carefully to protect the living environment from the noise and vibration that are generated. We have developed a method for repairing the embankments using "crushed and compacted soil produced by utilizing the mud soil of earth dams."

Outline of Crushed and Compacted Soil

It will soon become possible to harden soft soil using stabilization materials with cement and to obtain the required mechanical strength. Although the stabilized soil has a high strength, it can be failed by a small strain and suffer a larger deformation compared to that of the surrounding ground (embankment) soil making it difficult to use the soil as embankment materials (impervious materials) for the earth dams which require low permeability.

Figure 1 shows the outline of the newly developed method. A soil improvement material with cement is added to the mud soil of earth dams and the soil that is excavated from existing embankments and the natural ground. After mixing and solidifying, they are crushed to the required maximum grain size and compacted to construct embankments. The properties of the easily cracked, stabilized soil can be made similar to those of natural soil by crushing once. Figure 1 shows that in earth dam repairs, embankments are often widened and raised on the upstream and downstream slopes that need to be reinforced. Water core nature is not required for such embankments; rather, water permeability is preferred. It is ideal to obtain the required mechanical strength and permeability coefficient according to usage for the embankment materials that are to be used to repair earth dams. Necessary mechanical characteristics can be obtained with the crushed and compacted soil by varying the mixing ratios of the pond mud soil and the excavated soil from existing embankments and the natural ground, the amount of cement added, and the maximum size of the grains obtained by crushing.

In this paper, the mechanical characteristics of the embankment materials using purely pond mud soil are described, while multiple kinds of soil, together with the pond mud soil, are used in the actual embankment construction. Thus, with the newly developed technique earth dams can be renewed without incurring costs for discarding the pond mud soil and for purchasing other types of soils.

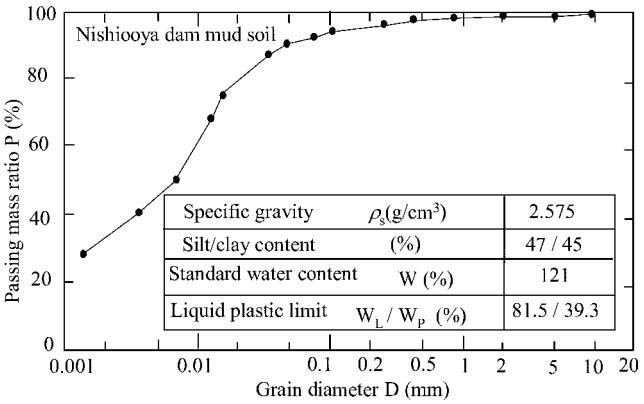

FIG. 2—*Grain size and physical characteristics of the earth dam mud soil.*

Mechanical Characteristics of Fracturing- and Rolling-Processed Soils

Crushed-compacted soil and initial-stabilized soil were developed by solidifying the pond mud soil obtained from the bottom dam reservoir in a pit for a certain period of time (t_s), excavating it, crushing the stabilized soil to the required maximum grain size (D_{max}), and compacting the crushed soil. Embankments with a deformation properties that are similar to those of natural soil can be constructed with this crushed-compacted soil. The curing time after crushing is denoted as t_{cc}. The curing time t is t_s (day) for the usual initial stabilized soil and t_s+t_{cc} for the crushed and compacted soil because the stabilization continues after embanking. In the following section, we describe the experimental results obtained from the mechanical tests for the specimens that were prepared in the laboratory and obtained from actual embankments. From the results, we examine the curing times till crushing, and the characteristics of strength, deformation, and water permeability of crushed and compacted soil using the results. In addition, we have carried out a dry-wet cycling processing test for endurance with the crush-compacted soil, leading to a study of their mechanical characteristics.

Curing Times

Earth dam mud soil that was obtained from the Nishiooya dam was used for testing. Considering the actual work operation, this state was defined as the initial one after the free water was removed from the mud soil. Figure 2 shows grain size curves and physical characteristics of the earth dam mud soil that was used in the tests. The soil consists of mainly fine grains that are less than 0.075 mm in diameter, and because of its high water content (w=121 %), the soil has not been considered to be suitable as an embankment materials. The stabilization material used in this test program was a cement stabilizer for soft soil improvement and the cement content was expressed by the additive ratio C_W (%) that a percent of the cement stabilizer to the wet unit weight of the mud soil.

Figure 3 shows the unconfined compressive strength (q_u) of the specimens that were prepared in a laboratory using a mold for initial stabilized soil and crushed-compacted soil on initial stabilization time (t_s). The specimens were 50 mm in diameter and 100 mm high. The initial stabilization soil was prepared by mixing prescribed amounts of stabilization material with cement and pond mud soil to fill a mold with no voids, and then cured. After curing for the necessary period, the stabilized soil was taken out of the mold, and crushed into grains with an approximate maximum size of 10 mm by a straight edge. Then, they were packed in the mold to be compacted according to the method A of JGS T071 (E_c=550 KJ/m^3) (Japanese Geotechnical Society, 2000), and cured for the necessary period. Unconfined compression tests were performed on these specimens. Figure 3 shows the dependence of unconfined compressive strength (q_u) on the curing time (t_{cc}) for initial stabilization periods t_s, 1, 3, and 7 days. As the initial stabilization

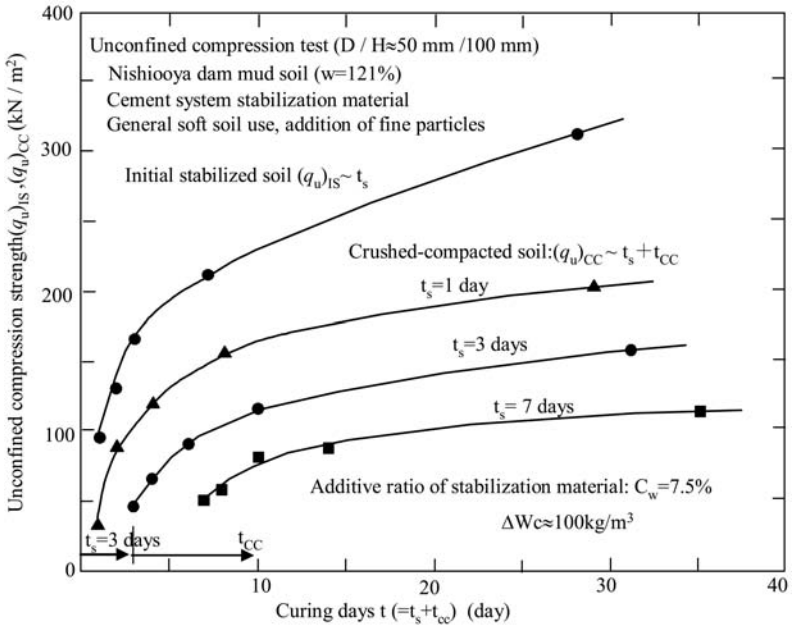

FIG. 3—*Effect of initial stabilization period on strength of initial stabilized soil and crushed-compacted soil.*

period increases, the strength immediately after crushing and compacting is reincreasing, while the final strength is small compared to that for shorter initial stabilization periods as these periods increase, indicating that the increase in the strength after crushing and compacting is small.

Figure 4 shows the effect of initial stabilization period on reduction in unconfined compressive strength (q_u)cc for a 28-day-old crushed-compacted soil obtained from the pond mud soil with different contents of fine grains Fc (i.e., weight fraction of the grains with the sizes less than 0.075 mm), which is

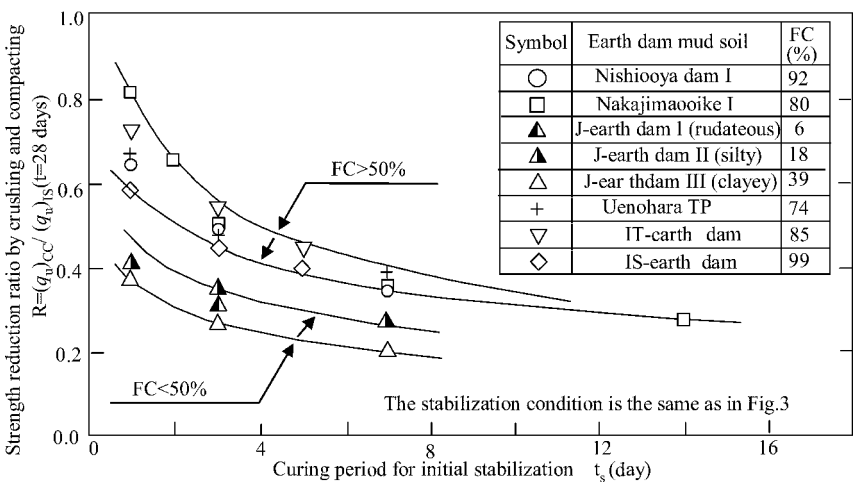

FIG. 4—*Effect of initial stabilization period* (t_s) *on strength reduction by crushing and compacting.*

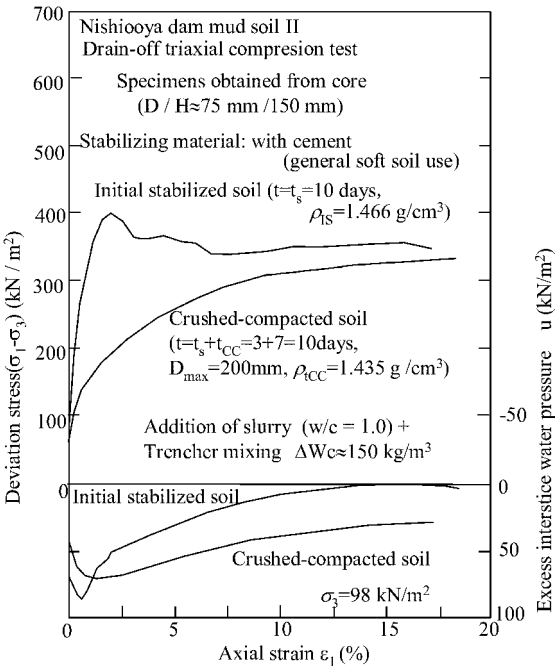

FIG. 5—*Example of relationship between initial stabilized and crushed-compacted soil.*

represented using a strength ratio, $R=(q_u)_{CC}/(q_u)_{IS}$. As the curing period of crushed-compacted soil (t_{cc}) increases, the strength $(q_u)_{CC}$ becomes small compared to that of the initial stabilization soil $(q_u)_{IS}$, and the strength ratio R decreases, e.g., for a curing period of three days, $R=0.3$-0.55.

Moreover, as Fc increases, R tends to decrease roughly. The strength immediately after crushing and compacting $(q_u)_{CC}$ is related to the trafficability of a compacting machine, and the final strength is related to the structural stability of the embankments and solidifying efficiency. Based on this information, the standard initial stabilization period t_s was determined to three days.

Strength Characteristics

Figure 5 shows examples of stress-strain curves that were obtained from the isotropically consolidated undrained triaxial compression tests [at a confining pressure, $\sigma_3=8(kN/m^2)$] for the initial stabilization soil at $t=t_s=10$ days) and the crushed-compacted soil at $t=t_s+t_{cc}=3+7=10$ days with the same composition. The initial stabilized soil exhibits a maximum strength at a strain of approximately 2 %, and the strength decreases at larger strains. On the other hand, the maximum strength of the crushed-compacted soil is smaller than that of the initial stabilized soil; however, it exhibits stress-strain curves similar to those of the ordinary soil, indicating that the deformability of the crushed-compacted soil is not much different from that of the ground or existing embankment soil.

Figure 6 shows the specimens after the triaxial compression tests. While the initial stabilized soil clearly shows the onset of a slip plane due to a local strain concentration, the crushed-compacted soil, as well as the ordinary soil, shows no strain concentration, but a barrel-shaped deformation. Figure 5 shows only the typical data; however, Fig. 7 shows all of the data concerning strains at peak stresses (i.e., failure strain) in the initial stabilized soils and crushed and compacted soils that were obtained from the triaxial compression tests. The additive ratio of the stabilization material is approximately $C_w=15$ %, the failure strain of the initial stabilized soil is 2 %, while that of the crushed and compacted soil is 7–15 % at below $C_w=15$ %. This indicates that the strength of the crushed and compacted soil is mobilized at a larger than that of initial stabilized soil (Fukushima, Kitajima, Tani, and Ishiguro, 2003).

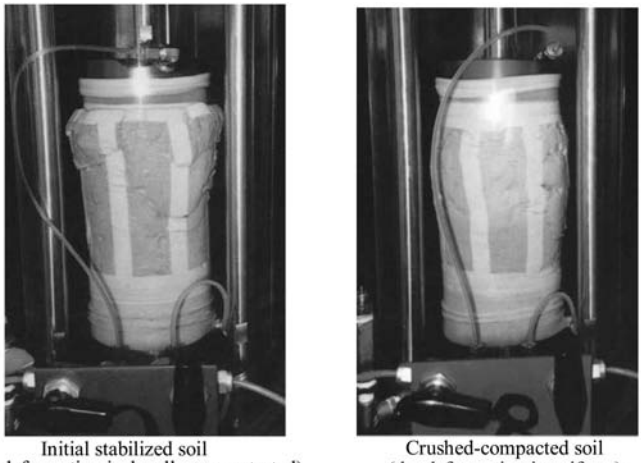

FIG. 6—*Specimens after triaxial compression test.*

Effect of Additive Ratio of Stabilization Material to Unconfined Compressive Strength

For initial stabilized soil ($t=t_s=10$ days) and crushed-compacted soil ($t=t_s+t_{cc}=10$ days), the unconfined compressive strength was compared at additive ratios of the stabilization material, $C_w=5.0$, 7.5, 10, and 15 %. As shown in Fig. 8, the strength of the crushed-compacted soil was lowered to approximately half that of the initial stabilized soil at each additive ratio.

Effect of Crushed Grain Size on Strength of Crushed-Compacted Soil

To examine the effect of the maximum size of grains that were obtained by crushing the initial stabilized soil with the strength of crushed-compacted soil, with the same pond mud soil as in Fig. 2, the crushed-compacted soil ($t=t_s+t_{cc}=10$ days) was prepared by crushing the initial stabilized soil (with a cement content C_w of 7.5 %, $t_s=3$ days) into three kinds of grain sizes ($D_{max}=10$, 20 mm, and less by a mixer), called "crushed grain." Unconfined compression tests were carried out with the crushed-compacted soil.

Figure 9 shows the grain size distribution for each specimen after crushing. The strength of the crushed-compacted soil exhibits approximately $q_u=120$ (kN/m^2) for the large grain size, 100 (kN/m^2) for the middle grain size, and 50(kN/m^2) for the small grain size, indicating that the strength depends considerably on the crushed grain size.

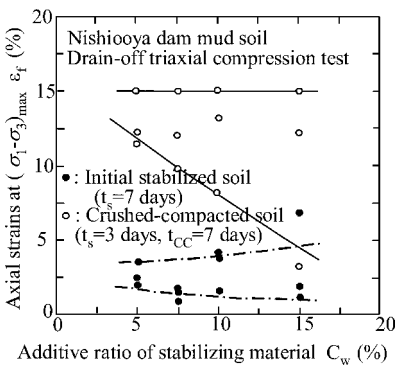

FIG. 7—*Comparison of failure strains for initial stabilized and crushed-compacted soil.*

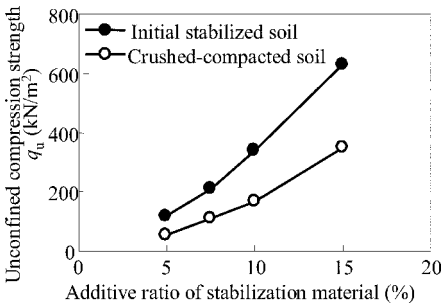

FIG. 8—*Effect of additive ratio of stabilization material to unconfined compression.*

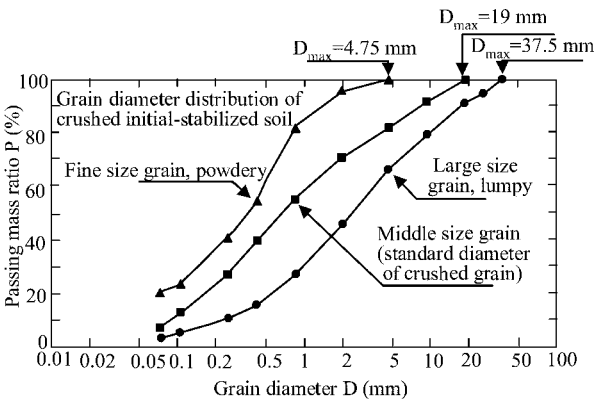

FIG. 9—*Grain size distributions of specimens after crushing (laboratory test).*

Figure 10 shows grain size curves for the soil that was crushed by a bucket-type crashing machine (Fig. 11) into three different sizes (D_{max}=50, 100, and 200 mm); the soil was prepared by solidifying (t_s=3 days) the same earth dam mud soil. Figure 12 shows relative strengths of undisturbed specimens ($t=t_s+t_{CC}=3+7=10$ days), having different maximum grain sizes that were obtained from a constructed embankment; the strengths were determined from unconfined compression tests (where the strength of the specimen with the maximum grain size of 200 mm is denoted by $[(q_u)_{(200)}]$. For $(q_u)_{200}=1.0$, $(q_u)_{100}$ and $(q_u)_{50}$ are approximately 0.85 and 0.65, respectively, indicating that the strength decreases with decreases in grain size. For large sized grains, large clusters exhibit a behavior as if rock materials formed a matrix, thus increasing the strength. This result shows a tendency that is similar to that for the specimens which were prepared in the laboratory mentioned above. As the required grain size increases, the in situ crushing efficiency by the machine increases, and in addition, larger strengths can be obtained for the specimens. These are the constructional and structural merits for embanking.

Characteristics of Permeability Coefficients

Figure 13 shows the results from the permeability tests using triaxial cells that were carried out by varying the additive ratio of the stabilization material (C_w) and the confining pressure in a triaxial cell. The specimens, 60 mm in diameter, and 60 mm high, are the crushed-compacted soil with D_{max}=10 mm and a compaction energy E_c of 550 (kJ/m^3) that were produced from the pond mud soil shown in Fig. 2. The permeability coefficients are slightly dependent on the additive ratio of the stabilization material, while they are clearly dependent on the constraining pressure.

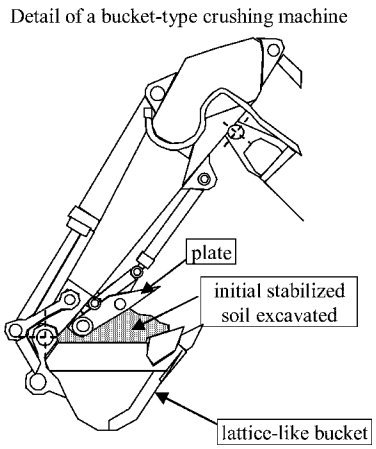

FIG. 10—*Grain size distribution of crushed soil by a bucket-type crushing machine. (Grain size distribution of specimens after in-situ crushing test of embankment.)*

According to a standard for fill dams, permeability coefficients of core materials k are less than 1.0×10^{-6} (cm/s) in a laboratory test, and less than 1.0×10^{-5} (cm/s) for actual embankments. According to a technical guideline for earth dam, k is less than 5.0×10^{-6} (cm/s) in a laboratory test, and less than 5.0×10^{-5} (cm/s) for actual embankments. The figure shows the results from the permeability test using triaxial cell. If the permeability coefficient k_{200} is defined as 1.0 for a grain size of 200 mm, $k_{100}=0.42$ for 100 mm, and $k_{50}=0.30$ for 50 nm, indicating that the permeability coefficient increases with grain size.

These results suggest that the grain size should be small for core materials so that the permeability decreases and should be large for embankment materials so that the strength increases. On the other hand, working site experiments $[k=5.0 \times 10^{-6}(\mathrm{cm/s})]$ suggested that if the content of fine particles of the earth dam mud soil is more than approximately 50 %, the required permeability can be obtained even for the grains with $D_{max}=200$ mm.

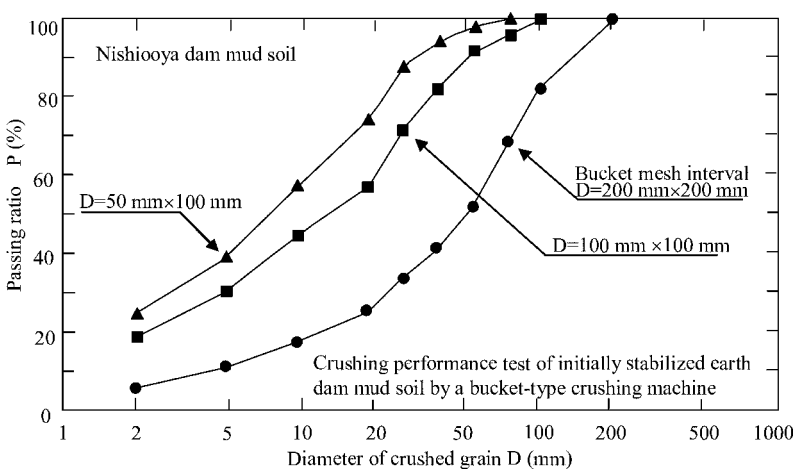

FIG. 11—*Schematic of bucket-type crushing machine.*

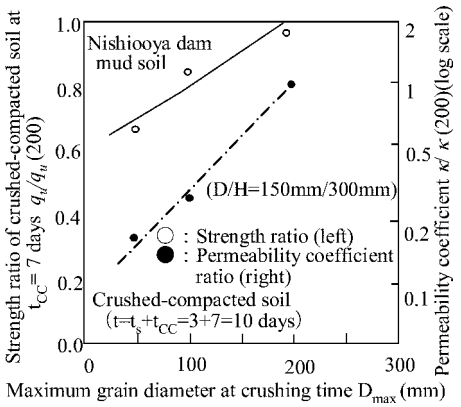

FIG. 12—*Permeability coefficient ratio and strength ratio of crushed-compacted soil (specimens prepared in laboratory).*

Characteristics of Consolidation and Settlement

After construction, embankments exhibit a consolidation-settlement behavior due to their own weight, and so a consolidation test was carried out to clarify such settlement characteristics. Specimens were 60 mm in diameter, and 60 mm high, and the preparation method was the same as that for the permeability test. Figure 14 shows the relationship between the settling strain ε_v and the consolidation pressure σ_v for the initial stabilized soil with various additive ratios of the stabilization material ($t=t_s=10$ days) and the crushed-compacted soil ($t=t_s+t_{cc}=3+7=10$ days). When σ_v exceeds a certain value, ϵ_v increases considerably for the initial stabilized soil, while it increases more gradually for the crushed-compacted soil, which is clearly seen particularly in low additive ratios, indicating a strain hardening behavior, as shown in the stress-strain curves that were determined from the triaxial compression test. Thus, the deformation of a new embankment that constructed the crushed and compacted soil can be considered to follow the settlement of the existing embankment without the local concentration of strain.

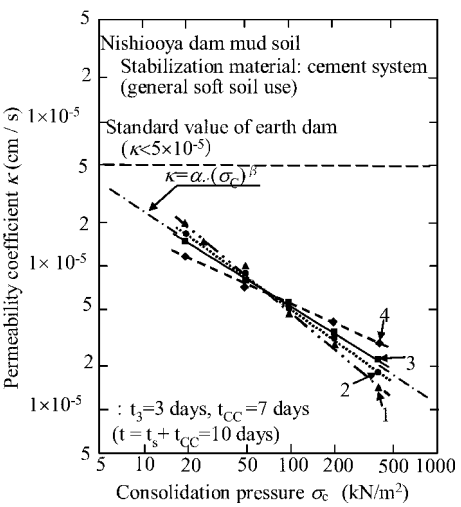

FIG. 13—*Effect of maximum grain size at crushing time on strength and permeability coefficient of crushed-compacted soil.*

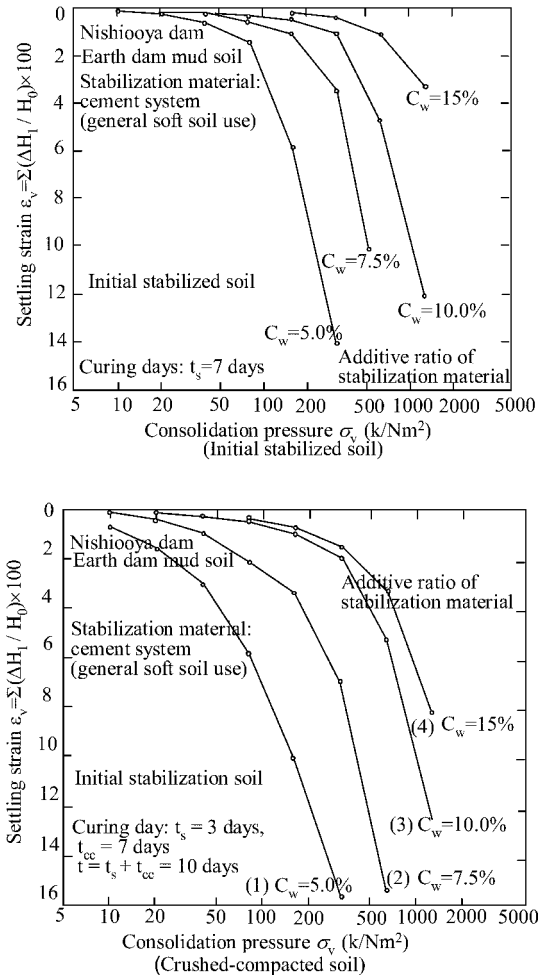

FIG. 14—*Relationship between settling strain* ϵ_v *and consolidation pressure* σ_v *(consolidation test).*

Effect of Dry-Wet Cycling Procedure

Earth dam embankment soil repeatedly undergoes dry and wet states due to the variation in the level of stored water or the weather. Thus, to examine the long-term stability of crushed-compacted soil, the unconfined compression tests were carried out for the soil by dry-wet cycling processing. For t_s=3 days and t_{cc}=28 days, $t=t_s+t_{cc}$=31 days, the unconfined compressive strength of the crushed-compacted soil is defined as the standard strength. Two types of dry-wet cycling procedure were executed for $t=t_s+t_{cc}$=3 +7=10 days; one is the repetition of a serial process of air drying –> water immersion–> air drying, and the other is the repetition of a serial process of 110°C oven drying –> water immersion –> oven drying. To execute the procedure of the cycle number for the remaining 21 days, e.g., for three cycles, the dry-wet state is repeated 21/3=7 days/1 cycle.

Figure 15 shows the relationship between the number of dry-wet cycles and the strength ratio (unconfined compressive strength of the crushed-compacted soil undergoing dry-wet cycling N times (q_uN)/ unconfined compressive strength of crushed-compacted soil (q_u) (t=31 days). The reduction rate in the strength for case (2), i.e., 110°C oven dry –> water immersion –> oven dry is larger than that for case

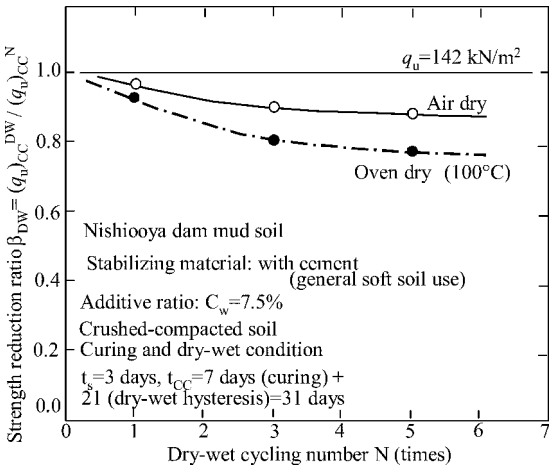

FIG. 15—*Effect of dry-wet cycling processing on unconfined compression strength of crushed-compacted soil.*

(1), i.e., air dry –> water immersion –> air dry, indicating that the reduction rate in the strength is larger for the soil at the more severe drying condition. However, the reduction rate is approximately 20 % at most, thus by considering the dry-wet cycling condition which can actually occur, there is no problem if the strength is designed to have a sufficient margin.

Improved soil using cement has long been used as a protective material for the slope of the dam pond beds, and its long-term stability has been verified. To examine the durability of the crushed-compacted soil, as mentioned above, the dry-wet cycling test was carried out with the specimens, and it was verified that no problems occur regarding the stability if the designed strength has a sufficient margin. However, in the actual construction, it is necessary for the cover soil layer of 30–50 cm thick to protect the embankment from the dry and wet weather conditions.

Next, we describe examples where the newly developed method has been applied, such as works for upgrading the water storage capacity of superannuated earth dams and the embankment repairing works for water leakage protection.

Design and Execution of the Embankment Construction Method with Crushed-Compacted Soil

Outline of the Construction Method

The embankment construction method using crushed-compacted soil is a technique to construct inclined core zones for water leakage protection and raising embankments using crushed-compacted soil which is prepared in the following manner: (1) "Initial stabilized soil" is prepared by adding a stabilization material with cement to the mud soil that has accumulated at the bottom of earth dams (pond mud soil) and cured for a certain period t_s (initial stabilization period) to acquire the required strength and the low permiability; (2) then the soil is crushed into grains with required maximum sizes D_{max}; and (3), the crushed soil is plowed and leveled to have a constant layer thickness, and then compacted afterward in the same manner of ordinary soil. The embankment soil, called crushed-compacted soil can have a deformability that is similar to that of the usual soil from crushing and compacting the once-stabilized soil.

The execution process of this method consists of three processes, initial stabilization of pond mud soil, crushing of the initial stabilized soil, and embanking with the crushed soil. The following procedure is standardized in the initial stabilization process, that is, after emptying out of the dam reservoir, slurry with a composition ratio of water to a stabilization material by weight, w/c=1.0 is added to the pond mud soil

for in situ stirring using a trencher-type mixer. In this process, homogenous stabilization mixing is most essential for constructing structurally homogenous embankments by the crushed and compacted with the required strength and the low permeability.

In the crushing process, the initial stabilized soil that has been cured for a certain period t_s (t_s=3 days is standard) is crushed into grains with required maximum sizes D_{max} using a bucket-type crushing machine which can do such operations as excavation -> crushing -> loading consecutively. This crushing machine has a skeleton bucket with a capacity of 0.7 m^3, having a soil extruding plate with a maximum power of 196 kN, (the bucket is replaced with that of a backhoe having a capacity of 0.7 m^3). The initial stabilized soil is pushed out of the skeleton by the extruding plate with a required mesh interval to execute the crushing and loading operations. (D_{max} is adjusted by changing the skeleton mesh interval.) D_{max} can influence the strength and core performance of the crushed-compacted soil, that is, by increasing D_{max} the strength increases, and the low permeability decreases.

In the embankment process, the crushed soil was plowed by a backhoe to mix the grains consisting of coarse to fine particles homogeneously and to obtain a constant layer thickness, leveled by a bulldozer, and compacted by a vibrating roller. Furthermore, the surface region of the slope was covered by soil with a thickness of 30–50 cm for green planting to protect the crushed-compacted soil from degradation due to the dry-wet state cycling and the prevention of alkaline elution from the embankment constructed by the crushed and compacted soil.

Setup of Target Strength

According to the "quality improvement method for general soil," the strength of the initial stabilized soil or the crushed-compacted soil is represented by an unconfined compressive strength q_u, and the strength parameter is indicated by the cohesion, neglecting the internal frictional angle ϕ.

$$C = q_u/2 \tag{1}$$

The strength of the pond mud soil stabilized by a stabilization material with cement usually increases with curing time t, while it decreases drastically after t=10 days. Thus, the target strength $(q_u)_{cc}$* is determined to be the strength at $t=t_s$=10 days after adding and mixing the stabilization material for the initial stabilized soil, and the strength $(q_u)_{cc7}$ at t_{cc}=7 days ($t=t_s+t_{cc}=3+7=10$ days) after crushing and compacting to obtain the crushed-compacted soil.

The strength $(q_u)_{CC^*}$ is examined using $(q_u)_{CCStability}$(=$2C_{Stability}$), which is transformed from the cohesion $C_{Stability}$ (estimated from a stability analysis) that is required for the crushed-compacted soil part of the inclined core zone so that the whole the embankment is stable or satisfies the safety ratio Fs^*. By using $(q_u)_{CCTrafficability}$ which is required for the trafficability of execution machines under construction.

$$(q_u)_{CC^*} = [(q_u)_{CCStability}, (q_u)_{CCTrafficability}]_{max} \tag{2}$$

The embankments of many earth dams are less than 10 m in height, and for these embankments, $(q_u)_{CCTrafficability}$ is usually larger than $(q_u)_{CCStability}$. The strength $(q_u)_{CCTrafficability}$ can be obtained as shown below. The strength required for the trafficability of execution machines at the time of embankment construction with crushed-compacted soil is $(qu)_{CC0}$ at t_{CC}=0 day immediately after crushing and compacting the initial stabilized soil. Thus, if $(q_u)_{CC0}$ must satisfy a bearing force (the cone index, q_C =490 kN/m^2, is the standard) where operation is possible on the embankment foundation ground of the earth dam, then using the transformation equation, $q_u=q_c/7.5$

$$(q_u)_{CC0} = 65 \text{ kN/m}^2 \tag{3}$$

As stabilization proceeds, $(q_u)_{CCTrafficability}$ changes from $(q_u)_{CC0}$ at the time of the embankment construction to $(q_u)_{CC7}$ generated at t_{cc}=7 days which is the day to set the target strength and can be determined using the equation $(q_u)_{CC7}=(q_u)_{CC0}$ that was obtained from the mixing proportioning test.

If the target strength $(q_u)_{CC}$* [=$(q_u)_{CCTrafficability}$] of the crushed-compacted soil can be transformed into the target strength $(q_u)_{IS}$* of the initial stabilized soil, using a strength reduction ratio R_3 due to the crushing and compacting of the initial stabilized soil (R_3 is the value at t_s=3 days which corresponds to the standard initial stabilization days)

$$(q_u)_{IS}{}^* = (q_u)_{CC}{}^*/R_3 \tag{4}$$

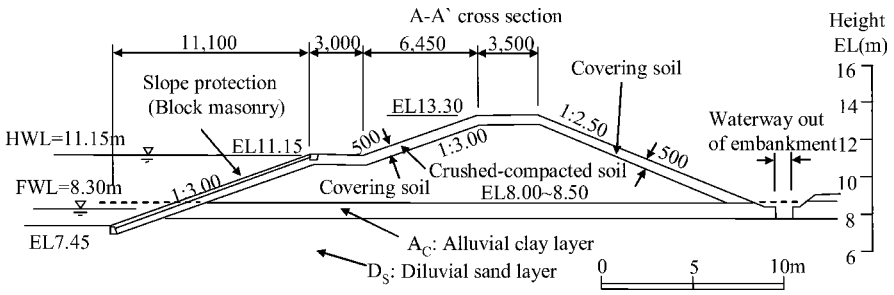

FIG. 16—*Standard cross section of Jige dam embankment.*

Determination of Amount of Stabilization Material Added

In the present construction method, stabilization material with cement (for soft soil use) is intended to be used, because it is suitable for the stabilization of the mud soil with high water content. The stabilization material can induce a large strength in the early stage of curing of such stabilized soil, and has characteristics suitable for the present construction method which involves crushing and compacting at approximately $t_s=3$ days. For convenience, at the time of execution of working, the additive amount of the stabilization material added is defined as the weight of the cement ΔW_C to weight of pond mud soil of 1 m^3. The cement was added to the pond mud soil by the slurry of w/c=1.0. The slurry method which is suitable for homogeneous mixing, is standard for pond mud soil stabilization.

The mixing condition test was carried out on the basis of water content $w=w_0$ that was expected at the actual execution for pond mud soil, and the effect of ΔW_c and curing times $t(=t_s)$ on the initial stabilization strength $(q_u)_{IS}$ of pond mud soil was examined to determine a linear relation between ΔW_c and $(q_u)_{IS10}$ at $t_s=10$ days which is the setting day of the target strength, that is

$$\Delta W_C = A + B(q_u)_{IS10} \tag{5}$$

The amount of stabilization material added in the actual working site ΔW_C^* can be obtained by substituting the extra strength $(q_u)_{IS}{}^*/\alpha_{FL}=1/1.5$. The value of α_{FL} is the field-laboratory strength ratio to correct the strength by consider the different between the actual working site mixing and the laboratory mixing conditions, we adopted especially $\alpha_{FL}=1/1.5$ from the results of the mixing tests in the construction cite.

Depending on the accumulation site of the pond mud soil, since the water content w before stabilization of mud soil is not constant, if the effect of w on $(q_u)_{IS10}$ is not considered, the strength of a stabilized mud soil is varied. Thus, for ΔW_C at the time of the actual execution, w at the time before stabilization is measured, and according to the difference from standard value w_0 *in* the mix proportioning test, ΔW_C^*at $w=W_0$ is adjusted in the following manner. The relationship between $(q_u)_{IS10}$ and w, which is obtained from the mix proportioning test, is approximated by the following equation, independent of the kind of pond mud soil and ΔW_C:

$$(q_u)_{IS10} = a^*(w/w_0)^b \ (b=-1.37). \tag{6}$$

Thus, using Eq 5, the strength $(q_u)_{IS10}$ at $w=w_0$ can be determined, and the effect of w on $(q_u)_{IS10}$ can be taken into account.

Applications to the Construction of Homogeneous-Type Embankment (The Repair Work of the Jige Dam Embankment)

The Jige dam is located in Suzuka city in the Mie prefecture. To add a water storage capacity of 120 000 m^3 for flood control to the present capacity of approximately 20 000 m^3 for irrigation, the peripheral region of the old earth dam was excavated for expansion, and the main embankment was moved 30 m downstream from the former embankment, and a new flat-bottomed earth dam embankment was constructed there. The standard cross-sectional view is shown in Fig. 16, and the structural parameters of the embankment are shown in Table 1. The embankment is a homogeneous type, because there are soft

TABLE 1—*Structural parameters of Jige dam embankment before and after repairing.*

Embankment specifications	Before repairing	After repairing
Type	Homogeneous	Homogeneous
Height (m^3)	4.5	5.3
Length (m^3)	90.0	4000
Volume (m^3)	7000	33 000
Amount of stored water (m^3)	20 000	140 000
Amount of crushed -compacted soil (m^3)	···	30 000
Slope gradient	1: 2.0 (upstream) 1:1.8 (downstream)	1:3.0 (upstream) 1:2.5 (downstream)

parts in the foundation ground, and also because it is necessary to decrease the amount of disposal portion of the excavated soil, as described below. In this earth dam, there is no place to discard the pond mud soil in the old earth dam, and the required amount of embankment soil with a high core performance cannot be obtained; therefore, the embankment construction method using crushed-compacted soil was applied, which can produce embankment soil artificially with the required performance of strength and core by solidifying the pond mud soil.

For the embankment construction method using the crushed-compacted soil, the embankment soil is basically produced by solidifying the mud soil that has accumulated at the bottom of the earth dam. However, for this earth dam, as the total amount of embankment soil is approximately 33 000 m^3, while the amount of excavated soil for the reservoir expansion is approximately 110 000 m^3, indicating that if only the pond mud soil is used, it would not be enough for the embankment. Thus, a mixed mud soil was newly prepared by adding the excavated soil (e.g., sand and sand filter soil) to the pond mud soil. The ratio of the amount of earth dam mud soil to that of excavated soil is defined as the volume ratio in the wet state $n_V = V_{Mud}/V_{Cut}$. The ratio n_V^* in the actual working site was also determined to satisfy the standard value of the permiability for the homogeneous type embankment, $k_{Lab} \leqq 1 \times 10^{-5}$ cm/s. The target strength $(q_u)_{CC}$* for the Jige dam, was $(q_u)_{CCTrafficability} = 118$ kN/m^2, which is required for trafficability, and not $(q_u)_{CCStability} = 35$ kN/m^2, because the embankment height is low, and the slope gradient is small.

In this construction, stabilization processing was carried out in a pit to conveniently control the mixing ratio of pond mud soil and excavated soil. As shown schematically in Fig. 17, four pits were set for the following stabilization processes; mixing, first day curing, second day curing, and third day crushing. Excavated soil and pond mud soil were carried in so that their mixing ratio was the required mixing ratio nV^*. Then the adding and mixing of the stabilization material were done by a trencher-type mixer. The dimensions of the pits were 4.5 m wide, 2.0 m deep, and 25–30 m long, corresponding to the amount of stabilized soil per day. The embankment after repairing is shown in Fig. 18.

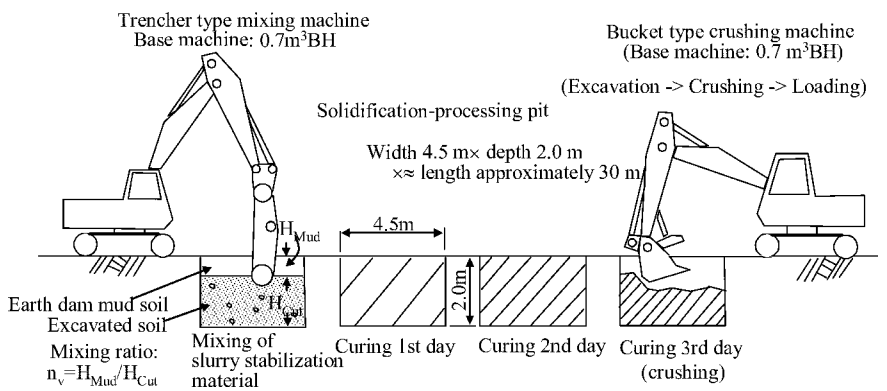

FIG. 17—*Initial stabilization by pit method.*

FIG. 18—*Jige dam embankment after repairing.*

The strength of the embankment was checked using the unconfined compression test for the undisturbed specimens sampled at intervals of embankment volume of $\Delta V = 1000 - 15\ 000\ m^3$ that was obtained from the embankment at each construction time. Figure 19 shows the relationship between $(q_u)_{IS10}$ at the setting day for the target strength, $t = t_s + t_{cc} = 3 + 7 = 10$, or $(q_u)_{CC}$ and the accumulated amount of embankment soil, where the symbol indicates the average value, and the vertical bars indicate the extent of data, from maximum to minimum. The figure shows a scatter of data, which is probably due to the inhomogeneous mixing of the stabilization material, and a variation of the values of n_V or w of the mixed mud soil. The scatter range of $(q_u)_{CC7}$ is 1/2 to ~1/3 that of $(q_u)_{IS10}$. This suggests that more homogeneous embankments can be constructed by crushing and compacting the initial stabilized soil rather than by simply using the initial stabilized soil. In addition, $(q_u)_{CC7}$ did not necessarily satisfy $(q_u)_{CC}$*; however, ΔW_C was not altered to suppress the strength, when the trafficability and the strength stabilizing the embankment $(q_u)_{CCStability}$ were satisfied. This construction method with the crushed-compacted soil aims to build the embankments having not only the strength required for stability but also the properties to have good contact with former embankments, while the usual methods for soil quality improvement only aim to achieve the required strength. However, compacted-crushed soil with strength stronger than necessary worsens the contact with the former embankment, and results in a loss of homogeneity of the embankment.

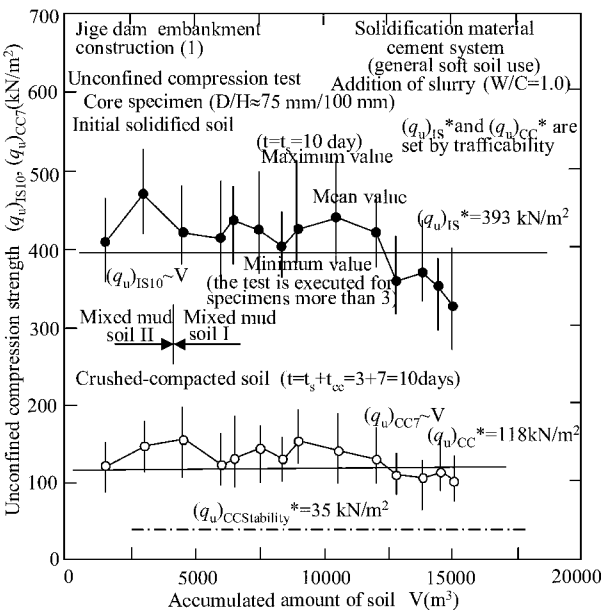

FIG. 19—*Relationship between* $(q_u)_{IS10}$ *or* $(q_u)_{CC7}$ *and V.*

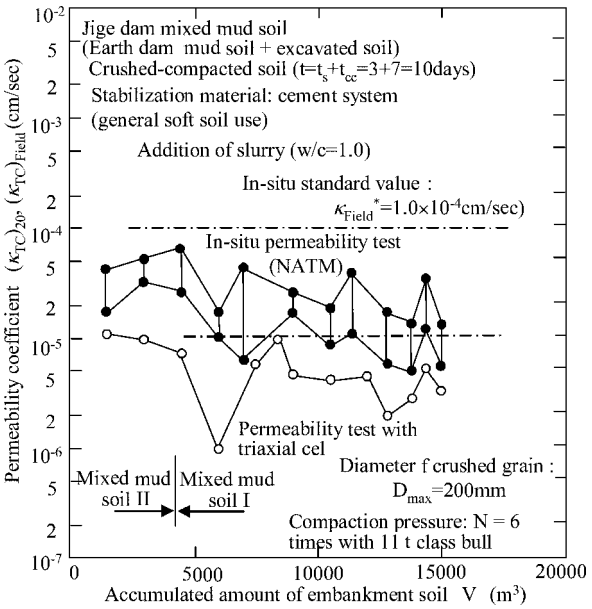

FIG. 20—*Relationship between* k_{Field} *or* $(k_{TC})_{20}$ *and V.*

The low permeability of the embankments was checked by the in situ permeability test of the soil with a certain volume of ΔV at the time of the embankment construction and the triaxial permeability test for the undisturbed specimens obtained from the embankment by (D/H=75 mm/100 mm). Figure 20 shows the relationship between the amount of the accumulated embankment soil V and the maximum and minimum values of permeability coefficients k_{Field}, which were obtained by the in situ permeability test according to JIS A 1218, or the permeability coefficients $(k_{TC})_{20}$ at σ_X=20 kN/m^2 obtained by the triaxial permeability test. This figure demonstrates that $(k_{TC})_{20}$ satisfies the standard value of permeability in the laboratory test, $k^*_{Lab}=1.0\times10^{-5}$ cm/s, although there are the scattering in data, and k_{Field} satisfies the standard value by the in situ permeability test, $k^*_{Lab}=1.0\times10^{-4}$ cm/s. This can be considered due to the setting of a strict condition that k^*_{Lab} should be one tenth of the in situ test value based on test data.

Application to the Construction of Sloping Impervious Zone for Water Leakage Protection

Repairing Work for Torakichizawa Dam Embankment

The Torakichizawa dam, located in Iide-cho, Nishiokitama-gun, Yamagata prefecture, was constructed in 1867, and has been used for irrigation. However, the embankment needed an oval repair because water was leaking from the edge of the embankment slope and the periphery of the bottom gutter due to aging, the cross-sectional deformation of the embankment, lack of height margin, the breakdown of the flood discharge outlet, and the reduction in flow performance. In this repair work, a large amount of pond mud soil was accumulated during excavation for the cut-off trench of the inclined core zone. Such excavated pond mud soil is highly hydrated and extremely soft, and thus must be taken to a treatment plant. However, it is very expensive and not desired environmentally. For the Torakichizawa dam, an inclined water core zone was constructed by the embankment construction method with the crushed-compacted soil, produced by solidifying the pond mud soil using a cement system stabilization material, and having the required strength and core performance (Fukushima, Tani, Kitajima, and Ishiguro, 2004).

Figure 21 shows the cross-sectional view of the embankment, and Table 2 shows structural parameters of the embankment before and after repairing. In the repair work, the central region of the embankment

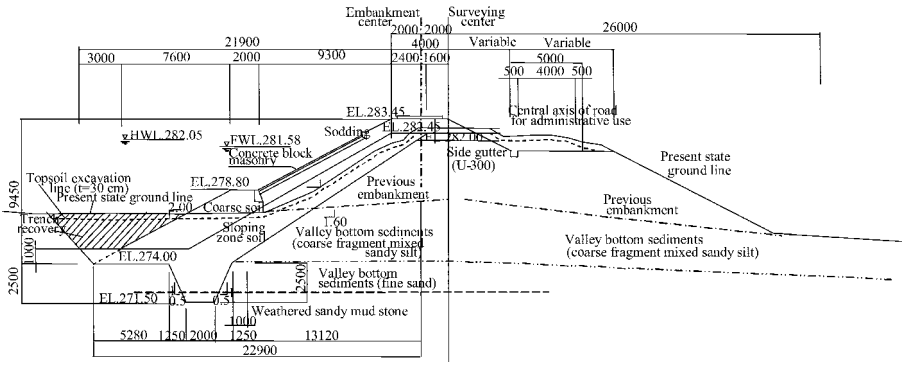

FIG. 21—*Standard cross section of Torakichizawa dam.*

was transversely excavated in the a V shape to repair the conduit, then the root part of the sloping impervious zone was excavated, with stepped-cut excavation of the former embankment, to construct a new sloping impervious zone. However, the target strength at that time, $(q_u)_{CC^*}$, was not $(q_u)_{CCStability} = 100$ kN/m^2, but $(q_u)_{CCTraficability} = 132$ kN/m^2.

Figure 22 shows the relationship between $(q_u)_{IS10}$ or $(q_u)_{CC7}$ that was determined from the uniaxial compression test for the undisturbed specimens of the initial stabilized soil and crushed and compacted soil ($D/H = 75$ mm/150 mm) which were obtained for each embankment volume of 500 m^3 and the accumulated amount of embankment soil V. The vertical line symbols indicate maximum and minimum values among the three types of specimens tested, and the symbols indicate the average values. This figure shows that although $(q_u)_{IS}^*$ and $(q_u)_{CC}^*$ which were set up for trafficability are not necessarily satisfied, ΔW_C was not altered because no problems can occur if the trafficability is kept during execution, and the strength required for the stability of the embankment $(q_u)_{CCStability} = 100$ kN/m^2 is satisfied.

Next, to check the water core performance of the inclined core zone, $(k_{TC})_{20}$ was determined by the triaxial permeability test for the core specimens that were obtained from the constructed embankment ($D/H = 75$ mm/150 mm), and k_{Field} was measured by the in situ permeablility test for each embankment volume of approximately 500 m^3. Figure 23 shows the relationship between the maximum and minimum values of $(k_{TC})_{20}$ and k_{Field} and the accumulated amount of embankment soil V. This figure shows that $(k_{TC})_{20}$ satisfies the standard value of the permeability, $k_{Lab} < 1 \times 10^{-6}$ cm/s, and k_{Field} satisfies the standard value of the permeability by the in situ test, $k_{Field} < 1 \times 10^{-5}$ cm/s, indicating that the constructed sloping impervious zone has the required permeability performance for the embankment.

Repair Work for the Embankment of the Kitatani Dam

The Kitatani dam is located in Matuzaka city in the Mie prefecture. The stability of the embankment cannot be maintained due to erosion and deformation, and because of the water leakage from the edge of

TABLE 2—*Structural parameters of Torakichizawa dam embankment before and after repairing.*

Embankment specifications	Before repairing	After repairing
Type	Homogeneous	Sloping sealing zone
Height (m)	7.0	8.4
Length (m)	65.5	70.0
Volume (m^3)	13 700	13 800
Amount of stored water (m^3)	3100	3100
Amount of crushed-compacted soil (m^3)	…	4000
Slope gradient	1: 1.5 (upstream) 1:1.8 (downstream)	1:2.0 (upstream) 1:2.0 (downstream)

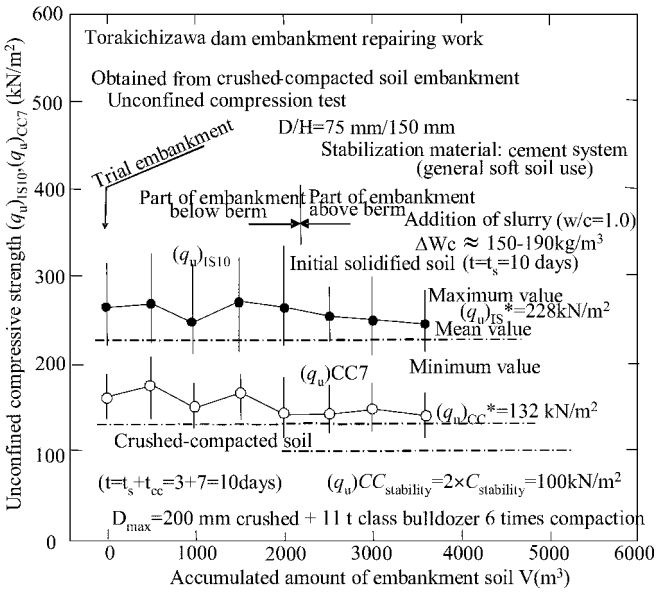

FIG. 22—*Relationship between* $(q_u)_{IS10}$, $(q_u)_{CC7}$ *and V.*

the embankment slope and the periphery of the bottom gutter due to aging. Thus, the water-leakage protection by the inclined core zone, and the overall repairs of the bottom gutter and flood outlet were needed. Figure 24 shows the cross-sectional view of the embankment after repairing of the Kitatani dam, and Table 3 shows structural parameters of the embankment before and after repairing.

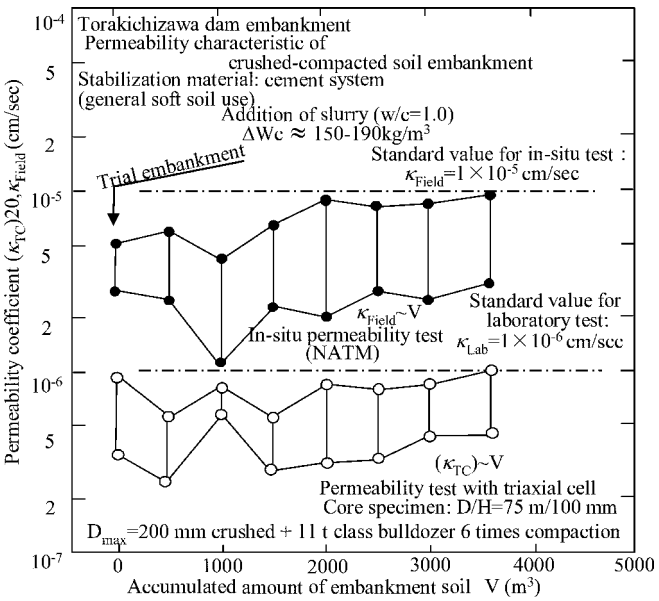

FIG. 23—*Relationship between* k_{Field} *or* $(k_{TC})_{20}$ *and V.*

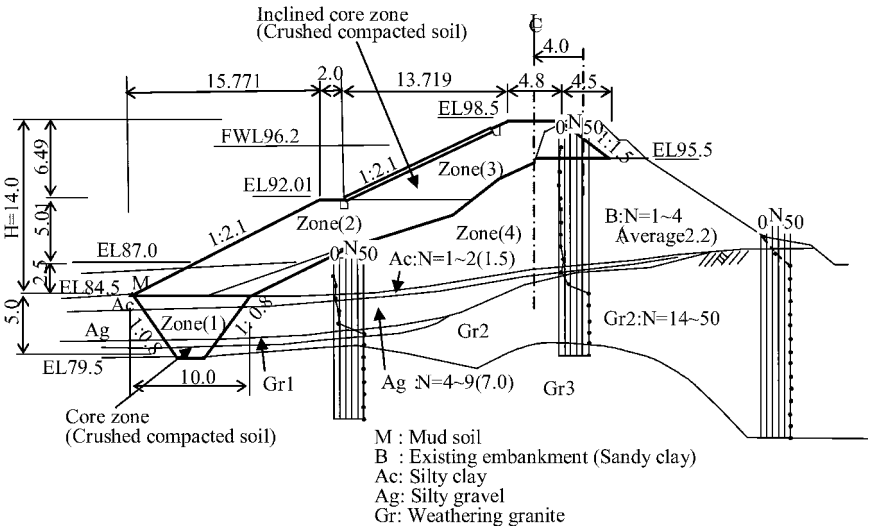

FIG. 24—*Standard cross section of Kitatani dam.*

The figure and the table show that the embankment is taller than 12 m, and is as large as the earth dam embankment. Thus, if the embankment is repaired using an available amount of embankment soil to keep the stability and the low permiability for the embankment, the resultant slope gradient must be small, i.e., more than 1:3.0. A large amount of embankment soil is required to repair this embankment, and the water storage capacity would be drastically reduced, so realistic repairs were considered to be impossible. Also, a large amount of pond mud soil was obtained by excavating the sloping impervious zone, but it was not possible to remove it without any processing. Even if it were possible, it would be difficult to secure a site for disposing of the soil. For these reasons, the embankment construction method with crushed-compacted soil was adopted for repairing this earth dam, which can artificially produce embankment soil with the strength required for embankment stability and low permiability capable of maintaining the water-storing function for the embankment by solidifying pond mud soil using a cement system stabilization material. Figure 25 shows the embankment of the Kitatani dam under repair.

Since the amount of embankment soil planned fell short for the Kitatani dam and Jige dam, mixed mud soil was prepared by adding earth and sand, which was obtained by excavating the earth dam bed to

TABLE 3—*Structural parameters of Kitatani dam embankment before and after repairing.*

Embankment specifications	Before repairing	After repairing
Type	Homogeneous	Inclined sealing zone
Height (m)	12.0	14.0
Length (m)	116.0	116.0
Volume (m^3)	25 500	36 000
Amount of water stored (m^3)	150 000	150 000
Amount of crushed -compacted soil (m^3)	-	16 000
Slope gradient	1: on average 1.6 (upstream)	1:2.1 (upstream)
	1: on average 1.5 (downstream)	1: on averave 1.8 (downstream)

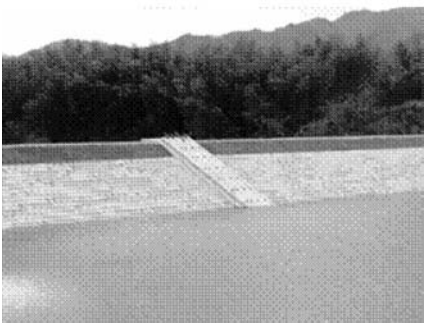

FIG. 25—*Kitatani dam embankment after repairing.*

compensate for the reduction in the water-storage capacity due to the embankment repairs, with pond mud soil. The mixing ratio of earth and sand to pond soil was determined to satisfy the required standard value of the permeability, $k_{Lab} \leqslant 1 \times 10^{-6}$ cm/s.

For earth dams which are lower than 10 m, the target strength of the crushed-compacted soil, $(q_u)_{CC}$*, is the strength that is necessary to keep the trafficability for the construction machines that were used. However, since the slope gradient was set to be steeply. i.e., (1:2.1), to keep the water-stored capacity, $(q_u)_{CC}$* was determined from the strength $C_{Stability} = (q_u)_{CCStability}/2$ that is required for a (the) embankment stability satisfying the (a) necessary safety stability, $(q_u)_{CCStability}$.

Since $(q_u)_{CC}^* = (q_u)_{CCStability}$ which was determined from a stability analysis is large, when the strength of the existing embankment is small, there appears to be a large difference between the strengths of the existing embankment and the newly constructed sloping impervious zone. Such a difference is not desirable for maintaining a close contact between the existing and new embankments. Thus, to reduce the difference in strengths of the existing and new embankments, $(q_u)_{CC}$* at the over and under layers of the berm in sloping impervious zone were made different for the Kitatani dam. That is, the strength of the layer over the berm, being affected significantly by the embankment deformation during an earthquake, was set to be the strength required for trafficability $(q_u)_{CC}^* = (q_u)_{CCTrafficability}$ and only the strength of the layer under the berm, being hardly affected by the embankment deformation during earthquake, was set to $(q_u)_{CC}^* = (q_u)_{CCStability}$, and the values were determined from the stability analysis. Furthermore, embanking of the under layer by using crushed-compacted soil with high strength leads to the widens the under layer, which is an advantage for stability analysis.

Concluding Remarks

Crushed-compacted soil is produced first by solidifying the earth dam mud soil with a cement stabilization material, and then by crushing and compacting the stabilized soil. Although conventional stabilized soil is apt to crack, crushed-compacted soil has properties that are similar to those that of ordinary natural soil.

In this paper, laboratory tests for crushed-compacted soil was performed to investigate the strength characteristics, the stress and strain behavior, permeability characteristics, consolidation characteristics, and durability. A new construction method was developed to use purely pond mud soil, but the size distribution of the grains of actual pond mud soil depends considerably on the water shed and the mud precipitation site in the earth dam, thus it is necessary to mix different types of pond mud soil. Thus, the grain size distribution of pond mud soil should be checked carefully to determine the mixing ratio and the sizes of the crushed grains according to its intended use for the embankment before execution. Although, we have mainly described the crushed-compacted soil using only pond mud soil in this report, in actual projects it is necessary to effectively use the excavated soil from the embankment and natural ground soil with the pond mud soil effectively. The construction method with the crushed-compacted soil is also applicable by determining the most appropriate mixing ratios of soil and additive ratios of cement. By this method, in principle, all the soil that was obtained in the construction site can basically be used.

At present, there are five examples where this construction method has been applied. Pond mud soil

and excavated soil from the former embankment and natural ground are used by mixing. All embankment materials are obtained inside the earth dam site, and there is no introduction of other new embankment materials and no removal of waste soil. Good execution management is necessary to determine the mixing design according to the types of soil obtained in the earth dam site, and the sizes of the crushed grains, which is possible by establishing a laboratory at the working site. The cost of the embankment construction with crushed-compacted soil is dependent on the cost of purchased soil and the cost of disposing of pond mud soil. Considering the previous cases, a 20–50 % reduction in cost is possible for the direct construction cost of the embankment. Also, as introduced in the case of the Kitatani dam, this method is suitable for high embankments; e.g., by increasing the strength of only the lower layer of the inclined core zone where the deformation is small, when an earthquake occurs, and the slip plane passes through, the difference between the strengths of the former embankment and the core zone can be reduced.

References

S. Fukushima, A. Kitajima, S. Tani, and K. Ishiguro, 2003, "Strength and Permeability Characteristics of Small Earth Dam Embankment Constructed by Cement-Stabilize d Muddy Soil," *J. Japan. Soc. Civ. Eng.*, No.750/3-65, pp. 205–221.

S. Fukushima, S. Tani, A. Kitajima, and K. Ishiguro, 2004, "Case Study of Sloping Core Zone Constructed by Cement-Stabilized Muddy Soil for Leakage 8 Control," *J. Japan. Soc. Civ. Eng.*, No.764/3-67, pp. 341–357.

Japanese Geotechnical Society, 2000, Standard Soil Test Method (JGS 0711).

Journal of ASTM International, Vol. 3, No. 7
Paper ID JAI13351
Available online at www.astm.org

Takeshi Suko,[1] *Tomonori Fujikawa,*[2] *and Tsuyoshi Miyazaki*[3]

Transport Phenomena of Volatile Solute in Soil during Bioventing Technology

ABSTRACT: Bioventing is one of the remediation techniques for volatile organic compound (VOC) contamination with VOC in the vadose zone. The object of this study is to investigate the pollutant transport and removal during aeration treatment focusing on convection, biodegradation, and volatilization. As for the result of 20-cm column experiment, dodecane removal ratio of the samples with aeration was about 20 % higher than those with no aeration. But after 30 days, the increasing rate of dodecane removal ratio decreased drastically in all cases. Total germ density increased after 10 days, but stopped increasing after 30 days. In the samples with higher water content, total germ numbers and dodecane removal ratio increased largely at the inlet of the air. From the estimations of the contribution of volatilization and biodegradation, the authors found that volatilization played a more important role on dodecane removal during the first 10 days of the column experiment, and biodegradation became predominant afterward.

KEYWORDS: bioventing, microorganism, andisol, volatilisation

Introduction

The problems of soil or groundwater pollution are occupying the interest of people all over the world lately. Bioventing is one of the remediation techniques for volatile organic compound (VOC) contamination in the vadose zone. The advantages of using this technique are that the remediation cost is low and complete remediation can be achieved. There have been several studies about bioventing. Most of these studies are conducted in the field contaminated with volatile organic compound, definitely the way pollutant mass removed is calculated from O_2 and CO_2 gas concentrations was indicated (Hinchee et al. 1992), monitoring O_2 and CO_2 gas concentrations and estimate of annual biodegradation ratio of pollutant using convective-diffusion equation and chemical formula were conducted (Lahvis et al. 1996). In most of the researches about bioventing so far, the target soils are almost limited within sand and sandy soil. We conducted the difference of remediation efficiency between sand and Andisol (Suko et al. 2004). This study aimed at investigating the pollutant transport and removal during aeration treatment in the aspects of biodegradation and volatilization.

Materials and Methods

We conducted aeration experiment by using a column filled with Tachikawa Loam soil (Andisol) polluted with dodecane, a component of light oil and kerosene. Andisol was sampled at 1-m depth of farming field at Nishi-Tokyo, Tokyo, Japan in order to consider the subsoil pollution. We added 1-mg dodecane per 1-g dry soil, mixed them, and stored at 4°C overnight. The column was made of acrylic plastic of 7.5-cm diameter and 20-cm height. We packed dodecane-polluted Andisol with bulk density of 0.50 Mg/m^3 by hand. Figure 1 shows the schematic figure of aeration experiment. Air was put into the column at the bottom using a pump with constant flow rate, 20 ml/min for 50 days. In order to stabilize the airflow and to add enough moisture to the air, a buffer was attached between the pump and the column. We installed gas samplers, which is made of porous stone, in the depth of 3, 9, 13, and 17 cm from the surface of the

Manuscript received March 30, 2005; accepted for publication October 19, 2005. Presented at ASTM Symposium on Contaminated Sediments: Evaluation and Remediation Techniques on 23–25 May 2006 in Shizuoka, Japan; M. Fukue, K. Kita, M. Ohtsubo, and R. Chaney, Guest Editors.

[1] National Institute of Advanced Industrial Science and Technology.
[2] National Institute of Rural Engineering.
[3] Graduate School of Agricultural and Life Sciences, The University of Tokyo.

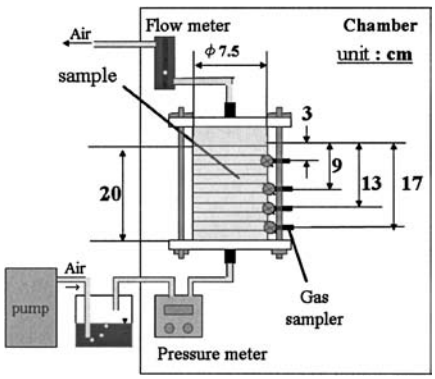

FIG. 1—*Schematic figure of aeration experiment.*

sample, extracted the gas in the soil gas phase by using syringes connecting with them every 10 days, and measured gaseous dodecane concentration in the extracted gas with gas chromatography (FID, Shimadzu GC-14A). After 50 days, we picked up the sample in the depth of 3, 9, 13, 17, and 19 cm from the surface, and measured the fluid dodecane concentration (mg-g^{-1} dry soil) with solvent (polychrolotrifluoroethylene, S-316) extraction method using fourier transform infrared spectroscopy (FTIR-8200PC, SHIMADZU) and the number of micro-organisms with direct count technique (Someya 1995). The experimental condition is shown in Table 1. We changed water content of the sample, that is to say, air filled capacity and evaluate the efficiency of pollutant removal. In order to observe the time series of these measurement indexes, we determined three kinds of aeration period, 10, 30, and 50 days for Runs 1 and 2, respectively. All the experiments were conducted under constant temperature, 30°C.

Result and Discussion

Comparison with Removal Ratio of Dodecane

Figure 2 shows the time series of removal ratio of dodecane from the samples. Removal ratio of dodecane in the sample (RR_{all}) mentioned here was calculated using the following equation:

$$RR_{\text{all}} = \frac{C_{f,\text{ini}} - C_{f,\text{res}}}{C_{f,\text{ini}}} \tag{1}$$

where $C_{f,\text{ini}}$ is the initial concentration of fluid dodecane (mg-g^{-1} dry soil), and $C_{f,\text{res}}$ means the concentration left in the sample at a given time (mg-g^{-1} dry soil). We give the average of the value measured at five sampling point for each point in Fig. 2. RR gradually increased in the whole experimental period, and the rate of the increase was smaller for 30- to 50-day period, compared with the 10- to 30-day period.

Result of Run 1

Figure 3 represents the distributions of removal ratio of dodecane as for Run 1. For the whole period of the experiments, almost uniform distributions of removal ratio was observed. Figure 4 shows the distributions of concentrations of gaseous dodecane. The concentrations decreased drastically after 20 days, and did not change afterward. We point out that the concentration at the surface was higher than that at the bottom in

TABLE 1—*Conditions of the experiment.*

Run No.	Water content, g g^{-1}	Air-filled porosity, m^3 m^{-3}	Saturation, m^3 m^{-3}
1	0.8	0.35	0.53
2	1.2	0.20	0.75

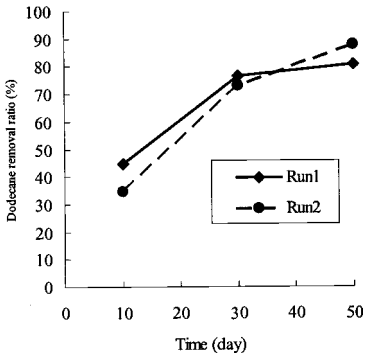

FIG. 2—*Time series of removal ratio of dodecane.*

every period. Figure 5 shows the distributions of the numbers of micro-organisms per 1-g dry soil. For first 10 days, micro-organisms decreased because the species of micro-organisms which cannot degrade dodecane as a substrate lost their activities. For the period from 10- to 30-day, the numbers were about twice as many as the initial value. For the period from 30- to 50-day, the number decreased slightly from the previous period because at this period much dodecane is removed from the sample by volatilization and biodegradation, so substance shortage happened to the micro-organisms there. The distributions in Fig. 5

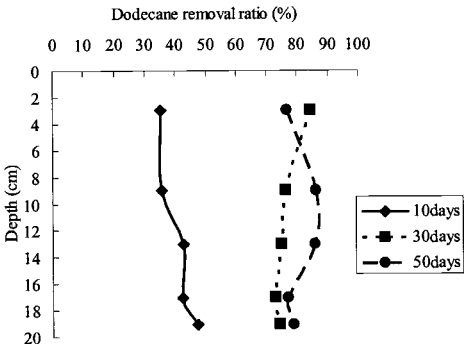

FIG. 3—*Distributions of removal ratio of dodecane (Run 1).*

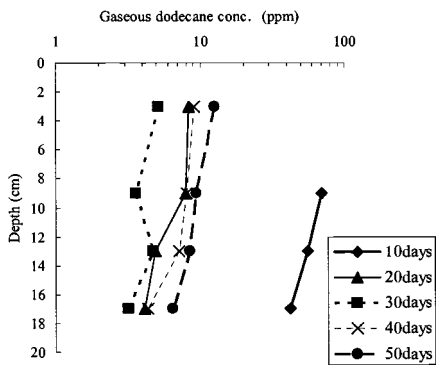

FIG. 4—*Distributions of concentrations of gaseous dodecane (Run 1).*

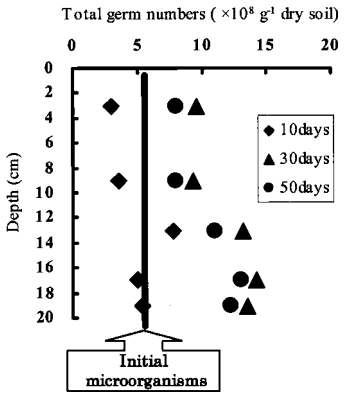

FIG. 5—*Distributions of the numbers of microorganisms (Run 1).*

suggest that the numbers of micro-organisms at the bottom of the column, the inlet of airflow, were larger than that at the surface. The reason is that micro-organisms living at the bottom can take fresh air more easily because of the air supplied from outside.

Taking every factor into consideration, biodegradation was the main factor of the remediation of dodecane at the inlet of airflow, and on the other side volatilization was at the surface. So the distributions of removal ratio were almost uniform.

Result of Run 2

In Run 2, the condition of lower air-filled porosity, Fig. 6 represents the distributions of removal ratio of dodecane. As time went by, the ratio at the bottom of the column was higher than that at the surface. Figure 7 shows the distributions of concentrations of gaseous dodecane. Similar to the result of Run 1, in that, the distributions were almost uniform. The values were lower than those in Run 1, and this can be because low air-filled porosity means the path of the airflow was restricted, in other words, the contact between air and fluid dodecane was restricted.

Figure 8 shows the distributions of the numbers of micro-organisms per 1-g dry soil. For first 10 days, micro-organisms were as many as initial values. For the period from 10 to 30 days the numbers was four times at a maximum as many as the initial value. For the period from 30 to 50 days, the number did not change. From the distributions in Fig. 8, it is pointed out that the number of micro-organisms at the bottom of the column was larger than that at the surface, the trend is similar to Run 1. In summary, at the bottom

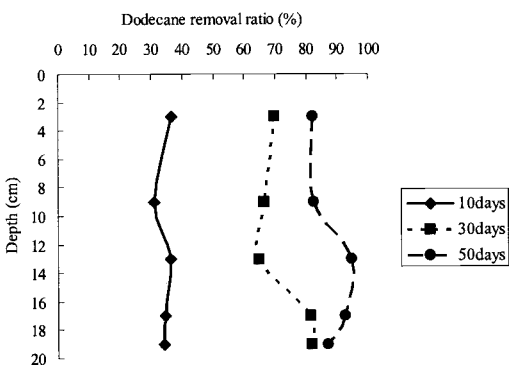

FIG. 6—*Distributions of removal ratio of dodecane (Run 2).*

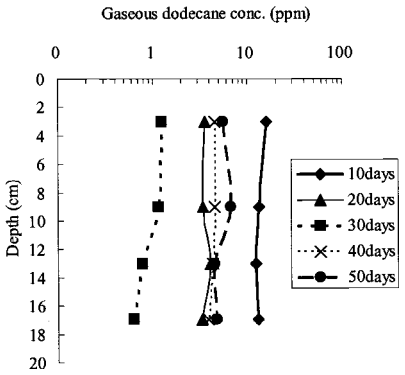

FIG. 7—*Distributions of concentrations of gaseous dodecane (Run 2).*

of the column biodegradation was dominant for removal of dodecane, but the influence of volatilization was low in this condition. Therefore we realized that the removal ratio at the bottom of the column was higher than that at the surface.

Contributions of Biodegradation and Volatilization to the Removal of Dodecane

Now we are going to separate the removal ratio of dodecane into two factors, i.e., biodegradation factor, which means the dodecane removal ratio only by biodegradation and volatilization factor, which means the one only by volatilization. We can calculate the volatilization factor from the results of gaseous concentration of dodecane using the following equation (Malina et al. 2000):

$$RR_{\text{vol}} = \frac{1}{2}\rho(C_{g,t1} + C_{g,t2})Q_a \tag{2}$$

where RR_{vol} is removal ratio by volatilization, ρ is the density of dodecane, $C_{g,t1}$ and $C_{g,t2}$ mean the gaseous concentration of dodecane at $t1$ and $t2$, and Q_a is the volume aerated between $t1$ and $t2$. We calculate the biodegradation factor by subtracting volatilization factor from the whole removal ratio of dodecane.

Table 2 shows the result of calculations. For the first 10 days, volatilization is the ruling factor in dodecane remediation, because microorganisms are trying to be accustomed with the environment where dodecane existed (so-called lag time). For the next period (10–30 days), biodegradation degrade more

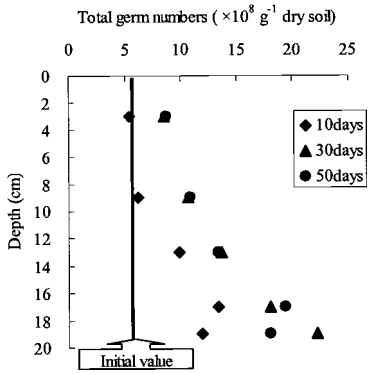

FIG. 8—*Distributions of the numbers of microorganisms (Run 2).*

TABLE 2—*Contributions of biodegradation and volatilization for removal of dodecane.*

Run No.	Period	Volatilization factor, %	Biodegradation factor, %
1	0～10 day	24	21
	10～30 day	6	25
	30～50 day	2	2
2	0～10 day	20	14
	10～30 day	4	34
	30～50 day	4	11

dodecane than before whereas volatilization decreased because of the decline of fluid dodecane. For the last period (30–50 days), fluid dodecane decreased remarkably and therefore the removal ratio decreased in both factor.

Considered with the difference of air-filled porosity, more dodecane was removed in the samples which had high air-filled porosity after 10 days, but afterward, the removal ratio of the sample with low air porosity was more than that with high porosity because the sample with low air-filled porosity have more fluid dodecane, namely, the sample have the power enough for indigenous micro-organisms to work for remediation.

Conclusion

We observed the remediation process of Andisol contaminated with dodecane by aeration treatment. The micro-organisms lived in the sample increased from 10–30 days after a lag-time period and degrade more dodecane than any other period of the experiment. On the other hand, volatilization occurred harder for the first 10 days, especially at the surface of the sample. The low air-filled porosity makes the contact between air and fluid dodecane restrict, so the contribution of volatilization for the removal of dodecane was lower than that of the sample with high air-filled porosity. But the high water content provide more micro-organisms with dwelling, therefore the sample of high water content, that is, low air-filled porosity exceeded that of high air-filled porosity in contribution of biodegradation.

Acknowledgments

We thank Hiromi Imoto at the University of Tokyo for his help in experiments. We also thank unknown reviewers for their advice.

References

Hinchee, R. E. and Ong, S. K., "A Rapid In Situ Respiration Test for Measuring Aerobic Biodegradation Rates of Hydrocarbons in Soil," *J. Air Waste Manage. Assoc.*, 42(10), 1305-1312 (1992).

Lahvis, M. A. and Baehr, A. L., "Estimation of Rates of Aerobic Hydrocarbon Biodegadation by Simulation of Gas Transport in the Unsaturated Zone," *Water Resour. Res.*, 32(7), 2231-2249 (1996).

Malina, G. and Grotenuis, J. T. C., "The Role of Biodegradation during Bioventing of Soil Contaminated with Jet Fuel," *Appl. Biochem. Biotechnol.*, 88, 59-76 (2000).

Someya, T., "Three-Dimensional Observation of Soil Bacteria in Organic Debris with a Confosal Laser Scanning Microscope," *Soil Microorganisms*, 46, 61-69 (1995).

Suko, T., Miyazaki, T., Imoto, H. and Mizoguchi, M., "Experiments of Bioventing for Soil Pollutant Removal," *Trans. Jpn. Soc. Irrig. Drain. Reclam. Eng.*, 72(1), 29-36 (2004).

Author Index

Subject Index

www.astm.org

ISBN: 0-8031-3408-8

ASTM Stock# STP148